A geological investigation of multispectral remote sensing data for the Mahd Adh Dhahab and Jabal said districts, western Saudi Arabia

Al-Sari, Abdulkader Mohammed


بسم الله الرحمن الرحيم

A GEOLOGICAL INVESTIGATION OF MULTISPECTRAL REMOTE SENSING DATA FOR THE MAHD ADH DHAHAB AND JABAL SAID DISTRICTS, WESTERN SAUDI ARABIA.

A thesis presented for the degree of

Doctor of Philosophy

by

Abdulkader Mohammed Al-Sari

University of Durham

Department of Geological Sciences.

August, 1989

DECLARATION

The work contained in this thesis has not been submitted elsewhere for any other degree or qualification and that unless otherwise referenced, it is the author's own work.

STATEMENT OF COPYRIGHT

This Thesis is dedicated to the memory of my Father, Mohammed Salem Al-Sari.

Also to my mother, wife, my daughter Nada, my sons Mohammed and Abdullah, and to my dear brothers and sisters.

ABSTRACT

This thesis examines the effect of spatial resolution on lithological and alteration mapping using remotely sensed multispectral data.

The remotely sensed data were obtained by the Thematic Mapper (TM) and Airborne Thematic Mapper (ATM) over two areas in the Arabian Shield. These were the Mahd Adh Dhahab and Jabal Said areas. The ATM data had a nominal spatial resolution of 7.5m, 5m, and 2.5m. In order to compare these data sets it was necessary to correct for sensor- and scene-related distortions. This was achieved by calibrating each data set and converting them to reflectance units using ground spectra with a similar spectral resolution obtained with the Barringer Hand Held Ratioing Radiometer (HHRR). The ATM data were also corrected for X-track shading by normalising the brightness of each column to that of the centre column.

The result of X-ray and laboratory spectral analysis of samples collected from the study areas, support the presence of characteristic minerals associated with the alteration zones.

The corrected data were analysed by a variety of techniques in order to enhance the geological information present in the data. These included false colour compositing, decorrelating stretching and band ratioing. The latter two techniques proved most effective for discrimination and several additional geological units and areas were identified which had not been mapped previously.

Results further indicate that the increased spatial resolution of the ATM data did not permit greater discrimination than the TM data. This suggests TM data should prove to be a cost-effective way of mapping and detection of alteration zones in the Arabian Shield.

ACKNOWLEDGEMENTS

The author is very grateful to the King Fahd University for Petroleum and Minerals, Saudi Arabia for their financial and moral support. I am grateful to Dr. Abdullah Dabbagh, Director of the Research Institute at King Fahd University for his continuous interest and support.

The author would also like to express his sincere thanks and gratitude to Dr. Timothy Munday for his supervision and invaluable advice and constructive criticism throughout. Thanks are also extended to colleagues at Durham University, especially Dr. Simon Hook for providing programs for data calibration and shade corrections.

Many thanks go to Dr. C.H. Emeleus for all his help and moral support and for acting as supervisor after the departure of Dr. Munday in November 1988. Special thanks to Mr. Ron Hardy for his help with the X-ray of samples and analysis; and to Dr. Mohamed Tawfiqe, Chief Geologist at the Ministry of Petroleum and Minerals, Jeddah (Saudi Arabia) for providing the ATM data and field support.

Finally, I am grateful to Carole Blair for her excellent typing and to Karen Atkinson for drafting the figures, and also to the technical staff in the Department of Geological Sciences, University of Durham. Thanks also to friends from the Mahd Adh Dhahab Gold Mine Project for providing the field support. Special thanks to my wife for her support and encouragement without which I would never have completed this work.

TABLE OF CONTENTS

CHAPTER ONE

CHAPTER 2

GEOLOGICAL SETTING

CHAPTER 3

PHYSICAL BASIS FOR THE USE OF

MULTISPECTRAL REMOTE SENSING DATA FOR

LITHOLOGICAL AND ALTERATION MAPPING IN THE STUDY AREA

CHAPTER 4

PRE PROCESSING AND PREPARATION

OF MULTISPECTRAL REMOTE SENSING DATA

CHAPTER 5

LITHOLOGICAL DISCRIMINATION AND THE INFLUENCE OF SPATIAL RESOLUTION ON LITHOLOGICAL MAPPING AND MINERAL EXPLORATION

CHAPTER 6

DIGITAL IMAGE ANALYSIS AND

INTERPRETATION

CHAPTER 7

CONCLUSIONS AND RECOMMENDATIONS

LIST OF TABLES

LIST OF FIGURES

CHAPTER 1

INTRODUCTION

1.1 Background

Remotely sensed data, particularly in the form of aerial photographs, have been used as a major tool of field geologists for about 50 years. Aerial photographs consistently provide a means for area-wide extrapolation of outcrop information and permit the integration of these data into the broader geological fabric. At the same time they provide excellent base maps, especially in the poorly-mapped areas, where adequate conventional maps are either poor, or completely non-existent.

Since NASA's first Earth Resources Technology Satellite (ERTS-1), now known as LANDSAT, was launched into orbit in July 1972, and followed by LANDSAT Series, they have delivered high-resolution, multispectral images of the earth, providing new sources of geological information and helping the geologist with new concepts and capabilities. The result of combining the spectral imaging capability as well as digital image processing was a significant turn away from the use of standard photo interpretation techniques on aerial photography to an expanded use of the spectral properties of surface materials for mapping, and discrimination (Goetz et al., 1981; Goetz, 1983). The Landsat carried a four-channel

Multispectral Scanner (MSS) and three Camera Return Beam Videcon (RBV), a data collection system, and two tape recorders for data storage. The four MSS channels had the following spectral intervals: Band 4 (0.5-0.6um); band 5 (0.6-0.7um); band 6 (0.7-0.8um); and band 7 (0.8-1.1um), and it recorded data at a nominal spatial resolution of 79 metres (NASA, 1972; see Appendix A10). MSS was designed primarily for agricultural applications, although much valuable geologic information has been derived from it.

Interpretation of Landsat images has been widely accepted by the geological community (e.g. Rowan et al., 1977). Excellent interpretations of regional structures can be made from the satellite images, based on surface texture, tone and geometric form (e.g. Boldget et al., 1978). In addition, a limited number of rock classes can be discriminated using the multispectral scanner (e.g. Lawrence et al., 1977; Price et al., 1985).

Much of the research in the late 1970's and early 1980's concentrated on determining spectral features in the visible and near infrared for most of the minerals and rocks on the earth's surface, and the work published by Hunt and his group was considered to be very important in identifying minerals and rocks using these spectral features (Hunt et al., 1970, 1974).

Further studies used spectral reflectance and spectral emittance characteristics of rocks and minerals in different wavelength regions. These were conducted

over various areas using either the Skylab S-192 scanner which had 12 bands in the 0.4-2.5um wavelength region, and a single broad-band thermal infrared band (Vincent, 1974), or field and laboratory spectra which covered 0.45-2.5um, or a Bendix 24-channel (MSDS) scanner (Abrams et al., 1977). Areas of hydrothermal alteration were mapped in the Cuprite Mining District of Nevada using MSDS data. This studey provided the basis for the selection of the seventh band (2.08-2.35um) to be incorporated in the Landsat 4 Thematic Mapper.

The Thematic Mapper (TM) (Landsat 4) was launched on July 16th 1982, comprising a seven band multispectral scanner system with six channels covering a wavelength range from visible to near infrared (0.45-2.35um), and one channel in the thermal infrared band region 10.4-12.5um. The spatial resolution of Landsat 4 and later Landsat 5, was 30m for the six reflective visible/ s.w. infrared bands and 120m for the thermal infrared band (Appendix A2).

The development of airborne multispectral scanners has moved in parallel to the satellite development, with an airborne scanner normally preceding a satellite scanner in order to test the design specifications. However, aircraft scanners have developed a role in their own right. An aircraft is more directly under the control of the operator in terms of where and when it will carry out the surveys. The aircraft's altitude is variable, within

limits, and this allows the spatial resolution of the data to be varied. Also the airborne scanners commonly have a wider spectral coverage than satellite systems and this can be modified if necessary.

Recently, more sensors have been designed by many companies according to their customers' needs. The AADS-1268 Airborne Thematic Mapper (ATM) is one of the most advanced scanner systems currently available, designed by the Daedalus Company (Daedalus, 1982). Data from this scanner will be used in this study.

In addition to existing earth resource satellite systems such as Landsat TM, there is a growing trend towards the use of high spectral resolution data which allows surface materials to be identified from detailed spectral signatures. For example, Collins (1978) made the first step by acquiring spectro-radiometer data in 512 channels in the 0.4-1.0um region and 64 channels in the 1.0-2.5um or in the 2.0-2.5um region (Collins et al., 1983). Goetz et al. (1982) acquired data from shuttle orbits with a radiometer covering the 0.5-2.35um region in 10 channels; the 2.1-2.35um region contained 5 channels, 3 were 0.02um wide and centred at 2.17, 2.20 and 2.22um.

The Space Shuttle Synthetic Aperture Radar Systems SIR-A and SIR-B which were flown on NASA's space shuttle, were an imaging radar. Radar has proved useful for mapping regional structural features in areas of moderate relief (Crane, 1987) and the arid regions, such as Egypt

and Saudi Arabia are considered to be excellent terrains for the use of radar imagery (Crane, 1987; Dixon et al., 1988).

The results of the research described in this study are primarily concerned with the applications of remote sensing in the visible and near infrared wavelength regions (0.4-2.5um), mainly using multispectral data recorded by the Landsat TM and Daedalus 1268 (ATM) sensors.

1.1.1 The application of remote sensing data in geological studies of arid regions.

The arid land such as the Precambrian Arabian-Nubian Shield, provides an excellent area to test the capabilities of remote sensing data from either satellite or airborne sensors for geological mapping. It includes a wide variety of rock types and structures. Individual rock units are frequently exposed in large and fairly homogeneous bodies. Due to the arid climate there is little chemical weathering and soil development, and most of the area is nearly devoid of vegetation (Smith, 1977).

The application of remote sensing techniques to map the different lithologies and mineralized zones requires complete knowledge about the spectral reflectance and spectral emittance characteristics of rocks and minerals in different wavelengths (Goetz et al., 1983). Previous researchers succeeded in identifying spectral features for

most of the common minerals and rocks using laboratory samples (Hunt et al., 1970, 1979). For example, a spectral absorption feature at 0.4um is indicative of the presence of iron (Hunt & Salisbury, 1973). An absorption feature between 0.85 and 0.92um, as well as the slope of the reflectance curve in the visible region is used to identify the presence of limonite in Landsat MSS images (Rowan et al., 1974; Rowan et al., 1977).

In-situ reflectance spectra have been used to bridge the gaps between laboratory data and those supplied by remote sensing aircraft and satellite scanners (e.g. Kahle et al., 1981; Podwysocki et al., 1983; Whitney et al., 1983; Gladwell et al., 1983). The application of remote sensing to map areas of mineralization requires such areas to exhibit distinctive spectral reflectance curves which may be recorded by satellite or aircraft sensors.

Usually the ore minerals themselves are not exposed on the earth's surface (Gustafson et al., 1975) and so cannot be located by remote sensing. Epithermal deposits, however, are sources of many minerals which occur as sulphides. Here, the surrounding host rock is mineralogically changed during the injection of the ore bearing fluids. The mineralogical changes, termed hydrothermal alteration, produce a series of mineralogical assemblage zones which surround the ore deposits (Lowell & Guilbert, 1970; Gustafson et al., 1975). The surface exposure of an altered/mineralogical rock unit is often

expressed as a series of alteration zones with the most intensely altered rocks located closest to the intrusion. An intense iron staining associated with each zone is produced by the oxidation of pyrite. Clay minerals are the major alteration minerals which are often exposed on the surface overlying ore zones (Hunt & Ashley, 1979).

Altered rocks produce spectra which contain an intense absorption feature near 2.2m due to the strong fundamental OH vibration which generally reflects the behaviour of hydroxyl-bearing minerals (Chapter 3). Clays in particular, exhibit decreasing spectral reflectance beyond 1.6um, and this broad band has been used to identify clay-rich areas associated with hydrothermal alteration zones. The presence of alunite, pyrophyllite and muscovite also reduce the reflectance in the region in the 2.1-2.4um (Podwysocki et al., 1983; Prost, 1980; Goetz et al., 1983).

The hydrothermal alteration of the Cuprite, Nevada district, was studied by several researchers (Abrams et al., 1977; Rowan et al., 1977; Ashley & Abrams, 1980). Abrams et al. (1977) utilized an aircraft-borne multi-spectral scanner, equipped to measure reflectance intensities in hydroxyl and Al-OH vibrational overtone region (2.2um) as well as in the ferric absorption band. Using the ratios 1.6/2.2um, 1.6/0.48um and 0.6/1.0um, hydrothermal alteration could be delineated with or without ferric oxide coating. This technique will be less

effective if unaltered rocks in the area also contained hydroxyl-bearing minerals, they would also be classified as altered.

In another study, Rowan et al. (1977) used a portable field spectrometer in the Goldfield Mining District. The field spectrometer was equipped to record reflectance spectra between 0.4 and 2.4um, thereby including ferric and hydroxyl absorption features. They found altered rocks to have an overall higher reflectance due to the high clay and alunite content. They also showed altered rock spectra to contain a reflectance minimum centred near 2.2um due to clay minerals and alunite. Using a ratio of reflectance intensities recorded at 1.6um and 2.2um, the clay content could be examined and altered areas could be defined whether they occurred with or without a ferric coating.

The 1.6um region was used because it is a reflectance maximum on most spectra. The major problem in this method was the inability to discriminate between altered rocks and iron-stained rocks, such as unaltered hematitic metasediments. The metasediments have a strong clay absorption due to the clay minerals originally contained in the rock before metamorphism.

Subsequent studies have used different statistical and computational treatment of Landsat and aircraft data to enhance the difference between altered and unaltered rocks and to discriminate between different lithologies

(Podwysocki, 1979; Conel et al. 1980; Abrams et al. 1984). As a result of this, different techniques have been developed to manipulate the remote sensing data. These new techniques have been widely used for geological mapping and for identifying areas of alteration related to the mineralized ore bodies (e.g. Rothery & Milton 1981, 1984, 1987; Rowan, 1982; Bird et al., 1985; Loughlin et al. 1985; Legg 1985; Sultan et al., 1986, 1987; and Greenbaum, 1987).

Study by Longshaw (1974) revealed differences between laboratory spectra and field spectra (acquired in situ). Comparison of the two kinds of spectra revealed that major spectral features are observed in both, but that the environmental effects can modify the field spectra to the extent that they no longer resemble the spectra of pure laboratory materials. This is due to surficial weathering and natural diagenetic processes (Abrams and Siegal, 1981). The presence of surface vegetation and lichens also affect the spectral signature. However, much of the research into the use of multispectral measurements for geological applications has been undertaken in arid and semi-arid land, to minimize the effect of vegetation. Despite the wealth of information collected on the potential applications of multispectral remote sensing for lithological and mineral mapping (Munday, 1985), surprisingly little research has been reported on the effects of weathering and desert varnish on the spectral signatures of rocks and minerals. Marsh &

McKeon (1983) showed that the characteristic spectra for the units reflect their mineralogical assemblages. Their results indicate that in situ measurements can be used to separate and characterise visibly similar, altered rocks. Buckingham & Summer (1983) studied penetration depths of electromagnetic radiation on rock surfaces. The penetration depth varies with absorbed concentration and the wavelength being measured, but generally it is only the upper 50um of a rock surface which contributes to the rock's reflectance spectrum. The results of this study indicate a need to know the composition of the minerals which form the weathered products on the surface of the rocks. These may change from one environment to another.

According to Mosser (1979) the content of trace elements in clays formed by alteration of various rocks including granites, is very similar to that observed for the parent rocks (Minarik et al. 1983). Previous research on lithological mapping of arid areas has avoided the consideration of spatial variability of the spectral response within a particular lithology. Since Landsat MSS was launched, many people believed, wrongly, that improving the spatial resolution of the satellite-derived data, would increase the amount of discriminatory information. In fact an improved spatial resolution has not necessarily resulted in improved classification accuracy. The Landsat MSS with its $79m^2$ resolution (considered to be coarse spatial resolution), combined

with its relatively coarse spectral resolution, may classify certain cover types as being spectrally homogeneous. Using any other system with high resolutions of $30m^2$ TM, for example, may indicate these to be spectrally heterogeneous, because of the latter's ability to resolve a great inter-class variation, considering the IVOF only and not the spectral resolution (Townshend, 1980).

Most of the previous researchers who studied the effects of spatial resolution on lithological mapping, used data acquired at fixed resolutions, which was then degraded via computer processing to a coarser resolution (Abrams & Brown, 1984). This procedure produced images of the same ground deminsions for each pixel which could be registered to each other, thereby enabling easy selection of the same test area at each resolution (Markham, 1981).

There have been very few studies attempting to fully evaluate the information of the Landsat MSS or TM for geological mapping purposes. Landsat MSS with 79m resolution has been used to produce maps equivalent to 1:500,000 and 1;250,000 geological maps. Abrams (1982) (e.g. USGS 1984) using Landsat TM (30m resolution) expected to achieve mapping at 1:100,000 scale. In general he stated that the effects of resolution on spectral signals should be systematically studied. However, relatively little is known about the incremental

advantages of increasing pixel resolutions beyond 30m for lithological mapping purposes.

1.1.2 Geological application of remote sensing data in the Arabian Shield.

1.1.2.1 Aerial photography

Remote sensing data of several types have been used for mapping the Arabian Shield and the Arabian Peninsula. Aerial photography was one of the first remote sensing tools used, starting in 1949. By 1951, 640,000 square km of eastern parts of the country had been photographed. The remaining 4 million square km were covered between 1954-1959 to provide controlled vertical photography at 1:60,000 scale. In addition, the necessary overlap was obtained to give complete stereoscopic coverage. This controlled photography was used to produce highly accurate geographic maps at several scales, and served as a base for all subsequent surface mapping and regional compilations.

Geological activity in the Arabian Peninsula did not start until the early 1930's and was largely as an indirect response to the large petroleum exploration concession granted by the government. Comprehensive geological mapping of large areas, mainly where there has been sedimentary deposition, started in the East. Reconnaissance mapping for the entire sedimentary section was completed in 1946, and by 1954 the entire Arabian

American Oil Company (ARAMCO) concession had been mapped at scales of 1;500,000 or larger (Power et al., 1966). Official mapping of the Arabian Peninsula started later when a nationwide air survey was initiated in 1949, and by 1959 controlled aerial photography at a scale of 1:60,000 was available for most of the sedimentary section of Arabian Peninsula.

Mapping the Arabian Shield was not stimulated by the same strong economic factors that provided the finance and personnel for the earlier work. A preliminary mapping programme was initiated during the second world war by the United States Geological Survey (USGS) in cooperation with the Kingdom of Saudi Arabia. This started with localized geological and hydrological studies by G.F. Brown between 1944 and 1946. In 1960 the USGS, under the direction of G.F. Brown, initiated a more comprehensive mapping programme for the Shield area of Saudi Arabia. The broad objectives of this were to investigate mineral and water potential in the western part of the Kingdom of Saudi Arabia. By 1955 the entire Arabian Shield had been mapped at the reconnaissance level and many areas of specific economic or hydrological interest had been studied in detail (Blodget, 1978). The earliest geological maps of the Shield were at the scale of 1:500,000 and were published between 1956 and 1963 jointly by the Ministry of Petroleum and Mineral Resources and the United States Geological Survey. These were the result of cooperation

between ARAMCO, who supplied data on the Phanerozoic rocks from their exploration records, and the USGS who had undertaken a photo-geological interpretation of the Arabian Shield supported by observations from ground traverses. This series is seen today as an exceptionally fine set of reconnaissance maps of a huge area, prepared by a small team of geologists in a short time. One of the first priorities in the early 1960's, was to produce more detailed maps for mineral exploration using a 30-minute quadrangle format and the scale of 1;100,000. By 1974 a new series of maps was planned at 1:250,000 using a module of one degree by one degree thirty minutes; more detailed maps were produced around the old mining areas and any other promising deposits.

1.1.2.2 Satellite data:

Satellite imagery of the Arabian Peninsula has been available since the launch of the earliest weather satellite, Nimbus-1, in 1964. Several photographs of the Arabian Peninsula were also taken during Gemini and Apollo space trips. Landsat MSS data first became available after the launch of Landsat-1 on 23 July 1972. This was followed by Landsat-2 in January 1975. Cloud-free MSS images, obtained for the entire Arabian Peninsula, were used by USGS to prepare base maps and compile geological maps (Killsgard, 1978). Landsat imagery proved very useful in studies of geological features, such as fault and fracture systems. Hardy (1973, 1974) and Blodget

(1977) compared Landsat images with published geological maps (1:100,000) for Sahl Al-Mutran and as a result of activity between the USGS and the Deputy Ministry for Mineral Resources (DMMR) an index map of Landsat imagery of the Arabian Peninsula has been published which covers paths 169 through 198 and rows 38 through 51 (Miscellaneous map 102. SA(IR)-402 (1980). Blodget et al. (1978), used computer-enhanced Landsat data (MSS) to discriminate between the rock classes and the alteration products in southwestern Saudi Arabia. A Landsat image map at 1:4,000,000 was produced for the Arabian Peninsula from an uncontrolled mosaic of computer-enhanced Landsat MSS band 7 imagery. By the end of 1980, similar Landsat image maps had been published at 1:500,000 for the 21 quadrangles covering most of the Arabian Peninsula. In 1984 the first colour-composite imagery map from computer enhanced Landsat MSS bands 7, 5 and 4, for the Southern Hijaz quadrangle and other quadrangles were published.

In 1984 Landsat image maps of the central part of the Arabian Shield, scale 1:250,000 were published (USGS, 1984). The Landsat MSS data was also used for various studies in the Arabian Shield, e.g. drainage studies (Pruett and Vandenakker 1985).

Unfortunately, there were very few applications for using Landsat TM in the Arabian Shield and in the Arabian Peninsula. Recently Al-Hinai (1988) studied the Quaternary aeolian sand mapping in Saudi Arabia using

different remote sensing data, including Landsat TM. Also Landsat TM data was also used for mapping structural features in the Arabian Sheild (Thaker, 1988).

1.1.2.3 Airborne multispectral data:

In 1984 the Deputy Ministry for Mineral Resources in Jeddah, carried out a programme to assist mineral exploration in the mineralized zones, particularly in the Samran area. The survey area is shown in Fig. 1.1 and covers an area of approximately 30,000 sq.km. This survey used the Daedalus 1268 Airborne Thematic Mapper (ATM) which is a passive remote sensor designed to collect and record radiation from the earth's surface using an airborne platform. The ATM sensor separates incoming radiation into eleven spectral bands, ranging from the visible to the thermal infrared (see Appendix A3).

Imagery assists volcanic facies mapping and the delineation of alteration zones and gossans associated with sulphide mineralization. The survey was also intended to test the ATM technique as an exploration and mapping aid under a variety of topographic and geological conditions. The ATM survey was performed by the Arabian Aerosurvey Co. and Hunting Survey Co. using Daedalus scanner AADS-1268, which employs 10 spectral bands in the visible to shortwave infrared, and one broad thermal infrared band. The sensor has a spectral coverage which includes the range of the seven bands of Landsat TM, (Loughlin et al. 1985). The Arabian Aerosurvey (1984) and

Legg (1985) studied the application of the ATM over the Jabal Said alteration zone and noted the ability of the ATM to discriminate alteration zones from other lithologies.

Bird et al. (1985) carried out another study from test sites in the Arabian Shield using ATM data. They ranked the surface types in the test area in order of brightness for each waveband and indicated the importance of bands 10, 9, 3 (2.2, 1.6, 0.56um respectively) for discriminating the different lithologies.

Although the ATM-survey in the Arabian Shield created a huge amount of data, little interpretation and analysis has been done. Most of the study seems to be general and no detailed work has been carried out to evaluate the spectra measured by ATM.

1.2 Statement of the problem

The background to the research has been outlined in the previous section and this has highlighted the following problem areas where further research is required.

1. More information is required on the spectral response characteristics of natural surfaces in arid regions. In particular, it is important to study the effect of desert varnish on the spectral response of the natural weathering products. This is because some weathering products tend to obscure the spectral

differences between the rock types. In other words, there is a need to characterise in more detail the nature and causes of spectral variation in arid regions for different lithologies. As well as the desert varnish and the weathering effects, more information is also needed on how spectral signatures can be affected by homogeneity or heterogeneity of rock units. This provides a physical basis for more detailed interpretation of broad band multispectral data and also for interpretation of high spectral resolution data.

2. Although in situ spectra have been evaluated by previous research, the relationship between the field spectra, laboratory spectra, and the spectra extracted from Landsat or airborne imagery should be studied in more detail.

3. The Landsat spectral bands cover a broad wavelength range, for example, TM band 7 covers the range 2.08-2.35um. These broad bandpasses could be examined in more detail and in general, using sensors with a narrow spectral range in order to study the effect of spectral resolution on lithological mapping.

4. The effect of spatial resolution on information extraction should be better understood. In other words assess the incremental advantages of increasing pixel resolution for mapping purposes and

discrimination between different rock types. In particular, there should be more emphasis on the study of alteration zones. The field of geology encompasses many sub-disciplines, each of which have their own requirements for the scale of information necessary to solve the problem. The requirement of resolution needed is dependent on the problem and specific site.

5. The ATM survey over the Arabian Shield is considered to be one the largest and most comprehensive with data acquired over rugged and arid terrain. Only a limited amount of research has been done on the evaluation and use of these data for mapping and mineral exploration.

1.3 Aims and Objectives

The aims and objectives of this thesis are to test the capability and ability of multispectral remote sensing data for lithological mapping and mineral exploration. Specifically the objectives are as follows:

1. To test the ability and potential of multispectral remote sensing techniques covering the visible, near and SW infrared portion of electromagnetic spectrum, to map the different lithological units in the Arabian Shield.
2. To discriminate the hydrothermally-altered rocks from surrounding unaltered rocks. Thus, a considerable

effort will be made to understand the relationship between the composition of the different lithologies and the shape of their spectral curves and, in particular, the spectral features of the minerals which form the alteration zone.

3. To measure the effect of weathering on spectral reflectance and compare weathered surface to fresh rock surfaces, chemically by using x-ray diffraction analysis on selected samples, and spectrally using the laboratory reflectance spectra.

4. To describe the use of ground radiometric measurements to develop an understanding of the energy and behaviour of the spectra. The TM satellite data and the ATM data have been calibrated using ground based radiometric measurements in the field, measured by the Hand-held Radiometric Radiometer (HHRR).

5. To evaluate the spatial and spectral characteristics of different sensors considered by the study. By using quantitative analysis of the data, to analyse the effect of increased spatial resolution on lithological mapping and detecting the alteration zone in the area.

It is not possible to fully address all of the problem areas described in the previous sections, but the research described here begins to consider important factors for geological mapping in arid terrain.

1.4 Study area selection

Two test sites were selected in the Arabian Shield for application for this study. The selection was based on a variety of technical considerations relating to the surface characteristics and geology of the area, and for the following reasons:

1. The two sites chosen, Mahd Adh Dhahab and Jabal Said are characterised by contrasting types of mineralisation and types of alteration. The mineralisation at Jabal Said is massive porphyry, copper and zinc, hosted in pyroclastic rocks, whereas Mahd Adh Dhahab is characterised by mineralisation associated with quartz veins (mainly gold and zinc) intruded into pyroclastic and rhyolitic rocks.
2. Previous studies suggest the type of mineralisation and the alteration associated with mineralization at Mahd Adh Dhahab may not be easily detected using satellite data (Hakerby, 1984). One of the limitations of the MSS system was its lack of proper spectral regions for testing certain mineralogies. The Mahd Adh Dhahab was chosen as a means for testing the improved capability of TM and greater spectral coverage of other new sensors.

   Other reasons for choosing Mahd Adh Dhahab were the availability of detailed maps and studies of the alteration zone around the main hill which show the variations within the alteration zone. This provides

a unique test site for remote sensing data and their ability to detect the variation within the alteration zone.

In Jabal Said there is no detailed map for the alteration zone, but a wide range of lithologies provide a good site for testing the ability to distinguish different lithologies.

3. The sites are well exposed and a wide range of rock types are available for checking and improving mapping capability for the available data.
4. Adequate background information is available for both sites, including geological maps, structural studies, and reports to support the analysis and the interpretation of various remote sensing data.
5. There is no problem of access to the sites, for field checking and field spectral measurement.
6. Availability of the remote sensing data, where both of these two sites were used as test sites for ATM data from three different elevations for three different resolutions (IFOV) and a Landsat TM subscene covered both of them.

1.4.1 Remote sensing data used in this study:

The Landsat multispectral scanner data (MSS) with its very coarse resolution (80m), has been used to give a general impression of the type of terrain in the Arabian Shield and the general geology of the area.

The Landsat Thematic Mapper (TM) has been used for more precise identification of the different lithologies and the change in the terrain, as well as to study the ability of such data to be used to determine the location of alteration zones around promising deposits. The high resolution of the TM data, (30m) along with its narrower wave bands, helps to discriminate between different lithologies.

Apart from the spectral resolution of the sensors, spatial resolution effects have been studied using the Airborne Thematic Mapper data (ATM), covering both Mahd Adh Dhahab and Jabal Said areas. The spectral bands covered by the ATM are narrower compared to TM data. The effect of spatial resolution has been studied using ATM data for the same area with three different spatial resolutions (7.5um, 5.0um, 2.5um pixel sizes).

These remote sensing data were supported by ground truth data using the Hand Held Ratioing Radiometer (HHRR), with 10 bands, six of which correspond with the TM bands whilst the other four cover narrow bands from 2.0um to 2.35 um.

Further support and confirmation for identification of the lithology was performed using the laboratory spectra obtained by measuring the spectral reflectance of samples from different lithologies within the study area, using an Infra-Red Intelligent Spectroradiometer (IRIS). These spectra were compared to the field spectra for a

detailed analysis of the location of the spectral features.

1.5 Structure of the thesis

The thesis is structured as follows: Chapter 1, the Introduction is followed by Chapter 2 which describes the geology of the study areas.

Chapter 3 briefly reviews the nature of the current knowledge concerning the physical basis for multispectral remote sensing over an arid region. Attempts were made to determine the physical features of the different lithologies in the study area, that may affect the spectra. Samples collected from these lithologies were analysed by x-ray to define the chemical composition of the rocks. With some samples efforts were made to separate the weathered surface from the fresh rock. The laboratory spectra over selected samples serve as invaluable aids to determine some of their inter-relationships, also their chemical relationships are discussed. In order to gain a greater understanding of energy-matter interactions over natural surfaces, field based spectral measurements were taken using a hand-held ratioing radiometer (HHRR) over the two sites.

The field spectra will serve later as a reference to calibrate the Landsat and airborne data to reflectance units for ground surface comparison. The information in

this chapter serves as a basis for interpreting both airborne and satellite data in the following chapters.

Chapter 4 describes the calibration procedure to reduce the Landsat and airborne data to reflectance units. A procedure for removal of the across track shading effect from the airborne images was performed.

Following pre-processing of the data, Chapter 5 describes the effect of spatial resolution on extracting spectral information for the different lithologies. Quantitative analysis of data was performed using discrimant analysis to study the effect of spatial resolution on spectral information extraction.

Chapter 6 describes the digital image processing techniques used in this study for Landsat and ATM data. This is followed by interpretation of the digitally processed images and an evaluation of different techniques for detecting alteration zones is also discussed.

Chapter 7 contains the conclusions and suggested implications.

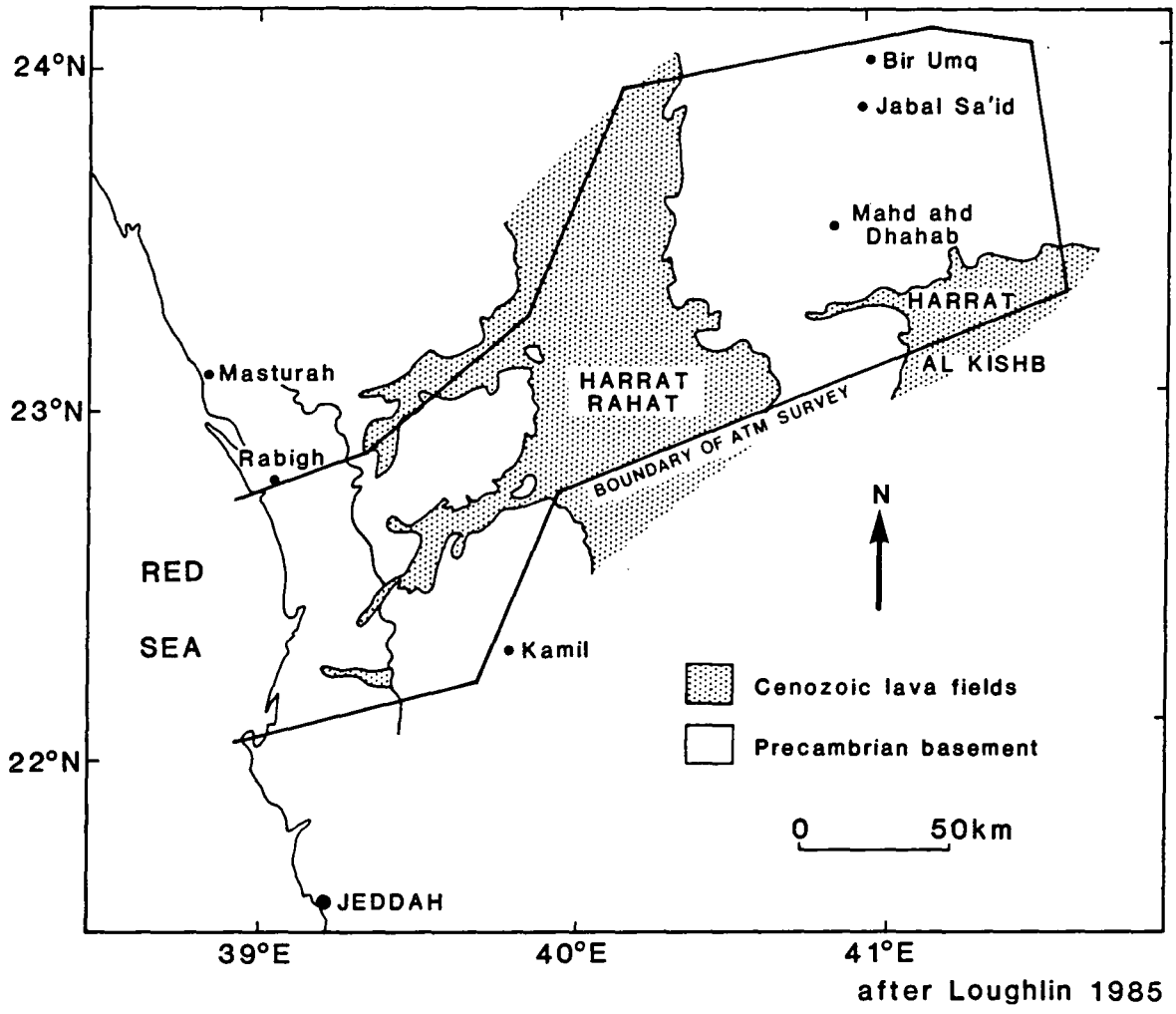

Fig. 1. The location of the area covered by ATM Survey (30,000 sq.km)

CHAPTER 2

GEOLOGICAL SETTING

2.1 Introduction

The study areas, "Mahd Adh Dhahab" and "Jabal Said" are located in the South Hijaz quadrangle in the west central part of the late Proterozoic Arabian Shield Fig. 2.1). This shield comprises a series of tonalitic and granodioritic batholiths with associated volcanogenic sedimentary rocks. The Proterozoic rocks are overlain by two large Tertiary-Quaternary basalt fields, Harrat Rahat in the west and Harrat Kishb east and south of Mahd Adh Dhahab and Jabal Said.

In this chapter, a general description of the regional geology of Mahd Adh Dhahab and Jabal Said is presented on a regional scale, followed by detailed descriptions of the geology around the deposit area and mine hill in Mahd Adh Dhahab, and the gossan and alteration zone in Jabal Said.

2.2 Geographical Setting

The Mahd Adh Dhahab goldmine lies about 270 km northeast of Jeddah and about 170 km southwest of Al-Madina Almonwra (Fig. 2.1). Jabal Said is located 45km northeast of Mahd Adh Dhahab.

The study area is predominantly rock desert, although some of the areas south and north of Mahd Mine Hill in Mahd Ahd Dhahab and north in the wadi to Jabal Said are

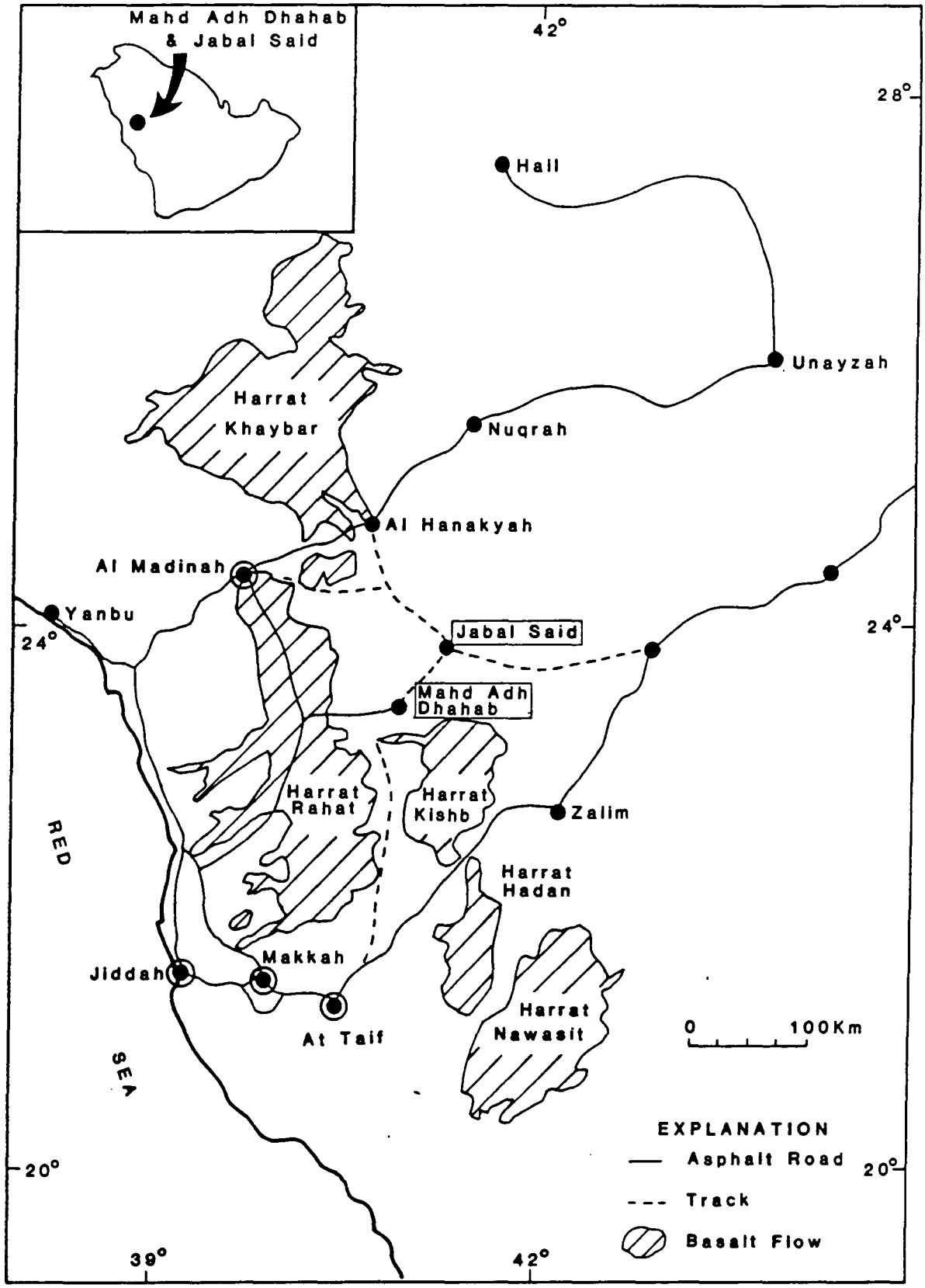

Fig. 2.1 Location map of Mahd Adh Dhahab and Jabal Said areas.

covered by sand. These wadis usually contain coarse sand derived from granitic rocks along with thin alluvial sand in the water courses.

The mine hill of Jabal Al-Mahd rises to 1238m above sea level and is surrounded by rocky hills rising to more than 1300m above sea level (Huckerby, 1984), whilst Jabal Said is much lower and rising only 900m above sea level (Saber, 1975).

2.3 Regional Geology of the area around Jabal Said and Mahd Adh Dhahab.

2.3.1 Introduction

The area was one of the earliest sites in Saudi Arabia studied by Brown et al., (1963) who prepared the first geological map of the south Hijaz Quadrangle at the large scale of 1:500,000. Recently Bowden & Smith (1981) mapped the area and prepared a reconnaissance geological map at a scale of 1:100,000. Kemp et al. (1982) compiled a map at a scale of 1:250,000 for the Mahd Adh Dhahab Quadrangle (1982). The regional geology mentioned here is based on the work done by Kemp et al. (1982), where they divided the Precambrian rock into different groups based on the similarity between the rocks and the composition of the minerals.

2.3.2 Arj Group

The Arj Group is considered to be the oldest volcano-sedimentary sequence in the study area and has a lithological content similar to the other volcano-sedimentary sequences in the Mahd and Ghamar Groups. It is divided into three different formations: Said Formation, Jabal Azlam Formation and Sumayir Formation (Fig. 2.2).

2.3.2.1 Said Formation

This formation named after Jabal sa'id Aswab in the northwest of the quadrangle, comprises volcanic and subordinate sedimentary rocks characterised by a dominant dark-grey to green colouration, and massive silicic rock bodies in which attitude and "way-up" are difficult to determine.

A unit of mainly quartz keratophyric composition occurs throughout the outcrop area composed of feldspar or quartz-feldspar phyric rocks. Fine-grained tuff, lapilli tuff and breccia also occur in this regional unit which is overlain by local units of similar silicic volcanic rock that include thick welded tuff and bedded vitric tuff.

Mineralisation is related to these local volcanic structures and is confined beneath an layer of sedimentary rock which includes lenses to extensive beds of chert including jasper grading into, or interfingering with lenticular carbonate beds. They also commonly contain tuffaceous chemical deposits, locally overlain by

sandstone with minor intercalated conglomeratic and mudstone beds.

2.3.2.2 Jabal Azlam Formation

This unit, named after Jabal Azlam in the northwest of the quadrangle, conformably overlies the Said Formation with only occasional local unconformities. The lower part of the formation in the west consists of thick, massive basaltic to andesitic breccia and tuff breccia containing fragments of amygdaloidal rock. In addition there is a large area covered by intrusive andesite.

The upper part of the formation in the west of the quadrangle is entirely sedimentary, and consists mainly of thick epiclastic breccia or coarse greywacke along with poorly-bedded sandstone and conglomerate.

2.3.2.3 Sumayir Formation

This is named after Wadi Sumayir near the north margin of the quadrangle. The contact of this formation with the Said and Jabal Azlam Formation cannot be seen, but is interpreted as lying stratigraphically above them. Most of the exposed rocks are composed of basaltic breccia tuff, limestone and chert and jasper. In some areas a few metres of epiclastic volcanic breccia varying to laminated siliceous siltstone and mudstone occurs.

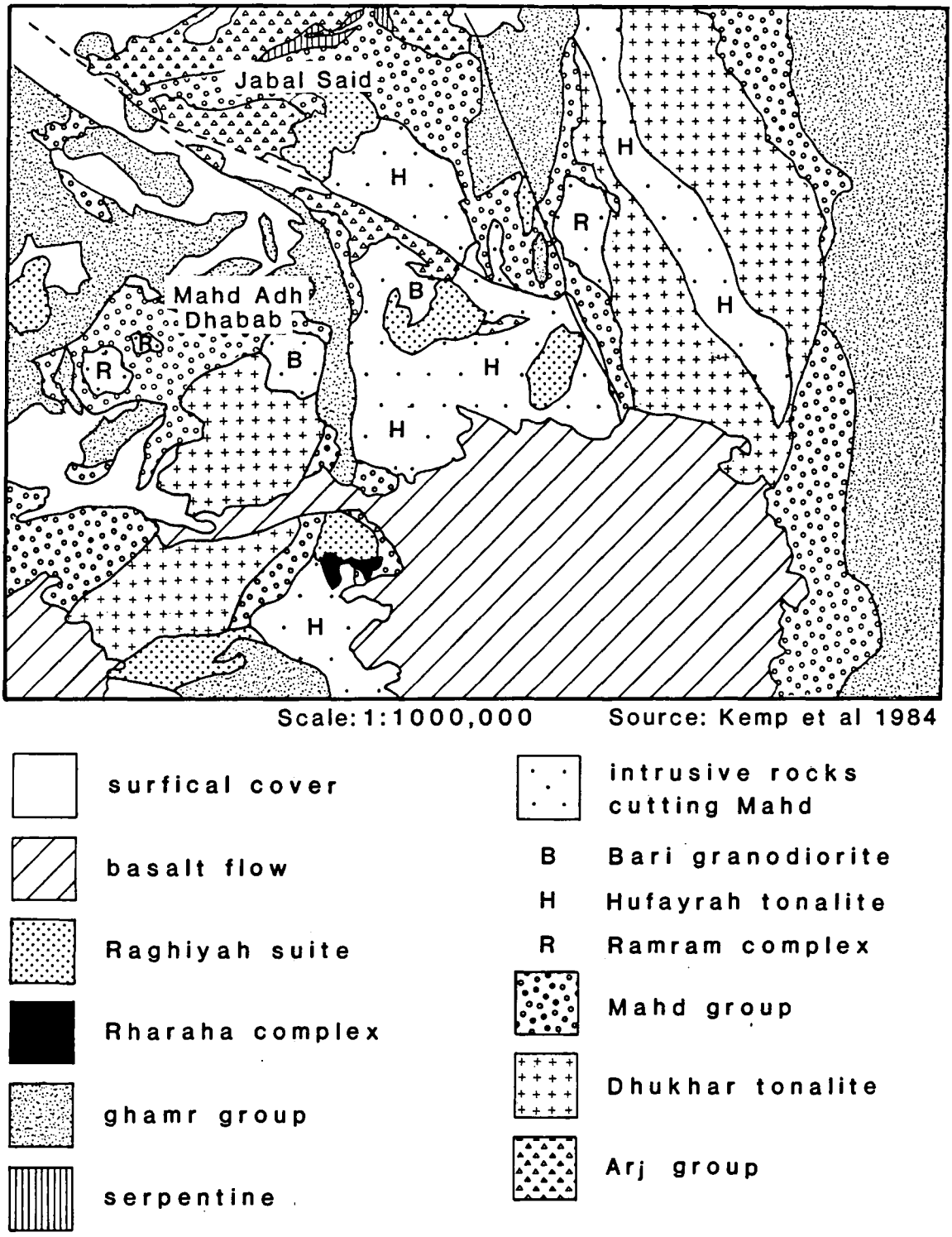

Fig. 2.2 Simplified geological sketch of the Mahd Adh Dhabab and Jabal Said area

2.3.3 Serpentinite Association

Serpentinite with minor gabbro occurs in two zones: around Bir'Umq and also in a zone trend southeast to northwest. The contact with the Sumayir Formation is commonly sheared and weathered whilst in other areas the contact has ultramafic chlorite rocks. The contact with the Tulaymisah Formation is commonly carbonated.

The serpentinite appears to be derived mainly from peridotite, relics of pyroxene, dunite and pyroxenite and disseminated chromite are also present (Rehaile & Warde, 1978).

2.3.4 Dhukhr Tonalite

Named after a hilly area in the southwest of the quadrangle, the tonalite occurs mainly in two areas: to the northeast of the quadrangle and north of Harat Kishb. It is a complex group of varied plutonic rocks, mostly tonalites but includes some granodiorites and gabbros. The bulk of the tonalites have a primary mineral fabric and may be pre- or syn-tectonic (Kemp et al., 1982). There are some younger non-foliated units within the tonalite and some associated gabbros of uncertain age.

2.3.5 Mughar Complex

This forms extensive areas of low relief and is composed mainly of metamorphic rocks (which appear to be

equivalents of the Arj group) and old plutonic rocks. It also contains schist and gneiss.

2.3.6 Mahd Group

The group named after the Mahd adh Dhahab gold mine and is composed of the Haf and Tulaymisah Formations.

2.3.6.1 Haf Formation

This consists of volcanic and sedimentary rocks that rest unconformable on the Dukhr tonalite. The Haf Formation is subdivided into three members:

Sa'anah member. This consists mainly of massive green to reddish-brown basaltic breccia and stuctureless basalt or andesite. The lower part contains some limestone beds.

Zur member. The lower part is composed of welded rhyolitic tuff associated with sedimentary rock. In some areas beds of sandstone and pebble conglomerate are also present. The upper part is predominantly red and red-brown and dominated by thick-bedded both welded and non-welded rhyolitic ash-flow tuffs ranging from uniform and flow-foliated to clast rich. A fine grained sandstone to mudstone is found near the top.

Juraysiyah member. This is composed mainly of rocks dominated by basaltic to rhyodacitic compositions. The rocks consist of green and red brown massive brecciated basalt to basaltic andesite.

2.3.6.2 Tulaymish Formation

This formation occurs mostly in the north of the quadrangle. It overlies unconformably the Said and Jabal Azlam Formations in the south and Sumayir Formation and serpentinite in the north. The lower part is composed of sandstone which shows some grading and cross lamination, followed by conglomerate which fines upward to a green, pebbly with mainly basaltic clasts. In some areas limestone beds also occur at the top of the conglomerate sandstone sequence. The upper arkose to quartz sandstone is overlain by basaltic or andesitic breccia and associated sedimentary rocks with rare, well-rounded tonalite clasts. The normal sandstone of the Tulaymisah Formation consists of angular to subangular lithic grains of plagioclase and quartz with sparse epidote and biotite and, in some instances, amphibole grains.

2.3.7 Rock Intrusive into the Mahd Group

2.3.7.1 Ramram complex

Named after Jabal Ramram, this consists mainly of coarse grained gabbro intruded into a fine grained marginal facies in apparent contact with quartz diorite. The gabbro is overlain by red granite to microgranite.

2.3.7.2 Hufayriyah tonalite

This intrusive unit varies in composition from quartz diorites to tonalite. The Hufayriyah tonalite consists of andesite, green hornblende/quartz, biotite and apatite.

2.3.7.3 Bari granodiorite

Named after a small intrusion close to the northwest corner of Harrat al Kishb, this consists mainly of normal oscillatory-zoned andesine to oligoclase and quartz with microperthite, biotite and some green-brown hornblende and accessory opaque minerals, mainly pyrite, and apatite, sphene and rare zircon. The rocks of the Bari granodiorite are typically medium to fine-grained, though those varieties with high quartz content are coarser grained. They are typically white, though varieties richer in potassic feldspar may be pink.

2.3.7.4 Ghamr Group

This is named after Wadi Ghamr and can be divided into two formations, Kharzah and Gharmati.

2.3.7.5 Kharzah Formation

The formation consists of a dominantly coarse clastic sedimentary sequence with subordinate rhyolitic and rhyodacitic volcanic rocks, commonly at the base but also at other levels. This is overlain by a sequence mainly of basaltic andesite to andesite.

2.3.7.6 Gharmati formation

The base of this formation is taken to be where the basaltic volcanic rocks of the Kharzah Formation give way to sedimentary silicic tuffaceous rock. The base starts with pillowed basalt with breccia and passes through upward-fining and increasingly well-bedded breccia. In the upper part of the breccia, red siltstone beds with

laminated siltstone to mudstone then appear and the coarser, epiclastic rock changes rapidly from green to dark grey-green in colour. The upper part of the formation is associated with green and red tuff or tuffaceous sandstone to siltstone beds. Thick green sandstone with epiclastic breccia occurs in places along with two or three pebbly to conglomeratic beds, which are distinctive in that they contain tonalite and granodiorite. Above this the red tuffaceous mixtite abruptly gives way to normal clastic sedimentary rocks, mainly of sandstone with which thin laminated calcareous beds and limestone are commonly associated.

2.3.7.7 Raghiyah Suite

All the rocks intruded into the Ghamr group in this quadrangle have been grouped into the Raghiyah suite, named after Jabal ar Raghiyah. The group consists of post-tectonic intrusive rocks ranging in composition from gabbroic to granitic. It is grouped into five different types based on the composition of the rocks:

1. The Rharaba complex of ultramafic and mafic rocks.
2. The Dumah granodiorite, consisting of rocks ranging from quartz to monzonite.
3. The Assharah monozogranite, consisting of monzogranite and red granite to microgranite, and locally peralkalic in composition.

4. The Dayahin granite, consisting of aegirine-riebeckite granite along with an aphyric and porphyritic variety.
5. The Zubaydah breccia, a single small intrusion of xenolith-rich aegirine-arfvedsonite granite.

2.4 Geology of Mahd Adh Dhahab Deposits

2.4.1 Introduction

The ore deposit of Mahd Adh Dhahab is located in a mountain called Jabal Almahd. The geology of Jabal Almahd has been studied by many geologists including Twitchell who visited the area and described the geology briefly (Twitchell, 1958). This was followed by: the first stratigraphic mapping of the area by Saudi Arabian Mining Syndicate (SAMA) geologists (Dirom, 1947); Goldsmith and Kother (1971) who studied the regional geology of the area; and by geochemical work on Jabal Almahd by the United States Geological Survey (USGS) which resulted in a new stratigraphical nomenclature (Theobald, 1965). Luce et al. (1975) from the USGS re-evaluated the mine area and proposed a new stratigraphic scheme, subsequently Hakim (1980) proposed another scheme which was similar to Luce et al. (1975). Worl (1979) modified the Luce scheme, but his changes have not been generally accepted (Hilpert et al., 1982). Chan (1980) carried out evaluation of the concession held by Goldfields Mahd Adh Dhahab Ltd. (GFMAD) when he prepared a geological map for the concession area

at a scale of 1:50,000. Chan mapped the area by adapting a litho-stratigraphic approach after the identification and mapping of two important marker units - the Lahof tuffaceous sediments and the Marker II chert unit. Only part of this map has been used in this research (Fig. 2.3), covering the most promising sites. The same area was covered with TM satellite data and comparisons will be discussed later in Chapter 6. The description of the geological units have been summarised here after Chan (1980) and adapted into new sub-group geological units. Only those units appearing in the study area will be discussed here.

2.4.2 Detail of Geological Units

1. The basement complex

This term is used to designate acid intermediate plutonic rock exposed along the eastern margin of the ara. The unit mainly consists of varieties of acid-intermediate plutonic rocks exposed on low hills and gentle terrain with occasional steep relief. The older lithological unit is a friable, coarse grained, white coloured granodiorite, which is easily eroded with resulting poor outcrop except where it has been strengthened by the intrusion of dykes of rhyolite to basaltic composition.

Small, massive amphibolite exposures are mapped on the east. Younger intrusions of fine grained granodiorite and quartz diorite have different exposures as small,

FIGURE 2.3

GEOLOGICAL MAP OF MAHD ADH DHAHAB AREA

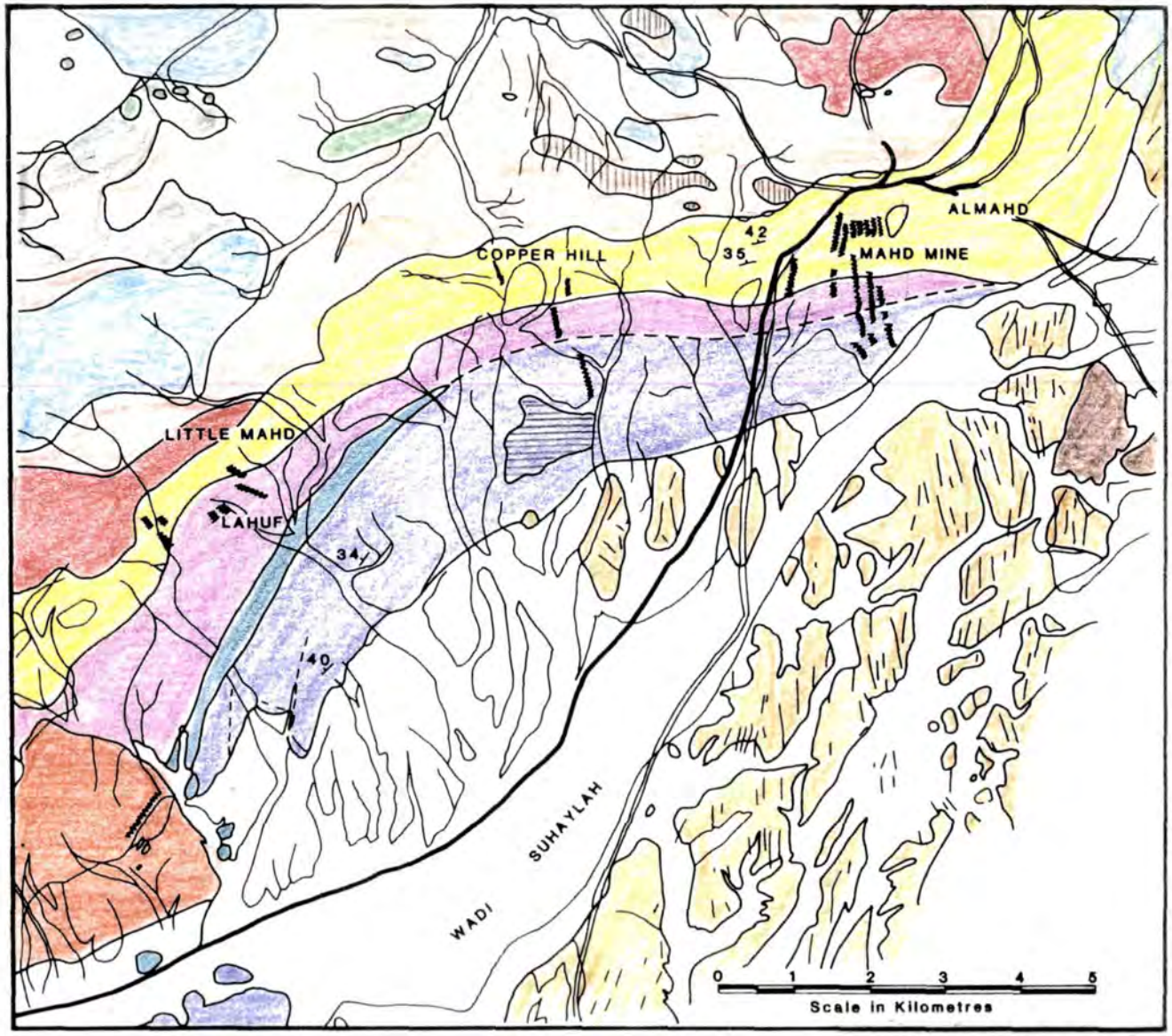

SOURCE:CHAN,1980

rounded boulders due to their massive nature and rare joints, with exfoliation as the major process of weathering.

2. **The Lahuf Subgroup:**

This consists of the upper and lower Lahuf, with the tuff sediments in between.

A. **The Lower Lahuf.** Consists of discrete hills, often with different rock types. Andesite, andesitic agglomerate, volcanic tuff and also one distinct patch of the sediments with tuff occur east of Lahuf. Granodiorite xenoliths are present well inside the Lower Lahuf unit, but only at low topographic levels. It appears that the lower Lahuf is joined together by separate andesitic units emplaced during an active volcanic period, together with sediments such as grit stone and feldspathic sandstone.

This period was followed by a volcanically quiet period, resulting in the deposition of the Lahuf sediment and tuff. The unit forms a topographic low resulting from differential erosion due to the soft nature of the tuff and sediment.

B. The tuff sediments are underlain by poorly consolidated volcanics consisting of weathered volcanic debris and occasional bands of metagreywacke which stand out on account of its distinct hardness.

C. **Upper Lahuf.** The Upper Lahuf overlies the tuff sediment unit over a substantial part of the strike length. On the eastern side, it overlies the lower Lahuf

due to the thinning out of the tuff-sediment. The unit consists of dominant andesite and minor agglomerate and are either flows or sills.

No sediments and relatively few tuffs were encountered within the unit. West of Lahuf, the unit is disconformably overlain by poorly stratified sands and gravel intruded by andesite and rhyolite sills. Most acid intrusions into the Lahuf subgroup are transgressive. Pink feldspar - rhyolite intrusions are common and often are associated with copper mineralisation, particularly around the east of the Lahuf.

The mineralisation is within the upper Lahuf and restricted to quartz veins systems and the alteration restricted in width within the mineralised zone.

3. **The M.A.D. subgroup.**

This consists of two major units, the mine sequence and the post-mine sequence, and a younger, less continuous sequence, namely the stratified sediment and meta-greywacke.

A. Around the mine area, the subgroup should logically start from the base of the lower agglomerate including the upper tuff and jasper acid tuff. This division excludes the andesite underlying the lower agglomerate of of Luce et al. (1975), and assigns it to the Upper Lahuf. In this way the mine sequence probably represents a distinct volcanic phase with two periods represented by the lower agglomerate, lower tuff and the upper agglomerate, and

then followed by a relatively quiet period with a limited sedimentation process as indicated by the presence of sediments above the upper tuff.

The western extension of the mine sequence is terminated at the west of Lahuf by the intrusion of the Lahuf rhyolite. The centre of the intrusions is located west of Lahuf and appears to run along the contact between the mine sequence and the overlying unit, the post mine sequence.

The southwestern extension of the mine sequence is obscured by the appearance of the poorly stratified sediments and metagreywacke unit. This unit is tentatively put as younger than the mine sequence, but it is quite possible that it may be the lateral sedimentary equivalent of the mine sequence.

The eastern extension of the mine sequence swings to the north where it changes from a thick agglomerate unit to a thick tuff unit.

A limestone lens with tuff outcrops in the east part of the mine sequence northeast of the old town and also west of the new Mahd.

B. **The post-mine sequence.**

This represents a period of active volcanism followed by a slow phase out. The base of this sequence north of the mine is agglomerate dominated, with numerous andesite sills with cooling joints. A prominent agglomerate unit occurs north-northwest of the old town with 1-2 metre

boulders; slump beds of tuff are also common within this sequence. Both the mine and post-mine sequences are heavily intruded by a young dyke swarm of acid and intermediate composition predominantly intruded in a north-south and a north-northwest direction.

Limestone lenses are of more frequent occurrences in the post-mine sequence but are seldom continuous.

C. **Metagreywacke**

These are generally associated with sediments and tuff and represents a change in the deposition process. They are found in the following stratigraphic horizons.

a. In wadis and as isolated outcrops indicating remnants of sediment left by erosion.

b. At the base of the lower Lahuf.

c. Below the Lahuf tuff-sediment.

d. At the base of the folded sequence or the top of the post-mine sequence, sometimes in low lying areas and occasionally as flat top mesa.

4. **The folded sequence.**

This includes the sedimentary units and volcanic intrusives and overlying sediment units resting unconformably on the M.A.D. subgroup. The practicality of mapping this sequence is related to the chert unit, referred to as the Mark II chert.

The Marker II chert was exposed in isolated locations in a topographic low or as a distinct flat top when

exposed on topographic highs on top of the post mine sequence.

The chert has a distinctive grey colour with bands 5-7cm thick, and often dips symmetrically with the topography of the underlying rocks. It is often underlain by volcanic debris and minor feldspathic sandstone. It has a wider distribution from north-northwest to west of Al Mahd and generally absent to the north of it. It has very limited exposure east of Al-Mahd. The chert unit is strongly folded west of the area appearing on the map.

5. **Intrusives and flows**

a. Lahuf rhyolite. This is an elongated body of rhyolite, located north of Lahuf. This body sent off a number of intrusions into adjacent areas and appears to be related to other rhyolitic intrusions near the mine. Similar intrusions are also located within the post-mine sequence.

A substantial part of the mine and post-mine sequences are intruded and metamorphosed by similar rhyolite intrusions.

b. Younger and intrusive volcanics. The flat-lying pyritic acid tuff intruded the folded sequence and the post mine sequence and appears to be related to the tectonics. The flat lying pyritic acid tuff could be the extrusive phase of the acid intrusion.

2.5 Geology of Jabal Almahd

2.5.1 Introduction

The geology of Jabal Almahd consists of a late Precambrian lensoid sequence of intermediate to felsic volcanic, volcanoclastic and epiclastic rocks. This sequence was dated by Clavez & Kemp (1982), as being between 813+3 and 748+22 Ma (Doebrich, 1984). The stratigraphic sequence from the south to the north (oldest to youngest) was originally described by Luce et al., (1975) and was the basis for subsequent studies. The main units in the area are andesite, lower agglomerate, lower tuff, upper agglomerate and upper tuff overlain by fine-grained thin-bedded clastic sedimentary rocks. These units are intruded by intrusive rhyolite (Fig. 2.4).

The description here is based on work by Doebrich and Leanderson (1984) and Huckerby (1984). Huckerby (1984) mapped the area, at a scale of 1:2,500 for GFMAD with similar stratigraphy to Luce et al. (1975). Doebrich & Leanderson (1984), from the USGS, studied the geology and the hydrothermal alteration in the area and mapped the area at a scale of 1:2,000.

2.5.2 Rock Unit Description

Andesite:

The outcrops in the south of the Jabal Almahd and consists of andesite flows, crystal tuffs, and crystal-lithic lapili tuffs, all intruded by andesite sills (Fig. 2.5).

The andesite flows contain phenocrysts of plagioclase and the volcaniclastic rocks contain crystal and lithic fragments of quartz, albite and andesite up to 1cm in diameter in a tuffaceous matrix.

The contact between the andesite and the lower agglomerate is a reddish-brown oxidation zone 3m wide (Doebrich & Leanderson, 1984). This contact has been regarded as conformable by some works (Dottin, 1974; Worl, 1978; Chan, 1980) whilst others report that the andesite is structurally and geochemically separate from the overlying rocks (Luce et al., 1979; Huckerby, 1984).

Lower Agglomerate:

This unit became more important when it was found to be the host rock to the recently-discovered mineralization in the southern area (Huckerby, 1984).

It is composed of massive to poorly-bedded, poorly sorted, immature, volcanic conglomerate. Crystal fragments of quartz, albite and orthoclase, and lithic fragments of andesite, rhyolite and local tuff and chert are enclosed in a siliceous, tuffaceous matrix. The thickness of these units is approximately 150m.

Bedding is better developed in the upper part of the sequence, and quartz veins indicate that the lower agglomerate was more competent than overlying and underlying units during deformation.

Fig. 2.4 Jabal Mahd Adh Dhahab "looking South". The Processing site is in the left of the picture. Notice where the quartz veins cut the rock units.

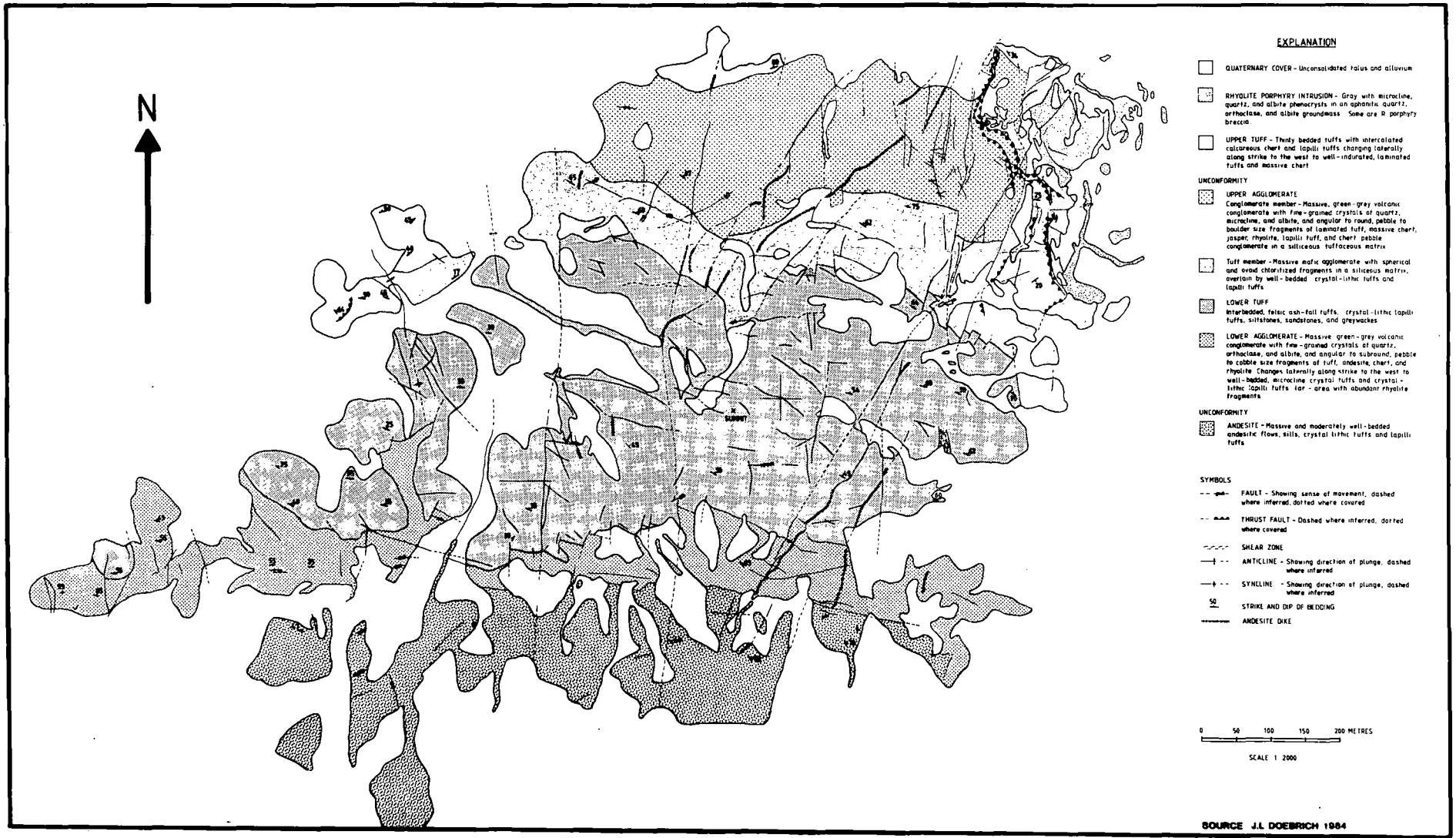

FIGURE 2.5 **GEOLOGY AND STRUCTURE AT THE MAHD ADH DHAHAB PRECIOUS-METAL DEPOSIT, KINGDOM OF SAUDI ARABIA**

Lower Tuff:

This unit, which is about 210m thick, and coloured grey, green or brown, is composed mostly of laminated, siliceous tuffs and interbedded crystal-lithic lapilli tuff, siltstones, sandstones and greywackes. It has a conformable and gradational contact with the lower agglomerate and the laminated tuff and lapilli tuff sequence are sandwiched between a well-bedded siltstone and sandstone with a minor tuff layer. This unit is less competent than the conglomerate unit which has fewer fractures and wide veins.

Upper Agglomerate:

The upper agllomerate unit is approximately 140m thick and forms an east-west ridge to the north of the area. It has been subdivided into a tuff member overlain by a conglomerate member (Worl, 1979).

The tuff member consists of a basal horizon, 30 to 40m thick of massive mafic agglomerate overlain by a moderately well-bedded sequence of intercalated crystal lithic tuffs and lapilli tuffs. The conglomerate member of the upper agglomerate unit is a siliceous, massive immature conglomerate. Most lithic fragments are between 2mm and 10cm in diameter and angular to subangular in shape although large rounded boulders, about 25cm in diameter are also present. This unit had more uniform competency and more uniform vein density along the strike than other units.

Upper Tuff:

This unit consists of well-bedded, thinly-laminated rocks. It lies unconformably over the upper agglomerate where a fault running along the contact brought the upper agglomerate alongside the upper tuff.

The upper tuff unit was incompetent and quartz veins in the upper agglomerate commonly terminate against the upper tuff contact. However, quartz veins cut the upper agglomerate-upper tuff contact at the same point, particularly in the north-central part of the Jabal Almahd. They tend to become thinner and occasionally terminate upward within the upper tuff.

Rhyolite Intrusive:

This crops out towards the north-east edge of Jabal Almahd in the northern zone where it is reddish on weathered surfaces due to oxidation of disseminated pyrite. This rhyolite also appears in the southern ore zone under the wadi where it is found in the drill core. The rhyolite contains microcline, quartz and albite phenocrysts, whic are commonly subhedral to euhedral.

The top of the rhyolite is capped by several metres of monolithic rhyolite breccia along its upper contact with the lower agglomerate in the southern zone. This rhyolite is related to the zone of mineralization in both orezones.

Andesite Dykes:

These cut Jabal Almahd trending north to northeast and can be up to 1.5m wide and several hundreds of metres long. The rock is easily-weathered and forms drainages and steeply-walled trenches, which cut the volcanic and rhyolite rocks, quartz veins, and mineralized zones.

2.5.3 Mineralization in Jabal Almahd Ore Deposits:

Mineralization is developed in a series of quartz veins which trend north-south and, in some areas, follow fault planes (Figs. 2.6, 2.7). The productive quartz veins are often crustified comb or cockade quartz-chlorite accompanied by banded base metal sulphides (pyrite, chalcopyrite, sphalerite and galena). The gold occurs within the base metal sulphides as native gold and gold-silver tellurides (Hopwood, 1979).

The ore deposits occurred in two locations, and form northern and southern ore deposits.

Northern ore deposits:

These occur in the upper agglomerate, underlying the incompetent upper tuff. Generally, three major low angle west-dipping mineralized veins and vein systems occur along the one important north-trending thrust fault. The thrust fault, which is several metres wide, dips 45 W and contains some high-grade ore. In the hanging wall, numerous small, higher-angle, west-dipping veins and shear zones are thought to be imbricated structures that were formed by movement on the fault.

Fig. 2.6 SAMS Old Shaft and mineralized quartz veins

Fig. 2.7 Quartz veins and silicification alteration in Jabal Al Mahd.

Southern Ore Deposits:

These occur in veins in the competent lower agglomerate immediately underlying the incompetent lower tuff. They are thought to be a north-dipping tabular body, 40m thick and 400m wide and extending 250m down the dip, giving a total reserve of about 1.1 million metric ore of one ounce gold per tonne of the ore (Worl, 1979). Similarly, the three major low angle fault systems also appear in the north zone where the high grade mineralization occurs in systems of veins that dip 40 to 45 W and may be up to 10m wide. These are not observed at the surface.

2.6 Alteration in Jabal Almahd

Most of the rocks in the Jabal Almahd area show weak alteration related to hypogene and supergene processes. The intensity of alteration is related to lithology. The coarse sediments are visually more altered than fine, probably because the coarse sediments had higher porosity and permeability which allowed passage of hydrothermal fluids into them.

The different types of alteration are related to the vein types in the area, but the structurally competent lower and upper agglomerates were host to the greatest variety and the most intense alteration. Six different types of alteration occur in the area: silicification, quartz- sericite-pyrite alteration, potassic alteration,

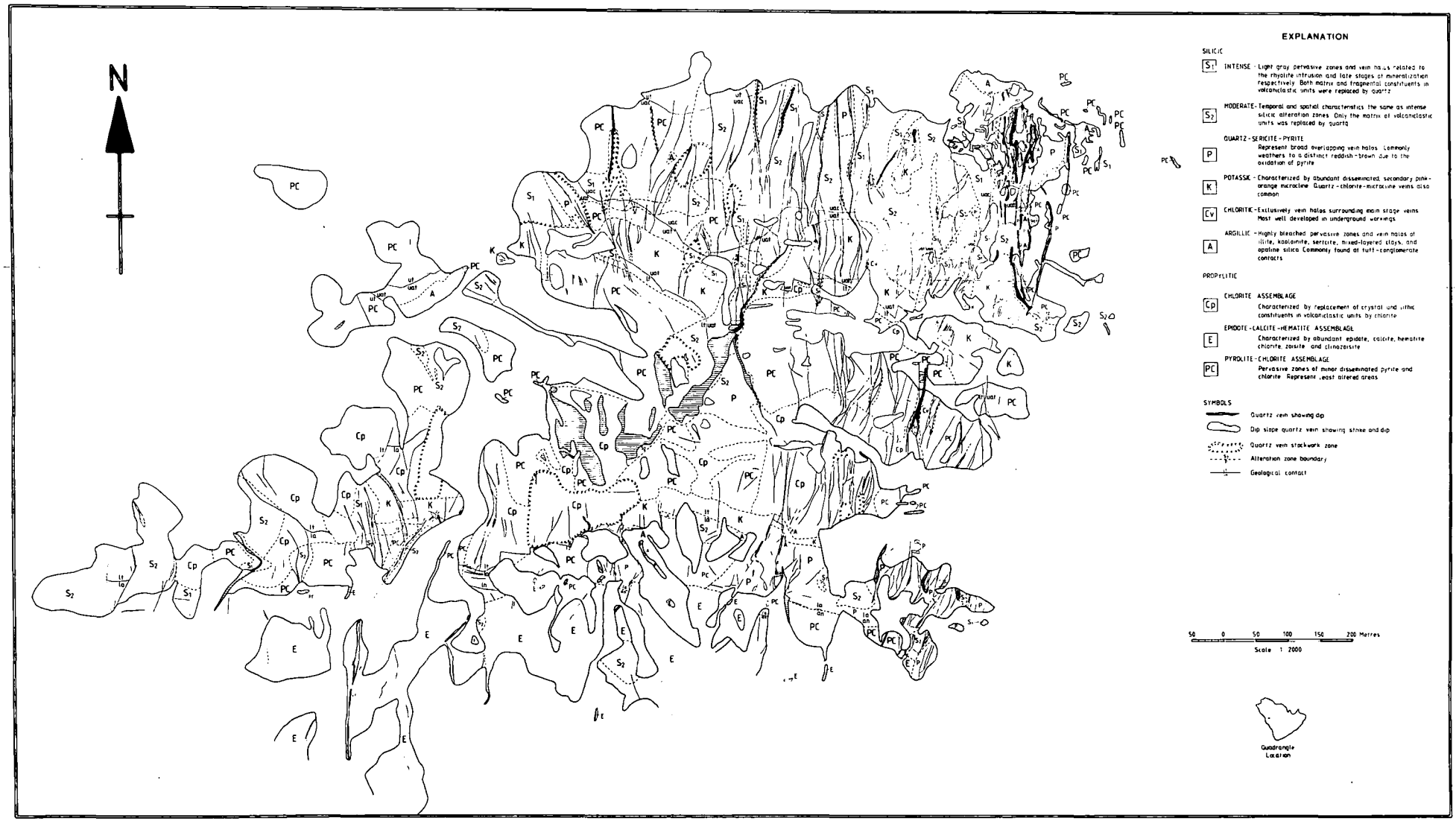

SOURCE : J.L. DOEBRICH 1984

FIGURE 2.8 DISTRIBUTION OF QUARTZ VEINS AND HYDROTHERMAL ALTERATION ZONES AT THE MAHD ADH DHAHAB PRECIOUS-METAL DEPOSIT, KINGDOM OF SAUDI ARABIA

TABLE 2.1 Generalized descriptions of the alteration types in Jabal Al Mahd.

Alteration type	Sample in the map	Description
silicic	S1 & S2	Intense light grey zone and vein halos related to the rhyolite intrusion. Intense silicic alteration either the matrix of the volcaniclastic units was replaced or both the matrix and fragmental units were replaced.
quartz-sericite-pyrite	P1	weathered to distinct reddish-brown due to the oxidation of pyrite.
potassic	K1	characterized by disseminated orange microcline.
Argillic	A	highly bleached zones and vein halos of illite, kaolinite, sericite, mixed layer clay and opaline silica.
chlorite assemblage	CP	chlorite replacing crystal and lithic constituents in volcaniclastic units.
epidote-calcite-hematite	E	characterized by abundant epidote, calcite, hematite, chlorite, zoisite, and clinosoisite.
pyrite-chlorite-assemblage	PC	minor dissemination pyrite and chlorite represent the least alteration units.

chlorite alteration, argillic alteration, and propylitic alteration (Doebrich 1984; Fig. 2.8). Table 2.1 summarizes the description of these alteration units.

2.6.1 Silicification

The silicification zones are commonly found in the lower and upper agglomerates where zones of light-grey to grey, moderately to intensely-silicified rocks formed around the veins related to the intrusion of rhyolite. Moderate silicification consists of partial to total replacement of the matrix only. Secondary chlorite, sericite and pyrite, and microcline are present in minor amounts in both intensely and moderately silicified rocks.

Replacement of the original siliceous, tuffaceous matrix resulted in an increase in grain size. Complete replacement of lithic fragments resulted in pseudomorphs of coarse-grained, crystal aggregates of quartz and chlorite.

The silicified rocks in the upper agglomerate in the northwest corner of Jabal Al Mahd are associated with a large, subvertical vein and with extensive stockwork veins.

2.6.2 Quartz-sericite-pyrite alteration

This type of alteration formed primarily in the lower agglomerate, upper agglomerate, and rhyolite units, where it is characterized by the relative abundance of quartz, sericite, and pyrite and minor chlorite and calcite.

Because of the weathering of abundant disseminated pyrite, these rocks crop out as distinct reddish-brown zones.

In the southeastern and northeastern corners of the map area, broad zones of quartz-sericite-pyrite alteration are associated with abundant veins which represent a network of overlapping veins related to different stage of origin. Similar alteration occurred in the lower agglomerate updip from the southern ore zone. This type of alteration coincides with rhyolite in the northeastern corner.

2.6.3 Potassic alteration:

This is characterized by the presence of abundant orange-pink secondary microcline that occurs with disseminated, lesser amounts of contemporaneous chlorite and with both earlier and later quartz; sericite and pyrite are also present. The chlorite is the same age as the potassium feldspar because they occur together in quartz vein west of the old mine area.

Two major east-trending zones of this alteration are present at tuff-conglomerate contacts which correspond to the radiometric survey of Gettings (1981). The alteration also appears in the south in permeable and competent lapilli tuff horizons in the transition zone.

In the northern part of the major zone the alteration occurs in the basal mafic agglomerate of the tuff member of the upper agglomerate where it is in direct contact with the lower tuff.

2.6.4 Chloritic alteration:

The chloritic alteration occurs in some veins related to the main stage of quartz veining. The alteration was very intense, it destroyed primary textures and also primary and secondary minerals to a distance of several centimetres from the vein. This resulted in a zone of massive chlorite accompanied by variable amounts of secondary quartz.

2.6.5 Argillic alteration

The argillic alteration resulted in bleached zones of illite, kaolinite, sericite, mixed-layer clays, and opaline silica along tuff-conglomerate contacts and veins.

In the southeastern and south-central part of the area, patches of argillically altered rocks are in the uppermost part of the lower agglomerate. The argillically altered rocks are often in contact with the overlying potassium feldspar-altered base of the lower tuff.

In the northeastern and west central part of the area there has been alteration along the upper agglomerate-upper tuff contact, also in the northeastern part of the area the base of the upper tuff and part of the rhyolite has also been intensely altered.

2.6.6 Propylitic alteration:

This type of alteration affects the largest part of the area and is found in almost all rock types. It can be divided into three categories: (a) mainly chlorite, (b) mainly epidote, calcite and hematite, (c) alteration of

minor pyrite, chlorite and sericite. Most of the chloritic alteration occurred in zones within an east-trending belt in the lower to middle sections of the lower tuff. Patches of chlorite-altered tuff are also in the upper section of the lower tuff immediately below the upper agglomerate.

The second category, the epidote calcite, hematite alteration, is almost exclusive to the andesite. It is characterized by a complete replacement of mafic minerals and a partial replacement of plagioclase.

The areas with minor disseminated pyrite, chlorite and sericite represent the least altered zones in the area. These alteration minerals are very fine-grained and characteristically found well away from zones of known ore grade mineralization.

2.6.7 Mineralogy of alteration units:

The mineralogy of the hydrothermally altered rocks depends on the composition of the original host rocks and physical conditions at the time of alteration, especially temperature, chemistry of the fluid phase (ph, salinity, fugacites of oxygen and sulphur) Hemel & Jones,(1964).

In the Mahd Adh Dhahab area there were about six types of epithermal alteration. These are vein-related alteration, consisting of quartz-sericite-pyrite, chloritic, argillic and silicic halos which were superimposed on broad pervasive alteration zones of silicic, potassic and argillic alteration. Broad

propylitic alteration was then superimposed on all alteration types, Dobreach (1984). Table 2.2 shows the mineral composition of all the units in Jabal Al Mahd.

Table 2.2 **The mineral composition of the rocks and alteration units in Mahd Adh Dahab area.**

Rocks and alteration type	Mineral composition
Silicic alteration	Silica-rich quartz-sericite pyrite zones.
Quartz sericite pyrite alteration	quartz, sericite and pyrite and minor chlorite and calcite
Potassic alteration	orange pink secondary microcline, chlorite, sericite and pyrite.
Argillic alteration	illite, kaolinite, sericite
Propylitic alteration: a. chlorite assemblage b. epidote calcite hematite c. pyrite chlorite & sericite	chlorite, epidote, calcite and hematite, or pyrite, chlorite, sericite.
Carbonate rocks	limestone, calcium carbonate

Source: Dobreach, 1984.

2.7 Geology and Mineralization of Jabal Sa'id

2.7.1 Introduction

Much work has been carried out in the Jabal Sa'id area since the regional map (1:500,000) of the south Hhijaz quadrangle by Brown et al (1963). This also provided the basis for stratigraphic column for the major Precambrian units in the Arabian Shield when Jabal Sa'id was correlated with the Halban andesite.

Aguttes and Duhamel (1971) mapped the area as pyroclastic Halban rocks, at a scale of 1:100,000. Later maps of the area and prospect were produced at scales of 1:50,000, 1:20,000, 1:2,000 and 1:1,000. Kemp et al. (1982) compiled a geological map for the area at 1:250,000. They included Jabal Sa'id in the Sayed formation which is part of the Arj Group, a Proterozoic group which comes between the Mughar complex and Mahd Group.

Hopwood (1979) prepared geological maps for the Jabal Sa'id prospect at scales of 1:20,000 and 1:5,000, but he described the stratigraphy in a different way. Bowden & Smith (1981) divided the volcanic rocks in the area into two volcanic cycles within the stratigraphic section of the rocks which are roughly equivalent to the Hulayfah and Murdama groups of the Bureau de Recherches Geologiques et Miniers (BGRM) classification. The rocks of the lower cycle have been divided into a lower felsic volcanic unit

(dominantly andesitic), a lower mafic volcanic unit, a lower diorite unit composed of a complex of interlensed mafic to felsic volcanic and volcano- sedimentary rocks, and a stratigraphically equivalent lower volcano-sedimentary unit. The lower cycles have been deformed and subjected to lower greenschist facies regional metamorphism.

The upper cycle rocks are divided into a basal volcano-sedimentary unit, a dominantly basaltic upper mafic volcanic unit and an upper felsic volcanic unit associated with alkaline lavas. A sedimentary unit overlying the upper mafic unit to the north and northwest of the district may be stratigraphically equivalent to rocks correlated with the Jabalah group in the northeast.

Recently, Riofinex (1984) reviewed all the previous work in Jabal Said district and implemented new classifications in the area.

2.7.2 Geology and Structure of Jabal Sa'id District

The geological description of the Jabal Sa'id deposit area which is presented here is based on geological mapping done by Sabir (1981), which was obtained from detailed surface mapping and subsurface diamond drilling.

The rhyolitic subunit which is host to the ore is made up of complexly folded and faulted volcano-sedimentary rocks comprising a differentiated assemblage of rhyolitic facies.

The zone character of the hydrothermal alteration and the presence of sedimentary features in the immediate vicinity of the deposits suggests a southeast to northwest lithological succession conformable with the structural interpretation (Fig. 2.9).

2.7.2.1 Lithostratigraphy

The following lithostratigraphic sequence from the base upward has been established:

1. Andesite: Black fine-grained andesite locally containing small crystals of pyrite.
2. Rhyolitic tuff and breccia: A differentiated pyroclastic assemblage comprising fragmental acidic rocks of rhyolitic tuff and breccia, intercalated with banded, thin-bedded or flow-textured tuff and locally thin beds of cherty tuffite. The rhyolitic tuff commonly contains crystals (quartz and feldspars) and lapilli (rhyolitic pumice) and ranges from massive to well-bedded. The rhyolitic breccia is massive, pumiceous, and commonly coarse-grained, with centimetre-size components. These facies are from the footwal of the Jabal Sa'id mineralization and are locally marked by hydrothermal alteration with the development of chlorite and pyrite giving way to bleaching and reddening by weathering. In a recent geological survey of the deposits in the area, Jurde (1976) recognized an andesite facies which marked the southern extremity of the rhyolitic assemblage. This

FIGURE 2.9

Regional Geology of Jabal Said

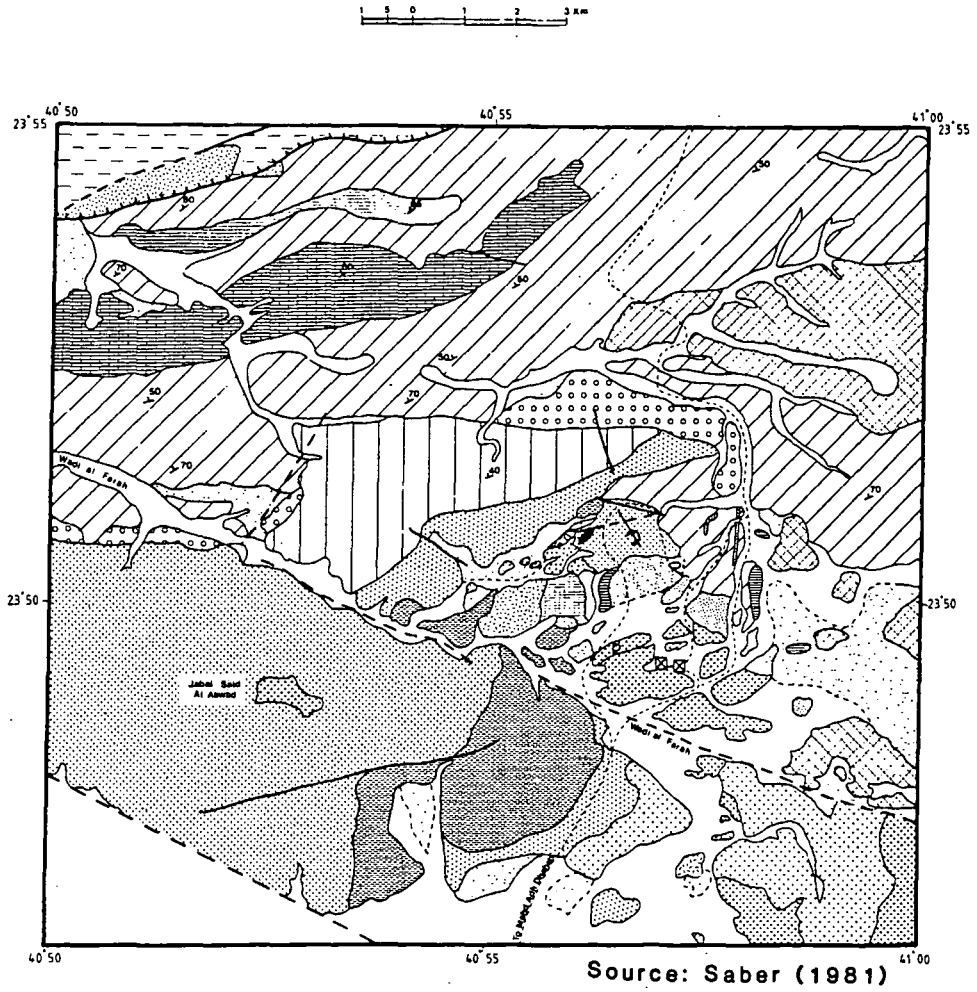

LEGEND

wadi ALLLVIUM

Sand and gravel

Intrusive rocks

White - gray alkaline granite

Red biotite granite

Granodiorite

Diorite microdiorite

Quartz vein

Silicic rocks

Zubaydah breccia

Volcano sedimentary rocks

Volcanic siltstone

Volcanic conglomerate

Coarse grain volcanic sandstone

Volcanic sandstone

Volcanic rocks

Andesite tuff

Andesite tuff & breccia

Andesite breccia

Andesite

Dacitic tuff

Graphitic tuff

Hydrothermally altered rocks

Black rhyotite

Green rhyotite

Welded rhyotite tuff with carbonate

Ignembrite

Jasper

Ophiolitic complex

Ophiolitic complex serpentinite

Map symbols

Geological contact

Fault

Reverse or upthrown fault

Strike and dip of bedding

Overturned anticlinal fold

Gossan

Road

P Pegmatite

Camp

is greenish and fine-grained and locally exhibits pillow-like structures, suggestive of submarine mafic flows. The hydrothermally-altered facies are intruded locally by small masses of rhyolite which occur in the form of stocks or continuous, relatively thick dykes which have well-defined contacts with the intruded fragmental acidic rocks. They are generally massive, schistose and strongly altered (silicified and chloritized). On their outcrop surfaces, these intrusive bodies locally show copper stains but where they are encountered in drill holes they are often barren or locally contain disseminated pyrite. Several types of rhyolite have been identified in the field. Generally they are greenish and contain well- developed quartz crystals. Where they occur in the zone of intense hydrothermal alteration, however they are reddish to pinkish, very fine-grained and completely silicified.

3. Chert (or Jasper): The footwall rocks are overlain by a layer of chert whose dominant facies consists of red or grey-black homogeneous masses that locally contain limonite and boxworks of pyrite. These siliceous rocks crop out forming discontinuous beds generally conformable to the stratification. However, toward the southwest of the main gossan, the chert is tectonized and fractured to small, rounded fragments that are set in a matrix rich in calcareous material. This chert layer (which forms the hanging wall of the mineralization) was encountered in

several drill holes where it was seen to be whitish-grey brecciated and locally intercalated with calcareous rock. It commonly incoporates small red jasper fragments and is cut by abundant veinlets of calcite.

4. Flow texture rhyolite (ignimbrite): This facies crops out mainly along the western face of the main gossan hill and comprises greenish-grey rocks that are often bedded or flow textured. At this locality it is intercalated with thin lenses of dolomite carbonate that are generally conformable to the stratification and is locally intruded by a flow of black aphanitic rhyolite. Eastward it grades into calcareous rhyolitic tuff.

5. Graphitic tuffite: The felsic sequence culminates in a thin layer of fine-grained material consisting of graphitic tuffite with reworked crystal and lapilli tuff to the northwest. This local tuffitic facies is overlain by dacitic tuff with quartz crystals that grade upward into the andesitic ensemble.

All of this sequence is intruded by small, but commonly continuous dykes of microdiorite, diabase, rhyolite and microgranite.

2.7.2.2 Structure

Folding

The complex structural pattern of the Jabal Sa'id area shows that it has been strongly and inhomogeneously deformed. The felsic facies enclosing the deposit show an

overall deflection in strike from north to south (south of the main gossan) and outline an assymetric semicircular arc in which the majority of the beds are very steeply dipping (70 -90). This deflection of the structure is well expressed by the fluidity, the stratification, and the red jasper bed (Sabir, 1981).

Most of the rhyolite, rhyolitic tuff and breccia are characteized by strong schistosities of variable orientation and genesis, excluding those schistosities that correspond to local shear zones (south of the main gossan). The most significant and well-developed schistosity observed in the area shows a dominant N.30 W trend with an average dip of about 85 SW, it presumably defines and conforms to the axial plane of an anticlinorium fold trending north to northwest and dipping steeply toward the southwest. The disposition of the axial plane apparently led to a diversion of the structure toward the east-northeast, which explains its asymmetric pattern (Sabir, 1975, 1981; Hopwood, 1979). The detail of this early phase of deformation is further complicated by the presence of minor folds. In the vicinity of the main gossan the strata are overturned and dip 60 to 90 . Delfour (1970) considered this attitude to be related to a faulted synclinal fold that affected the hydrothermally-altered rocks and associated sulphide masses. About 700m to the northeast the felsic volcanic rocks are again folded and merge in the core of a small anticlinal nose to

form the little fold situated to the north of the East Gossan. At this locality the beds show divergent dips of between 70 and 90 .

These minor folds can be related to a later phase of deformation that affected the felsic-rhyolitic sequence, and which were subjected to the N 65 E deformation phase which, as already outlined, marks the general structural trend in the area. According to Jurde (1976), this last phase was further affected by a fourth N 50 W deformation phase that brought about strong penetrative schistosity cutting across the whole formation.

Faults:

Two major faults are associated with deformation of the rhyolitic sequence. These are:

A N70 E-trending dextral fault that offsets the northern extremity of the main gossan and the flow-textured rhyolite for a distance of about 400m to the east-northeast. In the east valley area the trace of this fault is clearly marked by a fine-grained dyke of rhyolite, several tens of metres long. Here the east rhyolite can be seen to be in fault contact with the rhyolitic crystal and lapilli tuff and rhyolitic breccia that show evidence of strong hydrothermal alteration. In the main gossan area the trend of this fault is further illustrated by the development of several open fissures that have been filled with veins of hematite.

2. A N50 W trending fault that appears very clearly to the northeast of the east gossan where it displaces the flow-textured rhyolite and jasper for a distance of about 30m to the northwest.

Minor north-south to N10 E trending faults cut the pyroclastic rocks and the jasper particularly to the southwest of the main gossan where their presence is indicated by a shear zone of crushing and brecciation.

2.7.3 Jabal Sa'id Massive Sulphide Ore

Jabal Sa'id mineralization can be divided into four major ore bodies: Nos. 1, 2, 3 and 4 (Fig. 2.10). These fare further subdivided into two zones distinguished by their spatial and ore type parameters.

2.7.3.1 Sulphide deposits No. 1

This was the first to be discovered in the area, is expressed at the surface by a massive chert limonite gossan, capped by a jasper limestone breccia (Fig. 2.10).

The ore body forms an irregular lens of massive to submassive sulphide (mainly pyrite, pyrhotite, chalcopyrite and sphalerite), between 30m and 100m thick it dips 80 E strike N20 E and is believed to be overturned. The ore tonnages have been estimated (by the SERM-US Steel Corporation joint venture) to be 8,500,000 tons at a grade of 1.9% Cu 1.10%Zn (1976).

Fig. 2.10 Main gossan in Jabal Sa'id area.

Saber (1981) noticed that there are two different zones of mineralization; Zone 1 is the main ore body, whilst Zone 2 overlies this main ore body. He also noted that the chloritized footwall rocks below the massive ore body are traversed by veins and stringers of pyrite and chalcopyrite and sphalerite, together with disseminated sulphides which form the stockwork ore (Fig. 2.11).

2.7.3.2 Sulphide deposit no. 2

This is considered to be the northern part of ore body no. 1, offset by the eastern valley fault. The stratigraphic structural trends of this orebody are conformable to those of the other orebodies, but its wallrock association and ore type are more similar to orebody no. 3 than to nos. 1 or 4. The northern extension of no. 2 is truncated by a N70 E fault, which explains the discontinuity of the mineralized sequence toward the northeast.

The upper zone is composoed of small lenticular lenses of massive sulphides (mainly pyrite and sphalerite, with minor chalcopyrite and pyrhotite) intercalated in brecciated jasper. The massive sulphide zone grades downward into a network of sulphide veins (mainly pyrite and chalcopyrite).

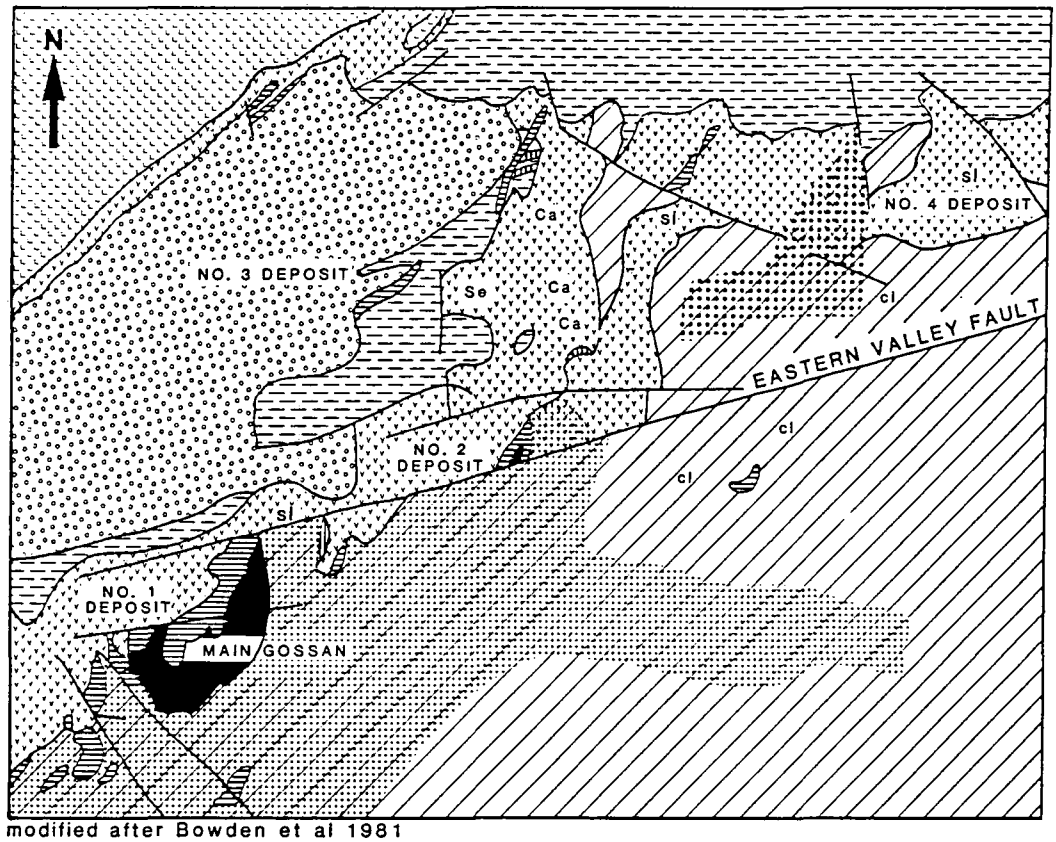

modified after Bowden et al 1981

LITHOLOGY

- Volcanic Conglomerate and Sandstone
- Andesite flow and fragmented rocks
- Predominantly rhyolitic flow rocks, welded tuff ignimbrite, lapilli tuff, chert, Jasper and Carbonate,
- Rhyolitic fragmented rocks, brecia and tuff
- Dacite with quartz phenocrysts
- Jasper and Chert
- Limestone and marble
- gossan

ALTERATION

- Areas with conspicuous quartz-eye development
- Ca Carbonate alteration
- Se Sericitization
- cl chloritization
- sl silicification
- Area of surface alteration including se, sl, cl, breathing and redding with copper

0 300 meters

1:5000

FIGURE 2.11 Geology and alteration of Jabal Said

2.7.3.3 Sulphide deposit no. 3

This deposit is characterized at the surface by hematite and limonite staining associated with jasper and black shale.

This deposit is the deepest and the most pyritic of all the ore bodies and consists of two superimposed zones of massive sulphides (mainly pyrite, pyrhotite with minor chalcopyrite and sphalerite). The thickness of the upper zone is 13-15m and has an average of 0.27% Cu and 0.7% Zn; the lower zone has an average thickness of 6m with grades varying from 0.88% Cu and 0.11% Zn and in other places, 0.6% Cu and 0.54% Zn.

2.7.3.4 Sulphide deposit no. 4

Ore body no. 4 strikes N 40 E. It is also divided into two distinct zones; an upper zone consisting of several lenses of massive sulphides, mainly pyrite and sphalerite with subordinate chalcopyrite or pyrhotite, intercalated mainly within brecciated jasper, although at depth they grade into a calcareous sequence. The average grade of Zn varies from 0.82 to 5.44% and high silver and tin concentrations are found in the sphalerite ore of this zone.

The lower zone represents the largest and the most continuous copper-rich stringer ore in the area. It is composed mainly of pyrite and chalcopyrite with minor sphalerite and pyrhotite that form veinlets and

dissemination in chloritic rocks. The average Cu grade varies from 2.0 to 3.0%.

The deposits are marked by extensive sericite and hematite alteration, leaching and silicification. At the surface it lies within the hydrothermally-altered host rock of the main gossan and consists mainly of massive and stringer mineralization. Bowen & Smith divided no. 4 deposit into nos. 4 (200m deep) and 4a (about 500m deep).

2.7.3.5 Types of deposits and minerals

The massive sulphide deposits at Jabal Sa'id are classified as stratiform-type deposits, "volcanic sulphide Mineralization of the Canadian type" deposits, and ore bedded with chert-carbonate horizons.

The mineral composition at No. 1 consists of nodular pyrite in a siliceous carbonate or chert-rich matrix with about 70% sulphide. The major sulphide minerals present are pyrite, pyrhotite, chalcopyrite and sphalerite with minor galena and magnetite. In deposit No. 4 the sulphide occupies 90% of the total volume of the rock and the principal sulphide minerals are pyrite, sphalerite and chalcopyrite, along with pyrhotite and galena as accessory minerals. The mineralization in No. 4 is not brecciated.

The stockwork mineralization associated with Nos. 1, 2 and 4 occurs as veins, stringers and dissemination, which cut across lithological boundaries and cover about 20% of the rock volume. The principal sulphide minerals

are pyrite and chalcopyrite with minor sphalerite (Table 2.3).

2.8 Summary and Conclusions

The mineral deposits at Mahd Adh Dhahab and Jabal Said both lie in a series of volcanic and volcaniclastic sediment which are intruded by different intrusions. The types and divisions of mineralogies are different; in Mahd Adh Dhahab the elements (Au, Ag, Zn) are associated with quartz veins through hydrothermal solutions, whereas in Jabal Said a syngenetic massive Zn-Cu sulphide deposits occurs as sulphide lenses in siliceous volcanic rocks.

There are marked variations in the appearances of the different lithologies. The mineralization associated with the alteration in Mahd Adh Dhahab appears to be related to mine sequence units which can be traced easily west from the mine hill and most of the other locations are associated with this unit. In Jabal Said the minerals are close to the gossan and they are restricted to standard zones east of the gossan.

Generally it seems that there are marked variations in the appearance of different lithologies which can be picked up by measuring spectral differences, despite the presence of desert varnish which can affect these measurements. The fact that there are distinctive alteration assemblages at the surface may also aid detection by remote sensing systems. Thus there is a

Table 2.3 Comparison between ore deposits in Jabal Sa'id.

Deposit	Ore body Miner.	Surface Miner.	Host rock
No.1	Mainly pyrite	massive-chert lim. quartz, calcite	chloritized tuff and breccias.
No.2	Pyrite and sphalerite with minor chalcopyrite, pyrite and brecciated jasper.	similar to No. 1	similar to No.1
No. 3	mainly pyrite,	* gossan characterized by hematite, limonite staining associated with jasper and black shell.	similar to No.1
No. 4	mainly pyrite, with subordinate sphalerite	extensive hematite	hydrothermally altered tuff and breccia.

* Gossan is dominated by goethite (FeOOH) and hematite (Fe_2O_3), with gangue minerals such as quartz, calcite and small amounts of gypsum, anhedrite and siderite.

possibily of finding hidden or unknown targets from surface alteration using remote sensing techniques. Before applying the remote sensing technique in the area, it is very helpful to have background information about the area. Knowledge of physical background of the different lithologies is very important for the interpretation of the images. Chapter 3 will examine questions concerning the relationships between spectral reflectance and different minerals in Jabal Said and Mahd Adh Dhahab.

CHAPTER 3

PHYSICAL BASIS FOR THE USE OF MULTISPECTAL REMOTE SENSING DATA IN LITHOLOGICAL AND ALTERATION MAPPING IN THE STUDY AREA

3.1 Introduction

The overall aim of this chapter is to establish the physical basis for the use of broad-band multispectral remote sensing data in lithological and alteration mapping in the Arabian Shield. In this context, the following objectives are considered:

1. To examine the nature and composition of the various rocks and surficial materials found in the study area. This is reviewed through the detailed laboratory analysis of samples taken from both the Mahd Adh Dhahab and Jabal Said areas.

2. To estabish the relationship between the spectral properties of those materials characteristic of the study area and their composition. This was achieved through (a) The use of a laboratory spectrometer and a field radiometer measuring reflectance over the 0.4-2.5um wave length range. The purpose of this element of the study was to determine whether the materials found in the area are characterised by diagnostic spectral absorption features. Such information provides the basis for interpreting broad-band multispectral data (Hunt 1979, 1980; Goetz et al., 1983; Abrams et al., 1984). This part of the research also provides an indication of the mapping

potential that may be offered by the new generation of remote sensing instruments, namely the imaging spectrometers (Goetz et al, 1985). (b) The use of a field radiometer with band passes pre-set to coincide with those covered by the six visible, near and shortwave infrared bands of the Landsat TM sensor. The primary purpose for acquiring in-situ reflectance data was used to define the potential and limitations of using satellite Landsat TM and Airborne MSS data sets for mapping purposes. In order to characterise the minerals which produce a rock's reflectance spectrum, the analytical procedure must be advised to analyse only the upper rock surface down to the optical depth. The weathered surface was separated from the fresh rocks and both were examined by XRD and XRF.

The examination of the results would note the mineralogical differences which existed between altered and unaltered rocks and the mineralogical differences between the weathered surfaces and fresh rocks. Such data would allow examination of the ability of remote sensing devices to discriminate hydrothermally altered rock from unaltered rocks.

3.2 Rock Geochemistry

As detailed in Chapter 2, the study area is characterised by a wide range of mineralogically (and presumably spectrally) distinct lithologies and surficial materials. These include granites, diorites, andesites,

tuffs, volcanic conglomerates and breccias, pyroclastics and various alluvial sands and gravels. Before measuring the spectral characteristics of these materials, a detailed geochemical study was conducted on samples taken from the field, in order to determine their composition qualitatively for interpretation of laboratory spectra. Two types of analysis were used, X-ray diffraction (XRD) and X-ray fluorescence (XRF) on the samples.

3.2.1 Sample acquisition

Only a limited time period was available for field investigations and sampling. Therefore, sample acquisition was largely controlled by the need to acquire rock and surface materials representative of both the Mahd Adh Dhahab and Jabal Said districts.

In the Mahd Adh Dhahab district, sampling was confined largely to the Mine Hill and its immediate surroundings. Particular attention was paid to acquiring samples from the different types of alteration as defined by Doebrich & Leanderson (1984) which characterises the area. Additional samples were collected from unaltered rocks surrounding Mine Hill. Figure 3.1 details the locations of the sampling points.

At Jabal Said the major concern was to acquire samples from the wide range of lithologies found in the area. Samples were also collected from the gossan and

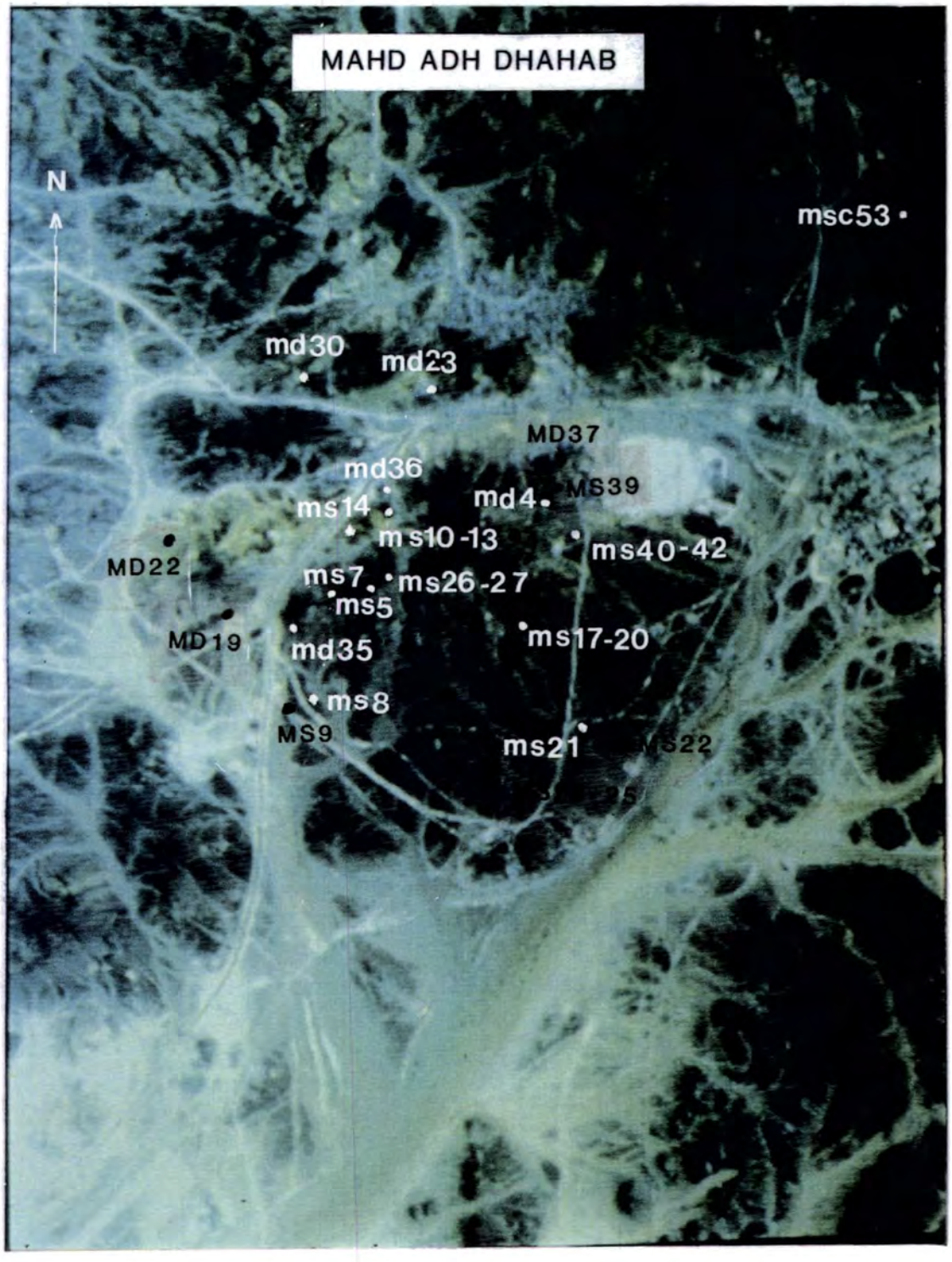

Fig. 3.1 Location map of the samples collected for XRD and Laboratory spectra from Mahd Adh Dhahab.

zones of known alteration. Sample points are located in Fig. 3.2.

3.2.2 Sample preparation

The methodology for determining the geochemical characteristics of those samples acquired in the field was in part constrained by a knowledge of how electromagnetic radiation interacts with natural surfaces. Remotely sensed data are generally obtained from the upper micrometres or millimetres of the surface because of the high opacity and scattering characteristics of natural materials (Goetz & Rowan, 1981). Buckingham & Sommer (1983) conducted a series of experiments to define that portion of a rock sample which contributes to the remotely sensed signal. They concluded that the depth to which the visible, near and shortwave-infrared radiation penetrated the surface was dependent in part on the actual mineralogy present, and in part on the concentration of certain minerals, most notable those which act as significant absorbers. A value of 50um was used as an approximate maximum penetration depth to include all mineral species which may contribute to the remotely sensed signal (Buckingham & Sommer, 1983).

Many of the samples returned from the study area were characterised by the presence of a weathered coating/ stain/rind. In many instances these coatings or rinds exceeded the critical 50um thickness. This implied that the remotely sensed signal recorded over naturally

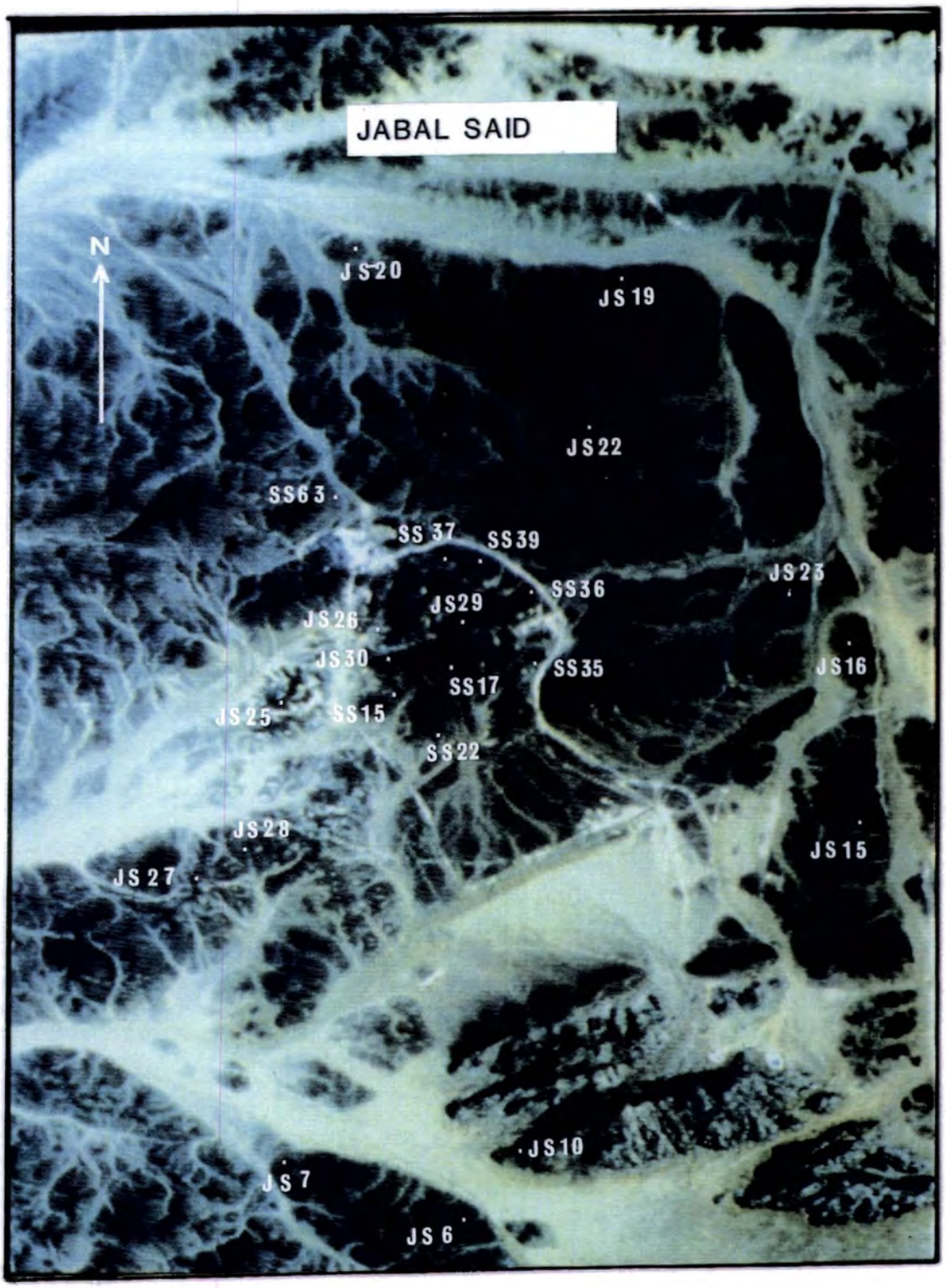

Fig. 3.2 Location map of the samples collected for XRD and Laboratory spectra from Jabal Said.

occurring materials in the study area would be largely determined by the chemical composition of the weathered surface, rather than the bulk chemistry of the rock. Therefore, in order to fully understand the physical basis for the spectral response characteristics exhibited by those lithologies, geochemical analysis was conducted on material from the upper weathered surface and the unweathered bulk.

Forty-four samples from the study area were analysed by XRD to determine the chemistry of their rocks. The samples from Mahd Adh Dhahab were selected on the basis of the type of alteration present, while the samples from Jabal Said were selected on the basis of differences in lithology (Figs. 3.1, 3.2).

In order to look at the effect of the chemistry of the weathering coating in relation to the whole rock chemistry, the weathered surface was separated from the fresh rock, either by cutting 2mm slices from the samples including the weathered surface, or scratching the surface with a small electric drill. The rocks were then crushed to a very fine grained powder.

Samples for XRD were prepared by mixing the powder with water on a glass slide and left until dry. Other procedures were used to increase the presence of clay minerals by mixing 50gm of the powder samples with 100mm distilled water in a small pitcher, leaving the heavy

minerals to settle, the fine particles were collected on glass slides placed carefully in the pitcher.

The second procedure was effective on samples from alteration zones to increase the amount of clay minerals on glass slides.

The samples under investigation were first crushed in a Storevant jaw crusher and then ground to a fine powder in a TEMA tungsten carbide disc mill. About 5 grams of powder was then mixed with about 7-8 drops of Mowoil (used as a binder) and then pelleted in a 5 tone hydraulic press.

The sample pellets together with selected igneous and sedimentary international geochemical standards were run on a Philips PW1400 X-ray spectrometer, using a Rhodium 3-kilowatt X-ray tube, and incorporating a PW1500 automatic sample loader.

The measured peak intensities were then processed by two computer programs:

a) XRF, CBI for the major oxides SiO_2, Al_2O_3, Fe_2O_3, MgO, CaO, Na_2O, K_2O, TiO_2, Mn, P_2O_5, and S. XRF, CBI is a FORTRAN program used at the University of Durham, which corrects the measured peak intensities for differences in matrices using a simple mass absorption model together with an iterative cubic bivariate interpolation to obtain the compositions.

b) K-factor for the trace elements Ba, Nb, Zr, X, Sr, Rb, Zn, Cu, Ni, Pb, U, Th, V, Cr, Nd, Ga, La and Ce.

K-factor is based on the method used by the GGU in Copenhagen and is outlined in a guide "X-ray fluorescence analysis", Trace Element Techniques in the Institute for Petrology, University of Copenhagen, by John Bailey (1976). Again the program used a simple mass absorption correction model to correct the measured peak intensities together with a simple linear regression to obtain the composition.

Only six samples from Mahd Ahd Dhahab were analysed for XRF due to the fact that XRF needs larger amounts of samples compared to XRD, and it was not feasible to get the required amount of weathered samples. Another constraint was the limited size of the samples.

More samples from Jabal Said were analysed by XRF for the weathered surface due to the size of the samples and the amount of weathered coating.

3.2.3 Geochemical characteristics of the Mahd Adh Dhahab District

A total of 31 samples were analysed from the Mahd Adh Dhahab area. These samples were mainly concentrated from the Mine Hill and collected from the different types of alteration there (Fig. 3.1).

The results of the XRF analysis of the bulk samples for major elements are presented in Table 3.1. The major elements identified by XRF were used in conjunction with XRD analysis to determine the minerals present.

Table 3.1. Major elements - Mahd Adh Dhahab Area.

Sample No.	SiO_2	Al_2O_3	Fe_2O_3	MgO	CaO	Na_2O	K_2O	TiO_2	MnO	P_2O_5	S	LOI	Total
MD30/1	79.70	10.10	2.30	0.00	0.00	3.17	3.18	0.18	0.09	0.12	0.03	1.20	100.02
MS5	80.83	10.04	1.19	0.02	1.21	5.15	0.71	0.11	0.05	0.05	0.00	0.67	100.03
MS53	10.88	1.57	0.74	4.55	47.36	0.00	0.00	0.06	0.56	0.03	0.02	34.21	99.98
MD4/3	66.01	12.10	8.29	6.50	0.75	0.10	4.06	0.91	0.13	0.15	0.03	0.97	100.00
MS6a	34.19	11.06	7.74	11.71	17.25	0.02	0.02	0.51	0.22	0.03	0.00	17.25	100.00
MS11b	84.05	8.69	1.27	0.98	0.00	0.00	4.01	0.14	0.04	0.07	0.01	0.75	100.01
MS10a	76.44	10.45	2.14	0.34	1.66	6.42	0.35	0.21	0.06	0.63	0.05	1.22	99.97
MD22/3	75.84	11.64	1.82	1.37	0.76	6.81	0.22	0.24	0.05	0.07	0.01	1.16	99.99
MS24	76.00	7.51	7.25	6.05	0.52	0.11	0.83	0.31	0.56	0.08	0.02	0.80	100.04
MS9	75.84	13.16	1.18	0.33	0.58	5.73	1.54	0.11	0.04	0.04	0.02	1.43	100.00
MD35/1	77.51	9.20	2.29	4.06	0.05	0.05	5.27	0.20	0.11	0.06	0.03	1.17	100.00
MD37/1	74.88	11.81	3.27	1.26	0.00	1.11	6.10	0.23	0.09	0.04	0.06	1.18	100.03
MS11a	80.66	11.08	1.65	2.14	0.00	0.00	3.76	0.21	0.04	0.03	0.00	0.42	99.99
MD38	82.07	8.15	2.61	5.00	0.15	0.00	1.78	0.16	0.05	0.03	0.00	0.00	100.00
MS7	75.35	13.15	3.85	3.69	0.00	0.03	2.29	0.37	0.07	0.08	0.00	1.01	99.99
MS40	87.62	6.08	1.96	0.75	0.26	0.00	2.63	0.11	0.04	0.07	0.03	0.75	100.02
MS6c	85.02	7.42	1.40	0.36	0.21	4.66	0.07	0.12	0.05	0.03	0.00	0.66	100.00
MS8	32.55	12.38	11.96	8.91	15.55	0.17	0.84	0.98	0.46	0.12	0.00	16.06	99.98
MS39	82.19	8.34	2.07	0.65	0.14	0.00	4.05	0.23	0.17	0.10	0.08	1.99	99.99
MS27	74.92	9.10	6.10	4.36	0.27	0.00	2.53	0.28	0.20	0.07	0.04	2.16	100.03
MS14	80.37	8.23	2.43	2.71	0.44	0.05	2.95	0.30	0.07	0.11	0.02	2.34	100.02
MD35/2	59.64	14.40	6.63	7.00	0.92	0.04	6.24	0.54	0.33	0.16	0.01	4.11	100.02
MD4/1	53.86	17.53	9.89	6.77	0.74	0.08	6.73	1.23	0.16	0.30	0.02	2.70	100.01
MD4/2	73.80	9.37	6.52	2.18	0.34	0.06	4.13	0.74	0.08	0.11	0.08	2.59	100.00
MD19/1	60.28	14.03	8.09	2.74	2.14	5.30	1.92	1.25	0.21	0.44	0.00	3.62	100.02
MD23/2	80.44	9.71	2.93	0.46	0.24	5.33	0.50	0.17	0.12	0.03	0.05	0.00	99.98
MD23/3	74.81	11.39	3.44	2.24	0.82	5.28	0.57	0.19	0.19	0.11	0.01	0.95	100.00
MS6b	73.88	10.06	4.76	6.68	0.00	0.00	3.50	0.39	0.14	0.09	0.00	0.60	100.00
MS10b	75.18	11.10	2.71	1.99	3.05	2.73	1.21	0.43	0.12	0.12	0.03	1.32	99.99
MD30/2	78.94	9.36	2.29	1.82	0.34	2.76	2.71	0.24	0.08	0.10	0.02	1.32	99.98
MD37/2	78.37	11.74	2.72	0.02	0.06	0.09	5.81	0.22	0.04	0.06	0.00	0.87	100.00

Generally, most samples show a high percentage of SiO_2 except the samples from the carbonate rocks, collected from the northeast of the Mine Hill (not shown on the map).

The results of the trace elements for the same samples shows high values for copper, zinc and lead mainly concentrated in the east side of the Mine Hill (Table 3.2).

The same bulk samples were analysed by XRD to determine the mineralogy of the samples. Chlorite seemed to be the dominant mineral in the area. Kaolinite was the dominant mineral present in the argillic alteration. Details of the mineral composition and the results of the XRD are shown in Table 3.3.

A comparison between the chemistry of the bulk samples and the weathered surface was run for six samples, from the area mapped as argillic alteration, Andesite, silicic alteration, pyrite chlorite alteration and chlorite alteration (Table 3.4).

A ratio between the major elements in the bulk samples and the weathered surface was calculated (Table 3.5), the results are shown in Figs. 3.3 to 3.5. The samples from MS11/2 Argillic alteration (Fig. 3.3b) show a small increase in the Al, Fe, Mg and K on the surface while the other samples from area mapped as Argillic alteration (Fig.3.3a) shows an increase in Ca on the surface and an increase in Na in the bulk rock sample,

Table 3.2. Trace Elements - Mahd Adh Dhahab Area.

Sample No.	BA	NB	ZR	Y	SR	RB	ZN	CU	NI	PB	U	TH	V	CR	ND	GA	LA	CE
MD30/1	1362	7	113	27	121	39	55	20	10	19	3	10	11	8	7	10	10	34
MS5	217	7	100	7	649	15	15	13	1	29	5	9	8	6	11	5	7	10
MS53	68	1	29	21	161	6	13	0	0	15	5	1	5	0	49	3	15	24
MD4/3	982	4	54	22	48	45	1745	522	6	19	1	2	154	19	3	16	5	4
MS6a	35	3	23	17	101	4	58	48	16	10	2	0	139	54	6	11	3	16
MS11b	549	7	125	26	97	63	20	16	5	19	0	7	24	6	17	10	13	42
MS10a	139	7	117	21	123	8	43	42	3	20	1	5	15	5	18	9	11	43
MD22/3	267	8	145	26	166	6	37	19	4	20	3	10	12	7	12	13	6	33
MS24	922	4	14	4	69	13	612	1061	20	50	1	0	99	45	1	9	4	11
MS9	421	4	78	7	171	33	21	26	3	17	0	0	1	5	3	7	8	9
MD35/1	1048	6	89	21	45	54	472	24	2	40	1	7	23	6	12	10	5	15
MD37/1	1098	11	267	69	49	71	172	18	4	32	2	6	13	8	26	19	17	47
MS11b	240	9	170	54	13	78	33	27	2	14	1	6	17	10	19	21	12	33
MD38	532	6	93	27	16	35	336	17	0	22	1	8	17	12	15	11	3	25
MS7	403	7	120	33	33	36	74	22	3	16	1	7	39	14	23	17	11	26
MS40	1499	5	56	14	52	31	743	2329	0	444	0	4	14	7	9	9	2	17
MS6c	119	8	132	34	52	4	42	22	7	19	1	8	10	6	12	10	12	30
MS8	182	5	55	27	93	16	84	67	10	11	1	1	67	11	0	12	4	33
MS39	736	3	70	17	26	44	3384	9566	2	3058	0	0	27	7	22	23	2	47
MS27	1663	6	115	15	46	32	217	16	6	21	1	5	71	14	0	14	7	21
MS14	1872	5	97	21	74	33	102	37	7	37	1	0	39	16	7	10	7	0
MD35/2	896	5	67	24	62	72	140	50	8	15	2	4	103	70	6	18	2	24
MD4/1	1958	5	102	47	68	87	811	5	0	18	0	0	166	14	8	20	0	28
MD4/2	1645	3	43	15	61	43	536	217	0	21	1	0	122	24	0	11	5	6
MD19/1	598	7	143	44	270	25	101	21	0	14	3	1	96	9	24	20	2	42
MD23/2	213	10	232	65	52	5	84	19	6	17	1	8	7	9	16	16	13	27
MD23/3	533	11	231	67	178	7	96	20	16	19	3	8	9	9	39	19	16	45
MS6b	614	7	115	23	35	47	785	73	9	56	1	4	79	16	19	13	13	31
MS10b	371	7	112	22	202	20	67	43	7	15	4	9	44	8	14	11	9	34
MD30/2	742	5	124	27	299	38	45	9	0	17	2	3	18	15	16	10	9	26
MD37/2	834	8	254	70	42	56	2223	2108	5	3896	0	0	15	6	32	43	12	82

Table 3.3. Result of the samples analysed for mineral composition using XRD from Mahd Adh Dhahab area.

Sample No.	Lithology	Alteration type (where mapped)	Minerals Id by XRD
Msc 53/1	Carbonate Rock		C,Q
MD 23/2	Silicified tuff		Q,P,K
MD 23/3	Breccia		Q,P,CH
MD 22/3	Rhyolite		P,Q,K,C
MD 30/1	Rhyolite		Q,P,K
MD 30/2	Rhyolite		Q,P,CH
MS 14	Upper Tuff	Chlorite Pyrite	Q,KF,CH,M
MS 27	Lower Agglomerate	Chlorite	Q,CH,M,KF
MS 39	Rhyolite Intrusion	Quartz,ser.pyr.	Q,KF,M,K
MS 6a	Lower Agglomerate	Chlorite	Q,C,CH
MS 6b	Lower Agglomerate	Chlorite	Q,KF,CH,M
MS 6c	Lower Agglomerate	Chlorite	Q,KF
MS 11a	Upper Tuff	Argillic	Q,M,C,K
MS 11b	Upper Tuff	Argillic	Q,H,CH,KF,G
MS 8	Andesite	Pyrophyllite	Q,C,CH,M
MS 40	Upper Agglomerate	Potassic	Q,K,KF,M
MS 7	Lower Tuff	Chlorite	Q,K,M,P
MS 10a	Upper Tuff	Argillic	Q,P,A,K
MS 10b	Upper Tuff	Argillic	Q,P,C,CH,M
MS 5	Lower Tuff	Silicic	Q,P,M
MS 24	Andesite		Q,KF
MD 4/3	Lower Tuff	Pyrite Chlorite	Q,K,CH,KF
MD 35/1	Lower Agglomerate	Silicic	Q,KF,CH,C
MD 37/1	Upper Tuff	Silicic	Q,P,C,CH,L,KF
MD 37/2	Upper Tuff	Argillic	Q,KF,M,CH
MD 36	Upper Tuff	Pyrite Chlorite	Q,H,CH,M
MD 19/1	Andesite		Q,P,A
MD 4/1	Lower Tuff	Pyrite Chlorite	Q,KF,G,M,K,L
MS 9	Andesite	Pyrophyllite	P,Q,M,C
MS 4/2	Lower Tuff	Pyrite Chlorite	Q,KF,M
MD 35/2	Lower Agglomerate	Silicic alt.	Q,P,CH

Key for minerals identified by XRD:

Q = Quartz
H = Hematite
K = Kaolinite
G = Goethite
M = Muscovite
L = Allunite
P = plag-feldspar
C = Calcite
CH = Chlorite
KF = K-feldspar
A = Apatite

Table 3.4. Major elements - Mahd Adh Dhahab area. Comparison between the fresh rock and weathered surface.
F = Fresh rock sample. W = Weathered surface.

Sample No.		SiO_2	Al_2O_3	Fe_2O_3	MgO	CaO	Na_2O	K_2O	TiO_2	MnO	P_2O_5	LoI	Total
MS11b	F	84.05	8.69	1.27	0.98	0.00	0.00	4.01	0.14	0.04	0.07	0.75	100.00
Argillic Alt.	W	84.93	8.19	0.99	0.79	0.23	0.00	3.99	0.16	0.00	0.01	0.75	100.04
MS8	F	37.58	12.29	9.72	7.26	14.81	0.07	0.65	1.12	0.34	0.11	16.06	100.01
Andesite	W	53.59	13.50	11.49	8.54	4.70	0.25	0.83	1.58	0.31	0.11	5.28	99.98
MD35/1	F	78.89	8.89	2.11	2.73	0.29	0.00	5.57	0.24	0.09	0.03	1.17	100.01
Silicic alt.	W	75.99	9.68	2.97	3.35	0.49	0.00	5.35	0.24	0.18	0.10	1.65	100.00
MS10b	F	75.18	11.10	2.71	1.99	3.05	2.73	1.21	0.43	0.12	0.12	1.32	99.99
Argillic Alt.	W	73.46	14.88	3.44	2.43	0.51	1.43	1.87	0.48	0.10	0.08	1.32	100.00
MS6c	F	85.02	7.42	1.40	0.36	0.21	4.66	0.07	0.12	0.05	0.03	0.66	100.00
Pyrite-chlorite	W	85.06	8.88	1.14	0.33	0.37	3.38	0.00	0.14	0.03	0.02	0.66	100.01
MD4/3	F	71.23	10.19	7.76	3.98	0.76	0.00	3.90	0.91	0.13	0.15	0.97	99.98
Chlorite	W	65.08	12.37	10.44	4.89	0.60	0.00	4.11	1.23	0.16	0.23	0.89	100.00

Table 3.5. Ratio of Major elements, Mahd Adh Dhahab area.

Sample No.	SiO_2	Al_2O_3	Fe_2O_3	MgO	CaO	Na_2O	K_2O	TiO_2	M_2O	P_2O_5
MS 11b	1.01	0.94	0.77	0.81	2.3	0.0	0.99	1.14	0.0	0.0
MS 8	1.42	1.09	1.18	1,18	0.32	3.6	1.28	1.4	0.91	1.0
MD 35/1	0.96	1.08	1.41	1.23	1.69	0.0	0.96	1.0	2.0	3.3
MS 10b	0.98	1.34	1.27	1.22	0.17	0.52	1.55	1.12	0.83	0.7
MS 6c	1.0	1.19	0.81	0.92	1.8	0.73	0.0	1.17	0.6	0.7
MD 4/3	0.9	1.2	1.35	1.23	0.78	0.0	1.05	1.35	1.23	1.53

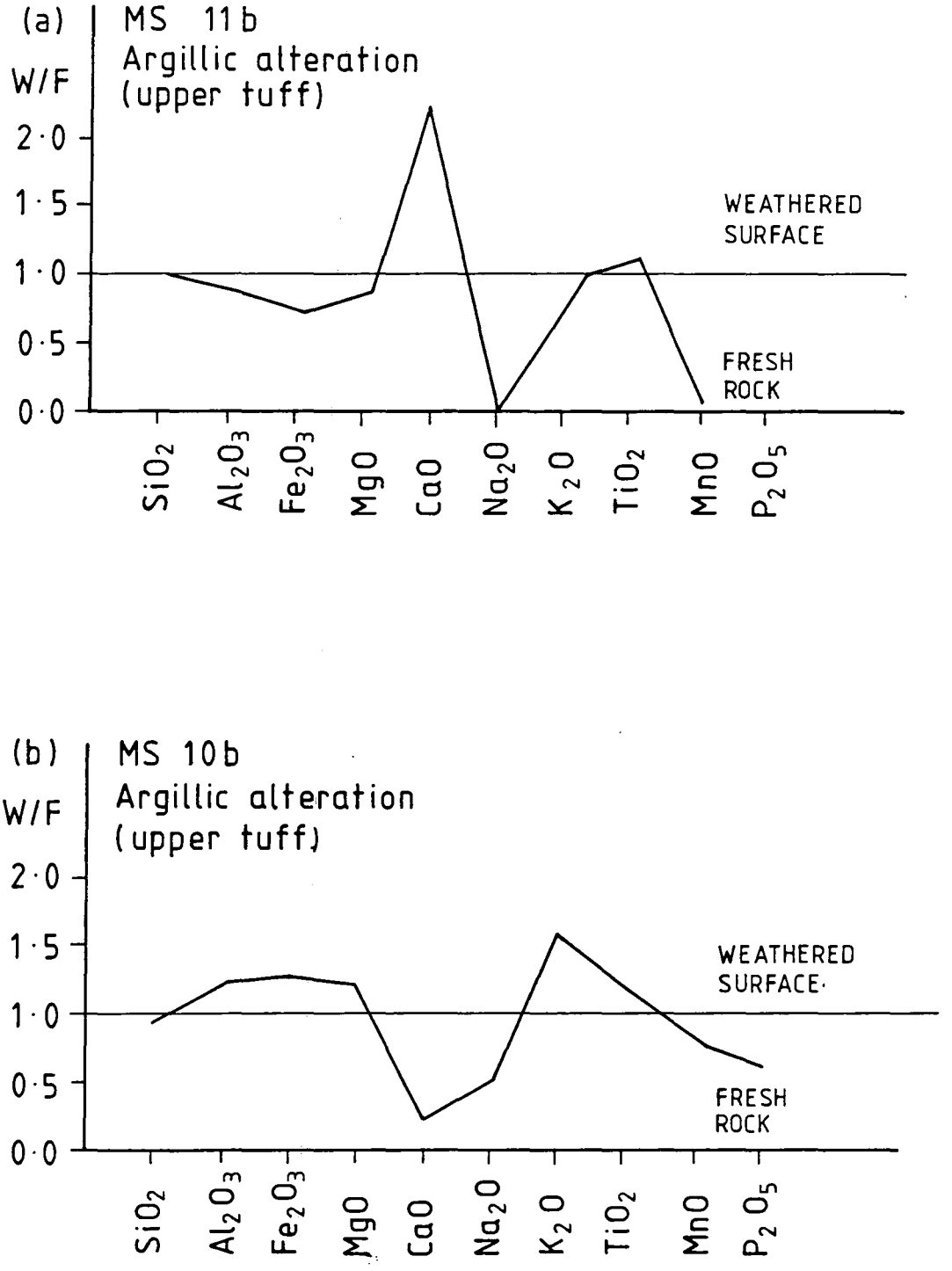

Fig. 3.3 Ratio of the major elements between weathered surface and fresh rocks - Mahd Adh Dhahab.

the proportions of other elements show now significant differences.

The sample from the chlorite alteration, MS6/3 (Fig. 3.5a) also shows an increase in Ca on the surface and an increase in K within the rock.

The sample from the andesite rocks MS8 from the south west part of the Mine Hill, was the only sample where all of the elements increased on the surface sample with the exception of calcium oxide and manganese oxide.

The samples of silicic alteration MD35/1 (Fig. 3.4a) show a decrease in Na and K and an increase in the other elements in the surficial sample. The pyrite chlorite alteration MD4/3 (Fig. 3.5b) shows a decrease in the Na and Ca and increase of the Al, Fe, Mg, K, Ti in the surficial sample.

XRD analysis was also carried out on the weathered surface of the 31 samples collected from Mahd Adh Dhahab. A comparison of the minerals identified in the weathered surfaces and the rock minerals is presented in Table 3.6.

Generally, the quartz, K-feldspar, plagioclase and carbonate show decreased in the surface compared to other minerals which show an increase in the surface like chlorite, kaolinite, calcite and mica (illite). The chlorite seems to be the dominant mineral in the altered rocks area, with the presence of the kaolinite.

Only one sample (MD37/1) collected from the argillic alteration zone shows about 30% of alunite on the surface.

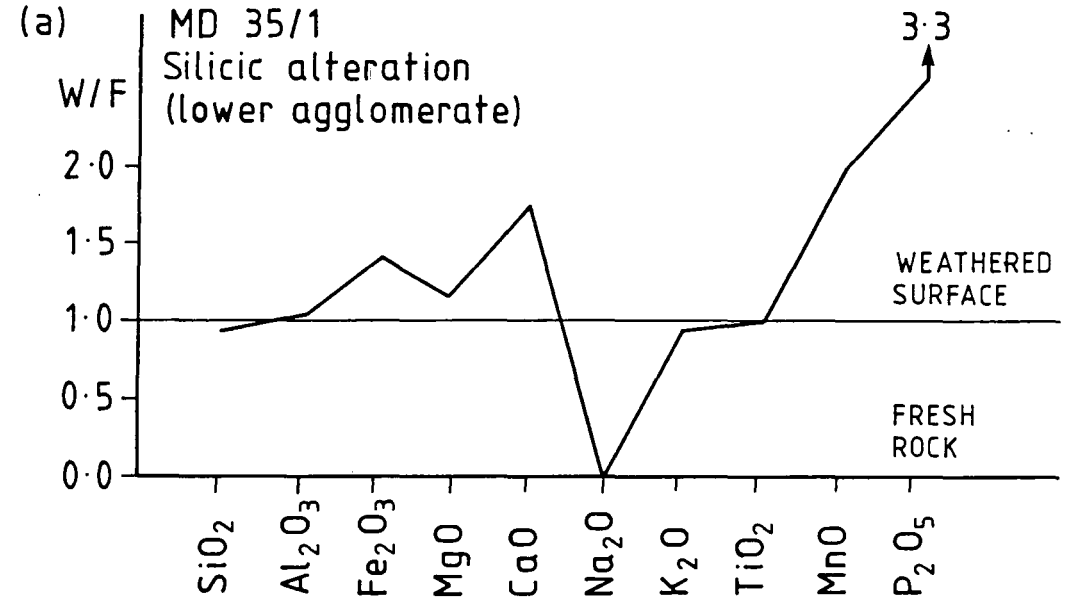

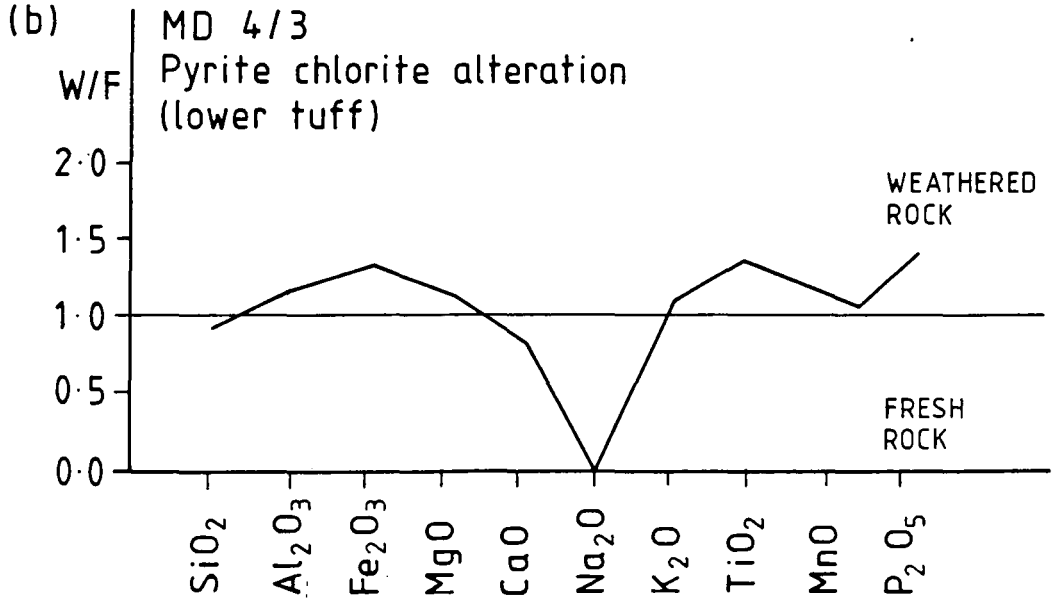

Fig. 3.4 Ratio of the major elements between weathered surface and fresh rocks - Mahd Adh Dhahab.

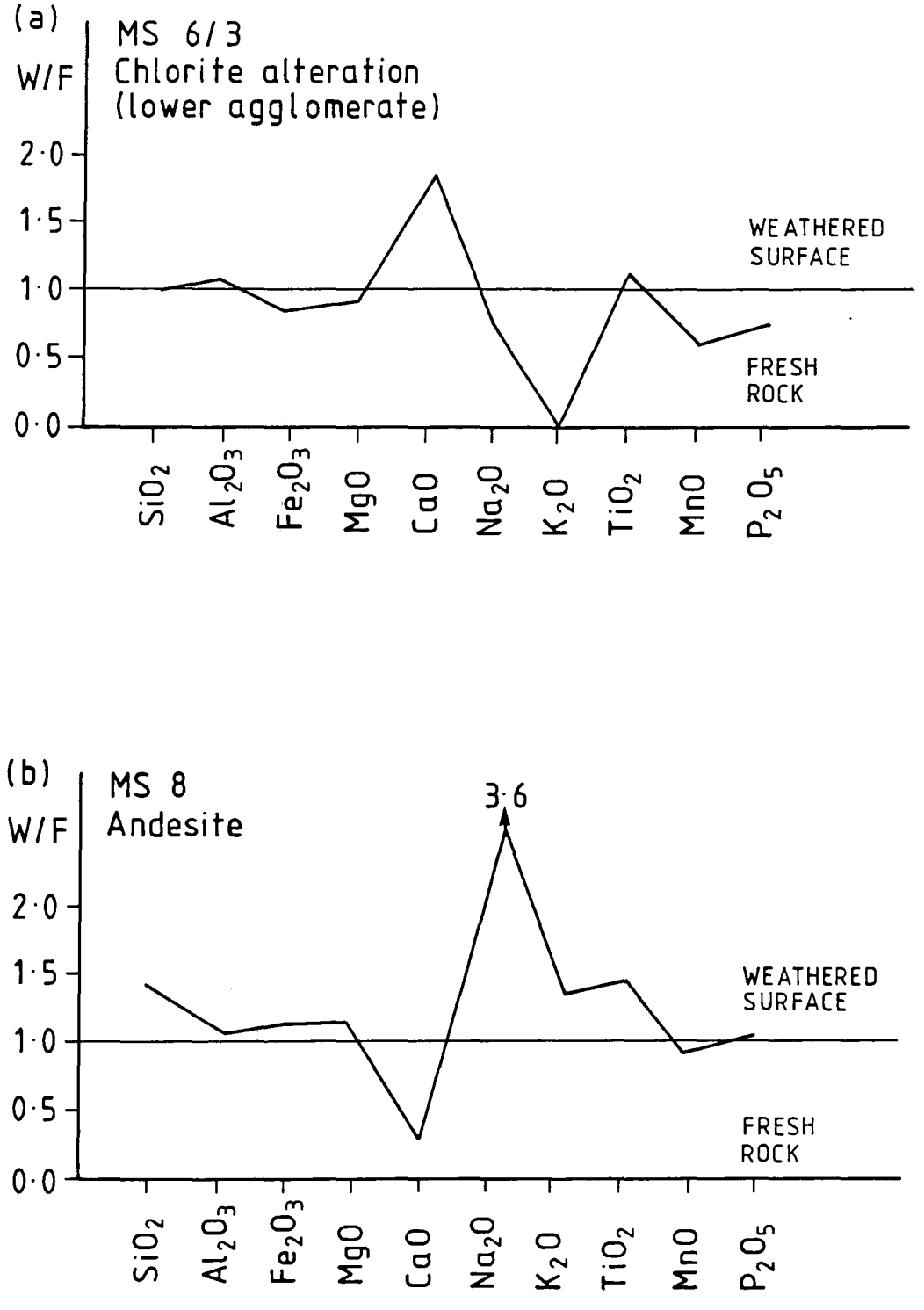

Fig. 3.5 Ratio of the major elements between weathered surface and fresh rocks - Mahd Adh Dhahab.

Table 3.6 Results of XRD, Mahd Adh Dhahab area. Comparisons between weathered surface and fresh rocks.

Sample No. and Lithology	Alteration type	Fresh rocks minerals	Weathered Surface
MD23/3 Breccia		quartz, plag. chlorite	some mineral reductn in plag. increase in chlorite
MD 4/1 Lower tuff	Chlorite	Quartz, K-feld, chlorite	increase in quartz and chlorite decrease in K-feld, + mica, absence of goethite
MD4/3 Lower tuff	Chlorite	quartz, K-feld, chlorite	decrease in K-feld, increase in chlorite + kaolinite
MS27 Lower Agglomerate	Chlorite	quartz, chlorite, K-feld, mica	increase in chlorite and mica
MS8 Andesite	Pyrophyllite	quartz, calcite, chlorite, mica	increase in quartz + chlorite, decrease in calcite
MS9 Andesite	Pyrophyllite	plag. quartz, mica	decrease in plag. increase in mica + calcite
MD22/3 Rhyolite		quartz, plag. calcite, kaolinite	high increase in kaolinite calcite disappears
MS53	Carbonate rocks	calcite, quartz, dolerite	decrease in calcite + kaolinite
M30/2 Rhyolite		quartz, plag., kaolinite	decrease in plag., increase in kaolinite
MD37/2 Upper tuff	Argillic	quartz, K-feld, mica	quartz + K-feld decrease, increase in mica + kaolinite
MD23/2 Silicified tuff		Quartz, plag. chlorite	no change
MD19/1 Andesite	Andesite rocks	quartz, plag., kaolinite apatite	no sample
MD30/1 Rhyolite		Quartz, plag. kaolinite	
MS7 Lower Agglomerate	(Lower Tuff) Silica	Quartz, kaolinite, mica plag.	no sample
MS5 Lower Tuff	(Lower tuff) Silica	plag. quartz, mica	no sample
MD4/2 Lower tuff	Andesite rocks	quartz, K-feldspar, mica	no sample
MS10a (Upper tuff)	Argillic	Quartz, plag., apatite	decrease in plag + kaolinite
MS10b (Upper tuff)	Argillic	quartz, plag., chlorite, mica, calcite	decrease in plag. increase in chlorite + mica. no calcite.
MS11a Upper tuff	Argillic	Quartz, mica	reduction in kaolinite + calcite
MS11b Upper tuff	Argillic	Quartz, K-feld, mica,	same + goethite
MS6a Lower agglomerate	Pyrite, Chlorite	Quartz, chlorite, calcite	increase in quartz and chlorite no calcite
MS6b Lower Agglomerate	Pyrite, Chlorite	Quartz, K-feld, chlorite mica	same + calcite
MS6c Lower Agglomerate	Pyrite, Chlorite	quartz, K-feld, chlorite	no change
MD35/1 Lower Agglomerate	Silicate alt	quartz, K-feld.	+ chlorite, calcite

Table 3.6 Continued.

MD35/2 Lower agglomerate	Silicate alt.	quartz, K-feld, chlorite	increase in chlorite
MS14 Upper tuff	Pyrite, Chlorite	quartz, K-feld, mica, chlorite	increase in chlorite, K-feld, mica.
MS24 Andesite		quartz, chlorite, K-feld	no change
MS40 Upper agglomerate	Potassic alt.	quartz, K-feld, mica, kaolinite	increase in kaolinite and mica
MD36 Upper tuff	Pyrite, chlorite	quartz, mica, chlorite hematite	no samples
MS39 Rhyolite	Quartz, sericite pyrite	quartz, K-feld, mica	increase in mica + kaolinite
MD37/1 Upper tuff	Argillic alt.	quartz, K-feld, chlorite, plag.	no plag. and chlorite + allunite and calcite

In some of the samples, there was no apparent change in the mineralalogical composition between the original rock and the weathered surface. This can be seen from the results of samples nos. MS24 and MD23/2 which are outside the mapped alteration area. It seems that the rocks furthest from the area of alteration appear to have very little surficial weathering on the surface and have no significant degree of weathering or even formation of desert varnish. This seems to suggest that rocks away from the altered zone have been subjected to weak natural weathering. However, further work needs to be done to elaborate this case.

3.2.4 Geochemical characteristics of the Jabal Said area

A total of 12 samples were analysed from Jabal Said. These samples were chosen to represent the major lithologies, including the main gossan and the alteration zone (Fig. 3.2).

The weathered surface was separated from all twelve samples. XRF and XRD analyses were performed on the samples, where XRF identified the major elements and XRD determined the mineral composition of the samples.

The results of major element analysis for the bulk samples and the weathered samples are presented in Table 3.7, the trace element composition of the same samples are presented in Table 3.8.

Table 3.7 Major Elements - Jabal Said Area.
A = Weathered Surface Samples: B = Fresh Rock Samples

Lithology	Sample No.	SiO_2	Al_2O_3	Fe_2O_3	MgO	CaO	Na_2O	K_2O	TiO_2	MnO	P_2O_5	S	LOI	Total
Alteration Z.	30/1B	78.52	11.44	2.62	2.60	0.20	0.21	2.32	0.12	0.12	0.03	0.04	2.00	100.02
Andesite T.	31/1B	56.22	14.45	9.00	6.90	7.41	3.21	0.05	0.44	0.14	0.06	0.00	2.13	100.01
M. Gossan	25/2	78.46	1.51	9.90	0.47	9.14	0.00	0.08	0.05	0.07	0.12	0.00	0.20	100.00
Diorite	27A	53.27	15.04	9.60	7.57	8.63	2.08	0.15	0.43	0.38	0.20	0.02	2.65	100.02
Diorite	27B	53.40	15.08	9.10	7.94	9.06	2.16	0.11	0.41	0.17	0.10	0.01	2.47	100.01
Rhyolite	28A	78.36	10.94	2.60	3.60	0.94	0.86	0.89	0.12	0.20	0.21	0.00	1.30	100.02
AlterationZ.	30/2A	80.26	10.18	3.75	2.51	0.08	0.14	2.05	0.11	0.04	0.04	0.02	0.81	99.99
Volcanic Sed.	20/1B	39.19	10.25	8.15	3.86	24.39	0.29	0.86	0.48	0.73	0.23	0.02	11.55	100.00
Volcanic cong.	18B	63.92	14.03	8.47	4.08	4.03	1.89	1.22	0.73	0.16	0.19	0.04	1.30	100.02
Rhyolite	15/2B	73.58	13.17	1.28	0.00	0.56	5.31	4.85	0.17	0.06	0.03	0.04	0.97	100.02
Z. Breccia	23/3B	75.69	7.44	4.81	0.32	0.83	7.08	1.77	0.65	0.11	0.08	0.04	1.20	100.02
Andesite T.	22A	53.21	17.30	8.78	5.19	8.29	2.73	0.91	0.36	0.27	0.43	0.02	2.52	100.01
Main Gossan	25/1	19.74	1.03	71.64	0.37	2.15	0.37	0.00	0.05	0.04	0.22	0.00	4.41	100.02
Volcanic congl.	19/2B	62.27	13.96	8.11	3.50	6.16	2.29	1.39	0.63	0.14	0.18	0.00	1.37	100.00
Andesite T.	22B	54.40	17.17	8.55	5.02	7.64	3.59	0.87	0.35	0.18	0.14	0.00	2.10	100.01
Rhyolite	28B	76.98	12.61	2.55	4.62	0.12	0.88	0.77	0.12	0.06	0.03	0.06	1.21	100.01
Alteration Z.	30/2B	80.86	8.31	3.52	5.43	0.23	0.17	0.46	0.11	0.19	0.03	0.03	0.68	100.02
Alteration Z.	30/1A	77.83	8.61	4.48	5.78	0.38	0.14	0.43	0.13	0.25	0.03	0.03	1.89	99.98
Rholite	15/2A	73.93	12.60	1.71	0.28	0.66	4.92	4.31	0.18	0.11	0.04	0.09	1.20	100.03
Volcanic Congl.	19/2A	63.46	14.05	8.65	3.25	5.30	1.66	1.43	0.75	0.19	0.20	0.01	1.04	99.99
Z. Breccia	23/3A	73.33	8.68	5.08	0.46	1.81	6.35	2.03	0.46	0.27	0.57	0.03	0.95	100.02
Andesite T.	31/1A	55.68	15.40	7.54	4.35	11.54	2.23	0.07	0.34	0.21	0.23	0.00	2.41	100.00

Table 3.8. Trace Elements Jabal Said area.

A = Weathered Surface Samples. B = Fresh Rock Samples.

Sample No.	BA	NB	ZR	Y	SR	RB	ZN	CU	NI	PB	U	TH	V	CR	ND	GA	LA	CE
30/1B	266	6	70	96	55	52	140	108	6	18	2	3	5	8	44	10	13	18
31/1B	148	3	28	10	188	5	76	41	62	13	1	3	166	96	0	13	5	22
25/2	383	3	17	1	147	8	86	81	7	253	5	0	71	19	0	3	8	25
27/1A	347	4	30	17	227	7	163	210	92	20	3	0	191	122	18	14	12	48
27/2B	119	3	24	10	213	6	77	100	77	12	0	1	187	124	14	12	1	0
28/1A	335	8	91	33	84	35	78	36	34	19	1	10	10	13	17	12	11	25
30/2A	231	6	68	64	52	49	140	146	12	16	1	3	2	5	24	10	16	19
20/1B	235	3	62	18	461	16	53	0	11	10	3	3	116	40	14	12	2	24
18/2	501	4	80	21	194	27	105	46	30	16	2	6	147	63	6	14	2	19
15/2B	860	18	132	27	207	444	44	11	3	98	5	10	10	5	6	17	19	44
23/3B	36	1519	9794	1910	84	264	2360	0	148	506	95	623	24	0	1774	31	946	3108
22/1A	749	4	84	17	534	19	79	11	41	15	1	1	128	51	11	16	11	23
25/1	126	0	22	2	126	5	362	169	0	5	0	0	392	64	12	8	15	33
19/2B	364	4	74	18	301	28	92	21	33	14	2	2	139	52	14	16	6	21
22/2B	546	3	80	11	555	16	71	5	15	10	4	1	113	45	18	16	9	35
28/2B	126	7	90	35	52	13	68	18	12	14	2	11	7	5	7	13	5	0
30/2B	131	5	46	24	25	7	114	551	2	15	0	11	4	5	11	8	9	14
30/1A	129	6	47	27	36	8	140	634	8	14	1	12	7	5	8	9	5	0
15/2A	753	19	133	16	136	405	94	100	23	31	7	21	18	8	13	17	32	79
19/2A	267	6	87	20	292	30	115	13	62	19	2	11	173	103	14	17	13	40
23/3A	191	922	6361	1123	91	262	3793	3717	130	451	57	431	50	35	1104	35	743	2283
31/1A	302	1	24	13	197	5	82	32	65	9	1	0	154	90	5	21	3	0

XRD analysis was carried out on both bulk rock samples and on the samples of the surficial weathered material (Table 3.9).

Generally, the most common minerals in the bulk rock samples are quartz, plagioclase, chlorite, and mica. Some samples contained some amphibole, epidote and potash feldspar. The samples from the gossan show the presence of the iron minerals hematite and goethite with quartz and calcite.

A comparison was made between the mineral composition of the bulk samples and the mineral composition of their weathered surface (Table 3.9).

Generally the weathered surface shows an increase in the chlorite. Two samples which show the presence of kaolinite in the surficial material are from the alteration zone (JS30/2) and the other from andesite tuff (JS31/1).

Detailed studies were carried out to define the mineralogical change in the weathered surface of each rock using the results of the major elements analysis. A ratio between the two compositions was calculated by dividing the composition for each mineral in the weathered surface by the composition of the bulk rock sample. The results are presented in Table 3.10. The ratios are also presented in graphical form in figures (Figs. 3.6, 3.7, 3.8).

Table 3.9. Comparison between minerals of the fresh rock and weathered surface - result of XRD from Jabal Said area.

Sample No.	Lithology	Bulk rock	Weathered surface
JS 22	Andesite t.	Quartz, chlorite, mica plag, amphibole	same min.plag.reduc. +goethite & epidote
JS 25/1	Gossan	Hematite, quartz, calcite	no sample
JS 27	Diorite	Plag, amphibole, chlorite quartz	same min. plag.reduc. + smectite
JS 25/3	Gossan	Quartz, goethite, calcite	no sample
JS 20/1	Volc. sed.	Quartz, epidote, calc.	same min. calc. reduc.
JS 31/1	Andesite t.	Quartz, plagi, chlorite amphibole, calcite	same min. + sedrite and kaolinite
JS 18	Volcanic conglom.	Quartz, plag, mica, chlorite	plag. reduced quartz chlorite, mic incre.
JS 19/2	Volcanic conglom.	Quartz, plag. mica, chlorite, amphibolite	no change
JS 30/2	Alteration zone	Quartz, mica, plag, chlorite	same min. + kaolinite chlorite increase
JS 28	Rhyolite	Quartz, chlorite, mica, plag.	chlorite increase
JS 15/2	Rhyolite	Quartz, K-feld, plag.	slight reduction in K-feld & plag.

Table 3.10. Major elements - Jabal Said area.

Sample No.	Lithology	SiO_2	Al_2O_3	Fe_2O_3	MgO	CaO	Na_2O	K_2O	TiO_2	M_2O	P_2O_5
30/3	Alteration Zone	0.99	0.75	1.71	2.22	1.9	0.66	0.19	1.1	2.0	1.0
31/2	Andesite Tuff	0.99	1.07	0.84	0.63	1.6	0.7	1.4	0.8	1.5	3.8
27	Diorite	0.99	0.99	1.05	0.95	0.95	0.96	1.4	1.02	2.2	2.0
28	Volcanic conglom.	1.02	0.87	1.02	0.78	7.8	0.98	1.2	1.0	2.2	7.0
30/2	Alteration Zone	0.99	1.23	1.07	0.5	0.38	0.82	4.5	1.0	0.2	1.3
15/2	Rhyolite	1.0	0.96	1.34	0.28	1.2	0.93	0.88	1.1	1.8	1.3
23/3	Z. Breccia	0.97	1.2	1.02	1.43	2.2	0.9	1.2	0.7	2.5	7.13
22	Andesite	0.98	1.0	1.02	1.03	1.1	0.76	1.05	1.02	1.5	3.1
19/2	Volcanic conglom.	1.0	1.0	1.02	0.93	0.86	0.72	1.03	1.19	1.36	1.1

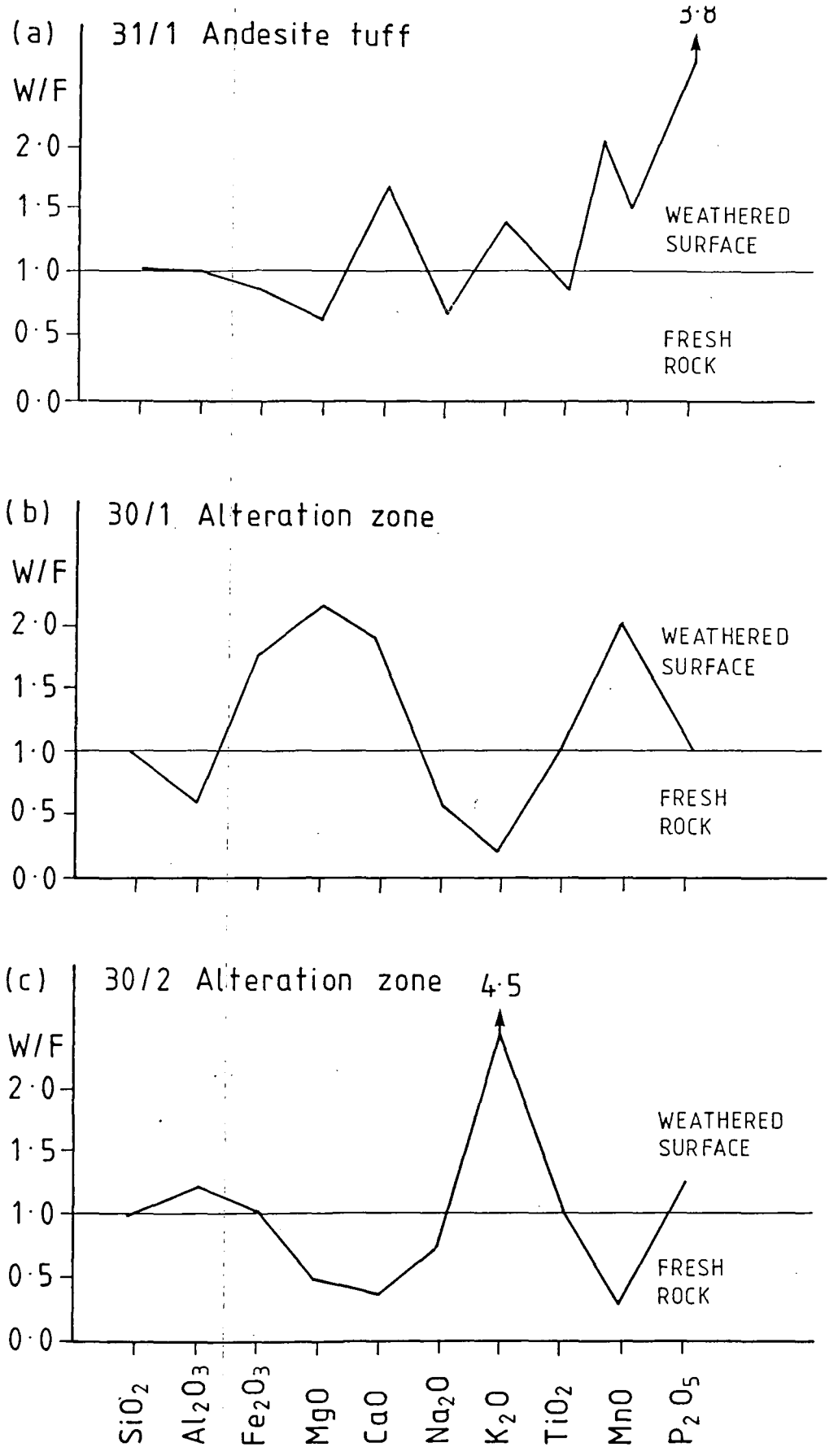

Fig. 3.6 Comparison of weathered surface and fresh rock, Jabal Said.

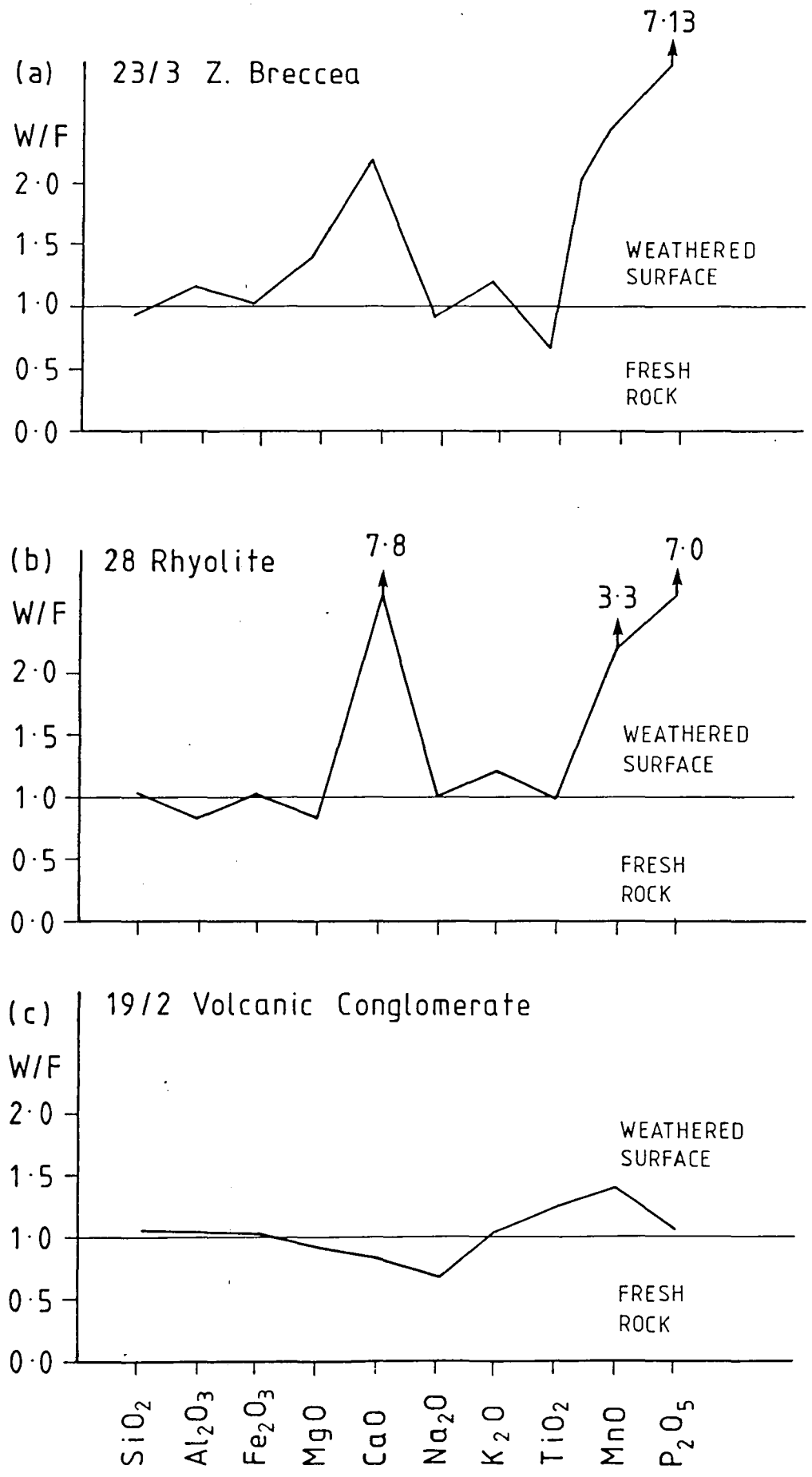

Fig. 3.7 Comparison of weathered surface and fresh rocks, Jabal Said.

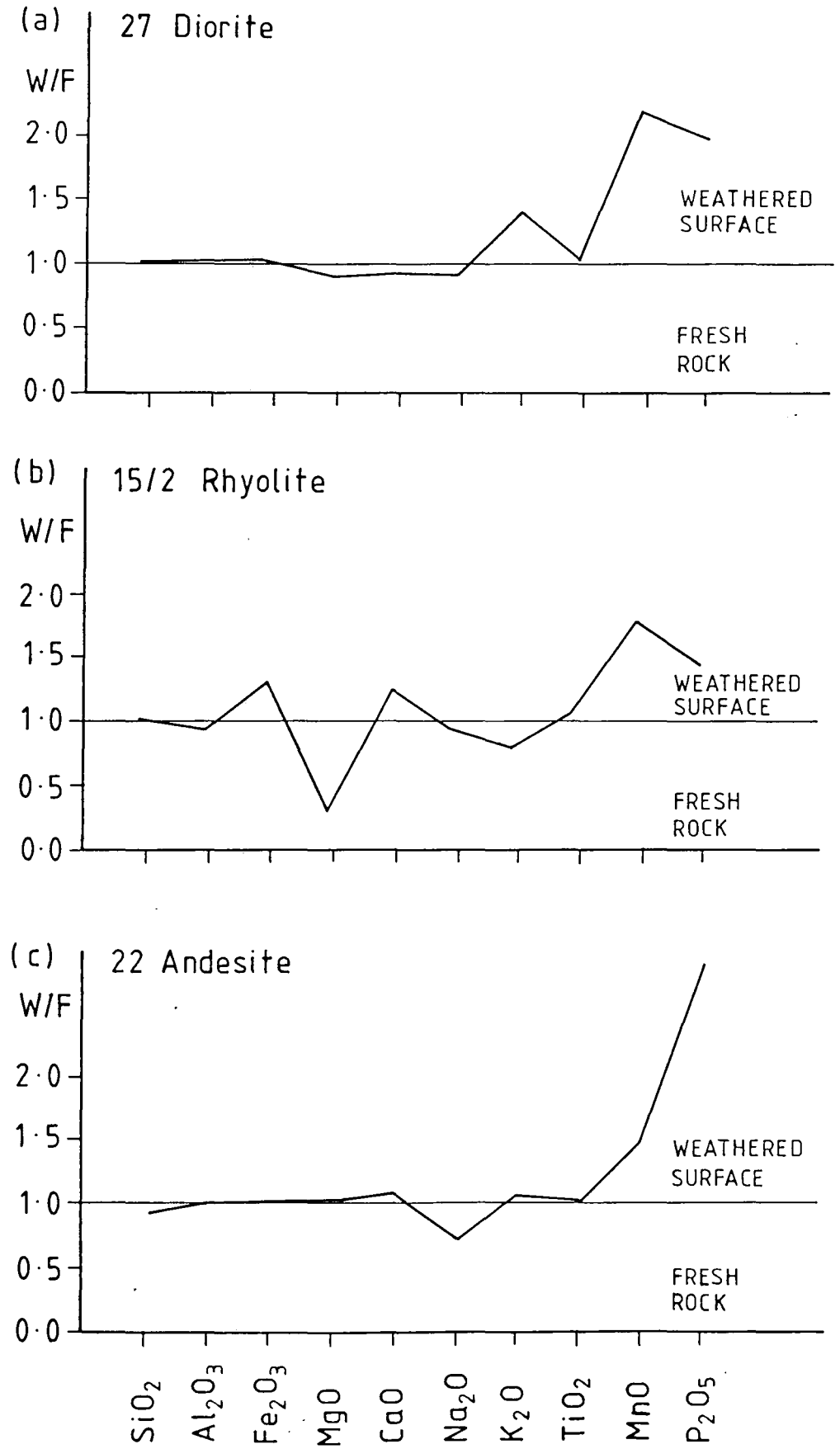

Fig. 3.8 Comparison of weathered surface and fresh rocks, Jabal Said.

This graphical presentation exaggerates the differences between the fresh rock and the weathered surface samples. However, it clearly illustrates the mineralogical changes which occur due to weathering and shows which elements are most affected by this process.

There are small changes in silica, iron, potassium and aluminium content. The two samples from the alteration zone show a different pattern however; one sample indicates the increase of potassium and aluminium oxides (Fig. 3.6c) while the other sample shows an increase in iron, calcium, magnesium and manganese oxides (Fig. 3.6b).

The bulk rocks and the weathered samples were expected to give a significantly different spectral response; where the weathered surface was rich in iron and magnesium oxides the fresh rock samples were richer in clay minerals.

3.3 Laboratory Spectral Analysis

3.3.1 Introduction

As a further step towards establishing the physical basis for spectral variations observed in the multi-spectral data covering the study area, detailed laboratory spectra were generated from samples representative of the main lithologies. Particular emphasis was given to the measurement of spectra from the natural (undisturbed) surfaces of the samples. Previous laboratory studies

(e.g. Hunt & Salisbury, 1970, 1971, 1976; Hunt et al., 1971a,b, 1972, 1973a,b, 1974a,b; and Salisbury et al., 1975) have concentrated on determining spectral characteristics of rock and mineral powders. In these studies, the main goal was to examine the spectral characteristics in relation to bulk composition. Given the high opacity and scattering characteristics of naturally occurring rocks and minerals, it was deemed appropriate to consider the variation in spectral response as a function of surface composition, because it is the surface which determines the nature of the radiation measured by airborne and satellite systems.

Many of the previous studies have concentrated on spectral properties of hydorthermally altered rocks because they mark the paths of migrating hot fluids that commonly contain base and precious metals (Lowell & Guilbert, 1970).

The surface exposure of an altered mineralized rock unit is often a series of alteration zones, the most intensely altered rock occurs closest to the intrusion, which is contained in the silicic and potassic zones. The degree of alteration decreases away from the intrusion through the phyllic and propylithic zones until unaltered host rock is reached. An intense iron staining produced by the oxidation of pyrite, pyrite oxidation produces hematite, geothite, and jarosite is often associated with each zone. Usually a gossan is the resultant assemblage

of alteration zones and iron staining. Table no. 3.11 shows an idealized list of mineral constituents for each zone (Buckingham, 1983; Hunt & Ashley, 1979; Lowell and Guilbert, 1970).

The intensity of alteration is expressed by the mineral assemblage, and most of the key minerals have diagnostic reflectance spectra. Figure 3.9 shows laboratory reflectance spectra for minerals that characterize different levels of alteration intensity. Fig. 3.9a shows the reflectance spectra of weak alteration, calcite, chlorite or epidote. The phyllic alteration is characterized by the presence of sericite or muscovite (Fig. 3.9c). In moderate and advanced intense argillic alteration, kaolinite, chlorite and alunite are the characteristic OH minerals (Fig. 3.9b, d).

3.3.2 Laboratory set-up and instrumentation

Laboratory spectra were measured using the Geophysical Environmental Research Inc. IRIS Mk IV Spectroradiometer (Milton & Rollin, 1987). The IRIS comprises two units: an optical head and a control unit. The optical head contains a telescope with a view finder for viewing the sampled areas and a Ba SO_4 reference panel was used to convert the radiance data to reflectance units. The light source used to illuminate the sample and the reference panel was a quartz-halogen lamp 1000W.

The spectral data are stored in removable non-volatile memory modules which can hold up to 96 sets of

Table 3.11 Idealised Mineral Assemblages associated with Alteration Zones. Compiled from Hunt & Ashley (1970) and Lowell & Guilbert (1970).

Zone	Mineralogy
Propylitic	Albitized plagioclase Chlorite Epidote Carbonate Montmorillonite
Argillic	Quartz Kaolinite Chlorite Montmorillonite
Phyllic	Quartz Sericite Pyrite
Advanced Argillic	Quartz Alunite Pyrophyllite Kaolinite K-mica
Silicified	Quartz Alunite Pyrophyllite Kaolinite K-mica

Source: Buckingham & Sommer (1983)

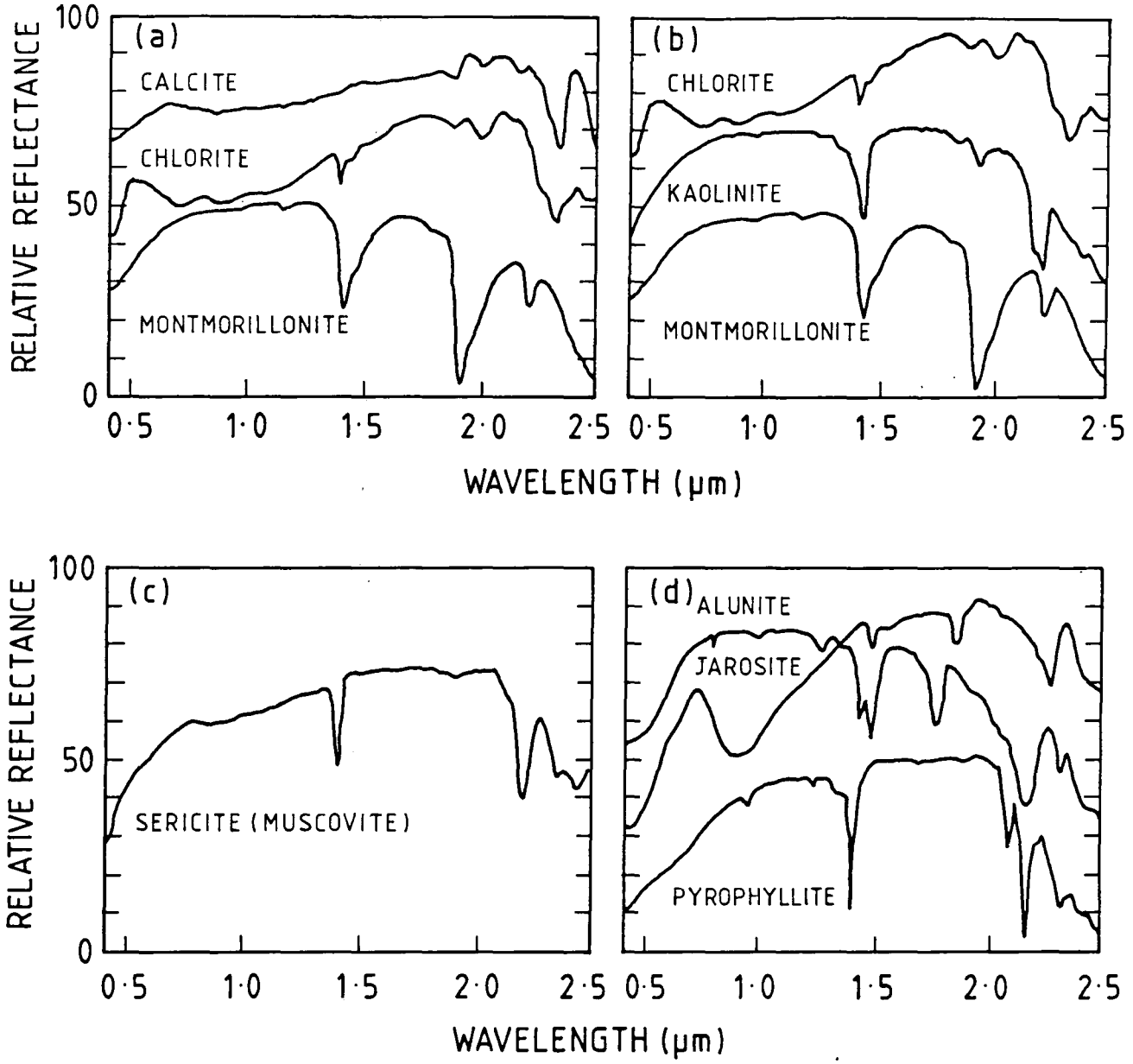

Fig. 3.9 Laboratory reflectance spectra of altered rocks; (a) minerals associated with propylitic alteration; (b) minerals associated with argillic alteration; (c) minerals associated with phyllic alteration; (d) mineals associated with advanced argillic alteration. Ater High-Resolution Imaging Spectrometer (HIRIS), EOS, Vol. II, p.32, NASA 1987.

measurements, termed files. Each file comprises a target spectrum, a reference spectrum obtained from the $BaSo_4$ panel, information on the date and time of measurement and details of the instrument configuration when the scan was made.

The normal route for the output of data is via an RS232 Serial Interface to a microcomputer, and software is provided for data transfer, calibration, analysis and display. (See Appendix A for more information regarding the IRIS instrument).

3.3.3 Laboratory Spectral analysis of Mahd Adh Dhahab

Relative reflectance spectra from 28 samples returned from the Mahd Adh Dhahab district were generated (Fig. 3.1). All the spectra were measured on the upper undisturbed surfaces of the samples. Table 3.12 lists the samples and their lithological characteristics. Selected samples were analysed by XRD to compare the results of the laboratory spectra with the mineral compositions of the rocks. The samples were collected from three different areas; (1) the alteration zones on the main hill, according to the map (Figs. 3.1, and 2.8); (2) samples from the area outside the mapped alteration zone; and (3) samples from carbonate rocks northeast of Mahd.
A list of all the samples and their lithologies, with types of alteration (where it is mapped) are shown in Table 3.12. The following is the description of the

Table 3.12 List of the samples analysed for laboratory spectra from Mahd Adh Dhahab area.

Sample No.	Lithology	"Alteration"
Msc 53/1	Carbonate Rock	
Msc 53/2	Carbonate Rock	
MD 23/2	Silicified tuff	
MD 23/3	Breccia	
MD 22/3	Rhyolite	
MD 30/1	Rhyolite	
MD 30/2	Rhyolite	
MS 14	Upper Tuff	Chlorite Pyrite
MS 27	Lower Agglomerate	Chlorite
MS 39	Rhyolite Intrusion	Quartz,ser.pyr.
MS 6a	Lower Agglomerate	Chlorite
MS 6b	Lower Agglomerate	Chlorite
MS 6c	Lower Agglomerate	Chlorite
MS 11a	Upper Tuff	Argillic
MS 11b	Upper Tuff	Argillic
MS 8	Andesite	
MS 40	Upper Agglomerate	Potassic
MS 7	Lower Tuff	Chlorite
MS 10a	Upper Tuff	Argillic
MS 10b	Upper Tuff	Argillic
MS 5	Lower Tuff	Silicic
MS 24	Andesite	
MD 4/3	Lower Tuff	Pyrite chlorite
MD 35/1	Lower Agglomerate	Silicic
MD 37/1	Upper Tuff	Silicic
MD 37/2	Upper Tuff	Argillic
MD 36	Upper Tuff	Pyrite chlorite
MD 19/1	Andesite	

spectral behaviour of the samples in each zone of the three groups mentioned above.

1. Alteration Zones

The first six samples show the spectral features of the chlorite alteration (Fig. 3.10). Strong spectral features occurring at both 1.4 and 1.9um indicate the presence of molecular water. The fall-off in reflectance towards the ultraviolet is caused by charge transfer bands, which normally indicates the presence of iron oxides (Hunt, 1977). Because of its distribution on the Earth's surface, iron is the most common cause of the charge transfer and electronic transmission absorption features seen in rocks and soil spectra (Hunt 1977; Goetz et al, 1983). The spectral features centre around 0.94um indicating the presence of hematite or geothite (Figs. 3.10b, d).

The absorption features around 2.2, 2.33um are recognized in most samples. Some are weak features (Figs. 3.10b, f). Others are very distinct and strong, as seen in samples MS7 and MS6b (Fig. 3.10c, d). These are Al-OH and Mg-OH vibration features; absorption at 2.2um indicates Al, while absorption at 2.3um is caused by vibration processes in the Mg-OH band occurring in chlorite and muscovite structures (Hunt & Salisbury, 1970).

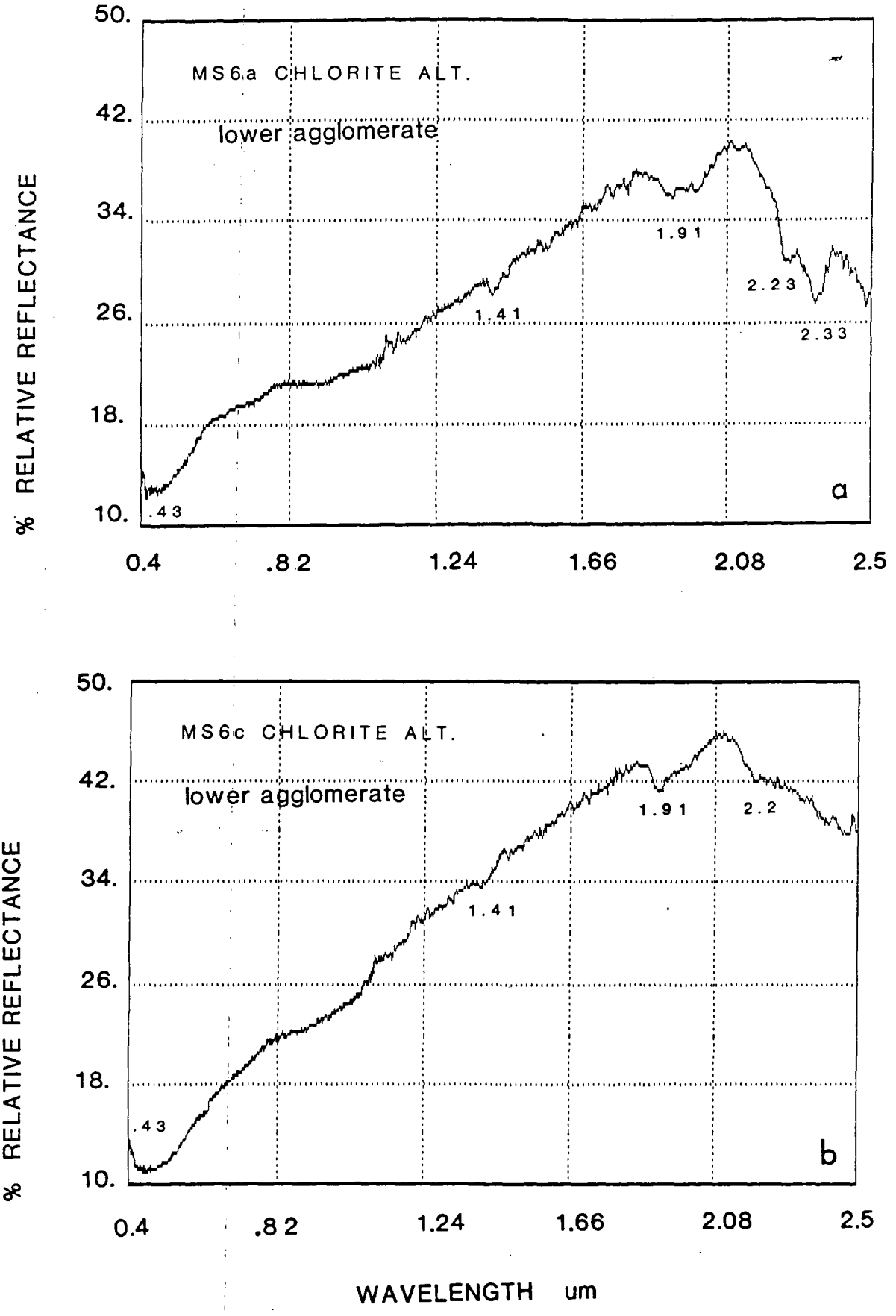

Fig. 3.10 Laboratory spectra using (IRIS) for samples from chlorite alteration - MAhd Adh Dhahab.

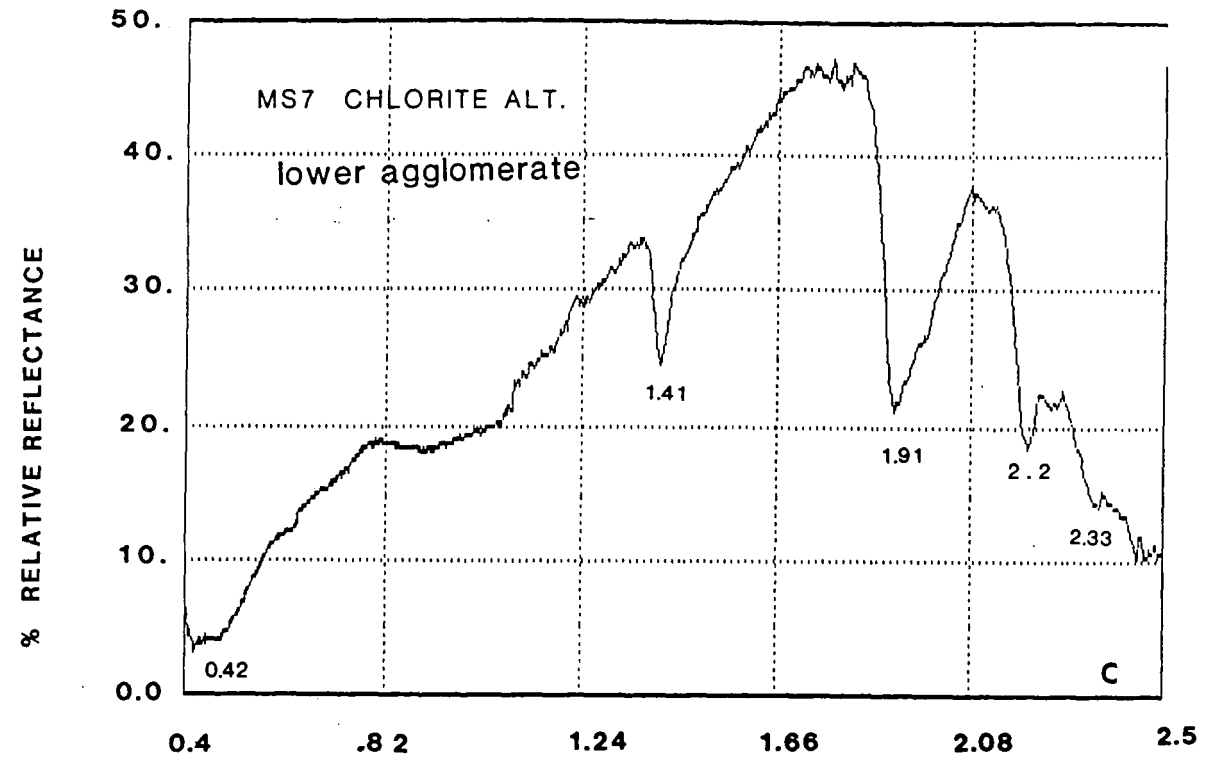

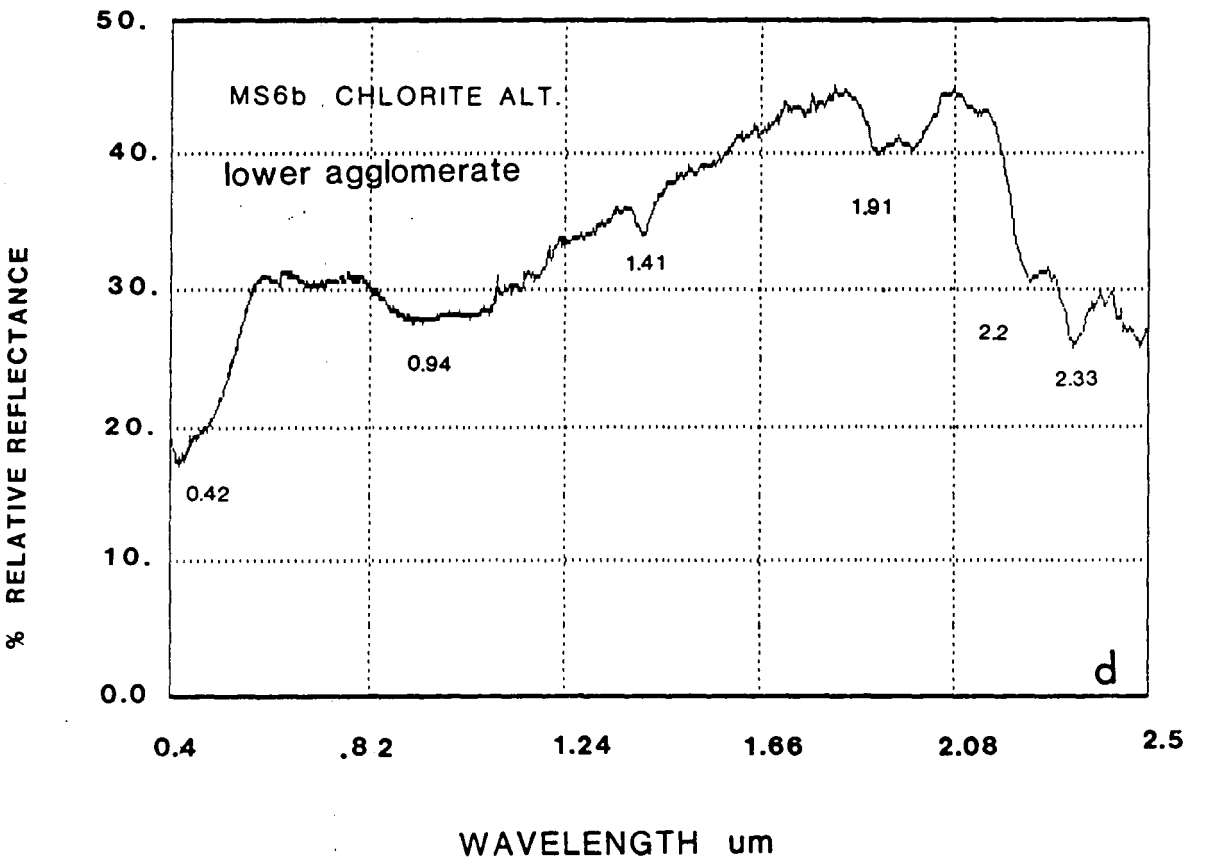

Fig. 3.10 Continued.

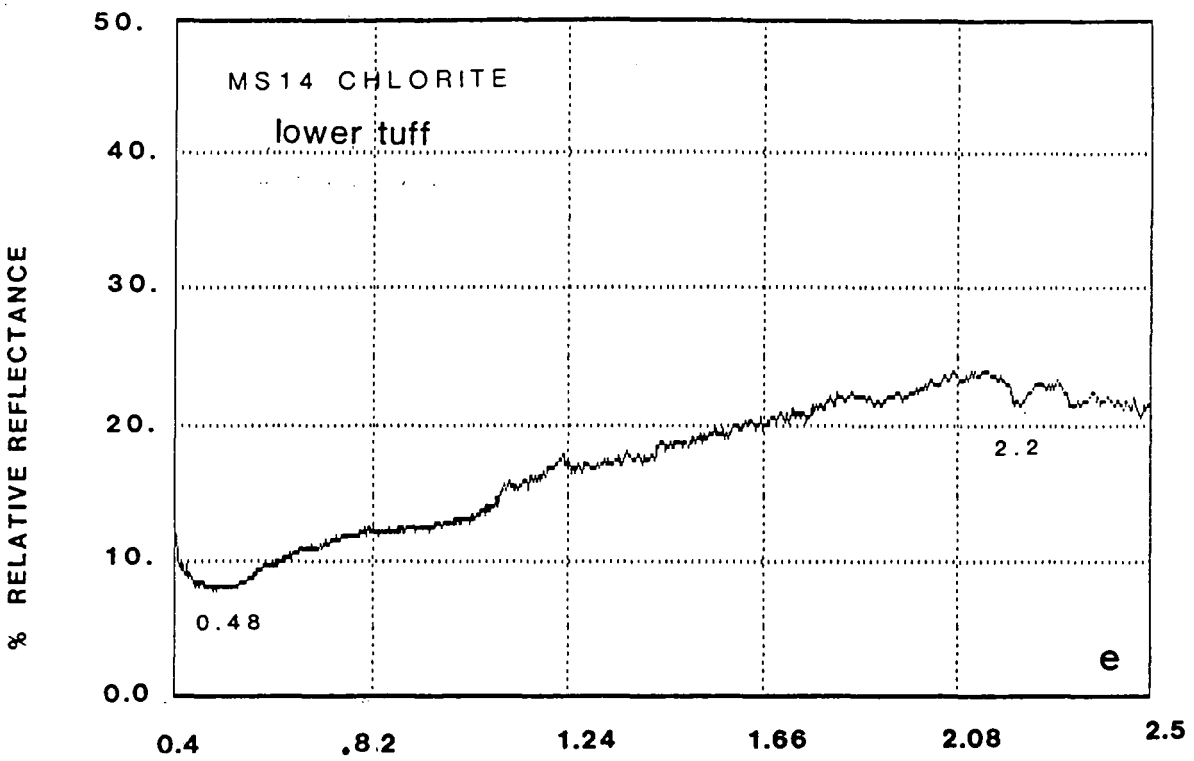

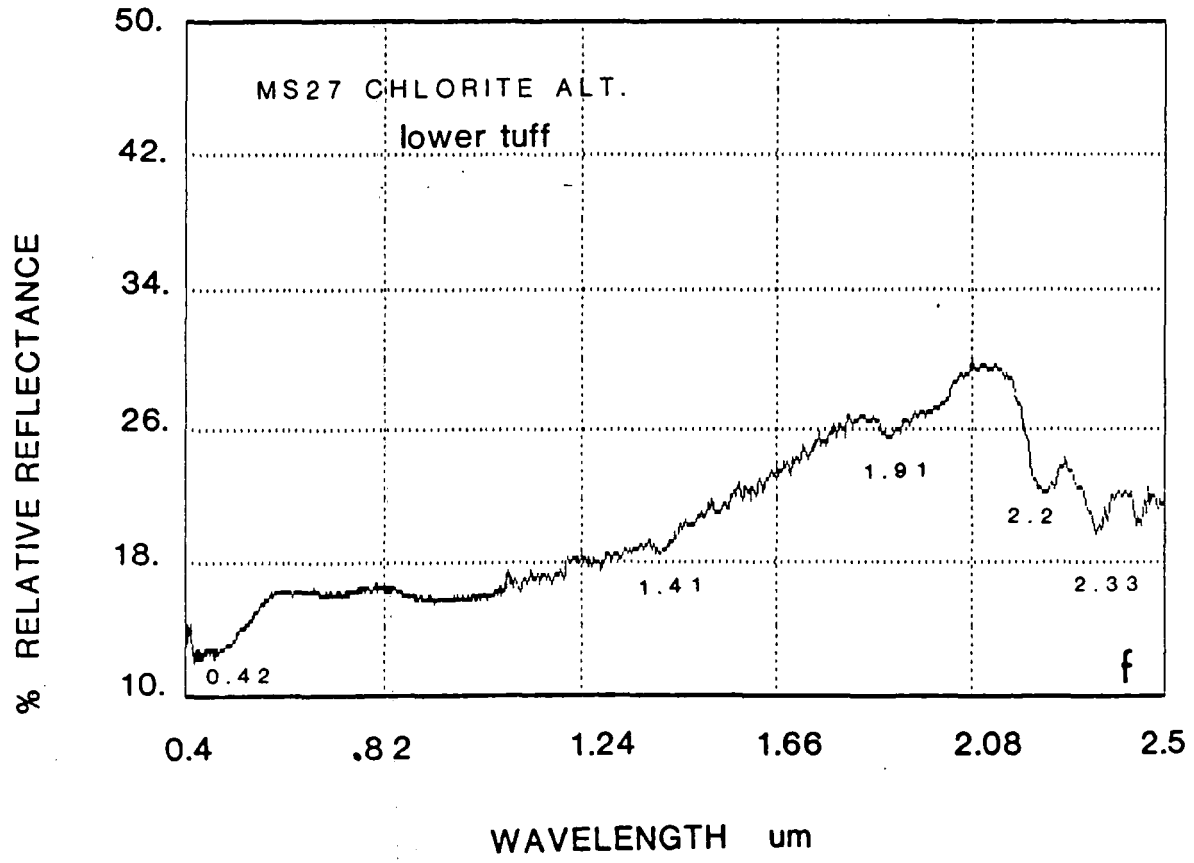

Fig. 3.10 Continued.

Sample no. MS14 from the upper tuff, shows an almost flat spectra, although the sample was taken from an area of chlorite alteration according to the alteration map (Fig. 3.10e). This flat spectra is an indication of opaque minerals such as iron. The chemical analysis of this sample (Table 3.6) indicates the presence of chlorite and micas, but the spectral features that are associated with these minerals are fairly subdued (Fig. 3.11).

Two samples were collected from pyrite-chlorite alteration (Figs. 3.12a, b). The sample MD4/3 shows well developed spectral features at 0.43 and 0.94um, indicating the presence of iron. The presence of chlorite is indicated by the absorption at 2.33um, which is very small in the other sample MD36 (Fig. 3.12a).

The spectrum of the silicic alteration samples MS5 and MD35/1 & MD37/1 (Figs. 3.13a, b, c) shows spectral features around 2.2um and 2.33um similar to the chlorite alteration with much clearer doublet absorption features at 2.2um, indicating the presence of kaolinite (Hunt & Ashley 1979). This similarity is related to the mineral composition of these zones (Table 3.11) and also to the fact that over- tone bending-stretching vibration of layered silicates for Al-OH and Mg-OH creates narrow spectral absorption bands within the 2.1 to 2.4um region (Goetz & Rowan, 1981).

The spectrum of the potassic alteration represented by sample MS40 (Fig. 3.14) is similar to the spectrum of the silicic alteration, but with lower albedo and stronger

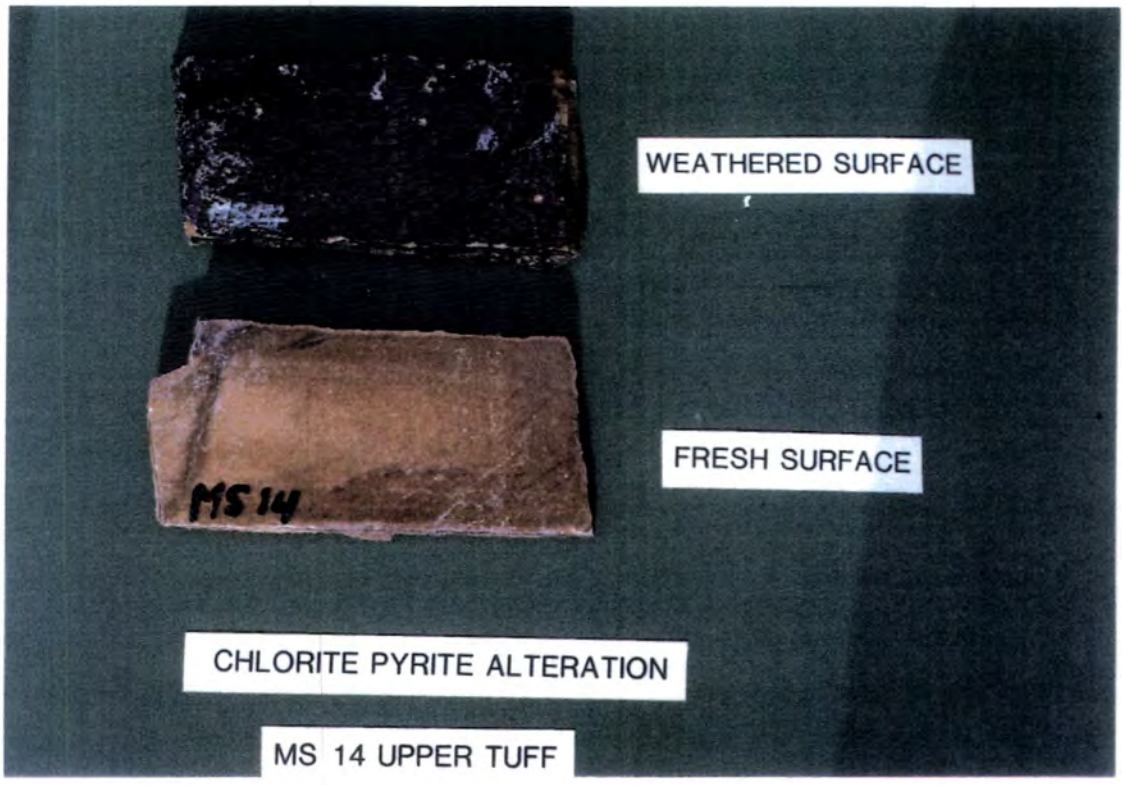

Fig. 3.11 Sample from Location MS14 showing the thickness of the desert varnish or the weather surface in some of the area (notice the difference in the colour of both surfaces).

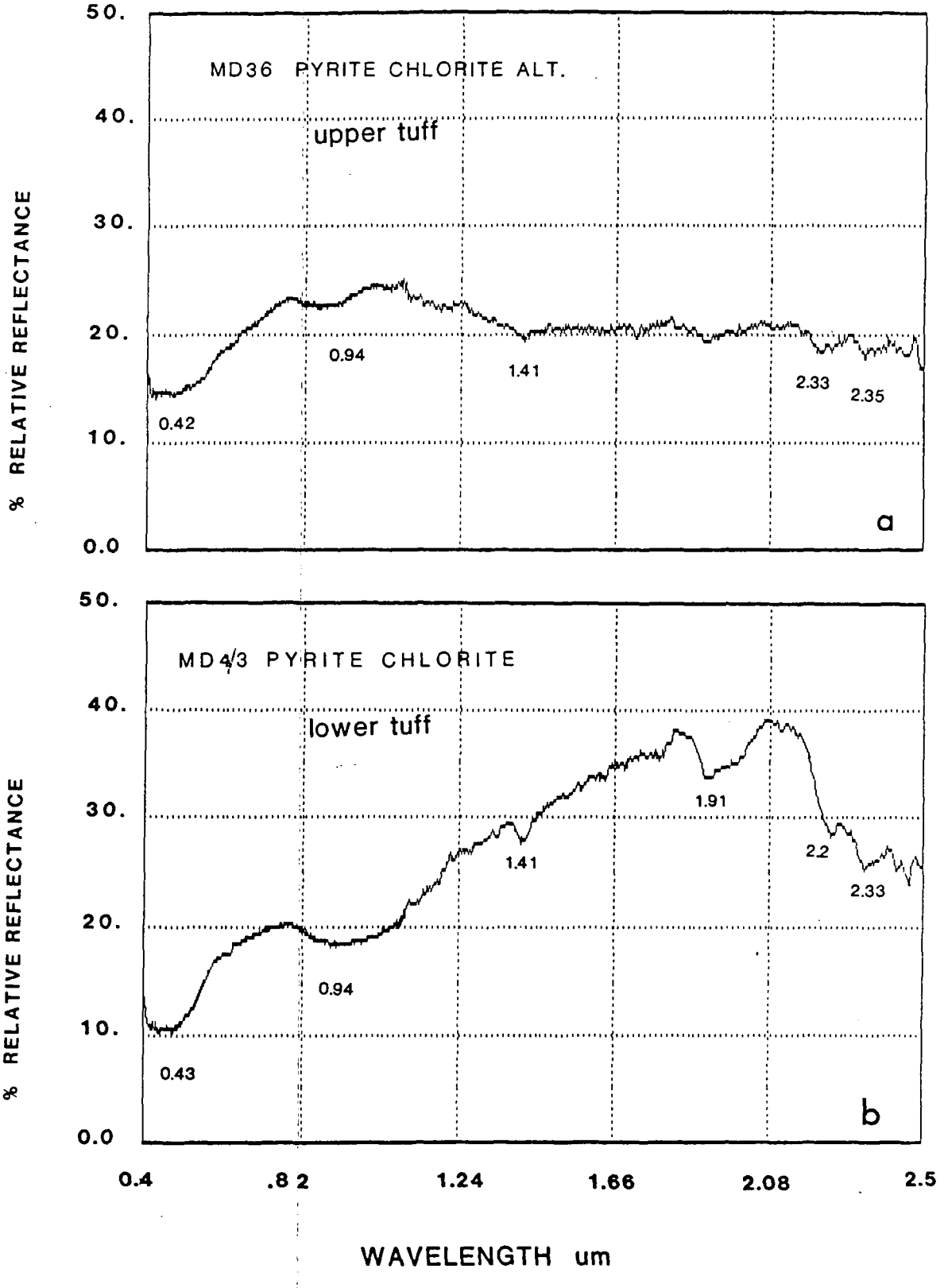

Fig. 3.12 Laboratory spectra using (IRIS) for samples from pyrite chlorite alteration - Mahd Adh Dhahab.

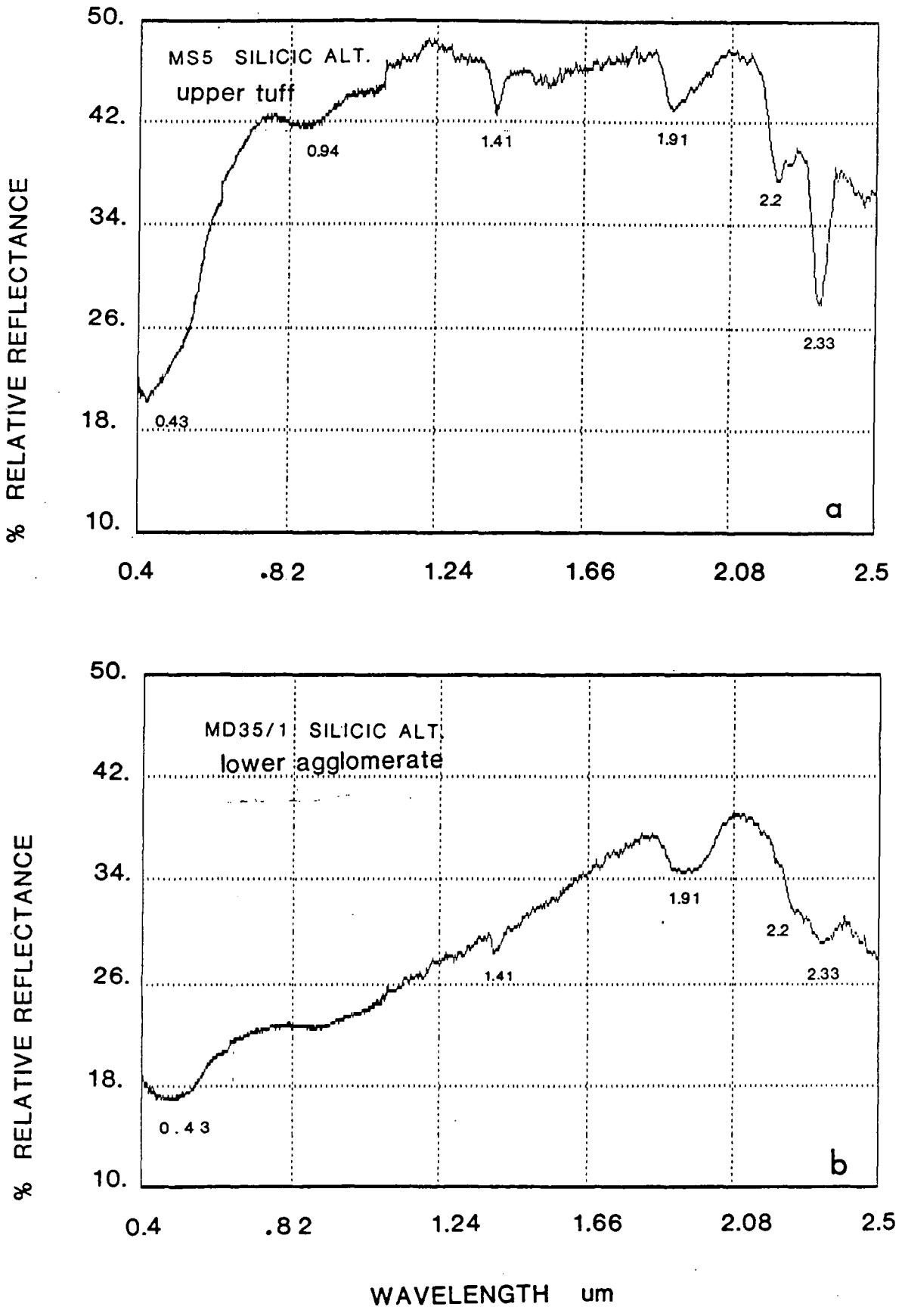

Fig. 3.13 Laboratory Spectra using IRIS for samples from sericite alteration, Mahd Adh Dhahab.

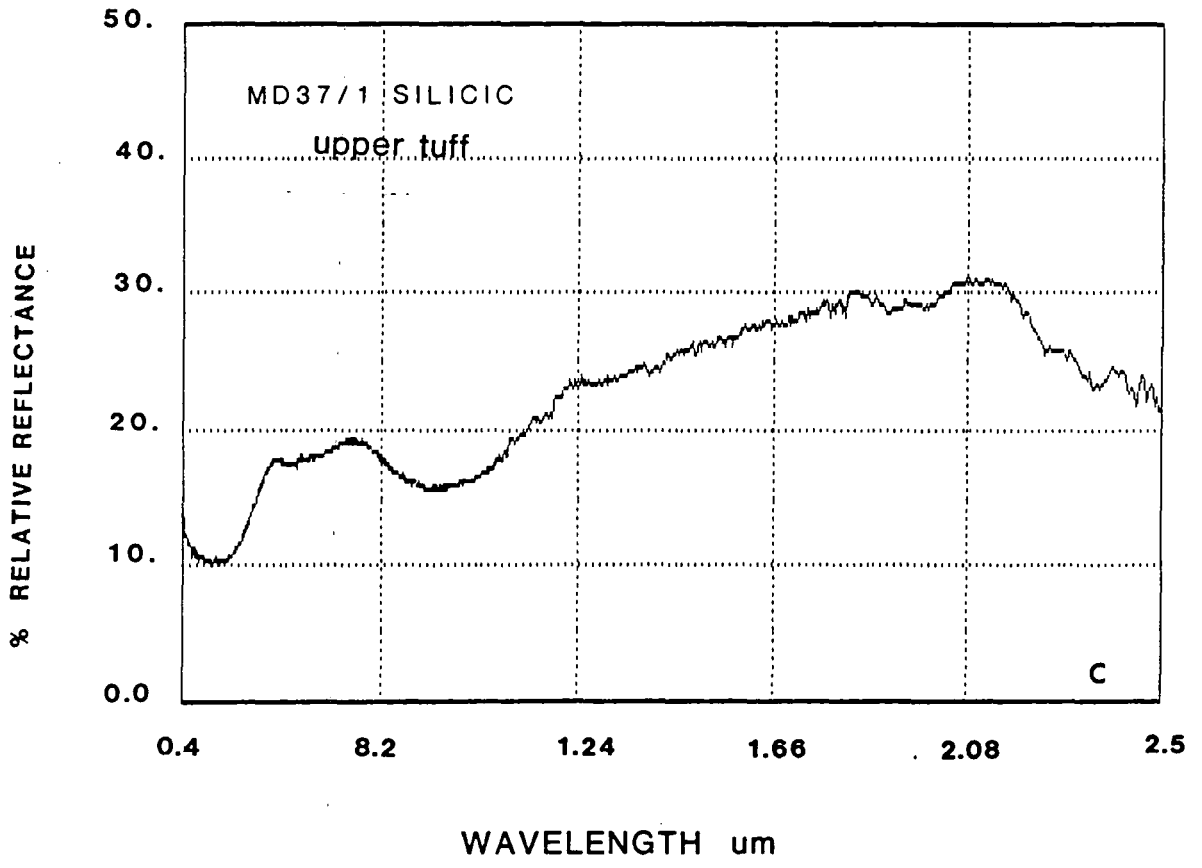

Fig. 3.13 Continued.

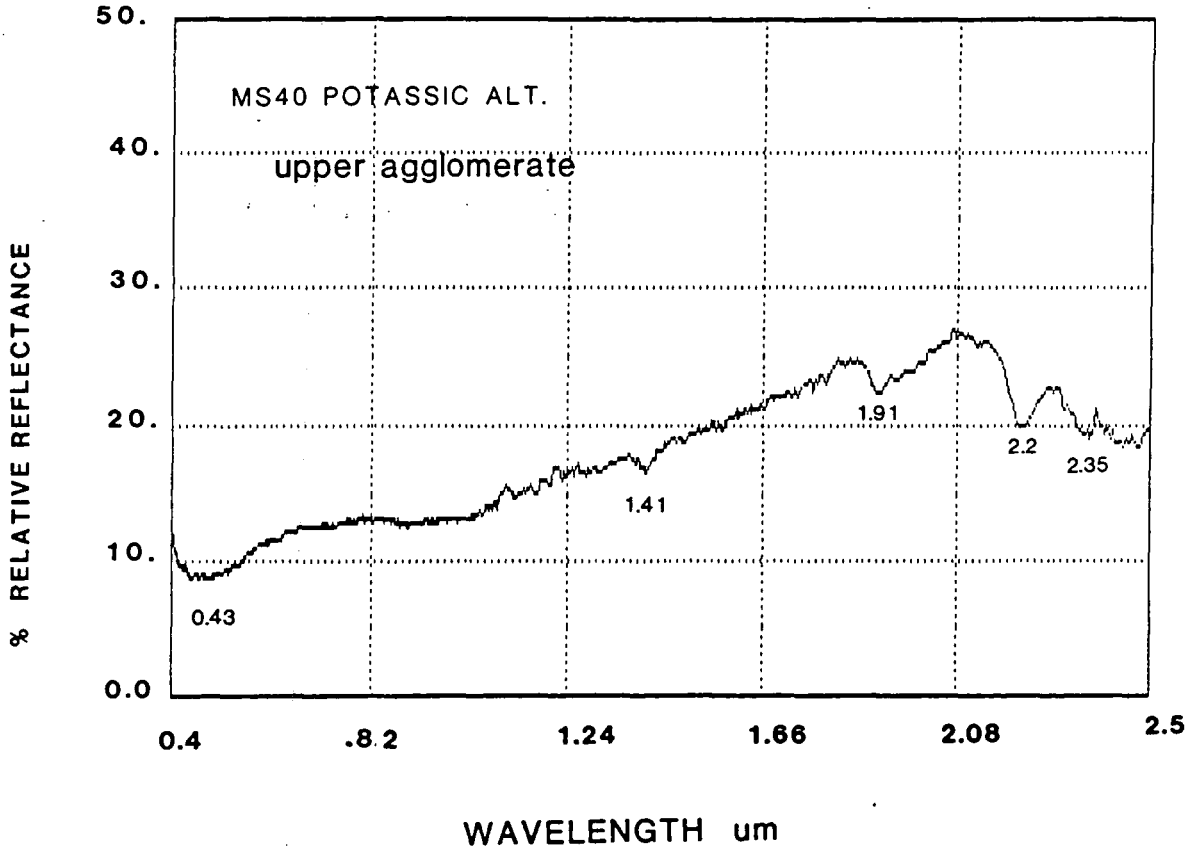

Fig. 3.14 Laboratory spectra from the potassic alteration Mahd Adh Dhahab.

absorption around 2.33um. The sharp fall-off towards 0.43um indicates the presence of iron. The minerals that characterize potassic alteration (K-feldspar and quartz) have no characteristic absorption features in this spectral region (0.4-2.5um) (Hunt, 1980). The spectrum is dominated by features due to silicic and argillic alteration mineral assemblage.

The spectrum of the quartz-sericite-pyrite alteration is shown in Fig. 3.15. This shows very weak absorption around 2.2um and strong fall-off toward 0.4um indicating the presence of the iron. The samples are from the rhyolite intrusion in the Main Hill of Mahd Adh Dhahab.

The spectrum of the argillic alteration (Fig. 3.16) has the typical overall appearance of intesely altered igneous rock, high reflectance at 1.6um, with large decreases towards both shorter and longer wavelengths (Abrams & Brown, 1984; Hunt & Ashley, 1979). Some samples show fall-off towards 0.4um. The strong absorption bands around 2.2um are considered to be indicative of the presence of clay minerals. Sample MS10b (Fig. 3.16d) shows the doublet features around 2.2um which strongly indicates the presence of kaolinite. Two samples, MD 37/2 and MS 11b show very high albedo compared to the rest of the samples (Fig. 3.16a, b). Sample MS 10a, (Fig. 3.16e) although being collected from the argillic alteration zone, shows no spectral features. This might be related

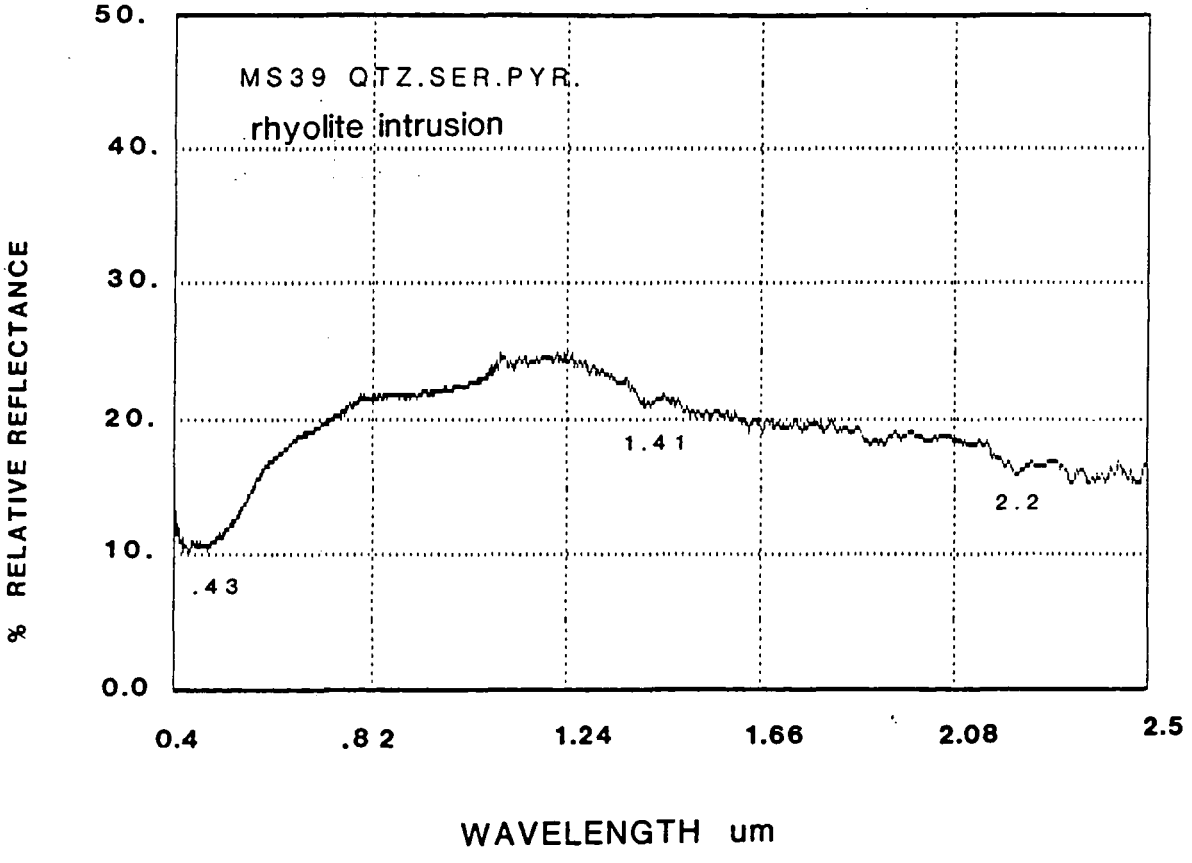

Fig. 3.15 Laboratory spectra from quartz-sericite-pyrite. Mahd Adh Dhahab.

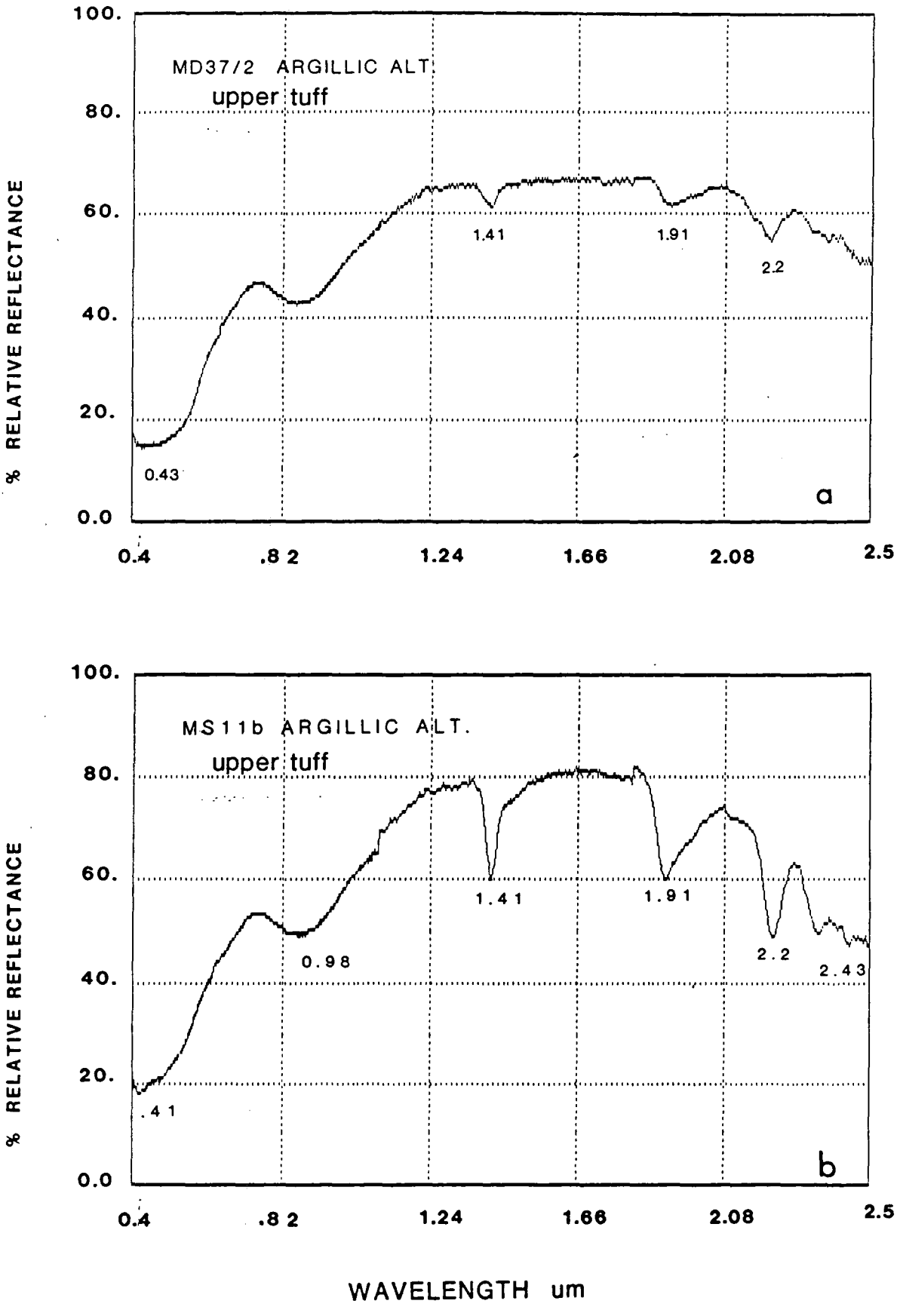

Fig. 3.16 Laboratory spectra using IRIS for samples from argillic alteration.

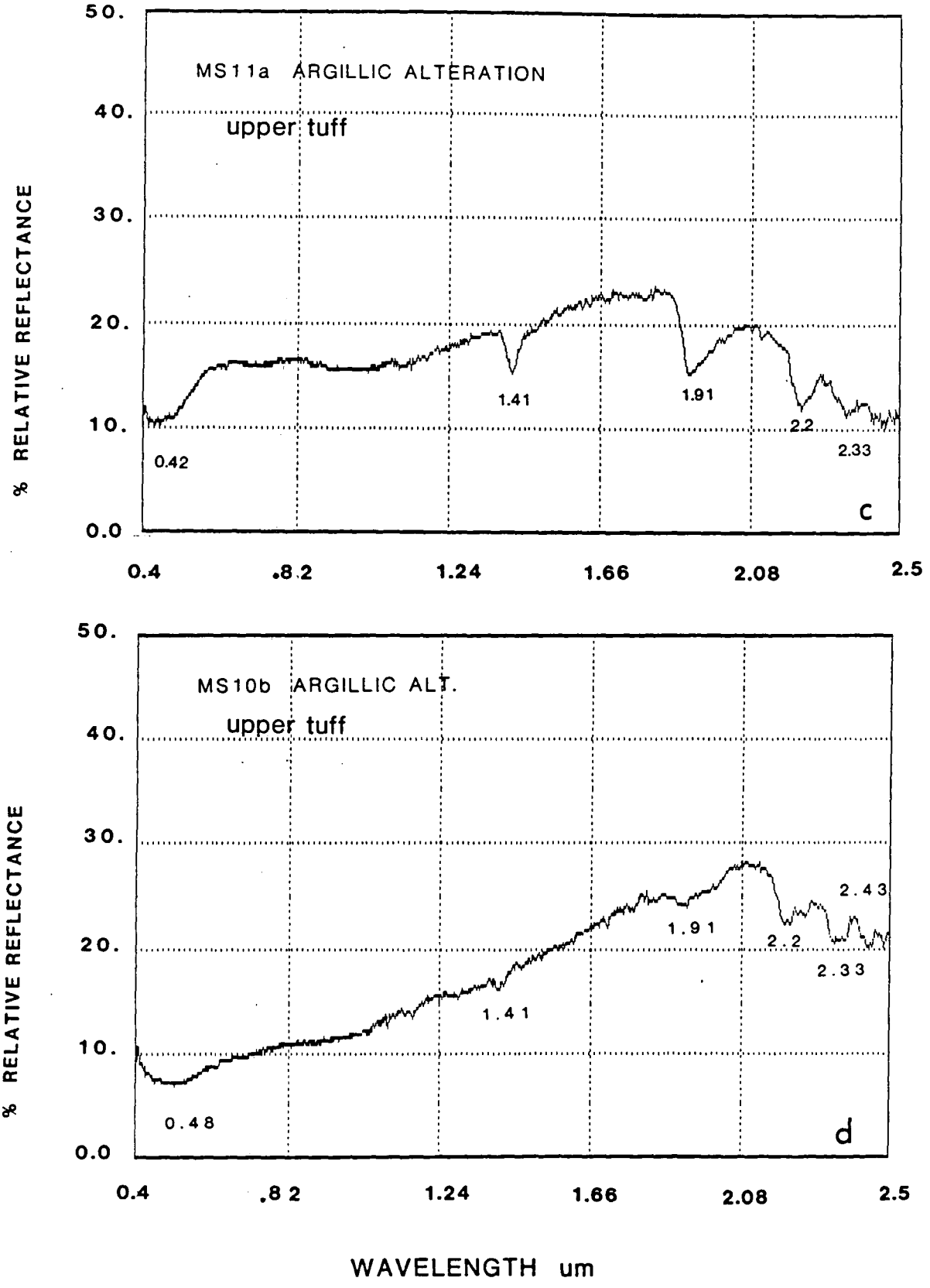

Fig. 3.16 Continued.

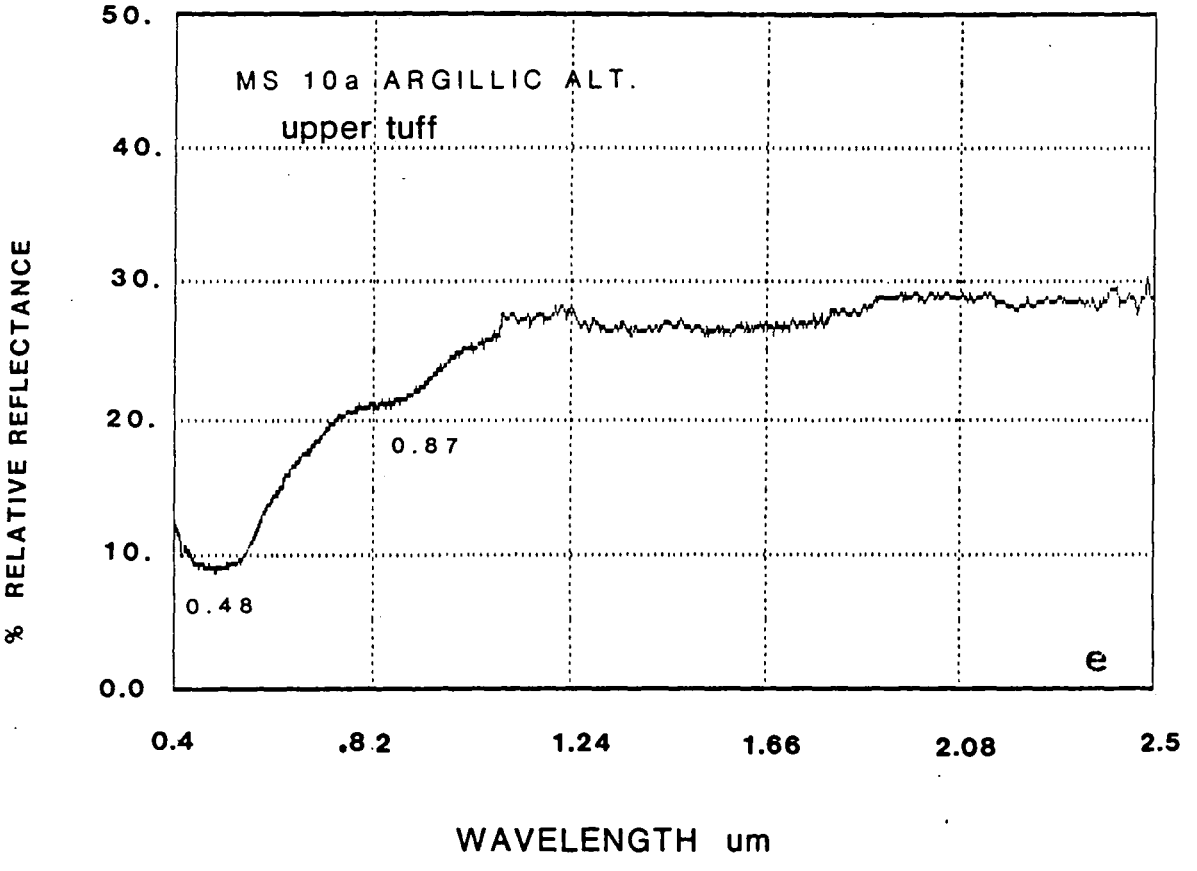

Fig. 3.16 Continued.

to the thickness of the weathered surface or desert varnish.

2. Samples from outside the mapped alteration zones.

These samples were picked randomly outside the alteration zone in the Main Hill. Two samples west of Al-Mahd (MD 22.3) are of rhyolite and andesite (MD 19/1). Fig 3.17a and Fig. 3.17g show flat spectra without any features except the fall-off towards 0.4um.

Samples were collected from the north and northwest of the main road and Mine Hill MD 23/3, breccia: MD 23/2 (Fig. 3.17 b, c), silicified tuff: MD 30/2, rhyolite:, and MD 30/1, rhyolite (Fig. 3.17 d, e). The silicified tuff is the only sample showing the spectral features around 2.2, 0.98, 1.41, 1.91um, with a sharp fall-off towards the 0.40um (Fig. 3.17b). The rest of the samples show no spectral features except for the sharp decrease in the albedo toward 0.4um (Fig. 3.17c, d).

Two samples were collected from the andesite, south of the Main Hill, MS 8, (Fig. 3.17f) and from the southeast andesite gravel MS 24 (Fig. 3.17h). Both of them show spectral features around 2.2 and 2.3um which is attributed to the weak alteration of the andesite to epidote. The sharp fall-off towards the ultraviolet is explained by weathered surface and black desert varnish, covering the andesitic rocks (Figs. 3.17f, 3.17h).

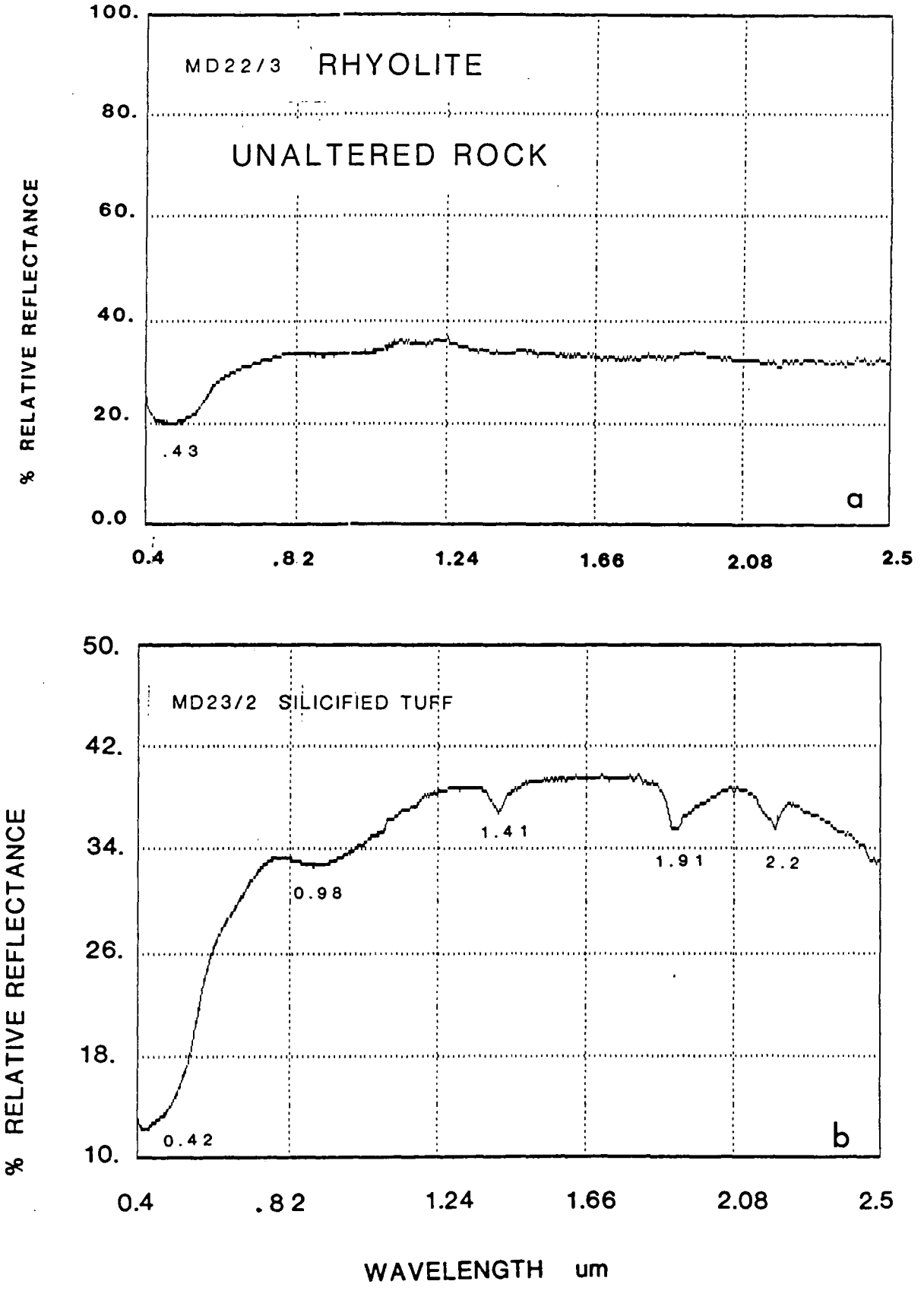

Fig. 3.17 Laboratory spectra using IRIS for Samples from the acid rocks.

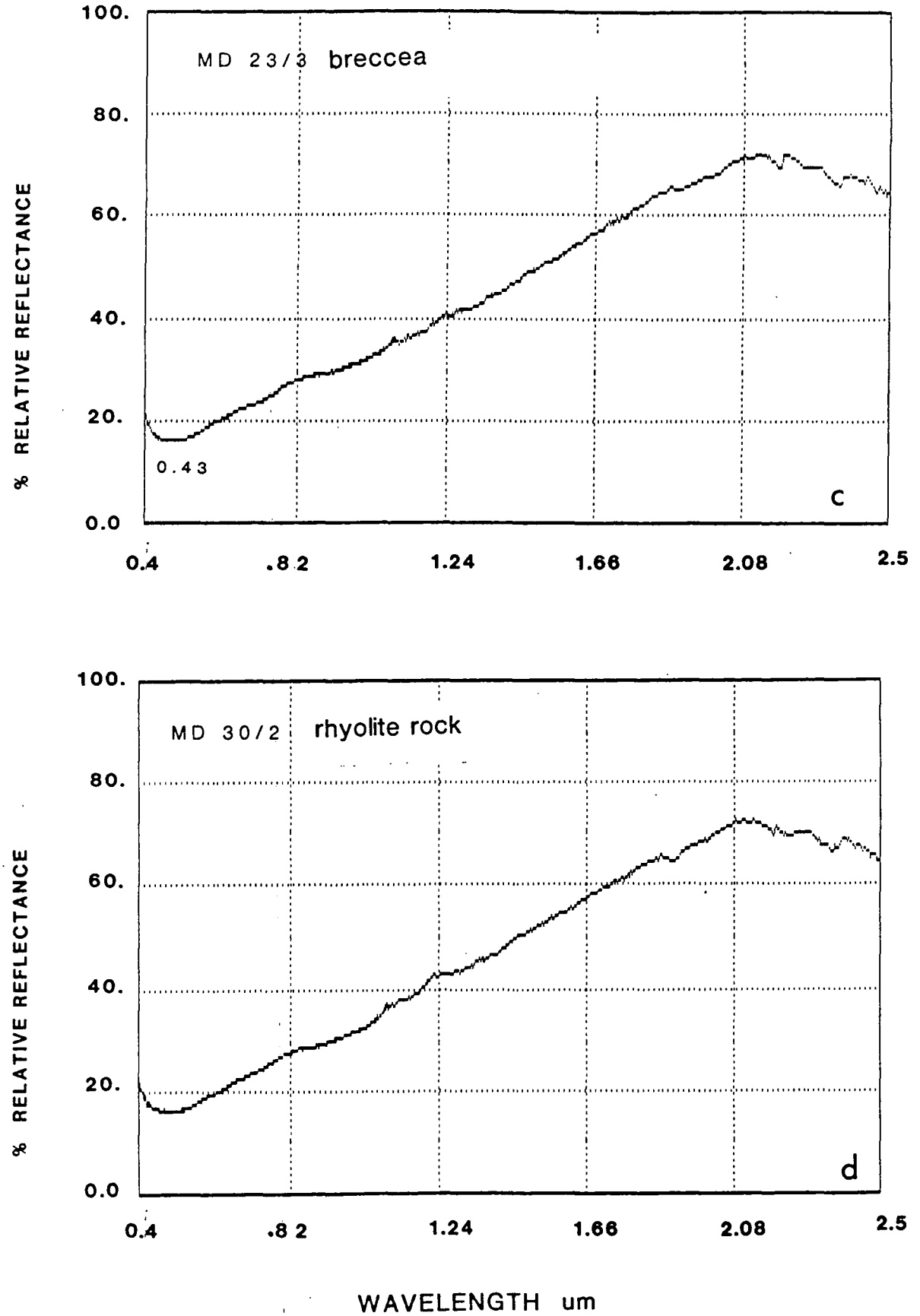

Fig. 3.17 Continued.

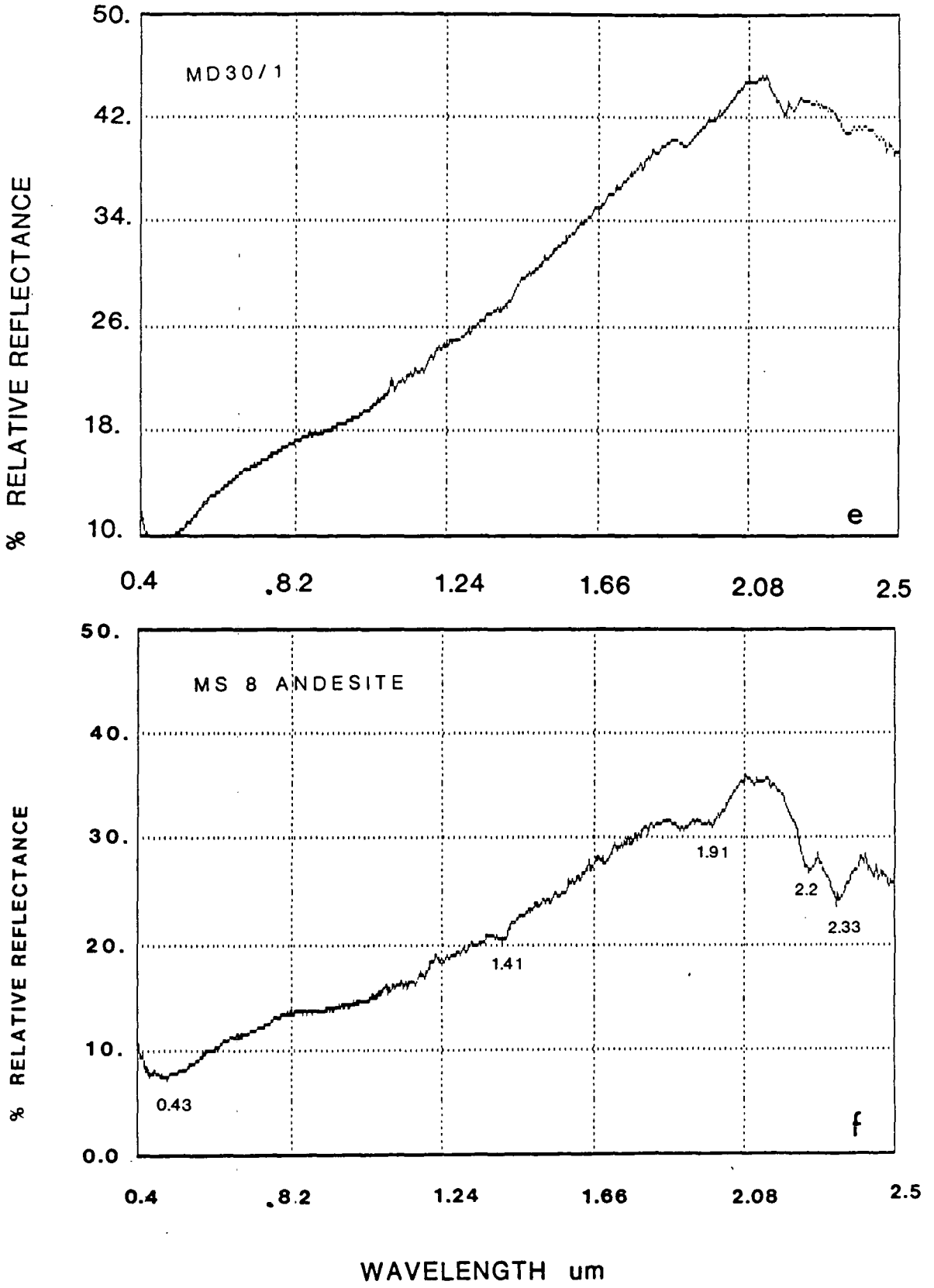

Fig. 3.17 Continued.

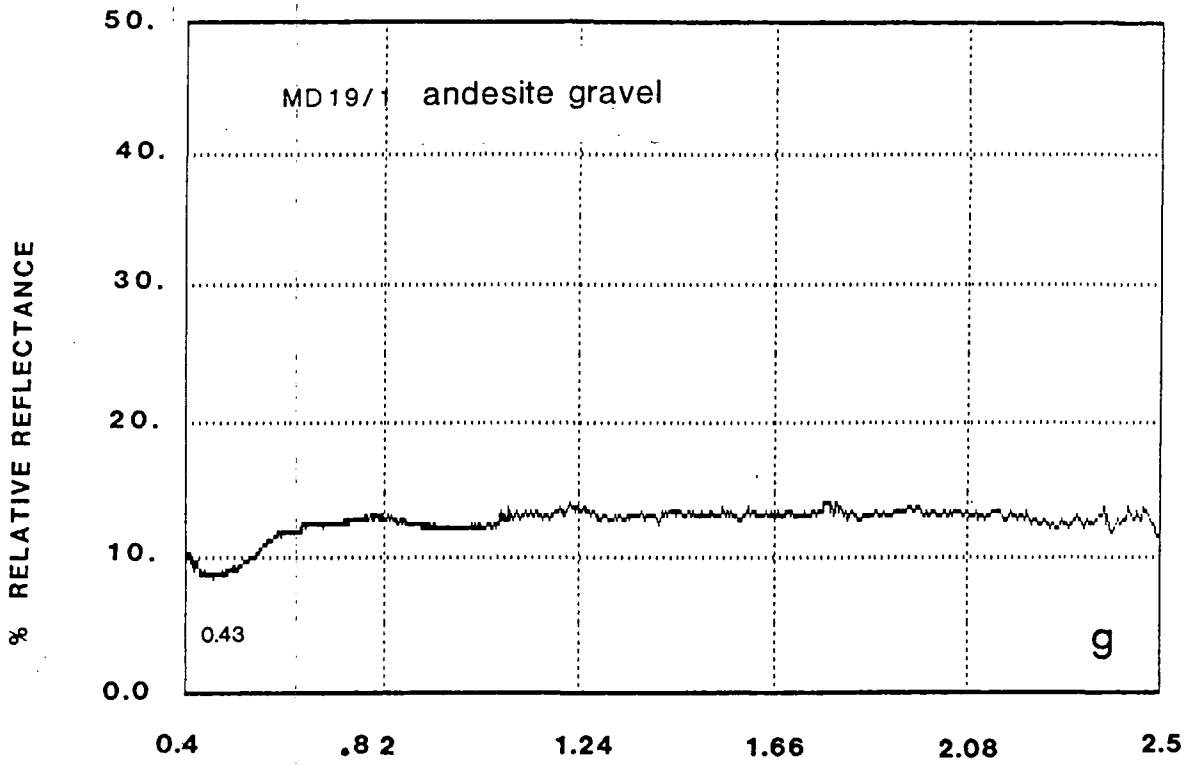

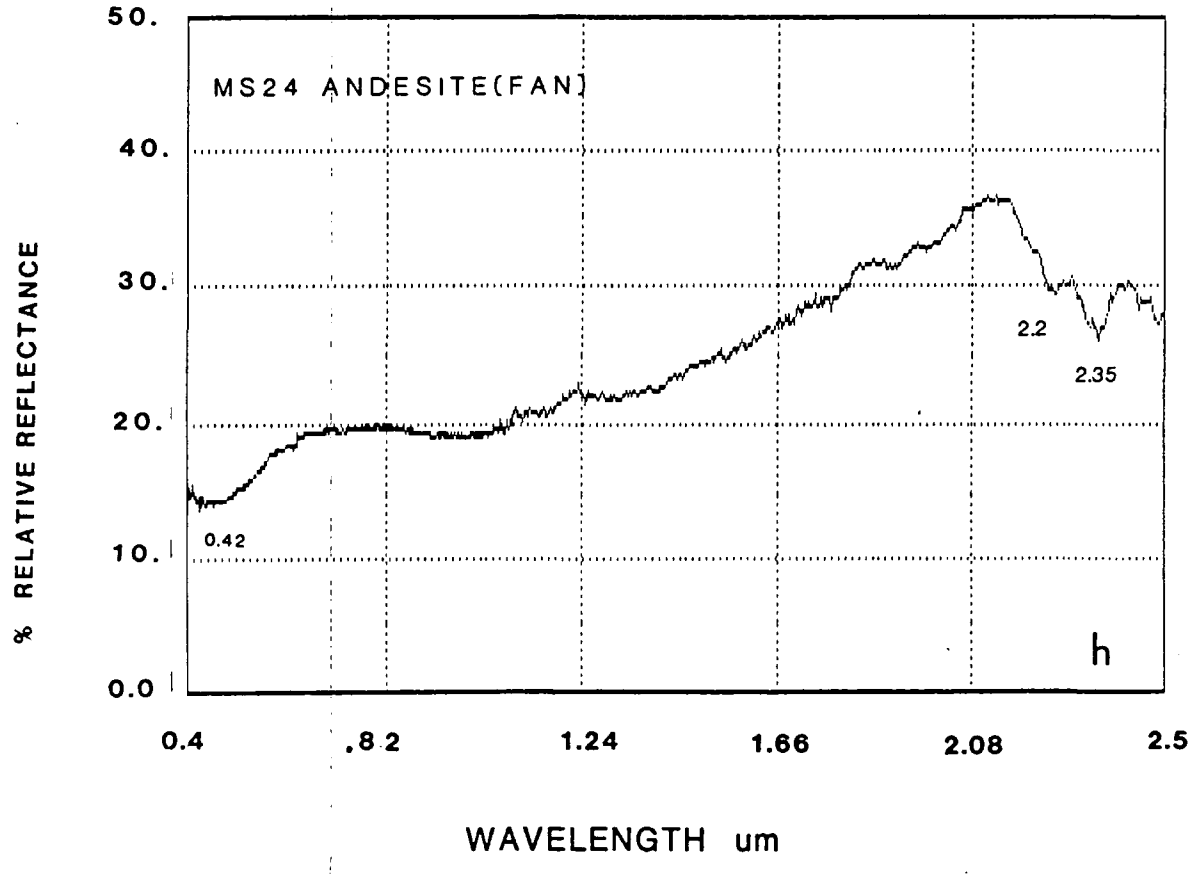

Fig. 3.17 Continued.

3. The carbonate rocks

The spectrum of the carbonate rocks samples MSC 53 (Fig. 3.18) is dominated by the presence of an intense absorption band near 2.35um. Due to the vibration process of the CO_3^{2} ion which result from electronic processes in the cation or impurity ions, or vibrational processes in the carbonate radical as an entity, or interactions of it with motions of crystal lattice, the sharp fall-off toward ultraviolet and the weak iron absorption bands indicates the presence of ferric minerals in the carbonate rocks (Hunt & Salisbury, 1971). A summary list of the main spectral features identified and the minerals associated with those features are given in Table 3.13. The chemical analysis of the same samples support the interpretations of the spectral features seen in the IRIS data. Table 3.14 shows the close agreement between minerals identified by interpretation of the spectra with those minerals identified by XRD analysis.

3.3.3.1 Implications for broad-band multispectral remote sensing in Mahd Adh Dhahab area

The spectral properties of materials can be used for identification purposes. The rocks in Mahd Adh Dhahab had their spectra taken from samples collected from an area which was mapped as altered and non-altered rocks. Spectral features diagnose certain mineral assemblages commonly found in association with alteration, including chlorite and kaolinite. These spectral features occur particularly at 2.2um and 2.33um.

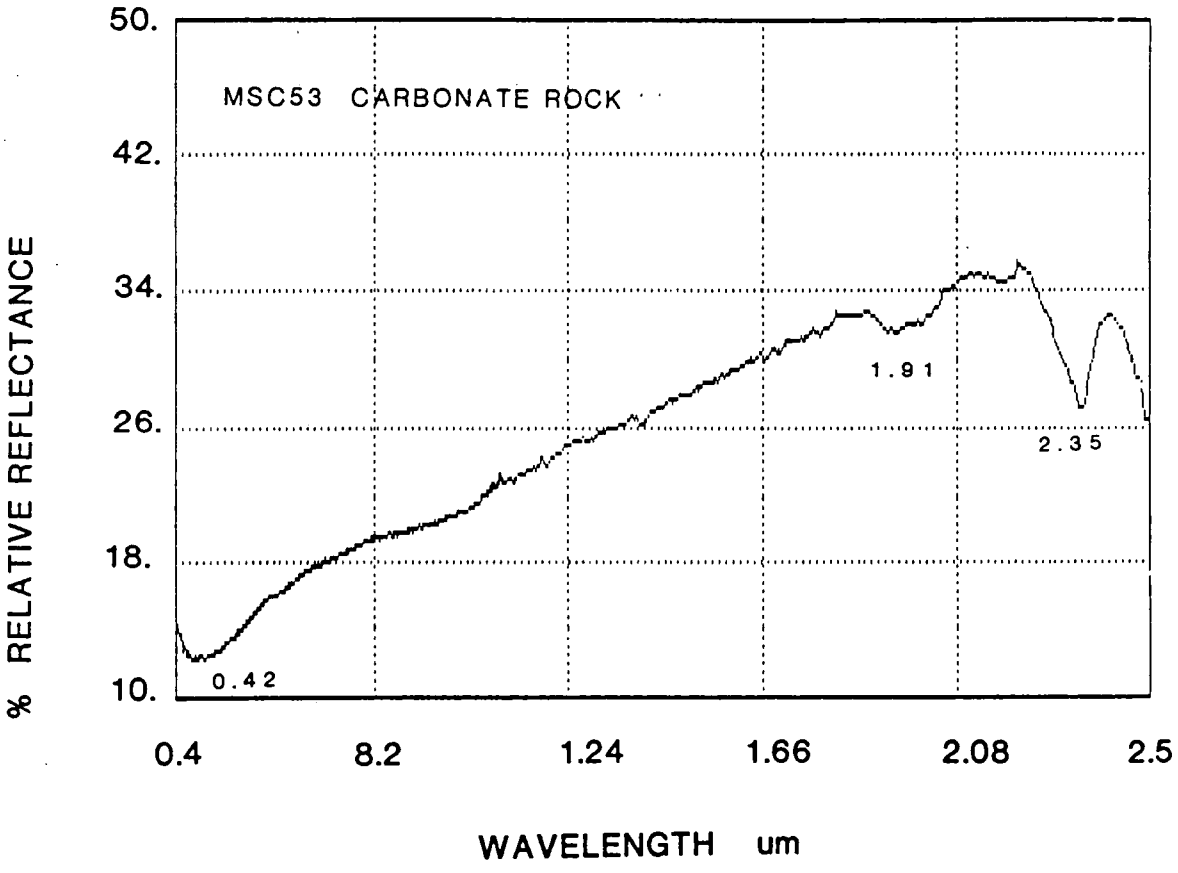

Fig. 3.18 Laboratory spectra using IRIS for samples from Carbonate Rocks, Madh Adh Dhahab.

Table 3.13. List of the samples analysed for mineral compositions using spectral features from Mahd Adh Dhahab area.

Sample No.	Lithology	Wavelength postn. of spectral features µm	Minerals
Msc 53/1	Carbonate Rock.	0.42,1.91,2.35	Fe,C
MD 23/3	Breccia	0.43	Fe
MD 22/3	Rhyolite	0.43	Fe
MD 23/2	Silicified Tuff	0.42,0.91,1.41,1.91,2.2	K,H
MD 30/2	Rhyolite	0.43	Fe
MS 14	Upper Tuff	0.48,2.2	H,L
MS 27	Lower Agglomerate	0.43,1.4,1.9,2.2,2.35	CH,C,M
MS 39	Rhyolite Intrusion	0.43,1.4,2.2	CH,H,Fe
MS 6a	Lower Agglomerate	0.41,1.4,1.9,2.2,2.35	CH,H,C
MS 6b	Lower Agglomerate	0.42,1.4,1.9,2.2,2.33	CH,H,M
MS 6c	Lower Agglomerate	0.43,1.9,2.2	CH,H,K
MS 11a	Upper Tuff	0.42,1.4,1.9,2.2,2.33	K,CH,Fe,C
MS 11b	Upper Tuff,	0.41,0.98,1.4,1.9,2.2,2.43	H,K,CH
MS 8	Andesite	0.48,1.4,1.9,2.2,2.33	M,CH,
MS 40	Upper Agglomerate	1.4,1.9,2.2,2.35	M,CH,K
MS 7	Lower Tuff	0.42,0.94,1.4,1.9,2.2,2.33	CH,M
MS 10a	Upper Tuff	0.48,0.87	G,H
MS 10b	Upper Tuff	0.49,1.4,2.21,2.2,2.33,2.43	CH,K,H,G
MS 5	Lower Tuff	0.43,1.41,1.92,2.2,2.33	M,CH,K
MS 24	Andesite	0.42,2.35,2.25	Fe,K,C
MD 4/3	Lower Tuff	0.43,0.95,1.4,1.9,2.2,2.33	H,G,M,CH
MD 35/1	Lower Gallomerate	0.43,1.4,1.9,2.2,2.33	Fe,M,CH
MD 37/1	Upper Tuff	0.47,0.96,2.3,2.4	H,G,M
MD 37/2	Upper Tuff	0.43,0.98,1.41,2.2	G,H,K
MD 36	Upper Tuff	0.43,0.94,1.4,2.2,2.35	Fe,CH
MD 19/1	Andesite	0.43	G,H

Key for minerals identified:

Q = quartz
H = hematite
K = kaolinite
G = goethite
M = muscovite
L = allunite
P = plag-feldspar
C = carbonate
CH = chlorite
KF = K-feldspar
Fe = iron oxides

Table 3.14. Comparison between minerals identified by spectra and XRD - Mahd Adh Dhahab area.

Sample No.	Lithology	Spectra	XRD
Msc 53/1	Carbonate Rock	Fe,C	Q,C
MD 23/3	Breccia	Fe	Q,P,CH
MD 22/3	Rhyolite	Fe	P,Q,K,C
MD 23/2	Silicified tuff	K,H	Q,P,K
MD 30/2	Rhyolite	Fe	Q,P,K
MS 14	Upper Tuff	H,	Q, KF, CH,M
MS 27	Lower Agglomerate	CH,C,M	Q,CH,M,KF
MS 39	Rhyolite Instrusion	CH,H,Fe	Q,KF,M
MS 6a	Lower Aggommerate	CH,H,C	Q,C,CH
MS 6b	Lower Agglomerate	CH,H,M	Q,KF,CH,M
MS 11a	Upper Tuff	K,CH,Fe	Q,M,C,K
MS 11b	Upper Tuff	H,K,CH	Q,H,CH,KF,G
MS 8	Andesite	M,CH,E	Q,C,CH,M
MS 40	Upper Agglomerate	M,CH,K	Q,K,CF,M
MS 7	Lower Tuff	CH,M	Q,K,M,P
MS 10a	Upper Tuff	G/H	Q,P,A,K
MS 10b	Upper Tuff	CH,K,H/G	Q,P,C,Ch,M
MS 5	Lower Tuff	M,CH,K	Q,P,M
MS 24	Andesite	Fe,K,C	Q,CH,KF
MD 4/3	Lower Tuff	H/G,M,CH	Q,KF,CH,C
MD 35/1	Lower Agglomerate	Fe,M,CH	Q,KF,CH,C
MD 37/1	Upper Tuff	H/G,M	Q,P,C,CH,L,KF
MD 37/2	Upper Tuff	G,H,K,	Q,K,KF,M
MD 36	Upper Tuff	Fe,CH	Q,H,CH,M
MD 19/1	Andesite	G/H	Q,P,A,CH

Key for minerals identified:

Q = quartz
H = hematite
K = kaolinite
G = goethite
M = muscovite
L = allunite
P = plag-feldspar
C = carbonate
CH = chlorite
KF = K-feldspar
Fe = iron oxides
A = Apatite

The rocks outside the alteration zone, in contrast, show relatively featureless spectral curves, with the exception of absorption around 0.4um related to iron coating in certain instances. In some spectra taken from andesite rocks there is evidence to suggest alteration to chlorite (see Fig. 3.17). The carbonate rocks show very clear spectral features around 2.35um and so can be differentiated from the clay mineral features (Hunt & Ashley, 1979).

All this suggests that in the TM spectral data with the spectral band covering the 2.2um region spectral absorption features should be observable. The absorption features associated with the alteration units are almost certain to be picked up, and these alteration units are likely to be discriminated with respect to the surrounding unaltered rock types which are characterized by the relatively featureless spectral curves. Unfortunately, using such broad band spectral data will not allow to discriminate between carbonate and alteration minerals.

3.3.4 Laboratory spectral analysis of Jabal Said

Thirty samples collected from Jabal Said were measured for their relative reflectance using IRIS. The location of these samples are shown in Fig. 3.2 and a list of the samples and their types of lithology are given in Table 3.15. The spectra were measured on the upper, undisturbed surface of the samples, except for one sample from the main gossan where spectra was also measured for

Table 3.15 List of the Samples analysed for laboratory spectra using (IRIS) from Jabal Said area.

Sample No.	Lithology
JS6, JS7/1	Dacitic tuff
JS7/2	Dacitic tuff
JS10	Granite
JS15/2, JS28	Rhyolite
JS27	Diorite
JS22, JS63	Andesite tuff
JS16	Volcanic sediments
JS19/2, JS20	Volcanic conglomerate
JS20/2	
JS23/1, JS23/2	Zubaiydh Breccia
JS25, JS25/1	Gossan
JS25.2	
JS26, JS29, JS30/2, JS35, SS22/2, SS22/1 SS15, SS17, SS26, SS36, SS37, SS39.	Alteration Zone

the fresh surface. XRD analysis was undertaken on selected samples, as mentioned earlier.

The samples in Jabal Said represent different types of lithologies, based on the intensity of the spectral features. The samples can be grouped into five main groups:

1. Alteration zone.
2. Gossan.
3. Andesite and dacite tuff.
4. Igneous rocks.
5. Volcanic sediments and breccia.

1. Alteration zone

The samples of the alteration zone were distributed randomly, but again these samples exhibit the behaviour of altered igneous rocks by giving high reflectance around 1.6um and sharp fall-off towards the ultraviolet and infrared (Hunt, 1979a). All the samples from the alteration zone exhibit spectral features around 2.2um and 2.33um. The intensity of these features are different from one sample to another, from being very sharp in sample SS 39 (Fig. 3.19a) to very weak in sample SS 37 (Fig. 3.19h). The presence of iron oxide is usually indicated by the fall-off of the curve towards the ultraviolet and the absorption around 0.87-0.94um (Fig. 3.19a). Several samples from the alteration zone do not show the fall-off towards the 0.4um and have a consistent reflectance in the range of 0.4-1.1um (e.g. JS 35, SS 36 (Fig.

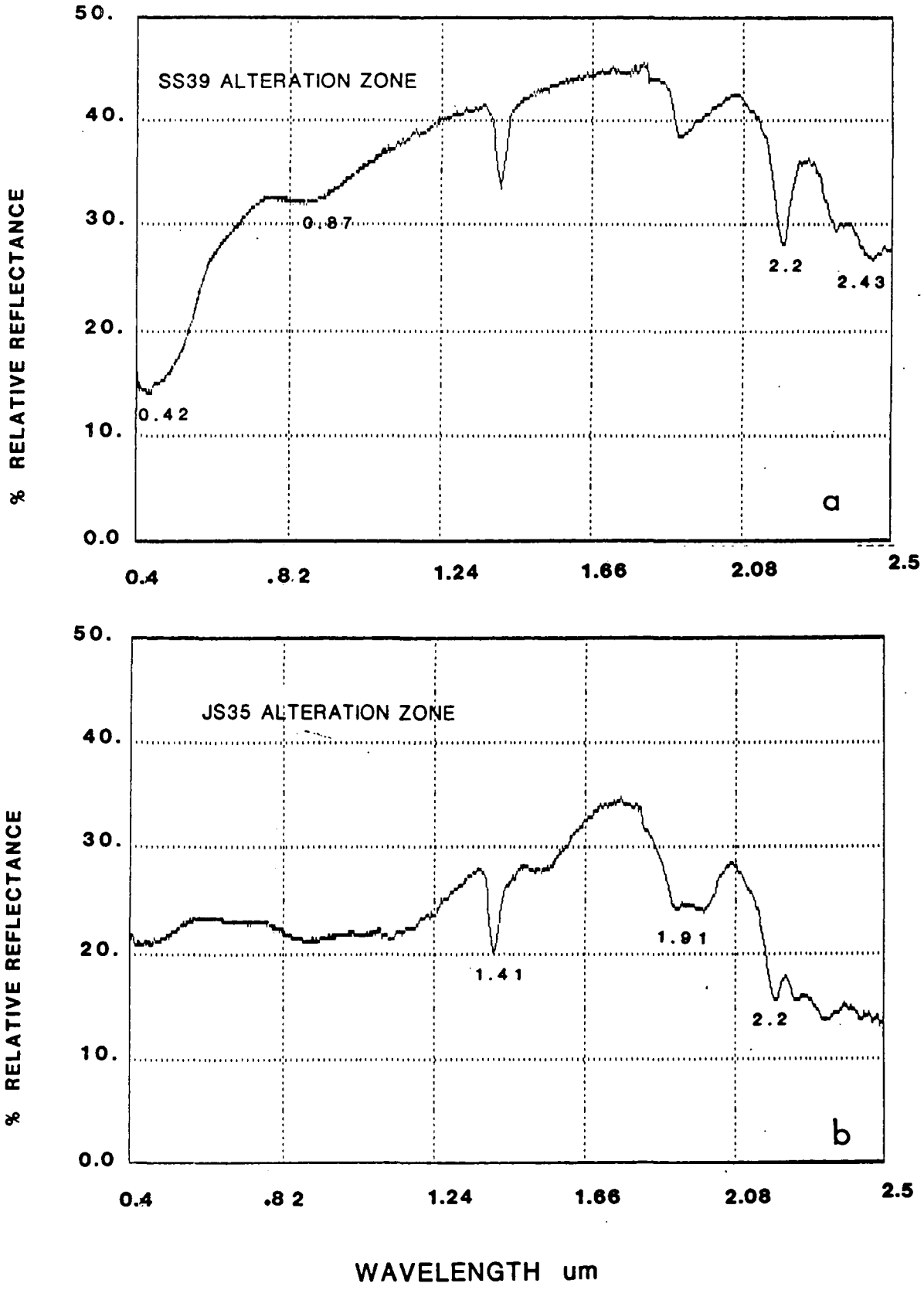

Fig. 3.19 Laboratory spectra using IRIS. Samples from alteration zone, Jabal Said.

3.19b,g) which might be explained by an increase in the amount of clay minerals and an absence of iron oxide.

2. The Gossan

Two samples were taken from the main gossan. Sample JS 25/2 is mainly limonite, spectral features around 2.2um indicate the present of clay minerals and the sharp fall-off toward 0.4um and the absorption features around 0.87um indicate the presence of iron oxide (Fig. 3.20a). The other sample JS 25, is composed mainly of hematite, but the spectra of the weathered surface exhibited absorption features indicative of clay minerals. The fall-off towards 0.4um, however, is indicative of iron oxide (Fig. 3.20b). The weathered surface of the sample JS 25 was removed and other IRIS measurements were made (Fig. 3.21). These show no absorption features at all around 2.2, but features are present around 0.85um and 0.42um indicative of iron oxide.

3. Andesite and dacite tuff

The samples from the andesite tuff exhibited spectral features around 2.2um and 2.33um, showing clay alteration JS22 and SS 63 (Fig. 3.22a, b), also, absorption around 0.87 and 0.42um is indicative of iron oxide as shown in sample SS 63.

The dacite tuff (sample JS 7/2) exhibited features around 2.2 and 2.35um indicating the presence of carbonate, also, spectral absorption is shown around

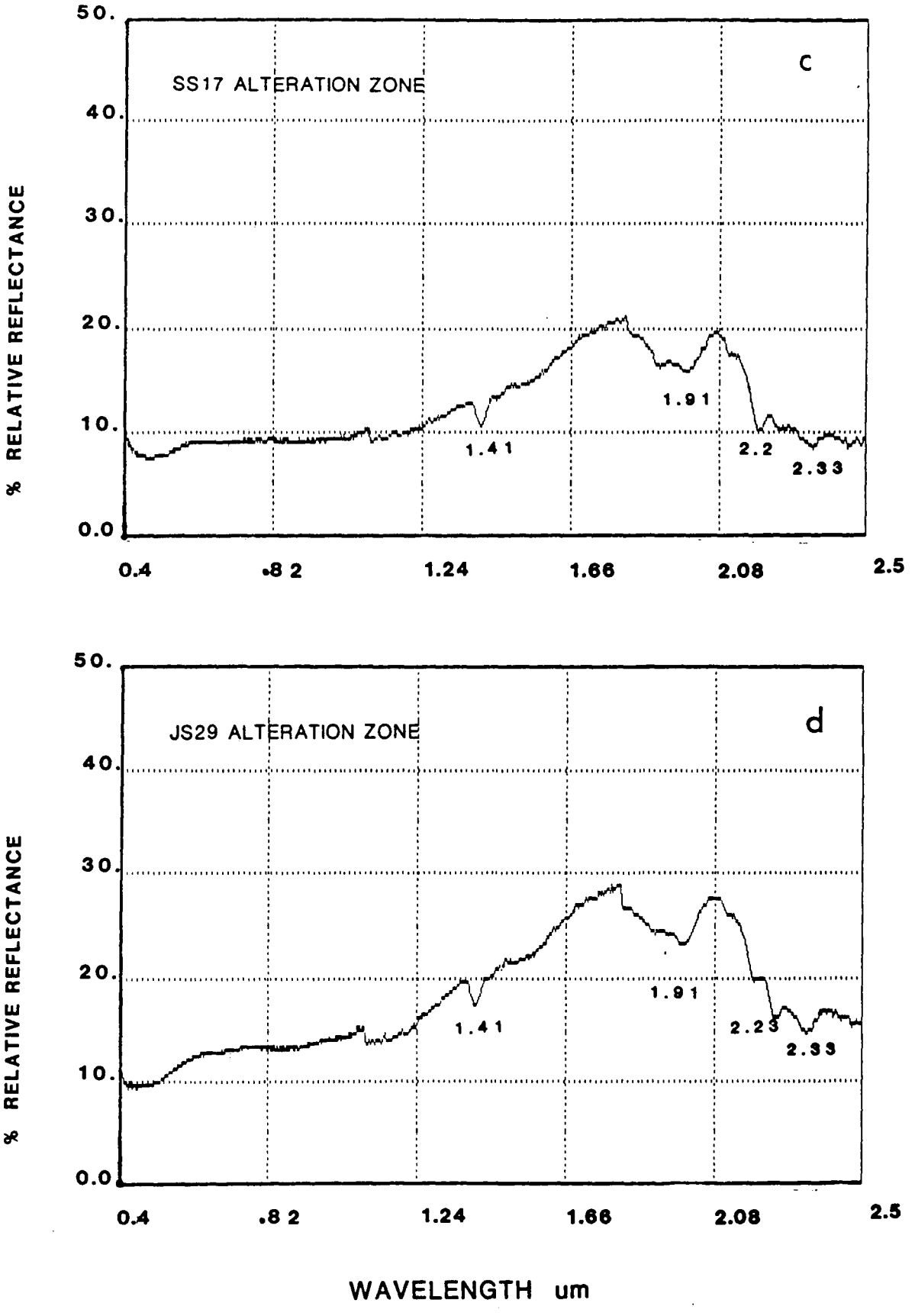

Fig. 3.19 Continued.

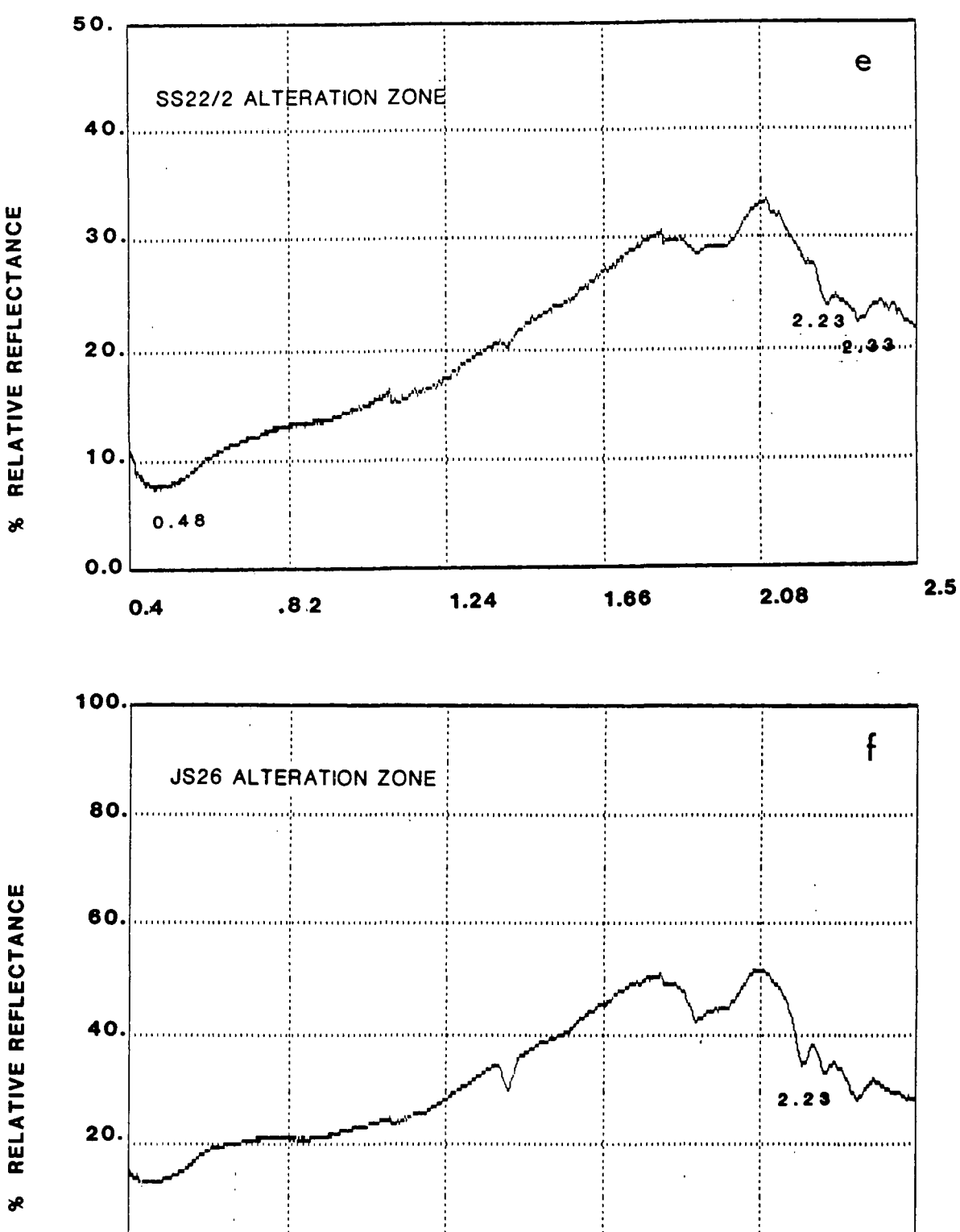

Fig. 3.19 Continued.

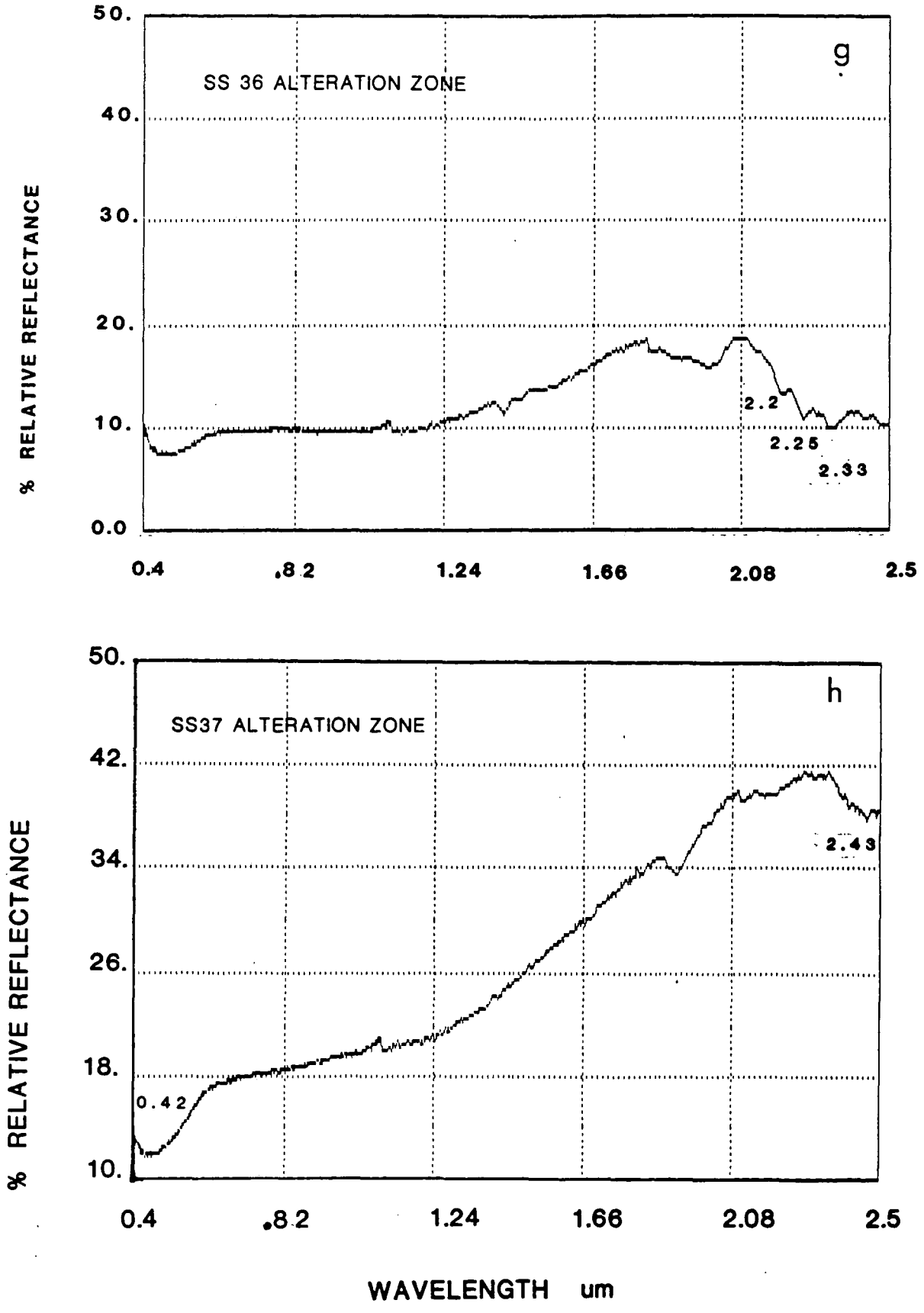

Fig. 3.19 Continued.

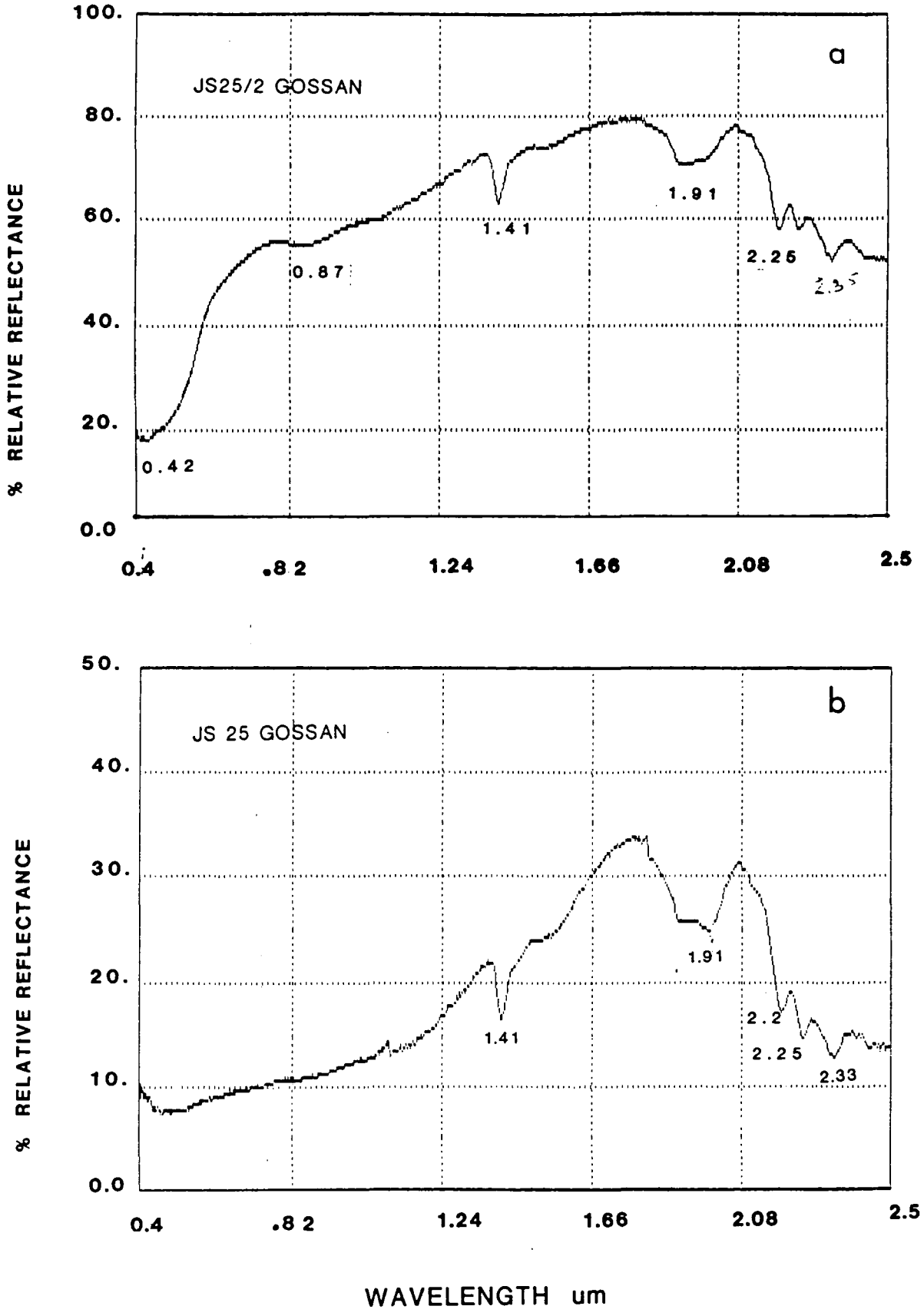

Fig. 3.20 Laboratory spectra using IRIS. Sample from the main gossan, Jabal Said.

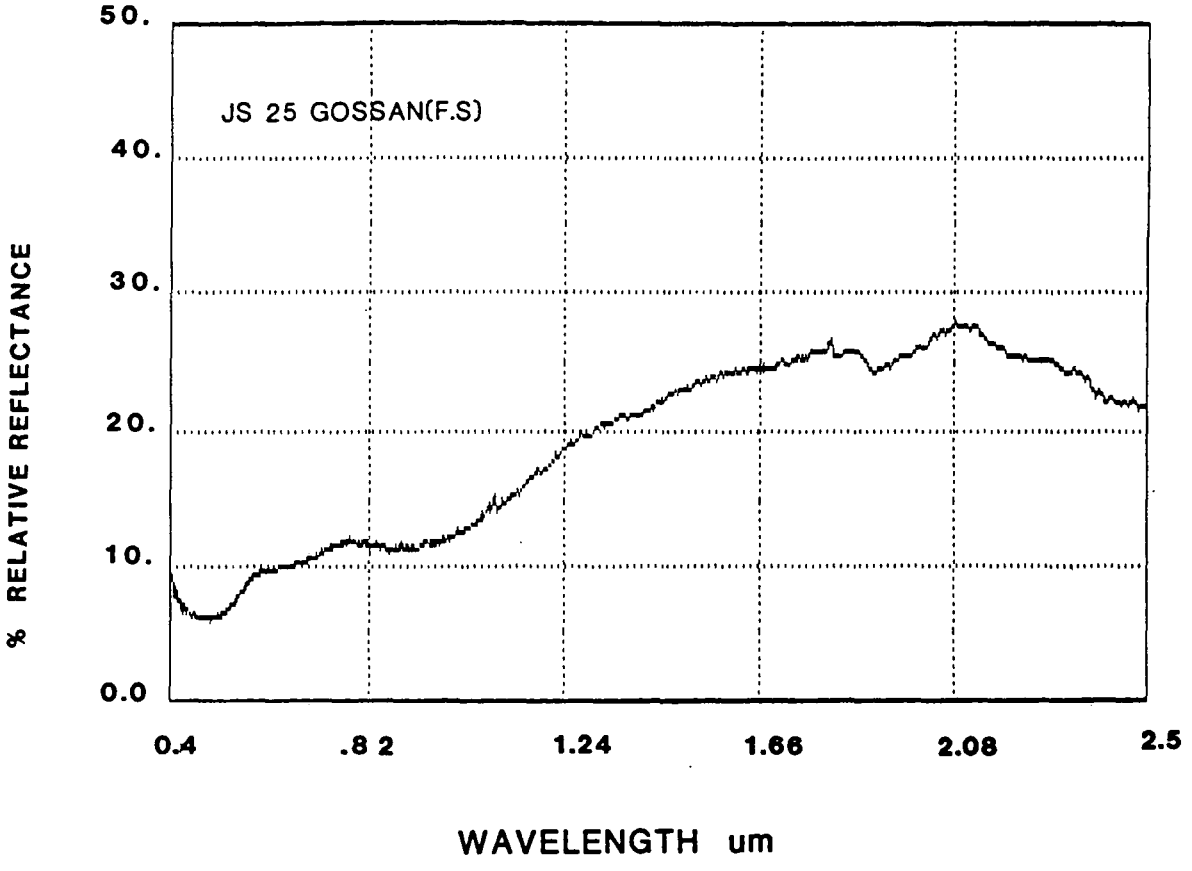

Fig. 3.21 Laboratory spectra using IRIS. Sample from the fresh surface of the main gossan, Jabal Said.

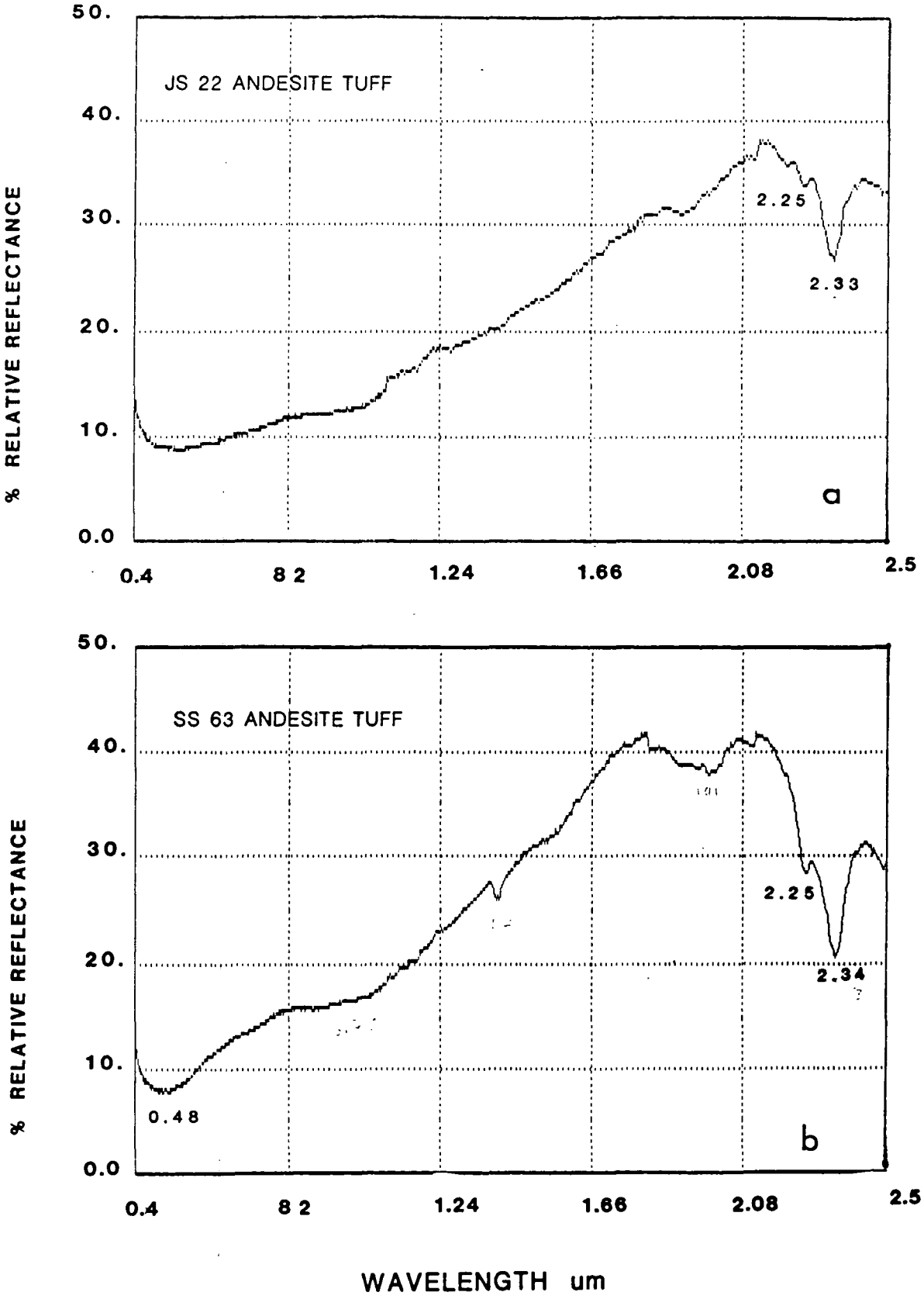

Fig. 3.22 Laboratory spectra using IRIS. Sample from Andesite tuff, Jabal Said.

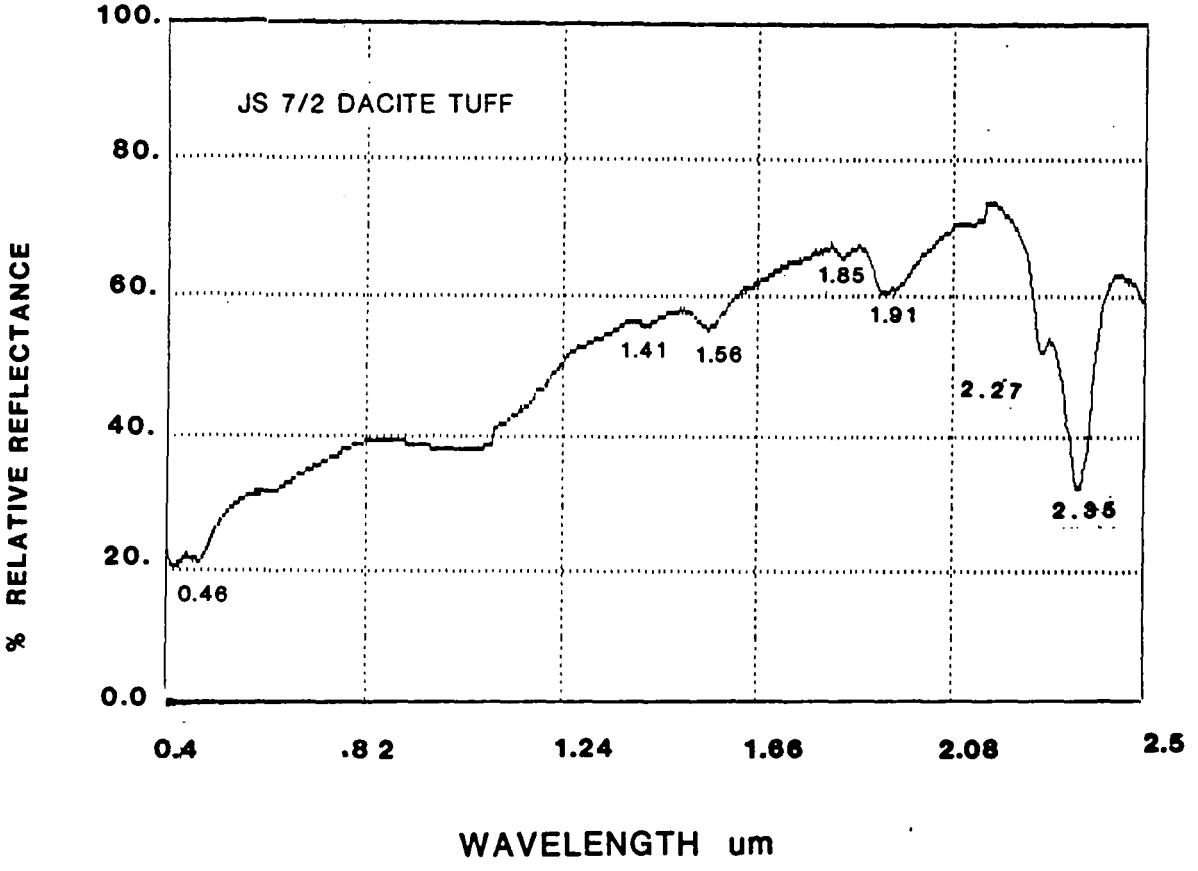

Fig. 3.23 Laboratory spectra using IRIS. Sample from Dacite tuff, Jabal Said.

0.87um and 0.46um indicating iron oxide presence (hematite)(Fig. 3.23).

4. Igneous rocks

Samples collected from different lithologies in Jabal Said include three types of igneous rocks - rhyolite, granite and diorite. Two samples were taken from the rhyolite, where there are two types of rhyolite according to the geologic map (Sabir, 1981); the black rhyolite and the green rhyolite. The spectra from the black rhyolite JS 15/2 covered with thick desert varnish show no spectral features, except the fall-off towards the 0.4um indicating the presence of iron oxide (Fig. 3.24b).

The green rhyolite show some spectral features, beside the iron oxide around 0.4um. A weak spectral feature exhibited at 2.2 and 2.37um indicated a weak alteration through the presence of clay and chlorite minerals (Fig. 3.24a).

The granite sample JS 10 collected from the granitic body in the area show sharp fall-off towards the ultraviolet, indicating the presence of the iron oxide as (Fig. 3.24d). The diorite sample also shows the iron oxide spectral features, and a wide spectral feature at around 2.33um (Fig. 3.24c).

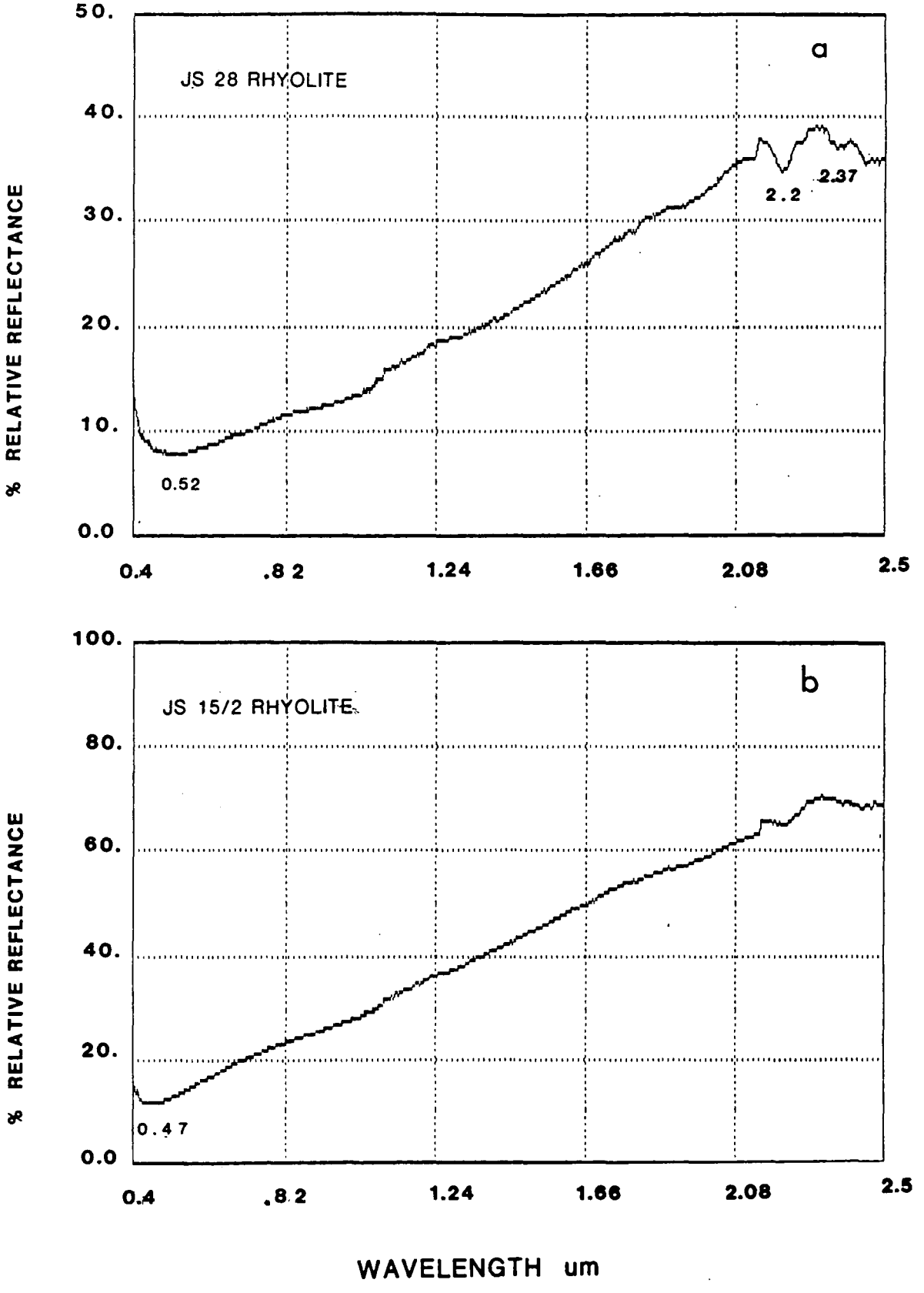

Fig. 3.24 Laboratory Spectra from igneous rocks in Jabal Said area.

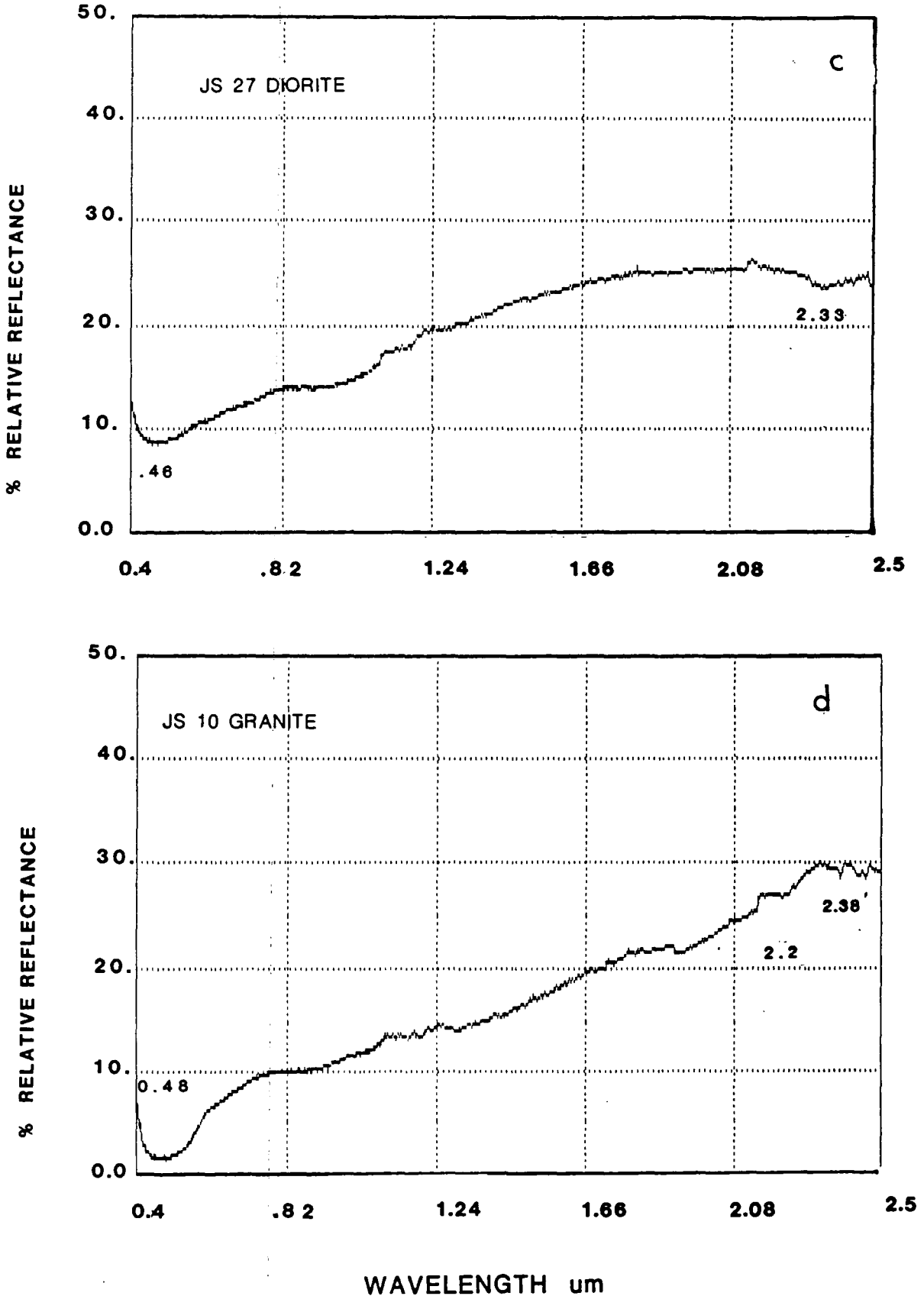

Fig. 3.24 Continued.

5. Volcanic sediments and breccia

Four samples were collected from the volcanic sediments and conglomerate east and north of the alteration zone and one sample from the Zabaidah breccia.

The first sample, JS 16, exhibited the sharp fall-off towards the 0.4um and showed high albedo at 2.5um, only very weak spectral features were shown at 2.2um (Fig. 3.25a).

The other sample JS 19.2 does not exhibit any features except the slight falling toward the 0.4um. This sample had a thick, black weathered surface (Fig. 3.25b).

Four samples from north of the alteration zone JS 20 and JS 20/1 also showed the presence of iron oxide. Sample JS 20 exhibited spectral features around 2.34um and 2.35um, indicating the presence of carbonate or Mg-OH minerals (Fig. 3.25c, d).

The sample from the Zabaidah breccia JS23/1, shows absorption around 0.42, 0.81, 1.24, 1.91um, and fall-off toward 2.5um.

The first three spectral features indicate the presence of iron oxide (Fig. 3.26). The Zabaidah breccia is rich in radio- active minerals as shown in Table 3.8.

A summary list of the samples and their main spectral features, and the identified minerals associated with these spectral features are given in Table 3.16.

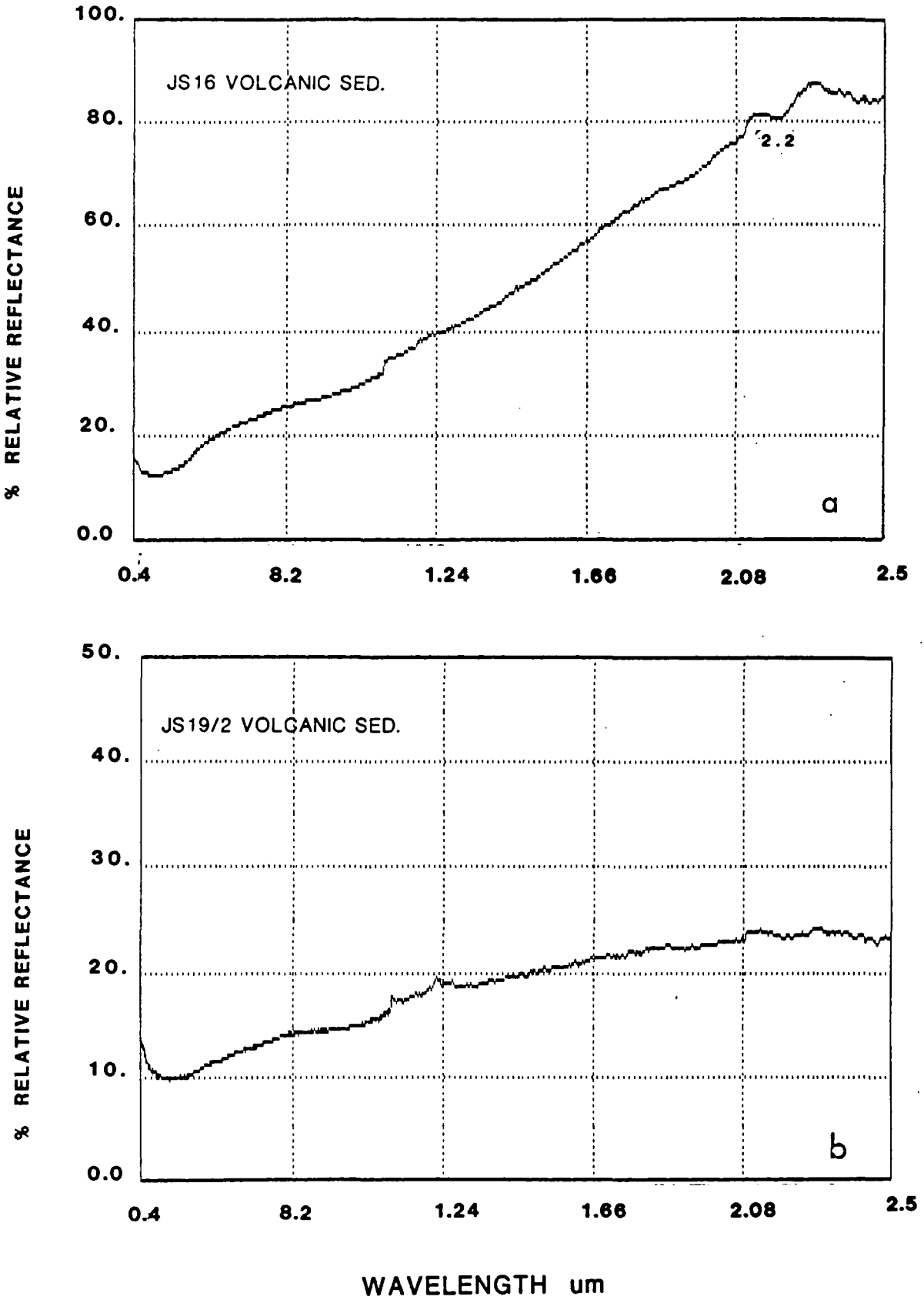

Fig. 3.25 Laboratory spectra of the volcanic sediments unit from Jabal Said.

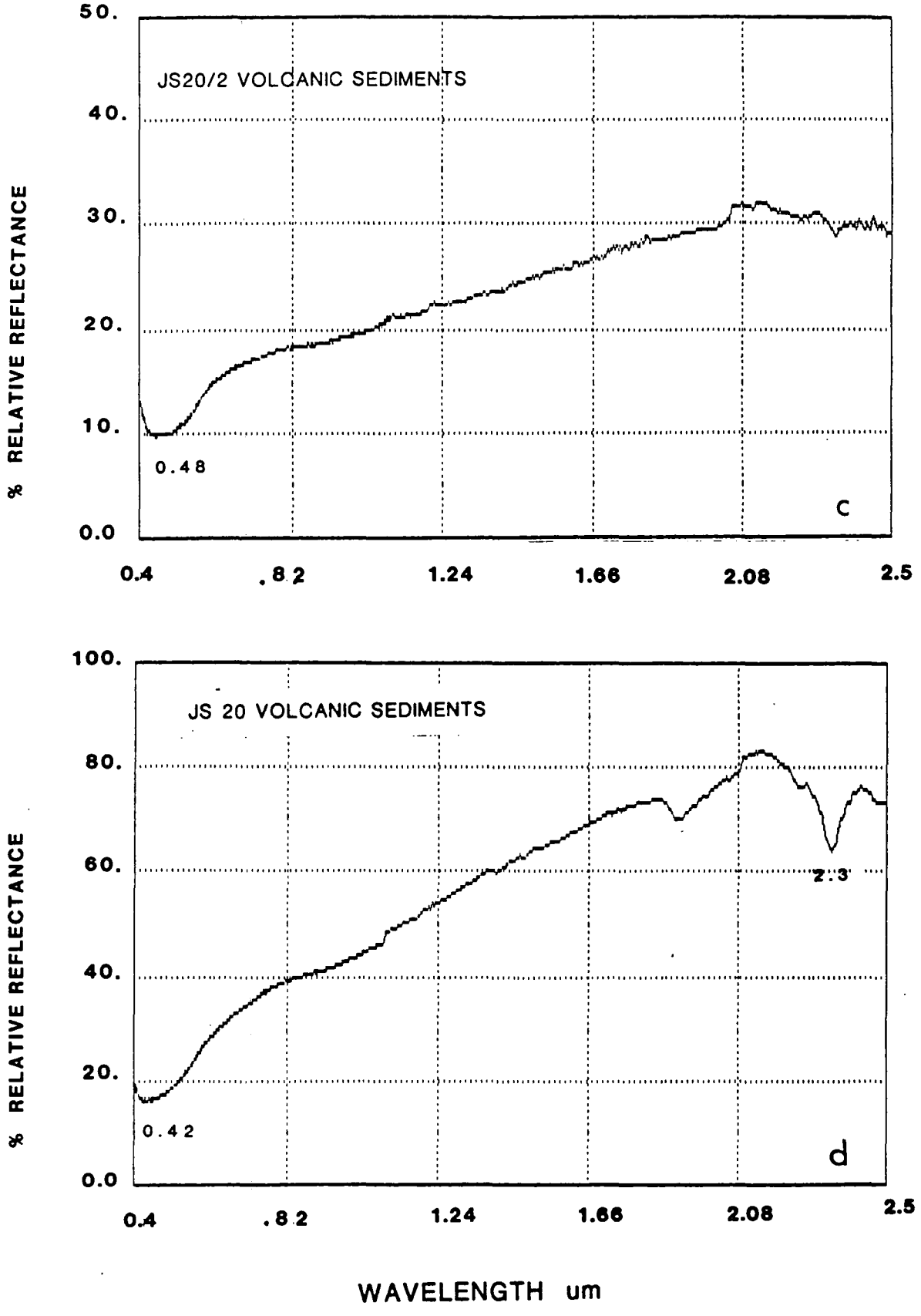

Fig. 3.25 Continued.

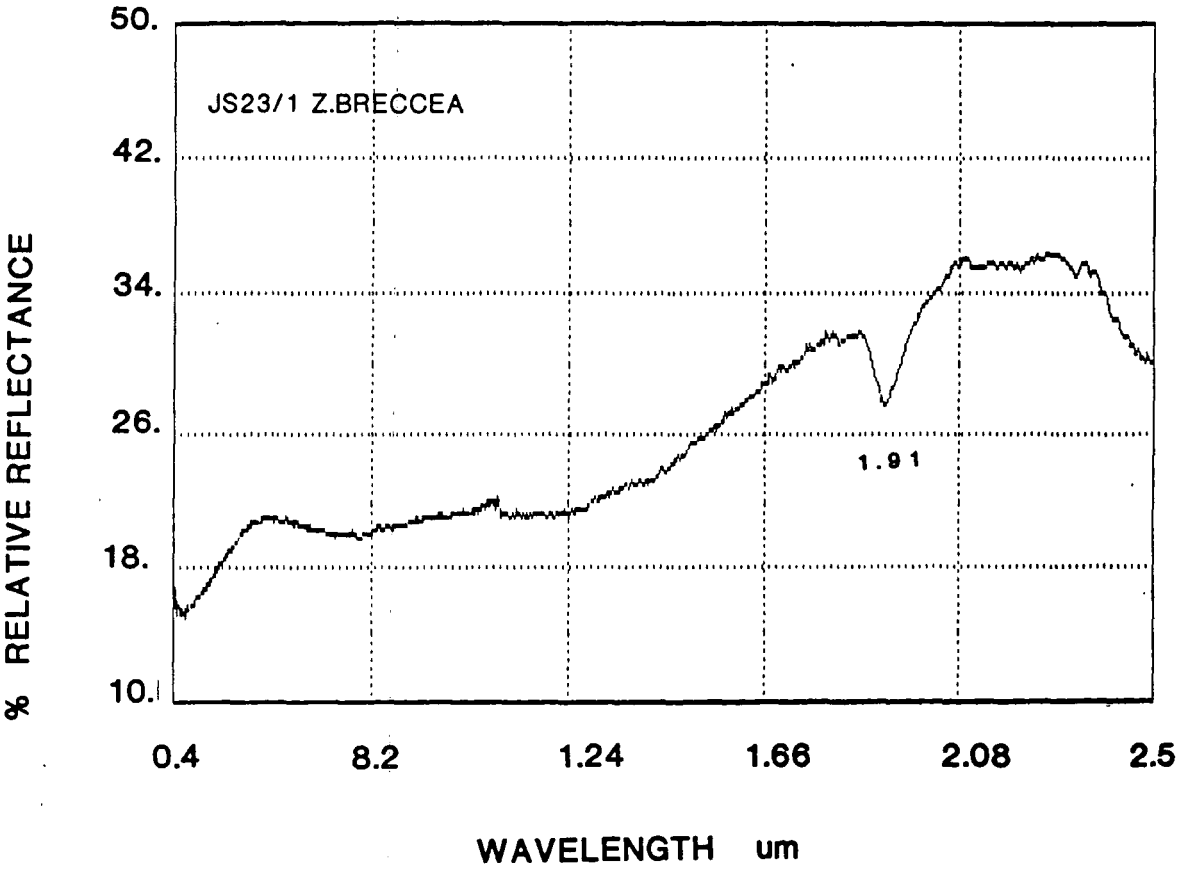

Fig. 3.26 Laboratory spectra of Z. breccia from Jabal Said.

Table 3.16. Mineralogy of rock samples collected from Jabal Said using visible and near infrared reflectance spectra measured by (IRIS).

Sample No.	Lithology	Wavelength position of sig.spectral features(μm)	Minerals
SS39	Alteration Z.	0.42,0.87,2.2,2.43	Fe,K,H
JS35	" "	1.41,1.91,2.2,2.33	K
SS17	" "	1.41,1.91,2.2,2.33	Fe,H,K,Ch
JS29	" "	1.41,1.91,2.23,2.33	Fe,H,K,Ch
SS22/2	" "	0.48,1.91,2.2,2.33	Fe,K,Ch
JS26	" "	0.43,1.41,1.91,2.2,2.33	Fe,K,Ch
SS36	" "	0.42,1.41,1.91,2.2,2.33	Fe,K,Ch
SS37	" "	0.42,1.91,2.43	Fe
JS25/2	Gossan	0.42,0.87,1.41,1.91,2.25, 2.35	Fe,H,K,CH,C
JS25	"	0.42,1.41,1.91,2.2,2.35	Fe,K,C
JS25(F.S)	"	0.42,0.87,1.91	Fe,G,H
JS28	Rhyolite	0.42,2.2,2.3	Fe,K
JS10	Granite	0.42	Fe
JS23/1	Z.Breccia	0.41,0.87,1.91	Fe,H
JS15/2	Rhyolite	0.47	Fe
JS16	Volcanic sed.	0.42,2.2	Fe,K
JS19/2	" "	0.42	Fe
JS20/2	" "	0.48,2.35	Fe,C
JS20	" "	0.42,1.91,2.35	Fe,C
JS27	Diorite	0.46,2.33	Fe,Ch
JS22	Andesite tuff	0.42,2.2,2.83	Fe,K,Ch
SS63	" "	0.48,0.78,1.41,1.91,2.35,	Fe,H,K,Ch,C
JS7/2	Dacite tuff	0.46,0.78,2.2,2.35	Fe,H,G,K,Ch,C

Key for minerals identified:

H = hematite
K = kaolinite
G = goethite
C = carbonate
CH = chlorite
KF = K-feldspar
Fe = iron oxides

3.3.4.1 Implication for broad band multispectral remote sensing in Jabal Said.

Jabal Said is considered to be a model area to test the ability of remote sensing techniques to discriminate between the different lithologies. The reason for this is because Jabal Said shows many different types of lithological units within a very small area. By studying the variation with this area it is possible to compare and contrast data which has been acquired by several different remote sensing platforms including satellite and airborne systems.

The spectal features diagnosed are associated with specific minerals. The alteration zone in Jabal Said has clearly shown spectral features around 2.2 and 2.3um, indicating the presence of alteration minerals, such as clay and chlorite.

The other rocks or lithologies in this area do not show spectral features in that range, or occasionally very weak absorption features.

The following section examines the spectral behaviour of rocks as measured in the field.

3.4 Field spectra acquisition, analysis & interpretation

Measurements of bidirectional reflectance were also made in-situ to further substantiate the findings from spectrometer measurements made in the laboratory. Acquisition of field spectra, particularly for natural

materials found in-situ, provides a more accurate and realistic indication of variations in reflectance that might be measured by an air- or space-borne multispectral sensor. The ability to control measurement conditions and parameters also allow such data to be used in establishing physical basis of ground surface reflectance (Milton, 1980; Lawrence et al., 1977; Jackson et al., 1980). When combined with detailed laboratory geochemical and spectro-radiometric studies, in-situ spectral reflectance measurements can provide valuable information linking mineralogy, and the spectral response of multispectral scanner data (Abrams & Bowen, 1984).

An additional, though no less important reason for acquiring field reflectance data was for the purpose of calibrating the airborne and satellite data sets used in this study. These aspects are examined in more detail in Chapter 4.

3.4.1 The instrumentation

The instrument used for acquiring the field spectra was called the Barringer Hand Held Ratioing Radiometer (HHRR) (Barringer, 1981), capable of acquiring spectral measurement in ten spectral bandpasses determined by filters (Figs. 3.27, 3.28). The first six filters used in this study are equivalent to Landsat 5 TM bands covering the spectral region from 0.45um to 2.5um. The last four bands cover the narrow spectral area from 2.088 to 2.34um. Table 3.17 show the band widths for filters used with the

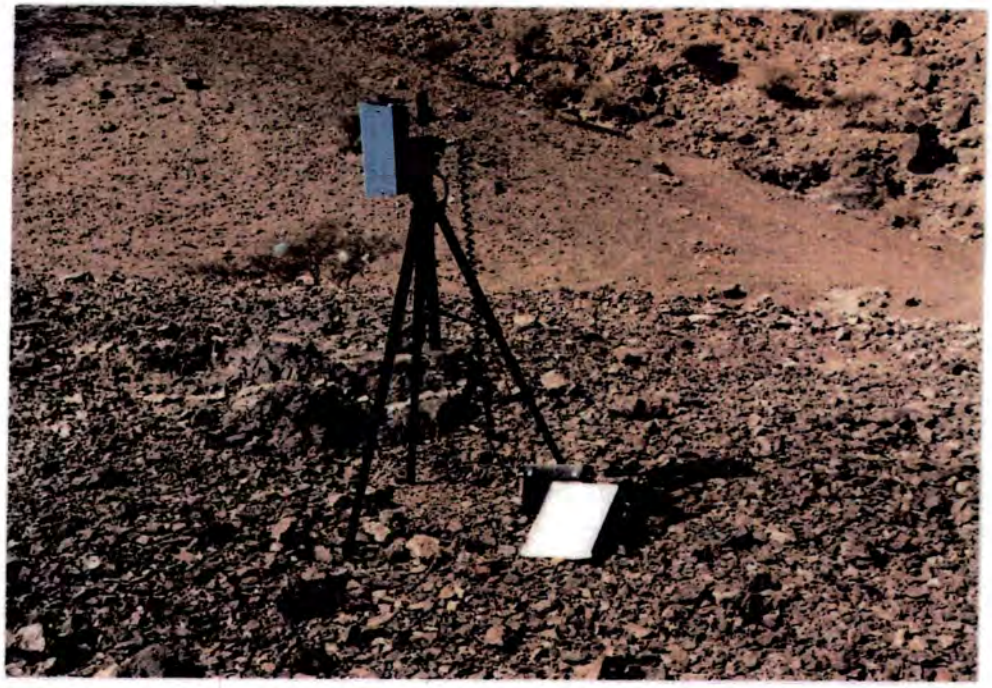

Fig. 3.27 A photograph showing the HHRR setup used in the field, the HHRR was aimed vertically downward and was positioned facing toward the sun. It is connected to the battery which is lying on the ground beside the white reference plate (Fiberflax).

Fig. 3.28 The back of the Barringer HHRR showing the display panel and detector controls.

Table 3.17 Bandpasses edges of the filters used in the field measurement with Baringer HHRR.

Filter No.	Equivalent to	Band edges	Centre Wavelength
1	TM1	0.45-0.52 um	0.48 um
2	TM2	0.52-0.60 um	0.56 um
3	TM3	0.63-0.69 um	0.66 um
4	TM4	0.76-0.90 um	0.83 um
5	TM5	1.55-1.75 um	1.63 um
6	TM7	2.08-2.35 um	2.22 um
7	---	2.0884-2.1204 um	2.10 um
8	---	2.160-2.180 um	2.17 um
9	---	2.180-2.220 um	2.20 um
10	---	2.314-2.340 um	2.32 um

HHRR in this study. The measurement was referred to a white artificial, fibrefax surface. The procedure was to record the reflectance from the target, followed by the reflectance of the fibrefax. The measurement was transcribed on a specially designed form (Appendix C). Relative reflectance was subsequently calculated for each band for each site by dividing the target measurement by the reference measurements.

For more information about the HHRR instrument see Appendix C.

3.4.2 Data Collection

Seventy-seven spectral measurements were made at 77 sites in the Mahd Adh Dhahab area, and 85 locations for field measurements were made in Jabal Said, several measurements were made in each of these locations over the same lithological units.

These measurements were averaged to determine a mean spectral curve in each bandpass. The benefits from this procedure of taking spectral measurements over several different sites within the given types of lithologies was to provide a typical spectral response from that lithology. However, given the limitations of time, it was not possible to acquire more than an average of six samples per site on each lithological type.

The assumption was made that the average spectra determined for each type of lithology was sufficient to characterize the nature of the surface in spectral term

would require a potentially higher measurement, dependent on the actual heterogeneity of that surface of lithology. In certain cases it may well be that the above assumption is invalid in part, because of the natural heterogeneity of the material concerned.

The other advantage of calculating a mean spectral response is more likely to be representative of the spectral record sense by aircraft or satellite sensor which record spectral radiance over large areas.

3.4.3 Analysis and interpretation of the ground spectra from Mahd Adh Dhahab

Field spectra were acquired for a total of 77 samples in the Mahd Adh Dhahab area. Particular emphasis was placed on sampling different type of alteration as defined by Dobreach & Leanderson (1984). An average of 3-6 locations were measure for each type of alteration. Spectral measurements were also recorded at locations surrounding the Mahd Adh Dhahab (Fig. 3.29). Only the result from the first six filters of the HHRR will be discussed and analysed here. These are equivalent to Landsat TM bands, the other four bands are narrow bands and will be discussed elsewhere.

The mean and standard deviation of the spectra of each band was calculated for the different types of alteration and other lithologies (Table 3.18). The average relative reflectance spectra were plotted for each mapped alteration units and lithological type. Generally the spectra of the altered rock in Mahd Adh Dhahab were of

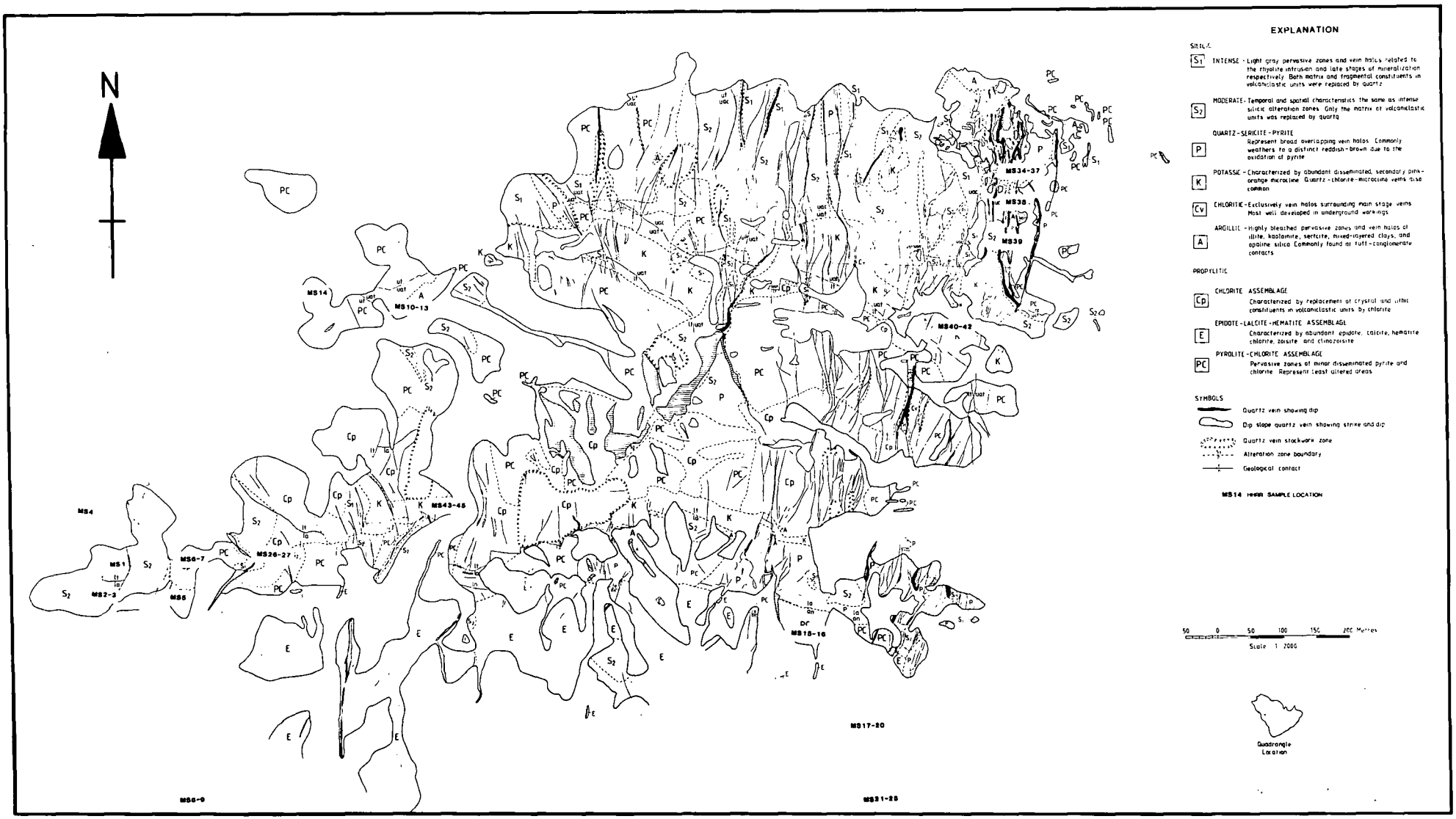

SOURCE : J.L. DOEBRICH 1984

DISTRIBUTION OF QUARTZ VEINS AND HYDROTHERMAL ALTERATION ZONES
AT THE MAHD ADH DHAHAB PRECIOUS-METAL DEPOSIT, KINGDOM OF SAUDI ARABIA

FIGURE 3.29 LOCATION OF FIELD SPECTRAL MEASUREMENT USING HHRR IN MAHD ADH DHAHAB AREA

Table 3.18. The means and standard deviation of ground spectra for different types of rocks and alteration zones in Mahd Adh Dhahab, bands equivalent to Landsat TM.

Type of Lithology	No.of samp.	Mean/st. deviation					
		TM1	TM2	TM3	TM4	TM5	TM7
Silicic alt.	4	11.0/4	15.2/6	17.4/6	19.9/7	27.9/9	25.2/6
Qtz.ser.pyr.	6	14.1/5	18.9/7	23.5/8	25.7/9	38.1/10	33.0/8
Pyrite chl.	3	10.5/1	12.8/2	14.5/2	17.0/3	22.6/7	21.9/6
Argillic alt.	4	16.2/2	26.7/3	34.5/3	37.3/3	58.7/7	38.4/4
Potassic alt.	6	12.6/5	16.9/8	20.1/9	22.4/11	31.8/13	28.8/1
Chlorite	4	12.1/2	15.8/3	17.5/4	18.4/3	23.9/4	19.2/3
Epidote cal.	2	09.4/3	12.0/5	14.4/6	14.2/10	18.8/8	17.1/8
Carbonate R.	3	16.4/5	21.9/7	27.0/8	32.9/9	43.9/11	38.8/1
West J.Almahd	2	12.2/5	15.9/7	18.4/8	22.1/8	39.6/17	35.7/5
Tallus	2	12.5/0	16.5/0	19.7/1	22.6/0	22.4/0	22.2/1
Wadi sediment	5	22.7/4	34.1/5	42.2/6	48.8/7	58.8/7	554.1/8
Andesite rock	5	11.9/2	15.2/3	17.8/3	19.7/4	20.3/4	18.9/4
Unaltered R.	8	10.4/2	13.8/2	16.2/2	18.6/2	28.7/3	31.2/4

a typical overall appearance of altered igneous rocks, high reflectance at 1.6um, with a large decrease towards both shorter and longer wavelengths (Hunt & Ashley, 1979).

3.4.3.1 Altered units

The spectra of the altered rocks, follow a similar pattern, but with a difference in albedo (Fig. 3.30). The argillic alteration unit shows the highest albedo where compared with the other types of alteration, and give the highest ratio between band 5 (1.6um) and band 7 (2.2um). The sharp fall-off towards 0.4um indicates the presence of iron oxide, which can be explained by the desert varnish in the area. The absorption in band 4 at 0.83um appears to be caused by the presence of hematite, the results of the XRD from samples collected from the area mapped as argillic alteration supports this interpretation. The mineral composition of the alteration units is shown in Table 3.19 which shows also that the argillic alteration unit sometimes contains kaolinite, chlorite, mica and calcite. All these minerals characterized by spectral absorption features covered by band 7 which centred at 2.2um. There is no way to differentiate between Al-OH features which characterize the kaolinite or the Mg-OH features which characterize the chlorite using the broad band spectra.

The spectra of quartz sericite pyrite alteration, exhibited high reflectance at bands 1.6um and low reflectance absorption at band 7 (2.2um). The ratio of

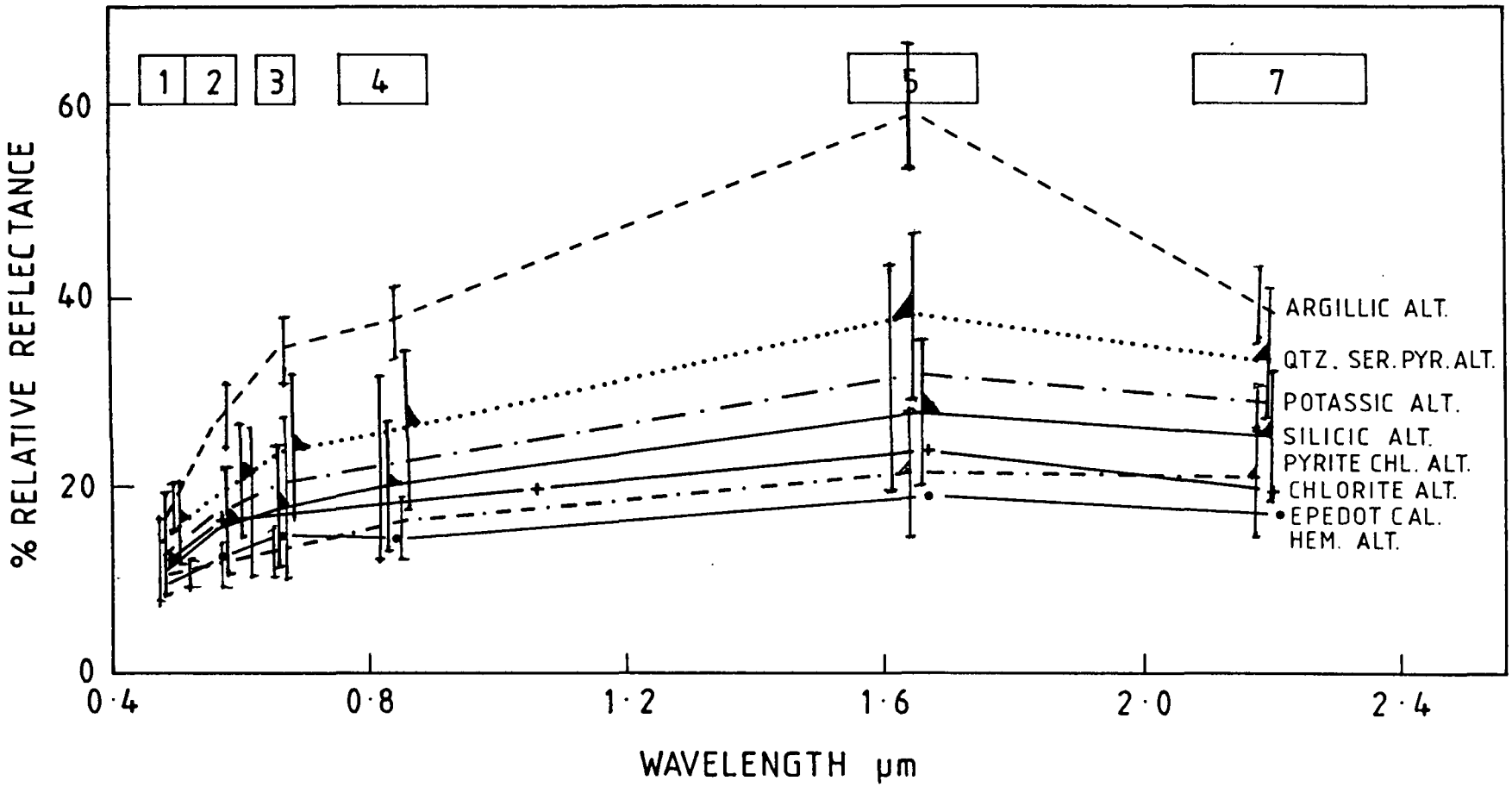

Fig. 3.30 Average HHRR spectra from Mahd Adh Dhahab area.

Table 3.19. Mineral composition of the different types of alteration in Mahd Adh Dhahab, identified by X-rd.

Alteration type where mapped	Mineral composition
Chlorite alteration	Quartz, chlorite, mica, K-feldspar, calcite, plagioclase
Silicic alteration	Quartz, plagioclase, mica, chlorite, K-feldspar, calcite
Quartz-sericite-pyrite	Quartz, K-feldspar, mica, kaolinite
Pyrite-chlorite	Quartz, K-feldspar, Mica, chlorite, goethite, hematite
Argillic alteration	Quartz, mica, chlorite, kaolinite, plagioclase, calcite
Potassic alteration	Quartz, K-feldspar, mica, kaolinite
Epidote-calcite alt.	Quartz, mica, chlorite, calcite
Carbonate rock	Quartz, calcite, chlorite
Andesite rocks	Quartz, plagioclase, mica, calcite, chlorite

band 5 to band 7 is very low compared to argillic alteration. It is the second highest in albedo after the argillic alteration (Fig. 3.30). The mica and kaolinite are responsible for this absorption at band 7 which is indicated by the chemical analysis of Table 3.19.

The spectra of the potassic alteration and the silicic alteration follows the quartz-sericite-pyrite alteration in the level of albedo. These two spectra are very similar although the chemical composition is different, but because the broad band centre is at 2.2um it is difficult to differentiate between them. The absorption around 0.48um indicates iron oxide, despite the absence of absorption around (0.76um, 0.90um) band 4 (Fig. 3.30).

The spectra of the chlorite and epidote calcite alteration also follow the same trend for the previous described types of alteration, but it expressed weak absorption at band 7, the spectrum of the epidote calcite exhibits the lowest albedo, which may be related to the presence of desert varnish. Most of these rocks are originally andesitic and are dark coloured. The spectrum also shows absorption in band 4 indicating the presence of hematite and a sharp fall off toward 0.48um indicating iron oxide. The iron oxide and chlorite alteration show the same absorption pattern except for the absorption in band 4.

The spectra of the pyrite chlorite alteration exhibit no absorption in band 7, although the chemistry indicates the presence of chlorite, it might be masked by the pyrite and iron oxide (Fig. 3.30 and Table 3.19).

3.4.3.2 Unaltered rocks

These samples were from outside the area which were mapped as an alteration zone. The Wadi sediment which was considered as light target showing the highest albedo but with very weak absorption around 2.2um, (band 7). In contrast it shows strong absorption around 0.48um indicating the presence of iron oxide (Fig. 3.31).

Andesite rocks exhibited the lowest albedo and show a relatively flat spectrum between bands 5 and 7 and fall-off toward the ultraviolet indicating the presence of iron oxides. The spectra of the talus are similar to the spectra of andesite, due to the fact that most of the talus are composed of andesite gravel (Fig. 3.31).

The spectra from rhyolite rocks west of Jabal Almahd exhibit no absorption in bands 5 and 7. In fact, the reflectance increases in band 7. This rock was analysed and the results were presented previously in Table 3.3, the XRD indicated the presence of kaolinite and calcite, which was also detected by spectral features in the laboratory sample. The field spectral data showed no indication of for any other mineral presence at all, this may be explained by the heterogeneity of the lithology.

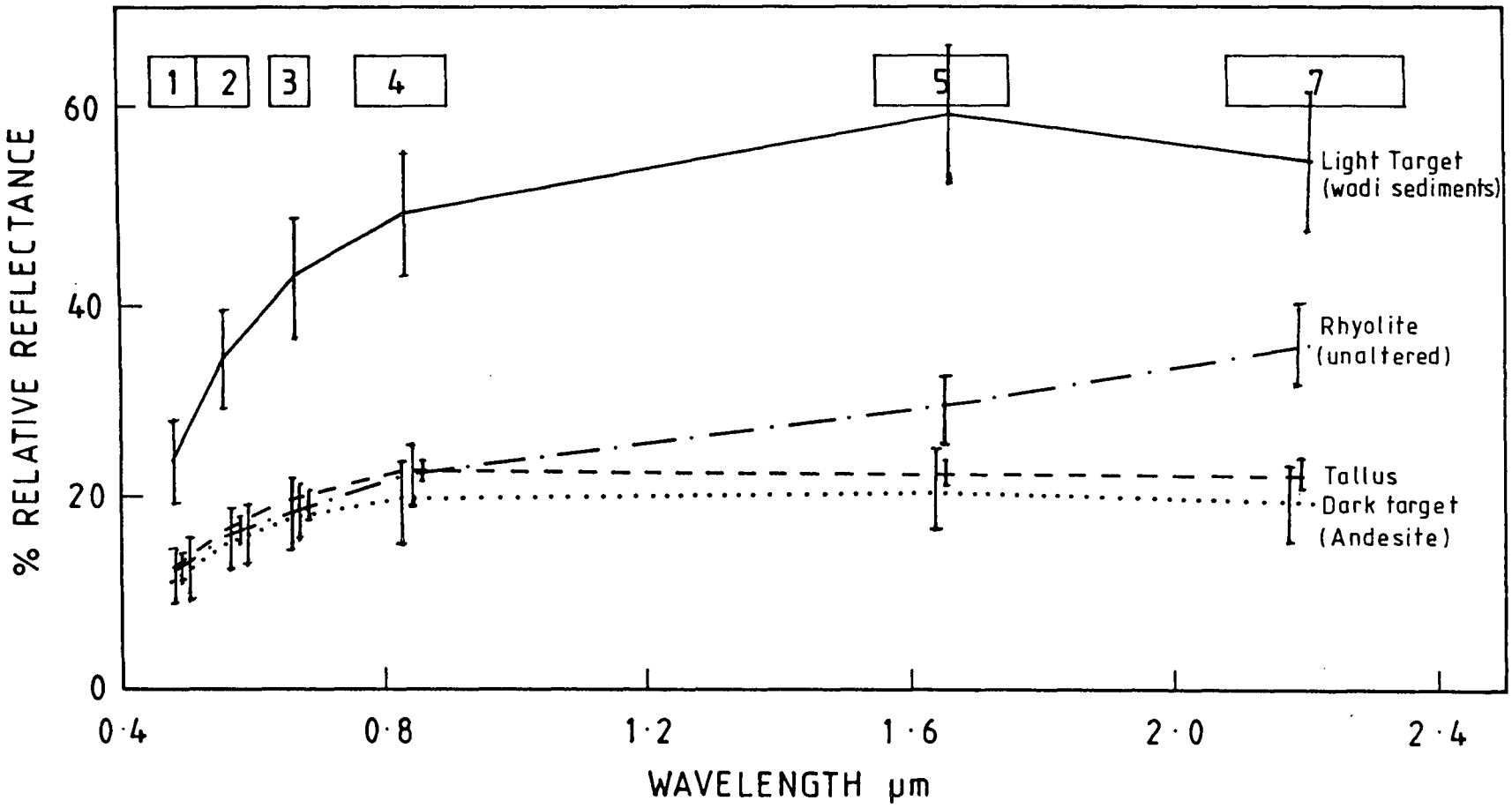

Fig. 3.31 Average HHRR spectra from Mahd Adh Dhahab area.

3.4.3.3 Carbonate rocks

The carbonate rocks display similar features to the alteration rocks between 1.6um and 2.2um (Fig. 3.32). This is due to combinations and overtones of the four fundamental internal vibrations of the planar CO_2-CO_3 ion (Hunt, 1985). Band 7 is a broad band covering the range from 2.08 to 2.35um, centred at 2.2um. This range covers absorption features for clay minerals, as kaolinite at 2.2um or chlorite at 2.33um. The carbonate give absorption features at 2.35um. The result of the laboratory spectra of the sample collected from the location of the carbonate rocks show this feature (Fig. 3.18). The chemical analyses of the samples also does not indicate any other minerals which explains these absorption features observed at band 7 (Table 3.3).

The carbonate rocks exhibit a high albedo compared to some types of alteration units like the potassic and silicic alteration.

The sharp fall-off towards the ultraviolet band (0.48um) indicated the presence of ferric minerals in the carbonate rocks (Hunt & Salisbury, 1971).

3.4.4 Analysis of the ground spectra from Jabal Said

Eighty five locations were selected to acquire ground spectra from Jabal Said using the HHRR. The measurements covered most of the different lithologies in the area (Figure 3.33). Much work was carried out on the

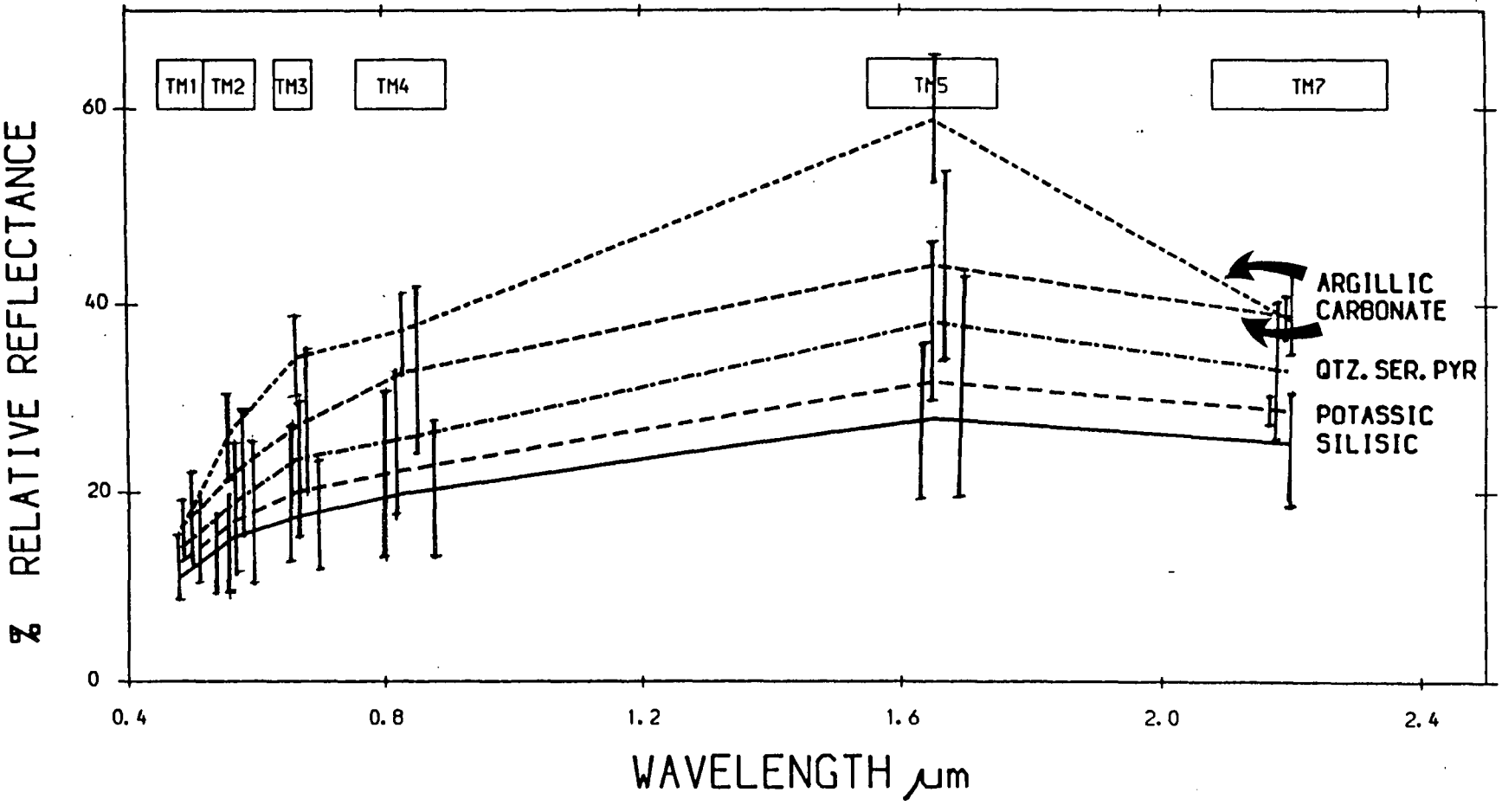

Fig. 3.32 Average HHRR spectra from Mahd Adh Dhahab area.

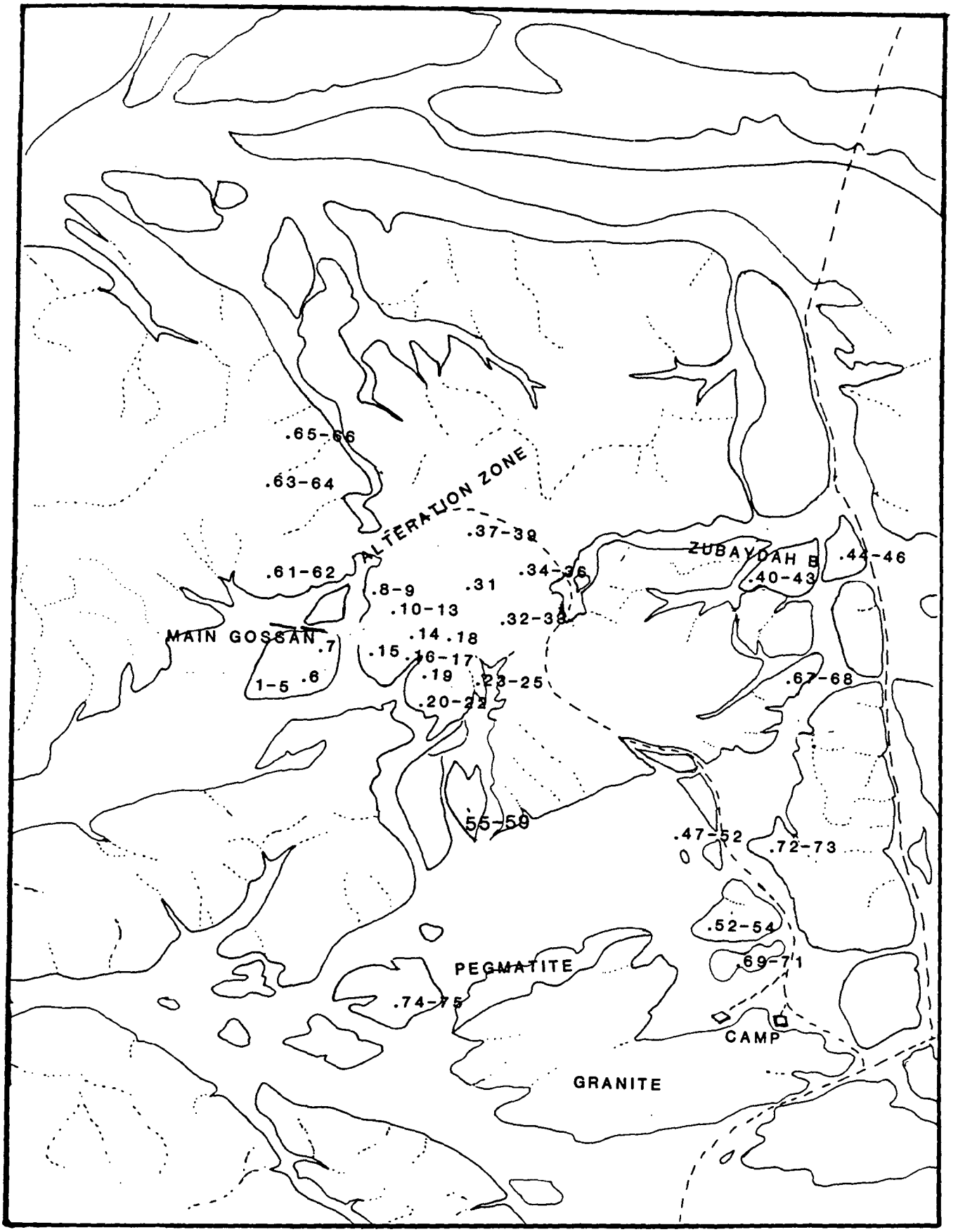

Fig. 3.33 Sketch map shows the location of the HHRR samples in Jabal Said Area.

alteration zone and the gossans, which are the landmark of the area.

The average reflectance spectra and their standard deviations were calculated for each lithological units which are presented in Table 3.20. The average mean of these relative reflectance spectra also plotted against the wavelength.

As in Mahd Adh Dhahab, only the spectra measured by the first six bands, which are equivalent to TM bands from HHRR bands will be discussed in this Chapter. The other four will be discussed in Chapter 7. The following is a description and interpretation of the behaviour of the relative reflectance spectra for each lithology.

3.4.4.1 The gossan

The relative reflectance spectra of the gossan exhibit a strong absorption in the visible range 0.43 to 0.83um, indicating the presence of iron oxides. The absorption around band 4 supports the presence of iron oxide. Fig. 3.34 indicates the presence of the hematite. The spectra have strong reflectance in band 5 and absorption inat band 7. This absorption can have many explanations, but the chemical analysis by XRD diffraction indicates the mineral composition of the gossan (Table 3.9) is predominantly hematite, geothite, quartz and calcite. The absorption at band 7 can be related to the calcium carbonate and possibly the presence of clay

Table 3.20. Mean and standard deviation for six bands of spectral reflectance measured by HHRR for 14 different lithologies in Jabal Said. (Names according to the geologic map).

Lithology	No. of samp	Mean/st. deviation					
		TM1	TM2	TM3	TM4	TM5	TM7
Pegmatite	2	13.6/3	17.6/4	21.5/4	23.9/5	27.2/7	24.7/6
Dacite tuff	2	11.9/2	13.8/2	15.4/2	19.2/5	30.0/15	30.9/13
Volcanic s.s	4	18.1/6	23.4/4	27.9/6	31.9/9	38.9/14	36.1/14
Andesite tuff	2	12.6/2	14.3/2	16.2/1	20.9/0	37.2/4	34.4/3
B. Rhyolite	3	14.6/3	18.6/3	21.8/2	23.7/3	31.4/4	30.9/4
Andesite grav.	6	11.7/4	17.3/2	19.9/2	21.9/3	32.1/4	31.3/1
Quartz gravel	6	21.2/1	29.0/1	35.4/2	38.9/2	45.8/1	48.3/1
Zubaydah B.	4	18.7/2	23.5/3	25.2/3	26.4/3	35.3/2	43.2/1
Andesite B.	2	10.4/2	12.3/2	13.7/3	14.7/2	21.2/5	23.4/5
Diorite	2	13.6/4	16.5/4	18.1/3	22.7/6	34.8/12	31.2/6
Granodiorite	2	16.9/2	17.5/4	19.4/4	20.8.4	28.2/2	21.4/6
Granite	3	20.0/4	25.7/4	29.5/4	32.2/3	35.1/2	38.5/2
Gossan	9	13.0/3	17.4/6	20.5/8	22.5/9	42.3/13	38.2/11
Alteration Z.	28	12.6/3	17.1/6	20.9/7	22.7/8	38.4/13	30.4/9

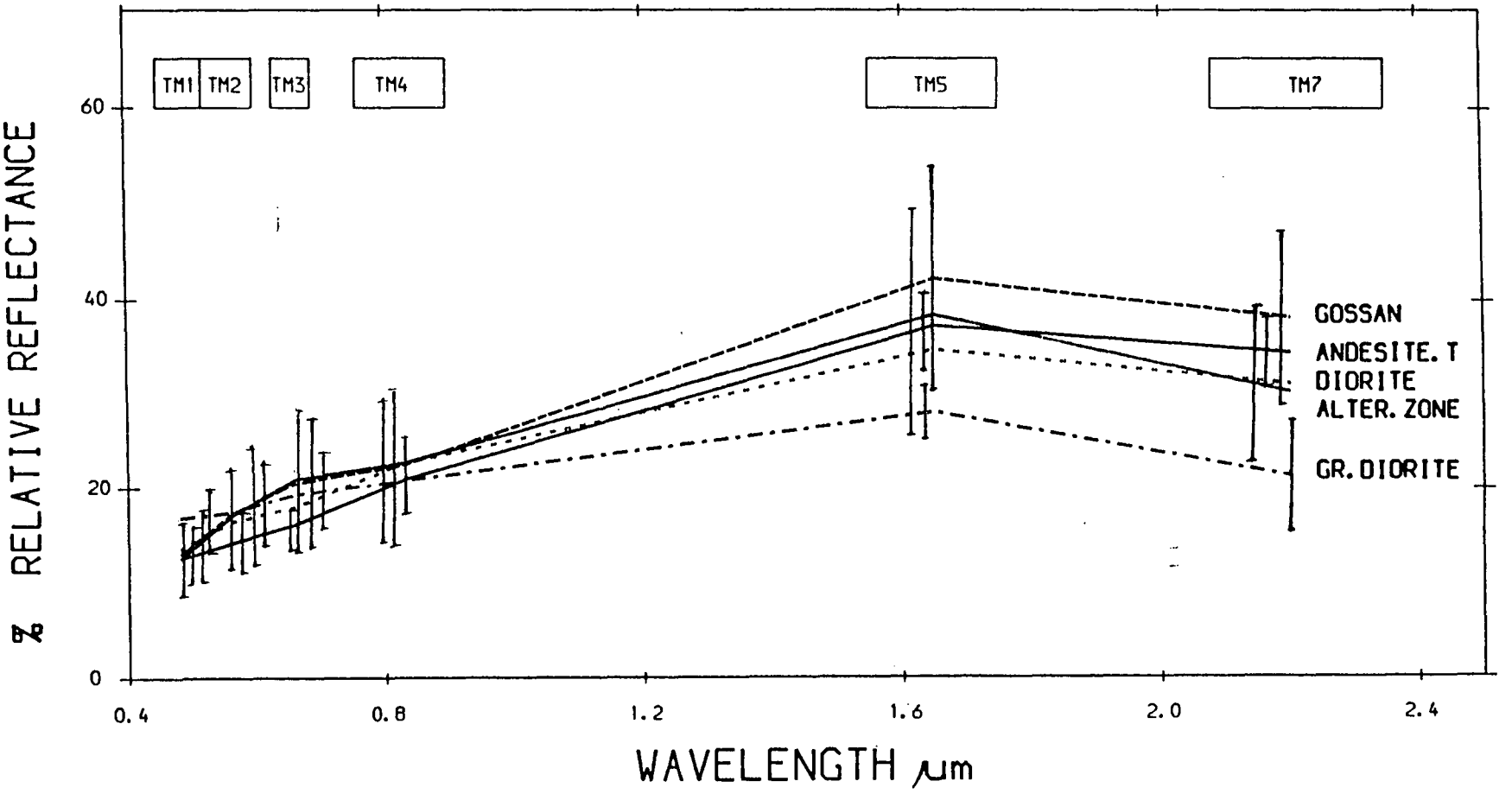

Fig. 3.34 Landsat TM equivalent ground spectra, Jabal Said.

minerals. This is confirmed by the IRIS spectral data for samples from the gossan. The absorption at 2.35um is considered characteristic to carbonate (Fig. 3.20). Part of the gossan is considered to be mainly of limonite with some clay minerals.

3.4.4.2 The alteration zone

The spectra of the alteration zone have the typical overall appearance of intensly altered igneous rocks, as suggested, by a high reflectance in band 5 with a large decrease toward both shorter and longer wavelengths (Hunt & Ashley, 1979). The chemical analysis of some samples from the alteration zone show that hydroxl-bearing minerals are present, such as; chlorite, kaolinite and mica (Table 3.9). The laboratory spectra for samples collected from the alteration zones also show very well-developed absorption in the 2.08 to 2.4um region indicating the presence of the hydroxl-bearing mineral (Fig. 3.19).

The 28 measurements acquired in the area mapped as a hydrothermal alteration zone were recalculated and divided into four groups based on the degree of the bleaching (Table 3.21).

1. strong bleach - mainly clay
2. moderate bleach - mixed clay and iron
3. unbleached - rich in iron
4. iron oxide.

Table 3.21 Mean and standard deviation of the Landsat TM equivalent for different types of alteration in the alteration within the alteration zone.

Lithology	No. of samples	Means/st. deviation					
		TM1	TM2	TM3	TM4	TM5	TM7
Str.Bleach	12	13.6/4	19.2/7	24.9/9	27.4/10	49.5/13	36.8/8
M.Bleach	11	11.6/4	15.9/6	18.8/4	19.9/4	32.4/8	26.9/6
UnBleach	4	13.4/2	16.5/3	18.4/3	20.1/5	31.6/6	27.2/6
Iron Oxides	2	11.5/2	14.9/3	17.2/3	18.4/4	30.3/7	25.5/5

A separate curve was plotted for each type (Fig. 3.35). The strong bleach exhibited the highest albedo and lowest absorption at 2.2um and 0.87um. This was followed by the unbleached and the moderate bleach, which almost overlapped and showed less absorption around 2.2 and 0.87um compared to the strong bleach. The iron oxide has the lowest albedo and the sharp fall-off toward the 0.4um.

3.4.4.3 Diorite and granodiorite

The spectra of the diorite and granodiorite exhibited a low albedo compared to alteration. The chemical composition of diorite shows some amphibole and iron (Fig. 3.8) and the laboratory spectra of the diorite samples exhibited very weak absorption at 2.33um.

The field spectra show weak absorption at band 7 due to the absence of OH-bearing minerals. The sharp fall-off of the granodiorite spectra indicated that this rock has a less amount of iron compared to the diorite.

3.4.4.4 Andesite and dacite tuff

The spectra of andesite and dacite tuff show very weak absorption in band 7 and strong absorption in band 3, followed by sharp fall-off towards the ultraviolet, indicating the presence of iron (Fig. 3.36). The XRD analysis of the andesite tuff shows the presence of chlorite, kaolinite and calcite (Table 3.3) which was confirmed by the results of the laboratory spectra showing absorption features in the range between 2.1 and 2.4um (Fig. 3.22).

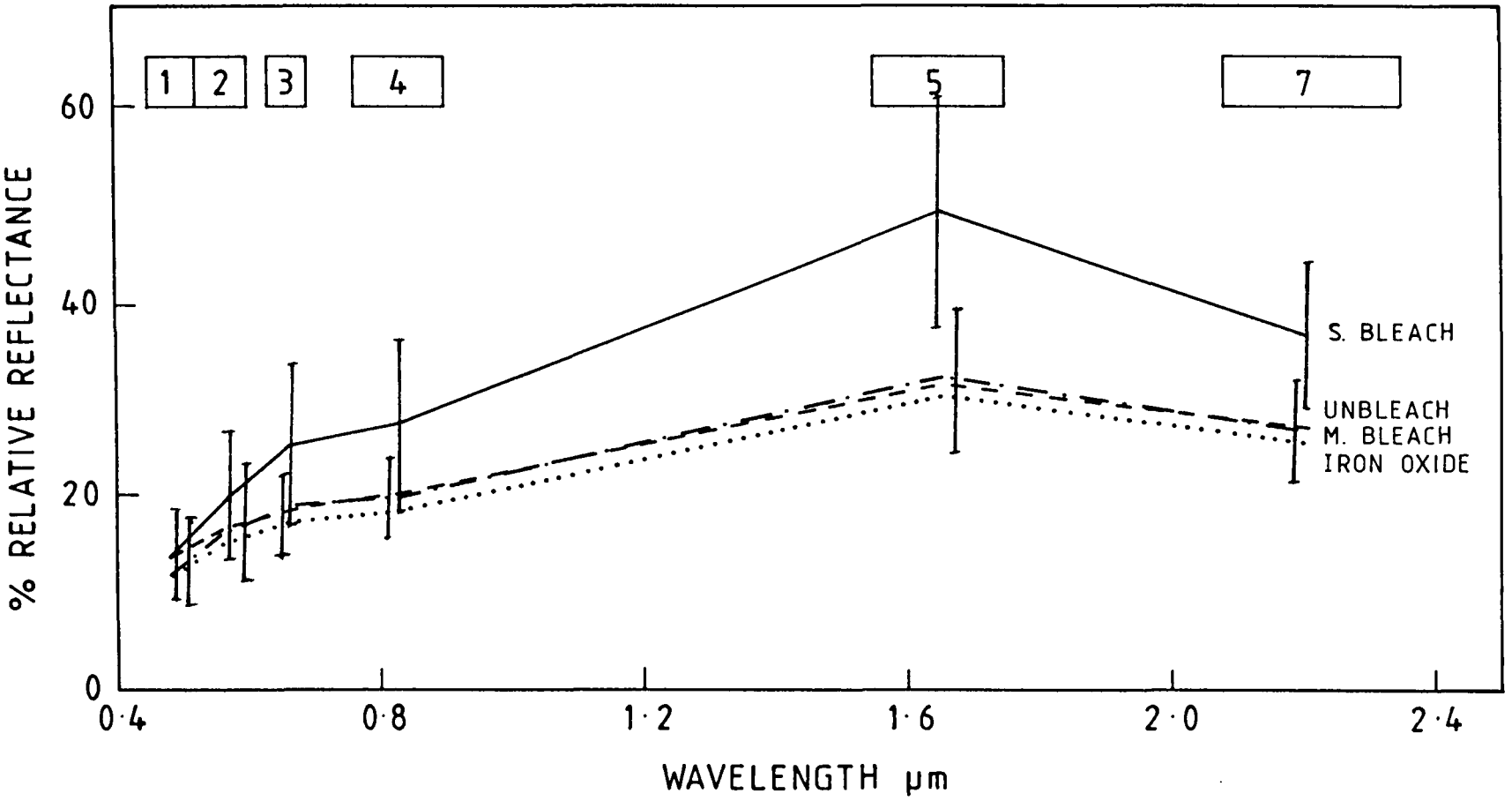

Fig. 3.35 Landsat TM equivalent ground spectra, Jabal Said.

3.4.4.5 The granitic rocks

The granite exhibited no features in band 7, in fact the granite showed a flat spectrum beyond band 4 with the spectra falling off towards band 1. The laboratory spectrum also showed no features.

3.4.4.6 Zubaydah Breccia

This breccia showed an increase in reflectance spectra from band 2 in the visible towards the infrared, a weak absorption feature in band 4 indicating a concentration of iron and a fall-off from band 2 to band 1 (Fig. 3.36). The analysis of this rock showed that it is rich in radioactive minerals, and the laboratory spectrum showed absorption beyond 2.5um (Fig. 3.26).

3.4.4.7 Quartz gravel

The spectrum of the quartz gravel shows the highest albedo among all the measurements made in Jabal Said. It is considered as a light target, exhibiting sharp fall-off towards the 0.4um, with a slight increase in band 7 (Fig. 3.36).

3.4.4.8 Andesitic breccia

This breccia exhibited the lowest albedo, which is considered as a dark target. The spectra had almost no spectral features, with slight increase of the reflectance in band 7 and weak absorption in band 1 (Fig. 3.36).

3.4.4.9 Black rhyolite

The relative reflectance of one type of the rhyolite was measured by HHRR. This is the black rhyolite (see the

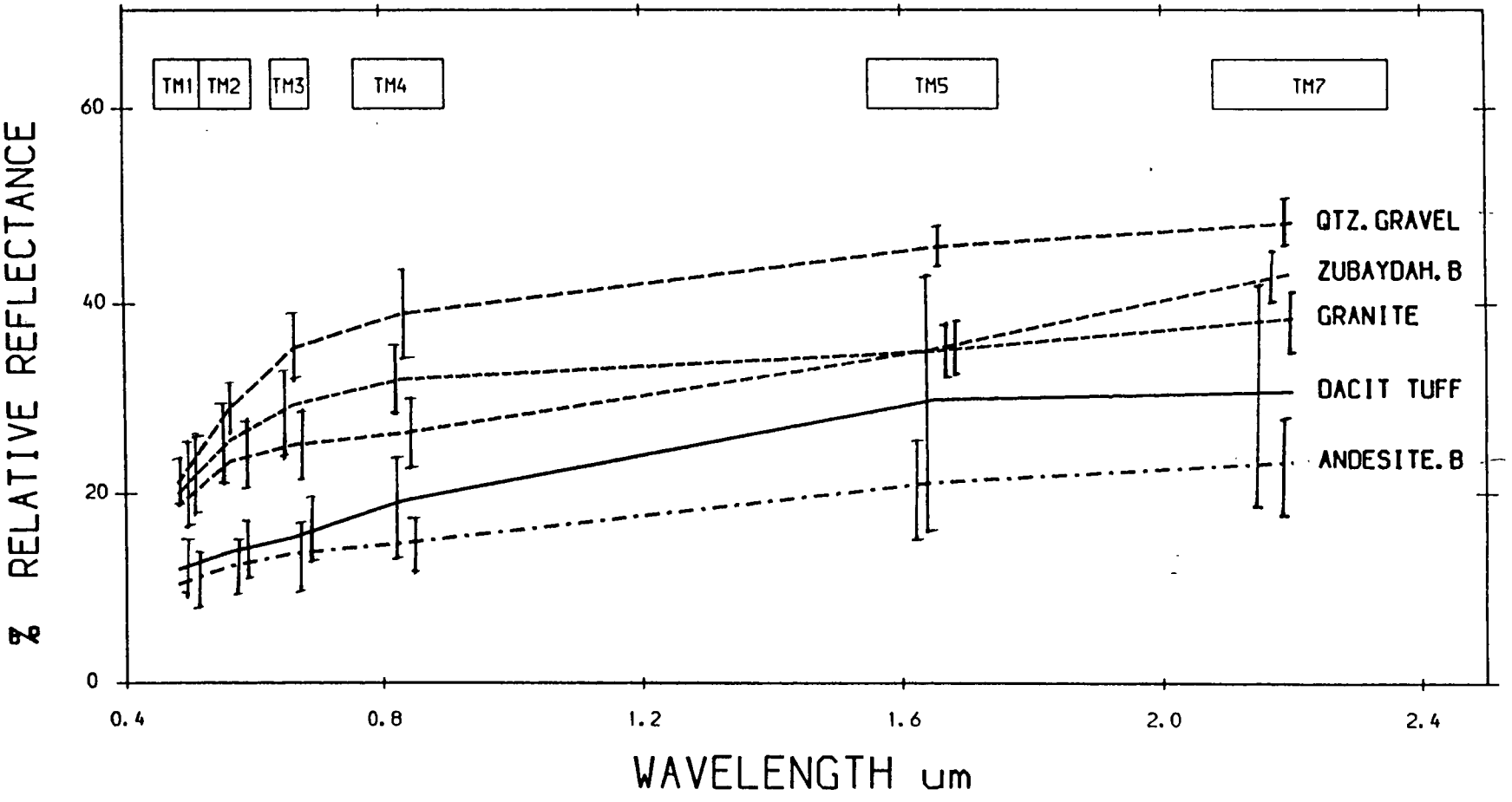

Fig. 3.36 Landsat TM equivalent ground spectra, Jabal Said.

geologic map). The spectrum exhibited spectral features in band 4 and sharp fall-off towards band 1, indicating the presence of iron, higher reflectance in band 5, but no absorption features in band 7 (Fig. 3.37). This was confirmed by the geochemical analysis presented earlier in Table 3.9 and also the result of the laboratory spectrum where no significant absorption features were recorded beyond 2.0um (Fig. 3.24b).

3.4.4.10 Andesitic gravel

This andesitic gravel gave a spectrum similar to the black rhyolite but without absorption features in band 4 (Fig. 3.37).

3.4.4.11 Pegmatite

The pegmatite rocks are dark in colour, the spectrum exhibited fall-off to band 1, reflectance in band 4 and 5, and less reflectance in band 7 (Fig. 3.37).

3.4.4.12 Volcanic sediments

This unit was composed of volcanic sediments and conglomerates. The spectrum showed a fall-off towards the ultraviolet indicating the presence of iron oxide. High reflectance in band 5 and weak spectral features in band 7 indicate the presence of calcite or chlorite (Fig. 3.37). This was confirmed by the chemical analysis (Table 3.9). Most of the laboratory spectra from this unit show no spectral absorption features between 2.0um and 2.4um, except one sample which showed a spectral absorption at 2.35um indicating the presence of carbonate (Fig. 3.25).

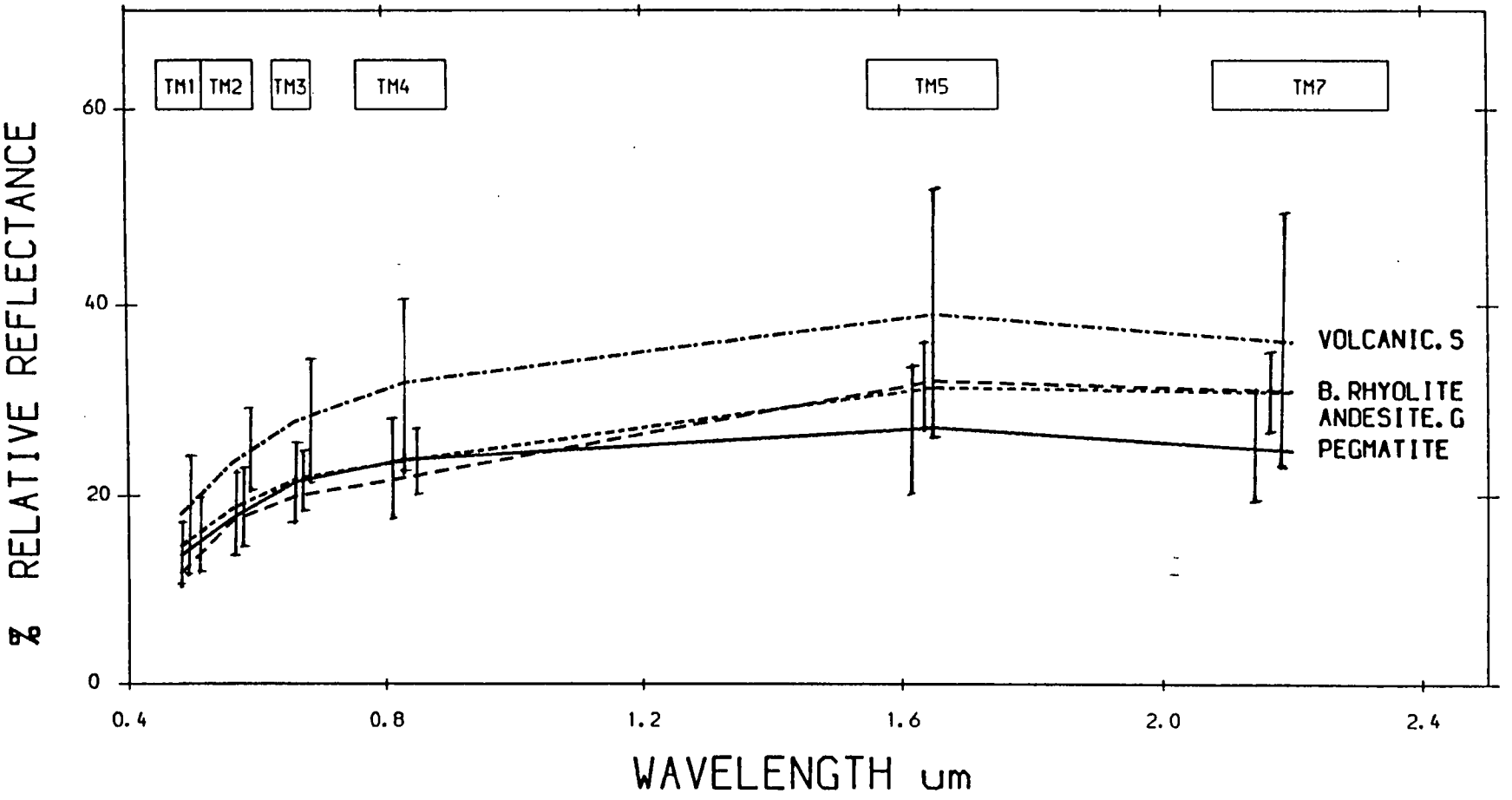

Fig. 3.37 Landsat TM equivalent ground spectra, Jabal Said.

3.5 Summary and Conclusions

The lithologies of the Mahd Adh Dhahab and Jabal Said areas comprise a complex mixture of materials having various physical and chemical properties which determined their spectral response characteristics. From the results presented in this Chapter, it is clear that certain parameters, either physical or chemical affect the variation in spectral reflectance between different materials.

The results of chemical and spectral analysis of the altered and unaltered rocks showed that some general differences exist. In general, the altered rocks contain a higher concentration of clay minerals than the unaltered rocks. This has implications for the performance capability of broadband sensors such as Landsat TM or any other sensor used to differentiate the altered rocks from the unaltered.

In the Mahd Adh Dhahab area the study concentrated on the discrimination between different types of alteration within the alteration zone and also the discrimination between the altered and unaltered rocks. The results of the XRD and XRF analysis showed considerable variation among the different zones of alteration based on their mineral compositions. Most of the rocks were affected by desert varnish, and some of these rocks showed change of in chemistry of the bulk of the rock and its weathered

surface, especially in the amount of iron oxide or the amount and type of the clay minerals present.

In certain cases there is no apparent difference between the bulk mineralogy and the surface mineralogy. The laboratory spectra from Mahd Adh Dhahab samples indicate that many of the materials in the different alteration zones exhibit diagnostic spectral features associated with clay minerals, such as kaolinite and chlorite. In fact, the laboratory spectra can differentiate between the alteration type based on their spectral features.

In Jabal Said area the study concentrated on the discrimination between different types of lithologies in the area and variation associated with the gossan and the massive sulphide. The result of the X-ray analysis indicate mineral variation for most of the lithologies in the area. Mineral variation between the weathered surface and the original rock itself was also noticed, though in some cases no apparent difference was noticed.

The results of the field spectra from both areas of Mahd Adh Dhahab and Jabal Said showed some diagnostic spectral features using the broad band sensor, especially to permitting differentiation between the altered rocks and unaltered rocks. The Laboratory spectra and the chemical analysis support the interpretation of the field spectra. The broad band spectra cannot really show detailed mineral variation especially in Band 7, centred

on 2.2um covering a wide range of spectral features for different types of minerals.

These results suggest that the Landsat TM and the airborne ATM sensor, may be able to discriminate between many of the lithologies based on their spectral features. Discriminatory power is limited because the broad band, especially band 7, covered the range from 2.08 to 2.35um, and centred at 2.2um where most of the spectral features related to altered rocks and their mineralsare located; also carbonate rocks show spectral features at 2.35um.

Preprocessing and preparation of multispectral remote sensing data is necessary for comparing different types of data. This will be discussed in Chapter 4.

CHAPTER 4

PRE-PROCESSING AND PREPARATION OF MULTISPECTRAL REMOTE SENSING DATA

4.1 Introduction

The sensors data in their raw DN forms, have no physical meaning and contain various effects due to different reasons; (e.g. variation in atmosphere, and in instrument response).

In order to provide a quantitative assessment of the ability of the different sensor systems for lithological mapping purposes and identification of the alteration zones, it is necessary to preprocess the digital data to render it into a form where comparisons can be made on a quantitative basis.

Chapter 3 described the techniques for the conversion of field spectral data, acquired in situ, to measure relative reflectance.

This chapter is concerned with the techniques used in calibration and correction of the airborne and satellite multispectral data used to measure ground equivalent reflectance. A description of the techniques and methods used in converting the data to ground equivalent reflectance is provided.

The steps described here were essential if comparisons were to be made between different data sets, acquired at different times using different instruments.

In order to study impact of the spatial resolution of MSS data for lithological discrimination and extracting of geological information, the data have to be calibrated to

a common reference. In this particular study a broad band ground spectral data equivalent to the spectral bands collected by TM sensors were used.

In addition an across track shade correction was applied to the ATM data because of its wide scan angle to remove the effects of systematic differences in brightness across the scene. The steps for calibration and correction are summarised in Fig. 4.1.

4.2 Airborne and satellite data set

The area of Mahd Adh Dhahab and Jabal Said are both covered by the same satellite data set (Landsat TM path 169, row 044, acquired on 17th July 1984). Although the area of Mahd Adh Dhahab and Jabal Said was covered by the same scene, a calibration curve was calculated separately for each district. This was done primarily for the purpose of comparing the satellite data (TM) with the ATM data.

The Landsat TM has seven bands, only six have been used in this study, the thermal band was not included. A list of the bands and their wavelength cover are summarised in Table 4.1. No consideration was given to the calibration of the thermal bands in TM or ATM.

The airborne data sets for Mahd Adh Dhahab and Jabal Said were acquired in March 1984, by the Daedalus Scanner (AADS 1268), by the Arabian Aerosurvey & Hunting Geophysical Company Ltd., with 11 band cover, 10 bands in visible, and shortwavelength infrared. Table 4.2 summarises the wavelength covered by each ATM band. Band

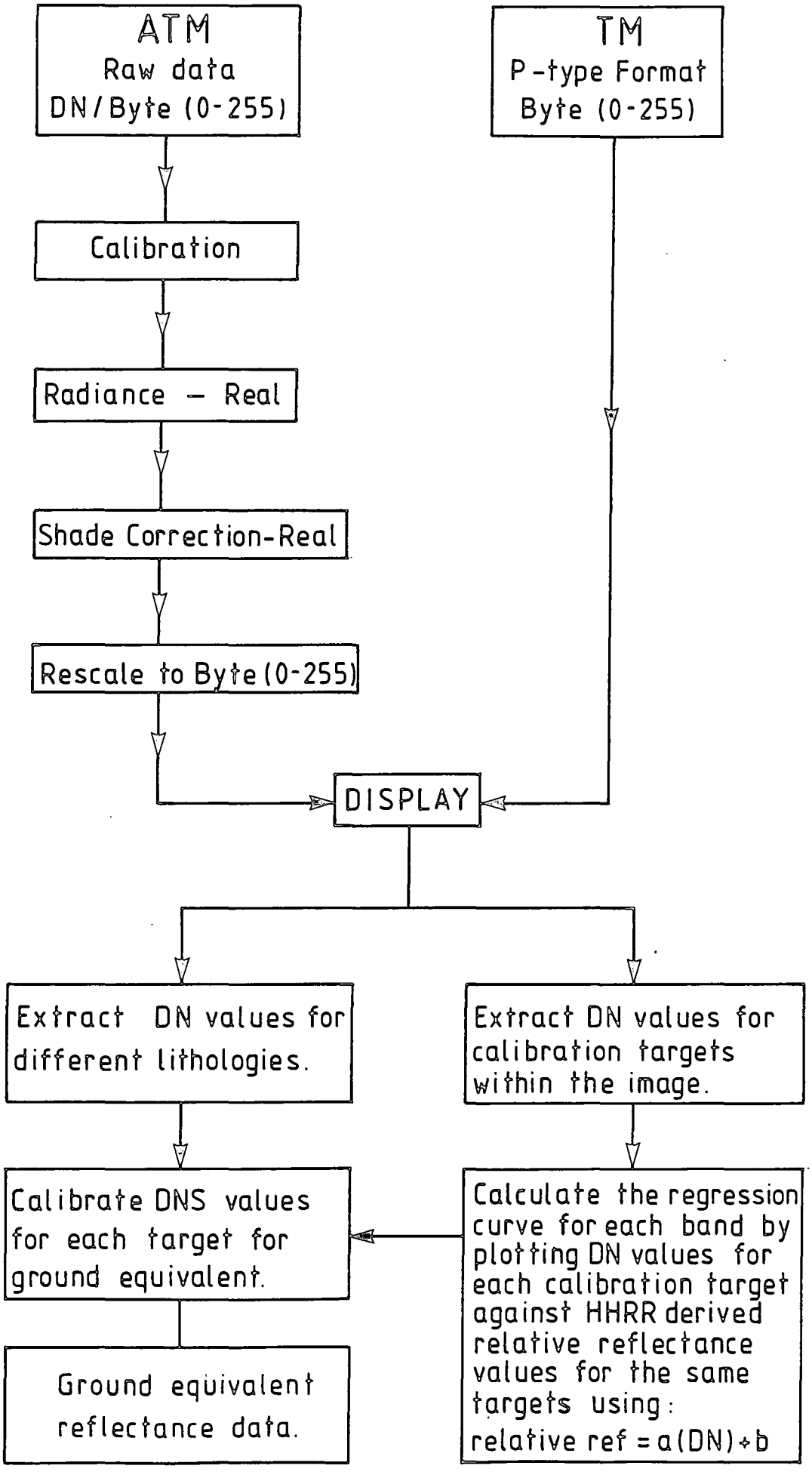

Fig. 4.1 A flow chart explaining the process of calibration for the data used in this study.

Table 4.1 Landsat TM bands and wavelengths

Band	Wavelength in Micron
Band 1	0.45-0.52
Band 2	0.52-0.60
Band 3	0.63-0.69
Band 4	0.76-0.90
Band 5	1.55-1.75
Band 7	2.08-2.35
Band 6	10.40-12.50

Table 4.2 ATM bands and their wavelengths.

Band	Wavelength in Micron
Band 1	0.42-0.45
Band 2	0.45-0.52
Band 3	0.52-0.60
Band 4	0.605-0.625
Band 5	0.63-0.69
Band 6	0.695-0.75
Band 7	0.76-0.90
Band 8	0.91-1.05
Band 9	1.55-1.75
Band 10	2.08-2.35
Band 11	8.50-13.00

one was not included in the study because it was badly transcribed from the HDDT's to CCT's.

4.3 Radiometric Calibration of ATM data

Radiometric calibration of ATM data transforms the digital numbers recorded by the scanner into radiance values. This is necessary to preserve inter-band relationships required for quantitative analysis. Fig. 4.2 shows instrument and atmospheric effects in the raw data prior to any type of calibration. Calibration is defined by the following relationship.

$$\text{Radiance}\,\lambda = \text{gain}\,\lambda\,(\text{DN}\,\lambda - \text{offset}\,\lambda)$$

Where the gain and offset parameters are determined separately for each band pass.

The ATM data have a fixed gain and offset for each bandpass. These were determined in the laboratory for a range of gain settings on the 21st December 1983 (Table 4.3) (Wilson, 1986). The gain settings for each band can be varied. These are commonly determined by the scanner operator at the commencement of each flight line in order to maximise the dynamic range of the data in each bandpass. Therefore calibration from DN to radiance has to take account of these.

The following calibration relationship was used:

$$\text{Gain G}\,\lambda = \text{Gain}\,\lambda/\text{Gain setting}$$
$$\text{offset G}\,\lambda = \text{offset}\,\lambda \times \text{Gain setting}$$

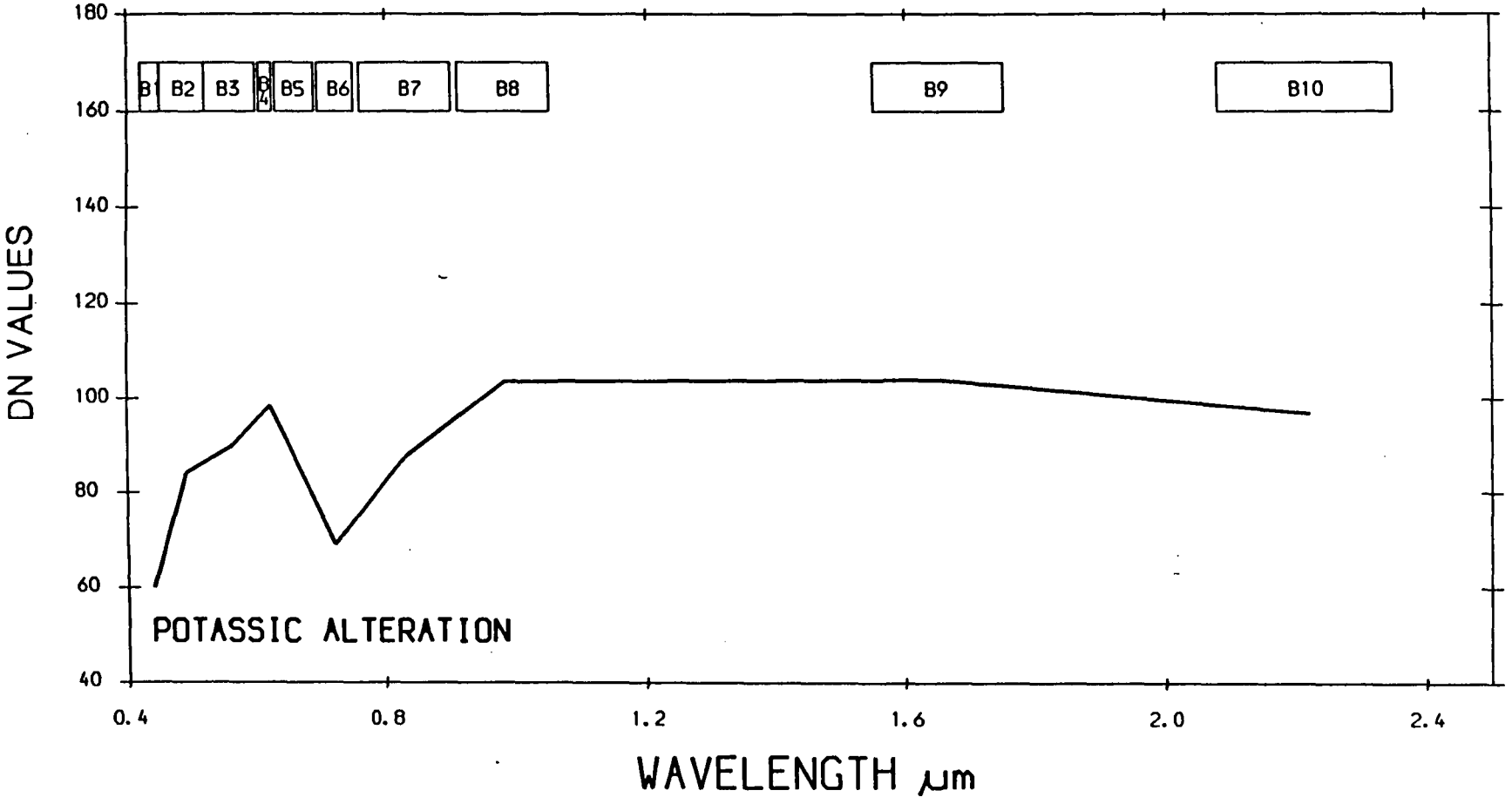

Fig. 4.2 Average ATM 1000m DN value, no. calibration & shade correction, Mahd Adh Dhahab.

Table 4.3 The gain and offset values derived from the laboratory calibration of the ATM Scanner prior to the flight.

Band	Gain	Offset
1	0.96	2.24
2	0.5831	4.16
3	0.7170	5.50
4	1.4221	4.35
5	0.4371	4.86
6	0.8053	5.50
7	0.4782	5.57
8	1.3517	4.99
9	0.2704	4.54
10	0.0731	5.63

Provided by Hunting (1984).

Radiance = Gain G λ (DN λ - offset G λ)

where G = corrected value for gain setting.

The value of the Gain G λ and the offset were calculated for each band and are presented in Table 4.4 These were then applied to the ATM data covering the study areas. Fig. 4.3 shows the ATM data after it is calibrated to radiance, notice that the instrument settings changes the shape of the spectral curve on calibration to radiance units. However, atmospheric effects remain.

Examination of the airborne data after calibration revealed an additional effect which has to be corrected prior to data analysis and interpretation. This is known as cross-track shading and is due to large scene angle and sun sensor geometry (Irons & Labovitz, 1982).

4.4 Shade Correction for ATM data

One of the major problems experienced when working with ATM data is the evidence of a cross-track shading within the scene. This can be caused by a combination of atmospheric, surficial and scanner effects which result in systematic differences in scene brightness, approximately orthogonal to the direction of flight (Donoghue & Hook, 1986). These cross-track shading effects must be removed before any quantitative comparison of spectral vectors across the image. Fig. 4.4 illustrates this effect for ATM data before any correction.

The severity of this across-track shading can be observed by plotting the column means of every 10 pixels

Table 4.4 Shows the calculated corrected gain settings and offsets for each band.

Band	Gain setting	Gain G	Offset G
1	2.0	0.48	4.48
2	1.0	0.583	4.16
3	1.0	0.717	5.50
4	2.0	0.71105	8.70
5	1.0	0.7371	4.86
6	1.0	0.8053	5.50
7	1.0	0.4782	5.57
8	4.0	0.337925	19.96
9	2.0	0.1352	9.08
10	2.0	0.03655	11.26

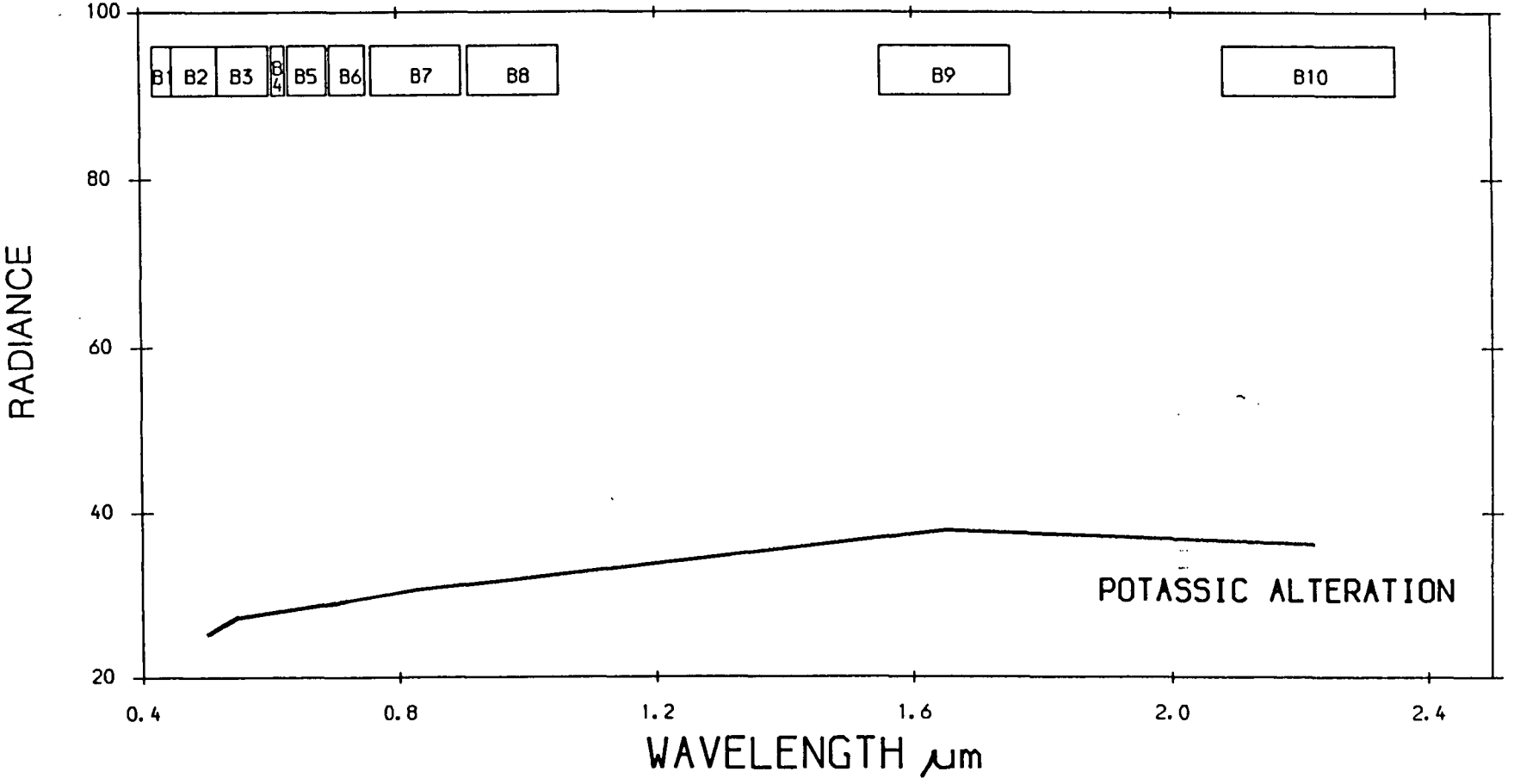

Fig. 4.3 Calibrated ATM Data 1000m M. Res. 2.5m, Mahd Adh Dhahab.

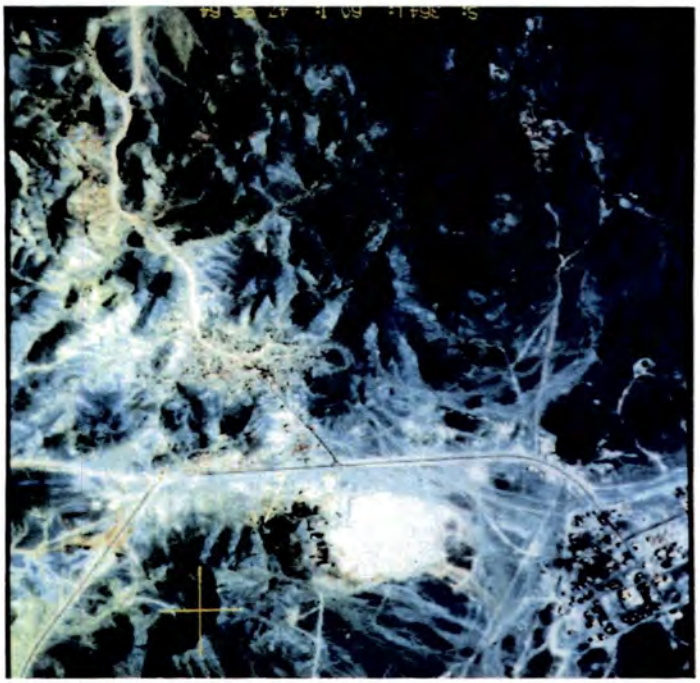

Fig. 4.4 Affect of the across track shading in ATM data (Mahd Adh Dhahab).

across the image. Fig. 4.5 shows the effect of across-track shading on calibrated ATM data from 3000m for some spectral bands. In some parts of the scene, in particular towards the centre, the effect of the across-track shading was not visually apparent, however the column means indicate that it is still present. Also, this figure indicates that there is a wavelength dependency in the shading process, where shorter wavelengths are most severely affected.

Similar patterns were observed in the raw radiance ATM data acquired from different heights from both Mahd Ahd Dhahab and Jabal Said areas, and these had to be shade corrected before analysing the data.

The correction method for across-track shading makes several assumptions:

i) that column means are equal, and

ii) that there is minimum shading at nadir.

The procedure used here for correcting the cross-track shading is as follows:

$$Sij = \frac{\sum_{i}^{nadir} \times j\lambda / C_{Samps}}{\sum_{j}^{h\ raws} \times ij\lambda / C_{Samps}}$$

S = shading coefficient

λ = wavelength

i = column

j = row

nadir = central column

Csamps = no. of pixels in each column of scene

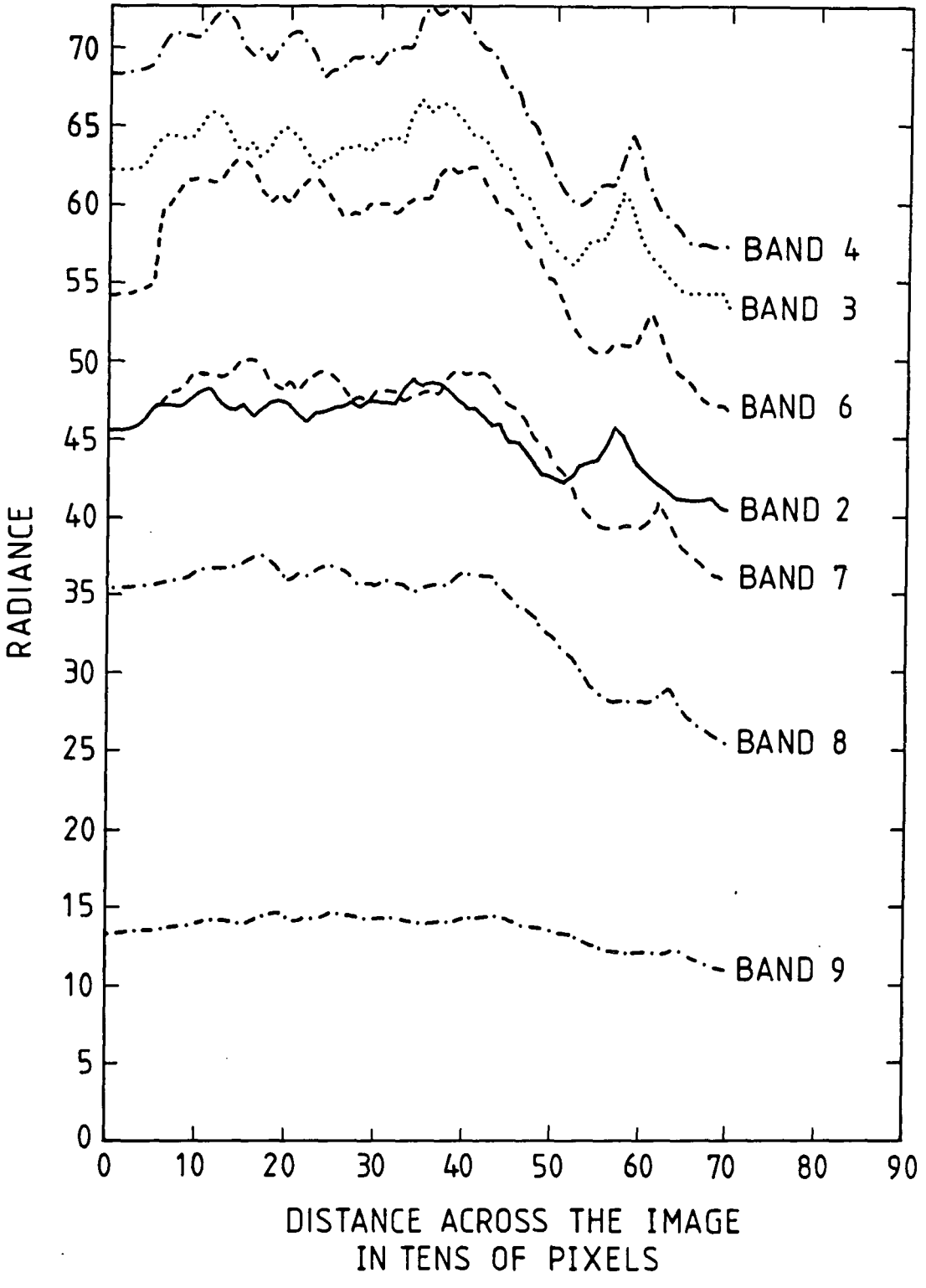

Fig. 4.5 Effect of across-track shading on calibrated ATM 3000m data from Mahd Adh Dhahab area.

This algorithm was applied to all ATM data sets in this study. The effect of removing this across-track shading is illustrated in Figs. 4.6, 4.7.

4.5 Calibrating airborne satellite remotely sensed data to ground equivalent reflectance.

4.5.1 Introduction

The ATM data from both the Mahd Adh Dhahab and Jabal Said areas were obtained from three different heights, 3000m, 2000m and 1000m. The TM data for the same area was obtained from a height of 720km.

Accurate and quantitative interpretation of airborne multispectral data requires the data are corrected for radiometric effects. These include sensor related effects (e.g. calibration) and scene related effects due to atmospheric and geometric relationships of the sun, sensor and target (Hook & Donoghue, 1988). In order to allow inter-scene comparison from different dates, the radiance data were calibrated against ground reflectance measurements acquired using the HHRR.

4.5.2 Correction procedure

The technique applied here required the identification of pixel areas on the image, which can be clearly identified on the ground, for which ground reflectance data have been collected in the spectral channels of interest. Only five targets were used in each area as a calibration target. Bidirectional ground reflectance measurements were made within each selected target area

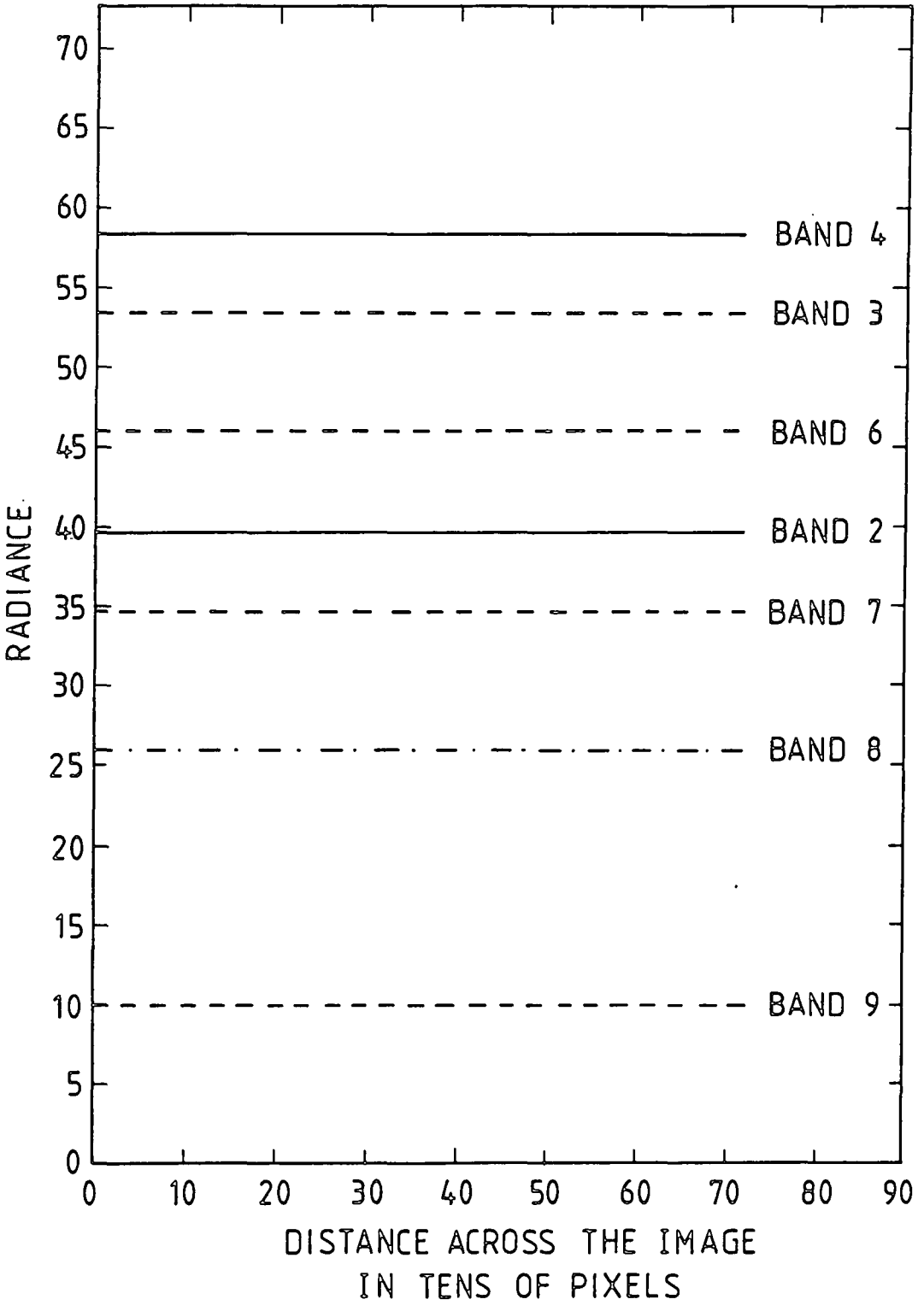

Fig. 4.6 Data corrected of across track shading calibrated ATM 3000m data from Mahd Adh Dhahab area (compare with Fig. 4.5).

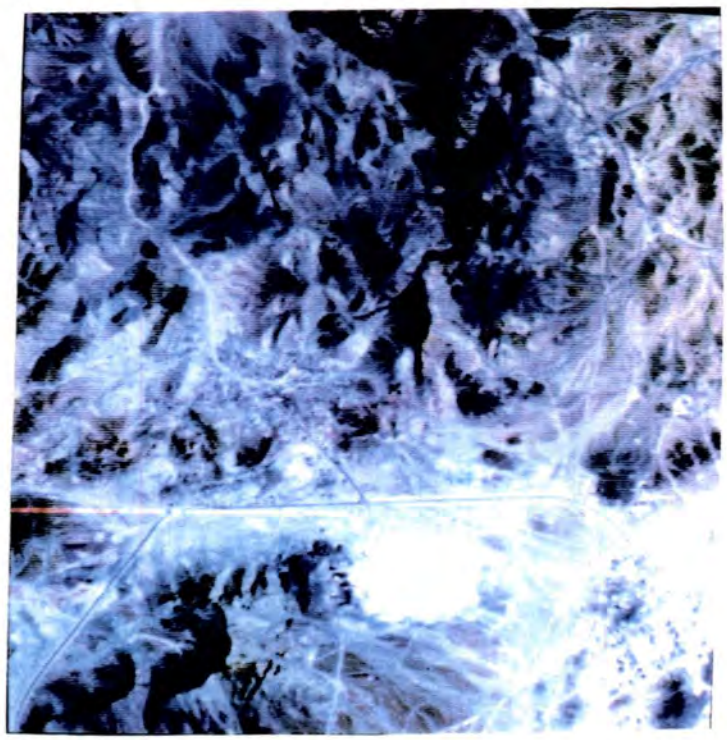

Fig. 4.7 Effect of the calibration on the across-track shading (after correction). Compare with Fig. 4.4.

using the HHRR. This has six filters that match the spectral coverage of TM bands (Appendix C).

These field measurements were acquired during January and February 1987.

In order to permit quantitative inter-scene comparison, the DN values collected from TM and ATM images were transformed using an empirically derived linear equation:

$$GER = a.\ DN + b$$

where

GER = Ground equivalent reflectance

DN = Digital values extracted from the image

a = constant

b = constant

(After Gillespie & Kahl, 1977; Conel et al., 1985)

4.5.3 Calibrating ATM digital data to relative reflectance (ground reflectance)

The correction procedure mentioned above was applied to the ATM data from the three different heights separately for both of the study areas, Mahd Adh Dhahab and Jabal Said.

Five calibration targets from each site were chosen to calculate the calibration curve for each height of the data. A digital value for each site was extracted from the shade corrected ATM images covering each of the two study areas, and these are presented with the bidirectional ground reflectance measurement (Tables 4.5 to 4.10).

Table 4.5 Summary of ATM-1000m (IFOV = 2.5m). DN value and equivalent TM band reflectance measured by HHRR, for the five lithologies used as calibration targets, Mahd Adh Dhahab area.

Lithology	ATM 2		ATM 3		ATM 5		ATM 7		ATM 9		ATM10	
	ATM	HHRR	ATM	HHRR	ATM	HHRR	ATM	HHRR	ATM	HHRR	ATM	HHRR
Wadi sediment	75.4	22.7	80.6	34.1	83.7	42.2	84.7	48.8	76.4	58.8	80.0	54.1
Andesite 1	47.5	11.9	42.8	15.2	40.8	17.8	39.8	19.7	34.4	20.3	35.2	18.9
Silicic alt.	46.7	11.0	44.9	15.2	43.8	17.4	42.0	19.9	48.7	27.9	43.2	25.2
Potassic alt.	37.2	12.6	32.2	16.9	29.9	20.1	30.6	22.4	37.9	31.9	36.2	28.8
Andesite 2	46.8	9.4	45.4	12.0	46.0	14.4	45.3	14.2	36.9	18.8	35.7	17.1

Table 4.6 Summary of ATM-2000m (IFOV=5.0m) DN value and equivalent TM band reflectance measured by HHRR, for the five lithologies used as calibration targets, Mahd Adh Dhahab area.

Lithology	ATM 2		ATM 3		ATM 5		ATM 7		ATM 9		ATM10	
	ATM	HHRR	ATM	HHRR	ATM	HHRR	ATM	HHRR	ATM	HHRR	ATM	HHRR
Wadi sediment	82.3	22.7	89.9	34.1	94.8	42.2	95.9	48.8	88.8	58.8	92.7	54.1
Andesite 1	50.8	11.9	46.1	15.2	44.3	17.8	44.6	19.7	39.6	20.3	40.8	18.9
Silicic alt.	41.4	11.0	41.0	15.2	41.2	17.4	39.8	19.9	42.1	27.9	39.3	25.2
Potassic alt.	54.0	12.6	52.5	16.9	48.4	20.1	45.2	22.4	48.8	31.9	46.2	28.8
Andesite 2	51.1	9.4	49.8	12.0	50.6	14.4	50.7	14.2	51.4	18.8	41.9	17.1

Table 4.7 Summary of ATM-3000m (IFOV=7.5m) DN value and equivalent TM band reflectance measured by HHRR, for the five lithologies used as calibration targets, Mahd Adh Dhahab area.

Lithology	ATM 2		ATM 3		ATM 5		ATM 7		ATM 9		ATM10	
	ATM	HHRR	ATM	HHRR	ATM	HHRR	ATM	HHRR	ATM	HHRR	ATM	HHRR
Wadi sediment	74.7	22.7	82.7	34.1	87.5	42.2	89.0	48.8	83.0	58.8	84.0	54.1
Andesite 1	50.7	11.9	47.0	15.2	45.0	17.8	45.0	19.7	40.5	20.3	41.0	18.9
Silicic alt.	46.2	11.0	45.8	15.2	46.3	17.4	44.7	19.9	47.2	27.9	43.7	25.2
Potassic alt.	58.2	12.6	57.2	16.9	54.7	20.1	51.5	22.4	54.8	31.9	52.3	28.8
Andesite 2	46.2	9.4	44.2	12.0	44.2	14.1	44.2	14.2	35.8	18.8	35.3	17.1

Table 4.8 Summary of ATM-1000m (IFOV=2.5m) DN value and equivalent TM band reflectance measured by HHRR, for the five lithologies used as calibration targets, Jabal Said area.

Lithology	ATM 2		ATM 3		ATM 5		ATM 7		ATM 9		ATM10	
	ATM	HHRR	ATM	HHRR	ATM	HHRR	ATM	HHRR	ATM	HHRR	ATM	HHRR
Andesite tuff	54.33	12.6	47.5	14.3	44.83	16.2	49.83	20.9	77.0	37.2	81.5	34.4
Andesite grav.	62.5	11.7	59.5	17.3	59.5	19.9	60.3	21.9	51.5	32.1	53.2	31.3
Quartz gravel	101.3	21.2	105.2	29.0	107.3	35.4	105.0	38.9	98.83	45.8	106.5	48.3
Pegmatite	74.3	13.6	71.3	17.6	73.5	21.5	72.3	23.9	64.2	27.2	60.83	24.7
Dacite tuff	68.83	11.9	66.2	13.8	64.83	15.4	66.0	19.2	69.2	30.0	73.83	30.9

Table 4.9 Summary of ATM-2000m (IFOV=5.0m) DN value and equivalent TM band reflectance measured by HHRR, for the five lithologies used as calibration targets, Jabal Said area.

Lithology	ATM 2		ATM 3		ATM 5		ATM 7		ATM 9		ATM10	
	ATM	HHRR	ATM	HHRR	ATM	HHRR	ATM	HHRR	ATM	HHRR	ATM	HHRR
Andesite tuff	54.3	12.6	47.5	14.3	44.8	16.2	49.8	20.9	77.0	37.2	81.5	34.4
Andesite grav.	62.5	11.7	59.5	17.3	59.5	19.9	60.3	21.9	51.5	32.1	53.2	31.3
Quartz gravel	101.3	21.2	105.2	29.0	107.3	35.4	105.0	38.9	98.8	45.8	106.5	48.3
Pegmatite	74.3	13.6	71.3	17.6	73.5	21.5	72.3	23.9	64.2	27.2	60.8	24.7
Dacite tuff	68.8	11.9	66.2	13.8	64.8	15.4	66.0	19.2	69.2	30.0	73.8	30.9

Table 4.10 Summary of ATM-3000m (IFOV=7.5m) DN value and equivalent TM band reflectance measured by HHRR, for the five lithologies used as calibration targets, Jabal Said area.

Lithology	ATM 2		ATM 3		ATM 5		ATM 7		ATM 9		ATM10	
	ATM	HHRR	ATM	HHRR	ATM	HHRR	ATM	HHRR	ATM	HHRR	ATM	HHRR
Andesite tuff	71.7	12.6	67.5	14.3	64.8	16.2	66.7	20.9	87.0	37.2	88.8	34.4
Andesite grav.	78.8	11.7	76.3	17.3	75.5	19.9	74.5	21.9	85.2	32.1	84.0	31.3
Quartz gravel	103.2	21.2	105.2	29.0	107.3	35.4	107.2	38.9	100.8	45.8	107.3	48.3
Pegmatite	86.2	13.6	85.3	17.6	84.2	21.5	86.0	23.9	76.7	27.2	75.8	24.7
Dacite tuff	73.3	11.9	70.7	13.8	69.5	15.4	71.7	19.2	76.2	30.0	83.7	30.9

Based on the data presented in these tables a linear equation: y = a (DN) + b was derived from least-square fit of DN versus band-averaged reflectance for each band, (Table 4.11 to 4.16). Calibration curves were produced for each of the three resolutions, from the two test sites and are shown in Figs. 4.8 to 4.13.

The correlation coefficients listed in Tables 4.11-4.16 show some variance in data from 3000m with 7.5m IFOV resolution greater than 0.93 in both sites, while the data from 1000m (2.5m resolution) gives a coefficient of 0.88. These are strong correlations, which suggest that the atmospheric, instrument and processing factors combine linearly in all bands.

The calibration values were used to calibrate the radiance data extracted for selected lithologies to relative reflectance. A comparison between the ground relative reflectance for some lithologies (Fig. 4.14) and the calibrated ATM data from other lithologies (Fig. 4.15) show very high similarities which indicate that targets measured in the field are representative of the measurements made by the ATM sensor. Comparing Figs. 4.14 and 4.15 with Figs. 4.2 and 4.3 will show the effectiveness of the calibration procedures on this type of data.

4.5.4 Calibrating Landsat TM digital data to ground equivalent reflectance

Following the same procedure used previously for transforming the ATM data, the lithological units used as calibration targets for ATM are used again to calibrate

Table 4.11 Least square parameter for the lines in the calibration curve for ATM 1000m (IFOV=2.5m). Mahd Adh Dhahab area.

Band	a	b	R
ATM2	0.3246	-2.91	0.8896
ATM3	0.4286	-2.377	0.8921
ATM5	0.4892	-1.504	0.889
ATM7	0.5806	-3.139	0.892
ATM9	0.877	-9.57	0.944
ATM10	0.614	+2.511	0.9338

Table 4.12 Least square parameter for the lines in the calibration curve for ATM 2000m (IFOV=5.0m). Mahd Adh Dhahab area.

Band	a	b	R
ATM2	0.3141	-4.064	0.9438
ATM3	0.4321	-5.436	0.9565
ATM5	0.49186	-5.086	0.9624
ATM7	0.5540	-5.594	0.9367
ATM9	0.7597	-8.07	0.9766
ATM10	0.628	-3.954	0.9604

Table 4.13 Least square parameter for the lines in the calibration curve for ATM 3000m (IFOV=7.5m). Mahd Adh Dhahab area.

Band	a	b	R
ATM2	0.416	-9.477	0.9657
ATM3	0.536	-11.03	0.9800
ATM5	0.609	-11.42	0.9918
ATM7	0.697	-13.27	0.9880
ATM9	0.865	-13.69	0.9961
ATM10	0.767	-10.53	0.9943

Table 4.14 Least square parameter for the lines in the calibration curve for ATM 1000m (IFOV=2.5m). Jabal Said area.

Band	a	b	R
ATM2	0.1903	+0.2215	0.836
ATM3	0.2850	-2.806	0.910
ATM5	0.3362	-2.7199	0.919
ATM7	0.4054	-6.544	0.904
ATM9	0.4599	-0.7634	0.923
ATM10	0.5808	-14.39	0.910

Table 4.15 Least square parameter for the lines in the calibration curve for ATM 2000m (IFOV=5.0m). Jabal Said area.

Band	a	b	R
ATM2	0.2063	-0.685	0.9270
ATM3	0.2636	-0.036	0.9244
ATM5	0.3219	-0.852	0.9298
ATM7	0.3552	0.145	0.9304
ATM9	0.3531	+8.984	0.8468
ATM10	0.3782	+5.494	0.8918

Table 4.16 Least square parameter for the lines in the calibration curve for ATM 3000m (IFOV=7.5m). Jabal Said area.

Band	a	b	R
ATM2	0.2897	-9.743	0.9322
ATM3	0.3892	-13.17	0.9692
ATM5	0.4548	-15.16	0.9678
ATM7	0.4705	-13.26	0.9532
ATM9	0.7094	-25.97	0.9691
ATM10	0.7437	-31.47	0.9990

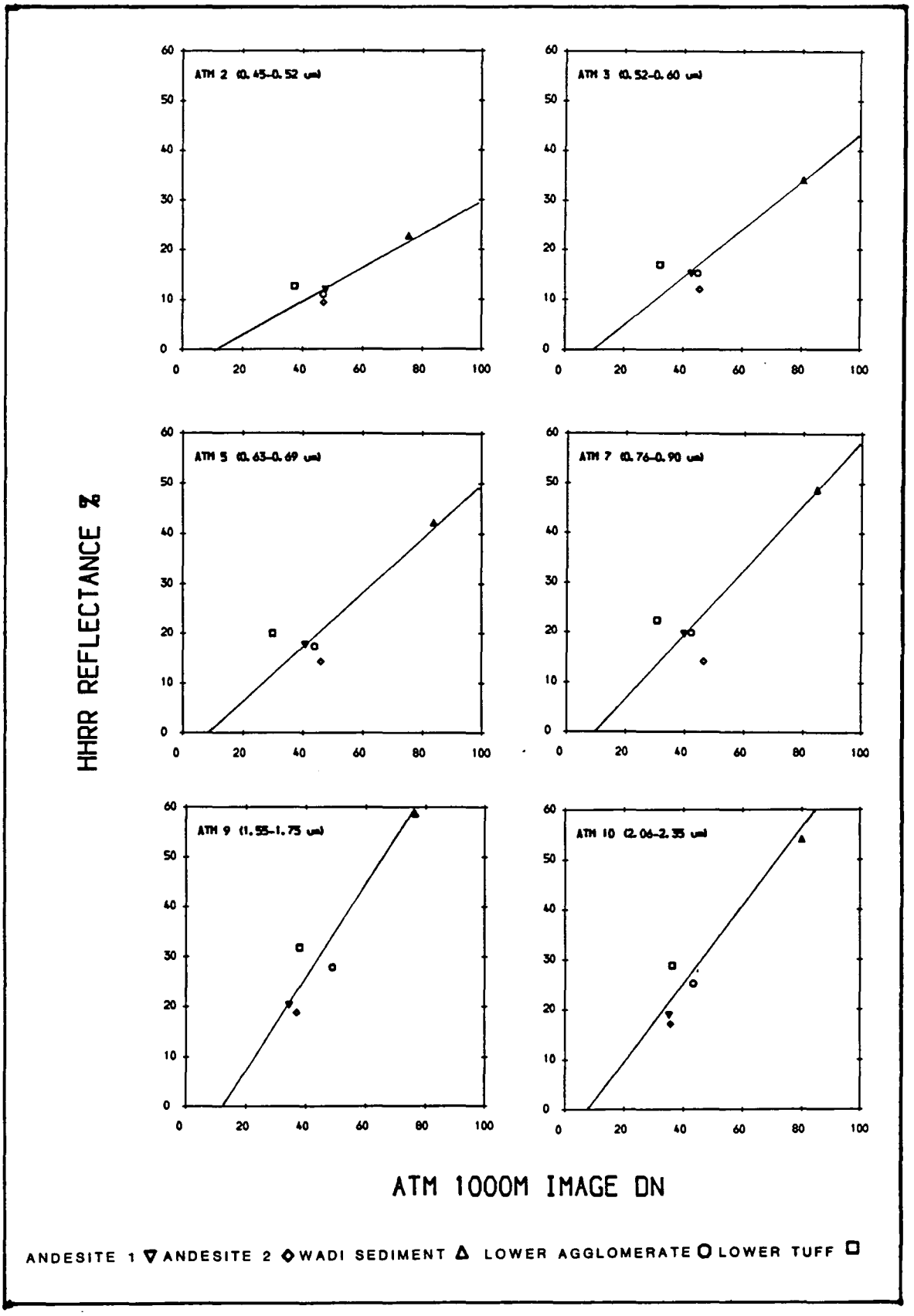

Fig. 4.8 Calibration curve for ATM 1000m data (resolution 2.5m) Based on HHRR field measurement, Mahd Adh Dhahab

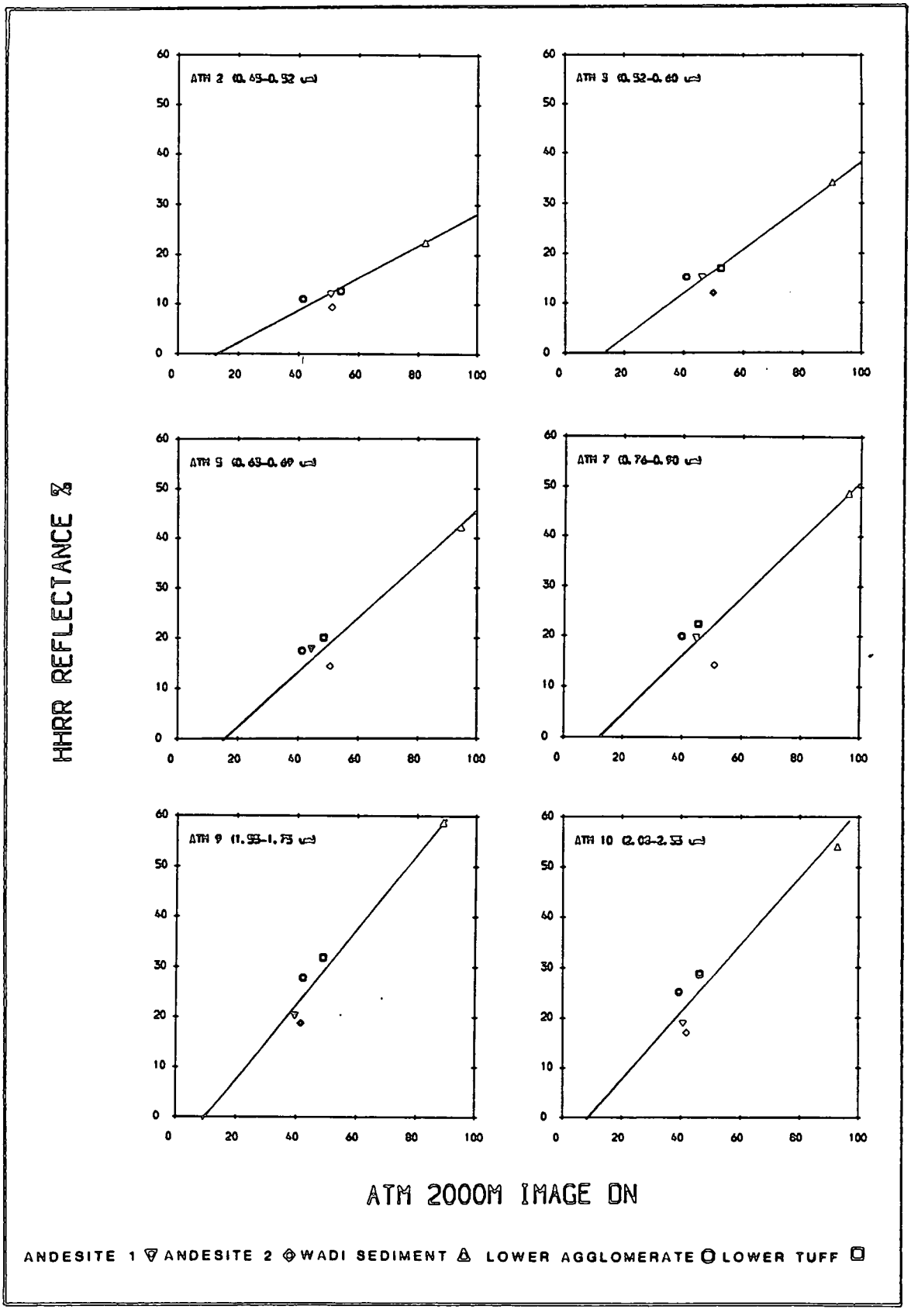

Fig. 4.9 Calibration curve for ATM 2000m data (resolution 5.0m) based on HHRR field measurement, Mahd Adh Dhahab.

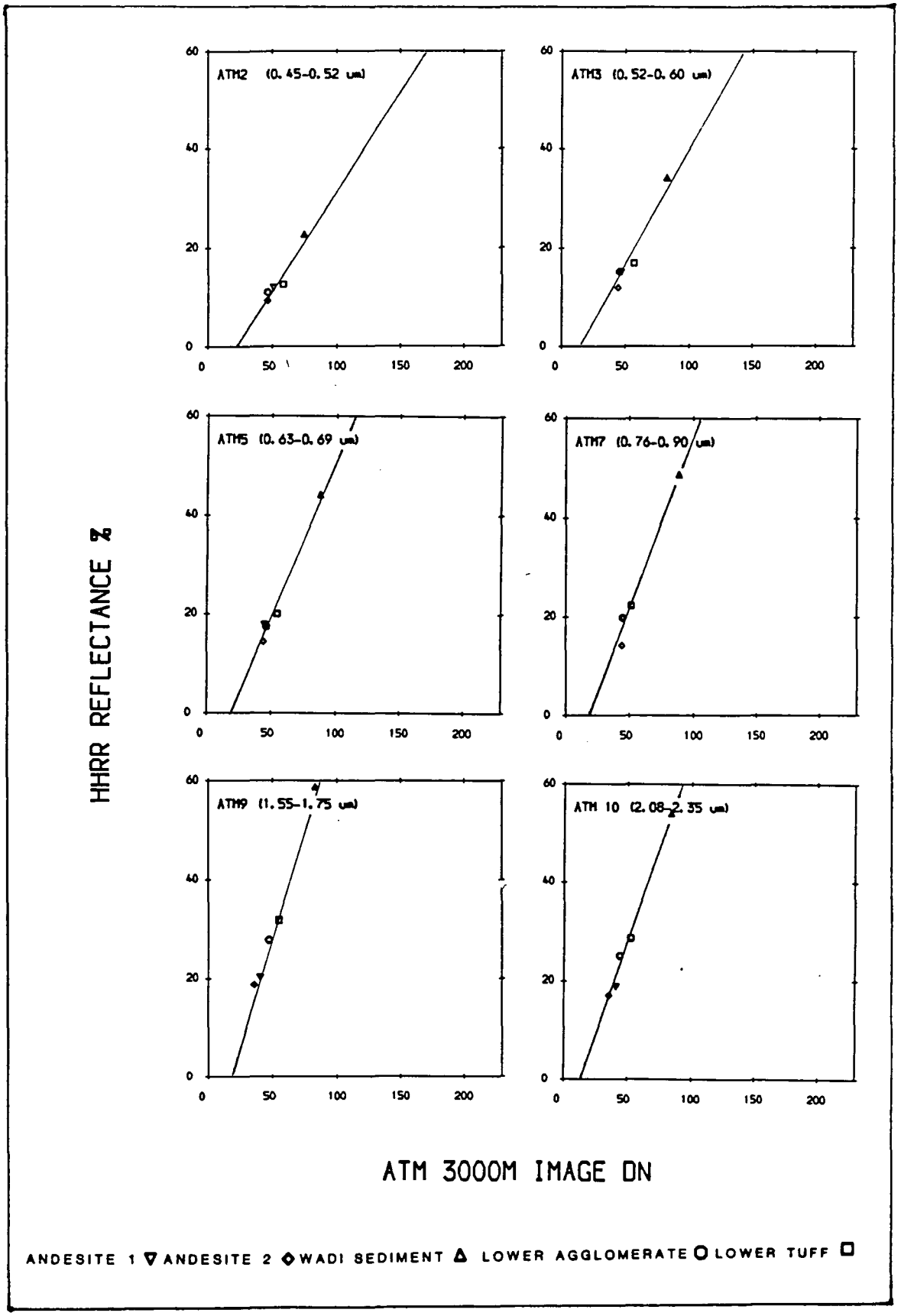

Fig. 4.10 Calibration curve for ATM 3000m data (resolution 7.5m) based on HHRR field measurement, Mahd Adh Dhahab.

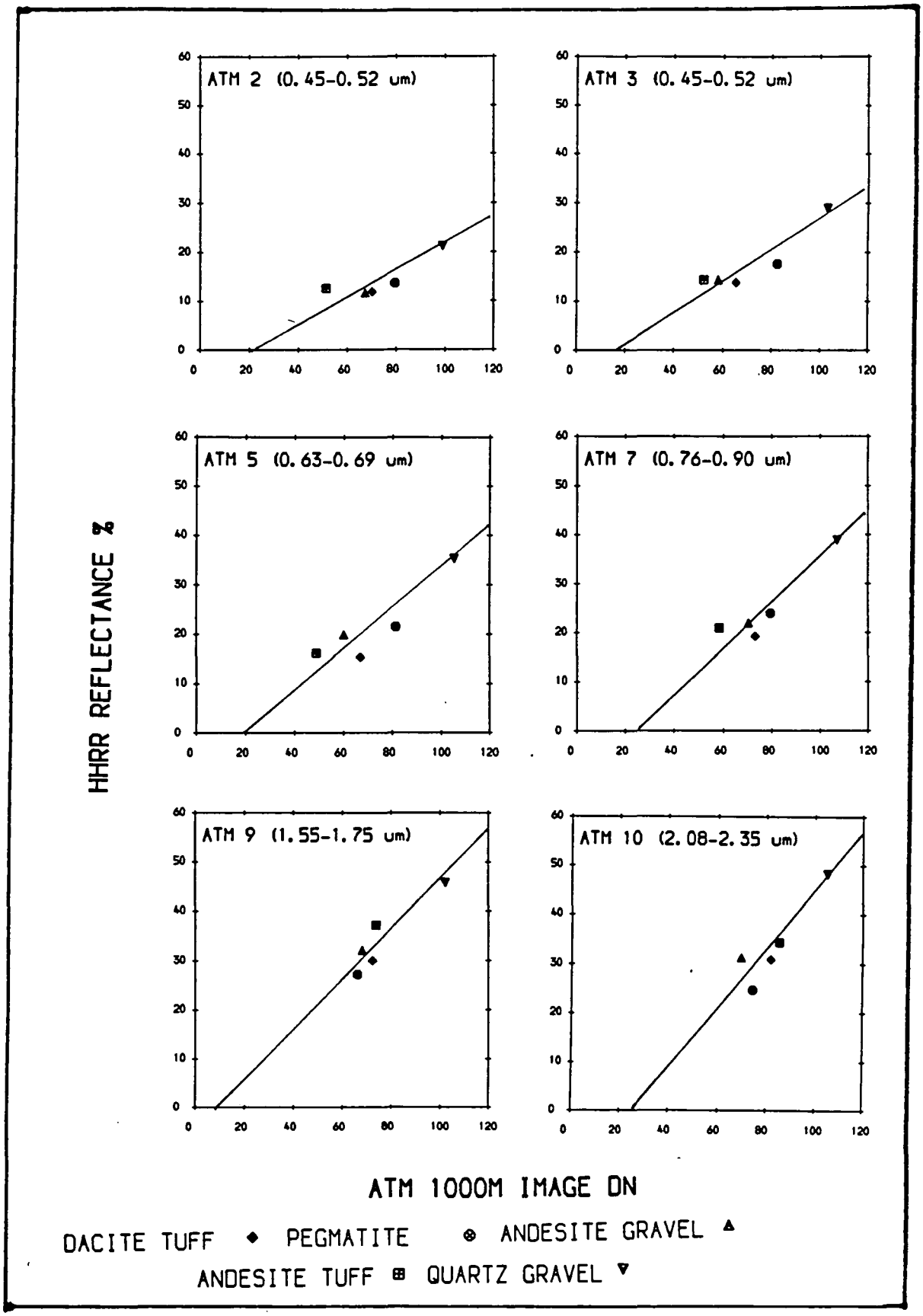

Fig. 5.11 Calibration curve for ATM 1000m data (resolution 2.5m) based on HHRR field measurement, Jabal Said.

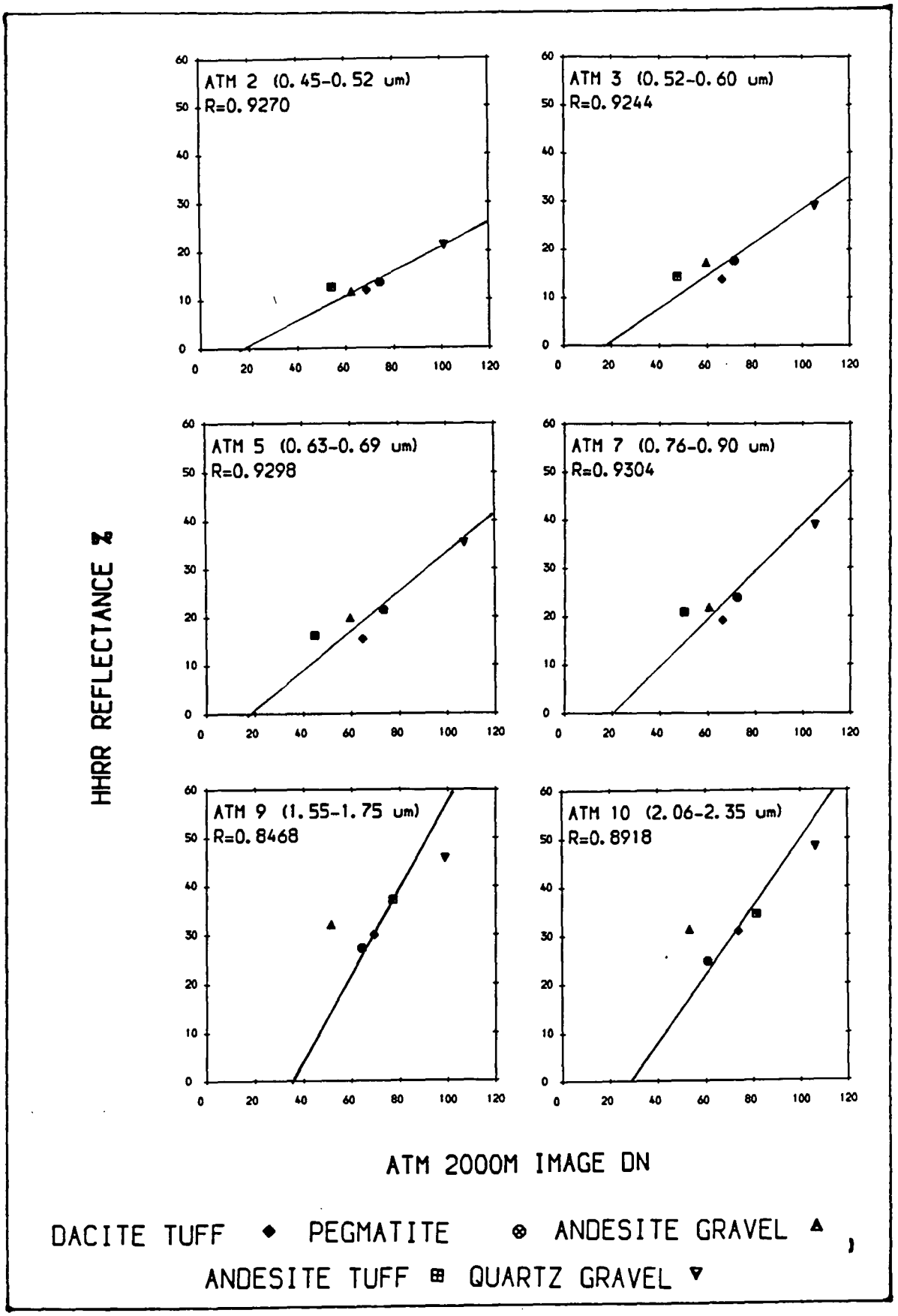

Fig. 4.12 Calibration curve for ATM 2000m data (resolution 5.0m) based on HHRR field measurement, Jabal Said.

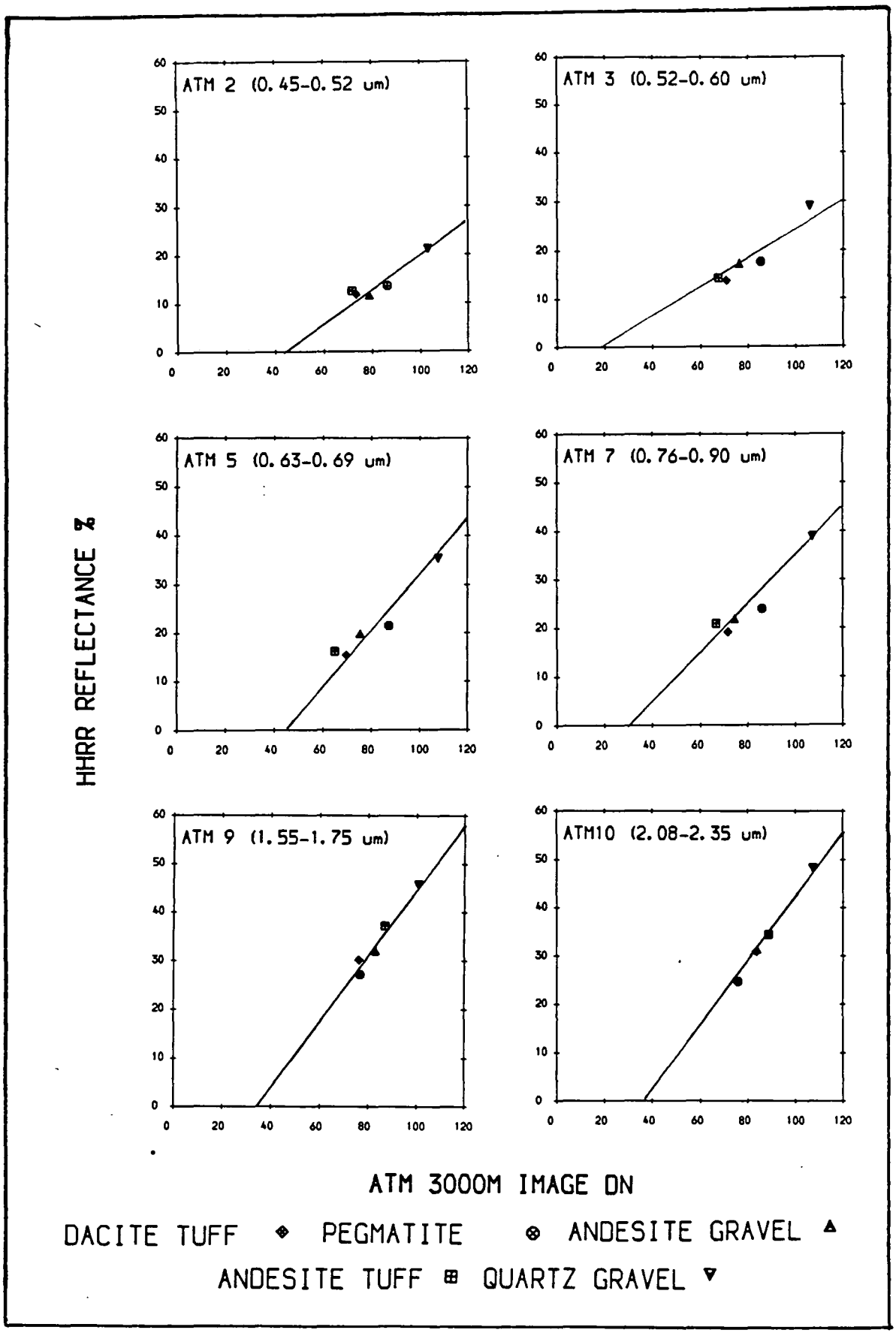

Fig. 4.13 Calibration curve for ATM 3000m data (resolution 7.5m) based on HHRR field measurement, Jabal Said.

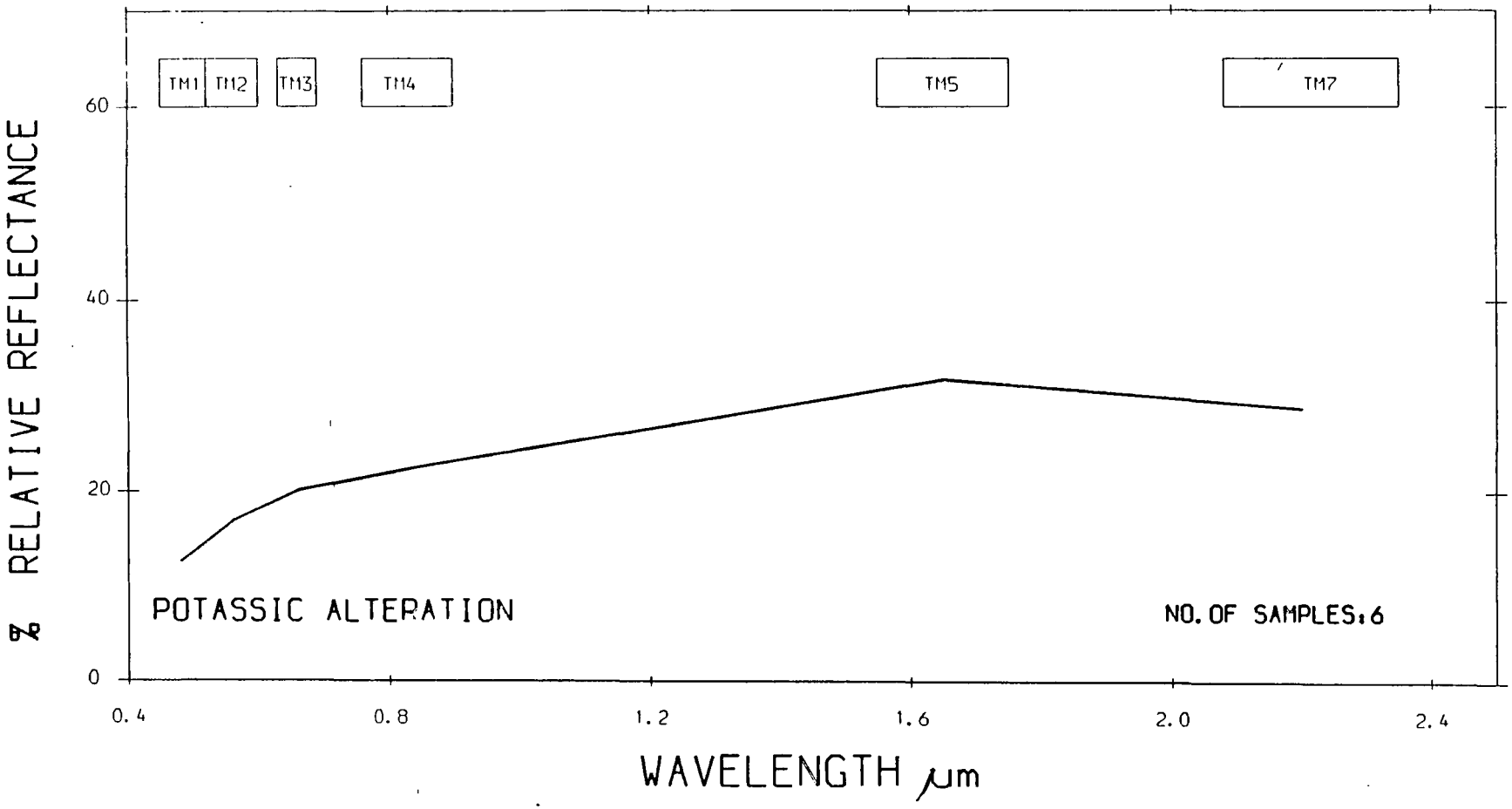

Fig. 4.14 Ground relative reflectance using the HHRR.

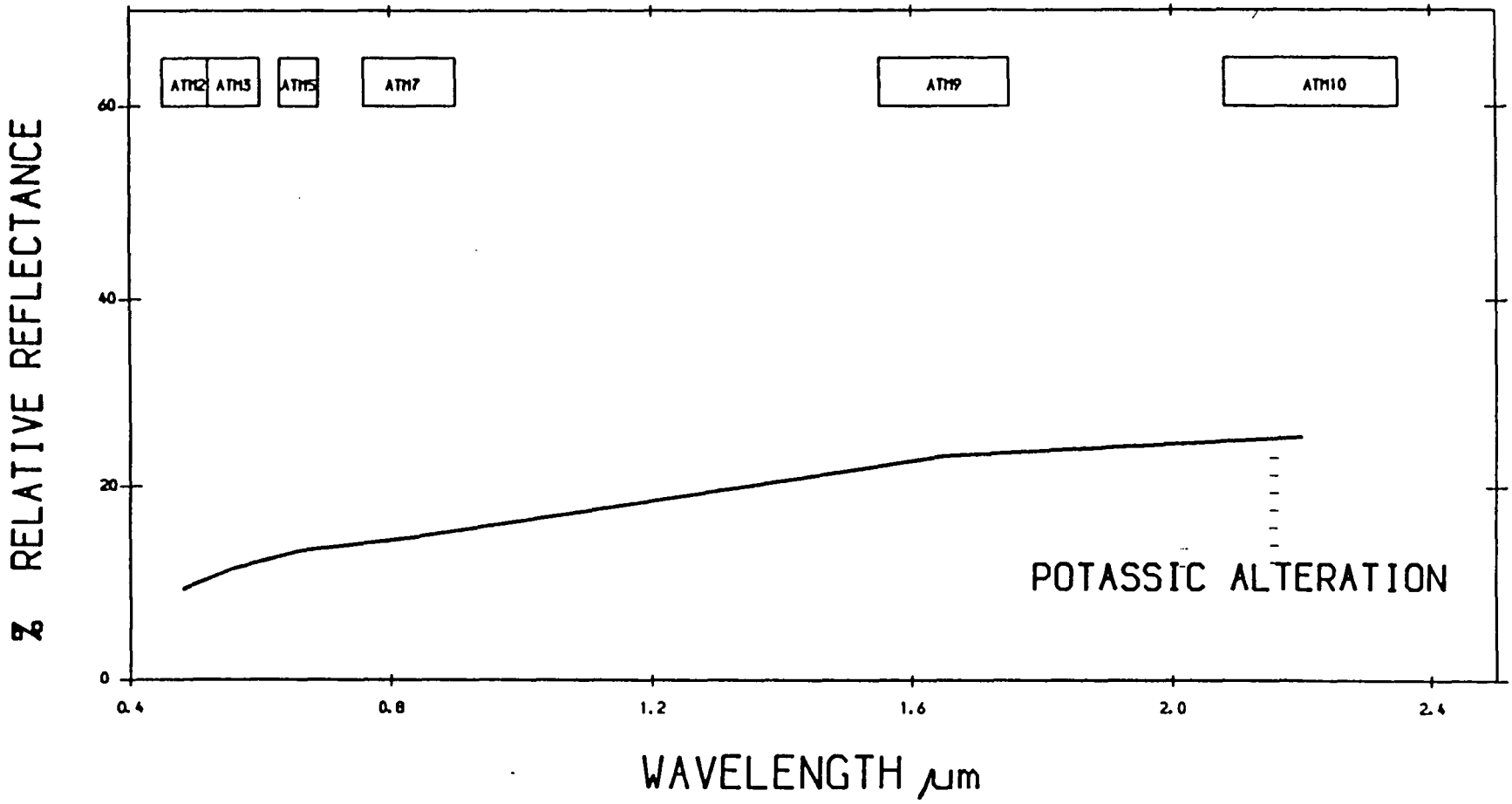

Fig. 4.15 ATM 1000m band equivalent to TM calibrated to relative reflectance using Claibration Curve, Mahd Adh Dhahab.

the TM. Digital values were extracted for these targets, five from Mahd Adh Dhahab and five from Jabal Said (Tables 4.17, 4.18).

Although the areas of Mahd Adh Dhahab and Jabal Said are covered by the same TM scene, a calibration curve was calculated for each district separately. This was done primarily for the purposes of comparing the satellite data with ATM data sets which were taken separately for each site. Such techniques were useful in comparing the results statistically, especially when the same calibration target was used in calibrating the TM and all ATM data sets.

Based on the data in Tables 4.17, and 4.18, and the calibration curves resulting from Fig. 4.16, 4.17, linear equations were derived from least square fits of DN versus band averaged reflectance for each band.

The correlation coefficients R listed in tables 4.19 and 4.20 are all greater than 0.90, which is considered excellent correlation and suggest that the function relating the Landsat TM scanner grey level (DN) of Mahd Ahd Dhahab and Jabal Said to the ground reflectance measured in the field are linear.

An example of the calibration result is provided in Fig. 4.18, which shows the ploting of Landsat TM data for one of the lithological units after it is calibrated to ground reflectance. This should be compared with Figs. 4.2 and 4.3.

Table 4.17 Summary of TM image (IFOV=30m) DN value and equivalent TM band reflectance measured by HHRR for the five lithologies used as calibration targets, Mahd Adh Dhahab area.

Lithology	TM 1		TM 2		TM 3		TM 4		TM 5		TM 7	
	TM	HHRR	TM	HHRR	TM	HHRR	TM	HHRR	TM	HHRR	TM	HHRR
Wadi sediment	176.0	22.7	102.2	34.1	156.7	42.2	126.7	48.8	221.5	58.8	138.5	54.1
Andesite 1	136.0	11.9	66.9	15.2	98.3	17.8	75.6	19.7	133.6	20.3	84.0	18.9
Silicic alt.	113.0	11.0	54.8	15.2	76.6	17.4	54.2	19.9	115.2	27.9	72.9	25.2
Potassic alt.	129.8	12.6	65.0	16.9	94.0	20.1	72.0	22.4	143.8	31.9	86.8	28.8
Andesite 2	126.7	9.4	61.0	12.0	86.5	14.4	67.0	14.2	118.7	18.8	86.0	17.1

Table 4.18 Summary of TM-image (IFOV=30m) DN value and equivalent TM band reflectance measured for HHRR, for the five lithologies used as calibration targets, Jabal Said Area.

Lithology	TM 1		TM 2		TM 3		TM 4		TM 5		TM 7	
	TM	HHRR	TM	HHRR	TM	HHRR	TM	HHRR	TM	HHRR	TM	HHRR
Andesite tuff	127.8	12.6	60.7	14.3	83.8	16.2	65.2	20.9	153.3	37.2	102.0	34.4
Andesite grav.	140.2	11.7	70.3	17.3	105.3	19.9	78.5	21.9	161.7	32.1	105.8	31.3
Quartz gravel	166.7	21.2	90.7	29.0	138.2	35.4	106.0	38.9	185.3	45.8	130.2	48.5
Pegmatite	133.3	13.6	63.2	17.6	93.0	21.5	75.0	23.9	122.5	27.2	80.5	24.7
Dacitic tuff	132.0	11.9	63.5	13.8	89.7	15.4	68.8	19.2	135.7	30.0	87.5	30.9

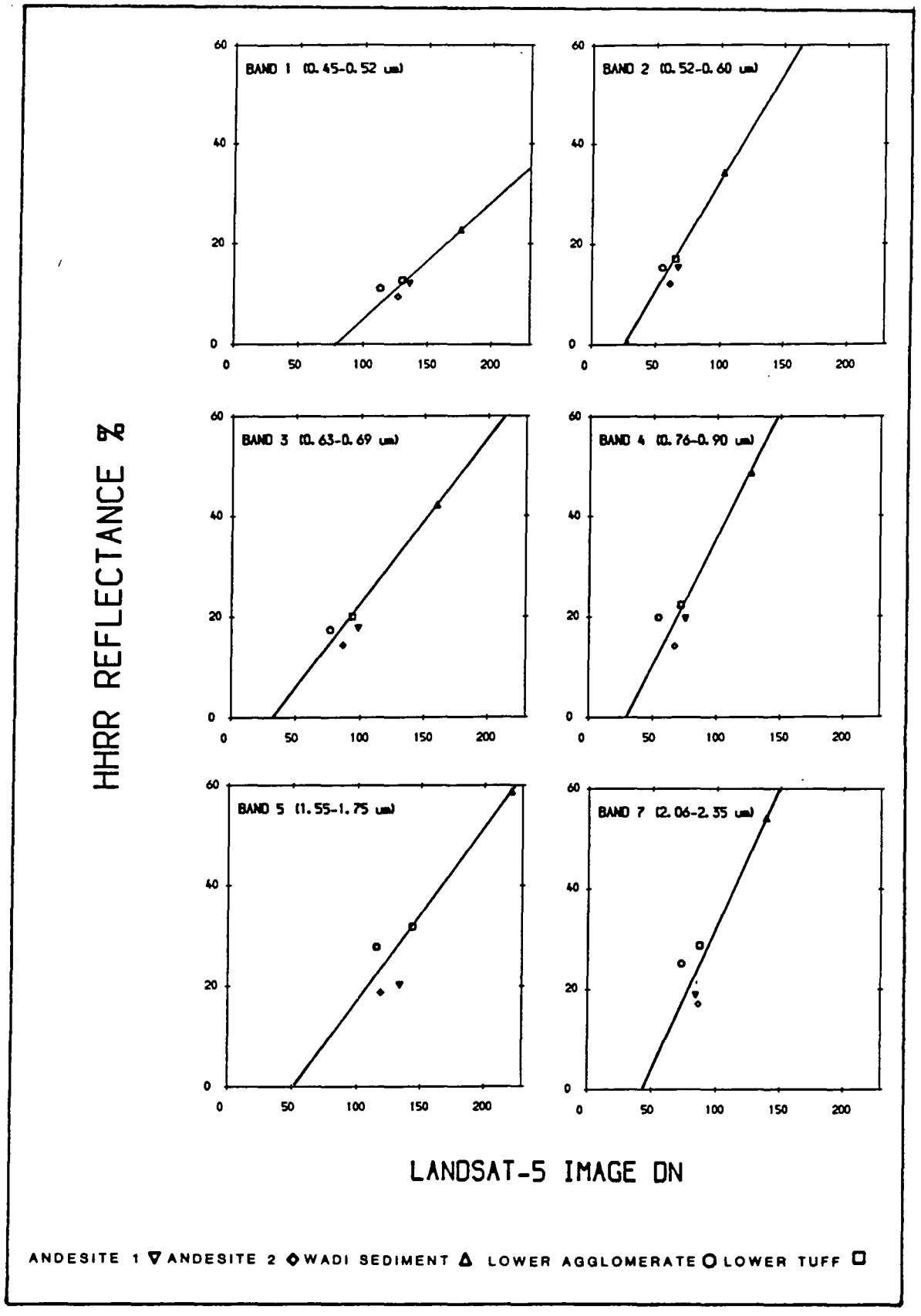

Fig. 4.16 Calibration curve for Landsat-5 TM data based on HHRR field measurement, Mahd Adh Dhahab.

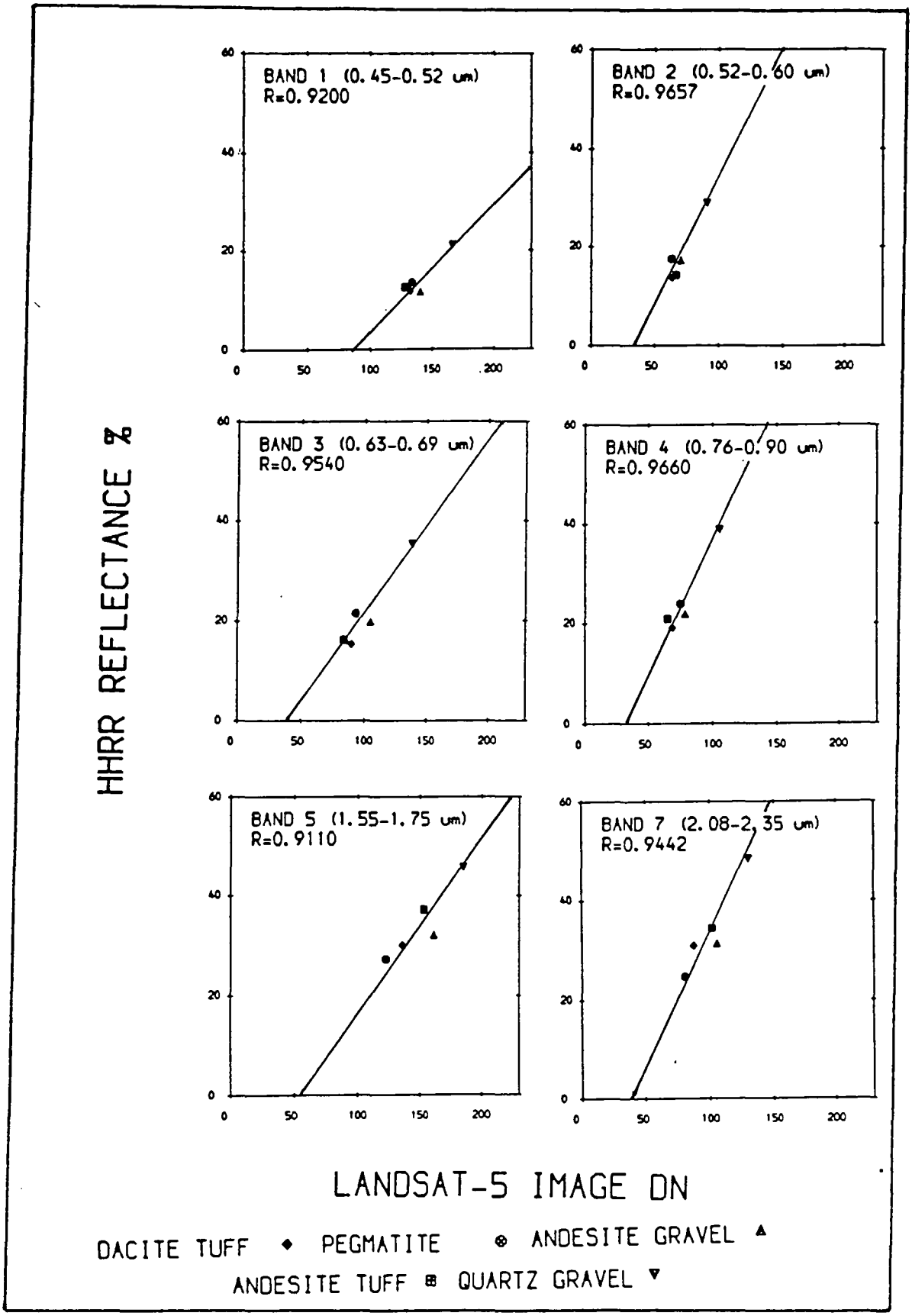

Fig. 4.17 Calibration curve for Landsat-5 TM data based on HHRR field measurement, Jabal Said.

Table 4.19 Least square parameter for the lines in the calibration curve for TM data (IFOV=30m). Mahd Ahd Dhahab area.

Band	a	b	R
TM 1	0.2083	-14.84	0.937
TM 2	0.4553	-13.15	0.960
TM 3	0.3332	-11.97	0.968
TM 4	0.4614	-11.48	0.940
TM 5	0.3520	-20.66	0.946
TM 7	0.5260	-20.49	0.909

Table 4.20 Least square parameter for the lines in the calibration curve for TM data (IFOV=30m). Jabal Said area.

Band	a	b	R
TM 1	0.235	-18.73	0.920
TM 2	0.485	-15.41	0.966
TM 3	0.355	-14.54	0.954
TM 4	0.478	-12.67	0.966
TM 5	0.275	-7.362	0.911
TM 7	0.435	-10.06	0.944

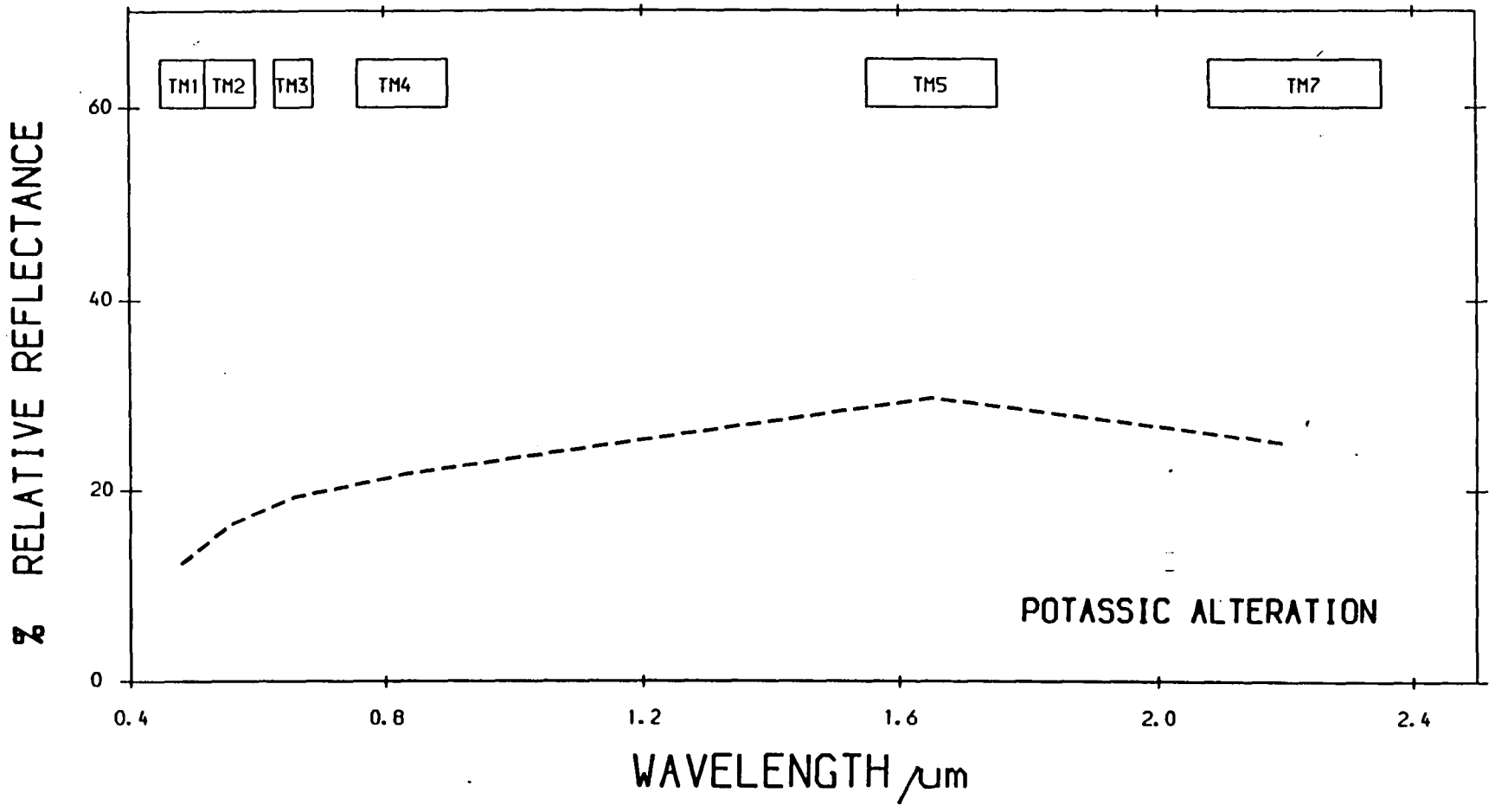

Fig. 4.18 Landsat TM calibrated to relative reflectance, Madh Adh Dhahab.

4.6 Summary and Conclusions

In order to compare quantitative data from different instruments, different heights acquired at different times, it is essential to transform the data and correct for the effects of atmosphere and instrument effect. This can be achieved through empirical calibration procedures to calibrate data to ground equivalent, reflectance based upon the use of spectra of known target measured by HHRR, removing the across track shading which was affecting the ATM data.

The result obtained from calibrating the TM and ATM data to ground equivalent reflectance show that the minimum correlation coefficients (R) are greater than 0.88 and in most cases, R is greater than 0.92, which is considered an excellent correlation between the ground spectral radiometric value measured by the HHRR, and the data extracted from the images of different resolutions (Fig. 4.19).

This excellent correlation might suggest that:

1) The Landsat 5 TM and ATM may be calibrated in terms of surface reflectance;

2) The targets measured in the field are representative of measurements made by the TM or ATM sensors; and

3) The function relating TM and ATM data to ground reflectance measured in the field is linear.

Using the calibrated data from different resolutions, the resulting data can be applied to separate lithologies based on their spectra. Discriminant analysis will be run between the different types of data for the selected

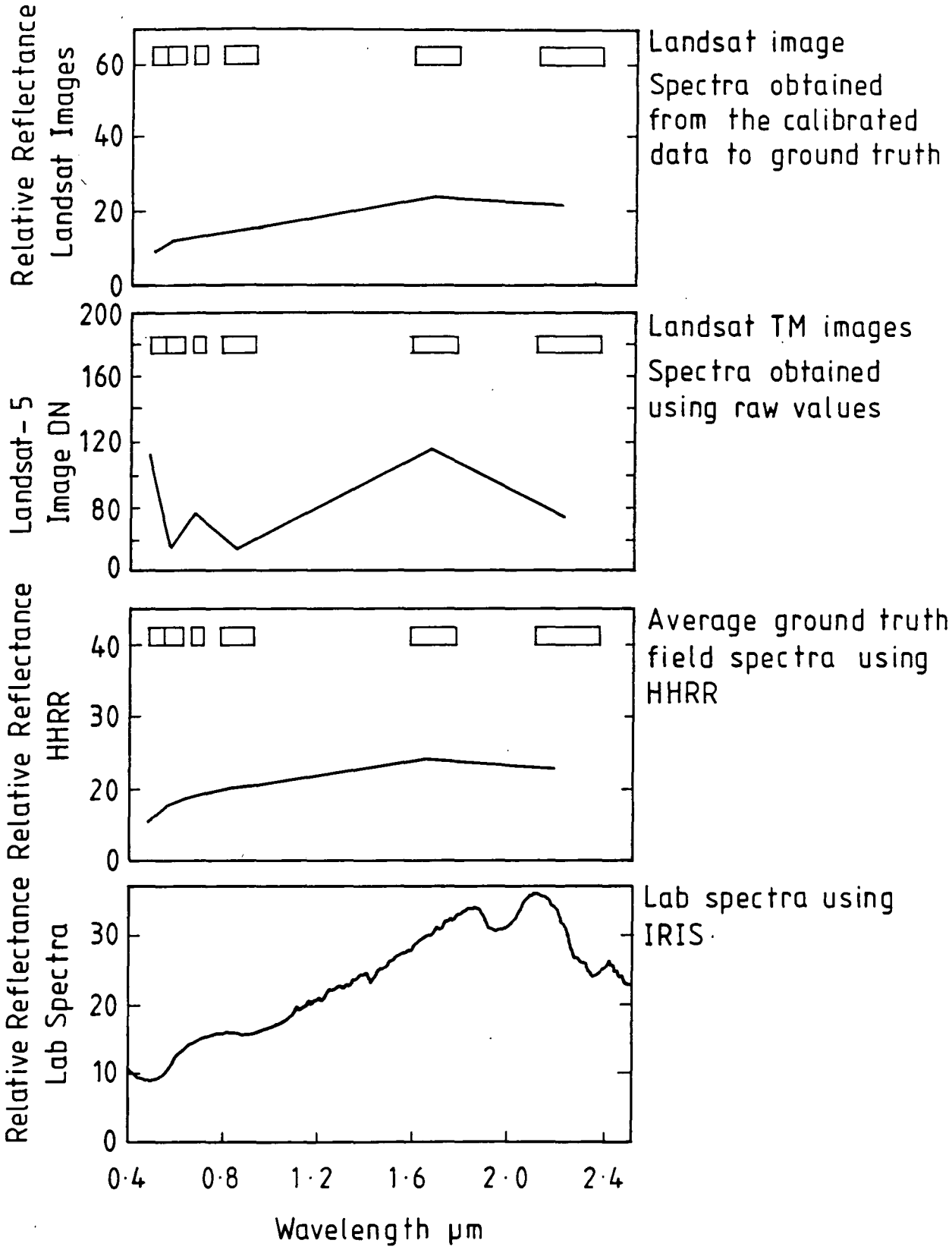

Fig. 4.19 Comparison between spectra from images before and after calibration with field spectra and laboratory spectra for silicic alteration in Mahd Adh Dhahab area.

lithological units. This will be examined quantitatively in Chapter 5.

CHAPTER 5

LITHOLOGICAL DISCRIMINATION AND THE INFLUENCE OF SPATIAL RESOLUTION ON LITHOLOGICAL MAPPING AND MINERAL EXPLORATION

5.1 Introduction

The spatial resolution refers to the fineness of detail depicted in an image; it is the minimum size of objects on the ground that can be separately distinguished or measured. For MSS, TM and ATM scanners, the spatial resolution can be expressed as the instantaneous field of view (IFOV) (Townshend, 1980)

The spatial resolution requirements for satellite remote sensing applied to geological applications have been debated since the 1960's (Settle et al., 1982). The discussion of those requirements necessary to solve geological problems continues today. Settle et al. (1984) state that no unique spatial resolution is appropriate for, or applicable to, all exploration problems. Data with a 15m instantaneous field of view (IFOV) is however sufficient for many problems. Abrams (1982) draws attention to the lack of studies on the effect that spatial resolution has on the extraction of geological information. This, he divides into two main areas; first, the effect of the IFOV on spectral reflectance and secondly, the effect of IFOV on the detection of spatial features within a scene.

This Chapter has two primary objectives. Firstly, to assess the influence of spatial resolution on discrimination. Spatial resolution is an important

consideration on geological mapping for a variety of reasons, such as the ability to resolve structural features in detail.

Today we are restricted to the acquisition of satellite data, resolutions ranging from 80m in the case of Landsat MSS to 30m for TM and, more recently, to the acquisition of data at 20m and 10m with SPOT.

The second main objective is to examine multispectral data, airborne and satellite systems to discriminate various lithologies, characterising the Arabian Shield and in particular, the two study areas, Mahd Adh Dhahab and Jabal Said. In relation to this objection, is an assessment of the ability of the data for separating the altered and unaltered lithologies, as related to the mineralization characterised in the two study areas.

Data is acquired at various spatial resolutions by operating remote sensing systems, comprising an airborne scanner and satellite system which give different spatial resolutions in similar parts of the spectra in the visible, near and shortwave infrared. Resolutions used in this study are shown in Table 5.1.

The major advantage of satellite sensors is that they provide the synoptic coverage at a relatively low cost per square km. Although the airborne system was capable of acquiring data at a high spatial resolution, it had the disadvantage of generating a large quantity of data for the same geographic area covered by satellite. Thus by adding data processing costs will inevitably rise for organising an extensive airborne survey. What is not

Table 5.1 Data type and its resolution

Type of Data	Resolution
Landsat MSS	80.0 m
Landsat 5-TM	30.0 m
ATM (3000 m)	7.5 m
ATM (2000 m)	5.0 m
ATM (1000 m)	2.5 m
HHRR (ground data)	0.96m

fully understood is the incremental advantages of increasing spatial resolution for lithological mapping on various scales, versus the problem of data handling and data acquisition costs.

These aspects are addressed in a quantitative manner in this Chapter. The first part of Chapter 5 examines and interprets the spectral curves derived from the different images which have different resolutions. The second part is concerned with differentiation and classification quantitatively, between different lithologies based on their characteristic features of spectra. There are many ways of looking at this problem and discriminant analysis is one of them. It is a powerful technique for such a purpose (see Section 5.4).

5.2 Methodology:

Several targets were selected from each area representing different lithologies. DN values for a total of 4 to 6 pixels were extracted from TM images for each lithology, in the case of ATM 9 pixels were extracted for the same lithology of each resolution. Taking into account that samples should be selected from some locations, the average of these DN values were calculated for each band using the calibration curve. They were then calibrated to the ground truth data (Chapter 4, Section 4.5).

Spectral relationships were plotted to show the percentage relative reflectance for each lithology and for each resolution.

The extracted DN values were examined using stepwise discriminant analysis, ranging from simple descriptive measures to multivariate discriminant analysis. This allowed the rocks and materials to be separated, and analysed for each of the spatial resolutions to be ranked by their usefulness. The same procedure was applied to both areas. Detailed studies of the spectral and statistical behaviour of data taken from different spatial resolutions were made in each area. The analysis involved two stages; first, the spectral curves were plotted and the curves representing the five spatial resolutions were compared for the same lithology. Secondly, using the same data, statistical discrimination among the different lithologies was carried out for each resolution.

5.3. Spectral analysis

Means of the calibrated data were calculated for each lithology for the Mahd Adh Dhahab and Jabal Said areas. These means were then plotted against each band. Absorption features evident in each spectral curve suggest the presence of certain minerals. Generally speaking, most of the altered rocks show absorption features around 2.2um, which indicates the presence of Al-O-H and Mg-O-H, or C-O-O bonds in the minerals. Unaltered rocks show no absorption in the visible bands, which might be related to the presence of desert varnish.

The spectra for each lithology in the MAhd Adh Dhahab area and the Jabal Said are will be discussed separately, and a comparative study for each resolution will be presented.

5.3.1 Spectral analysis of Mahd Adh Dhahab area

DN values were extracted from the Mahd Adh Dhahab images at each resolution for eleven lithologies (Tables 5.2-5.5). The spectral curves for each lithology were plotted separately for each resolution (Appendix D). Specific features for these spectral curves will now be discussed along with the effect of different resolution on the shape of curves.

The samples from Mahd Adh Dhahab were selected to represent the variation in spectral response for the different types of alteration in the area (see Chapter 2).

5.3.1.1 Wadi sediment

This was the lightest target in the area having the highest albedo at every resolution. The spectrum shows high reflection at 1.6um and low reflection around 2.4um. This relates to the presence of -OH absorptions. However, due to the large bandpass of TM band 7 (2.08 to 2.35um) it cannot be explained whether this relates to aluminium clay (absorption 2.22um) or to chlorite (2.33um) or to carbonate 2.35um). The drop off towards the short wavelength is attributed to the presence of iron in some form.

The spectra from the 5.0m IFOV exhibits the highest albedo compared with the other spectra (Fig. 5.1).

5.3.1.2 Altered rocks

The spectra of altered rocks is often characterised by the presence of a strong absorption feature around 2.2um. Generally, the spectrum of an altered rock typically has the appearance of an intensely altered

Table 5.2 Means of calibrated DN values to relative reflectance after extracted from ATM 3000m image (7.5m resolution), using only TM band equivalent, Mahd Adh Dhahab.

Lithology	ATM2	ATM3	ATM5	ATM7	ATM9	ATM10
Wadi sediment	21.58	33.28	41.86	48.76	58.25	53.90
Andesite 1	11.60	14.07	15.88	17.40	21.20	21.43
Argillic alt.	14.30	23.18	30.70	34.82	53.78	38.04
Silicic alt.	9.65	13.36	16.59	17.28	26.53	22.83
Potassic alt.	14.72	19.61	21.76	22.62	33.74	29.61
Chlorite alt.	10.69	14.52	17.30	19.02	26.96	23.98
Qtz.Ser.Pyrite	18.04	23.72	27.04	29.01	30.57	23.47
Pyrite Chlor.	12.57	18.63	23.18	26.57	40.37	34.21
Carbonate rock	12.91	18.36	22.27	24.25	40.95	31.27
Rhyolite rock	12.91	16.13	17.70	19.37	31.58	33.31
Andesite 2	9.72	12.73	15.47	17.51	17.30	16.57

Table 5.3 Means of calibrated DN values to relative reflectance after extracted from ATM 2000m image (5.0m resolution) using only TM band equivalent, Mahd Adh Dhahab.

Lithology	ATM2	ATM3	ATM5	ATM7	ATM9	ATM10
	Wavelength					
Wadi Sediment	22.05	33.88	41.72	47.87	60.74	53.93
Andesite 1	11.84	14.58	16.76	18.60	22.41	21.90
Argillic alt.	13.99	24.66	31.33	33.28	55.81	34.25
Silicic alt.	8.97	12.21	15.31	16.29	23.68	20.85
Potassic alt.	13.47	18.11	19.79	20.54	29.50	25.67
Chlorite alt.	7.97	8.53	9.24	10.56	18.24	17.29
Qtz.Ser.Pyr.	14.72	19.98	25.44	27.65	36.58	26.71
Pyrite Chlor.	12.47	18.33	22.90	25.06	39.62	32.05
Carbonate R.	12.79	17.10	21.18	23.21	35.82	25.25
Rhyolite R.	13.26	17.10	20.04	22.94	35.44	34.88
Andesite 2	11.74	15.73	19.47	22.20	22.92	22.32

Table 5.4 Means of calibrated DN values to relative reflectance after extracted from ATM 1000m image (2.5m resolution), using only TM band equivalent, Mahd Adh Dhahab.

Lithology	ATM2	ATM3	ATM5	ATM7	ATM9	ATM10
Wadi Sediments	21.55	32.07	39.40	45.87	57.37	51.63
Andesite 1	12.42	15.95	18.54	20.06	20.97	23.59
Argillic Alt.	14.15	25.15	31.50	33.49	58.25	36.69
Silicic Alt.	11.94	16.88	19.93	21.22	33.84	28.50
Potassic Alt.	9.18	11.39	13.16	14.55	23.31	25.33
Chlorite Alt.	8.86	12.38	14.95	15.51	19.22	22.46
Qtz.Ser.Pyrite	16.04	21.80	25.47	27.11	36.91	31.98
Pyrite Chlorite	10.75	16.88	21.31	23.54	38.37	31.57
Carbonate rocks	10.64	15.02	18.78	20.35	32.67	26.25
Rhyolite rocks	9.83	13.17	15.28	16.58	24.04	28.19
Andesite 2	12.21	17.09	20.90	22.96	21.70	24.30

Table 5.5 Means of the calibrated DN values to relative reflectance data extracted from TM image (30.0m resolution), Mahd Adh Dhahab area.

	TM1	TM2	TM3	TM4	TM5	TM7
Wadi Sediment	21.82	33.36	41.20	46.95	57.30	52.35
Andesite 1	13.83	18.03	21.72	24.42	28.15	25.35
Argillic Alt.	14.06	21.33	27.24	30.61	48.86	33.28
Silicic Alt.	8.85	10.63	12.75	13.77	19.90	17.76
Potassic Alt.	12.18	16.44	19.33	21.73	29.94	25.13
Chlorite Alt.	11.82	15.53	18.75	20.92	30.64	24.87
Qtz.Ser.Pyr.	12.91	16.33	18.91	19.31	24.30	17.90
Pyrite Chlor.	11.14	12.68	14.09	14.92	13.57	12.77
Carbonate Rock	22.60	32.94	40.23	42.95	54.49	51.56
Rhyolite Rock	11.09	13.48	15.54	16.59	23.78	23.95
Andesite 2	11.56	14.62	16.83	19.54	23.51	24.73

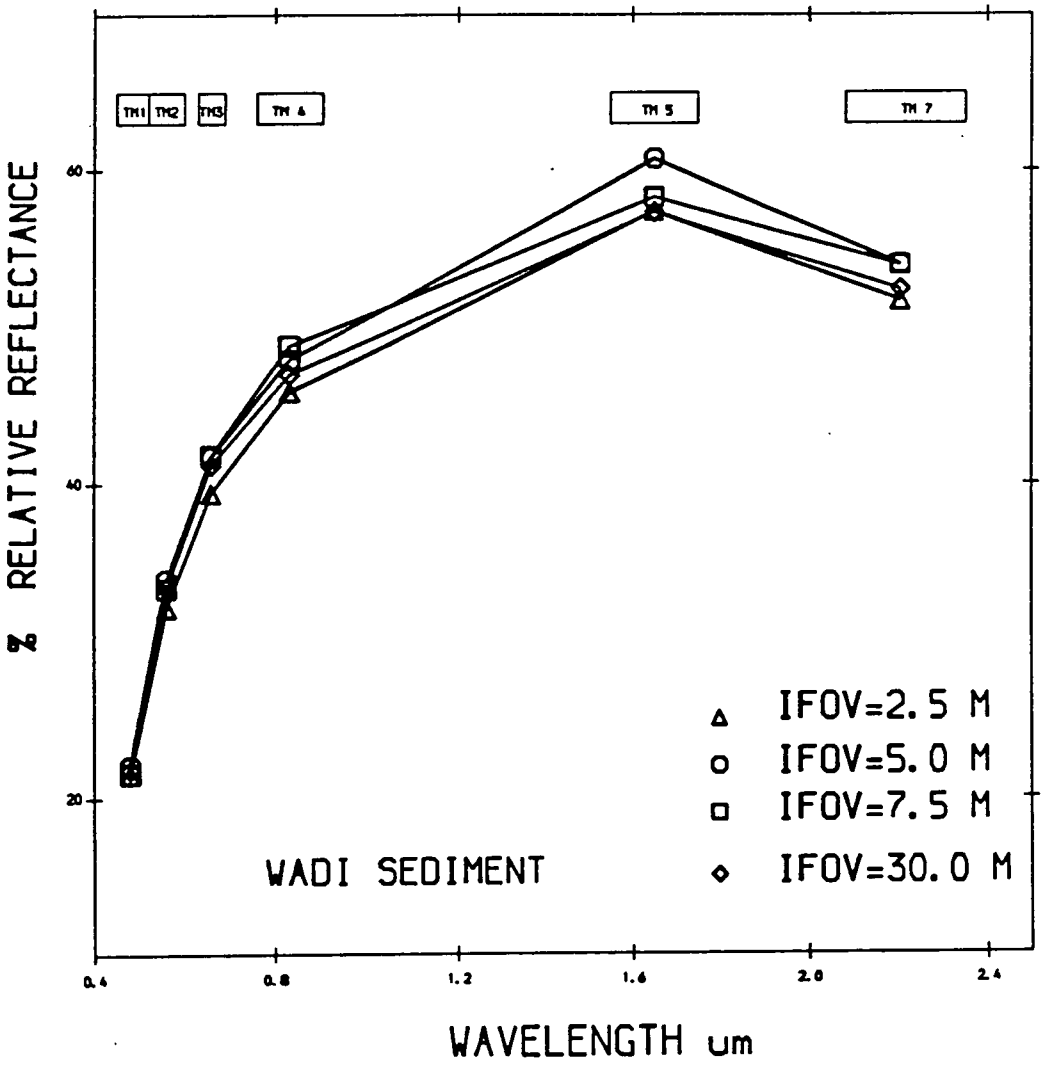

Fig. 5.1 Comparison of spectra from different spatial resolutions, Mahd Adh Dhahab.

igneous rock. High reflectance is observed at 1.6um, which decreases towards both the shorter and longer wavelengths (Hunt & Ashley, 1979). Ferric-iron absorption features are displayed by most of the altered rocks and for data of all spatial resolutions. All spectra display prominent features at wavelengths shorter than 0.6um, and at 0.65um and 0.9um all spectra decrease in intensity towards the ultraviolet which is a feature indicative of ferric-iron presence. The very clear features around 0.9um may be related to the varnish and iron staining of the weathered surface of the rocks.

i) Argillic alteration

These spectra show the drop off on both sides of 1.6um (Fig. 5.2). The albedo of the spectrum produces a pattern whereby the relative reflectance increases with increasing IFOV. The lowest albedo is given by the TM satellite data, while the highest is shown by the ATM (IFOV = 2.5m). The alteration here is homogeneous and only very minor internal variation is seen at visible wavelengths in bands 3 and 4, which might be explained by the low spatial resolution of the TM sensor resulting in spectral mixing.

ii) Quartz sericite alteration

Similar behaviour is shown in Fig. 5.3, for the quartz sericite alteration. The lowest albedo is given by the TM and the highest albedos are shown by the ATM data. The variation between the spectra from different resolutions reflect the heterogeneity of this type of alteration. The difference in the 30m resolution data is

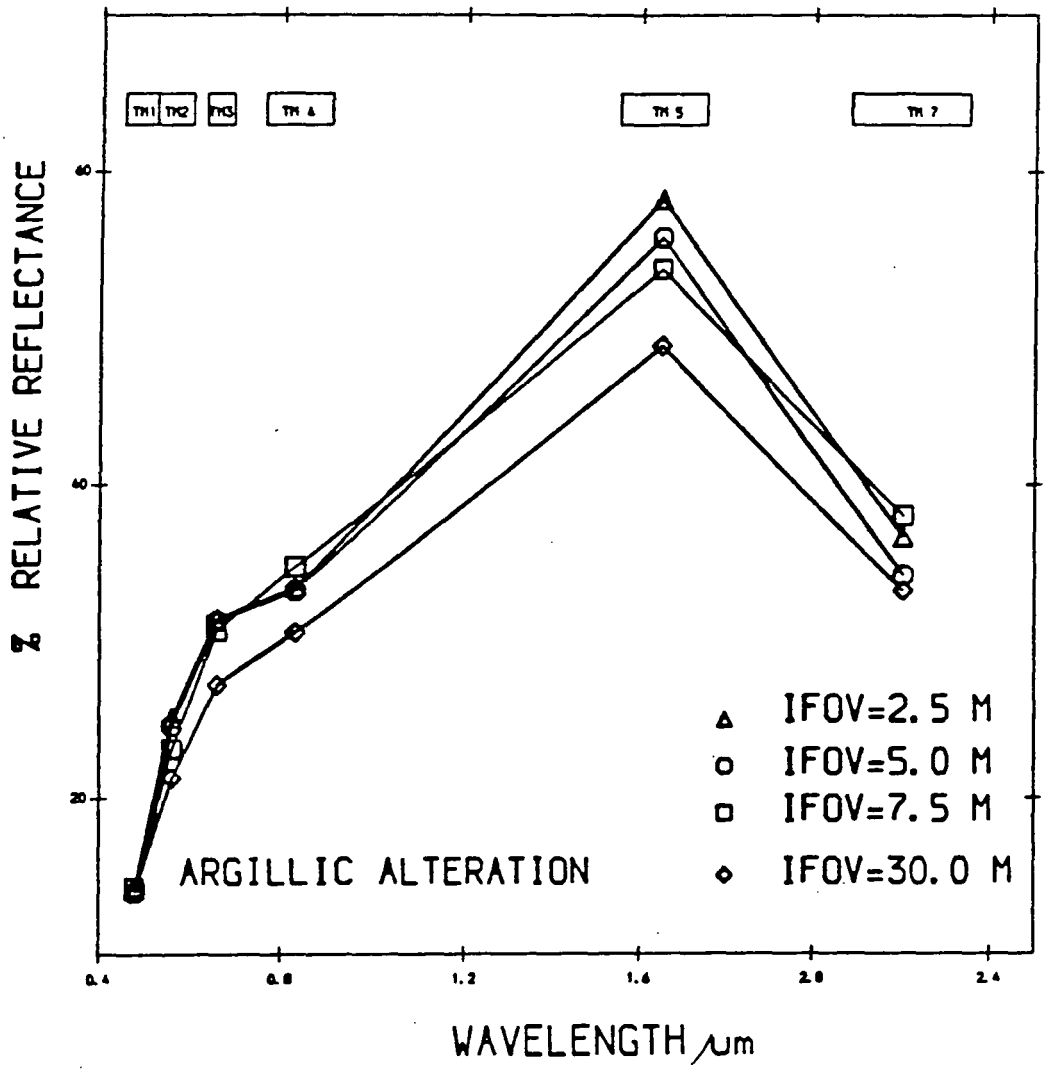

Fig. 5.2 Comparison of spectra from different spatial resolutions, Mahd Adh Dhahab.

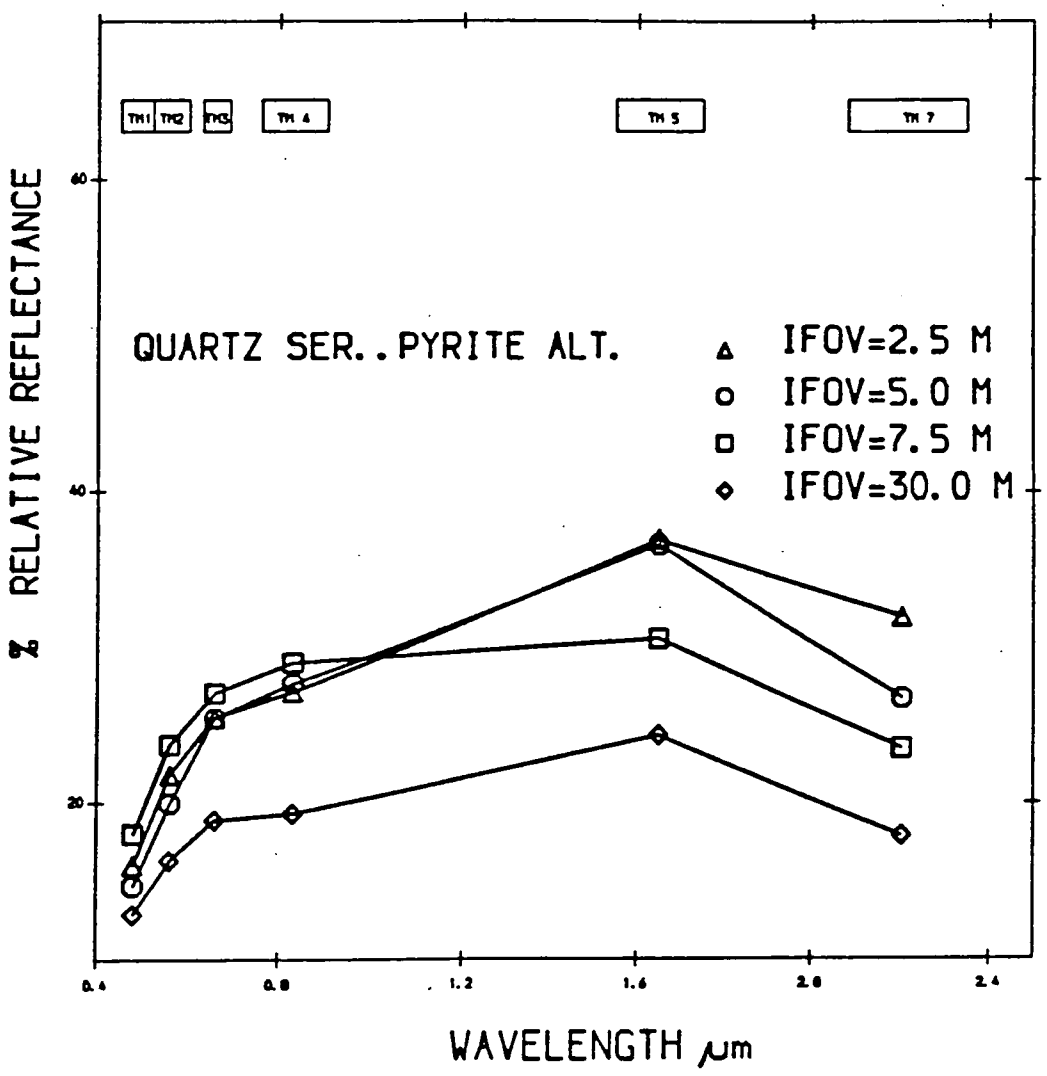

Fig. 5.3 Comparison between spectra from different spatial resolutions, Mahd Adh Dhahab.

attributed to the low resolution of the TM sensor, which means that this spectra reflect mixtures of the quartz alteration and surrounding area. The difference in the high resolutions, especially when the IFOV = 5m and 2.5m, is attributed to internal variation.

iii) Silicic alteration. Fig. 5.4 indicates that the ATM 2.5m resolution data has the highest albedo, but the ATM 5.0m and 7.5m curves are out of sequence; the 7.5m data having a higher albedo than the 5.0m data, but generally this reflects homogeneous types of alteration, where the shape of the four curves are similar, except for the degree of albedo.

iv) Potassic alteration

The highest albedo is given by the ATM data with 7.5m IFOV and the lowest by ATM with 2.5m IFOV. All values except that for an IFOV of 7.5m, are very similar when plotted against band 7. No absorption features are evidence around 2.2um when using the ATM data with 2.5m IFOV (Fig. 5.5). This reflects the internal variation within this alteration.

v) Chlorite alteration

Again the spectra show no absorption features around 2.2um, when using ATM data with 2.5m IFOV. This is due to the local variation in this type of alteration. However, here the highest albedo is produced by the TM data with a 30m IFOV, and the lowest albedo is given by ATM data (IFOV = 5.0m). The difference in the spectra of 5.0 and 2.5m is attributed to the internal variation of this unit, which appears only in the high resolution (Fig. 5.6).

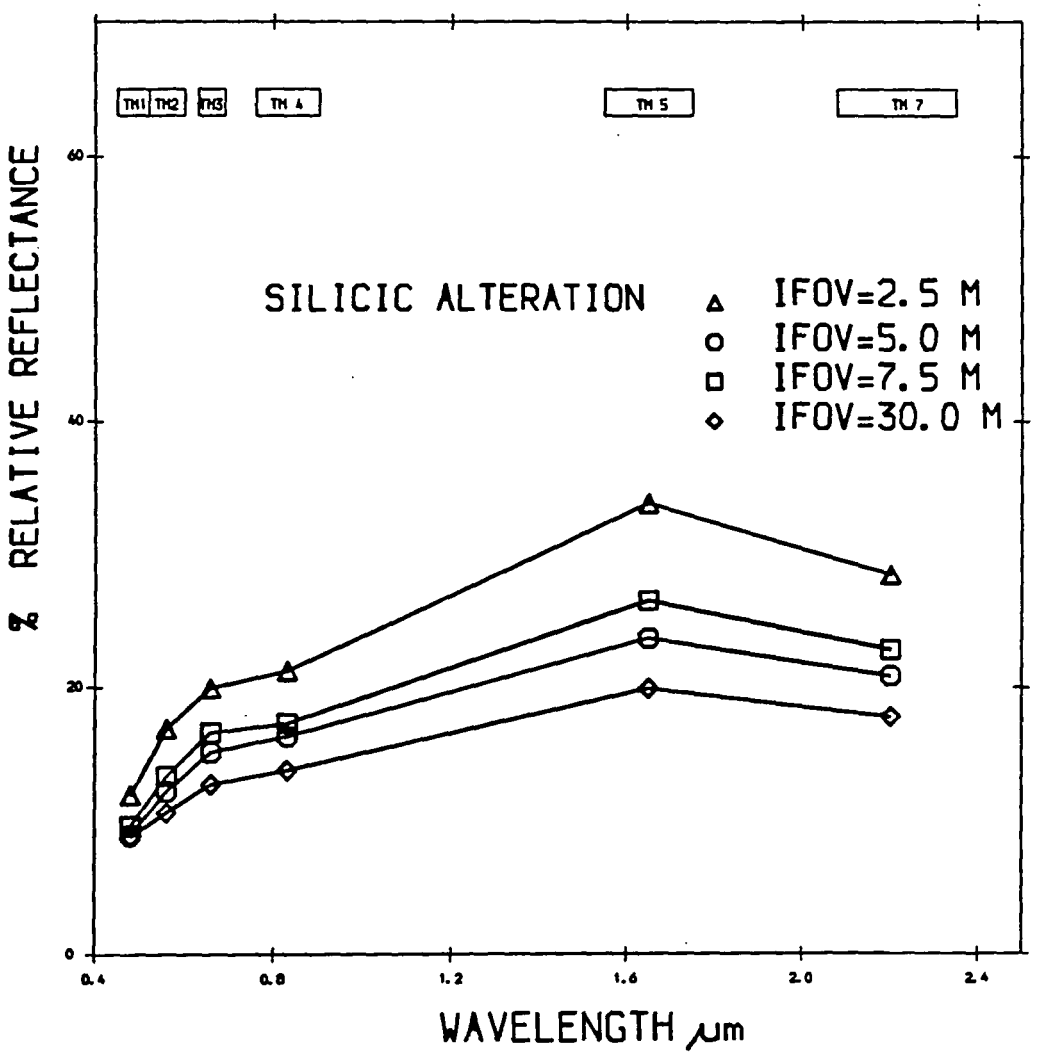

Fig. 5.4 Comparison of spectra from different spatial resolutions, Mahd Adh Dhahab.

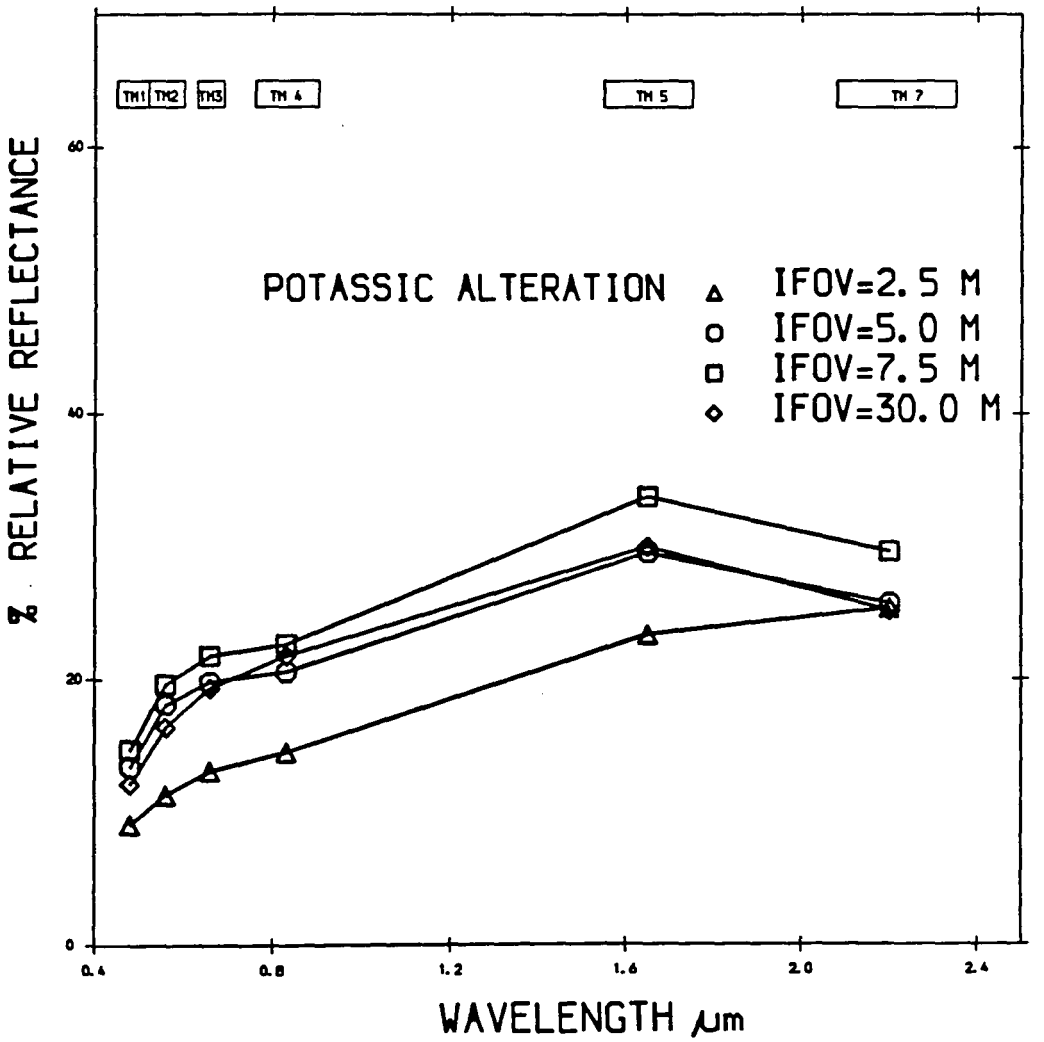

Fig. 5.5 Comparison of spectra from different spatial resolutions, Mahd Adh Dhahab.

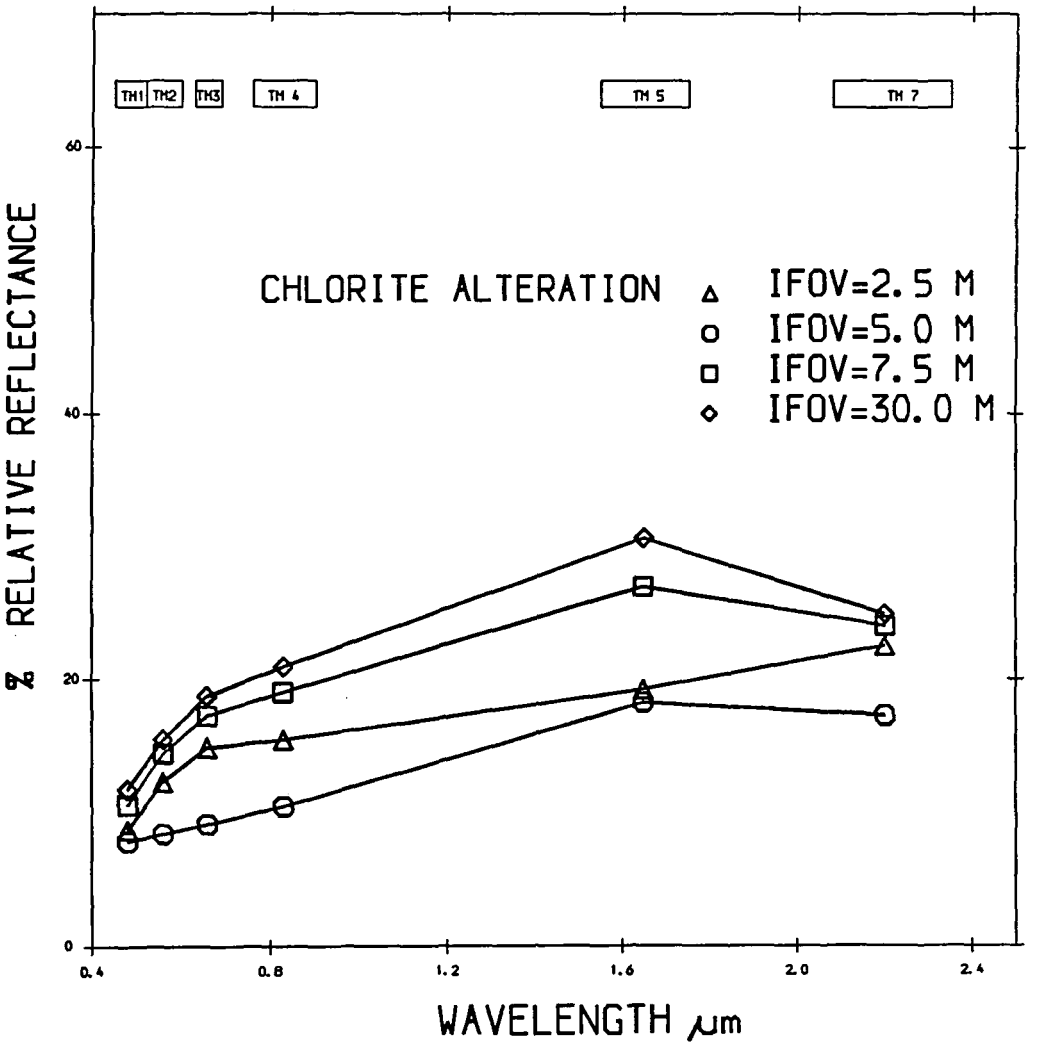

Fig. 5.6 Comparison of Spectra from different spatial resolutions, Mahd Adh Dhahab.

vi) Pyrite chlorite alteration

The spectra can be divided into two parts. The first part contains the spectra of the ATM data at 7.5m, 5.0m and 2.5m IFOV, and illustrates a clear absorption around 2.2um. The second part is produced by the TM data, and does not exhibit any absorption features around 1.65um and 2.2um (Fig. 5.7) and almost shows flat spectra behind band 3 and very low abledo compared to the ATM spectra. The difference in these curves between the ATM and TM sensors can be attributed to the low resolution of TM where the IFOV of 30m can easily cover the target and surrounding area, especially if the alteration unit sampled is very small. The curve might also reflect the heterogeneity of the rocks in this area (Fig. 5.7).

5.3.1.3 Carbonate rocks

The spectra of the carbonate rocks produces a different pattern to that illustrated by the altered rocks. Here the albedo increases as the resolution of the data is reduced. The TM data show the highest albedo but the absorption around 2.35um is weak compared to the features displayed by the ATM data at the same wavelength. The ATM data from all three resolutions, illustrated absorption around 0.9um and 0.43um.

The difference in the curves was attributed to the carbonate rocks themselves. In ATM data the selected pixel covers the carbonate rocks and falls within the outcrops. The selected pixel covered by TM data included materials surrounding the carbonate outcropping. Therefore, the TM spectral curve is not truely

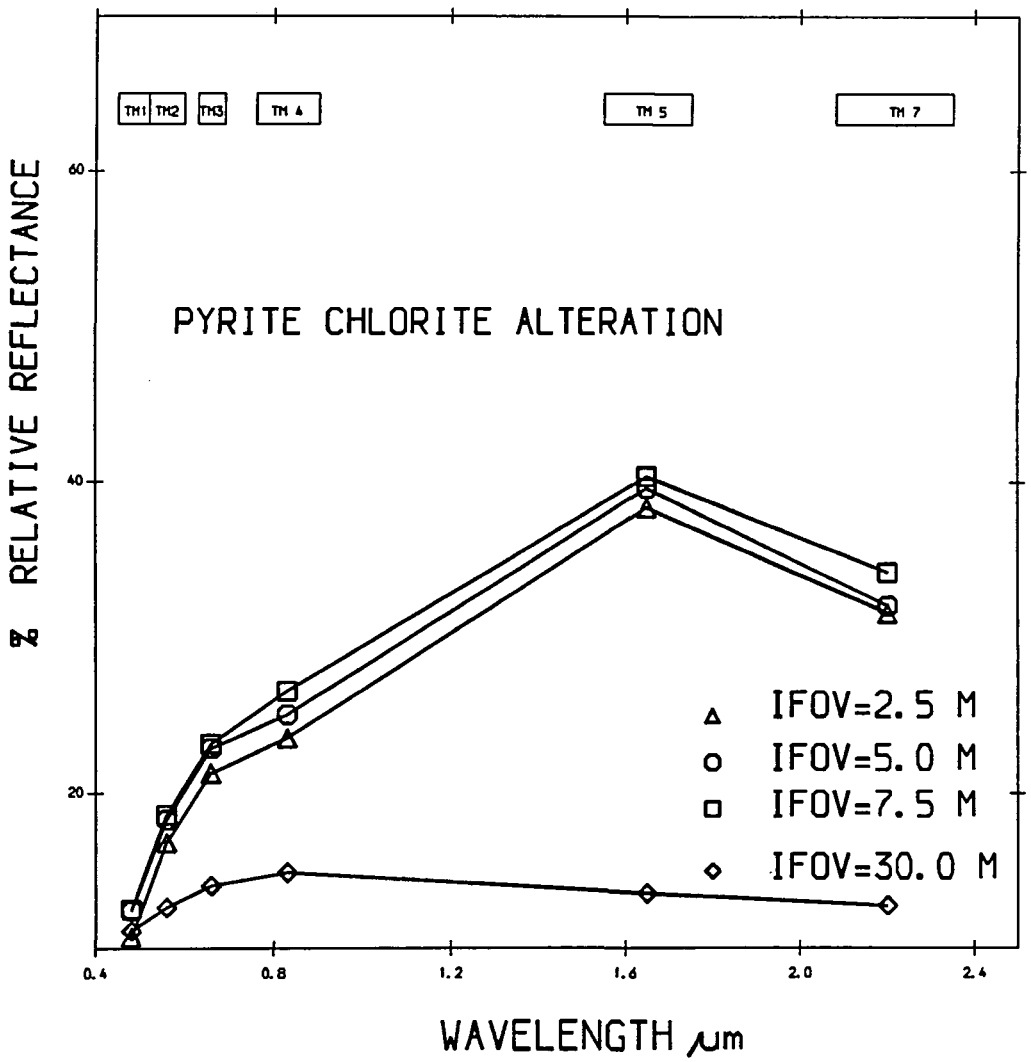

Fig. 5.7 Comparison of spectra from different spatial resolution, Mahd Adh Dhahab.

representative of the carbonate rocks. The variation in the ATM data can be attributed by a very local variation which was picked by 5.0m data (Fig. 5.8).

5.3.1.4 Andesite rocks

Two sites of andesite were sampled; Andesite 1 was from the Mine Hill, south of the alteration zone. The spectra of Landsat TM exhibited the highest albedo in all bands. The TM spectrum may not be truly representative of andesite rock because the area surrounding the outcrop may have contributed to the shape of the spectrum. Variation in the ATM spectra may be affected by internal variation (Fig. 5.9).

The second sample, Andesite 2, was from west of Mine Hill and outside the mapped alteration zone. Variation in the TM and ATM data is small. The ATM with an IFOV of 2.5m shows evidence of local and internal differences within the andesite rock (Fig. 5.10).

5.3.1.5 Rhyolite rocks

This rock is located west of the Mine Hill outside the mapped alteration zone and is an unaltered rock. The spectra have low overall albedos and show only a drop off towards the ultraviolet around 0.9um in the TM sensor spectra, and similarly with ATM data of IFOV 7.5m and 5.0m. The ATM IFOV 2.5m data displays a curve suggesting minor homogeneity in the rocks (Fig. 5.11).

5.3.2 Spectral analysis of the Jabal Said area

As for the Mahd Adh Dhahab area, eleven lithological types were chosen, and DN values for each lithology were

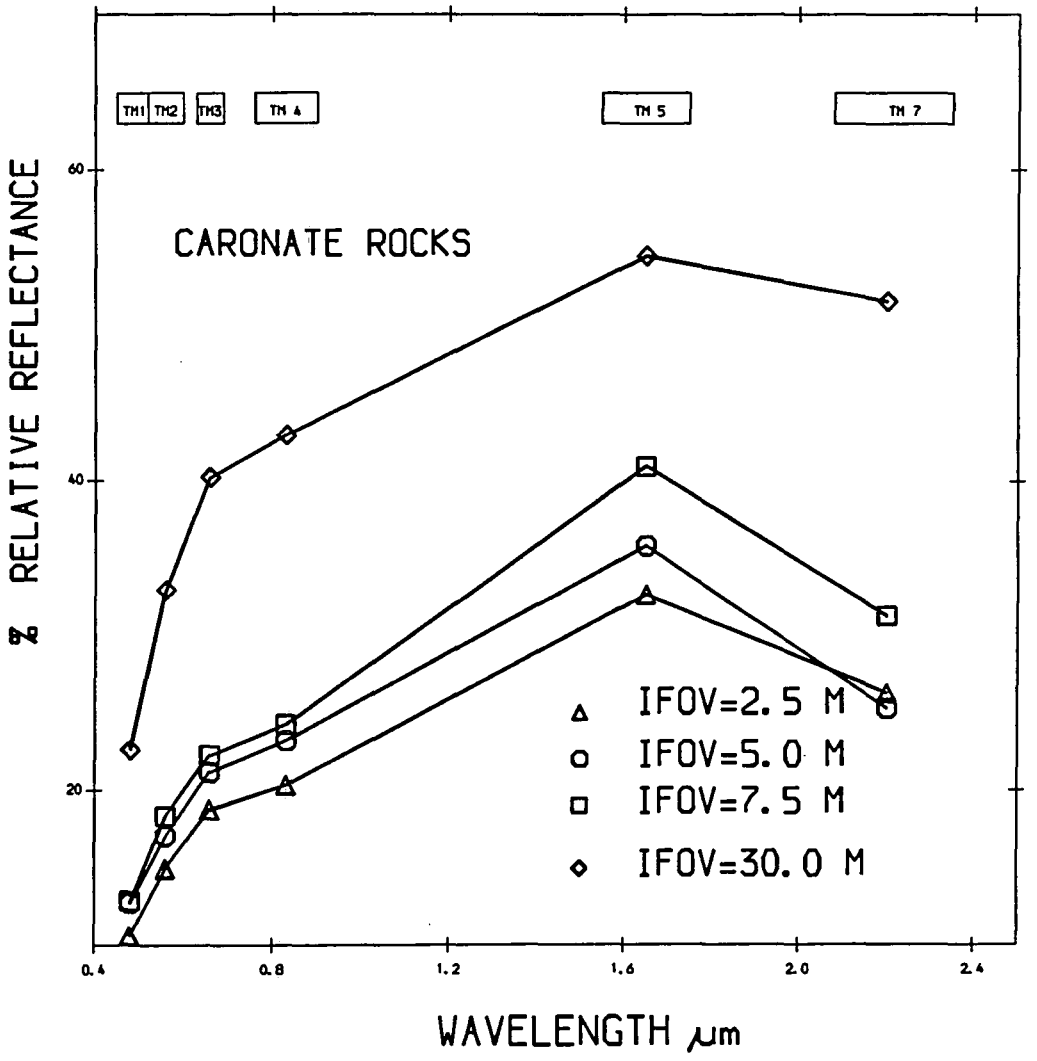

Fig. 5.8 Comparison of spectra from different spatial resolution, Mahd Adh Dhahab.

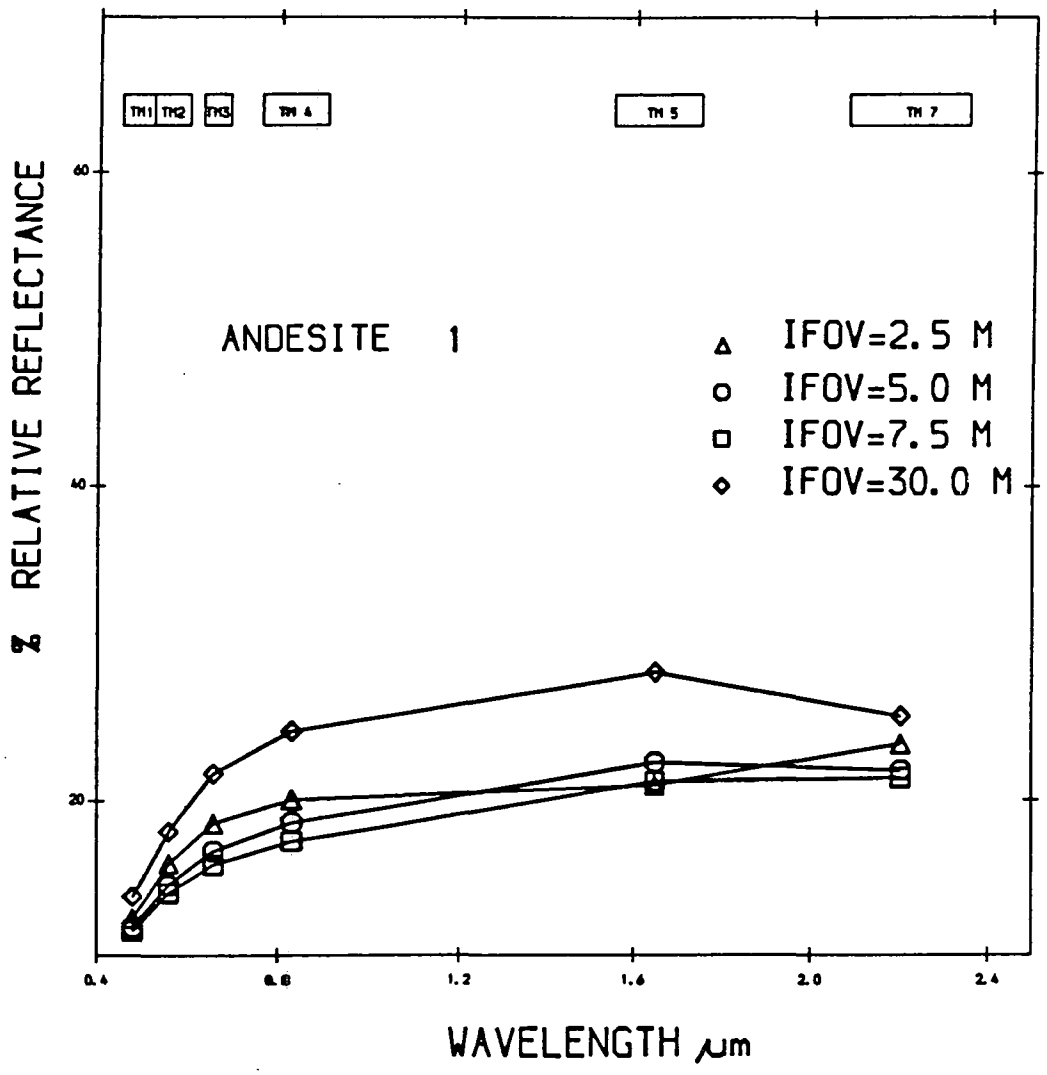

Fig. 5.9 Comparison of spectra from different spatial resolutions, Mahd Adh Dhahab.

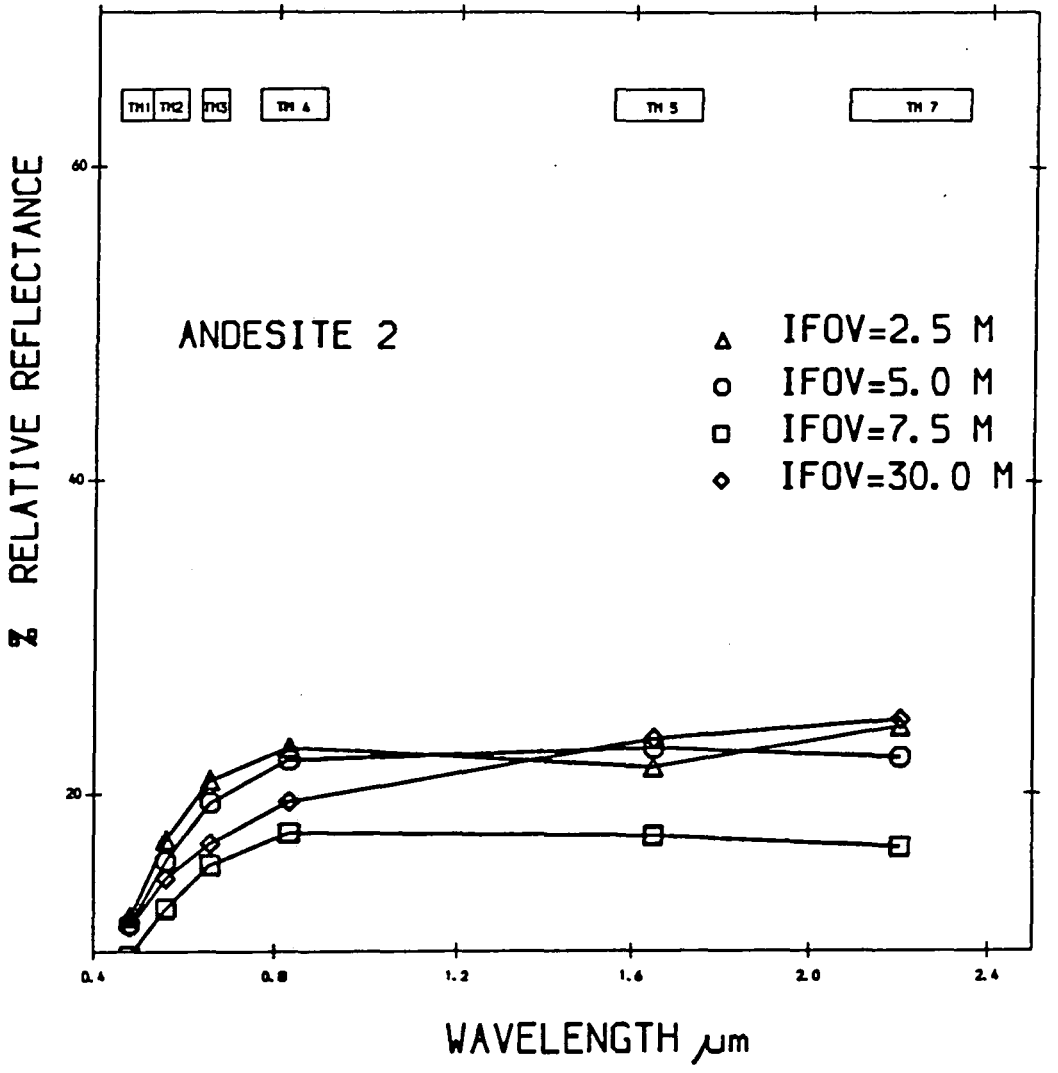

Fig. 5.10 Comparison of spectra from different spatial resolutions, Mahd Adh Dhahab.

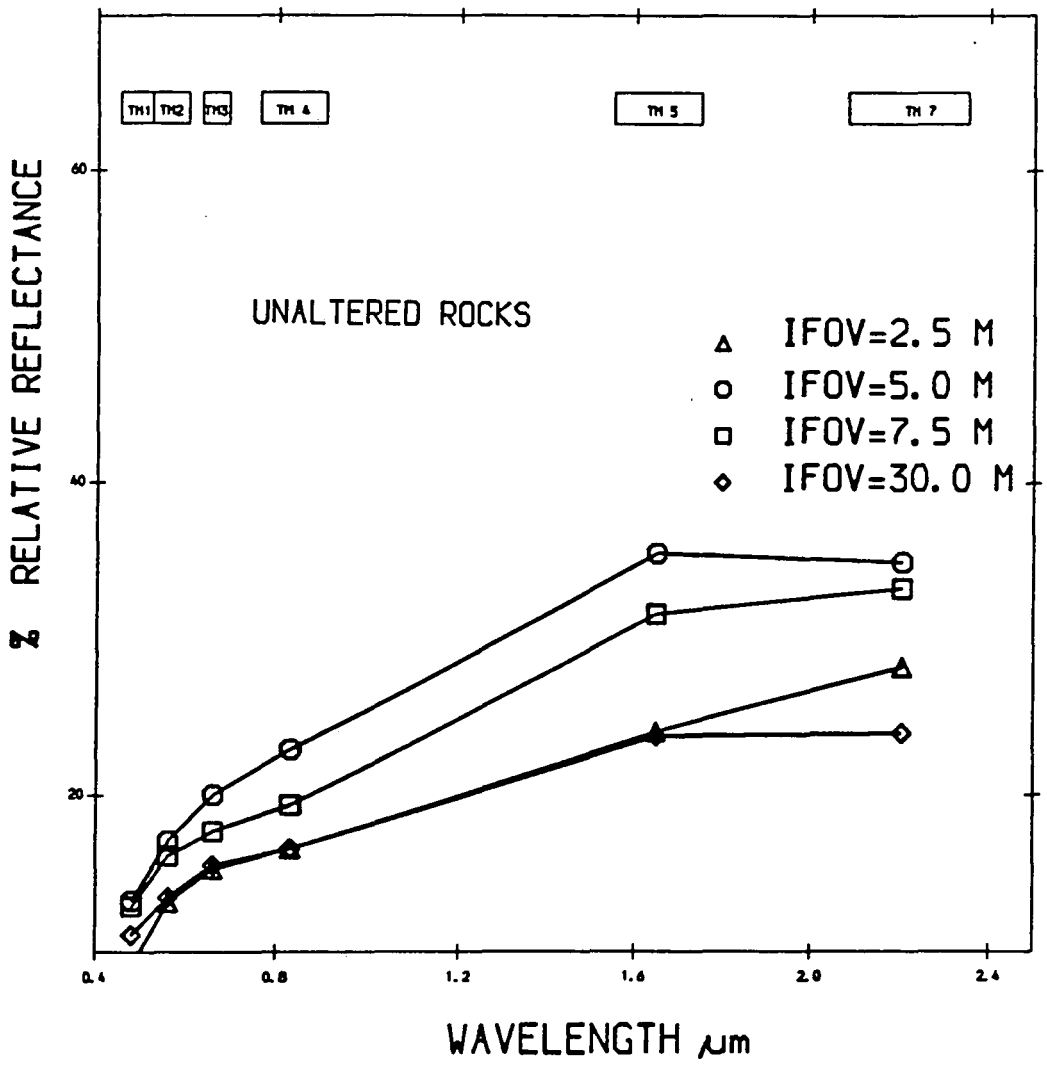

Fig. 5.11 Comparison of spectra from different spatial resolutions, Mahd Adh Dhahab.

extracted from the images for selected spatial resolutions (Tables 5.6-5.9). These spectra were plotted separately for each type of lithology (Appendix E). Many of the lithologies exhibit contrasting variations of spectral responses to Landsat TM bands, as seen in Chapter 3. These have been attributed to varying chemical and physical associations with different mineralogies. The samples from Jabal Said emphasise the variations between different lithologies in the area, including the alteration zone and the gossan.

The spectra produced from the 5.0m IFOV ATM sensor data seem to show the highest albedos for most of the lithologies, and the spectra from the 2.5m resolution data exhibit the lowest albedo. Significant features are evident around 0.9um in almost all the samples at the 2.5m IFOV resolution.

Generally the quartz gravel which was considered as the light target in the area, exhibits the highest albedo, while the andesite gravel, considered as the dark target, gave the lowest albedo.

5.3.2.1 Granite

The spectra of granite of the TM data and ATM 7.5m, coincided, which might suggest the homogeneity of the granite rocks which were sampled by 3.0m/pixel and 7.5m/pixel resolution. The spectra of the granite from ATM 5.0m and 2.5m IFOV resolution is attributed to internal variations with the granite rocks, where the 2.5m IFOV spectra shows a weak absorption around 2.5um. The internal

Table 5.6 Means of calibrated DN values to relative reflectance extracted from ATM 3000m image (7.5m resolution), using TM band equivalent, Jabal Said area.

Lithology	ATM2	ATM3	ATM5	ATM7	ATM9	ATM10
Granite	14.870	18.792	22.170	26.068	31.695	33.134
Dacite T.	11.450	14.319	16.482	20.495	28.032	30.778
Pegmatite	15.159	20.024	24.520	27.246	28.386	24.950
Rhyolite	12.172	14.449	15.420	17.747	14.324	9.822
Diorite	12.365	14.967	17.923	21.672	29.450	28.050
Andesite gravel	13.039	16.523	19.212	21.829	32.995	31.026
Gossan	12.606	16.523	20.501	22.850	46.702	45.410
Alteration zone	12.221	16.069	21.866	23.870	46.229	31.894
Andesite Tuff	10.968	13.087	14.359	18.140	35.713	34.622
Quartz gravel	20.072	27.999	33.924	37.215	45.520	48.386
Zubaidah B.	12.269	14.513	15.724	18.532	28.623	35.118

Table 5.7 Means of calibrated DN values to relative reflectance extracted from ATM 2000m image (5.0m resolution), using TM band equivalent only. Jabal Said area.

Lithology	ATM2	ATM3	ATM5	ATM7	ATM9	ATM10
Granite	18.404	22.100	26.006	29.143	36.575	38.943
Dacite Tuff	14.864	17.366	19.960	23.286	33.398	33.399
Pegmatite	15.997	18.725	22.742	25.534	31.633	28.485
Rhyolite	15.105	16.928	18.516	21.096	27.339	25.650
Diorite	14.864	17.410	21.405	23.226	32.634	33.273
Andesite gravel	13.560	15.613	18.248	21.274	27.162	25.587
Gossan	15.448	17.366	20.656	26.303	44.930	44.802
Alteration zone	13.834	16.314	21.619	23.522	46.636	37.431
Andesite tuff	11.877	12.457	13.450	17.546	36.164	36.297
Quartz gravel	21.559	27.623	33.603	37.131	43.871	45.747
Zubaidah B.	13.834	15.219	16.804	19.440	33.045	36.612

Table 5.8 Means of Calibrated DN values to relative reflectance extracted from ATM 1000m image (2.5m resolution), using TM band equivalent. Jabal Said area.

Lithology	ATM2	ATM3	ATM5	ATM7	ATM9	ATM10
Granite	14.028	17.690	21.025	22.886	30.602	27.853
Dacite Tuff	11.273	13.610	16.377	17.486	29.378	26.596
Pegmatite	8.106	8.378	9.657	8.036	13.236	5.426
Rhyolite	11.241	13.850	17.217	18.094	30.984	26.790
Diorite	9.753	10.970	13.297	14.381	29.990	24.276
Andesite gravel	11.304	13.898	17.497	17.891	30.525	25.920
Gossan	11.463	14.522	19.177	20.186	46.514	43.996
Alteration zone	10.323	12.554	15.369	12.963	28.613	11.710
Andesite tuff	9.278	9.722	11.393	11.748	25.782	21.860
Quartz gravel	15.231	20.522	25.001	26.193	34.503	32.976
Zubaidah B.	10.291	11.402	13.185	12.356	23.640	21.860

Table 5.9 Means of Calibrated DN values to relative reflectance extracted from TM image (30.0m resolution), Jabal Said area.

Lithology	TM1	TM2	TM3	TM4	TM5	TM7
Pegmatite	12.60333	15.55583	18.47500	23.18000	26.32550	24.95750
Quartz gravel	20.43667	28.56333	34.50917	37.99800	43.60467	46.56250
Andesite gravel	14.20917	18.70167	22.85333	24.85300	37.09633	35.97750
Zubaidah B.	11.89833	14.33667	15.33917	16.56767	25.46300	33.44000
Dacitic Tuff	12.29000	15.38750	17.29167	20.23233	29.94633	28.00250
Alteration zone	9.31333	10.45667	13.26833	14.65567	34.25467	25.61000
Diorite	10.09667	11.75000	14.74750	17.60333	31.22967	31.04750
Gossan	11.62417	14.01333	15.22083	18.47967	34.80467	34.31000
Andesite Tuff	11.31083	14.01333	15.22083	18.47967	34.80467	34.31000
Granite	15.34500	19.67167	22.61667	25.80900	31.22967	33.58500
Rhyolite	14.56167	19.26750	22.02500	25.33'00	29.21300	27.13250

variation reflected by 5.0m IFOV resolution data is much less than the variation reflected by 2.5m IFOV data. All the spectra have absorptions around 0.48um and 0.9um (Fig. 5.12).

5.3.2.2 Dacite tuff

All the spectra show absorption around 2.2um, except the 7.5m IFOV resolution data which have no features at all. The 5.0m IFOV data shows the hightest albedo; while the 2.5m IFOV data shows the lowest albedo except in band TM5, the 7.5m IFOV data are the lowest. The variation in the spectra suggests that this rock is heterogeneous, and have many local variations (Fig. 5.13).

5.3.2.3 Rhyolite rocks

The rhyolite spectra exhibit changes in albedo from the visible to the near infrared wavelengths. At visible wavelengths the highest albedo is given by the TM data, followed by the 5.0m IFOV ATM data. In the near infrared however, the highest albedo is given by the 2.5m IFOV ATM data followed by the TM data. The weak absorption around 2.2um might indicate the weathering of feldspar (Fig. 5.14). The spectra suggest that the rhyolite rocks are heterogeneous, but the local and internal variations are reflected by absorption features in the visible and in the infrared parts of the spectrum (Fig. 5.14).

5.3.2.4 Diorite rocks

Fig. 5.15 reflects the homegeneity of the diorite; except for the 2.5m IFOV ATM data which shows absorption features around 2.2um and 0.9um, the other resolutions exhibit no spectral features at all at 2.2um. The high

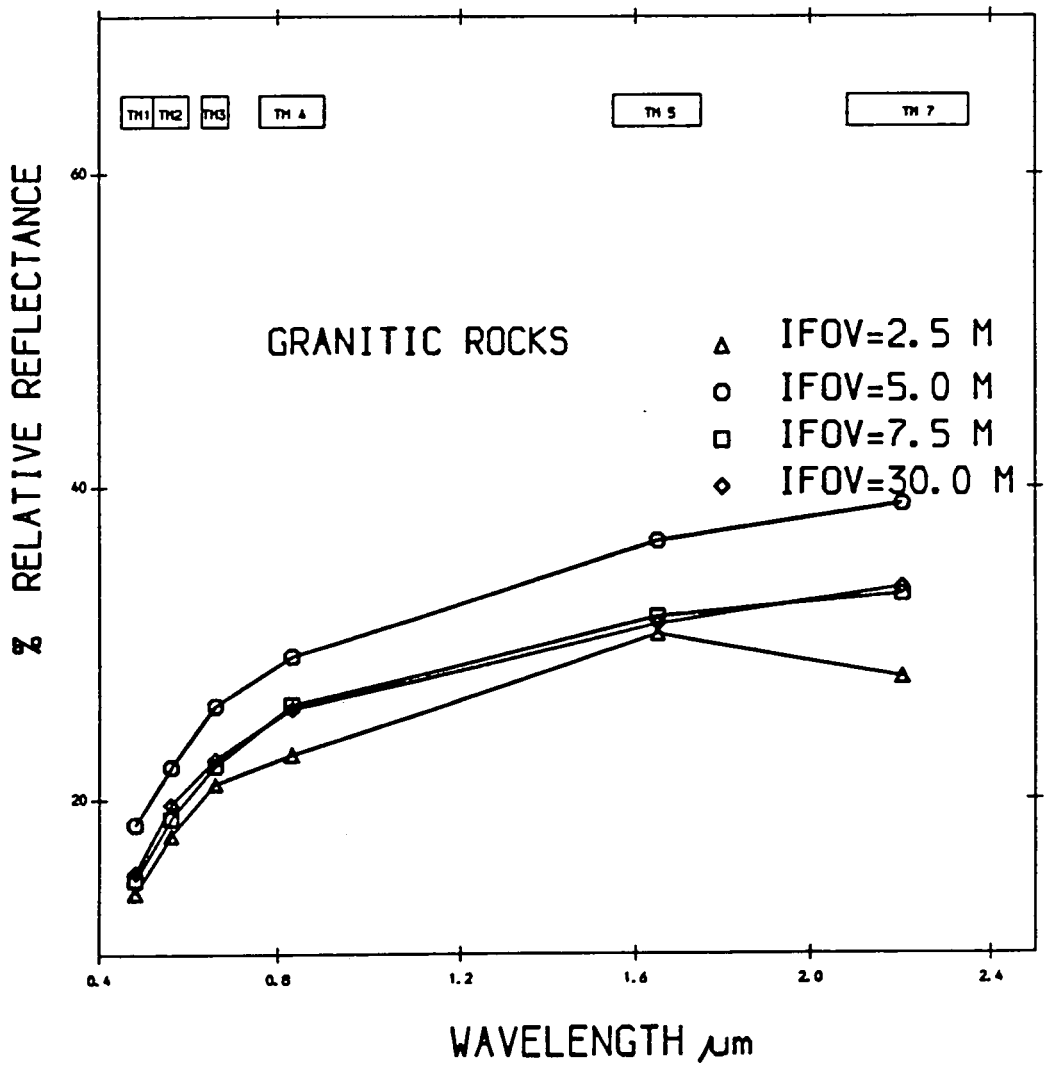

Fig. 5.12 Comparison of spectra from different spatial resolutions, Jabal Said.

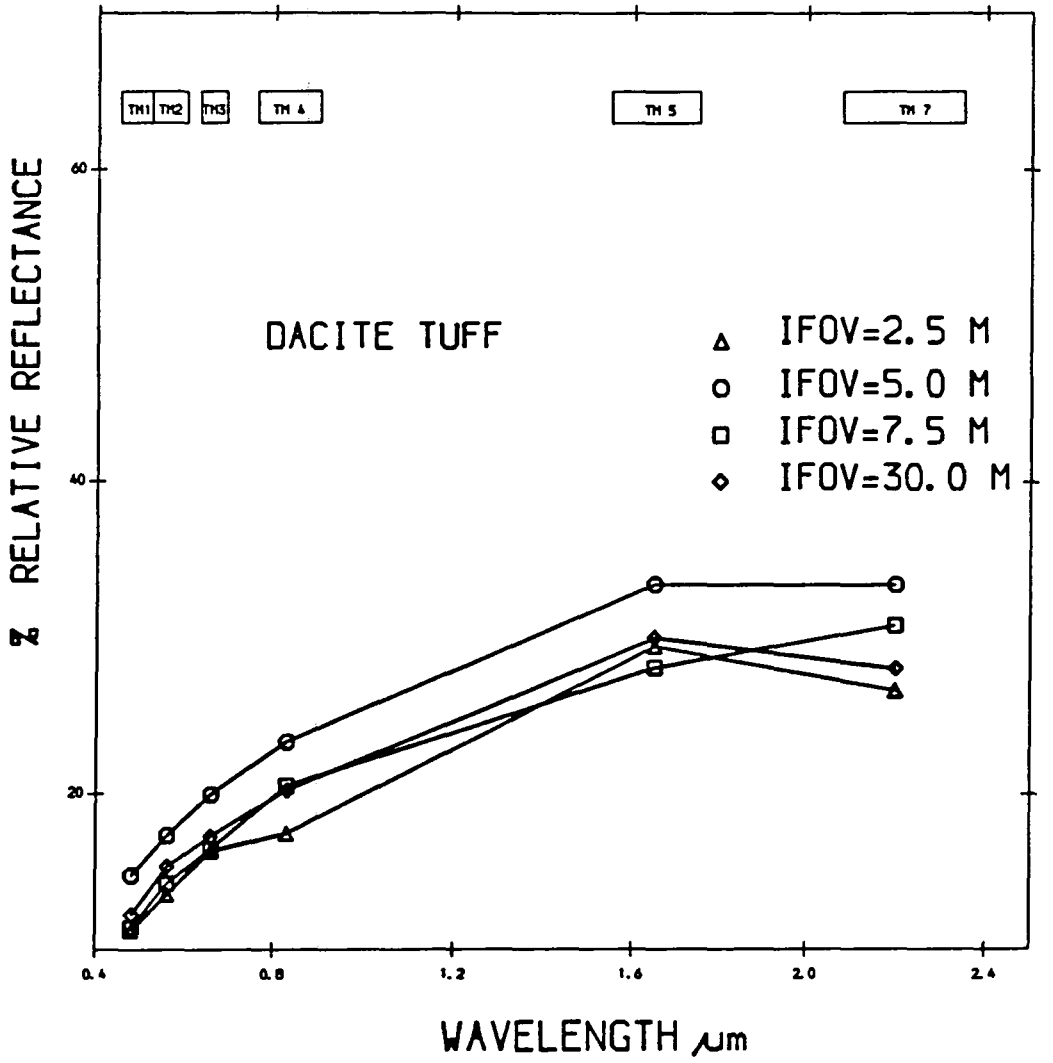

Fig. 5.13 Comparison of spectra from different spatial resolutions, Jabal Said.

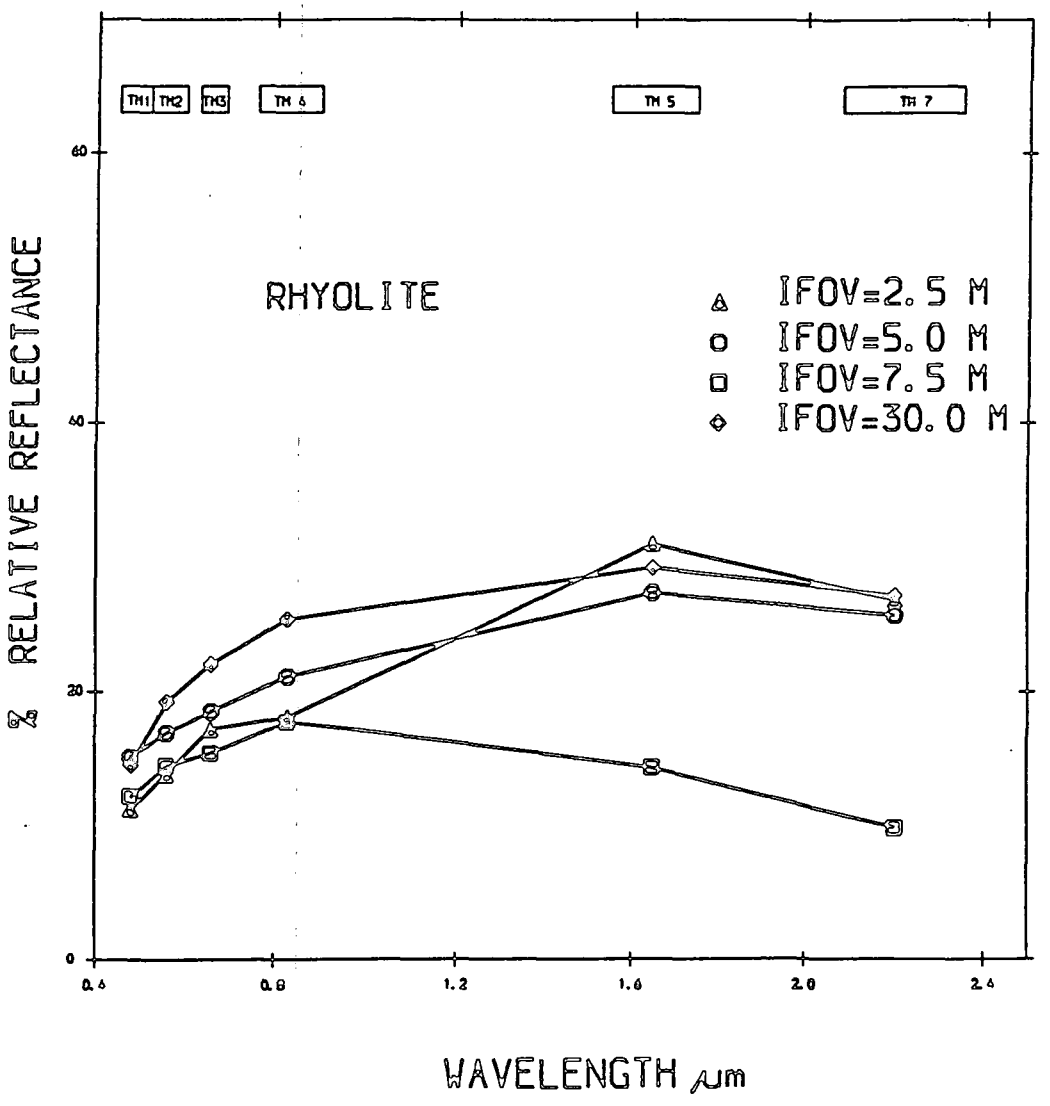

Fig. 5.14 Comparison of spectra from different spatial resolutions, Jabal Said.

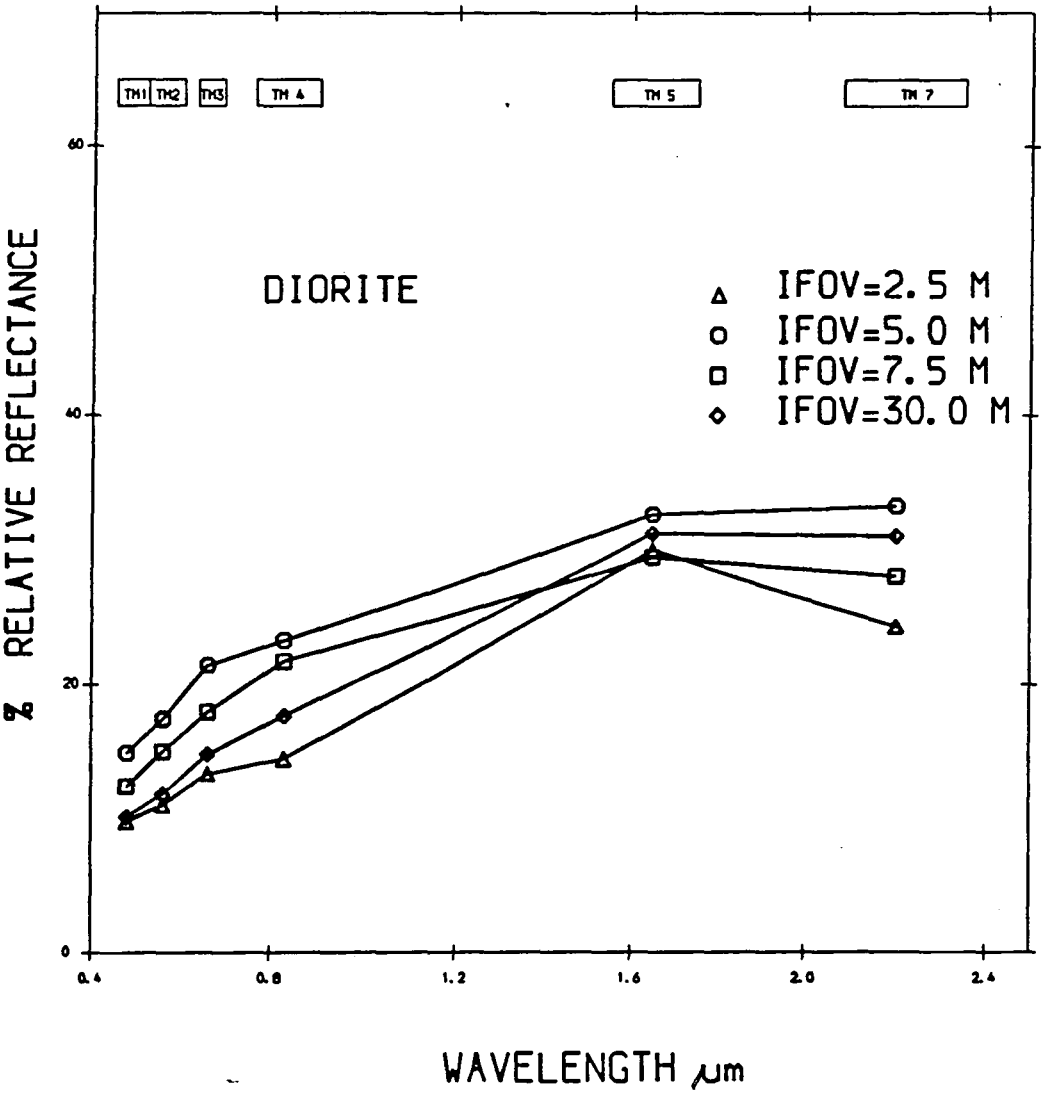

Fig. 5.15 Comparison of spectra from different spatial resolutions, Jabal Said.

resolution of the 2.5m IFOV ATM data may pick up the weathered rocks and the presence of a mineral such as chlorite, thus accounting for these absroption features. The absorption around 0.9um is due to iron staining appearing as local variation on the rocks in some places.

5.3.2.5 Andesite tuff

The spectra produced by the ATM 5.0m and 7.5m IFOV resolution data and the TM data are very similar. The drop off from the infrared towards the visible indicates the presence of iron. In addition to weathering and the presence of desert varnish, the curve produced by the 2.5m IFOV ATM data with absorption features around 2.2um, may indicate that siderite is found locally on the surface. XRD analysis has indicated the presence of kaolinite in the sample from this area, but carbonate would also account for the absorption feature. It must be a local feature however, otherwise it would be detected by data with larger IFOV such as TM (Fig. 5.16).

5.3.2.6 Alteration Zone

The general trend of the curve illustrates that both clay and iron absorption features were evident. This was confirmed by the result of XRD analysis (Chapter 3). The 5.0m and 7.5m IFOV resolution data show the highest albedos while the 2.5m IFOV ATM data gives a higher albedo than the TM data in the visible, but this is reversed in the infrared region around 1.6um. In general the spectra of all resolutions are very similar in the short wavelengths. The 5.0m and 2.5m IFOV data perhaps reflect the local variation in the alteration zone (Fig. 5.17).

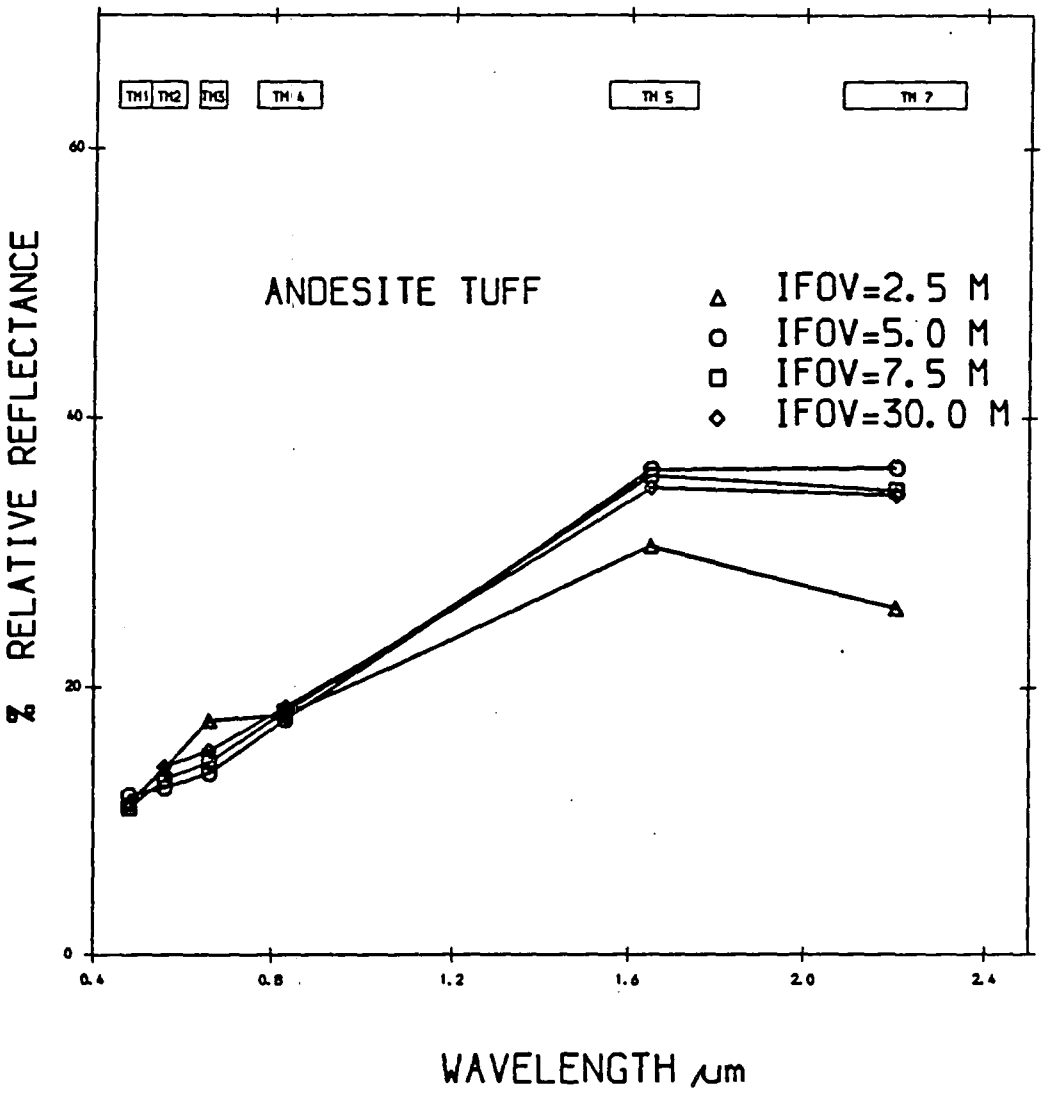

Fig. 5.16 Comparison of spectra from different spatial resolutions, Jabal Said.

5.3.2.7 Gossan

The main gossan spectra remained very similar, despite the change in resolution, suggesting homogeneity of the target. The rapid drop-off towards the visible wavelength is expected of a body rich in iron. The albedo remained similar at each resolution, but around 0.9um the 2.5m IFOV ATM data and the TM data do show absorption features (Fig. 5.18).

5.3.2.8 Quartz gravel

The spectra exhibit a high albedo. Great similarity shown by the TM 7.5m, and 5.0m IFOV ATM data, indicate the general homogeneity of the target. The 2.5m IFOV ATM data has a lower albedo than the other resolutions and also shows a weak absorption around 0.9um and 2.2um. This refelcts the fact that a high resolution may reflect internal variation, indicative of specific mineral composition (Fig. 5.19).

5.3.2.9 Andesite gravel

This represents the dark target in the Jabal Said area. The TM data shows the highest albedos followed by the 7.5m, 5.0m and 2.5m IFOV ATM data in the short wavelength region. At longer wavelengths the 2.5m ATM data shows a higher albedo than the 5.0m IFOV ATM data.

Absorption around 0.9um and 0.49um indicates the presence of iron, and the weak absorption around 2.2um may be indicative of weathering to chlorite or epidote (Hunt, 1979). Both features are picked up clearly by the high resolution sensor which suggests that these features reflect the local internal variations (Fig. 5.20).

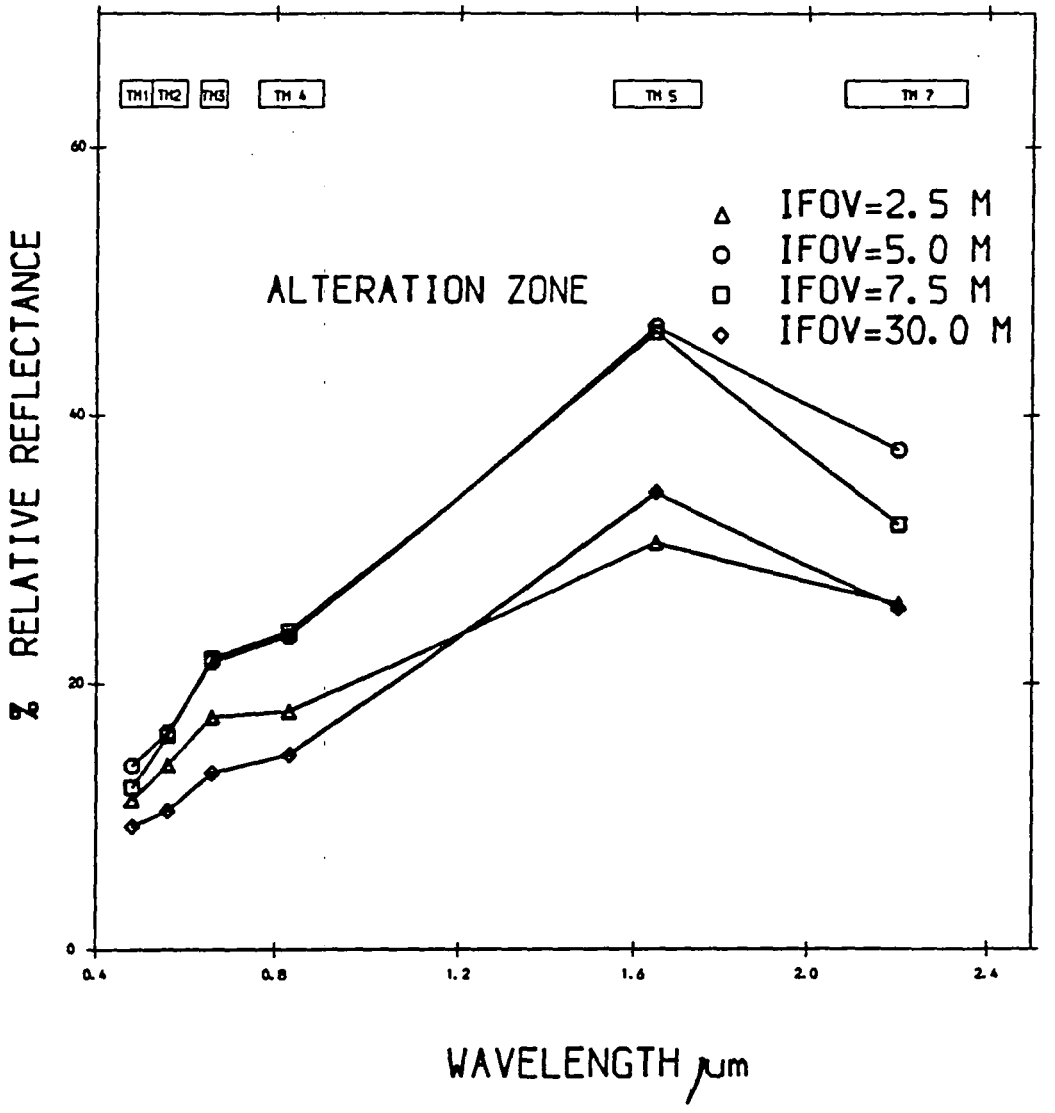

Fig. 5.17 Comparison of spectra from different spatial resolutions, Jabal Said.

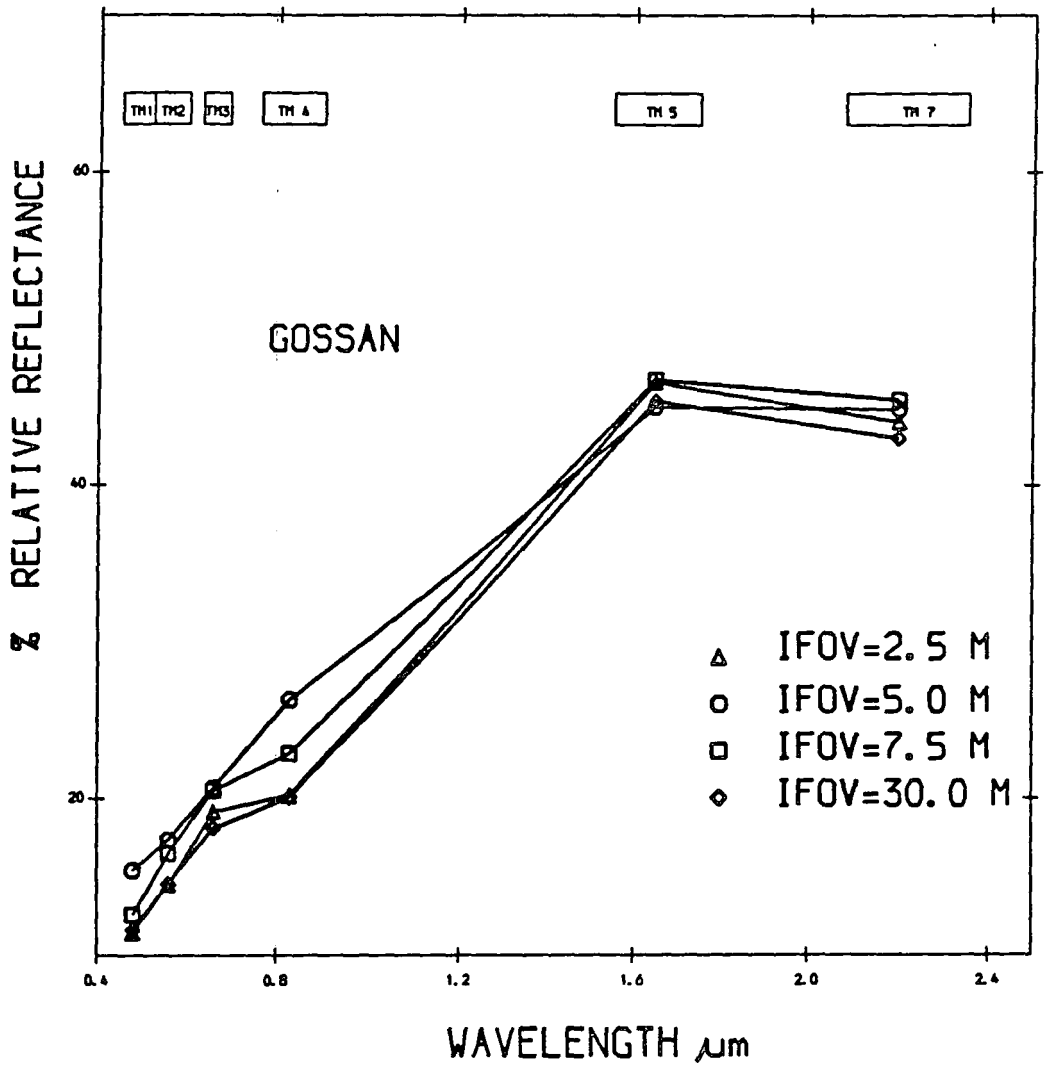

Fig. 5.18 Comparison of spectra from different spatial resolutions, Jabal Said.

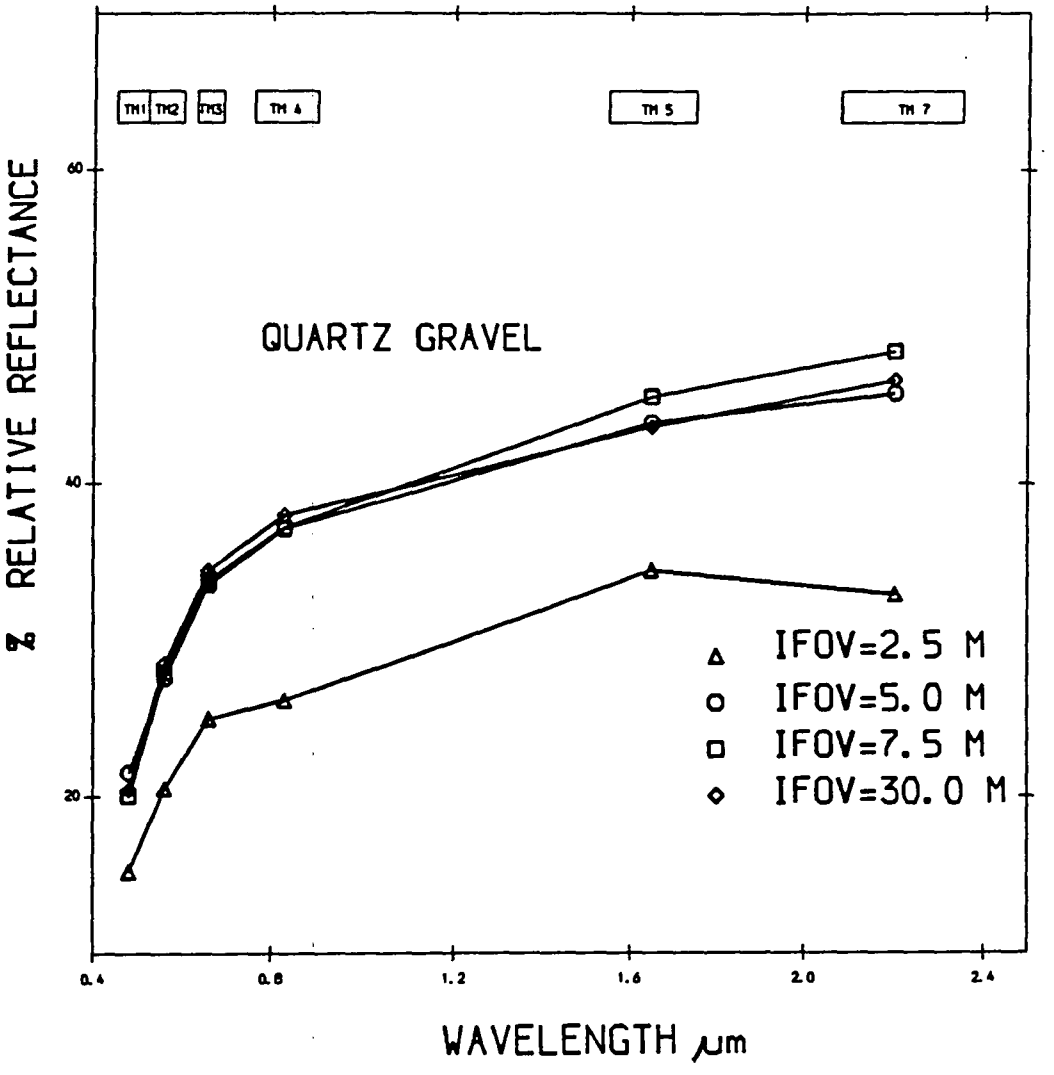

Fig. 5.19 Comparison of spectra from different spatial resolutions, Jabal Said.

5.3.2.10 Pegmatite

The similar curves shown by the TM data and the coarser 7.5m and 5.0m IFOV ATM data are evidence for the homegeneity of the rocks. The 0.5m and 2.5m IFOV ATM data picks up internal variation reflected by spectral features of the rocks. The 2.5m IFOV data show absorption features around 0.9um and 2.2um, again due to iron oxides and weathering of feldspar (Fig. 5.21).

5.3.2.11 Zubaydah breccia

There is great similarity between the spectra of the low resolution 7.5m, 5.0m IFOV ATM data and the TM spectrum; all being almost flat except for a drop off towards the visible wavelengths which is indicative of iron. The 2.5m IFOV ATM spectra shows absorption features around 0.83um and 2.2um. The difference in the spectral features between the curves attributed to the internal and local variation of the breccia (Fig. 5.22).

5.4 Discriminant analysis

As stated at the beginning of this Chapter, characteristic features of spectra can be used as a basis for differentiating between geological materials (Suits, 1983). An alternative or additional approach to visual interpretation or spectral interpretation is a quantitative approach using multivariate statistical analysis.

One of the most useful techniques of multivariate statistical analysis is discriminant analysis which helps to quantify the ability of multivariate remotely sensed

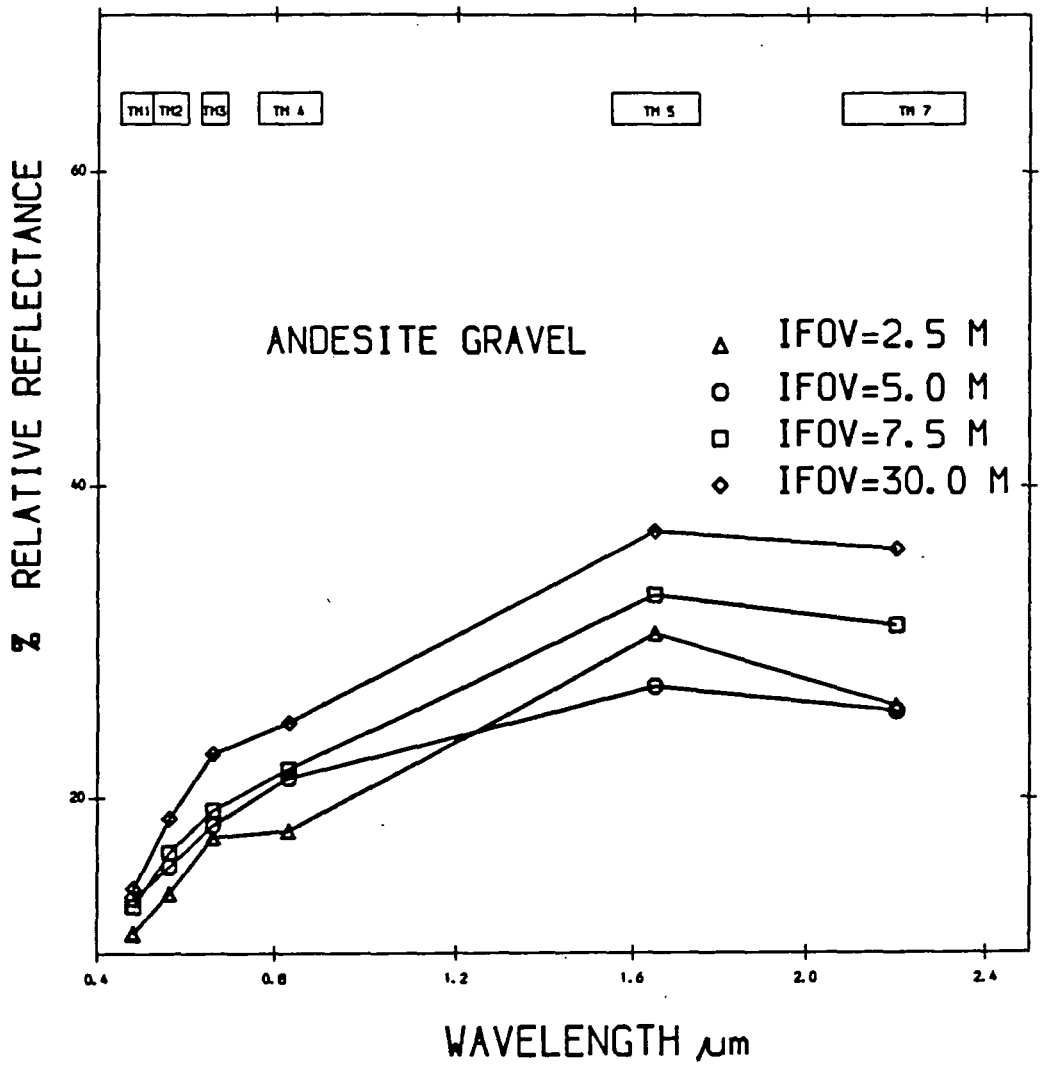

Fig. 5.20 Comparison of spectra from different spatial resolutions, Jabal Said.

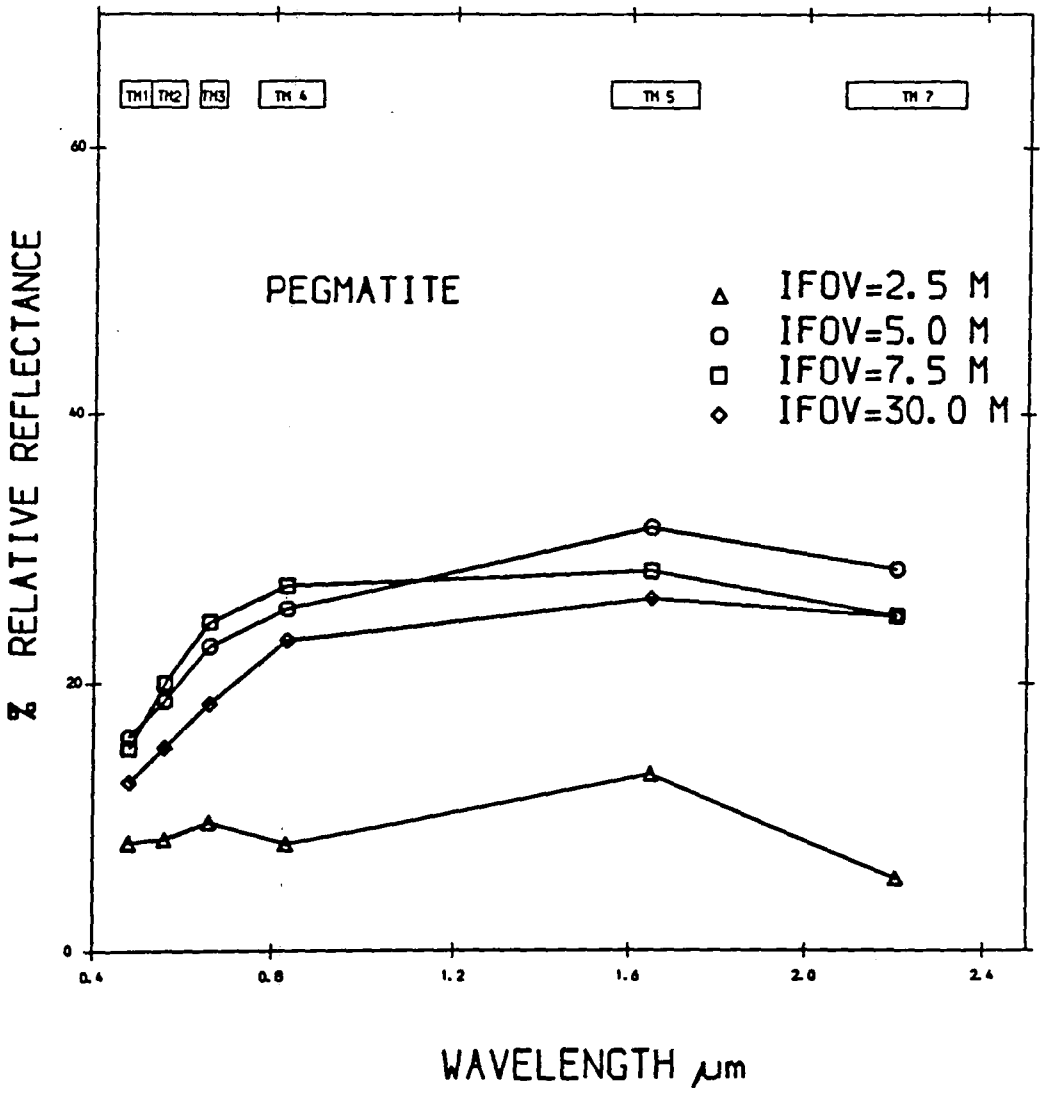

Fig. 5.21 Comparison of spectra from different spatial resolutions, Jabal Said.

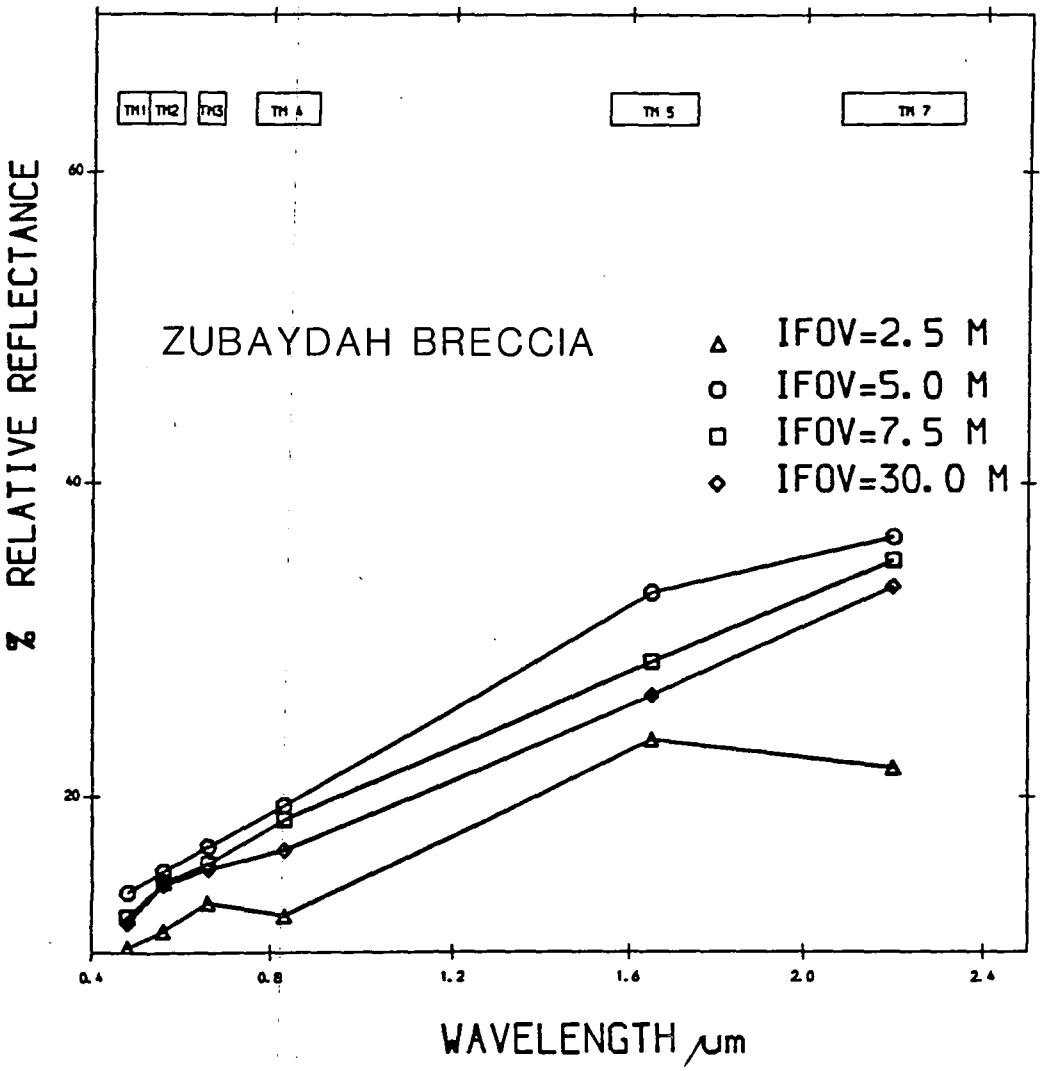

Fig. 5.22 Comparison of spectra from different spatial resolutions, Jabal Said.

data for distinguishing and separating different lithological units or surface materials.

For example, Conel et al. (1980) and Siegrist et al. (1980) used discriminant analysis on multispectral remote sensing data to distinguish between different lithologies.

The mathematics of discriminant analysis is discussed in detail by Kendall (1957) and Morrison (1967). This technique involves the weighting and linear combination of a set of discriminatory variables, forcing a set of established groups to become statistically distinct (Klecka, 1975). The linear transformations performed on the original variables are known as discriminant functions, and are constructed to provide an optimum statistical separation of specific groups.

The assumptions of discriminant analysis are that the selected groups or classes must have homogeneous variance-covarince matrices, and that the variables have normal distribution (Mather, 1976). The discriminant analysis is not seriously affected by limited inequality of variances or by limited departures from normality (Davis, 1975). As well as classifying each group, the technique calculates canonical variates which describe the optimum group separability. In particular this is attempted for different types of altered rocks with changes in resolution.

A stepwise discriminant procedure was performed on spectral data for both areas, Mahd Adh Dhahab and Jabal Said. Using the SPSSX computer progam on the University of Durham mainframe computer, the program defines a set of

linear functions of selected variates, thereby allowing a classification of spectral observation into one of a designated number of groups. This particular approach selects variation for inclusion in the discriminatory power. At each step, the spectral variable that added significantly to the separation of all the groups was entered, with that having the greatest discriminating power being entered first. As variables are selected for inclusion, some previosly selected may lose their discriminatory power. This occurs because the information they contain about group differences is now available in some combination of the other included variables. Such variables thereby become redundant, and are removed. A variable which has been removed at one step may re-enter a later step if it then satisfies the selection criterion being utilized (Klecka, 1975).

The selection criterion used in this case was the Mahalonobis D^2 statistic, which is a measure of overall similarity, between groups based upon all the variables (Mather, 1976). If D^2 is low then the two groups are similar, and conversely, if it is high they are well separated. An additional advantage of the use of this statistic was that it measures the equivalent euclidean distance in canonically transformed space (Merembeck & Turner, 1980), and as such was relatively easy to visualise as a measure of separability. The Mahalonobis D^2 distance is also used fairly frequently in classification algorithms which are applied to

multispectral remotely sensed data (e.g. Seigal & Abrams, 1976; Ballew, 1977; and Munday, 1984).

The statistical variates used in the stepwise are the TM sensor bands and their equivalent bands from the ATM sensor, and HHRR data and their ratios. It is necessary to bear in mind that each lithology has been defined as a matrix of 4 or 6 pixel values for each band.

5.4.1 Discrimination of lithologies in the Mahd Adh Dhahab area

The statistical variables used in the stepwise discriminant analysis were ATM bands 2 to 10, covering the region 0.4 to 2.35um, the TM equivalent bands, and the calibrated band ratios (Table 5.10). ATM band 1 was neglected in the analysis due to noise in the data.

Three different types of analysis were conducted. Firstly, uncalibrated data was used and analysis was performed on TM sensor data, ATM sensor data and HHRR radiometer data. Secondly the same data sets were used (Table 5.10), but prior to analysis the data were calibrated using ground truth measurements as described in Chapter 4. The third analysis involved the use of band ratios.

The above mentioned analyses were conducted for each type of resolution data; ATM 7.5m, 5.0m, 2.5m IFOV data; TM and HHRR data.

Although three types of analysis were conducted, the discussion will concentrate on the second analysis, where all the data were calibrated. Only a percentage of variance of the first and third analyses will be presented

Table 5.10 Spectral variables used in the stepwise discriminant analysis of data for Mahd Adh Dhahab and Jabal Said area.

a) Single band ATM

ATM2
ATM3
ATM4
ATM5
ATM7
ATM8
ATM9
ATM10

b) Single band TM and their equivalent from the ATM calibrated to ground reflectance

TM1
TM2
TM3
TM4
TM5
TM7

c) ATM Ratio (band equivalent to TM and calibrated to relative reflectance only)

ATM 2/3
ATM 2/5
ATM 2/7
ATM 2/9
ATM 2/10
ATM 3/5
ATM 3/7
ATM 3/9
ATM 3/10
ATM 5/7
ATM 5/9
ATM 5/10
ATM 7/9
ATM 7/10
ATM 9/10

d) ATM Ratio

ATM Ratio 2/3	ATM Ratio 3/5	ATM Ratio 4/8	ATM Ratio 6/9
ATM Ratio 2/4	ATM Ratio 3/6	ATM Ratio 4/9	ATM Ratio 6/10
ATM Ratio 2/5	ATM Ratio 3/7	ATM Ratio 4/10	ATM Ratio 7/8
ATM Ratio 2/6	ATM Ratio 3/8	ATM Ratio 5/6	ATM Ratio 7/9
ATM Ratio 2/7	ATM Ratio 3/9	ATM Ratio 5/7	ATM Ratio 7/10
ATM Ratio 2/8	ATM Ratio 3/10	ATM Ratio 5/8	ATM Ratio 8/9
ATM Ratio 2/9	ATM Ratio 4/5	ATM Ratio 5/9	ATM Ratio 8/10
ATM Ratio 2/10	ATM Ratio 4/6	ATM Ratio 6/7	ATM Ratio 9/10
ATM Ratio 3/4	ATM Ratio 4/7	ATM Ratio 6/8	

for comparison. This is because such data are not available for TM and HHRR data, nor is the data calibrated.

The discrimination and classification analysis was applied first on eleven lithologies from the Mahd area, representing different types of alteration and rock units. Secondly, these eleven lithologies were regrouped into three groups and the analysis was run again to discriminate between three groups of lithologies where all the alteration units were considered as one alteration unit.

5.4.1.1 Discrimination between eleven lithologies using ATM 7.5m resolution data

The results of the canonical discriminant functions are presented in Table 5.11. These show that the first three discriminant functions account for over 85% of the total variance among the groups. With the inclusion of the fourth function, the percentage rises to 99.7%. The relative importance of these functions can be interpreted from the eigen values, where the sum of the eigen values is a measure of the total variance existing within the discriminatory variables. The suggestion that the first four functions are the most significant, can be supported by looking at the canonical correlation coefficients for the four functions compared with that of the fifth function. The canonical correlation coefficients when squared, indicate the proportion of the variance in the discriminant function explained by the groups or classes (Klecka, 1975). Usually, high correlation coefficients

Table 5.11 Canonical Discriminant functions for the ATM 7.5m data

Function	Eigen Value	% of Variance	Canonical correlation
1	77.88	45.43	0.993
2	60.258	35.15	0.991
3	23.706	13.83	0.979
4	9.106	5.31	0.949
5	0.383	0.22	0.526
6	0.111	0.07	0.317

Table 5.12 Discriminant analysis of the ATM 3000m data (IFOV=7.5m) : standardised canonical discriminant function coefficients, Mahd Adh Dhahab area.

Bands	Function 1	Function 2	Function 3	Function 4	Function 5	Function 6
Band ATM 2 (0.43um)	0.37697	1.12863	0.64387	1.58161	1.32884	0.67882
Band ATM 3 (0.65um)	-0.33907	-0.66166	0.36641	-0.73328	-2.60991	-1.99599
Band ATM 5 (0.66um)	0.00704	-0.14539	-0.27834	-1.16952	0.27932	2.34430
Band ATM 7 (0.83um)	0.41004	0.78082	0.38485	-0.38420	0.97233	-1.02090
Band ATM 9 (1.65um)	-0.45010	-2.24280	0.67119	0.92213	0.25883	0.08064
Band ATM 10 (2.22um)	1.14285	1.24739	-1.30632	0.17231	0.10989	0.12378

reflect the importance of the functions in the discrimination of groups, while lower coefficients suggest a poorer discriminatory power. In addition, the low eigen value of the fifth function indicates that it will not improve the group discrimination.

Table 5.12 shows the standard canonical discriminant function coefficients for the ATM 7.5m data. It indicates that functions one and two are positively weighted for the shortwave infrared ATM band 10 (2.2um). These are considered the most significant contributions, followed by ATM band 7 (0.83um) and band 2 (0.48um). Function 3 is dominated by ATM band 9 (1.65um), followed by ATM band 2 (0.48um) and ATM band 7 (0.83um), while function 4 is affected by ATM bands 2 (0.48um) and 9 (1.65um). Function 5 indicates a similar pattern to that of function 3 and function 6 is dominated by ATM bands 5 (0.66um) and 2 (0.48um). It must be said that the interpretation of each discriminant function in terms of its physical relationship to spectral reflectance is particularly difficult (Munday, 1985).

5.4.1.2 Discrimination between eleven lithologies using ATM 5.0m IFOV data

The results of the discriminant analysis and the canonical discriminant functions for the calibrated TM equivalent data are presented in Table 5.13.

It can be seen that the first three discriminant functions account for over 95% of the total variance among groups. However, the eigen values and the canonical correlation coefficients suggest that the fourth and fifth

Table 5.13 Canonical Discriminant Function for the ATM 5.0m data

Function	Eigen Value	% of Variance	Canonical correlation
1	104.395	56.77	0.995
2	60.068	32.66	0.991
3	11.043	6.01	0.957
4	5.766	3.14	0.923
5	2.103	1.14	0.823
6	0.522	0.28	0.585

Table 5.14 Discriminant analysis of the ATM 2000m data (IFOV=5.0m): standardised canonical discriminant function coefficients, Mahd Adh Dhahab area.

Bands	Function 1	Function 2	Function 3	Function 4	Function 5	Function 6
Band ATM 2 (0.43um)	-1.33641	2.17504	-1.62214	1.08634	0.80431	0.14472
Band ATM 3 (0.65um)	-0.22781	-0.39126	3.22278	0.82615	-2.32480	-1.32782
Band ATM 5 (0.66um)	0.83710	-1.89484	-1.97561	-0.46403	0.81269	3.18633
Band ATM 7 (0.83um)	1.50242	-0.12057	-0.30226	-1.11086	0.00873	-1.84292
Band ATM 9 (1.65um)	0.12087	-0.45735	0.22569	1.04814	0.69588	0.52999
Band ATM 10 (2.22um)	-0.19250	1.41678	0.66904	-0.55954	0.03372	0.48505

functions also make a significant contribution to the discrimination of different lithologies, by raising the percentages of total variance to 98.57% and 99.72% respectively. The sixth function also has a low eigen value which suggests that little contribution can be made to further discriminate the data.

The standard discriminant function coefficients for the ATM 5.0m IFOV data are shown in Table 5.14.

Inspection of this table indicates that the first function is heavily weighted by the contribution of ATM band 7 (0.83um), followed negatively by band 2 (0.48um) and band 3 (0.56um) and band 9 (1.65um). Function 2 is dominated by ATM band 2 (0.43um) followed negatively by band 5 (0.66um) and positively by band 10 (2.2um). ATM band 3 (0.65um) dominates function 3, followed by the shortwave infrared ATM band 10 (2.2um) and ATM band 9 (1.6um). Finally, the fourth function which allows 98% of the discrimiantion, is dominated by ATM bands 2 (0.48um), 9 (1.6um) and 7 (0.83um).

5.4.1.3 Discrimination betweel eleven lithologies using ATM 2.5m IFOV data

The results of the discriminant analysis of the calibrated data are presented in Table 5.15. This indicates that the first three functions account for over 94% of the total variance whill addition of the fourth function improves this to 99%.

The standard discriminant function coefficients are given in Table 5.16. Here the first function is positively heavily weighted by ATM band 7 (0.83um),

Table 5.15 Canonical Discriminant function for the ATM 2.5m data

Function	Eigen Value	% of Variance	Canonical correlation
1	138.59	65.22	0.996
2	45.12	21.23	0.989
3	17.65	8.31	0.973
4	9.67	4.55	0.952
5	1.24	6.58	0.744
6	0.22	0.10	0.425

Table 5.16 Discriminant analysis of the ATM 1000m data (IFOV=2.5m): standardised canonical discriminant function coefficients, Mahd Adh Dhahab area.

Bands	Function 1	Function 2	Function 3	Function 4	Function 5	Function 6
Band ATM 2 (0.43um)	0.30952	1.01559	1.20225	1.18302	-0.69302	-0.66958
Band ATM 3 (0.65um)	0.22293	0.95113	1.26092	0.09527	1.18779	2.67366
Band ATM 5 (0.66um)	-0.42161	-2.19155	-2.52064	1.12949	1.29467	-3.47927
Band ATM 7 (0.83um)	0.79884	0.59152	-0.80454	-1.68194	-1.85186	1.73425
Band ATM 9 (1.65um)	0.42943	-0.77962	0.97558	0.23661	-0.41561	0.11070
Band ATM 10 (2.22um)	0.44132	0.90275	0.23019	-0.50175	0.48014	-0.27365

following by the infrared ATM band 10 (2.2um) and 9 (1.6um), and the visible ATM bands 2 (0.48um) and 3 (0.56um). The second function is determined negatively by band 5 (0.66um), followed positively by bands 2 and 3, followed by bands 10 (2.2um) and 9 (1.6um). The third function determined by negative band 5 (0.66um), but the visible bands ATM2 and ATM3 dominate, while the near infrared ATM bands 9 (1.6um) and 10 (2.2um) are of lesser importance.

From the results in this table it can be seen that the first three discriminant functions account for over 94% of the total variance among the groups. By including the fourth function the percentage of total variance increased to 99.77%.

5.4.1.4 Discrimination between eleven lithologies using TM data (IFOV = 30m)

The result of the discriminant analysis and canonical discriminant function for the calibrated TM bands to ground truth are presented in Table 5.17. From the result in this table, we can see that the first three discriminant functions accounted for over 94% of the total variance. This increases to 99.77% by including the fourth discriminant function. This is only analysis where we have only five variables where TM2 (0.65um) was removed from the analysis.

The standard discriminant analysis of TM data are given in Table 5.18, which shows that the first function dominated visible band TM 1 (0.48um), TM 3 (0.66um) followed by infrared TM7 (2.2um). The second function is

Table 5.17 Canonical Discriminant function for the TM data

Function	Eigen Value	% of Variance	Canonical correlation
1	47.40	70.15	0.989
2	12.15	17.98	0.961
3	4.58	6.79	0.906
4	3.27	4.84	0.875
5	0.157	0.23	0.369

Table 5.18 Discriminant analysis of the TM data (IFOV = 30m): standardised canonical discriminant function coefficients, Mahd Adh Dhahab area.

Bands	Function 1	Function 2	Function 3	Function 4	Function 5
Band TM 1 (0.43um)	0.54159	0.98977	0.07040	-0.44248	1.29670
Band TM 3 (0.66um)	0.77316	-0.20090	1.95500	-1.92230	-2.53121
Band TM 4 (0.83um)	-0.57850	-1.83198	-3.33986	1.80352	-0.96975
Band TM 5 (1.65um)	-0.06392	-1.16613	1.31335	-0.01537	0.91042
Band TM 7 (2.22um)	0.47058	2.31677	0.28413	0.80262	-0.27653

heavily weighted by TM7 (2.2um) followed by TM1, and the third function is dominated by TM3 (0.66um) followed by TM5 (1.65um) and TM7(2.2um), but also effected negatively by TM4 (0.83um).

5.4.1.5 Discrimination among eleven lithologies using HHRR data

The results of the discriminant analysis and canonical discriminant function of the hand-held radiometer data for the Mahd Adh Dhahab area are shown in Table 5.19. This indicates that the first three functions accounted for more than 89% of the total variance between groups. Although this is the lowest percentage discussed, including the fourth function does increase the percentage to 95.96%.

The standard discrimant analysis of the HHRR data is given in Table 5.20. It shows that the first function is heavily weighted by the equivalent bandpass of TM band 2(0.56um), followed by that of TM band 5 (1.6um). The second function is dominated by bands 3 (0.66um) and 4 (0.83um) , while the third function is weighted by bands 2 (0.56um) and 4 (0.83um).

5.4.1.6 Classification of eleven lithologies of the Mahd Adh Dhahab areas

One objective of this research is to evaluate the effect of spatial resolution on the ability to classify different lithologies within the study area.

Table 5.19 Canonical Discrimination functions for the HHRR data

Function	Eigen Value	% of Variance	Canonical correlation
1	6.83	48.26	0.933
2	4.09	28.96	0.896
3	1.83	12.23	0.796
4	0.92	6.51	0.692
5	0.41	2.90	0.539
6	0.16	1.14	0.372

Table 5.20 Discriminant analysis of the HHRR data (IFOV=0.96m): standardised canonical discriminant function coefficients, Mahd Adh Dhahab area.

Bands	Function 1	Function 2	Function 3	Function 4	Function 5	Function 6
Band TM 1 (0.43um)	-2.78292	-0.99943	0.23726	-0.38747	3.37583	1.79582
Band TM 2 (0.65um)	3.60119	-1.24709	1.37769	2.78850	-5.87086	1.79853
Band TM 3 (0.66um)	-1.26860	3.44579	-6.41300	-8.70138	3.14888	-1.15929
Band TM 4 (0.83um)	-1.57303	1.10702	3.19661	6.83234	0.74997	-2.73640
Band TM 5 (1.65um)	3.21830	-2.68394	1.11445	1.39175	0.74806	0.84758
Band TM 7 (2.22um)	-0.88931	1.10886	0.72963	-1.91105	-0.38794	0.08317

This objective was achieved using discriminant functions derived from the original spectral vectors. The analysis was applied to data extracted from the images and from ground measurements so that a comparison between classfications will reflect differences in spatial resolution.

Previous studies have indicated that there are two counteracting factors which affect the accuracy of classifications, as a function of spatial resolution (Townshend, 1980). First there is the spectral heterogeneity of the land cover classes, called 'scene noise' (Wiersma & Landgerbe, 1978) and secondly the percentage of boundary (mixed) pixels increases as spatial resolution is reduced. Martham et al. (1981) state that 'change in classification accuracy with spatial resolution will be a function of the relative importance of scene noise and boundary pixels, where a scene with a small uniform target would be expected to show classification accuracy improving with finer spatial resolution, while an image with a large heterogeneous target might show the opposite trend'.

The results of the classification of eleven lithologies using ATM 7.5m IFOV data are presented in Table 5.21. This gives the classification matrix for the discriminant analysis with the variable sequence of 2.2um, 1.95um, 0.48um, 0.63um, 0.66um and 0.56um. The overall percentage of lithologies correctly classified was 100%. This is based on data extracted for specific targets.

Table 5.21 Classification matrix derived from the discrimination analysis performed on data for eleven lithologies using band equivalent to TM bands from ATM 3000m (IFOV=7.5m) as the discriminatory variable with the entry sequence, and the percentage of classification.

Actual Group Membership \ Predicted Group Membership	Wadi sediment	Andesite 1	Argillic alteration	Silicic alteration	Potassic alteration	Chlorite alteration	Quartz seric.pyrite	Pyrite chlorite alt.	Carbonate rocks	Rhyolite rocks	Andesite 2
Wadi sediment	100	0	0	0	0	0	0	0	0	0	0
Andesite 1	0	100	0	0	0	0	0	0	0	0	0
Argillic alteration	0	0	100	0	0	0	0	0	0	0	0
Silicic alteration	0	0	0	100	0	0	0	0	0	0	0
Potassic alteration	0	0	0	0	100	0	0	0	0	0	0
Chlorite alteration	0	0	0	0	0	100	0	0	0	0	0
Quartz seric. pyrite	0	0	0	0	0	0	100	0	0	0	0
Pyrite chlorite alteration	0	0	0	0	0	0	0	100	0	0	0
Carbonate rocks	0	0	0	0	0	0	0	0	100	0	0
Rhyolite rocks	0	0	0	0	0	0	0	0	0	100	0
Andesite 2	0	0	0	0	0	0	0	0	0	0	100

Variable Entry Sequence:

ATM band 10

ATM band 9

ATM band 2

ATM band 7

ATM band 5

ATM band 3

Percentage of Classification:

100.00%

Pure statistical manipulation of the data does not necessarily lead to physical reasons for the choice of variates in the classification (Conel et al. 1980).

Table 5.22 shows the classification matrix for the ATM 5.0m IFOV data, and again the percentage of accurate classifications was 100%. The variable entry sequence was different from the previous analysis: 2.2um, 0.83um, 0.49um, 1.65um, 0.66um and 0.56um.

The canonical variate scatter diagrams for the ATM 7.5m and 5.0m IFOV data are given in Figs. 5.23 and 5.24. Discrimination of the lithologies using the first two functions gives a good separation of the different lithological group. The classification results for the ATM 2.5m IFOV data are presented in Table 5.23. This shows a lower level of variance explained at 98.84% but it is not a significant change, compared to the percentage of classification of other resolution data. The change in the accuracy of classification using the variable sequence 1.7um, 0.56um, 0.66um, 2.2um, 0.49um and 0.83um was due to the misclassification of the potassic altered rocks with the rhyolite unaltered rocks (Fig. 5.25).

The classification matrix derived from the discriminant analysis performed on the eleven lithologies using TM sensor data, is presented in Table 5.24. Here, 92.31% accuracy in classification was achieved, but about 16.7% of the andesite was misclassified with the potassic altered rocks, and 25% of the potassic alkaline rocks were also mixed with the chlorite alteration and 16.7% with the

Table 5.22 Classification matrix derived from the discrimination analysis performed on data for eleven lithologies using band equivalent to TM bands from ATM 2000m (IFOV=5.0m) as the discriminatory variable with the entry sequence, and the percentage of classification.

Actual Group Membership \ Predicted Group Membership	Wadi sediment	Andesite 1	Argillic alteration	Silicic alteration	Potassic alteration	Chlorite alteration	Quartz seric.pyrite	Pyrite chlorite alt.	Carbonate rocks	Rhyolite rocks	Andesite 2
Wadi sediment	100	0	0	0	0	0	0	0	0	0	0
Andesite 1	0	100	0	0	0	0	0	0	0	0	0
Argillic alteration	0	0	100	0	0	0	0	0	0	0	0
Silicic alteration	0	0	0	100	0	0	0	0	0	0	0
Potassic alteration	0	0	0	0	100	0	0	0	0	0	0
Chlorite alteration	0	0	0	0	0	100	0	0	0	0	0
Quartz seric. pyrite	0	0	0	0	0	0	100	0	0	0	0
Pyrite chlorite alteration	0	0	0	0	0	0	0	100	0	0	0
Carbonate rocks	0	0	0	0	0	0	0	0	100	0	0
Rhyolite rocks	0	0	0	0	0	0	0	0	0	100	0
Andesite 2	0	0	0	0	0	0	0	0	0	0	100

Variable Entry Sequence:

ATM band 10 (2.2μm)

ATM band 7 (.83μm)

ATM band 2 (.49μm)

ATM band 9 (1.65μm)

ATM band 5 (.66μm)

ATM band 3 (.56μm)

Percentage of Classification:

100.00%

D I S C R I M I N A N T A N A L Y S I S FOR ATM 3000 M MAHD ADH DHAHAB

NUMBER OF CANONICAL DISCRIMINANT FUNCTIONS.. 6

SYMBOLS USED IN PLOTS			LIST OF THE 6 VARIABLES USED..	
SYMBOL	GROUP	LABEL	VARIABLE	LABEL
			ATM2	
1	1	WADI.S	ATM3	
2	2	ANDESIT 1	ATM5	
3	3	ARGIL.ALT	ATM7	
4	4	SILC.ALT	ATM9	
5	5	POT.ALT	ATM10	
6	6	CHLORIT.ALT		
7	7	Q.S.PY		
8	8	PYRITE CHLORITE		
9	9	CARBONATE R		
0	10	UNALTERED R		
A	11	ANDESITE 2.		
*		GROUP CENTROIDS		

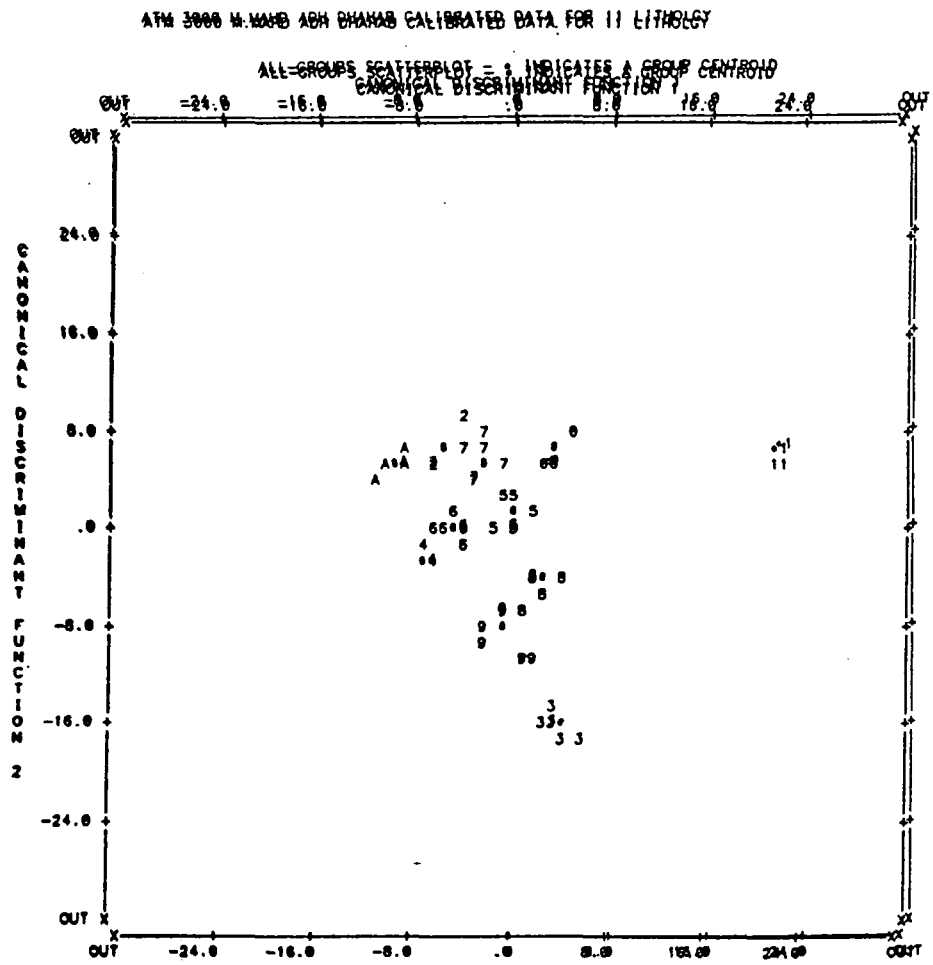

Fig. 5.23 The distribution of the eleven lithologies and alteration types in Mahd Adh Dhahab area, in canonically transformed feature space (derived from the transformation of ATM 7.5m values).

D I S C R I M I N A N T A N A L Y S I S FOR ATM2000 M MAHD ADH DHAHAB

NUMBER OF CANONICAL DISCRIMINANT FUNCTIONS.. 6

SYMBOLS USED IN PLOTS

SYMBOL	GROUP	LABEL
1	1	WADI.S
2	2	ANDESIT 1
3	3	ARGIL.ALT
4	4	SILC.ALT
5	5	POT.ALT
6	6	CHLORIT.ALT
7	7	Q.S.PY
8	8	PYRITE CHLORITE
9	9	CARBONATE R
0	10	UNALTERED R
A	11	ANDESITE 2.
∘		GROUP CENTROIDS

LIST OF THE 6 VARIABLES USED..

VARIABLE	LABEL
ATM2	
ATM3	
ATM5	
ATM7	
ATM9	
ATM10	

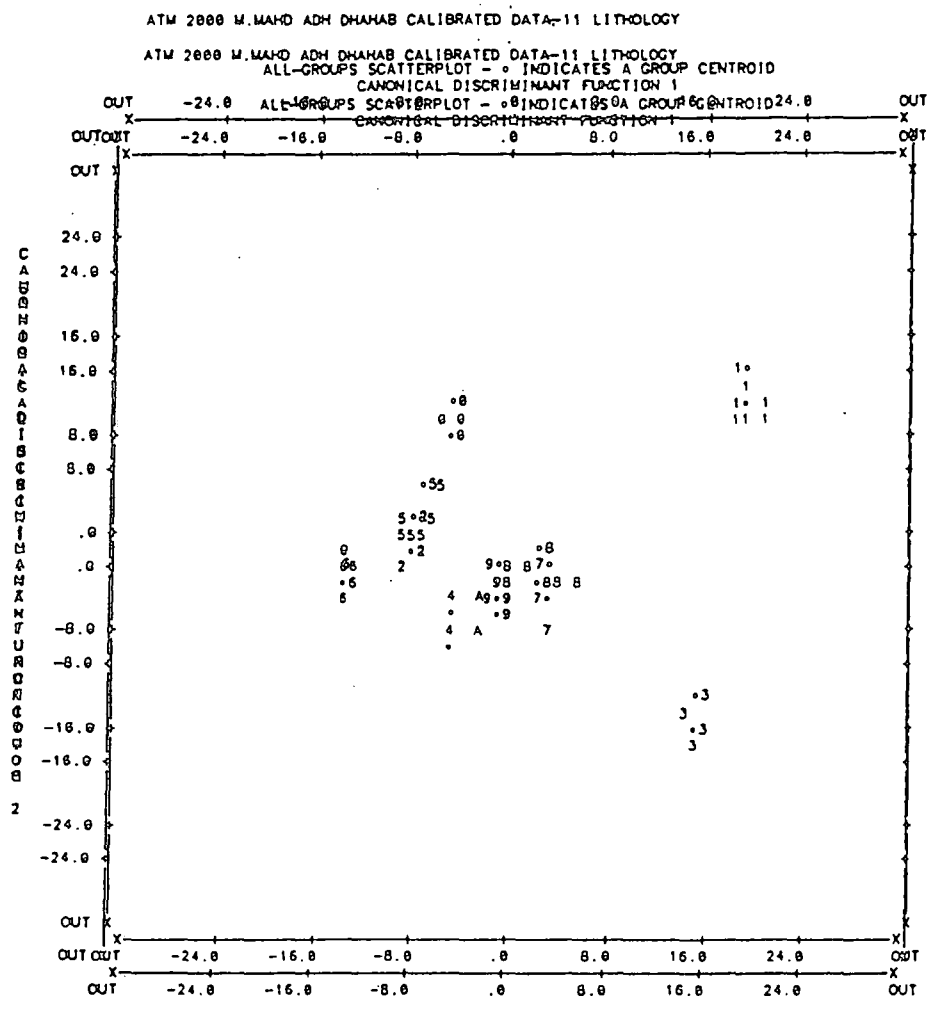

Fig. 5.24 The distribution of the eleven lithologies and alteration types in Mahd Adh Dhahab area. In canonically transformed features space (derived from the transformation of ATM 5.0m values).

Table 5.23 Classification matrix derived from the discrimination analysis performed on data for eleven lithologies using band equivalent to TM bands from ATM 1000m (IFOV=2.5m) as the discriminatory variable with the entry sequence, and the percentage of classification.

Predicted Group Membership / Actual Group Membership	Wadi sediment	Andesite 1	Argillic alteration	Silicic alteration	Potassic alteration	Chlorite alteration	Quartz seric.pyrite	Pyrite chlorite alt.	Carbonate rocks	Rhyolite rocks	Andesite 2
Wadi sediment	100	0	0	0	0	0	0	0	0	0	0
Andesite 1	0	100	0	0	0	0	0	0	0	0	0
Argillic alteration	0	0	100	0	0	0	0	0	0	0	0
Silicic alteration	0	0	0	100	0	0	0	0	0	0	0
Potassic alteration	0	0	0	0	83.3	0	0	0	0	16.7	0
Chlorite alteration	0	0	0	0	0	100	0	0	0	0	0
Quartz seric. pyrite	0	0	0	0	0	0	100	0	0	0	0
Pyrite chlorite alteration	0	0	0	0	0	0	0	100	0	0	0
Carbonate rocks	0	0	0	0	0	0	0	0	100	0	0
Rhyolite rocks	0	0	0	0	0	0	0	0	0	100	0
Andesite 2	0	0	0	0	0	0	0	0	0	0	100

Variable Entry Sequence:

ATM band 9 (1.7μm)

ATM band 3 (.56μm)

ATM band 5 (.66μm)

ATM band 10 (2.2μm)

ATM band 2 (.49μm)

ATM band 7 (.83μm)

Percentage of Classification:

98.48%

ATM 1000 M.MAHD ADH DHAHAB CALIBRATED -11 LITHOLOGY

SYMBOLS USED IN PLOTS

SYMBOL	GROUP	LABEL
1	1	WADI.S
2	2	ANDESIT 1
3	3	ARGIL.ALT
4	4	SILC.ALT
5	5	POT.ALT
6	6	CHLORIT.ALT
7	7	Q.S.PY
8	8	PYRITE CHLORITE
9	9	CARBONATE R
0	10	UNALTERED R
A	11	ANDESITE 2.
*		GROUP CENTROIDS

LIST OF THE 6 VARIABLES USED.

VARIABLE	LABEL
ATM2	
ATM3	
ATM5	
ATM7	
ATM9	
ATM10	

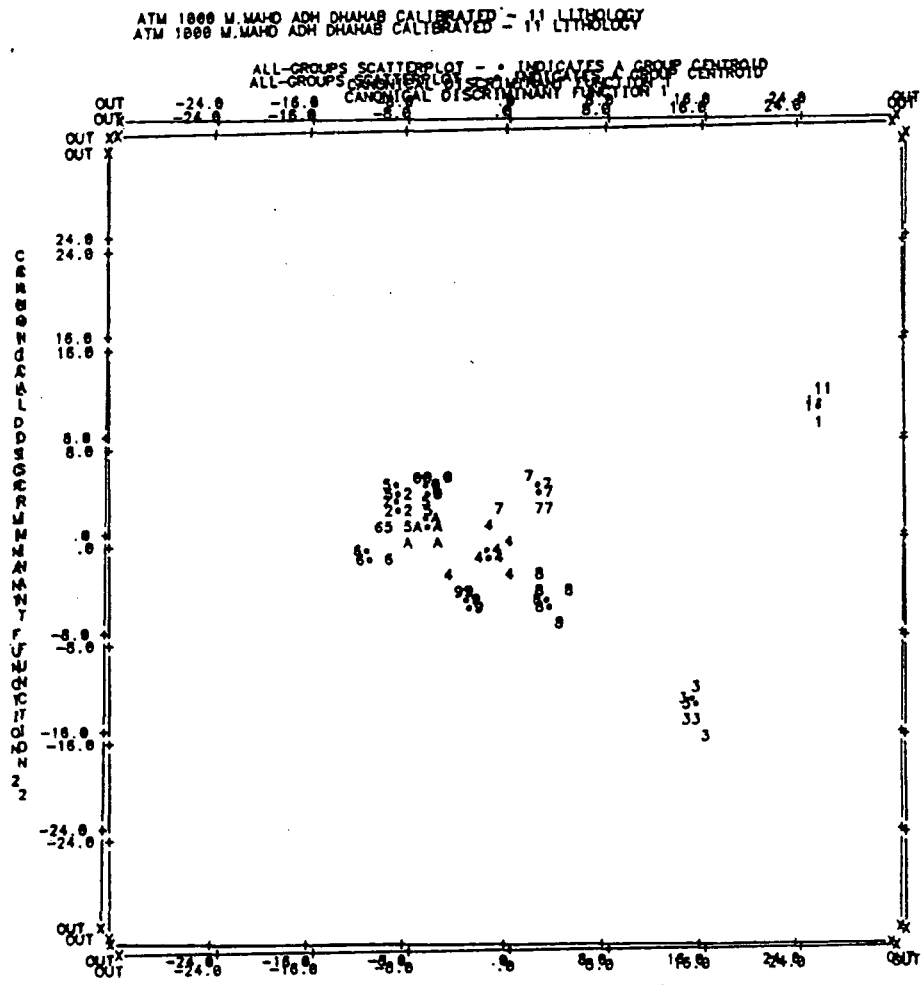

Fig. 5.25 The distribution of the eleven lithologies and alteration types in Mahd Adh Dhahab area. In canonically transformed features space (derived from the transformation of ATM 2.5m values).

Table 5.24 Classification matrix derived from the discrimination analysis performed on data for eleven lithologies using TM band (IFOV=30.0m) as the discriminatory variables with the entry sequence. Mahd Adh Dhahab area.

Actual Group Membership \ Predicted Group Membership	Wadi sediment	Andesite 1	Argillic alteration	Silicic alteration	Potassic alteration	Chlorite alteration	Quartz seric.pyrite	Pyrite chlorite alt.	Carbonate rocks	Rhyolite rocks	Andesite 2
Wadi sediment	100	0	0	0	0	0	0	0	0	0	0
Andesite 1	0	83.3	0	0	16.7	0	0	0	0	0	0
Argillic alteration	0	0	100	0	0	0	0	0	0	0	0
Silicic alteration	0	0	0	100	0	0	0	0	0	0	0
Potassic alteration	0	0	0	0	75.0	25.0	0	0	0	0	0
Chlorite alteration	0	0	0	0	50.0	50.0	0	0	0	0	0
Quartz seric. pyrite	0	0	0	0	0	0	100	0	0	0	0
Pyrite chlorite alteration	0	0	0	0	0	0	0	100	0	0	0
Carbonate rocks	0	0	0	0	0	0	0	0	100	0	0
Rhyolite rocks	0	0	0	0	0	0	0	0	0	100	0
Andesite 2	0	0	0	0	0	0	0	0	0	0	100

Variable Entry Sequence:

TM band 4 (.83μm)

TM band 5 (1.65μm)

TM band 3 (.66μm)

TM band 7 (2.2μm)

TM band 1 (1.49μm)

Percentage of Classification:

92.31%

unaltered rocks. The chlorite alteration was also mixed with the potassic altered rocks.

Only five variables were used for the TM data and the entry sequence was 0.83um, 1.65um, 2.2um and 0.49um.

Fig. 5.26 shows the scatter plot of the first two canonical functions for the lithologies.

Finally, Table 5.25 gives the classification derived from the analysis of the HHRR data. The accuracy of the classification was 72.92% although the IFOV was 0.96m. Generally it seems that the potassic altered rocks are mixed with other units (chlorite alteration and quartz sericite pyrite).

The low percentage of the accuracy of classification of HHRR compared to the other resolutions, indicates the heterogeneity of the lithologies where HHRR picked up the local and internal variations on each lithology.

The variables entered were 2.2um, 0.83um, 0.66um, 0.48um, 0.49um and 0.56um. The scatter plot of the first two functions show the separation of the argillic altered rocks and the wadi sediments (Fig. 5.27). The rest of the lithologies show poor separation.

The accuracy of the classification can be improved by taking the ratio of the band variables being used in the analysis. A comparison of the accuracies of the classification for each type of analysis and data type are presented in Table 5.26. It shows that the accuracy of classification is very high, indicating that these types of lithologies are almost completely separable from each other, based on their reflectance values.

DISCRIMINANT ANALYSIS FOR TM DATA MAHD ADH DHAHAB

SYMBOLS USED IN PLOTS

SYMBOL	GROUP	LABEL
1	1	WADI.S
2	2	ANDESIT 1
3	3	ARGIL.ALT
4	4	SILC.ALT
5	5	POT.ALT
6	6	CHLORIT.ALT
7	7	Q.S.PY
8	8	PYRITE CHLORITE
9	9	CARBONATE R
0	10	UNALTERED R
A	11	ANDESITE 2.
•		GROUP CENTROIDS

LIST OF THE 5 VARIABLES USED

VARIABLE
TM 1
TM 3
TM 4
TM 5
TM7

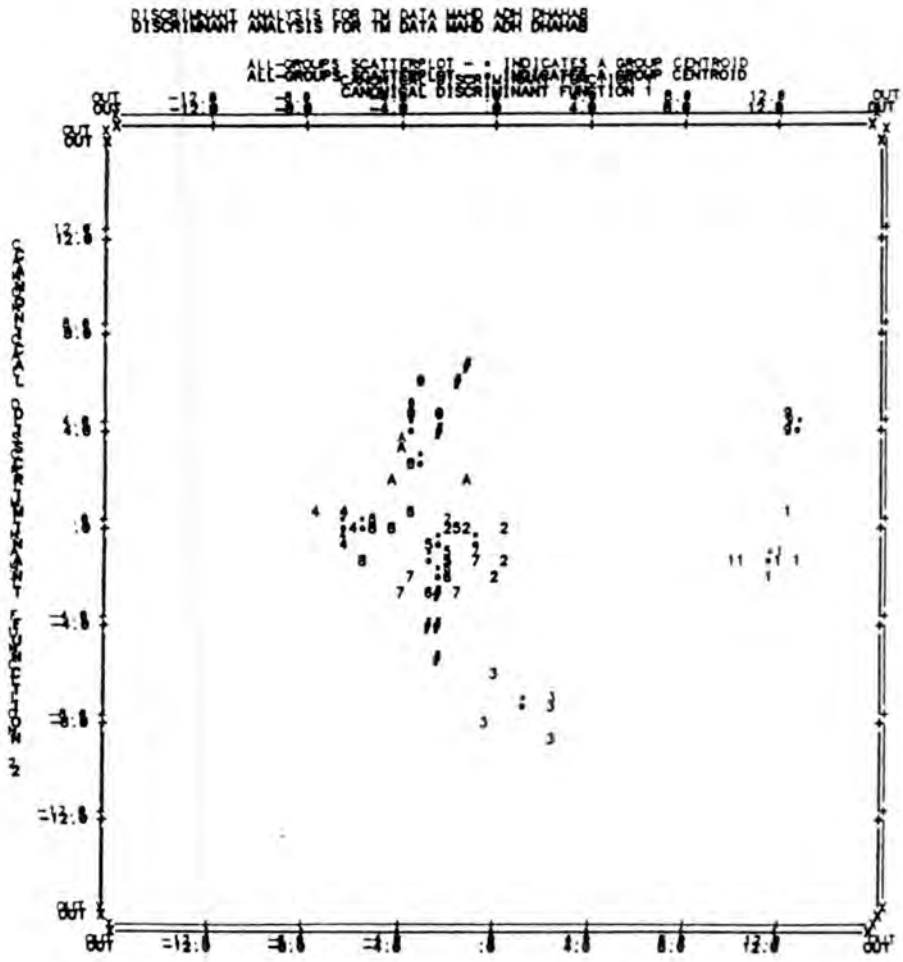

Fig. 5.26 The distribution of the eleven lithologies and alteration types in Mahd Adh Dhahab. In canonically transformed features space (derived from the transformation of TM values).

Table 5.25 Classification matrix derived from the discrimination analysis performed on data for eleven lithologies using band equivalent to TM bands from HHRR ground data as the discriminatory variable with the entry sequence, and the percentage of classification.

Predicted Group Membership / Actual Group Membership	Wadi sediment	Andesite 1	Argillic alteration	Silicic alteration	Potassic alteration	Chlorite alteration	Quartz seric.pyrite	Pyrite chlorite alt.	Carbonate rocks	Rhyolite rocks	Andesite 2
Wadi sediment	100	0	0	0	0	0	0	0	0	0	0
Andesite 1	0	100	0	0	0	0	0	0	0	0	0
Argillic alteration	0	0	100	0	0	0	0	0	0	0	0
Silicic alteration	0	0	0	75.0	0	0	0	25.0	0	0	0
Potassic alteration	20.0	0	0	20.0	20.0	20.0	20.0	0	0	0	0
Chlorite alteration	0	0	0	0	0	25.0	0	50.0	0	0	25.0
Quartz seric. pyrite	0	0	0	0	0	20.0	60.0	0	0	20.0	0
Pyrite chlorite alteration	0	0	0	0	0	0	0	66.7	0	0	33.3
Carbonate rocks	0	0	0	0	0	0	0	0	100	0	0
Rhyolite rocks	0	0	0	14.3	0	0	0	0	0	85.7	0
Andesite 2	0	33.3	0	0	0	0	0	0	0	0	66.7

Variable Entry Sequence:

TM band 7 (2.2μm)
TM band 4 (.83μm)
TM band 5 (.66μm)
TM band 1 (.48μm)
TM band 3 (.66μm)
TM band 2 (.56μm)

Percentage of Classification:

72.92%

DISCRIMINANT ANALYSIS FOR HHRR DATA FROM MAHD ADH DHAHAB

SYMBOLS USED IN PLOTS SYMBOL	GROUP	LABEL	LIST OF THE VARIABLES USED VARIABLE
1	1	WADI.S	TM1
2	2	ANDESIT 1	TM2
3	3	ARGIL.ALT	TM3
4	4	SILC.ALT	TM4
5	5	POT.ALT	TM5
6	6	CHLORIT.ALT	TM7
7	7	Q.S.PY	
8	8	PYRITE CHLORITE	
9	9	CARBONATE R	
0	10	UNALTERED R	
A	11	ANDESITE 2.	
*		GROUP CENTROIDS	

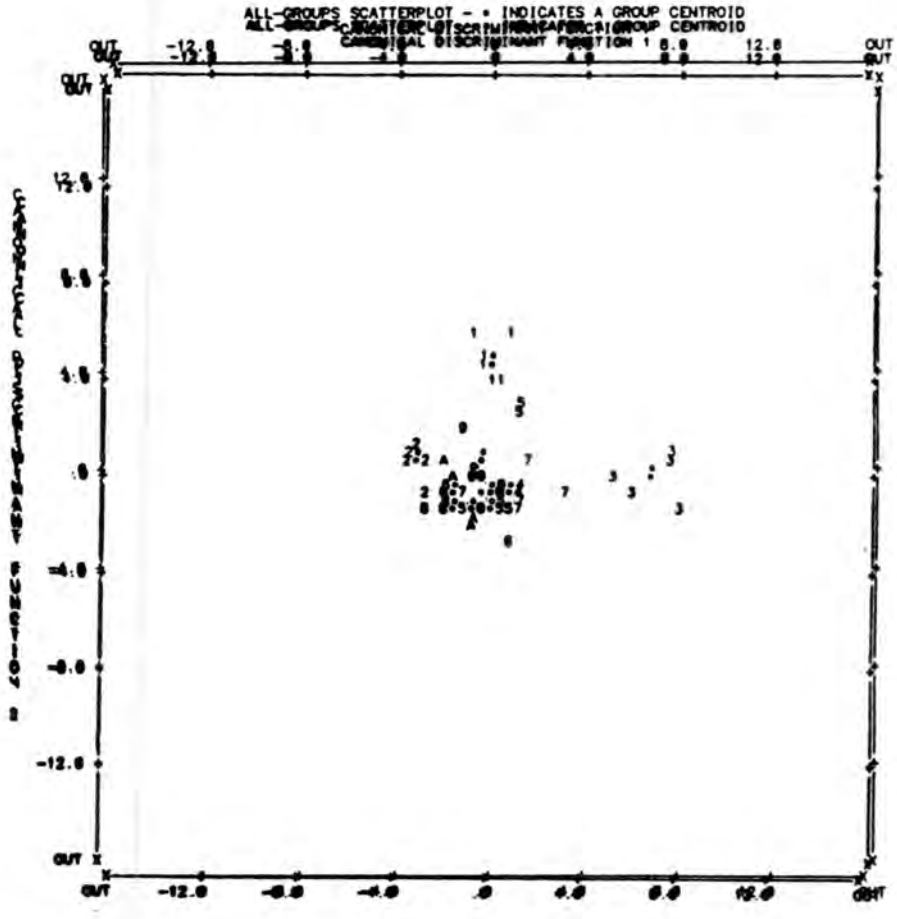

Fig. 5.27 The distribution of the eleven lithologies and alteration types in Mahd Adh Dhahab area. In canonically transformed features space (derived from the HHRR values).

Table 5.26. Comparison of the accuracy of classification and data type for the analysis of eleven lithologies using different variables.

Data type	Resolution	Classification analysis		
		Radiance	Ground reflectance	Ratio/Calibrated G.R.
ATM 1000m	2.5m	100% (9bands)	98.48% (6band)	100%
ATM 2000m	5.0m	100% (9bands)	100% (6band)	100%
ATM 3000m	7.5m	100% (9bands)	100% (6band)	100%
TM	30.0m	92.31% (6band)	92.31% (6band)	92.31%
HHRR	0.96m	72.92% (6band)		83.33%

The results of the accuracy of the classification of the calibrated data to ground reflectance using the TM sensor bands is equivalent only with the results of HHRR shown in Fig. 5.28.

5.4.1.7 A comparison of bands selected by discriminant analysis for eleven lithologies in Mahd Adh Dhahab

The discriminant analysis provide the order by which bands are selected, by ranking the ability of the data to separate the different lithologies. Fig. 5.29 shows the variables (bands) in the order they were selected plotted against the different resolutions.

Band selection can be categorized with reference to the spatial resolution of the data. Bands selected for IFOV 2.5m and less exhibits mixed and confused selection, which might be related to the fact that high resolution picked detailed local varation within the lithologies. The data from 5.0m and 7.5m IFOV exhibited almost similar selections, except for the second and fourth selection sequence. Band selection for 30m resolution shows different selection from the bands suggested above. Based on these results, it might be concluded that band selections can be limited by specific spatial resolutions.

5.4.1.8 Discrimination between three groups of lithologies in Mahd Adh Dhahab area.

The previous sections dealt with the discrimination of the different alteration types and lithological units in the Mine Hill and surrounding area. The six types of alteration studied separately earlier were grouped

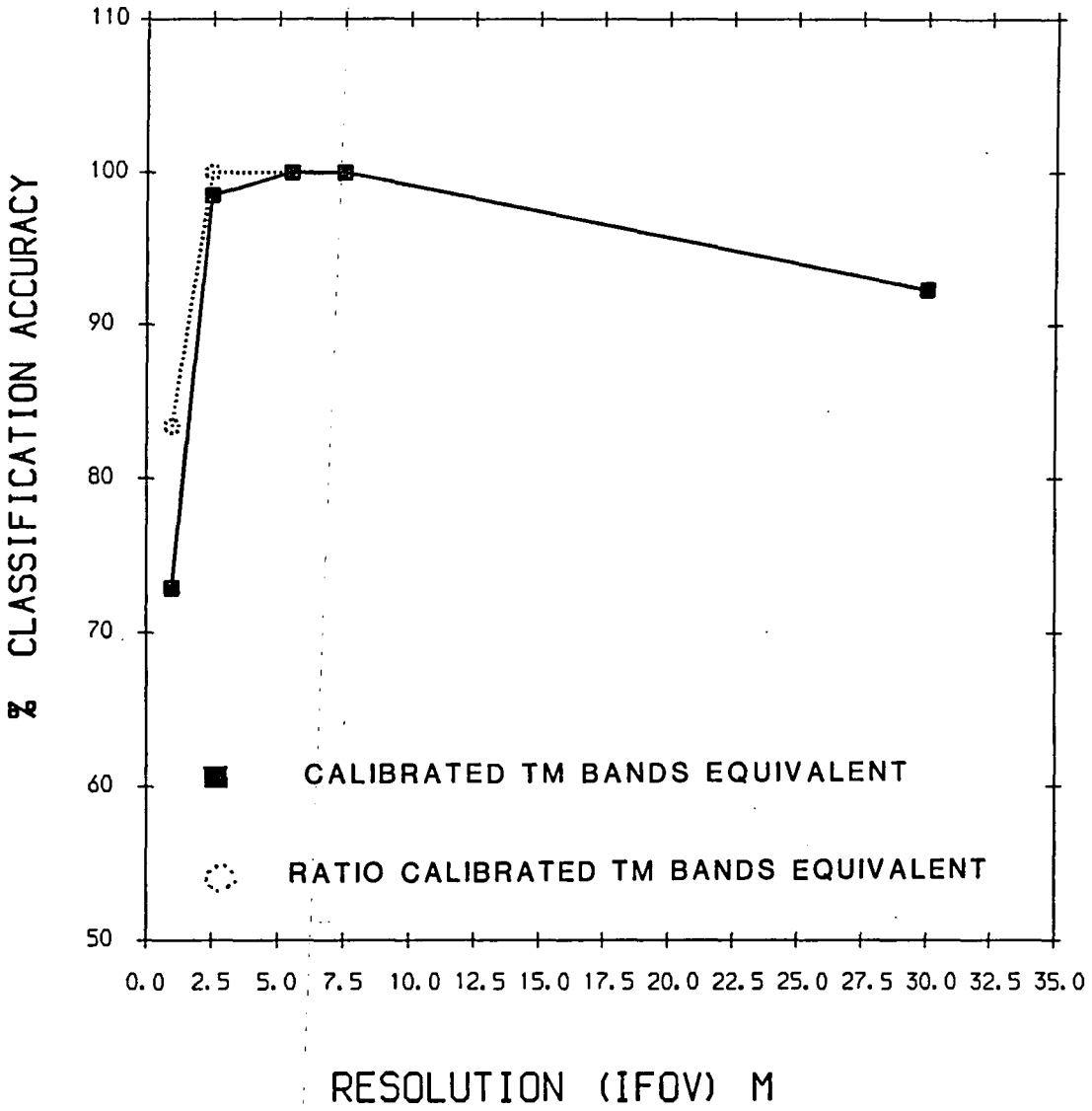

Fig. 5.28 Comparison of % classification accuracy using 11 lithologies, Mahd Adh Dhahab.

Fig. 5.29 Relation between bands selection for maximum discrimination with different resolutions used in Mahd Adh Dhahab.

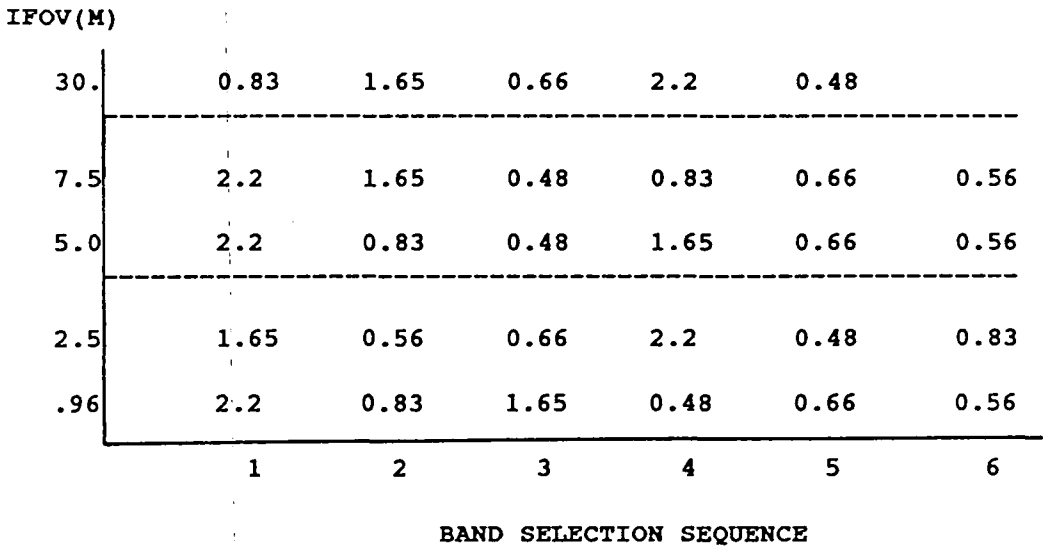

together. Generally as a first step, any mineral exploration mission will be looking for indications of alteration. Therefore, the data previously extracted from the images and measured on the ground for all eleven lithologies, has been grouped into three different lithological groups:

i) altered rocks.

ii) unaltered rocks.

iii) carbonate rocks

as shown in Table 5.27.

A stepwise linear discriminant analysis was done using these three groups and the calibrated spectral data as variables for each set of resolution data. The discriminant analysis is based on the analysis of the calibrated TM bands and the ATM band equivalent.

5.4.1.8.1 Discrimination of the three lithological groups using ATM, TM and HHRR data.

The results of the canonical discriminant functions for the calibrated ATM sensor 7.5m IFOV data are given in Table 5.28a and b. The first discriminant function accounts for over 95% of the total variance among the three groups. From Table 5.28b it can be seen that the first discriminant function is heavily weighted by visible band (0.83um) followed by the infrared band (2.2um).

The results of the discrimination of ATM 5.0m IFOV data are shown in Tables 5.29a and b. These show that the first function accounts for over 81%, while ATM band 7 (0.83um) is the largest contributor to both the first and

Table 5.27 Grouping of different lithologies

1.	Altered rocks	
	Argillic Alt.	Quartz sericite pyrite alteration
	Silicic Alt.	Chlorite alteration
	Potassic Alt.	Chlorite pyrite alteration
2.	Unaltered rocks	
	Wadi sediments	Andesite 2
	Andrites	Rhyolitie rocks
3.	Carbonate rocks	

Table 5.28
a. Canonical discriminant function for ATM 7.5m data

Function	Eigen Value	Percent of Variance	Canonical correlation
1	2.370	95.14	0.838
2	0.121	4.86	0.328

b. Standard Canonical Discriminant function coefficients

	Bands	Function 1	Function 2
0.43	ATM 2	1.179	6.125
0.56	ATM 3	-4.080	-10.796
0.83	ATM 7	4.298	2.539
1.65	ATM 9	-5.106	2.447
2.2	ATM10	3.827	0.319

Table 5.29
a. Canonical discriminant function of ATM 5m data

Function	Eigen Value	Percent Variance	Canonical correlation
1	1.535	81.53	0.778
2	0.347	18.47	0.507

b. Standard Canonical Discrimination function coefficients

Bands	Function 1	Function 2
ATM 2	-1.067	4.407
ATM 3	1.774	-5.414
ATM 5	-4.866	-5.974
ATM 7	5.629	6.53
ATM 9	-3.298	3.27
ATM10	1.987	-2.58

second functions. This can be interpreted as accounting for the variations in reflectance around 0.84um. The results for the ATM 2.5m IFOV data (Tables 5.30a and b) show that ATM band 5 (0.66um) dominates, followed by ATM band 9 (1.65um) and ATM band 2 (0.48um).

The first function allowed for over 85% of the total variance within the lithologies.

The results of the canonical discriminant functions for the TM data are given in Table 5.31a and b. This shows that the first function accounts for over 83% dominated by the infrared band central at 2.2um, while the second function was dependent upon the visible part of the spectrum.

Finally, the canonical discrimination of the HHRR data shows that the first function accounts for over 64% of the total variance; the lowest percentage recorded. The standard canonical discriminant function shows domination by TM bands 4 (0.83um) and 5 (1.65um) (Table 5.32a and b).

5.4.1.8.2 Classification of the three lithological groups of the Mahd Adh Dhahab area.

As previously stated the mineral geologist is looking for the ability to identify altered rocks from the surrounding country rocks. To see this more clearly, the eleven lithologies were regrouped into three groups: altered, unaltered and carbonate rocks.

The results of the classification using calibrated 7.5m IFOV ATM data are presented in Table 5.33. The overall percentage of correctly classified lithology was

Table 5.30

a. Canonical discriminant function for the ATM 2.5m data

Function	Eigen Value	Percent Variance	Canonical correlation
1	1.832	85.66	0.804
2	0.321	14.94	0.493

b. Standard Canonical discrimination function coefficients

Bands	Function 1	Function 2
ATM 2	3.335	-3.169
ATM 3	-8.889	12.34
ATM 5	6.697	-2.04
ATM 7	-3.877	-8.06
ATM 9	4.499	-1.32
ATM10	-1.657	2.26

Table 5.31

a. Canonical Discrimination function for the ATM 30m data

Function	Eigen Value	Percent of Variance	Canonical correlation
1	3.891	83.33	0.891
2	0.778	17.67	0.662

b. Standard Canonical Discrimination function coefficients

Bands	Function 1	Function 2
TM 1	2.884	-0.248
TM 3	2.488	10.352
TM 4	-7.564	-10.269
TM 5	-1.21	2.25
TM 7	3.94	-1.958

Table 5.32

a. Canonical discriminant function for the HHRR data (IFoV = 0.96m)

Function	Eigen Value	Percent Variance	Canonical correlation
1	0.833	64.78	0.674
2	0.453	35.22	0.558

b. Standard Canonical discrimination function coefficients

Band	Function 1	Function 2
TM 1	2.841	0.326
TM 3	-10.923	-9.654
TM 4	4.877	10.346
TM 5	6.19	-0.492
TM 7	-2.96	-0.296

over 86%. The carbonate rocks were fully classified, while 95.8% of the unaltered rocks and 77.8% of the altered rocks were correctly classified. The largest single error occurred where six types of altered rocks were classified as carbonate rocks.

Table 5.33 shows the variable entry sequence: 1.6um, 0.83um, 2.2um, 0.48um and 0.56um.

The classification results for the ATM 5.0m IFOV data are given in Table 5.34. The overall accuracy of the classification was 84.85%; the carbonate rocks being fully classified, while 95.8% of the unaltered and 75% of the altered rocks were correctly classified. Again the error is caused by 8 altered rock types being classified as carbonate rocks.

The band entry sequences was 0.48um, 2.2um, 0.56um, 1.7um and 0.83um. Table 5.35 shows the classification matrix for the three lithologies when using the ATM 2.5m IFOV data.

An overall acuracy of 80.30% was achieved. Ten samples of the altered rocks were distributed among carbonate and altered rocks, resulting in a classification of 72.2%. Again the carbonate rocks were correctly classified, but some samples of unaltered rocks were misclassified as altered rocks.

The band entry sequence was 0.56um, 1.89um, 0.66um, 0.48um, 2.2um and 0.83um.

The classification matrix for the HHRR data gave an overall accuracy of 77.08%. Several of the unaltered

Table 5.33 Classification matrix derived from the discrimination analysis performed on data for three lithologies using bands equivalent to TM bands from ATM 3000m (IFOV=7.5m) as the discriminatory variables, with the entry sequence, Mahd Ahd Dhahab area.

Actual Group Membership \ Predicted Group Membership	Altered rocks	Carbonate rocks	Unaltered rocks
Altered rocks	77.8	16.7	5.6
Carbonate rocks	0	100	0
Unaltered rocks	4.2	0	95.8

Variable Entry Sequence:

ATM band 9 (1.6um)

ATM band 7 (.83um)

ATM band 10 (2.2um)

ATM band 2 (.48um)

ATM band 3 (.56um)

Percentage of Classification: 86.36%

Table 5.34 Classification matrix derived from the discrimination analysis performed on data for three lithologies using bands equivalent to TM bands from ATM 2000m (IFOV=5.0m) as the discriminatory variables, with the entry sequence, Mahd Abd Dhahab area.

Actual Group Membership \ Predicted Group Membership	Altered rocks	Carbonate rocks	Unaltered rocks
Altered rocks	75.0	22.2	2.8
Carbonate rocks	0	100	0
Unaltered rocks	4.2	0	95.8

Percentage of Classification: 84.85%

Variable Entry Sequence:

ATM band 2 (0.48μm)
ATM band 10 (2.2μm)
ATM band 3 (0.56μm)
ATM band 9 (1.7μm)
ATM band 7 (0.83μm)
ATM band 5 (0.66μm)

Table 5.35 Classification matrix derived from the discrimination analysis performed on data for three lithologies using bands equivalent to TM bands from ATM 1000m (IFOV=2.5m) as the discriminatory variables, with the entry sequence, Mahd Ahd Dhahab area.

Actual Group Membership \ Predicted Group Membership	Altered rocks	Carbonate rocks	Unaltered rocks
Altered rocks	72.2	13.9	13.9
Carbonate rocks	0	100	0
Unaltered rocks	12.5	0	87.5

Percentage of Classification: 80.30%

Variable Entry Sequence:

ATM band 3 (.056μm)

ATM band 9 (1.7μm)

ATM band 5 (0.66μm)

ATM band 2 (0.48μm)

ATM band 10 (2.2μm)

ATM band 7 (0.83μm)

rocks were classified as altered rocks producing an accuracy of 80% (Table 5.36).

Table 5.37 illustrates the classification matrix derived from the discriminant analysis when using the TM data. This exhibits the highest overall accuracy of 92.31%. 95.8% of the altered rocks were correctly classified while only 87.5% of the unaltered rocks were. The variable entry sequence was 2.2um, 1.65um, 0.66um, 0.58um and 0.83um.

The discriminant analysis of the three lithologies was also performed for the radiance values of the 9 available ATM sensor bands, the 6 TM sensor bands and for the band ratios of the six calibrated TM sensor bands.

The accuracy of the classification can be improved by using band ratios in all the data sets except for the TM sensor data. A comparison of the accuracy of classification for each type of analysis and for each data type is shown in Table 5.38. Fig. 5.30 shows the relationship between the IFOV and the accuracy of classification for the three lithologies in the Mahd region. It shows a decrease in the accuracy of classification with an increase of in spatial resolution, this might be related to the fact that the low resolution data increases the homogeneity of the lithologies, whilst in the high spatial resolution data, increases the levels of local and internal heterogeneity.

Table 5.36 Classification matrix derived from the discrimination analysis performed on data for three lithologies using TM bands equivalent of the HHRR data (IFOV=0.96m) as the discriminatory variable, with the entry sequence, Mahd Adh Dhahab area.

Actual Group Membership \ Predicted Group Membership	Altered rocks	Carbonate rocks	Unaltered rocks
Altered rocks	72.0	12.0	16.0
Carbonate rocks	0	100	0
Unaltered rocks	20.0	0	80.0

Variable Entry Sequence:

TM band 7 (2.2μm)

TM band 5 (1.65μm)

TM band 3 (0.66μm)

TM band 4 (0.83μm)

TM band 1 (0.48μm)

Percentage of Classification: 77.08%

Table 5.37 Classification matrix derived from the discrimination analysis performed on data for three lithologies using TM band (IFOV = 30.0m) as the discriminatory variable, with the entry sequence - Mahd Adh Dhahab area.

Actual Group Membership \ Predicted Group Membership	Altered rocks	Carbonate rocks	Unaltered rocks
Altered rocks	95.8	16.7	4.2
Carbonate rocks	0	100	0
Unaltered rocks	12.5	0	87.5

Variable Entry Sequence:

TM band 7 (2.2μm)

TM band 5 (1.65μm)

TM band 3 (0.66μm)

TM band 1 (0.43μm)

TM band 4 (0.83μm)

Percentage of Classification: 92.31%

Table 5.38 Comparison between % of classification and data type for classifying 3 lithologies

Data Type	% Classification		
	Radiance	Six TM equivalent calibrated bands	calibrated band ratio
ATM1000	83.33 (9bands)	80.30	84.85
ATM2000	86.36 (9bands)	84.85	90.91
ATM3000	86.36 (9bands)	86.36	98.48
TM	92.31 (6bands)	92.31	86.54
HHRR	(6bands)	77.08	79.17

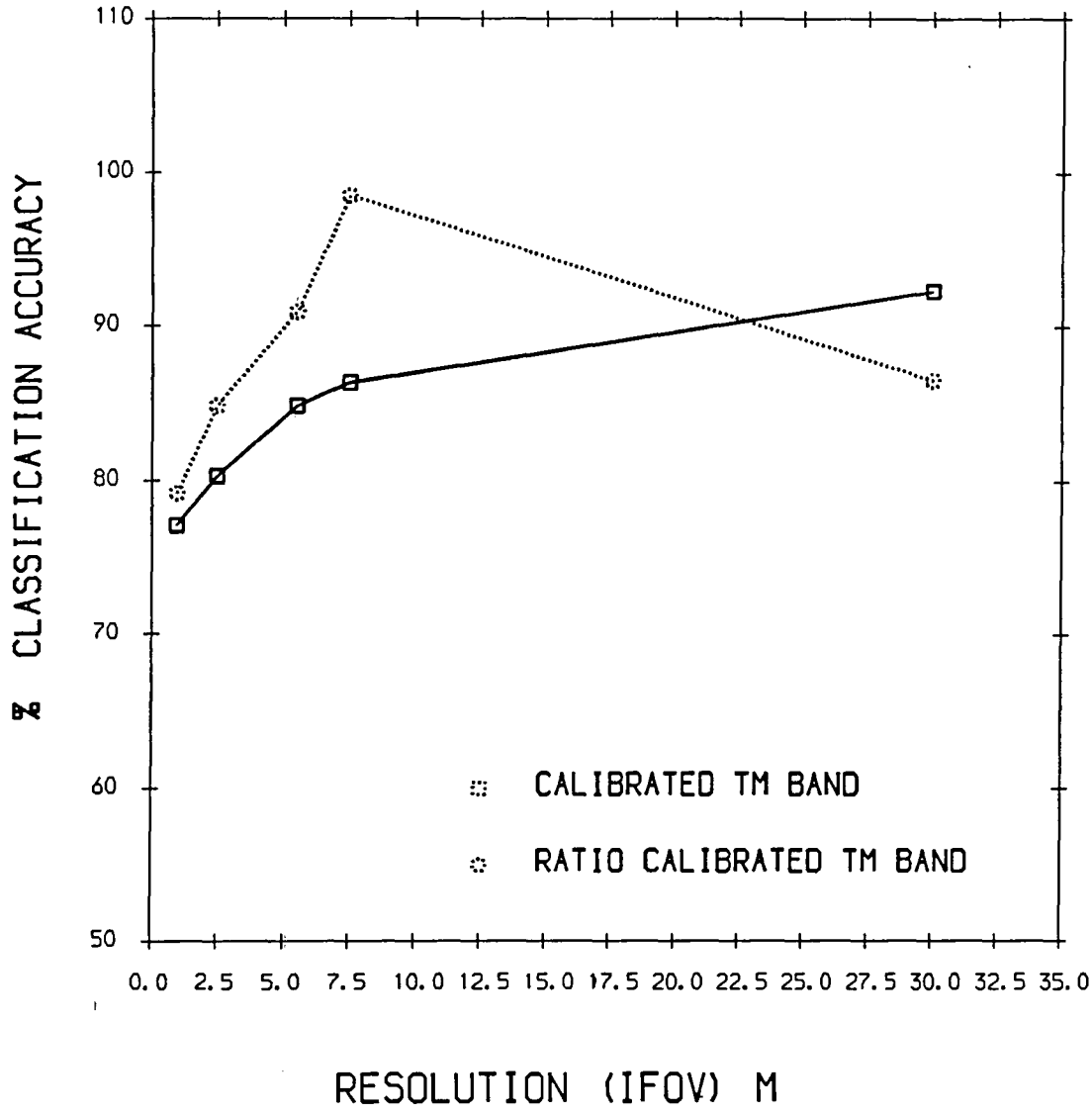

Fig. 5.30 Comparison of % classification accuracy using 3 lithologies, Mahd Adh Dhahab.

5.4.1.8.3 A comparison of the bands selected by discriminant analysis of the 3 lithologies

The discriminant analysis ranked the bands selected on their ability to separate the lithologies. Fig. 5.31 shows the bands which best classify the data for each resolution. The band selection does not change systematically, despite the same bands being selected for the HHRR and TM sensor data.

5.4.2 Discrimination and classification of eleven lithologies from Jabal Said data

As with the Mahd Adh Dhahab area, eleven lithologies were selected from Jabal Said, by a stepwise discriminant analysis. The selected targets from Jabal Said represent rock units and not alteration units. There is one target known as the alteration zone, but without any detail of the type of alteration, it will be considered as one lithological unit.

ATM bands 2-10 and TM sensor bands were used, as well as the HHRR data. One type of analysis was conducted for each type of data using the calibrated TM band equivalents only. As in Mahd Adh Dhahab area, the ATM data have three different resolutions: IFOV 7.5m, 5.0m, and 2.5m.

5.4.2.1 Discrimination between eleven lithologies using ATM 7.5m IFOV data

The canonical discriminant functions were calculated and summarised in Table 5.39. This shows that the first three functions accounted for 96.44% of the total variance among groups, but after adding the fifth function, this is increased to 97.84%. The relative importance of these

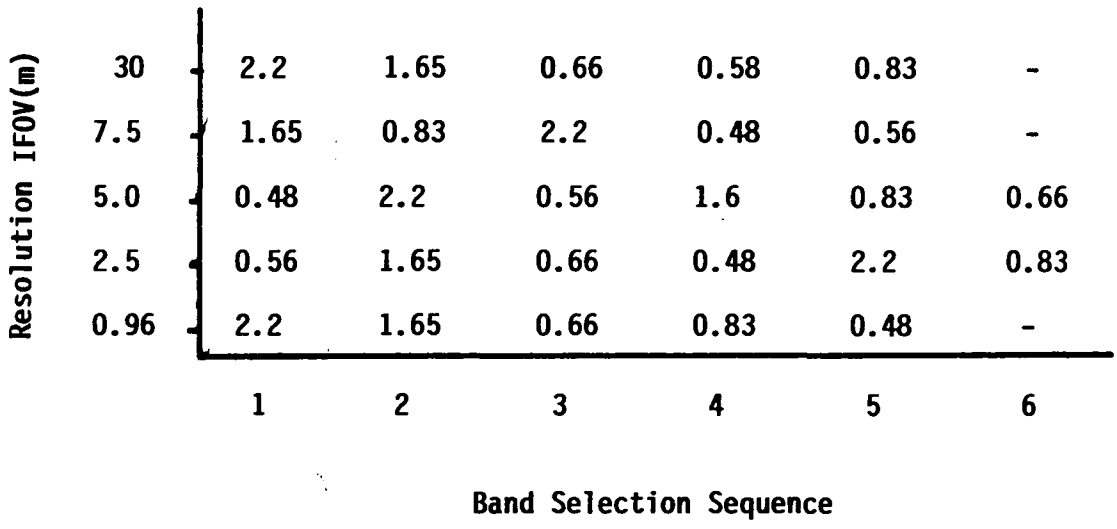

Fig. 5.31 Showing the bands which were selected for best classification for each resolution.

functions can be interpreted from the eigen values. The first of these functions contribute to the discrimination between groups but the fourth function does not contribute significantly to the separation of the lithology. This was evident by the low eigen value and canonical correlation coefficient observed in Table 5.39.

The standard canonical discriminant functions coefficients are presented in Table 5.40. This indicates that the first function is weighted positively by the shortwave infrared ATM band 9 (1.6um), and negatively by bands 7 (0.83um) and band 10 (2.2um), followed by ATM bands 3 and 5 (0.66um and 0.56um). The most significant contribution in the second function came from ATM band 7 (0.83um) followed by bands 10 (2.2um) and 3 (0.56um), while in function three the visible ATM band 5 (0.66um) dominated, followed by bands 2 (0.48um) and 7 (0.83um) negatively, and ATM band 9 (1.65um) positively. The last three functions were heavily dominated by visible wavelengths followed by near infrared ATM band 9 (1.65um).

5.4.2.2 Discrimination between eleven bands using ATM 5.0m IFOV data.

The results of the canonical discriminant analysis of the calibrated data are given in Table 5.41. This demonstrates that the first three discriminant functions account for over 95% of the total variance among the different lithological groups at Jabal Said. This rises to over 99% when the fourth function is included. The fifth and sixth functions do not contribute significantly to the lithological separation.

Table 5.39 Canonical discriminant function for the ATM 300m (IFOV=7.5m) data, Jabal Said.

Function	Eigen Value	% of Variance	Canonical correlation
1	72.67	58.04	0.9931
2	28.37	22.06	0.9820
3	20.50	16.37	0.9764
4	1.783	1.42	0.8004
5	1.1409	0.92	0.7300
6	0.732	0.58	0.6502

Table 5.40 Discriminant analysis of the ATM 3000m data (IFOV=7.5m): standardised canonical discriminant function coefficients, Jabal Said area.

Bands	Function 1	Function 2	Function 3	Function 4	Function 5	Function 6
Band ATM 2 (0.43um)	-1.06150	-1.11956	-2.13481	1.77299	2.00972	-2.30813
Band ATM 3 (0.65um)	0.38693	1.02689	0.70694	-0.23691	0.99171	4.10203
Band ATM 5 (0.66um)	0.38616	-0.61083	2.96100	0.64437	-2.50205	-2.44182
Band ATM 7 (0.83um)	-1.50314	1.36537	-1.04461	-2.01597	1.62803	0.58178
Band ATM 9 (1.65um)	1.50153	-0.91277	0.51038	0.46290	0.89575	0.36888
Band ATM 10 (2.22um)	0.46668	1.09590	-0.74066	-0.15833	-0.55465	-0.30243

The standardised canonical discriminant function coefficients show that ATM 10 (2.2um) and ATM 9 (1.65um) are the most significant contributors to the first function. This is interpreted as an indication of the importance of the shortwave infrared wavelengths 1.65-2.2um for discriminating between the lithology. Also it might relate to the composition of these lithologies (Table 5.42). The second function is also dominated by ATM10 (2.2um), followed closely by the visible wavelengths which might indicate the importance of iron and desert varnish. The third function is dominated by the infrared ATM 9 (1.65um) followed by the visible bands ATM 5 (0.66um), ATM 3 (0.56um) and ATM 2 (0.48um). The fourth discriminant function which explains only 3.74% of the total variance and may account for the variation in the visible part of the spectrum, particularly in ATM3 (0.56um) and ATM 5 (0.66um). Discriminant functions 5 and 6 are dominated by the visible band ATM 2 (0.48um).

5.4.2.3 Discrimination of eleven lithologies using ATM 2.5m data

The results of the canonical discriminant analysis of the ATM 2.5m data equivalent to the TM bands only, are given in Table 5.43. This shows that the first three functions account for over 93% of the total variance among the different groups. This rises to over 97% by including the fourth function, and to over 99% when the fifth function is added. The sixth function does not contribute significantly to the separation of the lithology.

Table 5.41 Canonical discriminant functions for ATM 2000m (IFOV=5.0m) data, Jabal Said.

Function	Eigen Value	% Variance	Canonical Correlation
1	51.986	53.78	0.990
2	24.612	25.46	0.980
3	15.518	16.05	0.969
4	3.616	3.74	0.885
5	0.816	0.84	0.6703
6	0.108	0.11	0.312

Table 5.42 Discriminant analysis of the ATM 2000m data (IFOV=5.0m): standardised canonical discriminant function coefficients, Jabal Said area.

Bands	Function 1	Function 2	Function 3	Function 4	Function 5	Function 6
Band ATM 2 (0.43µm)	-0.25987	0.64918	0.03465	0.50411	0.87581	1.01659
Band ATM 3 (0.65µm)	0.22282	0.64207	0.27782	1.33404	0.58885	-1.58034
Band ATM 5 (0.66µm)	-0.20033	0.19848	0.33632	1.27446	-1.41957	0.75478
Band ATM 7 (0.83µm)	-1.60467	-1.24319	-0.12449	-3.37351	-0.08739	-0.09300
Band ATM 9 (1.65µm)	0.13246	-1.62524	1.04301	0.52585	0.59848	-0.09837
Band ATM 10 (2.22µm)	1.73733	1.86983	-0.47180	-0.07976	-0.47980	0.05835

Table 5.43 Canonical discriminant functions for ATM 1000m calibrated bands to ground , Jabal Said.

Function	Eigen Value	% of Variance	Canonical correlation
1	68.825	46.81	0.992
2	40.509	27.55	0.987
3	28.515	19.39	0.982
4	6.007	4.09	0.925
5	3.011	2.05	0.866
6	0.158	0.11	0.370

Table 5.44 Discriminant analysis of the ATM 1000m data (IFOV=2.5m): standardised canonical discriminant function coefficients, Jabal Said area.

Bands	Function 1	Function 2	Function 3	Function 4	Function 5	Function 6
Band ATM 2 (0.43um)	-0.07580	0.07406	1.38632	-0.67001	1.37834	-1.53787
Band ATM 3 (0.65um)	-0.08939	0.31671	-0.14469	-1.27742	0.46934	3.29075
Band ATM 5 (0.66um)	0.10231	1.20959	-1.95251	-0.68609	-2.39087	-1.89284
Band ATM 7 (0.83um)	-1.05809	-0.53563	1.18828	3.27216	0.38206	0.08556
Band ATM 9 (1.65um)	0.17585	0.60469	-1.05007	0.26349	0.86704	0.04382
Band ATM 10 (2.22um)	1.52081	-0.69674	0.81364	-0.81562	-0.54333	0.11231

The standardized canonical discriminant function coefficients (Table 5.44) show that the first function was dominated by the infrared bands and especially ATM 10 (2.2um) and ATM 9 (1.65um). This was similar to the ATM data for Jabal Said which indicated the importance of the reflectance of the IR radiation. The second function is heavily weighted by the visible bands, ATM 5 (0.66um) followed by ATM 3 (0.56um) and ATM 2 (0.43um). The near infrared band ATM 9 (1.65um) also contributes to the discrimination. The third function is dominated by the visible band ATM 2 (0.43um), followed by the near infrared band ATM 10 (2.2um). This indicates the importance of these two bands in separating clay alteration from the lithology and in identifying the presence of iron, which covered most of the arid surface. The fourth function which accounts for only 4.09% of the total variance among the eleven lithologies is dominated by band ATM 7 (0.83um). The last two functions did not contribute significantly to the discrimination, their total contribution being less than 3%.

5.4.2.4 Discrimination of eleven lithologies using TM sensor data

The results of the canonical discriminant functions using calibrated TM sensor data in Jabal Said are given in Table 5.45. This demonstrates that the first three discriminant functions account for over 96% of the total variance between the different lithologies in Jabal Said. This rises to over 99% when the fourth discriminant function is included.

An examination of the canonical correlation coefficients indicates that the first four functions contribute to the discrimination while the other two functions do not contribute significantly.

The standardized canonical discriminant function coefficients (Table 5.46) show that the first functions are dominated by the visible bands; TM 2 (0.56um), TM 1 (0.43um) and TM 3 (0.35um), followed by near infrared band TM 7 (2.2um). This pattern is completely opposite to that of the ATM sensor data and can be explained by the large size (30m) of the TM pixels. These cover large parts of the lithology and allow other parts of the lithologies to be included which effect the pixels digital value. This accounts for variations in reflectance for different materials in the visible band.

The second function is also weighted by the visible band TM 2 (0.56um), but is followed by the near infrared band TM 7 (2.2um) and TM 5 (1.65um). Discriminant function three was interpreted as accounting for variations in reflectance in the visible and the near infrared, particularly in TM 3 (0.66um) and TM 4(0.83um). The fourth function explained only 3.74% of the total variance among the lithologies, and was interpreted as accounting for variations in reflectance in the visible wave bands TM 3 (0.66um) and TM 4 (0.83um) and TM 7 (2.2um) is also significant here but of less importance than the visible. The last two discriminant functions only explain less than 1% of the total variance and do not

Table 5.45 Canonical discriminant functions for TM data (IFOV=30m). Calibrated band to ground, Jabal Said.

Function	Eigen Value	% of Variance	Canonical correlation
1	28.996	67.74	0.9831
2	8.458	19.76	0.9456
3	3.813	8.91	0.8900
4	1.172	2.74	0.7346
5	0.240	0.56	0.4406
6	0.121	0.28	0.3296

Table 5.46 Discriminant analysis of the TM data (IFOV=30m): standardised canonical discriminant function coefficients, Jabal Said Area.

Bands	Function 1	Function 2	Function 3	Function 4	Function 5	Function 6
Band TM 1 (0.43um)	0.40028	0.27259	-0.53630	-0.24886	-0.20845	2.48733
Band TM 2 (0.65um)	0.77138	0.56902	0.73244	-2.37353	0.40497	-1.86970
Band TM 3 (0.66um)	0.35547	0.15502	1.40204	2.22706	-1.50227	-0.40790
Band TM 4 (0.83um)	0.06209	-0.11583	0.44328	0.53820	1.49206	-0.06900
Band TM 5 (1.65um)	-1.58306	0.34695	0.57688	-0.69598	0.05502	0.25102
Band TM 7 (2.22um)	0.11998	0.39765	-1.12619	0.73482	0.08131	-0.15426

contribute significantly to the separation of the lithology.

2.4.2.5 Discrimination between eleven lithologies using HHRR data

The results of the canonical discriminant analysis of the HHRR data are given in Table 5.47.

Only five functions were used here, as TM band 2 0.65um) was removed from the analysis. The first three discriminant functions account for over 96% of the total variance between different surface lithologies. This rises to over 98% when the fourth discriminant function is included.

Examination of the canonical correlation coefficients indicates that the first three discriminant functions contribute to the discrimination, but the fourth and fifth do not contribute significantly to the separation of the lithology.

The standardized canonical discriminant function coefficients (Table 5.48) show that the first discriminant function is dominated by the visible and near infrared bands TM 3 (0.66um) and TM 7 (2.2um). TM1 (0.43um) is also important. The second function is heavily weighted by TM 3 (0.66um), followed by TM 5 (1.65um), while the third function is dominated by the red part in the visible part of the spectrum. The fourth discriminant function explains less than 2% of the total variance among the lithology groups, although it is dominated by TM 4 (0.83um) and TM 5 (1.65um). Generally, the fourth and

Table 5.47 Canonical discriminant functions for HHRR data, Jabal Said.

Function	Eigen Value	% of Variance	Canonical correlation
1	6.153	74.83	0.927
2	1.229	14.94	0.742
3	0.579	7.04	0.605
4	0.151	1.89	0.362
5	0.111	1.35	0.316

Table 5.48 Discriminant analysis of the HHRR data (IFOV=0.96m): standardised canonical discriminant function coefficients, Jabal Said Area.

Bands	Function 1	Function 2	Function 3	Function 4	Function 5
Band TM 1 (0.43um)	0.4971	-0.0693	-0.614	-0.0100	1.4144
Band TM 3 (0.66um)	2.8723	6.4545	0.1033	0.9387	-0.7015
Band TM 4 (0.83um)	-2.9768	-6.8936	1.5458	1.1114	-0.5799
Band TM 5 (1.65um)	-2.7911	1.1758	-0.1278	0.9514	1.0378
Band TM 7 (2.22um)	2.8713	-0.4868	-1.2980	-0.1307	-0.8512

fifth functions do not contribute significantly to the separation of the lithologies.

5.4.2.6 Classification of eleven lithologies in Jabal Said

The potential of the TM sensor and ATM sensor data to discriminate between, and classify the eleven lithologies from Jabal Said was assessed using the divergence statistics. This indicates the ability of the statistical technique to separate the classes on the bases of differences between their mean vectors and their variance-covariance matrices (Swain & Davies, 1978).

Using the same procedure as that used for the Mahd Adh Dhahab data, a discriminant analysis was applied to the Jabal Said data using the 'SPSSX' computer program. This also gave the results of the classification of the different lithologies. A separate classification was calculated for each resolution for these eleven lithologies.

The results of the classification of ATM 7.5m IFOV data are presented in Table 5.49. This gives the classification matrix derived from the discriminant analysis, with the variable entry sequence as follows: ATM 5 (0.66um), ATM 9 (1.6um), ATM 10 (2.2um), ATM 7 (0.83um), ATM 2 (0.49um), and ATM 3 (0.56um).

The high percentage classified (98.48%) was evidence for a reliable classification for most of the lithological groups. The only lithology which had a percentage error

Table 5.49 Classification matrix derived from the discrimination analysis performed on data for eleven lithologies using bands equivalent to TM bands from ATM 3000m (IFOV=7.5m) as the discriminatory variable, with the entry sequence, Jabal Said Area.

Predicted Group Membership / Actual Group Membership	Granite rock	Dacite Tuff	Pegmatite	Rhyolite	Diorite	Andesite Gravel	Gossan	Alteration zone	Andesite Tuff	Quartz Gravel	Zubaidah Breccia
Granite rock	83.3	0	0	0	16.7	0	0	0	0	0	0
Dacite Tuff	0	100	0	0	0	0	0	0	0	0	0
Pegmatite	0	0	100	0	0	0	0	0	0	0	0
Rhyolite	0	0	0	100	0	0	0	0	0	0	0
Diorite	0	0	0	0	100	0	0	0	0	0	0
Andesite Gravel	0	0	0	0	0	100	0	0	0	0	0
Gossan	0	0	0	0	0	0	100	0	0	0	0
Alteration zone	0	0	0	0	0	0	0	100	0	0	0
Andesite Tuff	0	0	0	0	0	0	0	0	100	0	0
Quartz Gravel	0	0	0	0	0	0	0	0	0	100	0
Zubaidah Breccia	0	0	0	0	0	0	0	0	0	0	100

Variable Entry Sequence:

ATM band 5 (.66um)

ATM band 9 (1.6um)

ATM band 10 (2.2um)

ATM band 7 (.83um)

ATM band 2 (.49um)

ATM band 3 (.56um)

Percentage of Classification:

98.48%

was the granite, where 16.7% had been misclassified as diorite.

The classification matrix for the ATM 5.0m IFOV data is presented in Table 5.50. This shows the overall classification as 98.48%. The variable entry sequence was ATM 5 (0.56um), ATM 2 (0.49um), ATM 7 (0.83um), ATM 9 (1.65um), ATM 10 (2.2um) and ATM 3 (0.56um).

The diorite is the only lithology which shows 16.7% misclassified as dacite-tuff. The canonical variable scatter diagram is shown in Fig. 5.32 and Fig. 5.33, for eleven lithologies using the ATM 7.5m and 5.0m IFOV data. This clearly indicates the separation of the different lithologies that was achieved.

100% classification of the ATM 2.5m was achieved, and Fig. 5.34 clearly shows the separation of the different lithologies. The variable entry sequence was ATM 7 (2.2um), 5 (1.65um), 3 (0.56um), 10 (2.2um), 9 (1.6um) and 2 (0.48um) (Table 5.51).

The classification of the TM sensor data for Jabal Said (Table 5.52) shows an overall classification of 98.48%, and again it is the granitic rocks which show 16.7% misclassified as rhyolite. The same table indicates the variable entry sequence. Table 5.53 summarises the results of classification of all data from Jabal Said.

5.4.2.7 Bands selected by discriminant analyses for eleven lithologies in Jabal Said

The discriminant analysis which was applied to each type of resolution data (to discriminate between the eleven lithologies) in Jabal Said provides the order of

Table 5.50 Classification matrix derived from the discrimination analysis performed on data for eleven lithologies using bands equivalent to TM bands from ATM 2000m (IFOV=5.0m) as the discriminatory variable, with the entry sequence, Jabal Said Area.

Actual Group Membership \ Predicted Group Membership	Granite rock	Dacite Tuff	Pegmatite	Rhyolite	Diorite	Andesite Gravel	Gossan	Alteration zone	Andesite Tuff	Quartz Gravel	Zubaidah Breccia
Granite rock	100	0	0	0	0	0	0	0	0	0	0
Dacite Tuff	0	100	0	0	0	0	0	0	0	0	0
Pegmatite	0	0	100	0	0	0	0	0	0	0	0
Rhyolite	0	0	0	100	0	0	0	0	0	0	0
Diorite	0	16.7	0	0	83.3	0	0	0	0	0	0
Andesite Gravel	0	0	0	0	0	100	0	0	0	0	0
Gossan	0	0	0	0	0	0	100	0	0	0	0
Alteration zone	0	0	0	0	0	0	0	100	0	0	0
Andesite Tuff	0	0	0	0	0	0	0	0	100	0	0
Quartz Gravel	0	0	0	0	0	0	0	0	0	100	0
Zubaidah Breccia	0	0	0	0	0	0	0	0	0	0	100

Variable Entry Sequence:

ATM band 5 (.66um)

ATM band 2 (.49μm)

ATM band 7 (.83um)

ATM band 9 (1.6um)

ATM band 10 (2.2um)

ATM band 3 (.56um)

Percentage of Classification:

98.48%

ATM 3000 J.SAID AREA CALIBRATED IMAGE

SYMBOLS USED IN PLOTS

SYMBOL	GROUP	LABEL
1	1	GRANIT
2	2	DACITE.T
3	3	PEGMATITE
4	4	RHYOLITE
5	5	DIORITE
6	6	DARK TARGET
7	7	GOSSAN
8	8	ALTERATION ZONE
9	9	ANDESITE TUFF
0	10	LIGHT TARGET
A	11	ZUBAIDAH B.
•		GROUP CENTROIDS

LIST OF THE 6 VARIABLES USED.

VARIABLE	LABEL
ATM2	
ATM3	
ATM5	
ATM7	
ATM9	
ATM10	

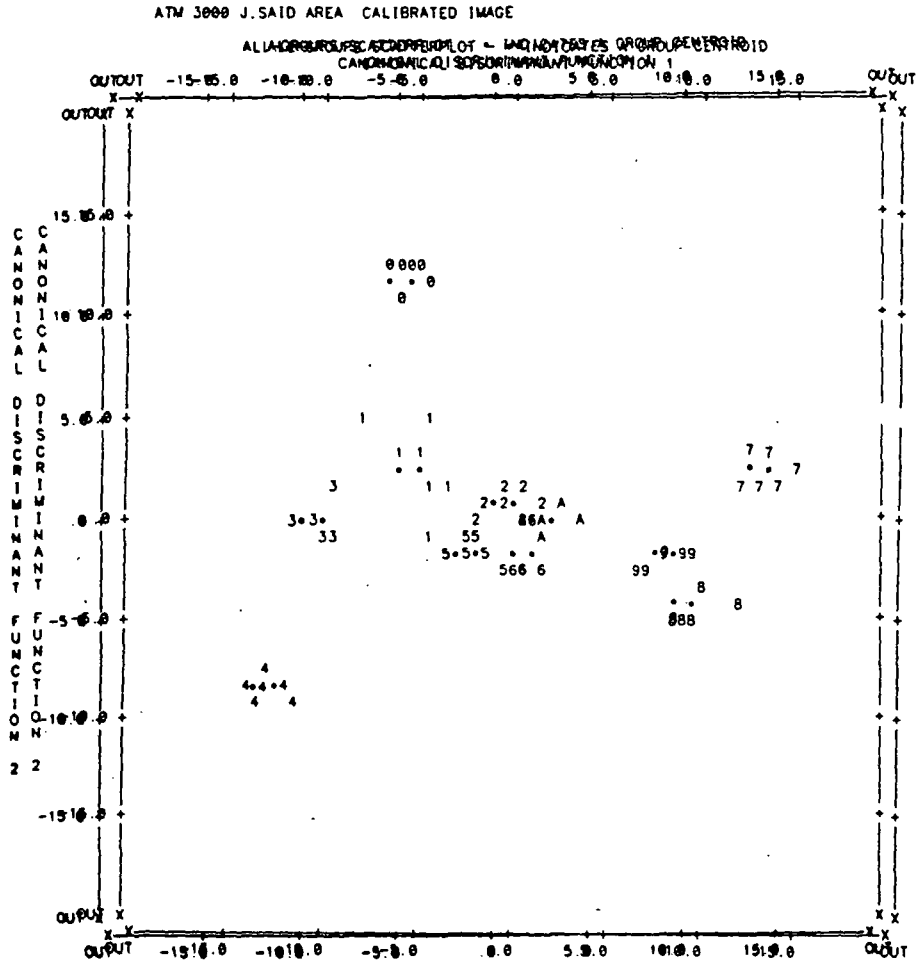

Fig. 5.32 The distribution of the eleven lithologies in Jabal Said area. In canonically transformed features space (derived from the transformation of ATM 7.5m data).

DISCRIMINANT ANALYSIS ATM 2000 M JABAL SAID.

SYMBOLS USED IN PLOTS			LIST OF THE VARIABLES USED
SYMBOL	GROUP	LABEL	VARIABLE
			ATM2
1	1	GRANIT	ATM3
2	2	DACITE.T	ATM5
3	3	PEGMATITE	ATM7
4	4	RHYOLITE	ATM9
5	5	DIORITE	ATM10
6	6	DARK TARGET	
7	7	GOSSAN	
8	8	ALTERATION ZONE	
9	9	ANDESITE TUFF	
0	10	LIGHT TARGET	
A	11	ZUBAIDAH B.	
*		GROUP CENTROIDS	

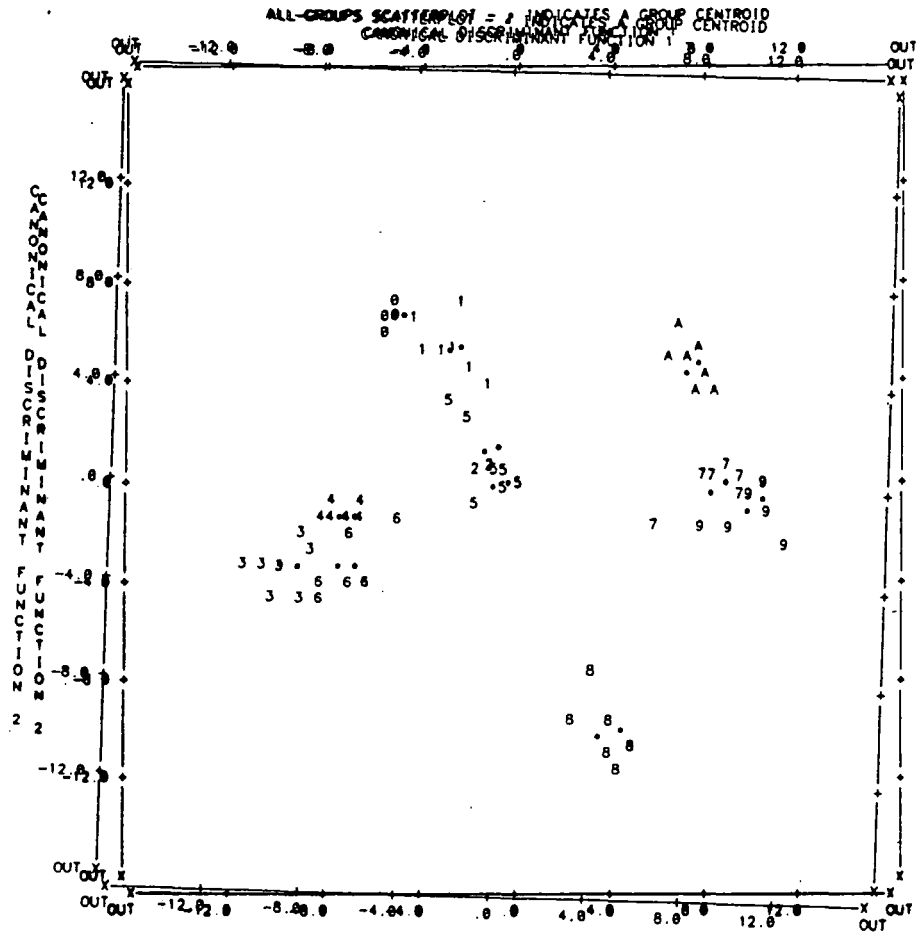

Fig. 5.33 The distribution of the eleven lithologies in Jabal Said. In canonically transformed features space (derived from the transformation of ATM 5.0m data).

SYMBOLS USED IN PLOTS		
SYMBOL	GROUP	LABEL
1	1	GRANIT
2	2	DACITE.T
3	3	PEGMATITE
4	4	RHYOLITE
5	5	DIORITE
6	6	DARK TARGET
7	7	GOSSAN
8	8	ALTERATION ZONE
9	9	ANDESITE TUFF
0	10	LIGHT TARGET
A	11	ZUBAIDAH B.
o		GROUP CENTROIDS

LIST OF THE 6 VARIABLES USED..
VARIABLE
ATM 2
ATM 3
ATM 5
ATM 7
ATM 9
ATM10

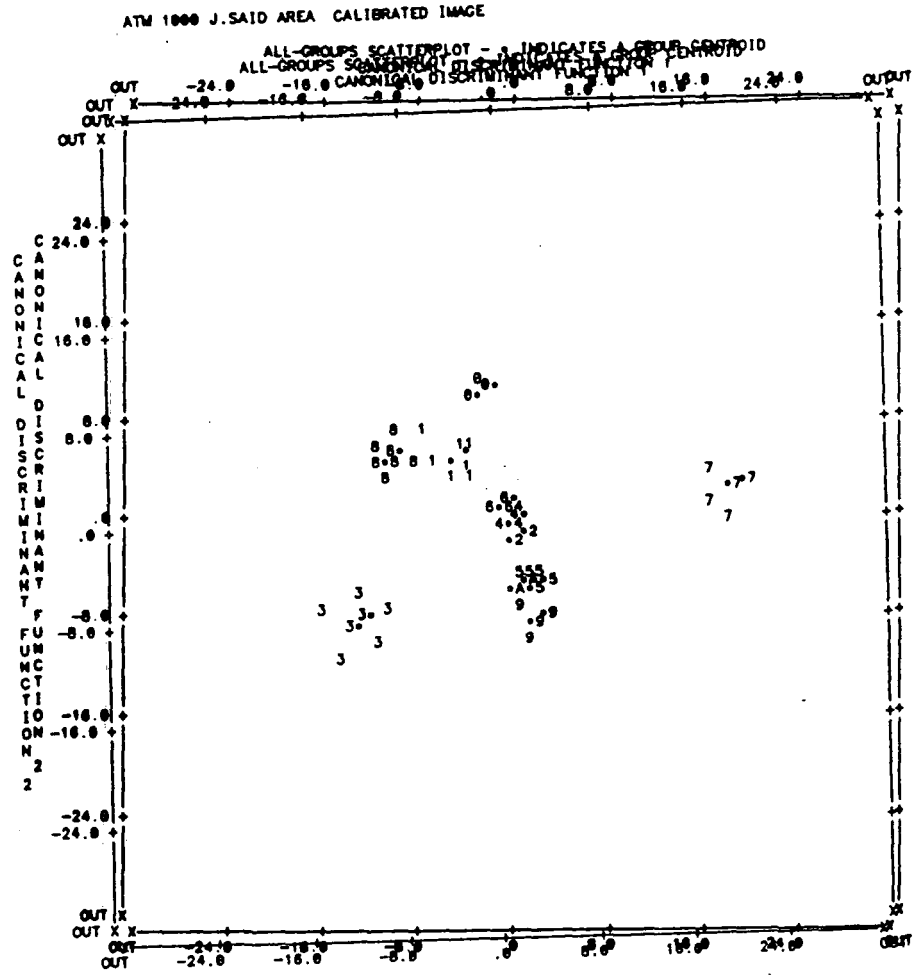

Fig. 5.34 The distribution of the eleven lithologies in Jabal Said. In canonically transformed features space (derived from the transformation of ATM 2.5m data).

Table 5.51 Classification matrix derived from the discrimination analysis performed on data for eleven lithologies using bands equivalent to TM bands from ATM 1000m (IFOV=2.5m) as the discriminatory variable, with the entry sequence, Jabal Said Area.

Actual Group Membership \ Predicted Group Membership	Granite rock	Dacite Tuff	Pegmatite	Rhyolite	Diorite	Andesite Gravel	Gossan	Alteration zone	Andesite Tuff	Quartz Gravel	Zubaidah Breccia
Granite rock	100	0	0	0	0	0	0	0	0	0	0
Dacite Tuff	0	100	0	0	0	0	0	0	0	0	0
Pegmatite	0	0	100	0	0	0	0	0	0	0	0
Rhyolite	0	0	0	100	0	0	0	0	0	0	0
Diorite	0	0	0	0	100	0	0	0	0	0	0
Andesite Gravel	0	0	0	0	0	100	0	0	0	0	0
Gossan	0	0	0	0	0	0	100	0	0	0	0
Alteration zone	0	0	0	0	0	0	0	100	0	0	0
Andesite Tuff	0	0	0	0	0	0	0	0	100	0	0
Quartz Gravel	0	0	0	0	0	0	0	0	0	100	0
Zubaidah Breccia	0	0	0	0	0	0	0	0	0	0	100

Variable Entry Sequence:

ATM band 7 (.83μm)

ATM band 5 (.66μm)

ATM band 3 (.56μm)

ATM band 10 (2.2μm)

ATM band 9 (1.6μm)

ATM band 2 (.49μm)

Percentage of Classification:

100.00%

Table 5.52 Classification matrix derived from the discrimination analysis performed on data for eleven lithologies using Landsat-5 TM bands (IFOV=30.0m) as the discriminatory variables, with the entry sequence, Jabal Said area.

Predicted Group Membership / Actual Group Membership	Granite rock	Dacite Tuff	Pegmatite	Rhyolite	Diorite	Andesite Gravel	Gossan	Alteration zone	Andesite Tuff	Quartz Gravel	Zubaidah Breccia
Granite rock	83.3	0	0	0	16.7	0	0	0	0	0	0
Dacite Tuff	0	100	0	0	0	0	0	0	0	0	0
Pegmatite	0	0	100	0	0	0	0	0	0	0	0
Rhyolite	0	0	0	100	0	0	0	0	0	0	0
Diorite	0	0	0	0	100	0	0	0	0	0	0
Andesite Gravel	0	0	0	0	0	100	0	0	0	0	0
Gossan	0	0	0	0	0	0	100	0	0	0	0
Alteration zone	0	0	0	0	0	0	0	100	0	0	0
Andesite Tuff	0	0	0	0	0	0	0	0	100	0	0
Quartz Gravel	0	0	0	0	0	0	0	0	0	100	0
Zubaidah Breccia	0	0	0	0	0	0	0	0	0	0	100

Variable Entry Sequence:

TM band 7 (2.2μm)

TM band 5 (1.6μm)

TM band 4 (.83μm)

TM band 2 (.56μm)

TM band 3 (.66μm)

TM band 1 (.49μm)

Percentage of Classification:

98.48%

Table 5.53 Comparison between % of classification and data type for analysis of 11 lithologies, Jabal Said area.

data type	Resolution (m)	Classification %		
		Radiance	Calibrat. TM	Cal. Ratio TM
ATM 1000	2.5	98.48% (9 bands)	100%	96.97%
ATM 2000	5.0	98.48 (9 bands)	98.48	96.97
ATM 3000	7.0	100% (9 bands)	98.48	98.48
TM	30.0	98.48 (6 bands)	98.48	100%
HHRR	0.96		76.81	82.61

bands selected for discrimination based on their spectral ability to separate these lithologies (Fig. 5.35). In contrast to the Mahd Adh Dhahab data, it is difficult to group any selected bands here. There are no similarities between the bands selected for maximum classification, except in the ATM 5.0m IFOV, 7.5m IFOV and HHRR data where the 0.66um band was selected. The TM data is the only data which considers 2.2um the best band by which separation of the altered rocks from the other lithologies can be achieved. Comparison between percentage of classification accuracy using eleven lithologies and the different resolutions for Jabal Said is shown in Fig. 5.36.

5.5 Conclusions

Examination of the spectral curves for different lithologies for both the Mahd Adh Dhahab and Jabal Said areas, do not show systematic changes with the different resolution data for the same lithology. However, absorption features are very clear, especially around 2.2um for the altered rocks, and the strong absorption near the visible band is indicative of iron oxide. No relationship between albedo and spatial resolution for any lithology was observed.

Using stepwise discriminant analysis on various ATM sensor and TM sensor data, where bands were ranked by their ability to separate specific lithological types and alteration types present in the Mahd Adh Dhahab and Jabal Said areas. The accuracy of the classification was almost

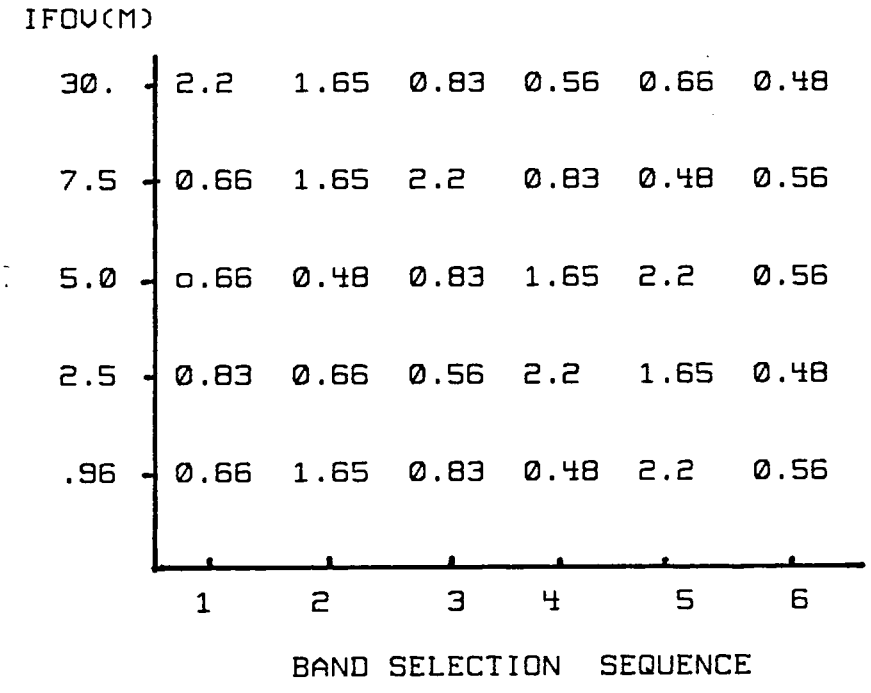

Fig. 5.35 Relation between bands selected for maximum discrimination with different resolutions, Jabal Said.

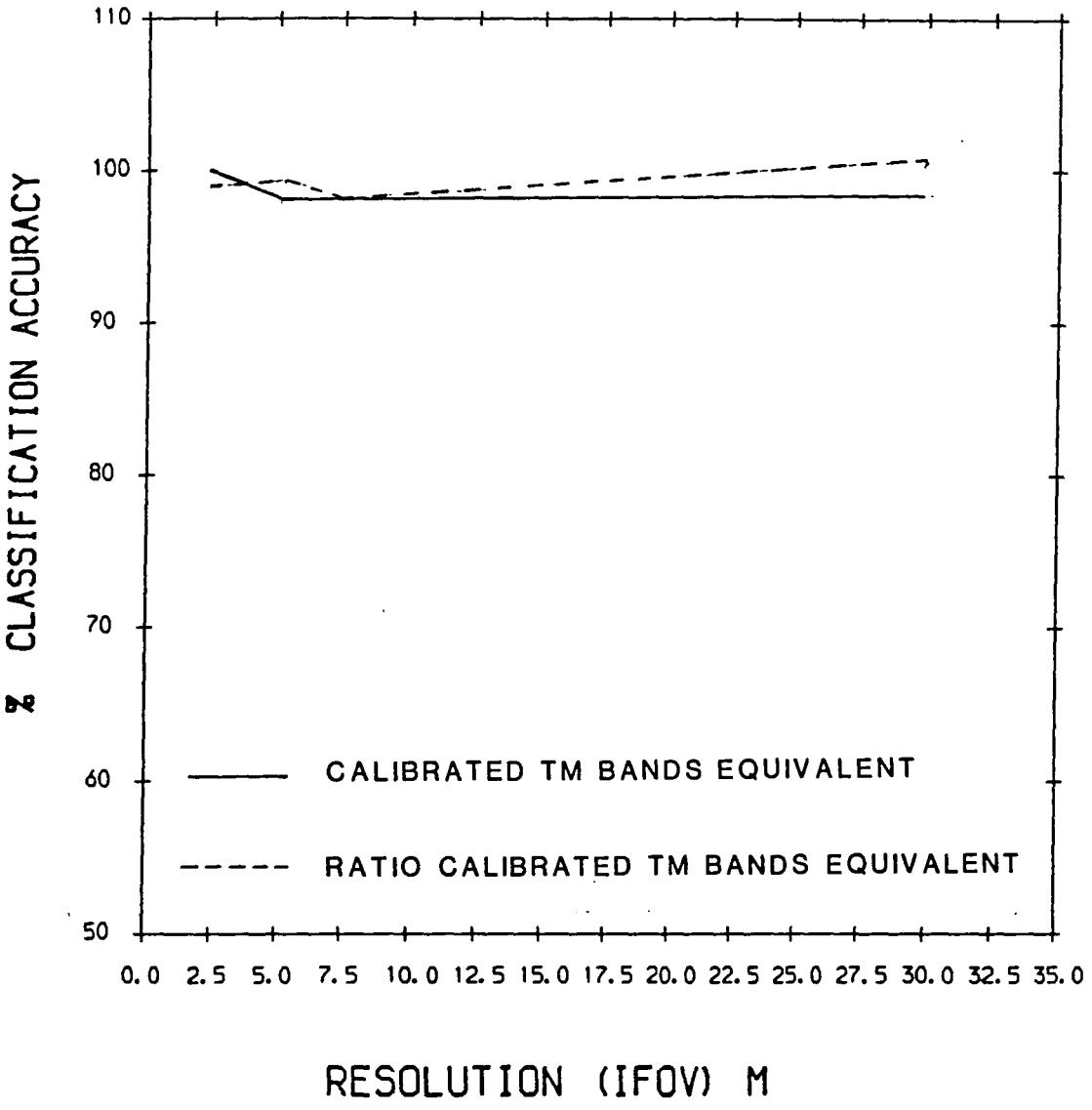

Fig. 5.36 Comparison of % classification accuracy using 11 lithologies, Jabal Said.

100% except for the results from the ground HHRR data. Generally the results suggest that successful rock discrimination, including that of altered rocks, may be influenced by the mineralogical composition of the lithology.

The entry of bands 2.2um, 0.83um, and 1.65um as the most discriminatory variable, supported the conclusion drawn in Chapter 3, namely that these bands were the most sensitive to changes in physical and chemical properties of different materials.

A comparison of the results derived from the analysis and interpretation of the spectral reflectance data with different resolutions, indicates that the TM sensor data can give similar results to those of the ATM sensor data, for identifying and discriminating certain types of lithologies (especially altered rocks). The result of the discriminant analysis for the data extracted from the different resolution data for the Mahd Adh Dhahab area did not go below 86.35% for the calibrated TM ratio data, and 92.31% as an overall accuracy for the calibrated TM sensor data. In Jabal Said the accuracy of the classification rose to 98.48% for the TM sensor bands and 100% when using the calibrated band ratios.

This indicates the ability of the TM sensor data to discriminate between the different lithologies although it has a coarser resolution than the ATM sensor data. In all cases the accuracy is significantly greater than 85%, which was recommended by Anderson (1971) as the minimum

level required in the discrimination of land cover categories using remotely sensed data.

The eleven targets chosen in Mahd Adh Dhahab contains six different types of alteration. Statistically it was possible to discriminate these types from each other, the types of lithologies or alteration, even the carbonate rocks. The results of classication was almost 100% in all the data types.

The classification accuracy of the eleven lithologies chosen over Jabal Said proved that a very high accuracy of classification can be obtained used any type of data used here.

The changing spatial resolution does not effect the accuracy of classification, as the most accurate classification of the TM data is similar to that of the ATM 2.5m data in Mahd Adh Dhahab. In Jabal Said the accuracy of classification of the TM data is similar to ATM 7.5m and ATM 5.0m IFOV data.

The acquisition of reflectance spectra in the short wavelength infrared allowed the more effective separation of those surfaces studied in both areas. Data from around 2.2um sepctral region was show to provide very useful discriminatory information.

Statistically, the discrimination of different lithologies is considered extremely successful. This indicates the ability of this technique and its success in Mahd Adh Dhahab and Jabal Said area, for identifying and discriminating altered from unaltered rocks. Results arising from the classification of various material types

supported the premise that Landsat TM sensor data was likely to provide a more effective tool for discriminating between different lithologies in the Arabian Shield. In other words, the TM sensor will give comparable results to those given by the ATM sensor. Considering the cost and processing time, any sugestion for using ATM data for lithological discrimination may be questionable.

Finally, improved spatial resolution does not necessarily result in an improvement in the accuracy of classification of selected lithologies.

CHAPTER 6

DIGITAL IMAGE ANALYSIS AND INTERPRETATION

6.1 Introduction

The preprocessing and preparation of the data have been discussed in Chapter 4. In Chapter 5, the ability of remote sensing data for lithological mapping were tested quantitatively, using discriminant analysis and classification techniques. In this Chapter the discussion will concentrate on the techniques of digital image processing which can greatly enhance the value of remotely sensed data. The result of applying these techniques was a significant turn away from the use of standard photo-interpretation and has proven valuable for different geological applications such as mapping and the detection of hydrothermal alteration (Goetz et al., 1983), especially in arid and semi-arid land.

This chapter has two principal aims. First, to test the capabilities of the variety of image enhancing techniques to separate between different lithologies on one hand, to differentiate between the areas of alteration and non-alteration, and also to test the suitability of satellite data in searching and high-lighting areas of alteration and possible areas of mineralization. Secondly, to test and evaluate whether these data could be used in lithological mapping in Shield-type terrain.

In discussions about the Mahd Adh Dhahab deposits (Huckerby et al., 1984), Dr. W.J. Phillips asked about

the potential of satellite imagery to identify similar tectonic features which would be targets for gold exploration. The authors replied that Mahd Adh Dhahab differs from other vein-typed gold deposits (for example, those in the western U.S.A.) in that the mineralization is not surrounded by widespread pervasive alteration that could be discriminated in a satellite image (Page B.158 - Applied Earth Science, v.93).

In this chapter, digital techniques used in this study for mapping the different lithologies and detecting alteration zones, are introduced and theoretically reviewed. A discussion of the application of results of these techniques to lithological mapping in Mahd Adh Dhahab and Jabal Said is presented.

Interpretation of these images (ATM and TM) as a result of applying the different techniques, were presented in transparency overlays, a comparison among the results of the different techniques is given at the end. The increased number of TM and ATM bands increase the possible number of colour composite and ratio combinations. Therefore careful selection for combinations was made using data collected from the field, including the field spectra and laboratory spectra. The results of the statistical analyses (Chapter 5) were also used.

6.2 Processing methods for lithological mapping and alteration detection

Digital image processing involves the manipulation and interpretation of digital images with the aid of a computer. Generally the process for digital data can be achieved using different techniques, one of which is Image Enhancement which involves techniques for increasing the visual distinction between features in a scene. The objective is to create a new image from the original image data in order to increase the amount of information that can be visually interpreted (Lillesand & Kiefer, 1987). Recently there have been various broad approaches to enhance the image.

In this study the image enhancement was adapted and the following type of processing techniques were applied: False Colour Composite, Ratio Images and Decorrelation Stretching.

6.2.1 Image Enhancement:

Image Enhancement is the modification of an image to alter its impact on the viewer. Enhancement generally distorts the original digital values, therefore enhancement is normally performed after restoration processes are complete and prior to visual interpretation.

The enhancement techniques were used to improve the capability of images to detect and and discriminate between the different lithologies in the study area.

Interactive processing of the multispectral data MSS, TM and ATM in this study were performed using the International Imaging System (IIS) at the University of Durham.

6.2.1.1 Contrast Enhancement

The contrast enhancement is defined as an image-processing procedure that improves the contrast ratio of images. The original narrow range of digital values is expanded to utilize the full range of available digital values.

Contrast enhancement was performed on the images prior to visual interpretation. One method used was a linear contrast stretch. It is a simple point operation that redistributes the pixel values so that a narrow range is expanded to cover the full dynamic range of the display system enabling an important evaluation of radiometric detail (Fig. 6.1).

6.2.2 False Colour Composite Production:

Since the human eye is more sensitive to coloured images than to monochrome images, visual interpretations of colour differences in a composite image becomes easier.

The false colour compositing image can be defined as a colour image consisting of three bands, assigned to three colour filters; red, green and blue, one for each band (Fig. 6.2).

The most common bands selected for LANDSAT MSS data to form colour composites are MSS bands 4,5 7 and assigned to blue, green and red filters respectively.

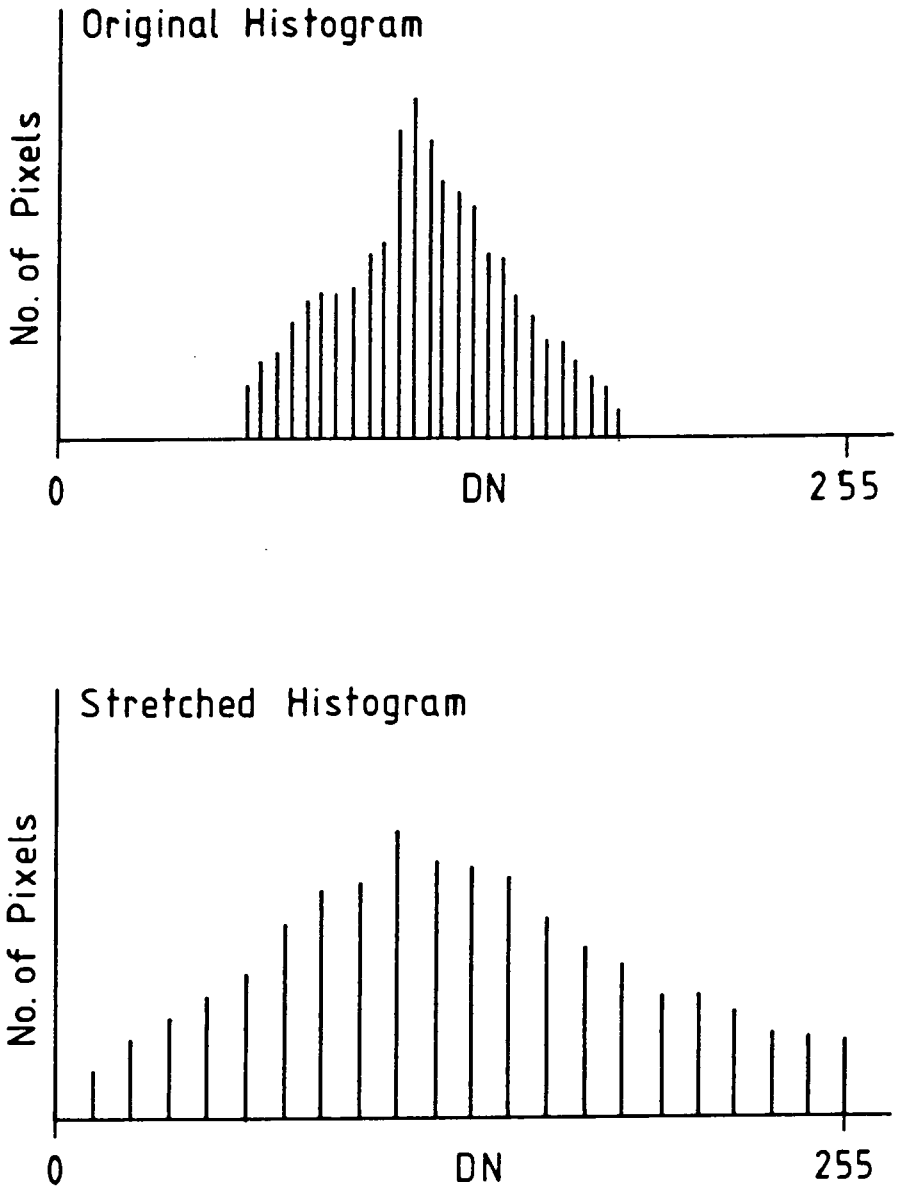

Fig. 6.1 Linear stretch of a single band.

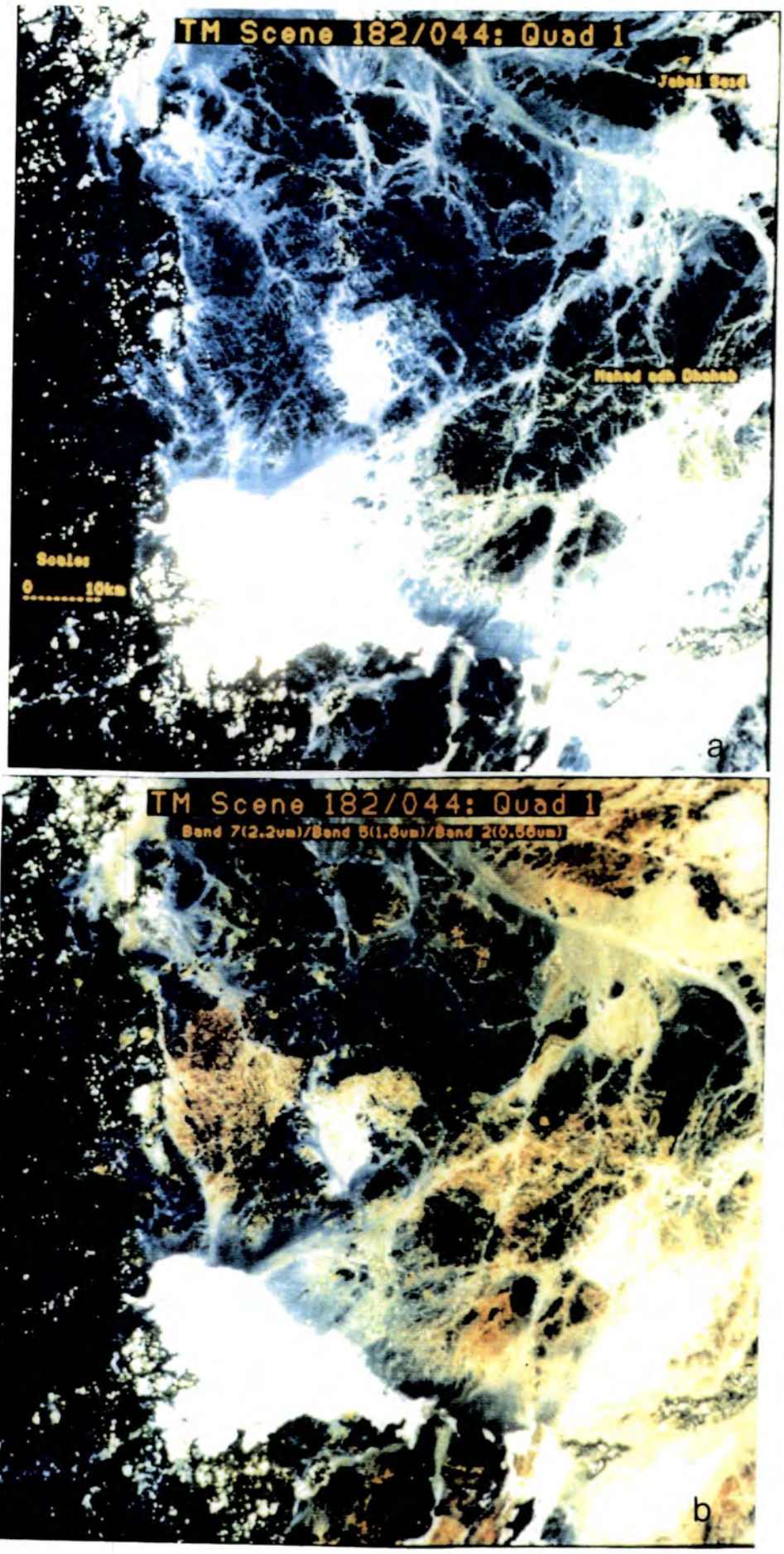

Fig. 6.2 a. Simulated true colour of TM using band 3.2.1. Image cover both areas Mahd Adh Dhahab and Jabal Said.
b. TM False Colour Composite using bands 7, 5 and 2 in RGB respectively.

This is also considered the best combination for the lithological discrimination (Blodget et al., 1978; Rothery, 1987).

The Landsat TM sensors and Daedalus ATM sensors have more bands and so producing a false- colour composite requires a careful choice of the available bands.

Two methods have been adapted for band selection; the statistical method which was discussed in Chapter 5, and visual analysis based on the experience and the type of lithologies in the area.

For geological interpretation in arid terrains, a previous worker suggested false colour composites using 2.2, 0.83 and 0.56um (TM, 7,4,2) or 2.2, 1.65, and 0.83um (TM 7,5,4), displayed in red, green and blue respectively (Rothery, 1987). Others, including Loughlin and Tawfique (1985), believe that 2.2, 1.6 and 0.56um (TM bands 7,5 and 2; ATM 10, 9 and 3) are best for discriminating argillic and ferrugineous alteration.

Different combinations were tested from the visual interpretation on the interactive system, however most of the interpretations used the combination of 2.2, 1.6 and 0.56um (TM bands 7,5 2 equal to 10,9, 3 in ATM). Legg (1985) compared colour composite images of ATM 10, 9 and 3 (2.2, 1.95, 0.56um) and bands 10, 7, 3 (2.2, 0.83, 0.56um) over Jabal Said for mapping the alteration zone.

The false colour composite of bands 7, 5, 4 (2.2, 1.65, 0.83um) were reported to be useful in mapping and subdividing the units (e.g. Abrams, 1986; Rothery, 1987). This band selection supports the results of statistical

analyses of TM data of Jabal Said (see Chapter 5). Results from the ATM data show that the near infrared bands contain more information than the short wavelength bands in Mahd Adh Dhahab, and in Jabal Said.

ATM 5,3,2 which is equal to TM bands 3,2,1 false colour composite simulates a true colour image (Fig. 6.2). Huntings (1984) reported also that ATM 10 (2.2um), 9 (1.65um), 8 (0.98um) is a useful geological combination.

6.2.3 Band Ratioing

Ratioing is a processing technique in which two spatially registered spectral images are divided, pixel by pixel (Abrams & Siegal, 1980). The resultant data are rescaled to fill the dynamic range of the display by contast enhancement techniques which are mentioned above.

Ratios can also be defined as a method of enhancing minor differences between materials by defining the slope of the spectral curve between two bands.

The DN at any pixel represents the ratio of the DN from two channels:

$$DN_{ls} = \frac{DNi_{ls}}{DNj_{ls}} + b$$

DN = ratio of the DN from channels i and j at line sample s.

a,b = constant

Ratio values can range from zero to infinity, but because reflectivity in terrestrial scenes is strongly correlated across much of the spectrum, most observed ratio values lie between about 0.25 to 4.0 (Gillespie, 1980).

The geological application of ratio techniques was first reported by Rowan et al. (1974) using MSS images. The ratio images have the effect of suppressing the detail in a scene which is caused by topographic effects, while emphasising colour boundaries. This is one of the reasons which has made ratio images useful in geological applications (Abrams et al., 1983; Abrams et al., 1984).

The earliest study over the Arabian Shield using the band ratio was done by Blodget et al. (1978) where an area in the south of the Arabian Shield was studies, using MSS data. They claimed that the enhancement ratio image 4/5 (0.55/0.65um), 5/6 (0.65/0.75um) and 6/7 (0.75/0.95um) permitted the best overall visual identification of lithologies and alteration products.

The ratios found to be most useful in this study were 1.6/2.2um, 0.66/0.56um, and 0.83/1.6um. These ratios are then combined in a colour composite image allocating each ratio to the red, green and blue filter respectively. The effect of the ratioing process will show areas rich in iron-oxide as green, due to the presence of an Fe^{3+} absorption band at wavelengths less than 0.56um. The clay-rich areas will appear in red due to the hydrous minerals absorption band near 2.2um. The area with hydrothermal alteration with mixture of clay,

sericite, chlorite and iron oxides will appear in orange to yellow due to the combination of red and green components (Abrams & Siegal, 1980).

The success of the ratioing technique depended on the nature of the area or the composition of the minerals in the area. A band ratio is a useful technique where iron oxides, minerals containing OH, H_2O, CO_3 and SO_4 molecules are present.

Clay minerals containing bound or unbound water, micas, carbonates, sulphates and hydrates (e.g. gypsum) are enhanced by the band ratio 1.65/2.2 where these appear as bright areas in the imagery. The most effective signal enhancements which relate to the ferric and ferrous iron are provided by the band ratios 2.2/0.83, 2.2/0.49 or 1.65/0.83, 1.65/0.49 due to the major electronic transition bands in the NIR (at 0.87um) and the visible, and charge transfer bands in the ultraviolet in contrast to the unaffected SWIR range. The common band of the ferrous ion near 1.0um is not covered by the TM sensor.

Kaufmann and Pfeiffer (1988) reported that the band ratio 0.66/0.49 (Landsat TM 3/1), used by many authors to enhance ferric iron, often failed because the slope between these two bands is too weak in comparison to combinations of the SWIR bands with 0.49um or 0.83um.

One of the disadvantages of ratio imaging was the accentuated noise, making interpretation more difficult. In addition, dissimilar materials having similar spectral slopes but different albedos, which are easily separable

on standard images, may become inseparable on ratio images.

6.2.4 Principal Component Analysis:

Principal component analysis (PCA) has been used for many years in various statistical applications. Applications of using principal components in remote sensing have been described by many investigators (e.g. Podwysocki et al., 1977; Blodget, 1978).

PCA is a procedure that determines a linear transformation that can condense the scene variance in the original data into a new set of variables (axes or principal components) that are uncorrelated. In addition, the scene variance tends to be concentrated into fewer new variables that still contain all of the original variability of the bands. This dimensionality reduction is the usual reason for using PCA on multivariate data.

The principal components analysis was used as an initial input image for calculating decorrelation stretch imagery for interested areas.

6.2.5 Decorrelation Stretching

This technique is now becoming widely used for lithological mapping (e.g. Kahle and Rowan, 1980; Rothery, 1987; Abrams et al., 1985). It is considered to be an excellent means of accentuating colour variations within an image as an aid to visual interpretation. The decorrelation stretch can be defined

as a method to exaggerate colour saturation and intensity, while preserving hue information.

Usually the absorption features in the reflectance spectra which give rise to variations within and between rock units are comparatively minor, so there is a high degree of correlation between the spectral responses of these surfaces in each spectral band (Soha & Schwartz, 1978; Rothery, 1987; Gillespie & Kahle, 1986).

Figures 6.3(a-c) explaines the effect of the stretching on the data. This shows the conventional contrast stretching. The results will be imaged with a full range of brightness colour and saturated hues.

The principal component image will be performed by constrast stretch along the principal axes as mentioned above. This will achieve a spheroidal distributions. Figures 6.3(d-f) gives the disadvantages of the principal component image that the colours are not related to spectral features. Decorrelation stretching can be achieved by projecting the principal component image back to the original red, green and blue axes (Rothery, 1987; Gillespie, 1986).

6.3 Image analysis and interpretation of Mahd Adh Dhahab

6.3.1 Introduction

The different techniques explained at the beginning of this Chapter were applied to the TM data and the three data types of ATM data covering the Mahd Adh Dhahab area. The analysis of the images included analysis of single band, colour composite, ratioed and decorrelation

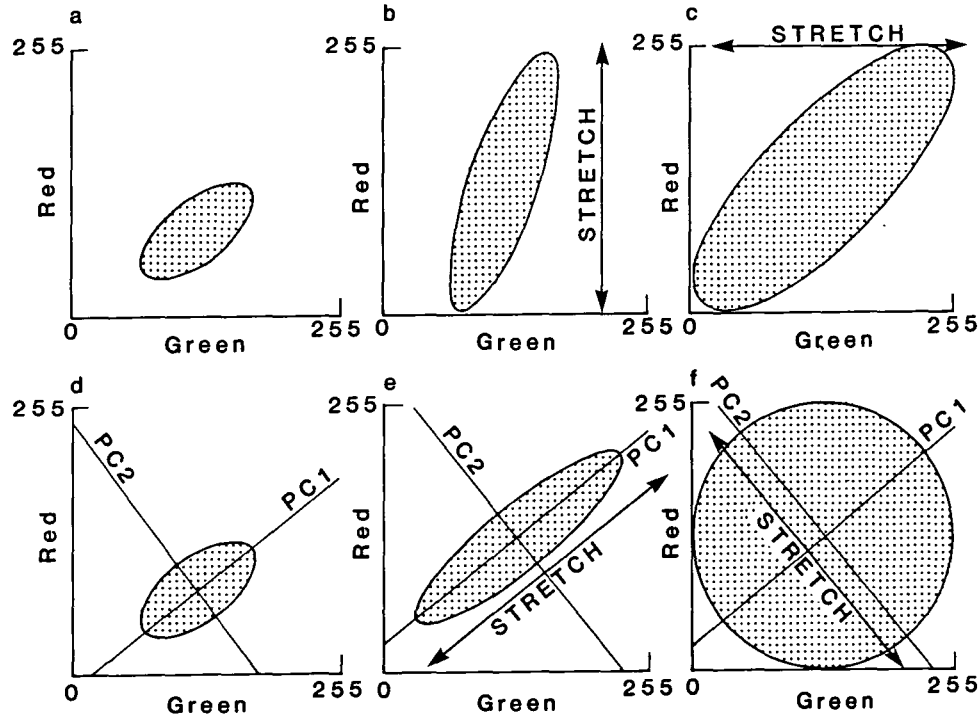

Fig.6.3 Conventional contrast stretching (a-c) and decorrelation stretching (d-f) of multispectral data, shown in the red-green plane. The values of 0-255 on each axis are the DN (digital numbers) used in 8-bit processing. (a) Raw data typically has a restricted DN range, and is also correlated. (b,c) Conventional contrast stretching is performed parallel to the input band axes which yields an image with a full range of DN in each channel, but the bands are still correlated. (d-f) In decorrelation stretching principal component axes are defined parallel to the principal axes of the ellipsoidal data distribution, and stretching is done along these directions. This produces a spheroidal, decorrelated, data distribution which makes fuller use of colour space and the resulting image is more colourful. Source: D. Rothery (1987).

stretched images and a comparison of these techniques is presented.

One of the problems was the management of the image due to the number of bands and different resolutions. Sometimes it was difficult to select the combinations for colour composite, even when using the results of the discriminant analysis which was discussed earlier (Chapter 5).

Effort in the analysis and interpretation of the images were not equally distributed, but was concentrated on those images which offered the highest potential value to mineral exploration in the Mahd Adh Dhahab area. The type of information extracted from TM images were general lithological separation and mapping capabilities, an indication for the presence of alteration. On the other hand, the ATM data covered a limited size of area, mainly the Mine Hill, and all the image interpretation was focussed on the separation of the alteration zone and different types of alteration, together with local structure features.

6.3.2 Airborne thematic mapper image analysis

The ATM data covering Mahd Adh Dhahab were available in three different resolutions as mentioned previously at 2.5m IFOV, 5.0m IFOV and 7.5m IFOV and taken from altitudes of 1000m, 2000m and 3000m respectively. Due to the increase of the resolutions, the area covered was decided by one flight line from 3000m. The other data were limited to the size of the first flight line which means an increase in the flight line to cover the

interested area, so data from 2000m was covered by two flight lines and data from 1000m covered by three flight lines (Fig. 6.4). The higher resolution data is divided into several different flight lines which makes it difficult to analyse, bearing in mind that the width of every flight line is 716 pixels and there is considerable overlap (see 2.5m IFOV data in Fig. 6.4).

One of the primary objectives was to see if it was possible to map the alteration and also to discriminate and map the various types of alteration. The character of the alteration in Mahd Adh Dhahab has been discussed in Chapter 2.

6.3.2.1 Interpretation of Single band images

A single band image from ATM 3000m with resolution 7.5m was contrasted, stretched and evaluated individually. In this case ATM bands equivalent to TM bands were selected for comparison with each other. Different geological features were recognised on each band (Fig. 6.5). In the first two bands, 0.49um and 0.56um, the volcanic rocks and the granodiorite can be discriminated from the wadi sediments and talus which, in the Mine Hill, show a darker colour than the wadi sediments east and south of the Mine Hill. The granodiorite in the each can be discriminated from the volcanic rocks. These two bands do not distinguish the altered rocks. The third band, 0.66um is similar to the previous bands except the tones of the volcanic rocks are much lighter and the wadi sediments are brighter.

FIGURE 6.4

COMPARISON BETWEEN DIFFERENT RESOLUTION

OF ATM DATA -MAHD ADH DHAHAB AREA

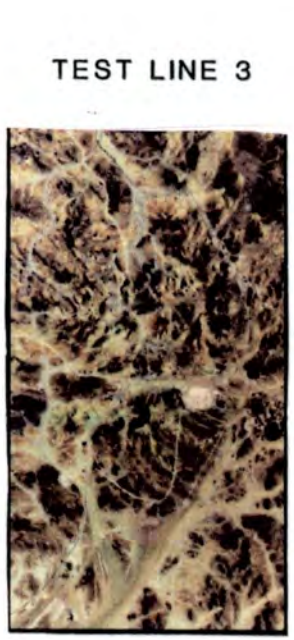

3000 M DATA

RESOLUTION 7.5m

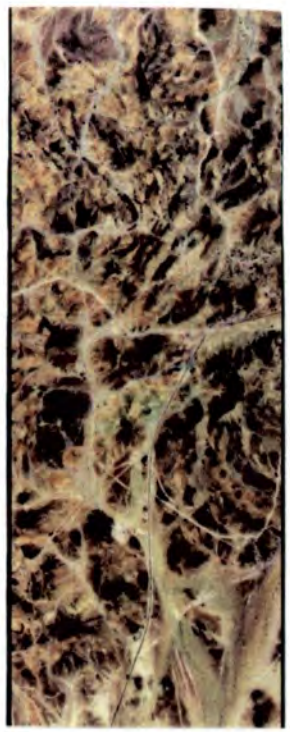

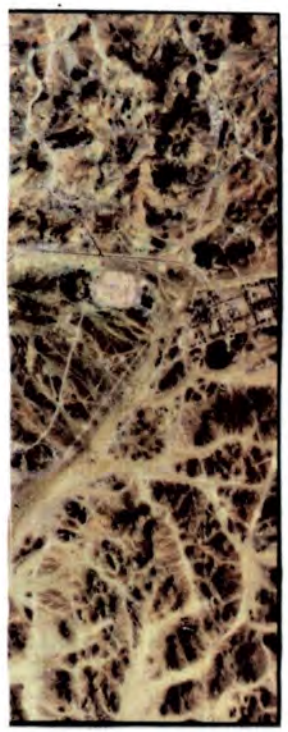

RESOLUTION 5.0m 2000 M DATA

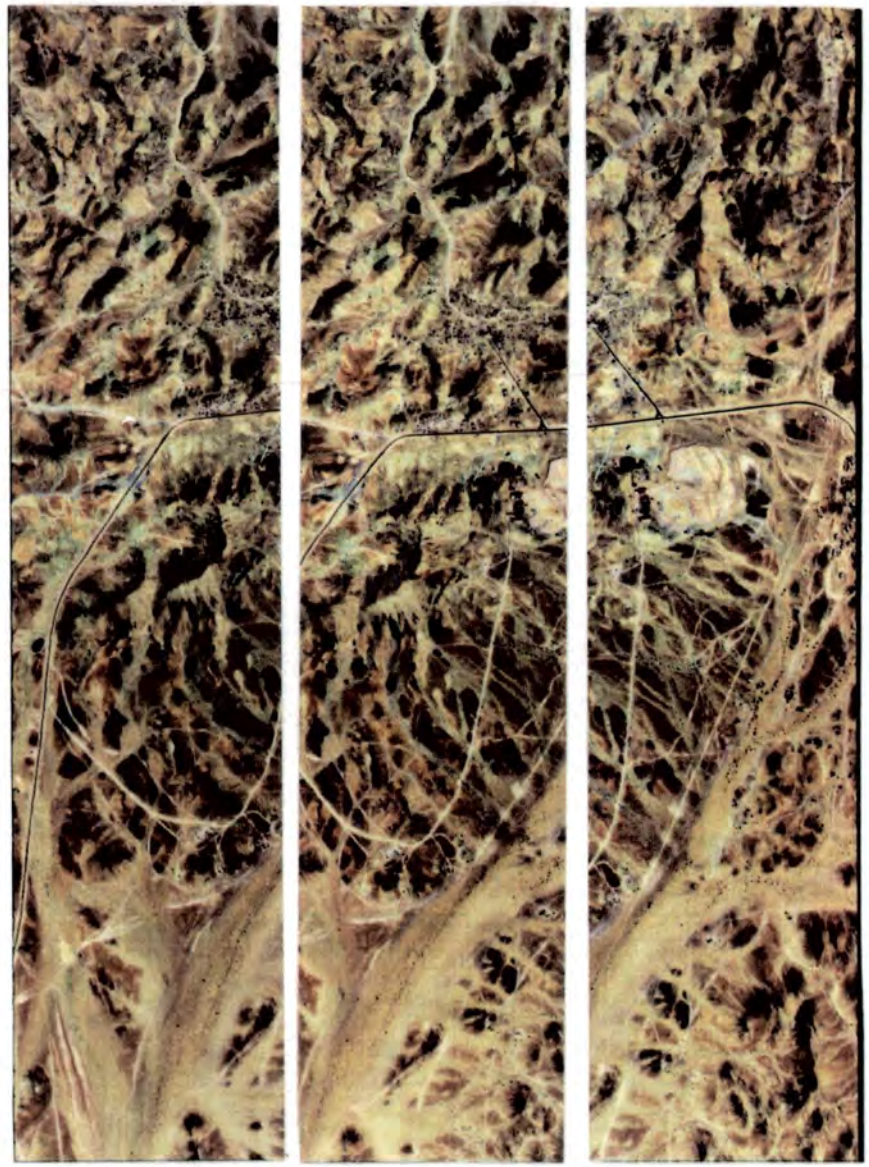

1000 M DATA RESOLUTION 2.5m

Source:The Arabian Aerosurvey Co. 1984

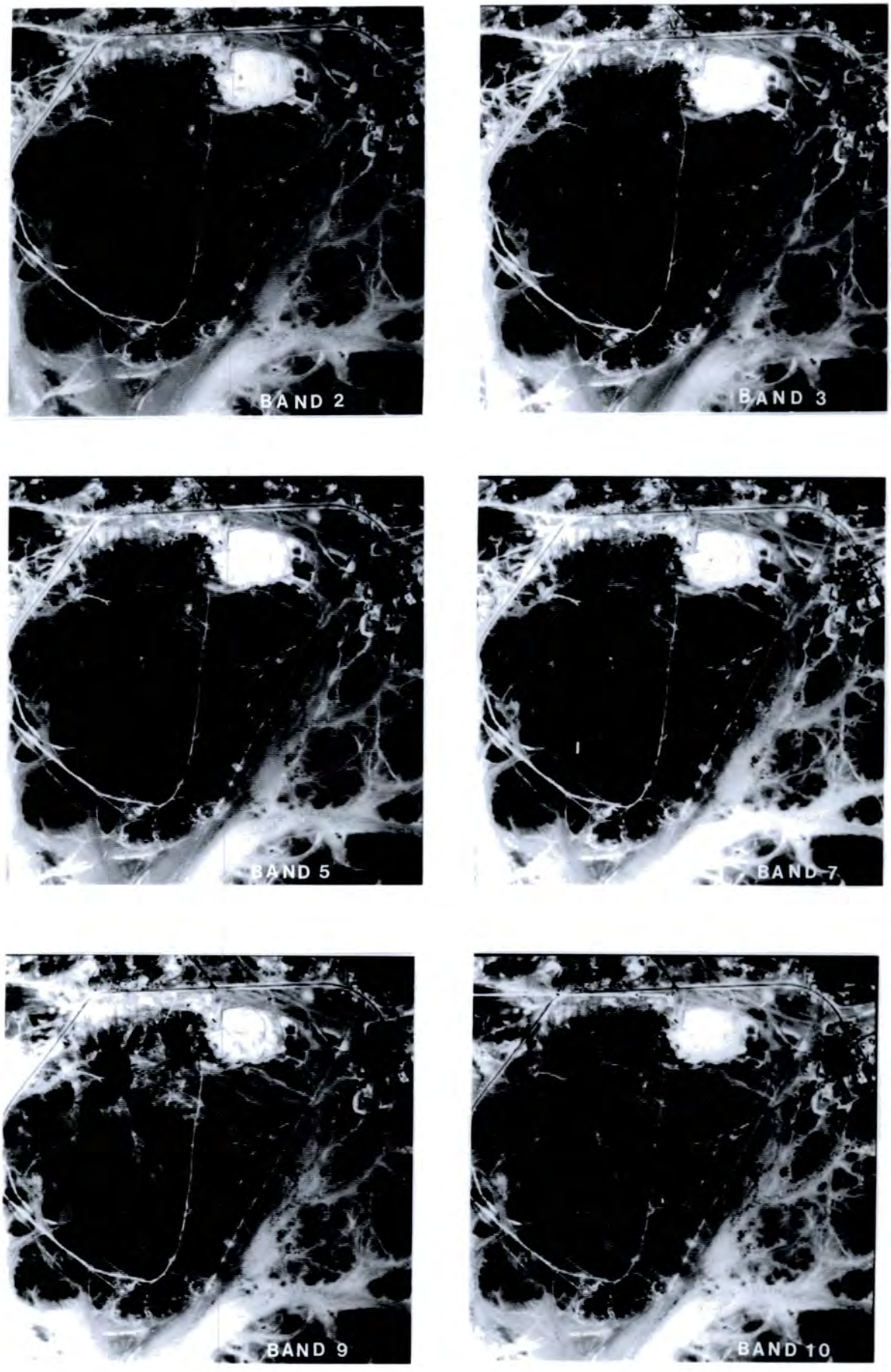

Fig. 6.5 Comparison between ATM 3000 m (IFOV 7.5m) single bands over Mahd Adh Dhahab area. Bands equivalent to TM bands only.

In band 4 TM (0.83um), which is similar to ATM 7 (0.83um), it is possible to discriminate the volcanic rock in the Mine Hill from the granodiorite rock in the east. It is also possible to discriminate between the volcanic rocks and the talus. Band 9 ATM (TM band 5)(1.65um) show much better discrimination between volcanic rocks and talus, and the andesite shows a much darker colour. The alteration zone in the Mine Hill appears lighter and whiter compared to the previous local structure and quartz veins can be picked up. The dark areas in the alteration zone are due to the shadow of the mountain and the low sun angle.

Band 10 ATM (2.2um) (TM band 7, 2.2um) show good discrimination between volcanic rocks and talus, the alteration zone have a darker tone compared to band 9 ATM due to the low spectral features of this band. It also showed the local structures, especially the quartz veins. The detail within the granodiorite can be picked up.

6.3.2.2 <u>False colour composite</u>

Choosing the best 3 bands to form a false colour composite from multispectral sensors is dependent on the geology of the area.

The Hunting Company used bands 10 (2.2um), 7 (0.83um), 3 (0.56um) in red, green and blue, and also bands 10 (2.2um), 9 (1.65um), 3 (0.56um) in red green and blue respectively. This has been claimed as the best combination for discriminating argillic and ferruginous alteration in the Arabian Shield. The combinations of

bands 5 (0.66um), 3 (0.56um) and 2 (0.48um) is simulated, the true colour is also used by Loughlin & Tawfiq (1985).

In this study more than one type of combination has been tested, including the results from statistical analysis (see Chapter 5, Fig. 5). The best band for discrimination between different types of alteration suggested in Chapter 5 are ATM 5 (0.66um), 10 (2.2um), 9 (1.65um) for data with 7.5m IFOV and 5.0m IFOV resolutions, while the higher resolution data suggests 9 (1.65um), 3 (0.56um) and 5 (0.66um) as the best bands.

The ATM 10 (2.2um), 9 (1.65um), 3 (0.56um) combination displayed in R, G, B respectively, highlight the altered rocks in distinctive greenish or turquoise colours. This alteration is distinguished from the rest of the lithologies which show a gradual change from light brown to very dark brown (Fig. 6.6). Detailed examination of the alteration zone in the image indicated variation between different types of alteration (Fig. 6.7). The yellow colour in the 10 (2.2um), 9 (1.65um), and 3 (0.56um) images is related to the iron oxides, which are probably due to relatively high reflectance in ATM 9 (1.65um) and 10 (2.2um) which is shared by siliceous and carbonate rocks (Bird et al., 1985) (Fig. 6.8). It was found that this confusion could be removed by producing images in which ATM band 7 (0.83um) is substituted for band 9 (1.65um) of the 10 (2.2um), 9 (1.65um), 3 (0.56um) in R, G, B images. The resulting 10 (2.2um), 7 (0.83um), 3 (0.56um) (R, G, B) image (Fig. 6.9) displayed iron oxides in reddish-brown, due to relativley high iron

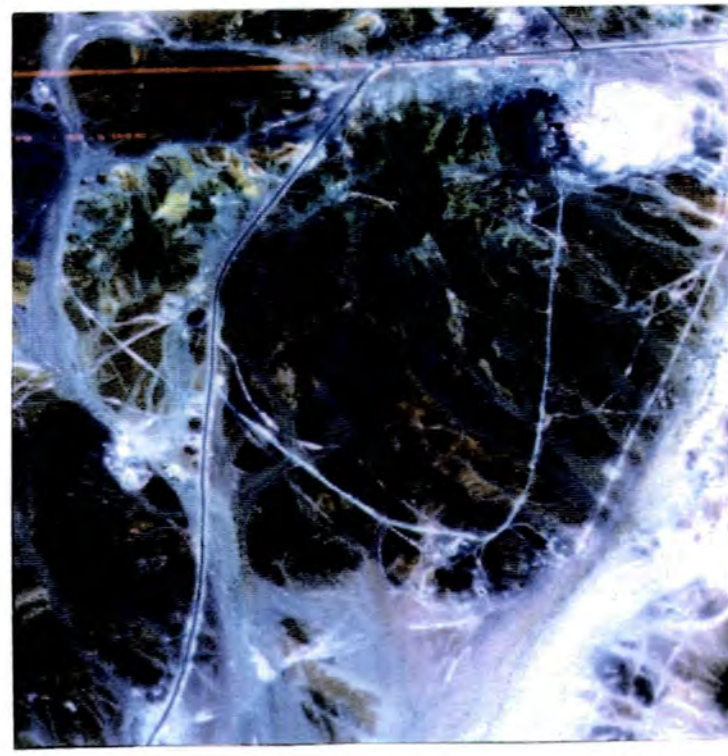

Fig. 6.6 In the composition 10,9,3. The alteration zone appears to have the greenish-blue colour in the Mine Hill and continues to the west of the road.

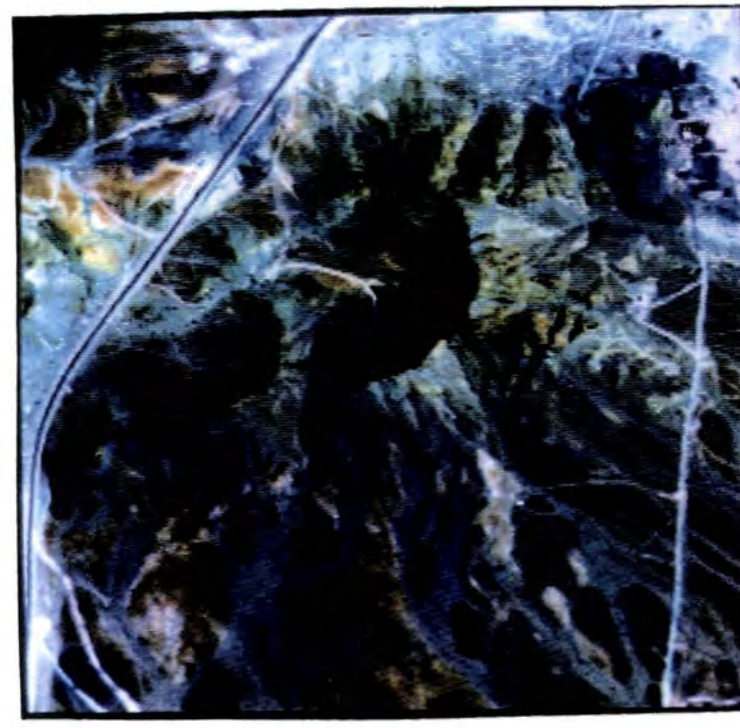

Fig. 6.7 Zoom from the previous figure over the alteration area, showing more variation with the alteration zone.

Fig. 6.8 10,9,3 composite colour in R.G.B, of ATM 1000m (resolution 2.5m) showing part of the alteration zone in the Mine Hill. The yellow colour appears to be related to iron oxide and siliceous and carbonate rocks.

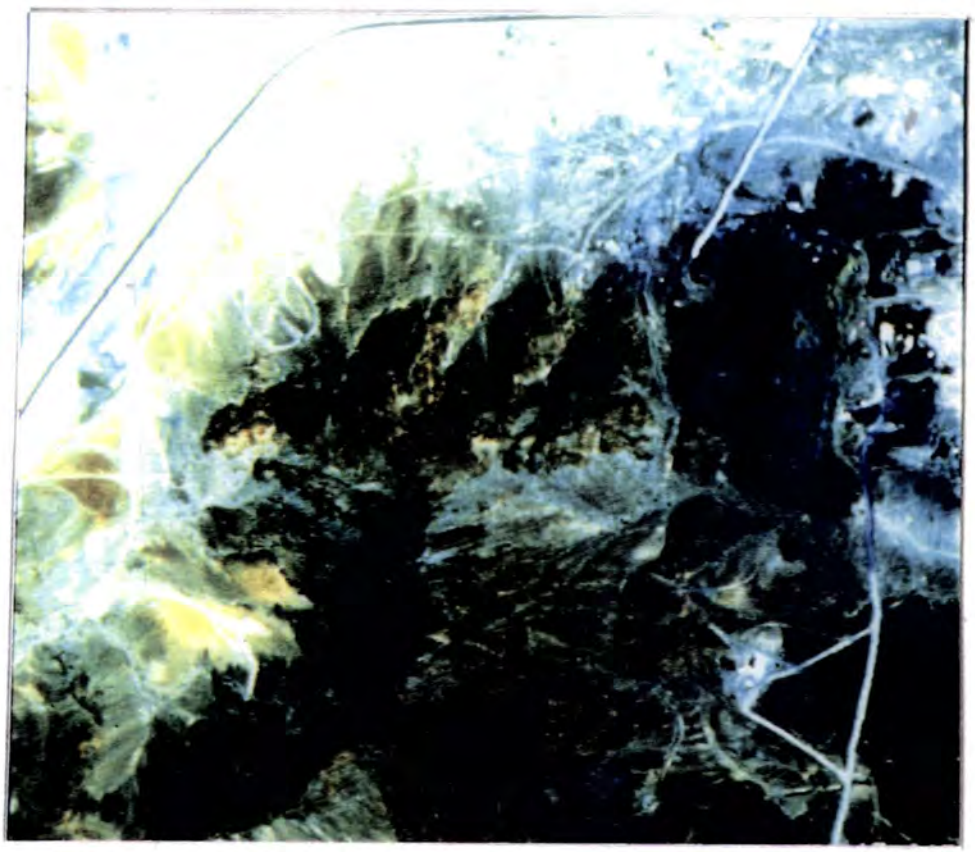

Fig. 6.9 10,7,3 colour composite in R.G.B. of ATM 1000m (resolution 2.5m) showing part of the alteration zone in the Mine Hill. The reddish-brown colour is related to the iron oxide and ferruginous alteration (Compare with Fig. 6.8).

oxide reflectance in band 7; the siliceous and carbonate rocks do not have this low reflectance in band 7 (0.83um). Therefore the 10 (2.2um), 7 (0.83um), 3 (0.56um) combination can highlight ferruginous zones. This was proved with the comparison to the spectral analysis in Chapter 3 (see Figs. 3.22 and 3.24).

Other combinations were also tested, 9 (1.65um), 5 (0.66um), 3 (0.56um) in R, G, B (Fig. 6.10) and 9 (1.65um), 8 (0.98um), 2 (0.48um) in R, G, B including band 8 (0.91-1.05um) which is not available on the TM sensor. This last combination seems to give an indication to the alteration zone in reddish-orange colour, and some detail of the alteration zone can be picked up (Fig. 6.11).

One of the problems of using broad band sensors such as band ATM 10 (2.08-2.35um)(7 TM) is that using this band will not only indicate the minerals with the hydroxyl-bearing, but also the carbonate minerals, where CO_3 can be reflected by spectral features around 2.33um. Therefore, the yellowish-greenish colour or turquoise colour which appear in the ATM 10 (2.2um), 9 (1.65um), 3 (0.56um) colour composite, should be carefully interpreted in relation to the ground truth. Fig. 6.12 shows the carbonate rocks north of the Mahd Adh Dhahab Mine.

6.3.2.3 Band Ratio Images

Band ratioing is a powerful technique for extracting spectral information from multispectral imagery (Rowan et al., 1974). It is an effective method for distinguishing

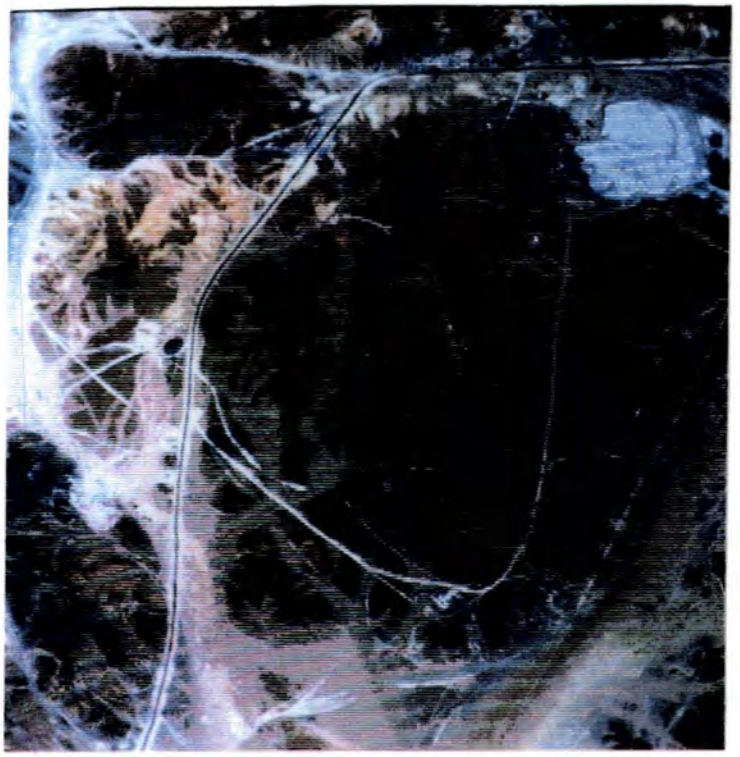

Fig. 6.10 9,5,3 in R.G.B of ATM 300m showing the Mahd Adh Dhahab area.

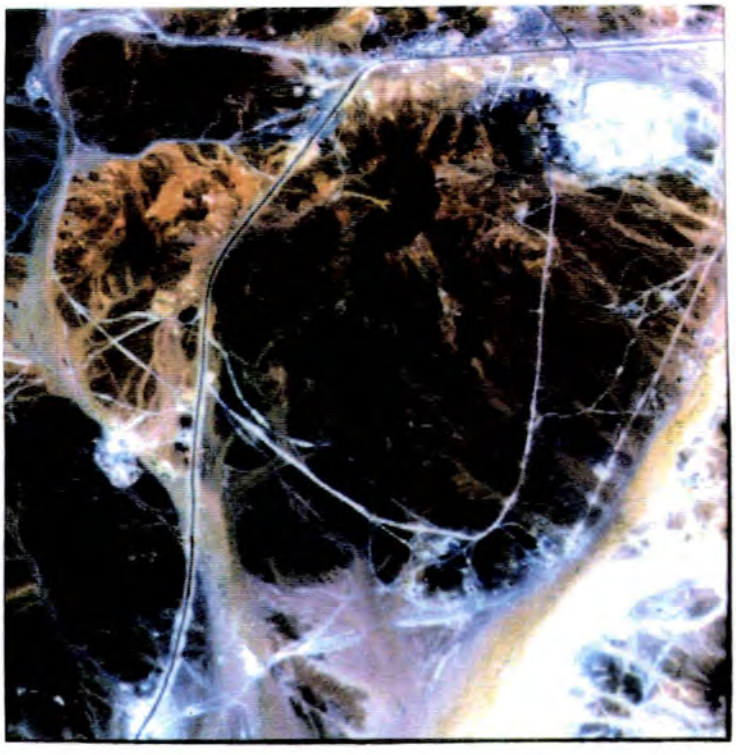

Fig. 6.11 The combination of 9,8,2 in R.G.B respectively of ATM 3000m, showing the alteration zone in reddish-orange colour. Some details of the alteration type can be picked out.

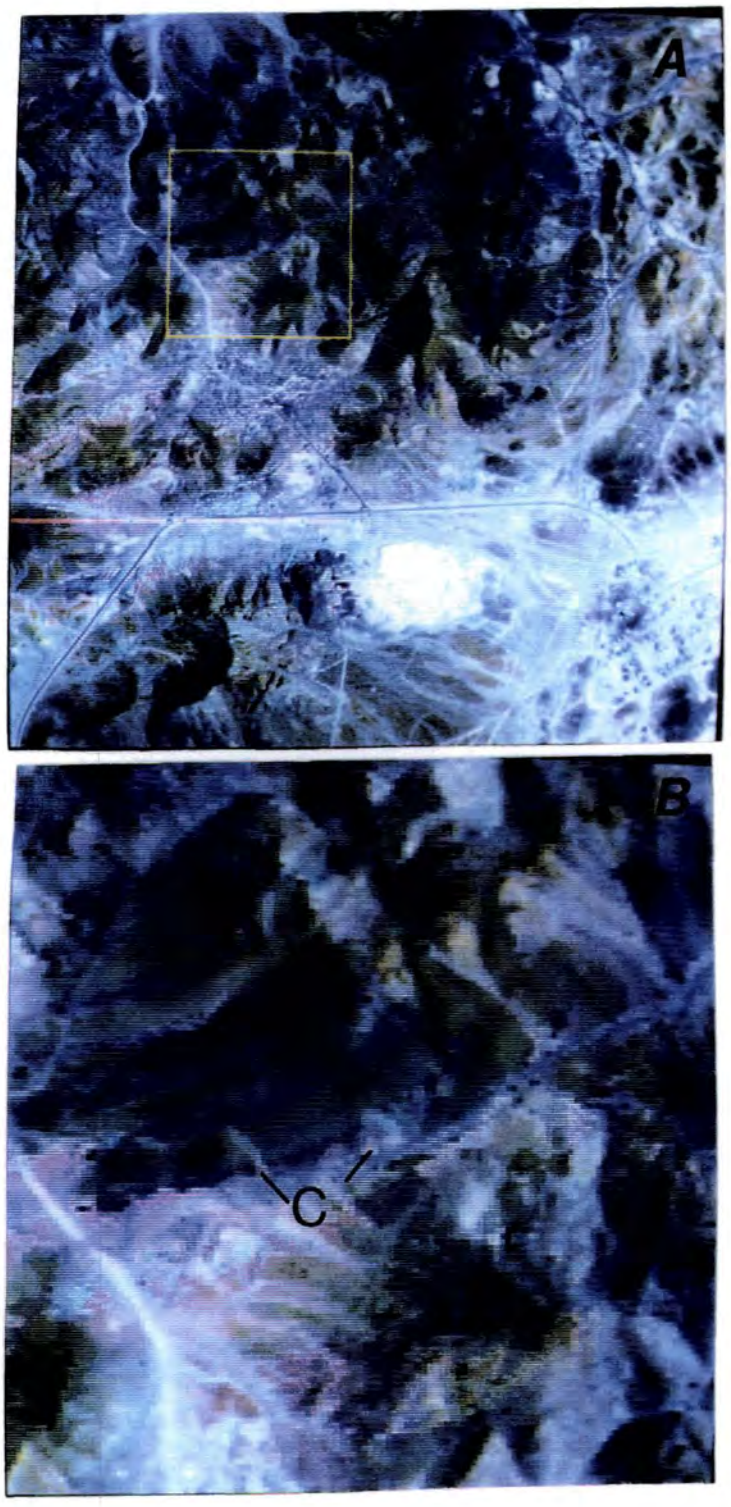

Fig. 6.12 (a) The greenish-colour indicates the presence of carbonate rocks, north of the wadi. (b) a zoom image showing the carbonate lenses (c).

between rock types because the main spectral differences in visible and near-infrared spectral regions are found in the slopes of the reflectivity curves.

The examination of the spectral reflectance data in Chapter 3 determines that the ratios; 9/10 ATM (1.65/2.2um) would provide an effective means for discriminations of hydroxyl-bearing minerals, related to hydrothermal alteration. This ratio displayed areas of alteration in the Mine Hill with white colour, due to Al-OH and Mg-OH absorption in the 2.0-2.5um region (Fig. 6.13a). The other types of ratio suggested, was 7/9 ATM (0.83/1.65um), which contrasts with the previous ratios. It displays the alteration zones which are rich in hydroxyl-bearing minerals and the iron rich rocks in a dark colour, due to the absorption of the iron at 0.85um. The granodiorite appeared in white colour (Fig. 6.13b).

Ratio 5/3 ATM (0.66/56um) displays areas with hydroxyl bearing minerals in white and the area rich in iron oxide which are very dark in colour (Fig. 6.13c).

A false colour ratio image was created by using red, green and blue for band ratios 1.65/2.2um, 0.66/0.56um and 0.83/1.65um respectively. This combination was also suggested by Abrams et al. (1977) and portrays an iron oxide-rich area in green due to the presence of the ferric ion charge transfer band in the ultraviolet, and clay rich areas, or hydroxyl bearing minerals in beds, due to the presence of the hydrous mineral absorption band near 2.2um, but where both clay and iron oxides are present, the area will appear yellow or orange. The

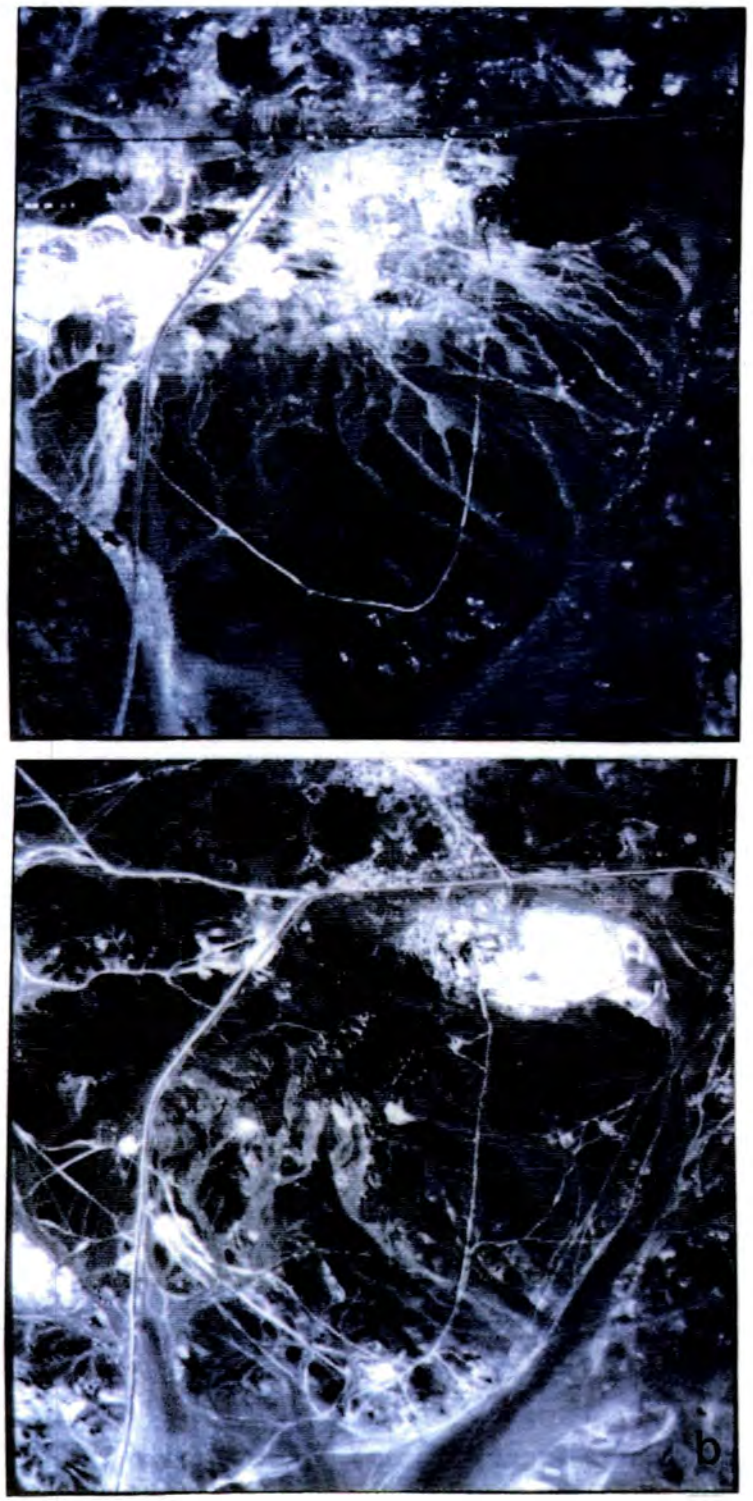

Fig. 6.13 ATM ratio (a) showing ATM 9/10 (1.65/2.2um) ratio image to display the alteration in white. (b) ATM 7/9 (0.83/1.65um) showing the alteration in darker colour.

effect of the ratioing process is to enhance iron oxide rich areas in green due to the presence of the Fe^{3+} absorption band short of 0.56um, and clay rich areas in red, due to the hydrous minerals absorption band near 2.2um. Areas of hydrothermal alteration, with mixutre of clay, sericite, chlorite and iron oxides, show up as orange to yellow areas, due to the combination of red and green colour components.

The Mine Hill is completely outlined as a yellowish-orange area, notably this coincides with the border of the alteration map discussed earlier in Chapter 3 (Fig. 6.14). The area west and north of the Mine Hill also suggests possible alteration.

6.3.3 TM Image Analysis

The subscene of the TM image of the Mahd Adh Dahahab area covered a wider geographical area compared to the ATM coverage. though the analysis of the TM image covers the different types of geological units and not limited to alteration zones only, as in the ATM images.

The interpretation and the analysis of TM images of Mahd Adh Dhahab deposits was commissioned to investigate the potential of Landsat Thematic Mapper Imagery to map areas of hydrothermal alteration associated with gold mineralization in Al Mahd and map the different types of lithologies in the area. Three different techniques were used in the TM images, false colour composite production, ratioing and decorrelation stretching.

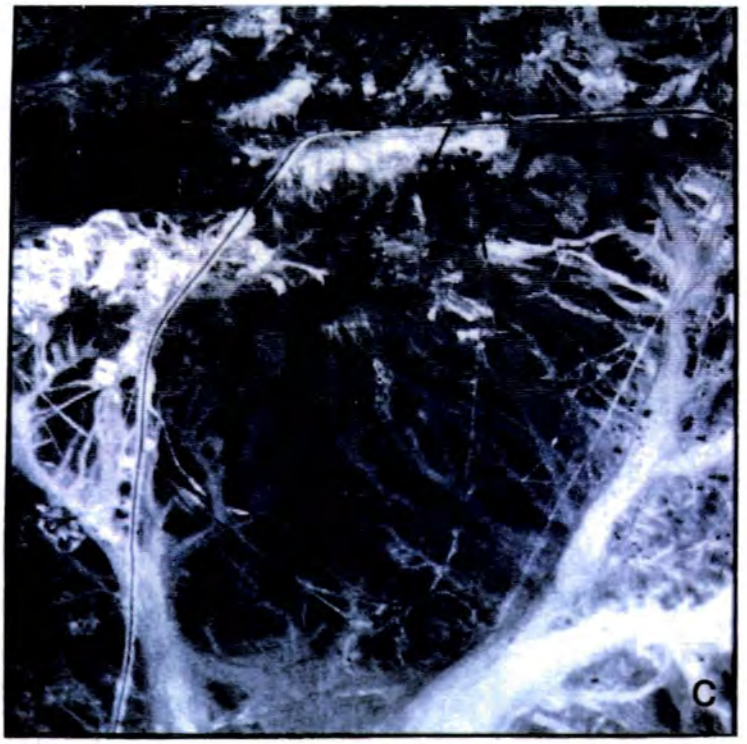

Fig. 6.13 (c) ATM 5/3 (0.66/0.56um) showing the clay in white and the iron oxide much darker.

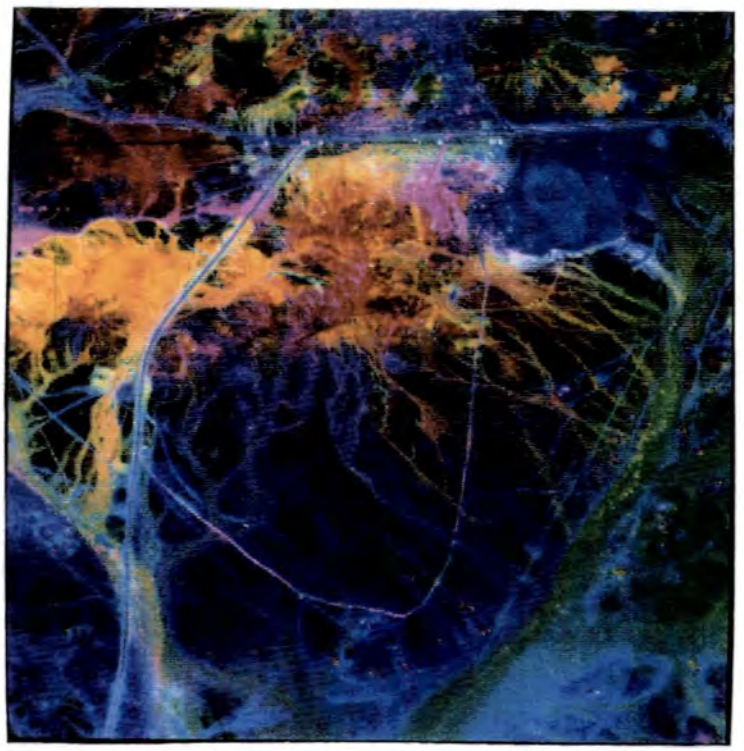

Fig. 6.14 Colour ratio composite of Mine Hill in Mahd Adh Dhahab of ATM 3000m (resolution 7.5m), Ratios 1.61/2.2um, 0.83/1.6um, 0.66/0.56um, displayed as red, green and blue respectively.

6.3.3.1 False Colour composite images

The thematic mapper subscene which covered the Mahd Adh Dhahab deposits was analysed using the same bands used with ATM band 7 (2.2um), band 5 (1.65um) and band 2 (0.56um) and displayed in R.G.B. respectively (Fig. 6.15). The most easily recognizeable features are the alteration areas around the Mahd Adh Dhahab mine (compare the image with Fig. 2.3). The mine sequence, with patches of alteration in Little Mahd and Little Copper Hill can be traced easily, the post mine sequence showed a mixture of volcanic rocks, agglomerate, acid and intermediate dykes and limestone lenses. The greenish-blue and cyan patches appear in the post mine sequence and the acid tuff might be alteration in the tuff or some of the carbonate lenses where it gives absorption features at 2.35um and can be picked up by the broad band, band 7 (2.08-2.35um). Generally, no alteration has been reported in the post-mine sequence.

The enlargement of the area around the Mahd mine, mainly the Mine Hill shown in Fig. 6.16 as a zoom-in of Fig. 6.15. It still showns the hydrothermal alteration in greenish-blue colour, even with the low spatial resolution of the TM data.

6.3.3.2 False colour ratioing image

The false colour ratio composite used here with TM data is the same ratio used before on ATM data. The following ratio used: band 5/7 (1.65/2.2um), band 3/2 (0.66/0.56um) and band 4/5 (0.83/1.65um) in red, green

Fig. 6.15 False colour composite of Mahd Adh Dhahab deposit; TM data, band 7,5, 2 in red, green and blue respectively. The hydrothermal alteration appears in greenish-blue colour (inside the yellow sequence), the boundary of the mine sequence can be followed easily.

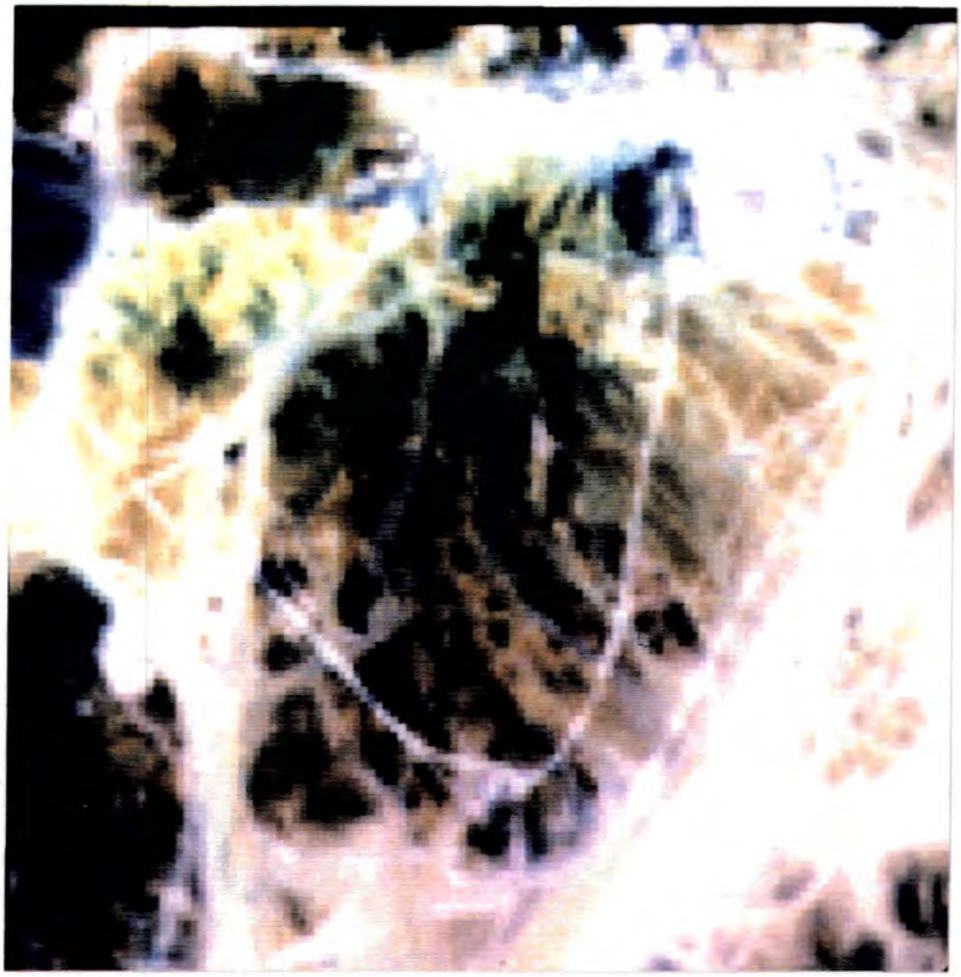

Fig. 6.16 Zoom over the Mine Hill, Mahd Adh Dhahab area of TM image bands 7,5, 2 in R.G.B respectively, still showing the greenish-blue colour of the hydrothermal alteration. The rhyolite intrusive appears blue in colour in the top of the image. Compare this with yellow sequence in Fig. 6.15.

and blue respectively, to study the ratioing technique in separating the different lithologies in the area.

Unlike the ATM ratio (Fig. 6.14), the ratio produced with the TM data is very noisy, however it is still useful in separating different lithologies (Fig. 6.17). The ratio image clearly separates the mine sequence from the other lithologies, but it was difficult to separate the Lahuf units, the upper and lower Lahuf and the tuff sediment. Comparing the ratio image with the geological map, it was noticed that the poorly stratified sediment units in the southwest corner of the image, appeared in the ratio image as an extension of the Lahuf subgroup.

It is not possible to locate the hydrothermal alteration in the Mahd mine, the yellow colour which supposedly means the presence of iron oxide and clay minerals, was exaggerated and showed all the wadi sediments in yellow colour to the fact that these sediments could be affected easily by the slope of 5/7 (1.65/2.2um).

A zoom over the Mine Hill area showed the location of the Mahd Mine. The image is very noisy by the distribution of the yellow colour (Fig. 6.18).

6.3.3.3 Decorrelation stretched TM imagery

Decorrelation stretching of bands covering 2.2um, 1.6um and 0.56um in red, green and blue are shown in Fig. 6.19, but colours have been intensified at the expense of a certain amount of albedo information. The decorrelation stretching technique forces an almost complete range of possible colours into the image

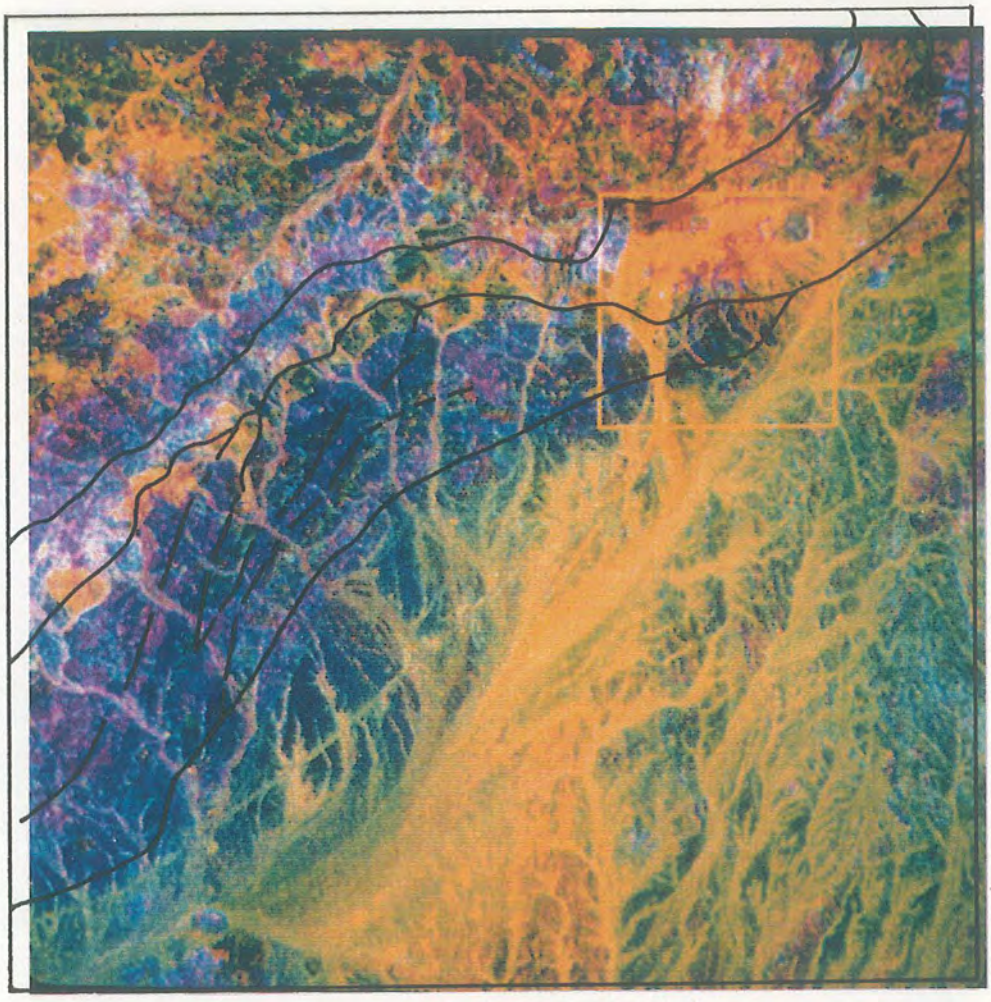

Fig. 6.17 TM Ratio image for Mahd Adh Dhahab ratio bands 5/7 (1.65/2.2um), 3/2 (0.66/0.56um), and 4/5 (0.83/1.65um) in red, green and blue respectively. Notice the Mine Hill sequence and the stratified sediments have been interpreted as an extension to the Lahuf units.

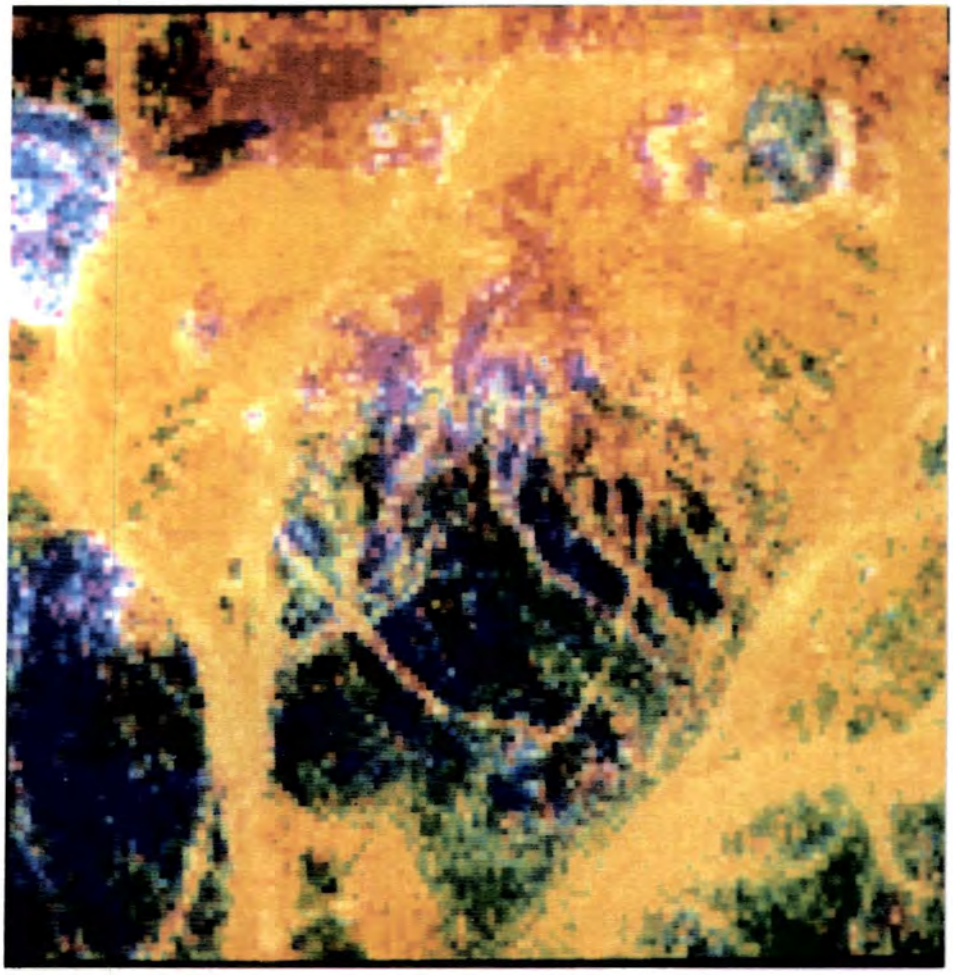

Fig. 6.18 TM Ratio 5/7, 3/2, and 4/5 in red, green and blue respectively of the Mahd Adh Dhahab area. The image is zoomed to this size.

(Rothery, 1987). The colours in the stretched image should be interpreted by considering the possible absorption features affecting the bands. Table 6.1 shows the primary and complimentary colours which result from the possible combinations of absorption features in TM bands 7 (2.2um), 5 (1.65um), 2 (0.56um), red, green and blue decorrelation stretched composite (Fig. 6.19).

This technique proved very effective in subdividing the volcanoclastic sequences whilst at the same time, enhancing differences between altered and unaltered areas. Comparing the decorrelation stretched image of Mahd Adh Dhahab (Fig. 6.19) with the map of the area discussed earlier in Chapter 2 (Fig. 2.3), and shown again in Fig. 6.20, it can be seen that the decorrelation stretched image shows more variation within the different units. An attempt was made to interpret the image and create a map based on the change of the colours in the image and the available information (see overlay Fig. 6.19). A comparison was made with the map by Chan (1980).

The mine sequence is picked out remarkably well in the bluish-green colour with yellow-orange colour. The cyan colour is an indication of the presence of hydroxyl minerals, while the yellow indicates the presence of iron oxide and desert varnish. The Lahuf sediment and tuffs appearing in red colours indicate the presence of iron oxide on the surface and the flat spectra at bands 5 (1.65um) and 7(2.2um). The lower Lahuf shows some variation in orange colour. The image also shows a lot

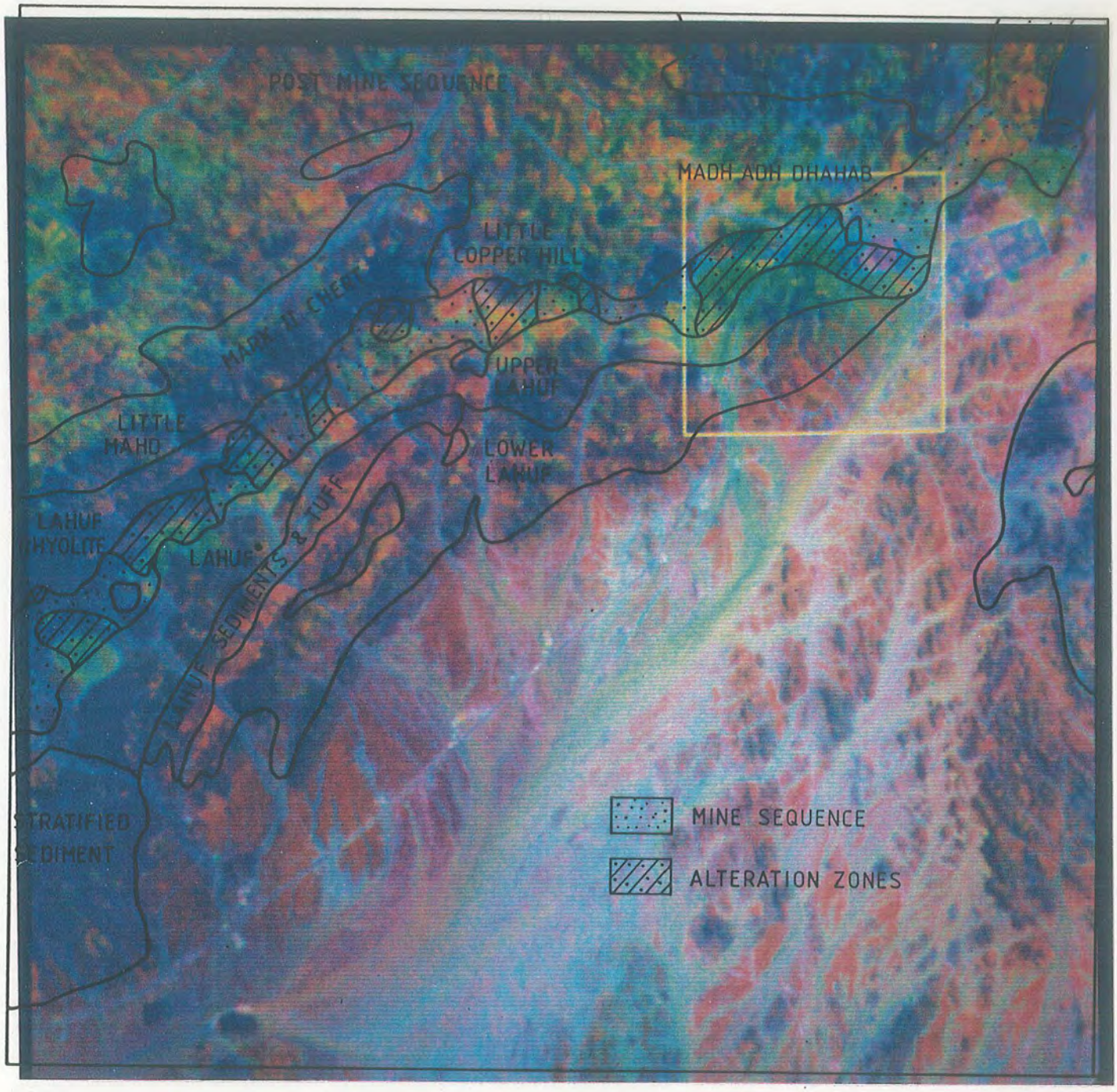

Fig. 6.19 Decorrelation stretched image of TM data, bands 7,5, and 2 in red, green and blue respectively. Colours are similar to Fig. 6.15, but more intense, enabling lithological differences to be mapped more easily.

Table 6.1 Colour shown by rock samples in a Landsat TM band 7,5, 2 in red, green and blue composite image and the mineralogical features responsible. These colour tendencies are accentuated by decorrelation stretching and may not be apparent in Ordinary Images.

Colour	Reason	Minerals
Blue	low in 5 and 7	Dark minerals almost flat in 5 and 2
Green	low in 2 and 7	Iron oxide
Yellow	low in 2	Iron oxide and clay minerals
Red	low in 2 and 5	Fe^{+2}
Magenta	low in 5	Minerals have no spectral features
Cyan	low in 7	Hydroxyl-bearing mineral such as clay, chlorite and carbonate.

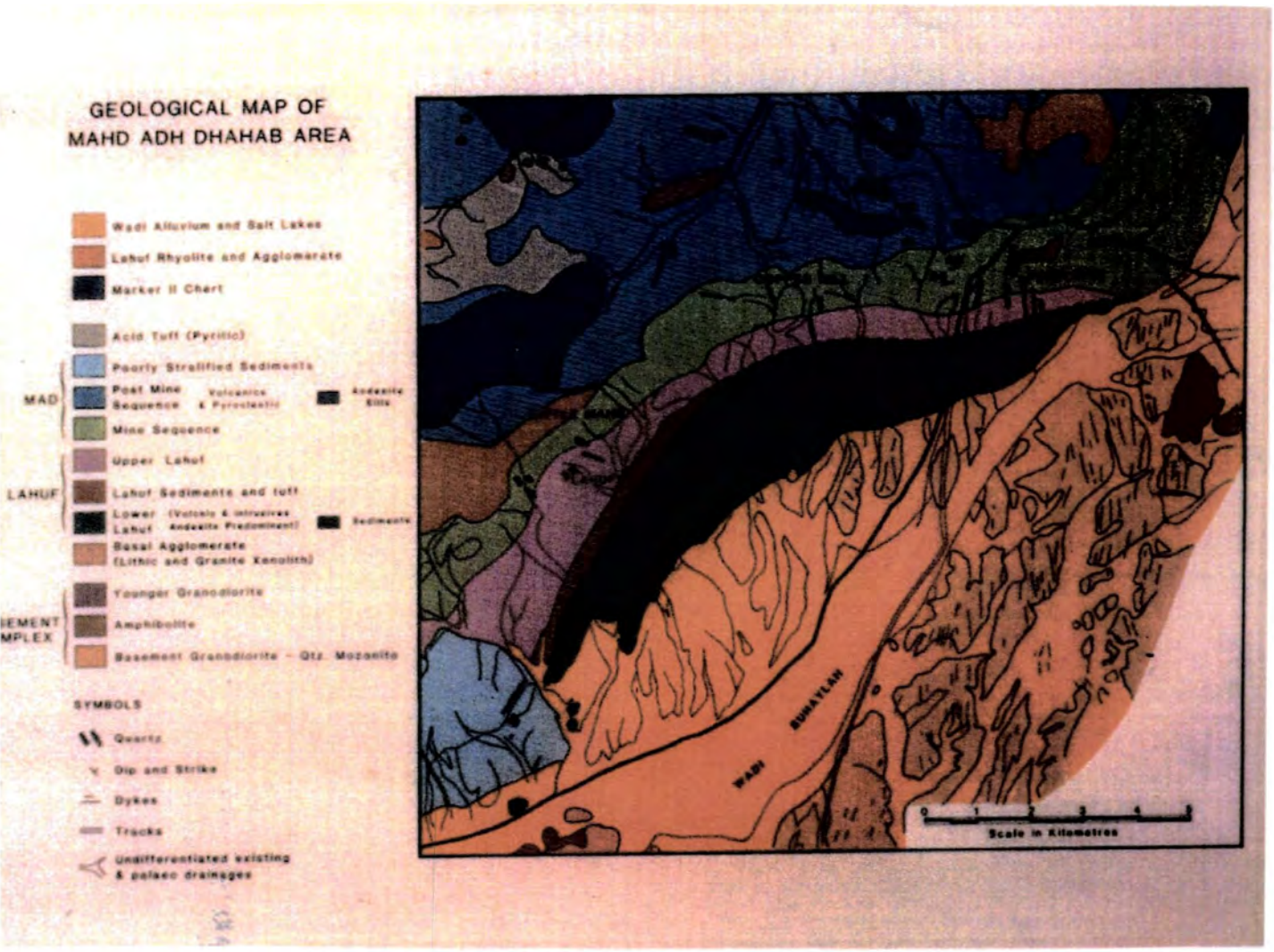

Fig. 6.20 Geological Map of the Mahd Adh Dhahab area.

of variation in the post mine sequence, especially in the cyan colour - greenish-blue, which might be interpreted as altered rocks. Careful study of the mineral composition of the post mine sequence indicated the presence of limestone lenses distributed in these units, due to the CO^{3-}. The limestone shows absorption features at 2.33um. This range is covered by band 7 (2.08um-2.35um).

Chan (1980) surveyed the area and examined a number of prospects in the Mahd Adh Dhahab area (Table 6.2). Most of these prospects were associated within the mine sequence, they showed malachite stains and had varying degrees of alteration.

Only two of these prospects are encouraging, Little Copper Hill and Little Mahd (Fig. 6.21).

Little Copper Hill

A small low hill appears to have been worked previously, situated 5km west of the Mahd. The outcrops of altered rock show widespread malachite and boxworks of quartz and oxidized sulphides according to Chan (1980).

Little Mahd

Located further south on the mine sequence, NW of Lahuf, alteration and silicification appear to spread out, but with limited presence of malachite.

Looking at the location of the Little Copper Hill and Little Mahd and the rest of the prospects suggested by Chan, comparing these locations with the colour in the decorrelation stretched image (Fig. 6.21). The locations

Table 6.2 List of the Prospects suggested by Chan (1980). [See Fig. 6.21 for location].

No.	Locality Name	Visible mineralisation	Remarks
1	N.E. Little Copper Hill	Malchite specks	Jasper with argillic alteration
2	Little Copper Hill	Malchite	Wide argillic alteration
3	S.W. New Mahd	Malchite	Pink feldspar-intrusive Rhyolite
4	Lahuf North	Malchite	Pink feldspar-intrusive Rhyolite
5	Little Mahd	Malchite	Pervasive alteration
6	Lahuf	Malchite	Silicic, argillic, quartz vein in andesite
7	Lower Lahuf	Malchite specks	
8	Mahd Mine	Malchite specks	Quartz specks

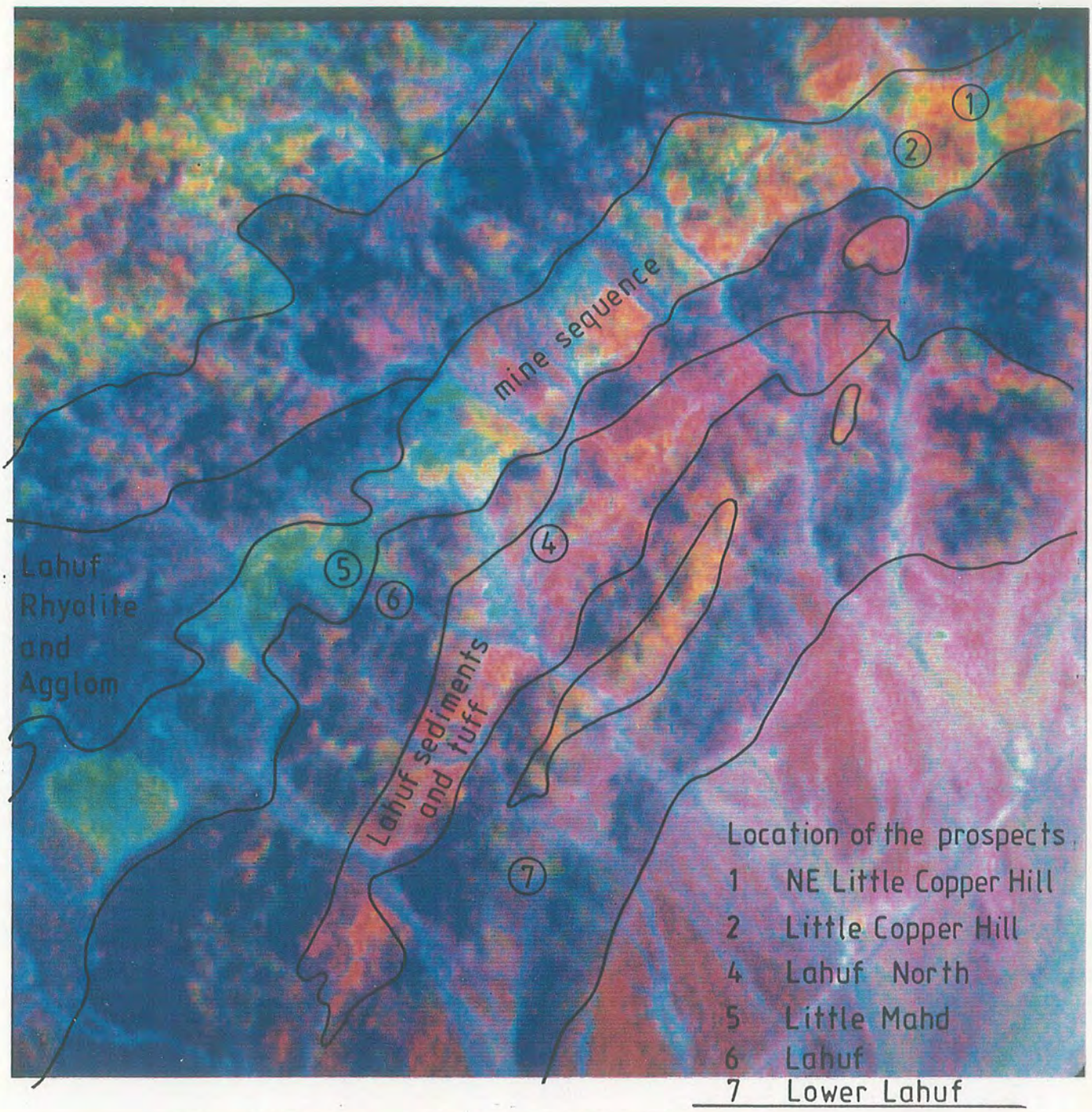

Fig. 6.21 The west of Mahd Adh Dhahab Mine (see Fig. 6.17 for location). Zoom over the mine sequence and other lithologies. Decorrelation stretched image 7,5,2 in R.G.B show the location of the prospects (see Table 6.2).

coincide with cyan colour (bluish-green) within the mine sequence of the Lahuf units.

Based on this interpretation it is suggested that locations which appear in the decorrelation image in a cyan colour (greenish-blue) show potential alteration targets, especially the location on the left side of the image, south of the Little Mahd and along the Mine sequence.

A zoomed image of the mine hill using the decorrelation stretched image as before, show the cyan colours concentrated on the area mapped as hydrothermal alteration (see Fig. 6.22). Huckerby et al. (1984) suggested that Mahd Adh Dhahab differs from other vein type gold deposits in that the mineralization is not surrounded by widespread, pervasive alteration that could be discriminated in a satellite image. Results here suggest otherwise (Fig. 6.22).

It is essential to further investigate all the locations appearing in the greenish-blue colour in the decorrelation stretched image of Mahd Adh Dhahab. Some of these locations are already known as mineral prospects or occurrences.

6.4 Image analysis and interpretation of Jabal Said area

6.4.1 Introduction

The analysis and interpretation of the imagery from Jabal Said was undertaken using the same techniques as were applied to Mahd Adh Dhahab. The major difference here was that the images from the ATM and TM sensors were

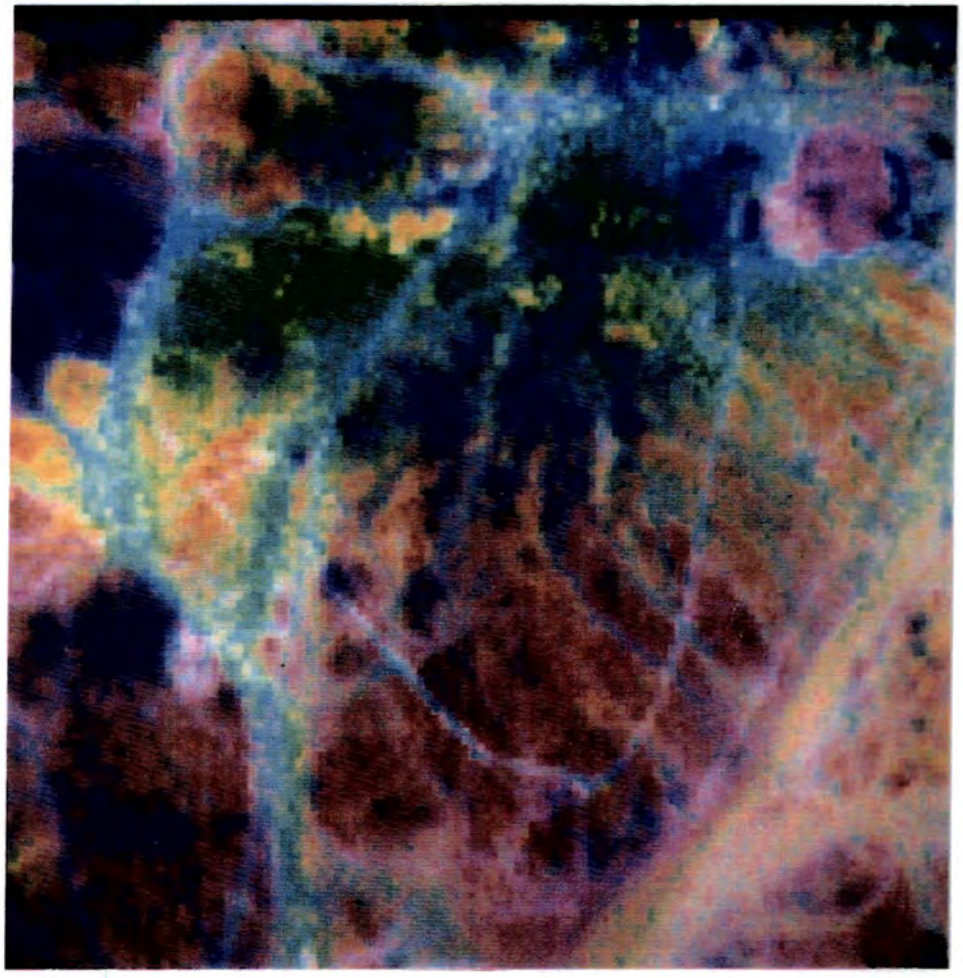

Fig. 6.22 A zoom of the Mine Hill area from the decorrelation stretched image bands 7,5,2 in R.G.B. scan image in Fig. 6.19.

evaluated for mapping the different lithologies in the area, and not for mapping the different types of alteration as was the case in Mahd Adh Dhahab. The effect of spatial resolution for the discrimination between rock types and alteration zones will be studied using the different resolution ATM sensor data, 7.5mIFOV, 5.0m IFOV and 2.5m IFOV, and the TM 30m IFOV data. Landsat MSS was used here for comparing low resolution data (80m IFOV) with the higher resolution data. However, relatively little is known about the incremental advantage of increasing pixel resolutions beyond 30m IFOV for lithological mapping purposes.

6.4.2 Analysis of the Airborne Thematic Mapper Images

As with the ATM sensor data for the Mahd Adh Dhahab area, the ATM data from Jabal Said area was taken from three different elevations, 3000m, 2000m and 1000m with resultant spatial resolutions of 7.5m, 5m and 2.5m IFOV (Fig. 6.23). The across-track scan width of the ATM data was 716 pixels. A comparison between the three resolutions indicated that the high resolution ATM flight lines offer a limited geographic coverage, which prevented the examination of the large structural features around the deposit.

6.4.2.1 Interpretation of single band images

The airborne thematic mapper has eleven bands (see Chapter 3 and Appendix C), covering the range from 0.435 to 2.35um. The first band (0.42-0.45um) was not used in this study due to the copying problem. Fig. 6.24 shows the images acquired with the nine ATM bands over Jabal

FIGURE 6.23

COMPARISON BETWEEN DIFFERENT RESOLUTION OF ATM DATA-JABAL SAID AREA

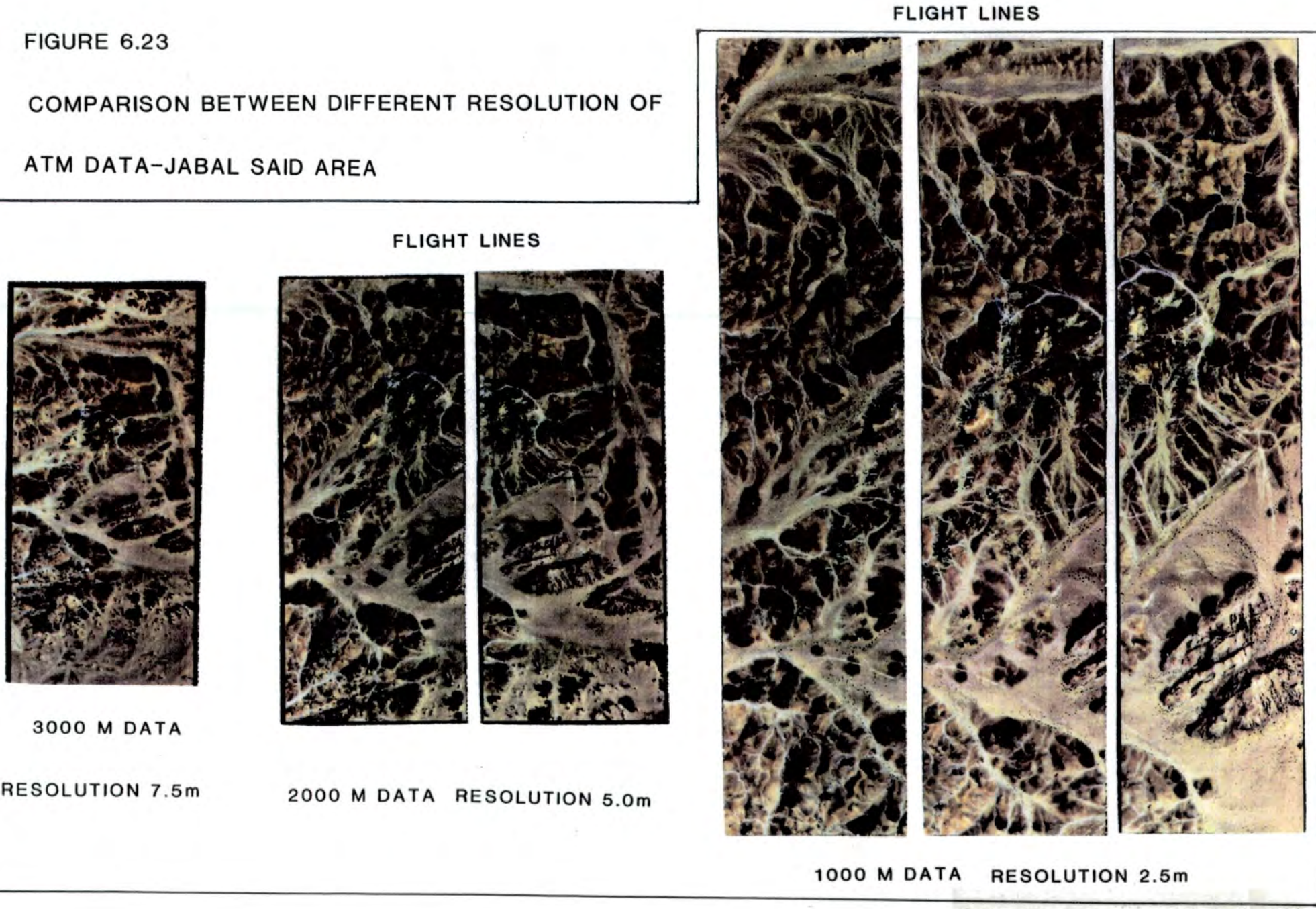

Source:The Arabian Aerosurvey Co.1984

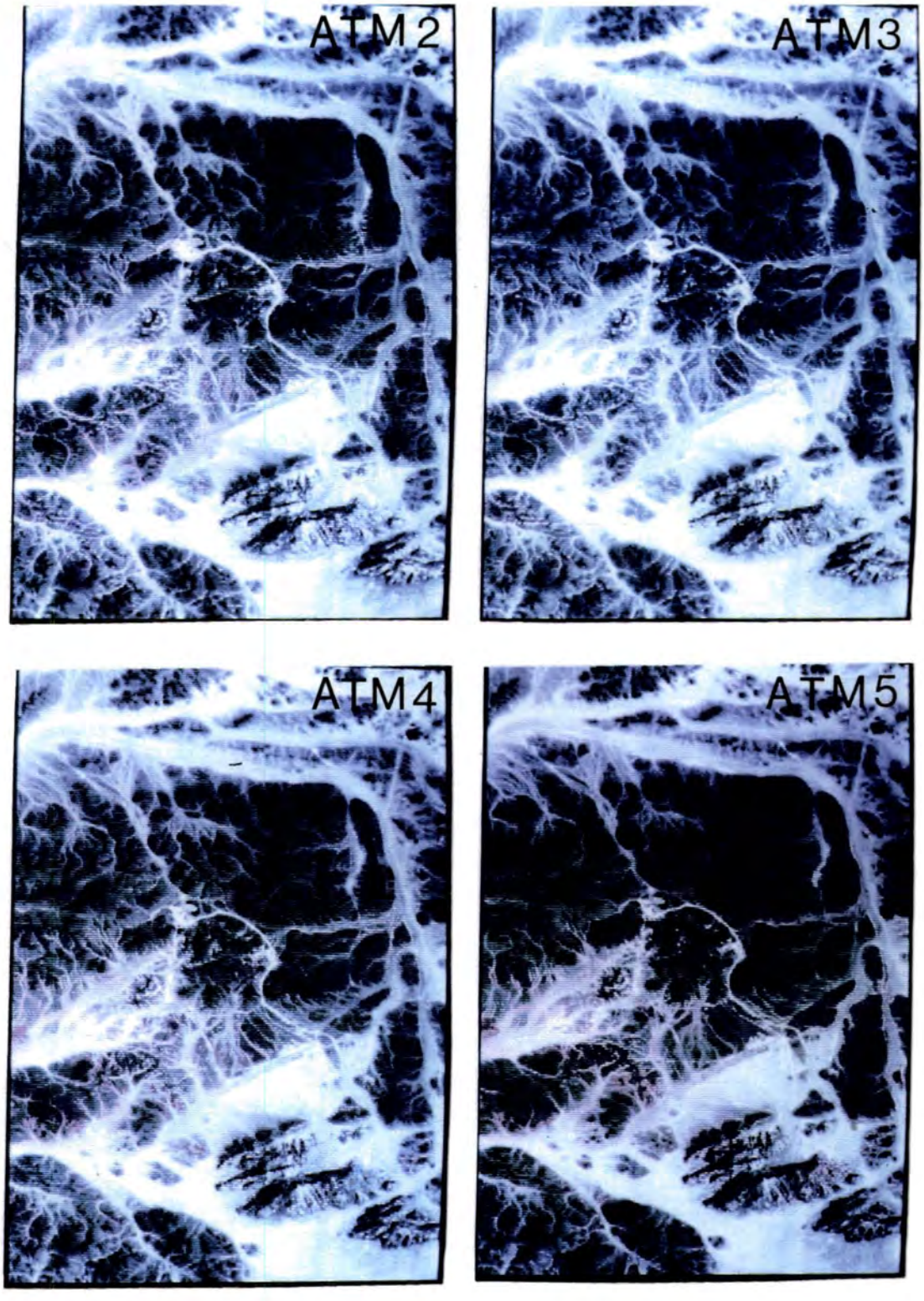

Fig. 6.24 Nine bands of Airborne thematic mapper images over Jabal Said.

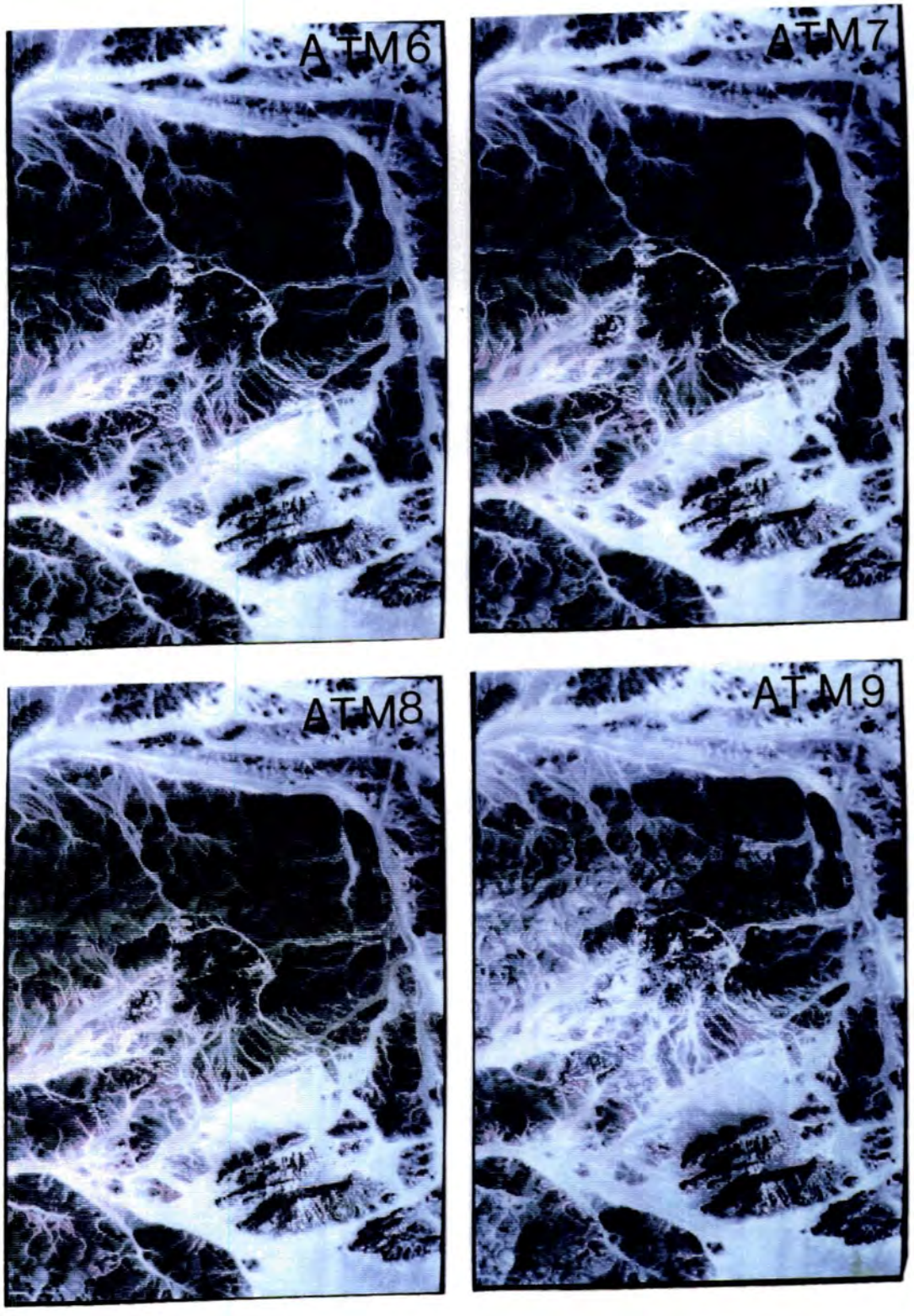

Fig. 6.24 continued.

Fig. 6.24 continued

Said area. Various lithological features are imaged differently in the individual bands. Generally it shows very good contrasts between the different lihtologies and wadi sediments. In the visible and the near infrared bands, the alteration area and the gossan shows a distinct tonal reversal between them and the rest of the lithologies.

Tones were reversed again between the near infrared and the shortwave infrared band, where all the alterations appear with a light tone in band 9 (1.65um), but look much darker in band 10 (2.2um).

6.4.2.2 ATM False Colour Composite

The analysis of the ATM images mainly concentrated upon the alteration zone and the gossan of Jabal Said due to the limited geographic coverage of the ATM flightlines. The result of the discriminant analysis which were discussed earlier (Chapter 5) suggested the best bands for lithological separation in each type of data, and particularly colour composite band 10 (2.2um), band 9 (1.65um) and band 3 (0.56um). The colour composite used for the 7.5m IFOV resolution data was also suggested by Hunting Co. (1985).

The ATM colour composite 10 (2.2um), 9(1.65um), 3 (0.56um) in R.G.B respectively has successfully targeted gossans and alteration zones associated with known mineralizations at Jabal Said (Fig. 6.25). The main lithologies of the area can be differentiated easily, although the images have limited spatial coverage. More internal detail of the variation within each lithology

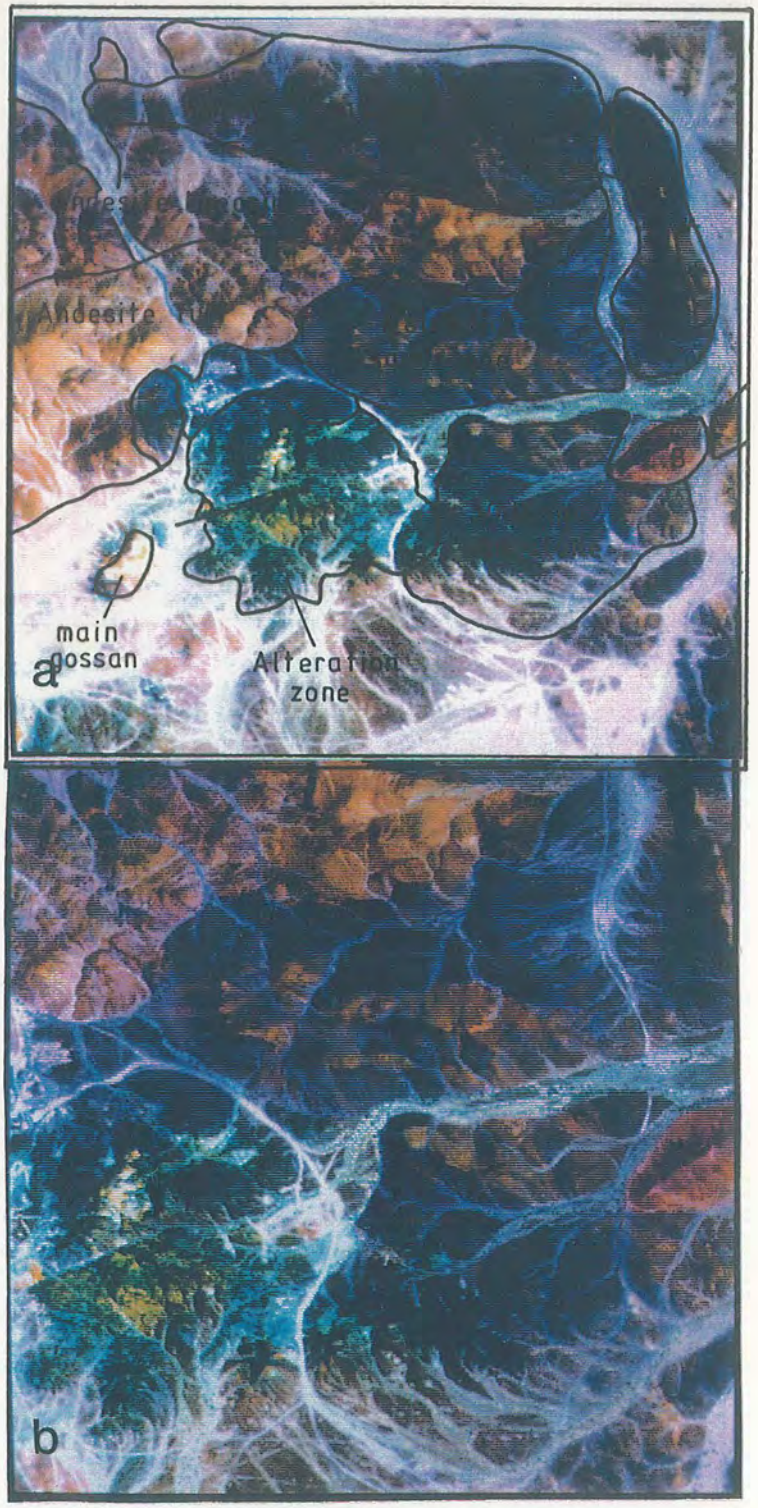

Fig.6.25 ATM colour composite of bands 10,9,3 in R.G.B. respectively showing the main lithologies in Jabal Said area. The alteration zone appears in a greenish-blue colour and the gossan a yellow colour. (a) colour composite from 3000m data resolution 7.5m. (b) colour composite from 2000m data resolution 5.0m. Compare the interpretation in the overlay with Fig. 2.9.

can be picked up using the higher resolution data as shown in Fig. 6.25.

The massive sulphide ore bodies in Jabal Said discussed in Section 2.7.3 earlier, show four ore bodies. An alteration zone covered the area between ore bodies 1 and 4. The application of ATM imagery to the alteration in Jabal Said has been reported by Legg (1985) and discussed by Loughlin and Tawfiq (1985). Legg also drew attention to a large alteration zone south of the no. 4 orebody across the Eastern Valley Fault, which has been reported by previous workers but never investigated at depth. The colour composite 10 (2.2um), 9 (1.65um), 3 (0.56um) is believed to be the best for discriminating alteration zones. The 10 (2.2um), 7 (0.83um), 3 (0.56um) ATM band composite image highlighted ferruginous zones, while the 10 (2.2um), 9 (1.56um), 3 (0.56um) composite highlighted the argillic and ferruginous zones. Fig. 6.26 shows the comparison between the two combinations. The main gossan does not show solid yellowish or reddish colours, compared to the small gossan. This is due to the disturbance of the surface, caused by the exploration work and the drilling over the main gossan. As a confirmation of the effect of the 10 (2.2um), 7 (0.83um), 3 (0.56um) combination and how important it is to identify the iron oxide, detailed comparisons over the gossan were made and the change of colour from yellow to red was effective only over the gossan, but not in the surrounding area which also showed yellow in the 10 (2.2um), 9 (1.65um), 3 (0.56um) combination (Fig. 6.27).

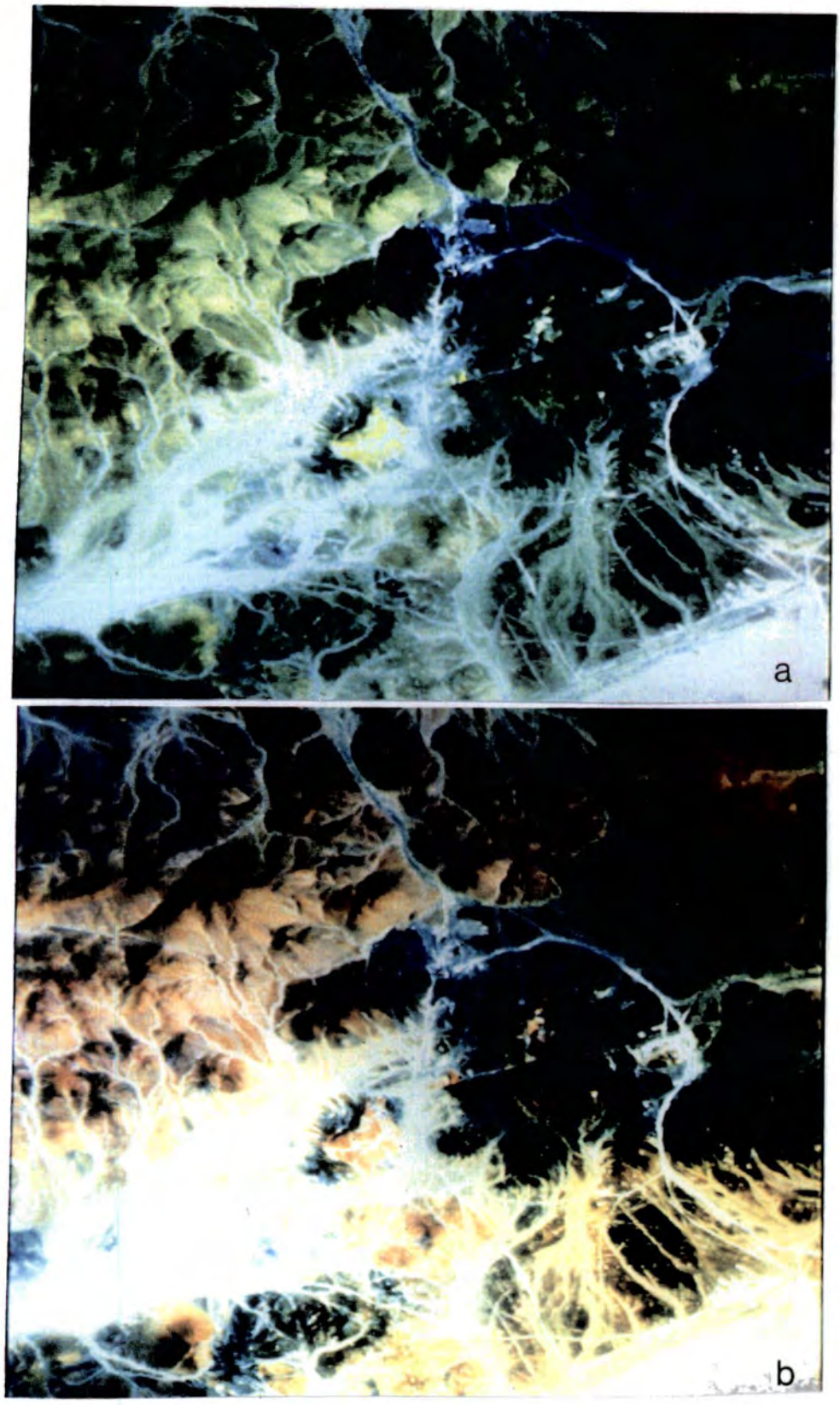

Fig.6.2 6 Comparison between the ATM 10,9,3 in R.G.B bands. Colour composite (a) and ATM 10,7,3 bands in R.G.B. colour composite (b) the gossan and iron oxide appear a yellow colour, in the first combination but in the second combination the iron oxide can be distinguished with the red colour.

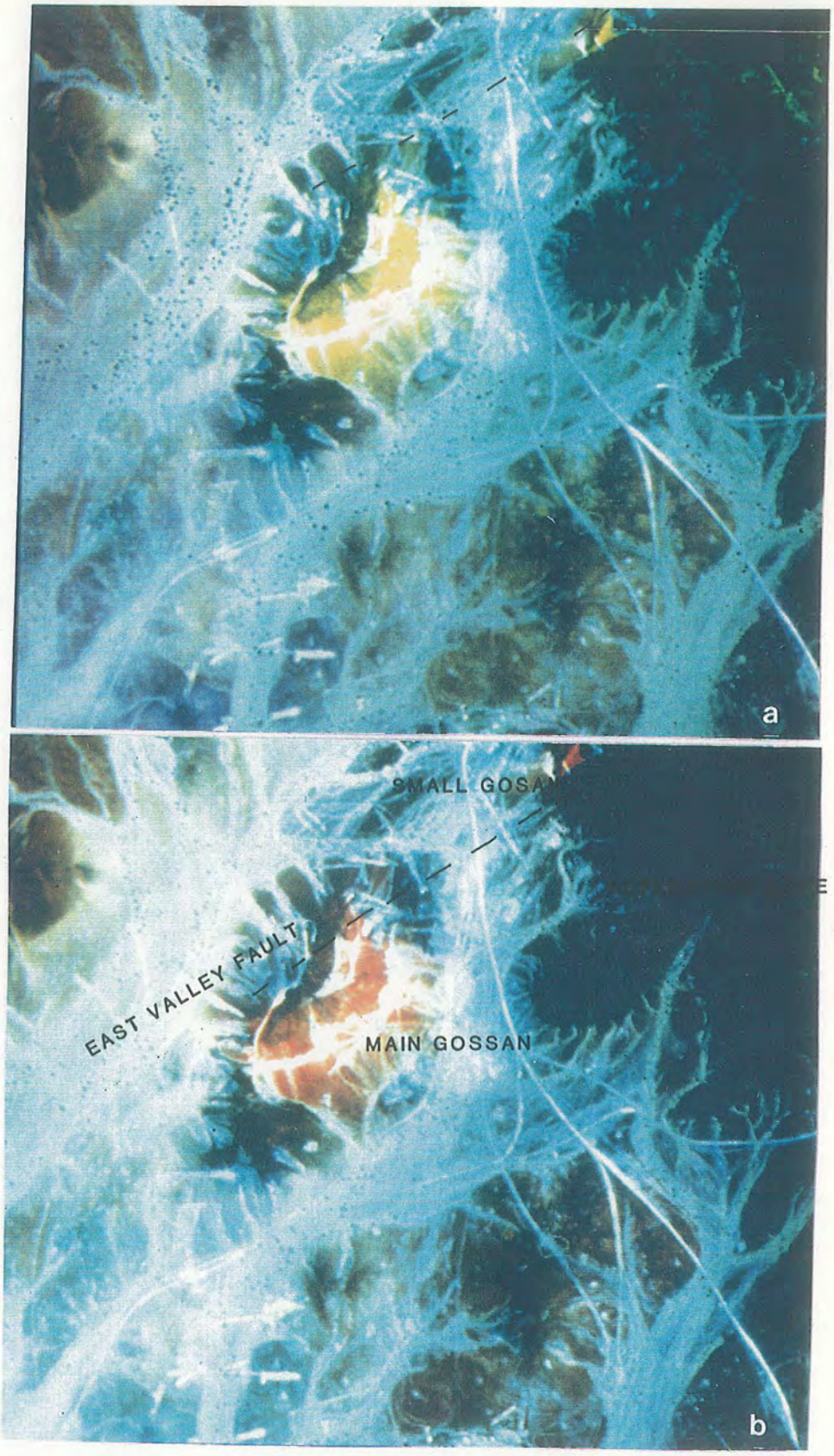

Fig. 6.27 (a) The main gossan and the small gossan appears as yellow in the colour composite with bands 10,9,3. (b) The gossans have a red colour using combination of 10,7,3.

The interpretation of Legg (1985) of the alteration zones in Jabal Said, using 10 (2.2um), 9 (1.65um), 3 (0.56um) and 10 (2.2um), 7 (0.83um), 3 (0.56um) combinations, indicated that the southern part of the Eastern Valley Fault area has mineral potential. Previous workers gave evidence supporting this interpretation. Bournat (1981) referred to ferruginous alteration, and a small, ancient copper working south of the Eastern Valley Fault has been reported by Hopwood (1979) to have alteration in the form of iron oxides, chlorite, sericite and silicification over a broad area south of the fault. Bowden and Smith (1981) reported a lithogeochemical anomaly extending southwards from the Eastern Valley Fault, with marked enrichment in copper and zinc. Legg (1985) also pointed out that previous geophysical surveys had revealed a coincident gravity and self-potential anomaly immediately south of the small gossan, which was located over the orebody No. 2 (Fig. 6.33). The interpretation of the ratio composite image giving more evidence of extending the alteration zones, will be discussed later.

Various band combinations on the Image Processing system were tested. One of the combinations which also effected the determination of the iron oxide-rich areas was 10, (2.2um), 4 (0.615um), and 2 (0.485um) in R.G.B respectively. This combination shows the gossan in a very bright red colour, due to the absorption features of the iron at band 4 (0.615um) and band 2 (0.485um) in green and blue (Fig. 6.28).

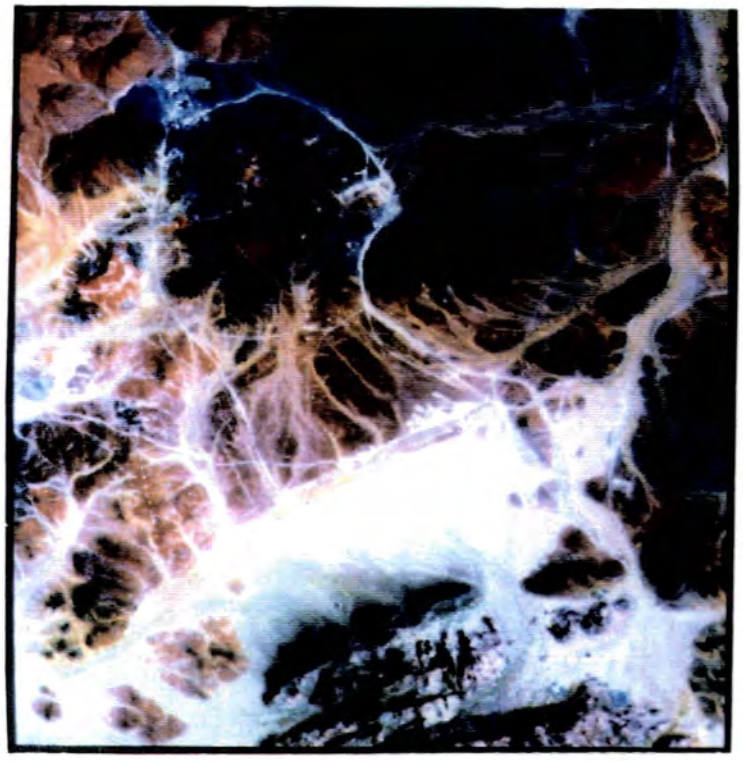

Fig. 6.28 Colour composite of ATM 3000m bands 10,4 and 2 in R.G.B respectively. Notice the colour of the gossan.

The ATM sensor composite image 10 (2.2um), 9 (1.65um), 3 (0.56um) is considered to be very valuable for mapping the different lihtologies in the area, using the ATM 3000m data with resolution 7.5m IFOV, the interpretation of the different colours in the image is related to the different lithologies using the geologic map of Jabal Said which was mapped by Saber (1981) (Fig. 2.9 in Chapter 2). Fig. 6.25a shows the area north of the alteration zone, and Fig. 6.29 shows the lithologies south of the alteration zone including the granite. The ATM images show considerable internal variation within each lithological unit. This may be used to increase the accuracy of geological mapping. In higher resolution data, substantial internal variation can be depicted (Fig. 6.25b).

6.4.2.3 <u>ATM Decorrelation stetched image</u>

The decorrelation stretching of bands 10 (2.2um),9 (1.55um), 3 (0.56um) in R.G.B, again give more internal variation. The previous image (Fig. 6.29) was decorrelation stretched and is shown in Fig. 6.30. A comparison between the two figures indicates that the colours shown in Fig. 6.30 are the same as those shown in Fig. 6.29, but they are more intense and saturated. The decorrelation stretch image shows more variation in lithologies especially in the top right corner of the image, in the volcanic sandstone east of the alteration zone, and in the andesitic tuff in the northwest. The dacite, diorite and andesite tuff and breccia in the south shows more internal variation. The alteration zone

Fig. 6.29 ATM 3000m colour composite of bands 10,9 3 in R.G.B. respectively showing the different lithologies in the Jabal Said area. See the interpretation in the overlay.

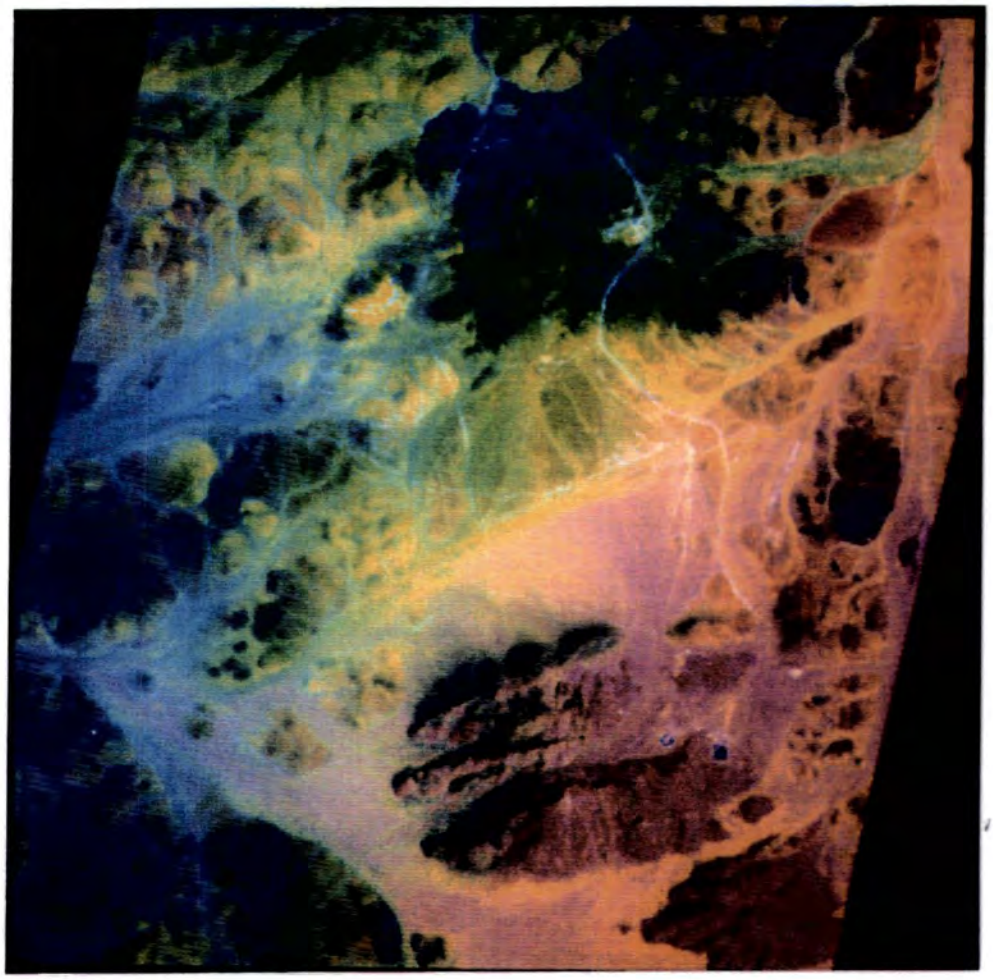

Fig. 6.30 ATM 3000m decorrelation stretched image of colour composite bands 10, 9, 3 in R.G.B. respectively showing the Jabal Said gossans and different lithologies, compared with Fig. 6.29.

appears in a greenish-blue colour, and other areas are highlighted with this colour, indicating a new alteration area, especially in the rhyolite unit south of the main gossan.

6.4.2.4 ATM band ratio images

The band ratios used over Mahd Adh Dhahab area were 9/10, 7/9 and 5/3, were also used with Jabal Said data. The choice of these ratios were based on the shape of the spectral curves from Jabal Said field data or the laboratory spectra discussed earlier in Chapter 3.

The Hunting Co. report (1984) suggested that the bands ratio 10/9 (2.2/1.65um), 9/8 (1.65/0.98um), 8/7 (0.98/0.83um) as the best bands for discriminating the alteration zones. This suggestion was supported by Loughlin & Tawfiqe (1985) and Bird et al. (1985) who claim that it is possible to distinguish iron-stained material from gossan material on the basis of the ratio 10/9 (2.2/1.65um), in which gossans would appear brighter than iron-stained targets (Fig. 6.31).

The ratio used in this study are in R.G.B ATM 9/10 (1.6/2.2um), 7/9 (0.73/1.6um), and 5/3 (0.66/0.56um) respectively. This ratio was also suggested for arid areas by Lepley et al. (1984) and Abrams et al. (1984). The ratio image shows the gossan in green colour, the weak iron oxide appears to have a light green colour. The red colour indicates the clay minerals and the yellow colour is mixed minerals of clay and iron oxides (Fig. 6.32).

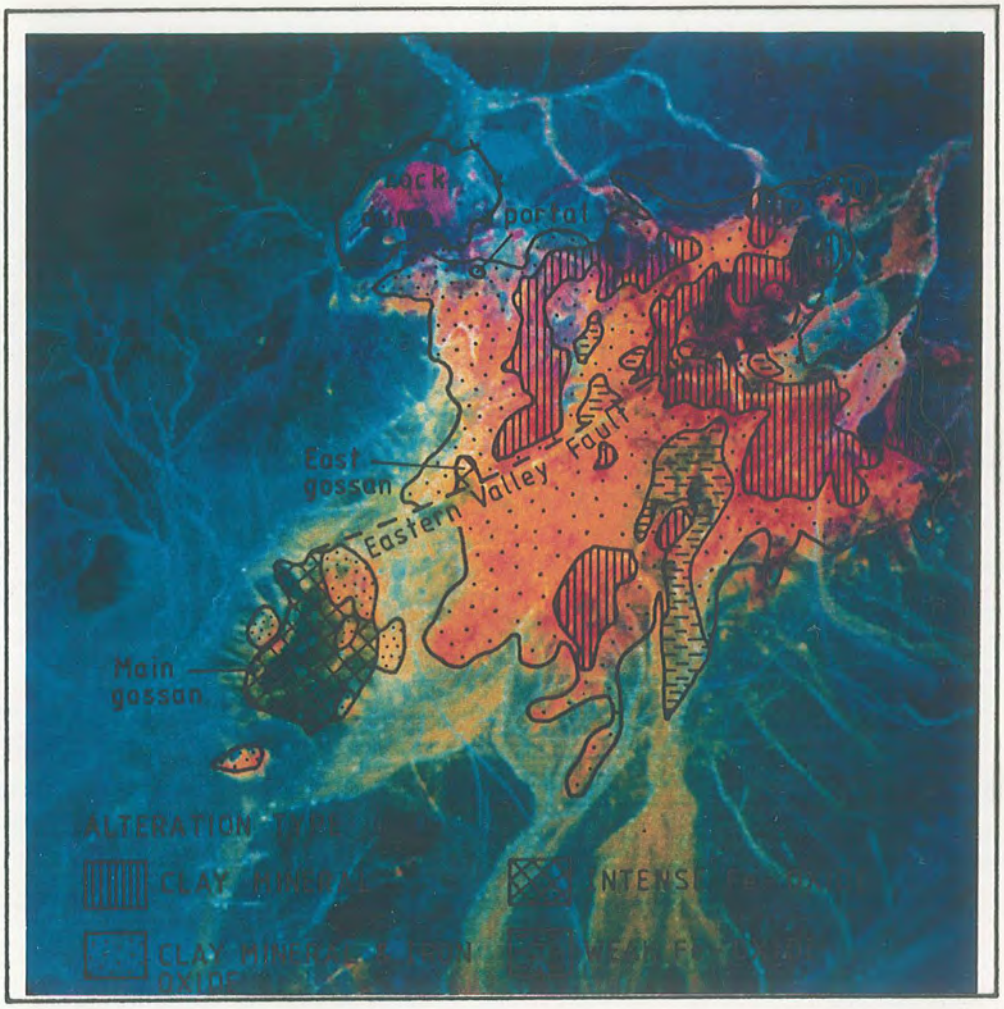

Fig. 6.32 ATM 2000m data (resolution 5.0m) ratio colour composite for Jabal Said. Band ratios 9/10, 7/9 and 5/3 are displayed as red, green and blue respectively. This combination highlights the presence of minerals associated with alteration (see the overlay and Fig. 6.33c for the interpretation).

The interpretation of the ratio image from Jabal Said was compared to the previous interpretation of the colour composite image 10, 9, 3 by Legg (1985)(Fig. 6.33 a and b). The results (Fig. 6.33c) show the power of this ratio combination for discriminating the alteration zone from the surrounding area and variation within the alteration zone.

6.4.3 Analysis of TM data

The subscene of TM Image covering Jabal Said area show the different lithologies surrounding the alteration zones and the area around it, which were covered by a limited cover of the ATM data. The subscene covered approximately 10km x 10km. The Jabal Said area was considered to be ideal to test the satellite data for lithological mapping, due to the different types of rocks available in the area, which were similar to that used earlier. Three different techniques were applied to the Jabal Said data; false colour composite, band ratioing and decorrelation stretch.

6.4.3.1 TM False Colour Composite

A combination of bands 10 (2.2um), 9 (1.65um), 3 (0.56um) displayed in red, green and blue respectively, form a false colour composite of the Jabal Said area. The subscene covered approximately 10km x 10km and showed all the other lithologies surrounding the alteration zone due to low resolution compared to the ATM images. The gossan gave the yellow colour and the alteration zone can be easily distinguished (Fig. 6.34). The other

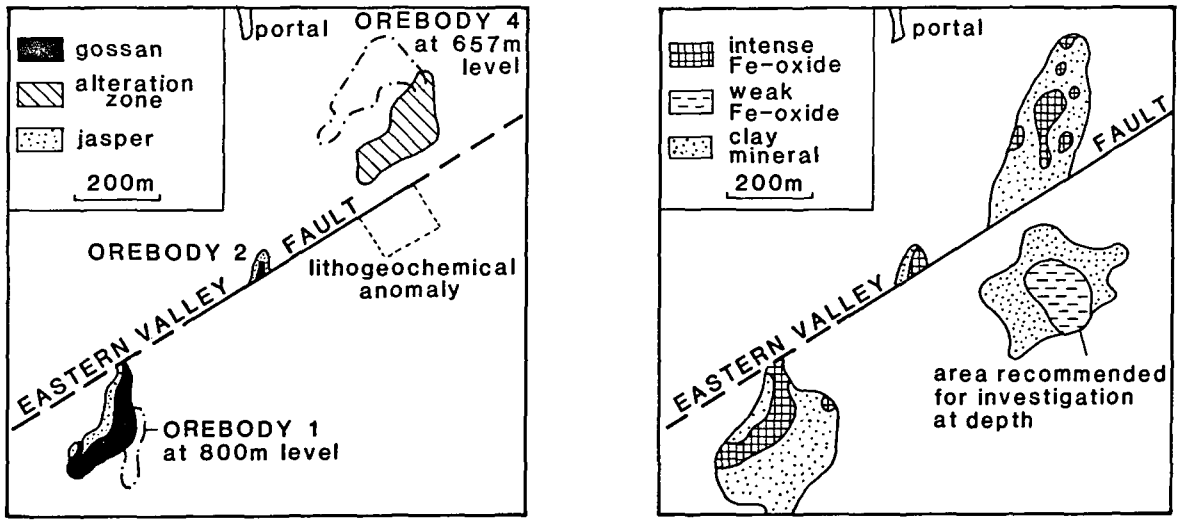

(after Legg 1984)

A. Distribution of orebodies, gossans, and alteration

B. Alteration zones inferred from ATM imagery

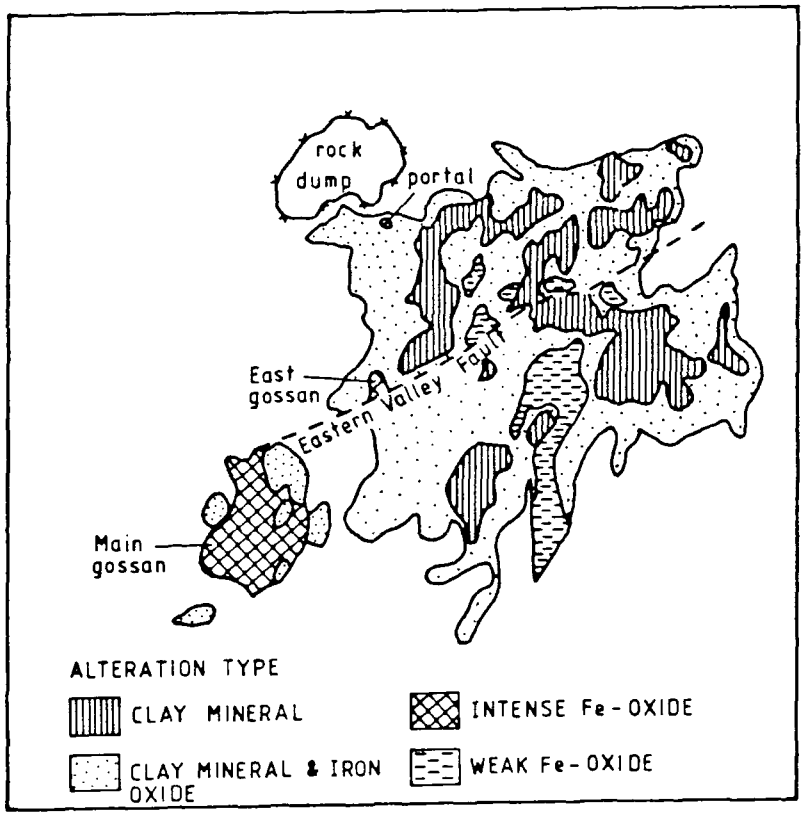

C ALTERATION ZONES INFERRED FROM ATM RATIO IMAGERY

Fig. 6.33 Comparison between interpretation of the alteration zones of Jabal Said from the colour composite and from the ratio imagery.

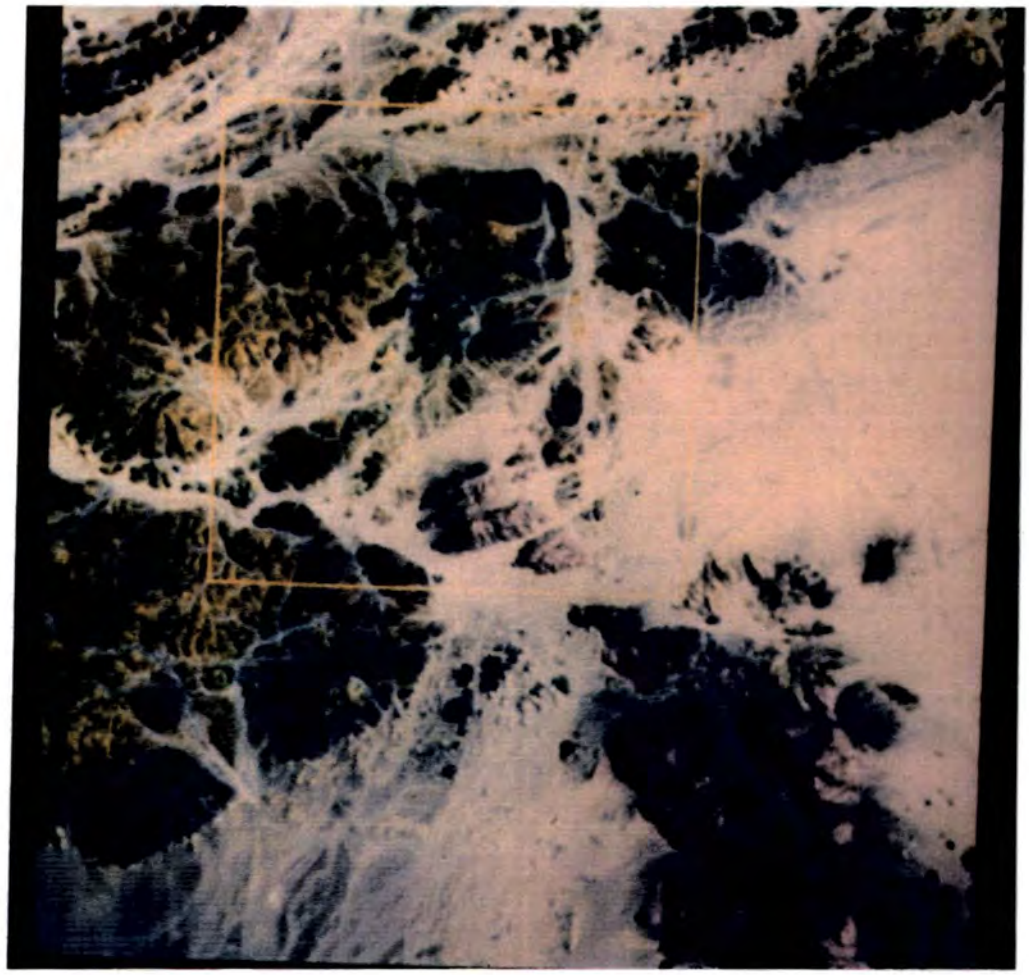

Fig. 6.34 Landsat TM colour composite of 10x10km subscene covering the Jabal Said deposit area. The composition consists of bands 7, 5, 2 displayed in red, green and blue respectively. Notice the distinct colour of the alteration zone.

lithologies also can be discriminated from each other based on the differences in colour. For example separating the alkali granite from the biotite granite can be achieved with the two different colours assigned to each lithology. The alkali granite appears pink and the biotite granite dark blue. Comparing this image with the geological map (Fig. 2.9) confirmed the discrimination of the lithologies.

An enlargement of part of the colour composite along the marked frame appears in Fig. 6.34, showing that many details of the ground and the lithologies still can appear with higher resolution from TM images (Fig. 6.35).

6.4.3.2. TM Decorrelation Stretches

The same colour composite discussed above the Jabal Said area has been decorrelation stretched using band 7 (2.2um), 5 (1.65um), 2 (0.56um) in red, green and blue respectively (Fig. 6.36). The decorrelation stretched images indicate that this technique is very useful in mapping and discriminating the different lithologies in the area. Comparing this technique with the colour composite, the lithologies appear in the image with a very distinctive colour. The interpretation of the image in the overlay, show some more internal variation in each unit. The two types of granite can be discriminated very easily from each other. The alteration zone appears in greenish-blue colour, very distinguishable in the image.

Fig. 6.35 Enlarged Landsat TM subscene of Jabal Said deposit consisting of composition of bands 7, 5, 2 displayed as red, green and blue respectively. Compare with Fig. 6.3 .

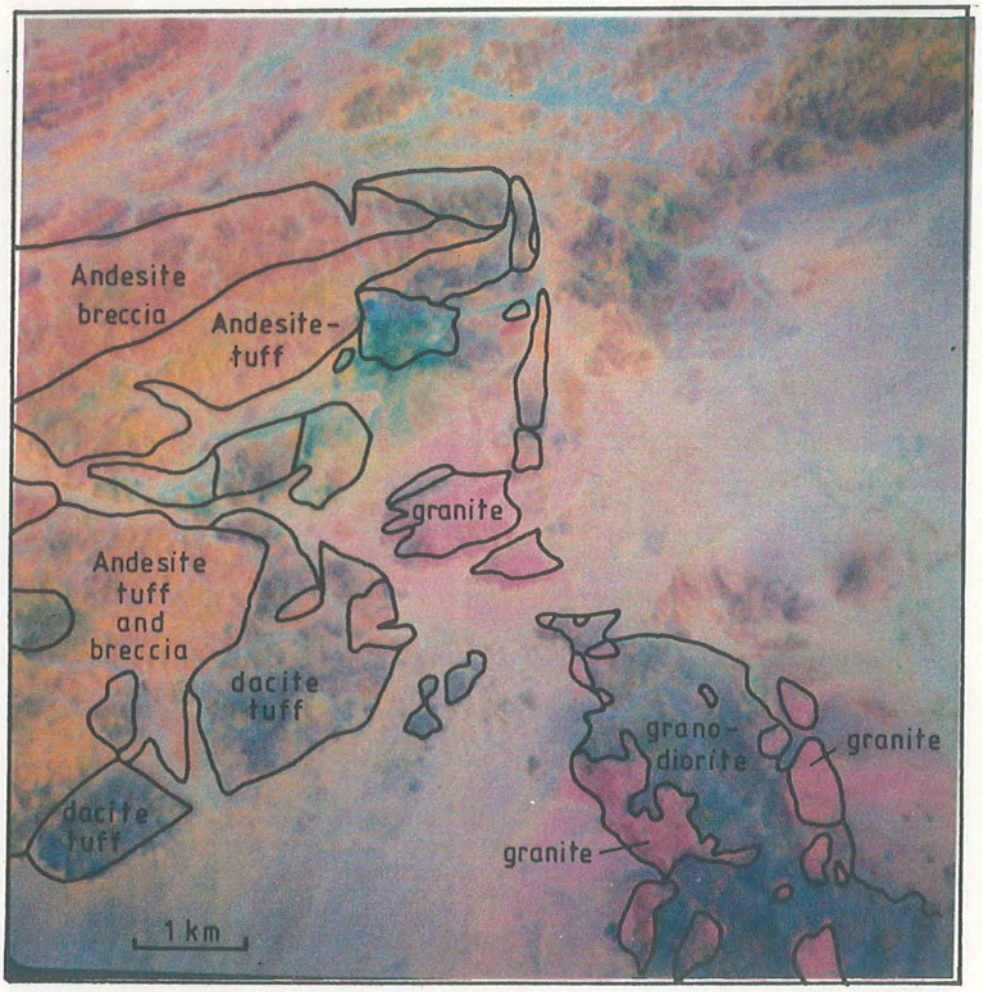

SCALE: 1:60,000

Fig. 6.36 Decorrelation stretched image of Landsat TM image band 7, 5, 2 in R.G.B. respectively. The colours are the same as in Fig. 6.35 but more intense, enabling lithological differences to be better mapped.

6.4.3.3. TM bands ratio images

The ratio used in Jabal Said are the same used earlier in Mahd Adh Dhahab. Generally three different ratios were used for TM data, mainly to enhance the alteration zones and the lithological differentiation. Ratio 5/7 (1.65/2.2um) was used to enhance the area rich in hydrous material, (Fig. 6.37a) where the alteration zone and the area rich in clay minerals appear bright. The second ratio was 3/2 (0.66/0.56um) (Fig. 6.37b), where the area rich in iron oxide will appear brighter than the surrounding areas. The third ratio was 4/5 (0.83/1.65um), where the iron oxide and the alteration zone will show darker tones, but the gray scale was darker in iron oxide compared to the alteration zone (Fig. 6.37c).

The ratio colour composite of Jabal Said was very successful in discriminating the alteration zone from the surrounding lithologies. The alteration zone appears in yellow colour indicating the mixture of the clay and iron oxides. The other lithologies also can be differentiated based on the different changes in the colour or in the colour tone (Fig. 6.38).

An enlargement of Fig. 6.38 shows more detail especially for the alteration area. The red colour related to the clay minerals which spread over most of the alteration zone (Fig. 6.39). The image does not show any green colour, indicating the iron oxide, due to the low resolution of the TM data. Comparison was made between this image with the ratio image from ATM data

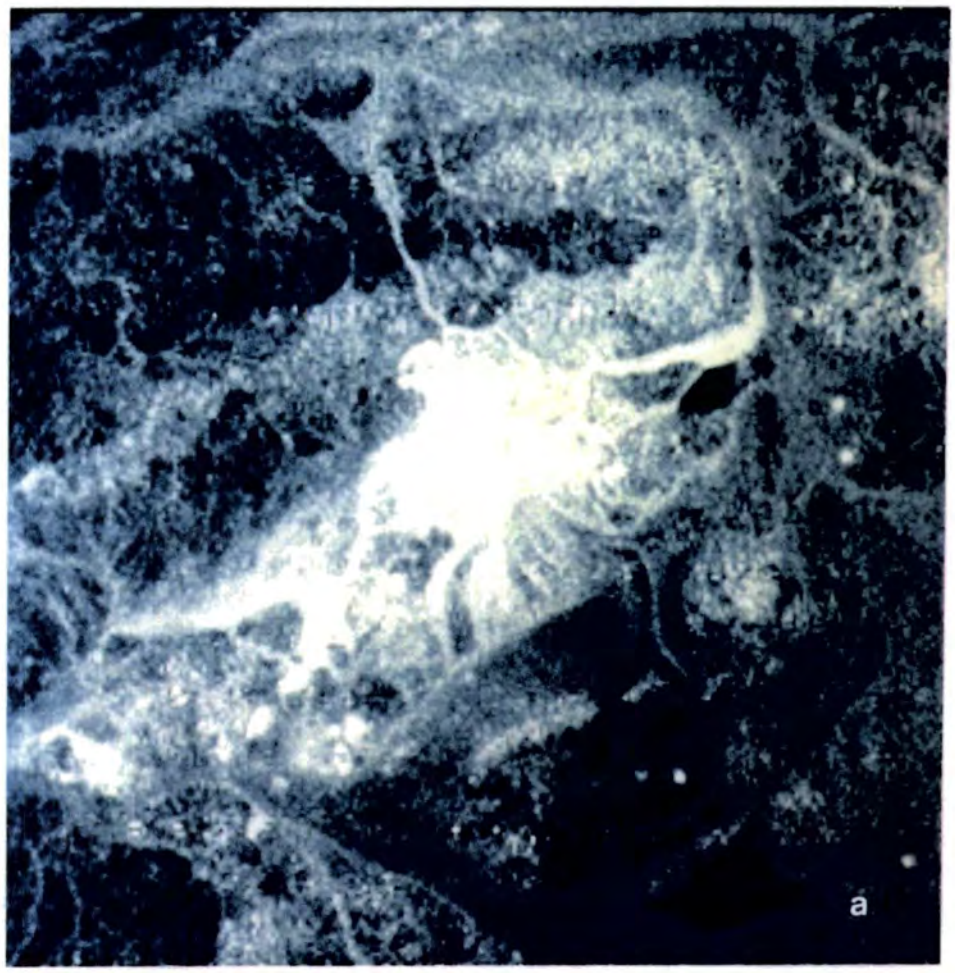

Fig. 6.37 (a) Ratio image of TM satellite data over Jabal Said. Every type of ratio provides special lithological information. (, ratio 5/7 (1.6/2.2um), b ratio 3/2 (0.66/0.56um), and c. ratio 4/5 (0.83/2.6/2.2um).

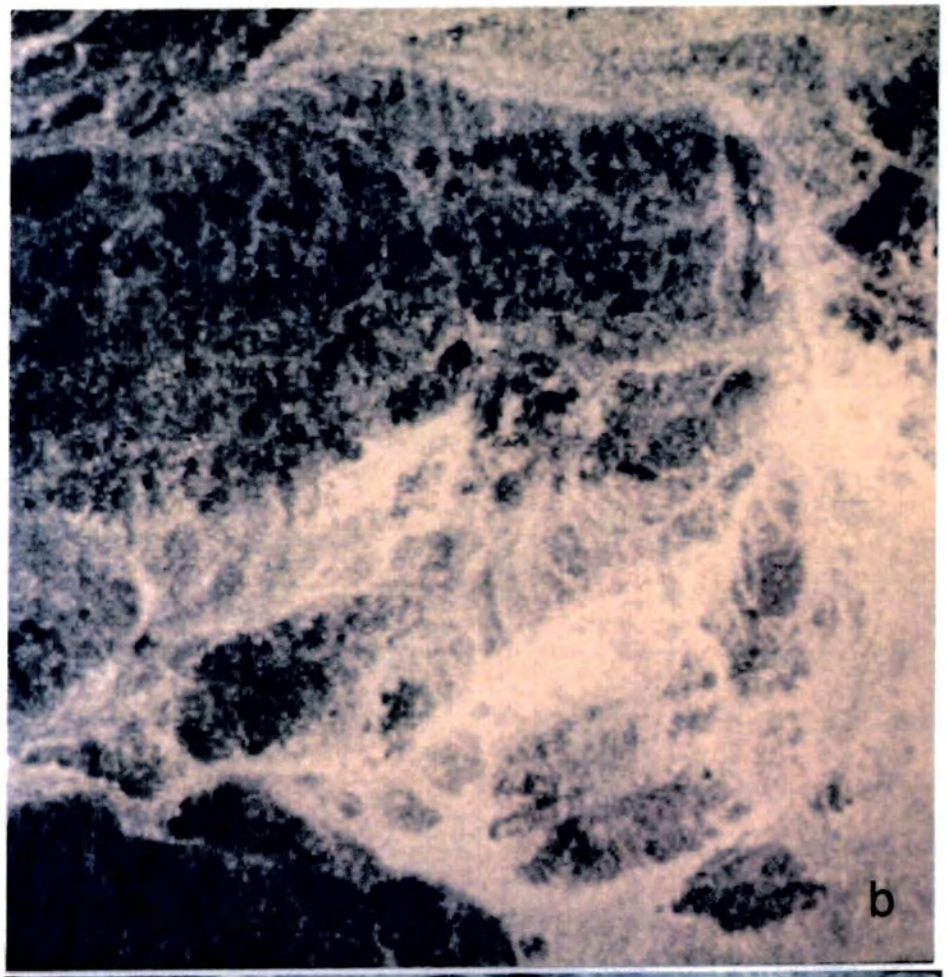

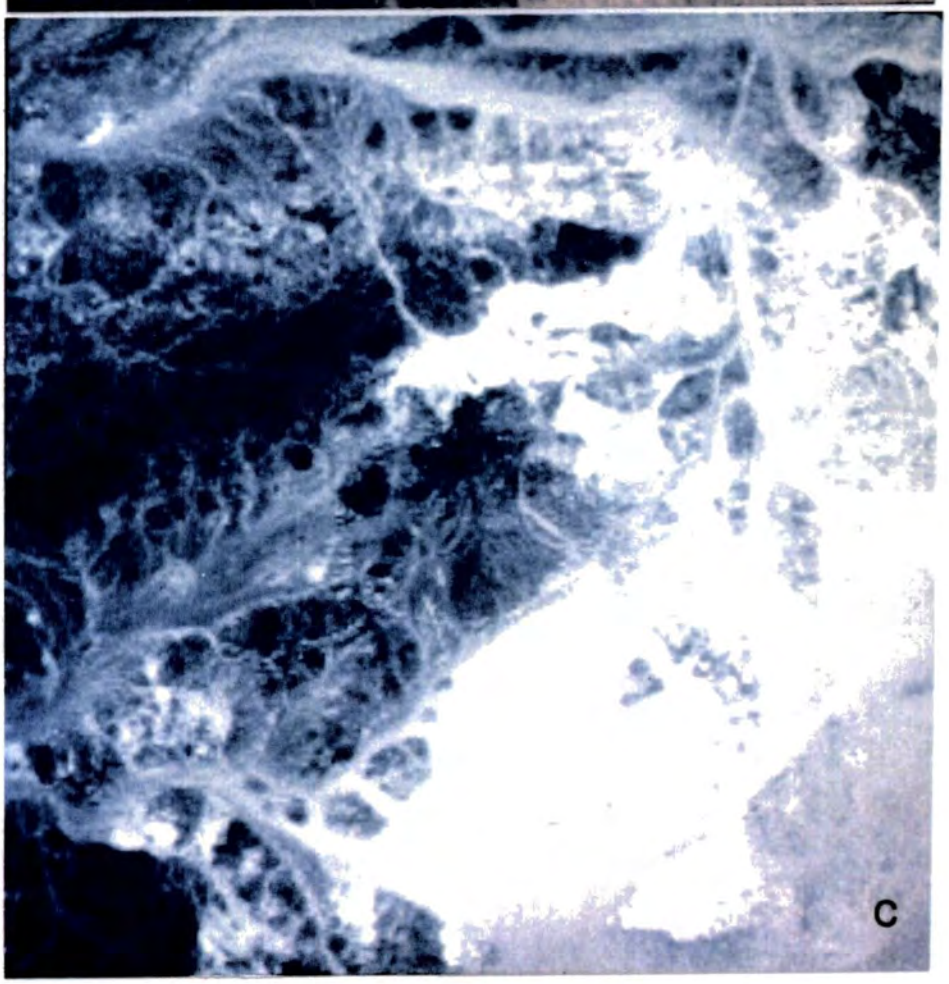

Fig. 6.37 continued.

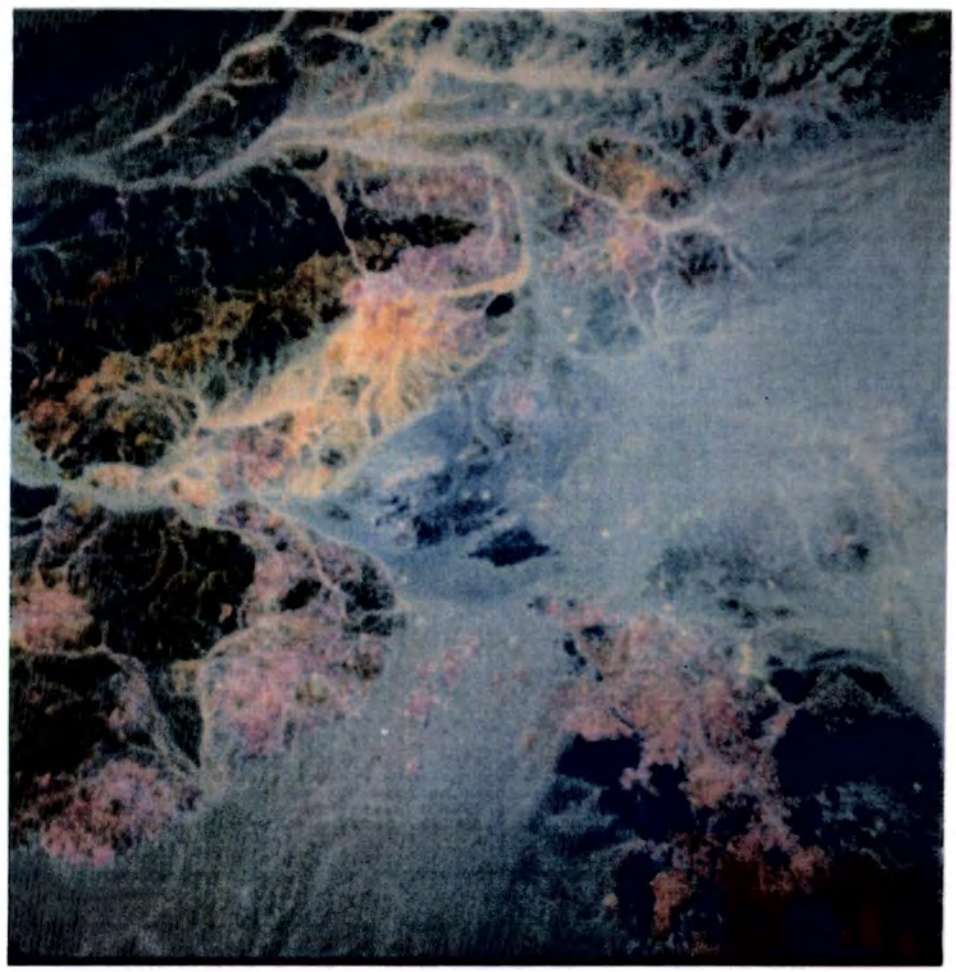

Fig. 6.38 Landsat TM ratio colour composite of subscene covering Jabal Said deposits. Bands ratios 5/7, 3/2 and 4/5 are displayed as red, green and blue respectively.

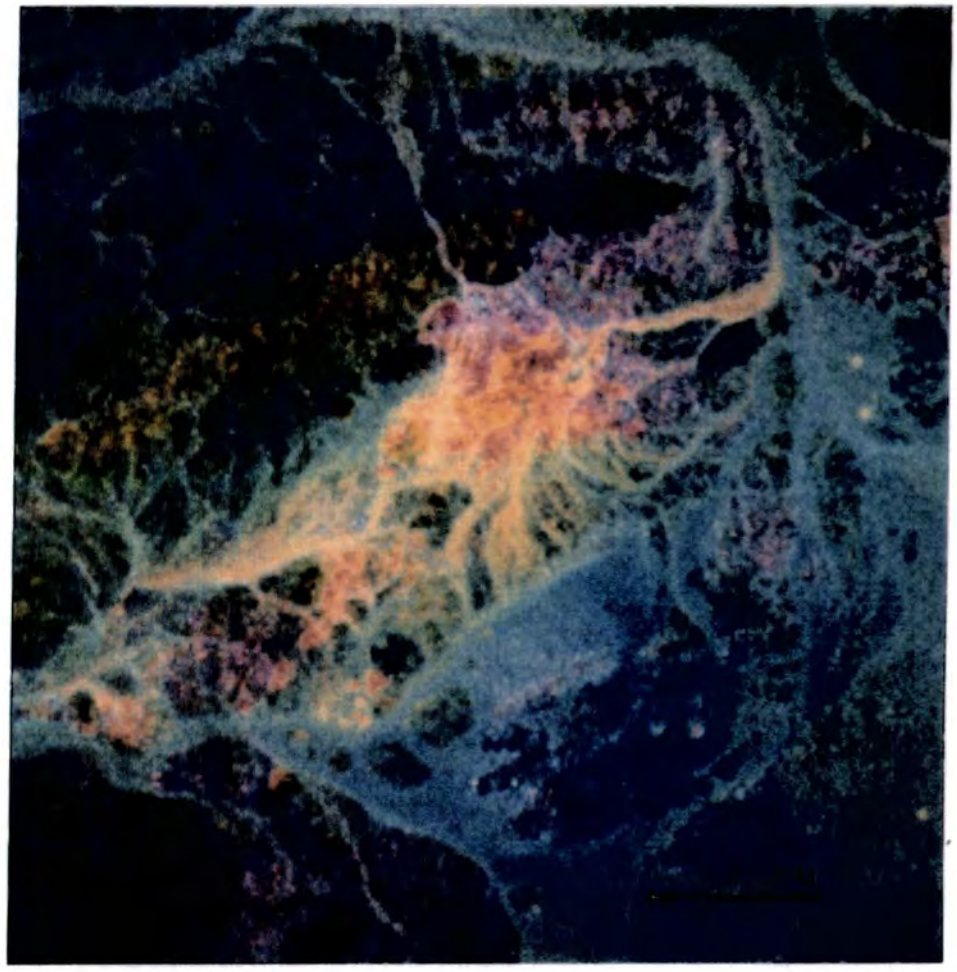

Fig. 6.39 Landsat TM ratio colour composite of a 7.5x7.5km subscene covering the Jabal Said deposit. Bands ratio 5/7, 3/2 and 4/5 are displayed as red, green and blue respectively.

(Fig. 6.32) which shows the green colour related to the iron oxide.

6.5 The influence of spatial resolution on lithological mapping in the Arabian Shield

6.5.1 Introduction

Systematic quantitative studies on the effect of spatial resolution for the discrimination between rock types and alteration zones using multispectral remotely sensed data are notably lacking (Abrams, 1982, 1984). This is despite a continuing demand for better spatial resolution in such data sets. It is generally recognised that an increase of the nominal-spatial resolution from 80m in the case of Landsat MSS to that of 30m for Landsat TM was particularly beneficial to the application of TM data in geological studies. However, relatively little is known about the incremental advantages of increasing pixel resolutions beyond 30m for lithological mapping purposes, or for the extraction of detailed structural information on small scale fractures, faults and joints, whilst retaining the spectral coverage afforded by the TM system.

The ATM data over Mahd Adh Dhahab and Jabal Said acquired at three nominal spatial resolutions; these are 7.5m, 5.0m and 2.5m IFOV from three different altitudes 3000m, 2000m and 1000m, respectively.

The availability of such data gives the ability to compare the spatial resolution from these ATM sensor data sets with TM and MSS sensor data.

6.5.2 Impact of spatial resolution on discrimination and mapping hydrothermally altered rocks and general geological mapping

Ultimately, the geological map is the end product for remote sensing data. Landsat, MSS data with 80m IFOV resolution are used to produce maps equivalent to 1:250,000 scale which are useful for regional mapping. Mapping for exploration purposes needs to be carried out at a scale of 1:48,000 or better (Settle (ed.), 1982). The Jabal Said area was mapped by Sabir (1981) on a scale 1:50,000 (see Fig. 2.9). Part of the mapped area is shown in Fig. 6.39, which is a ratio image of the TM subscene. The approximate scale of this image is 1:44,000. The TM imagery discussed in the previous section, for interpretation, also has the same scale.

6.5.3 Comparing the resolutions of Landsat MSS to TM

The Landsat TM ratio colour composition of 7.5x7.5km subscene covering the Jabal Said prospect. Bands ratios 5/7 (1.63/2.2um), 3/2 (0.66/0.56um) and 4/5 (0.83/1.63um) are displayed as red, green and blue respectively. This combination highlights the presence of minerals associated with hydrothermal alteration (Fig. 6.39).

In this image the various colours can be related to particular mineral assemblages. Areas with iron oxides are displayed as green; areas dominated by hydroxyl-bearing minerals appear as red; and areas where both occur are yellow and orange in colour.

For comparison, the same area was extracted from the Landsat MSS sensor and is presented as a colour ratio.

The composite consists of band ratios 4/5 (0.55/0.65um), 5/6 (0.65/0.75um) and 6/7 (0.75/0.95um) displayed as blue, green and red respectively (Fig. 6.40).

A comparison of the Landsat image in Fig. 6.40 with the geological map of the area, indicates that separation of the alteration associated with Jabal Said deposits with respect to surrounding unaltered lithologies, is not easily achieved. On the other hand, a comparison of the TM images with the available map, indicates that the TM image clearly delineates the general area of known surface alteration, and also differentiates between different lithologies.

6.5.4 Comparing the spatial resolution of Daedalus ATM data.

The ATM data acquired from the different elevation, 3000m, 2000m and 1000m with spatial resolution of 7.5m, 5.0m and 2.5m IFOV covered Jabal Said (see Fig. 6.23). Due to the limited geographical coverage of the higher spatial resolution, the examined area was separated into different flight lines. The 7.5 m IFOV resolution data covered one line only.

To compare the effect of higher spatial resolution on extracting geological information, the previous ratios used with MSS and TM have been applied to the ATM sensor data using ATM bands 9/10, 5/3 and 7/9 in the red, green and blue respectively from all the three nominal resolution over the alteration zone of Jabal Said. These bands ratios have the same spectral coverage as the bands

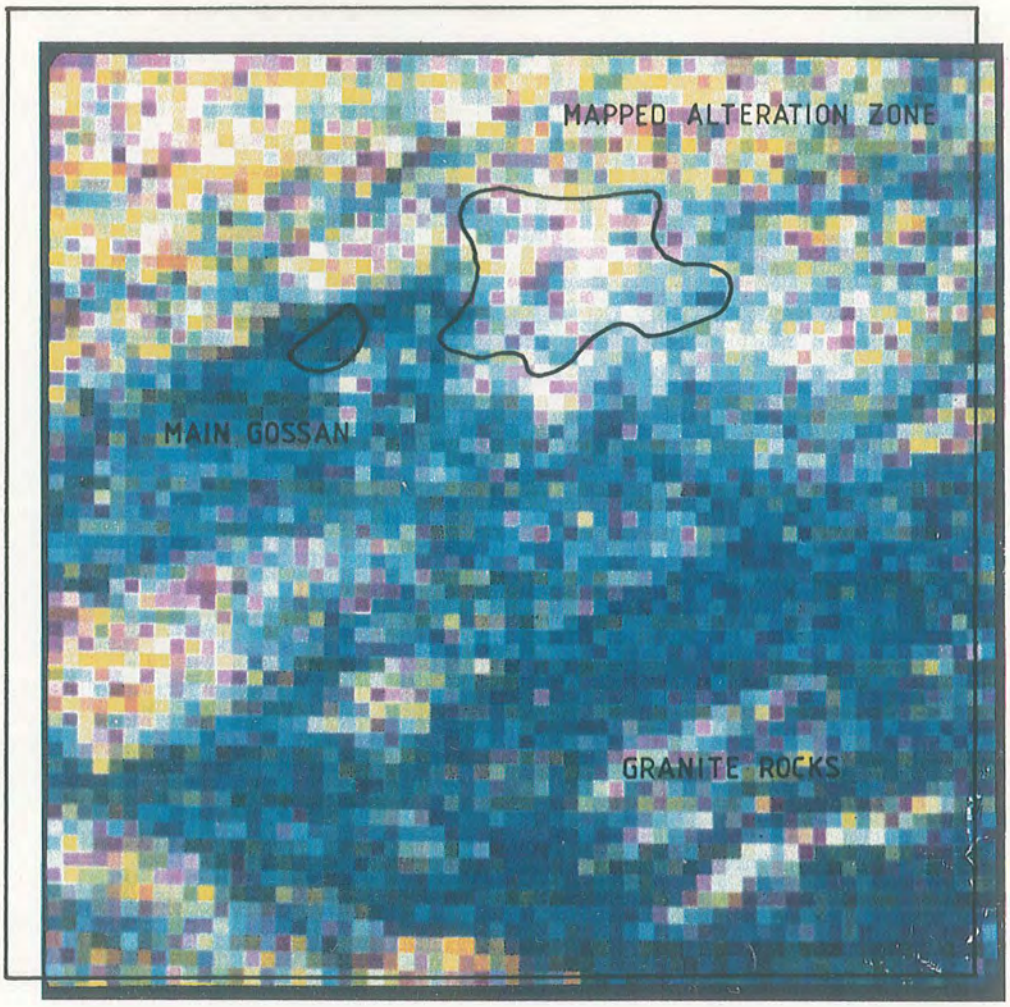

Fig. 6.40 Landsat MSS Ratio Colour Composite of a 7x7km subscene covering the Jabal Said massive sulphide deposit consisting of band ratios 4/5, 5/6 and 6/7 displayed in blue, green and red respectively. The area of coverage is approximately equivalent to that shown in the TM composite Fig. 6.39.

ratios used with TM data. The interpretation of the ratio image was discussed earlier (see Fig. 6.32). Generally, the colours can be related to particular mineral assemblages, the green related to the presence of iron oxides, red - hydrous minerals, the yellow or orange related to a combination of hydrous and iron oxide minerals (Fig. 6.41).

A comparison of the three ATM data sets suggests that while fine details are apparent in the 1000m data with resolution 2.5m, the 3000m data (resolution 7.5m) show many of the geological features to be maintained. It is clear that the image with 2.5m IFOV resolution shows considerable detail, for example the red colour in the alteration zone relates to the hydroxyl-rich minerals, and can be discriminated clearly from iron oxide (green) or from the mixture of the iron minerals and hydroxyl minerals (yellow/orange) in the 2.5m image. All these details are not shown in the 7.5m resolution image (Fig. 6.40). Another result of the higher resolution, is the detail of structural features such as lineaments which can be picked up around the alteration area.

Figure 6.42 shows an enlargement of the ratio images of the Jabal Said area. The main gossan appears very clear in all three resolutions. Notice that the 7.5m IFOV resolution image still maintains all the detail around the main gossan and the altered area around the gossan and within the gossan itself.

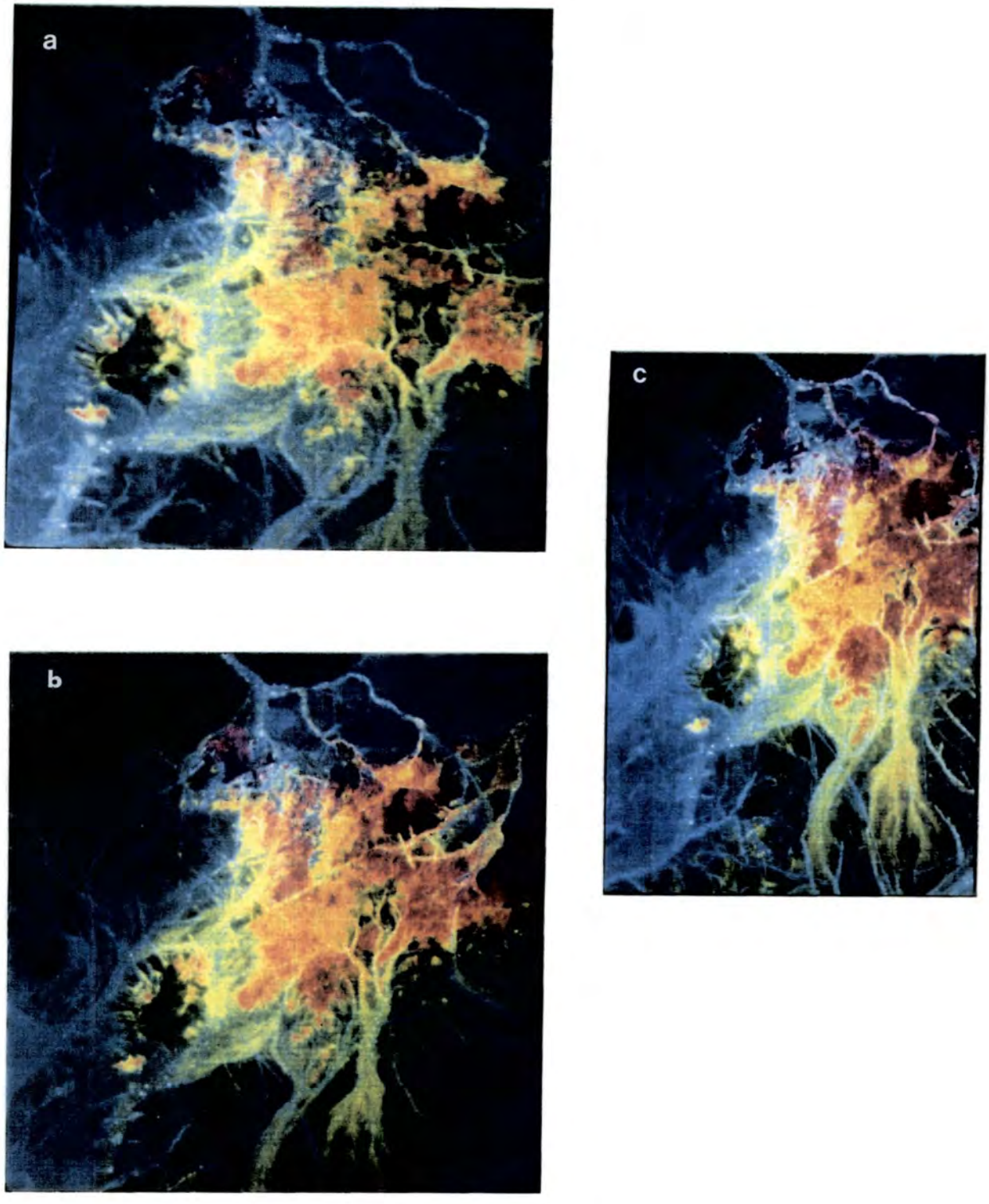

Fig. 6.41 Colour composite images of ATM bands ratio, bands 9/10 (red), 5/3 (green) and 7/9 (blue) of the alteration zones and the main gossan in Jabal Said, from three spatial resolutions. (a) 3000m data (resolution 7.5m), (b) from 2000m data (resolution 5.0m), (c) from 1000m data (resolution 2.5m). See text for explanation of colour assemblage.

Fig. 6.42 Enlargement of colour composite images of the ATM ratio in Fig. 6.41, covering the main gossan in Jabal Said deposit. (a) ATM 1000m (resolution 2.5m), (b) ATM 2000m (resolution 5.0m), (c) ATM 3000m (resolution 7.5m).

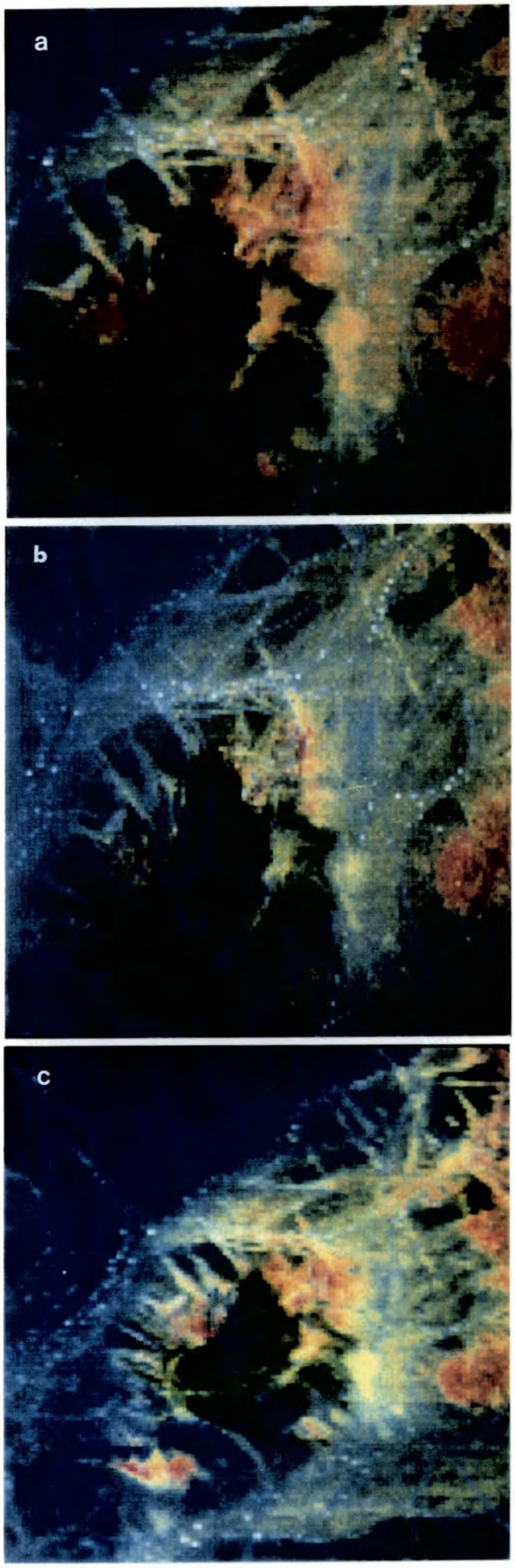
a
b
c

Generally the visual comparison of ATM data acquired at the three spatial resoltuion 7.5m, 5m and 2.5m IFOV suggests that the incremental advantages did not effect extraction of general geological information between the 7.5m and 2.5m IFOV data sets.

Comparison between the TM ratio image and the ATM image show that the alteration zones are still detectable in TM data, but the detail of the alteration zones are lost due to the low resolution. The other geological units can be discriminated and mapped from TM image using the ratio images or colour composites. A comparison between ATM (7.5m IFOV resolution) and an enlarged TM colour composite (to maintain approximately the same resolution) shows that the TM imagery is capable of detecting not only the large area of alteration zones, but also discriminating the gossan from the surrounding lithologies (Fig. 6.43)

6.6 Summary and Conclusions

The results of analysis of ATM and TM data over Mahd Adh Dhahab and Jabal Said suggest the following:

1. The best colour composite for separating altered rocks from unaltered and also mapping the different lithological units were bands 10 (2.2um), 9 (1.65um), 3 (0.56um) for ATM which are similar to 7 (2.2um), 5 (1.65um), 2 (0.56um) of TM. Other techniques such as decorrelation stretches and band ratioing especially 10/9 (2.2/1.65um), 5/3 (0.66/0.56um), 7/9 (0.83/1.65um) are

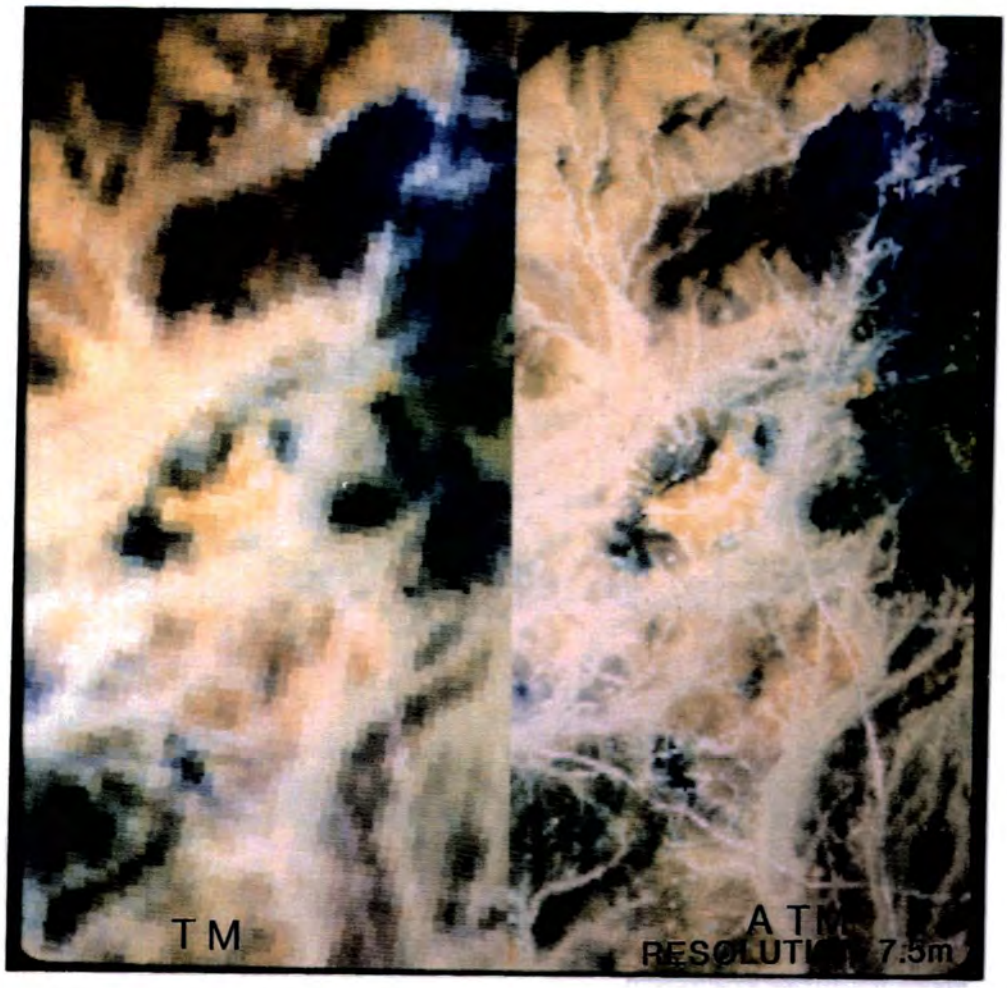

Fig. 6.43 A comparison between a false colour composite of 2.2um, 1.65um and 0.66um in red, green and blue respectively of ATM (7.5m) and TM data. Notice the ability of the TM enlargement to show the gossan in yellow colour. The greenish colour in the right is part of the alteration zone.

very useful for separating the alteration zone from the surrounding areas.

2. Variation within the alteration zone, in both areas can be picked up using high resolution data.

3. Many of the structural features recognised in higher resolution can still be detected in TM images.

4. Landsat TM could be used as a very effective geological map at a scale of 1:50,000 or higher.

5. One of the major drawbacks with the higher resolution ATM flight lines is that they offer only a limited geographic coverage, thereby preventing the area from being examined in a wider structural context.

6. The decorrelation stretched technique of bands 7 (2.2um), 5 (1.65um), 2 (0.56um) of TM sensor data are particularly effective in subdividing the volcanoclastic sequences, whilst at the same time enhancing differences between the altered and unaltered areas. A significant advantage of the decorrelation stretches over band ratioing is that it maintains a high signal to noise ratio and retains useful topographic information.

7. Results from the band ratios and decorrelation stretched techniques represent an effective means for highlighting alterations. This suggests that Landsat TM data could be used as a very effective exploration tool in arid regions such as the Arabian Shield. It is also suggested that TM data would serve as a targeting tool for more detailed studies using airborne multispectral systems.

8. Examining the images from different resolutions indicates that certain lithologies exhibit a higher internal spectral variability as higher resolutions, suggesting that the natural heterogeneity of these rocks is being resolved.

9. Comparison of the ATM data acquired at three spatial resolutions (7.5m, 5.0m and 2.5mIFOV) suggest that the incremental advantages in terms of a geological interpretation, of the higher spatial resolution may not be justified when factors such as higher data rates and increased costs are taken into account.

10. Huckerby et al. (1984) suggested that Mahd Adh Dhahab differs from other vein-type gold deposits in that the mineralization is not surrounded by widespread, pervasive alteration that could be discriminated in a satellite image. Results here suggest otherwise.

CHAPTER 7

CONCLUSION AND RECOMMENDATION

7.1 CONCLUSION

The aims and objectives of this study which was mentioned in the first chapter, was to test the capability of multispectral remote sensing data for lithological mapping and mineral exploration and specifically the objectives can be summarized as follows:

1. To test the capability of multispectral remote sensing techniques for lithological mapping in the Arabian Shield;
2. To discriminate the hydrothermally altered rocks from the surrounding unaltered rocks;
3. To evaluate the effect of weathering on the spectral reflectance characteristics of surficial materials;
4. To describe the use of ground radiometric data for sensor calibration and lithological discrimination;
5. To analyse the effect of spatial resolving power of increased multispectral data for lithological mapping and the detecting of alteration zones.

The multispectral remote sensing data used in this study were Landsat 5, TM data and Daedalus 1268 ATM data. The ATM had three nominal spatial resolution 7.5 m, 5.0 m and 2.5 m and covering 10 bands from (0.43 to 2.35 um). The data covering two test site Mahd Adh Dhahab and Jabal Said. The availability of these data afforded an opportunity to evaluate the utility of the wavelength range 0.43 - 2.35 um for lithological mapping and mineral

exploration and analyse the effect of varying the spatial resolution of the data.

The above objectives were achieved and the results can be summarized in the following points:

1. The ATM data sets were affected by a cross-track which can be caused by a combination of atmospheric, surface and scanner effects. This results in systematic differences in brightness, approximately orthogonal to the direction of flight. This serious radiometric distortion was corrected for using a nadir normalisation technique.

2. Initially the data were reduced to a meaningful parameter, that is reflectance units using the spectra of known targets measured by a Barringer HHRR. This permitted direct quantitative comparison of the various sensor data sets.

3. Variation in spectra reflectance between different lithologies in Mahd Adh Dhahab and Jabal Said areas were primarily a function of physical and chemical parameters affecting the relative brightness of the surface. The result of XRD and XRF analysis of samples collected from the area show the difference between the altered rocks and unaltered rocks. In general, the altered rocks contain a higher concentration of the Al-oH + Mg-oH + Co bearing minerals than the unaltered rocks. The laboratory spectra of the samples analysed by XRD and XRF from Jabal Said and Mahd Adh Dhahab indicate that many of the materials in the different alteration zones exhibit diagnostic spectral features associated with clay minerals, such as kaolinite and chlorite. In fact, the laboratory spectra can

differentiate between the alteration types based on their spectra features. In situ spectra from the HHRR broad band sensor, permit differentiation of altered and unaltered rocks. This implies that broad band sensors centred at 2.2 um such as band 7 in Landsat TM or band 10 in ATM should be capable of discriminating altered and unaltered rocks.

Samples collected from Mahd Adh Dhahab showed considerable geochemical variation among the different zones of alteration based on their mineral composition.

4. Most of the rocks in the area are undergoing considerable weathering and are covered by desert varnish. An attempt was made to separate the weathered surface from the bulk samples of materials collected from Mahd Adh Dhahab and Jabal Said. These samples were analysed by XRD. However, only a few samples showed the presence of iron oxides. This may be attributed to a lack of crystallinity inhibiting their identification by XRD analysis alone. On the other hand, iron oxide presence could be confirmed by XRF analysis.

A mineralogical variation between the weathered surface and the bulk rocks was noticed in the samples collected from both areas especially in the amount and the presence of iron oxides and clay minerals.

It is difficult to establish a clear pattern between the bulk rock mineralogy and the rock surface mineralogy in the areas under investigation. However, since the presence of a thick desert varnish can mask the spectral

features exhibited by altered rocks, this area needs further investigation.

5. The corrected ATM and TM data were analysed by a variety of techniques aimed to enhance differences in lithology and extract relevant geologic information about the presence and abundance of iron oxides and Al-oH + Mg-OH + Co bearing minerals. Areas particularly abundant in these minerals often result from hydrothermal alteration. Such hydrothermal systems are commonly mineralised and represent valuable targets for mineral exploration. The techniques utilized with the ATM and TM data were false colour compositing, bands ratioing and decorrelation stretching. All these techniques were evaluated over both areas, Mahd Adh Dhahab and Jabal Said. In Mahd Adh Dhahab the techniques were used in differentiate between different types of alteration, while in Jabal Said the methods were aimed at lithological discrimination.

Areas of iron oxides were enhanced in the ratio of two bands centred at 0.66 um and 0.56 um. This was due to iron minerals absorbing radiation around 0.56 um and having a reflectance peak at around 0.66 um, hence their red appearance. Therefore, areas of iron oxides had high values in this ratio compared with other materials. Areas of Al-OH + Mg-OH + Co bearing minerals were enhanced using the ratio of two bands centred at 1.65 um and 2.2 um. Areas of OH + Co bearing minerals have a reflectance peak around 1.65 um and absorption radiation around 2.2 um. This resulted in these areas having high values in this

ratio compared with other rocks. Band ratios calculated with these data were successful in enhancing areas of alteration especially using the ATM data over Jabal Said.

Decorrelation stretch data have been successfully used to discriminate various lithologies in Jabal Said and Mahd Adh Dhahab. Using the decorrelation stretch of TM data over the Mahd Adh Dhahab area it was possible to discriminate the majority of the known lithologies and identified alteration zone associated with the Mine sequence, and the presence of new alteration targets.

These locations have not been reported before. Due to the size of the targets seen in the ratio and decorrelation stretch data, these areas appear promising and deserve further investigation such as geochemical sampling.

6. The effect of an increased spatial resolution on lithological mapping and alteration zone detection was studied both statistically and visually. Statistically, the result of discriminant analysis and classification were compared and visually the interpretation of different resolution image were studied.

The results of the discriminant anlaysis to differentiate among eleven lithologies in Mahd Adh Dhahab and Jabal Said were very encouraging. The percentage of discrimination is very high in all types of data regarding the change in resolution. The TM data, despite its low spatial resolution (30 m) gave high discrimination statistics.

Classification of different lithologies as a function of their measured spectral response in the TM and the three resolutions of ATM data show very high percentage of accuracy of classification. The changing spatial resolution did not substantially alter the accuracy of classification.

The classification of the HHRR data shows the lowest percentage of accuracy of classification which might be related to the very low spatial resolution and to the fact that measured spectra picked up internal variation, perhaps from the effects of desert varnish.

The results of the statistical analysis and the classification suggested that the highest spatial resolution does not necessarily result in an improvement in the accuracy of classification for selected lithologies.

The spectral bands centred at 1.6 um and 2.2 um are very valuable in lithological mapping, particularly in alteration zones.

Using the TM data and its equivalent of ATM data, discrimination between different types of alteration was achieved in Mahd Adh Dhahab and the change in spatial resolution did not substantially effect the discrimination.

Interpretation and analysis of the digital images suggest that the best colour composite for discriminating different lithologies in both areas of Mahd Adh Dhahab and Jabal Said are 10 (2.2 um), 9 (1.65 um), 3 (0.56 um) of ATM which are similar to 7 (2.2 um), 5 (1.65 um), 2 (0.56

um) TM bands. These selected bands may not be the same bands selected by the statistical analysis due to the fact that the analysis was based on selected lithologies only.

Different techniques were checked in both areas. The ratio technique shows very good results at Jabal Said, but at the Mahd Adh Dhahab the ratio images appears very noisy, although it does indicate the presence of potential alteration zones.

The best digital techniques were decorrelation stretching using band 7 (2.2 um), 5 (1.65 um), 2 (0.56 um) TM or their equivalent ATM images where it retained the topographic information and discriminated between the different lithologies.

The results of the interpretation of the TM data over Mahd Adh Dhahab and Jabal Said show the ability of the TM to be used as a very effective exploration target tool in arid regions such as the Arabian Shield.

The spatial resolution of 30 m IFOV presented enough detail for all geomorphic features to be recognized and utilized in the image interpretation. The lithological units were also separable and distinguishable from each other. Using a subscene over Mahd Adh Dhahab indicated that Landsat TM could be used for very effective geological mapping at a scale of 1:50,000. The ATM data can be used for more detailed studies, especially in structure and mineralogies of the selected areas.

The analysis and the interpretation of the ATM images were useful in adding more information about the distribution of the alteration zones in the area, for

example, the new alteration zone south of the Eastern Valley Fault in Jabal Said, which coincided with the geochemical and geophysical anomaly in the area. The detailed study of the high resolution images can also help in mapping the alteration zone according to the percentage of clay and iron oxide. This could not be achieved using the TM due to the low spatial resolution.

The 2.5 m IFOV data shows much more detail in the area, and in some places it seems to show the internal variation of certain lithologies. This effect is less apparent in the lower spatial resolution of ATM data, the 5.0 m resolution and the 7.5 m resolution data.

The major drawback of the high resolution ATM flight lines data set is that they offer only a limited geographic coverage, thereby preventing the interested target to be examined in a wider structural context.

Another major constraint against the high resolution ATM flight lines data set is the cost of operation and computer work involved. All these factors should be taken into account, especially if the comparison between ATM data and TM proved that incremental advantages in terms of a geological interpretation is not very essential.

7.2 Implications to Mineral Exploration in the Arabian Shield

The value of using Landsat Tm and the airborne multispectral remote sensing was demonstrated in the preceding chapters. The study indicated that remote sensing techniques are good tools for mineral exploration,

where it indicated new areas of alteration in both the Mahd Adh Dhahab and Jabal Said region.

Using Landsat TM data on any mineral exploration programme over the Arabian Shield should give good results and would reduce the need for extensive fieldwork. Analysing such data for potential targets will result in an economical use of resources. False colour compositing of TM 7 (2.2 um), 5 (1.65 um), 2 (0.56 um) or decorrelation stretch techniques for the same combination, or even the ratio technique, should give an indication of alteration targets in the early stages of an exploration programme. Naturally the choice of particular techniques will depend on the type of lithologies and alterations needed to be enhanced. Identifying the location of the alteration zone is one of the aims in the mineral exploration and that can be solved by applying any of the techniques mentioned above. Processing of Landsat TM data will enable the user to produce a map of scale 1:50,000 or even better. Producing such maps means saving time and money especially to cover a large area such as the Arabian Shield.

The Airborne Thematic Mapper data also gave very good results, especially in studying the interested areas in more detail. The use of such data as an exploration tool may not be economically visable when TM data may give similar results.

7.3 RECOMMENDATION FOR FURTHER WORK

Based on the results of this work several areas for further study can be recommended.

The capability to map alteration zones needs to be tested over other areas in the Arabian Shield. A logical extension of this study is to examine deposits of related minerals. Hydrothermal alteration minerals are associated with many types of ore deposits, and so the results of this study should have wider applicability.

The techniques used here can be very useful for studying the detail of structure features in the area, using high resolution data such as from the ATM sensor.

The effect of extending the spectral region beyond the range of the TM and ATM sensors for lithological mapping was studied briefly. For example, TM band seven, which equals to band ten of ATM (2.2 um) is not ideal for lithological mapping because it was impossible using such a broad band to differentiate between different types of alteration and the presence of carbonate rocks.

Laboratory work by Hunt (1979) defined the location of spectral features between 2.08 - 2.35 um which is normally covered by band TM 7. For example, the pyrophyllite shows intense sharp features at 2.166 um. Alunite features appear at 2.152 and 2.178 um and kaolinite at 2.2 um. The carbonate rock shows intense absorption at 2.35 um (Hunt and Salisbury, 1971).

From the above discussion the shapes of the carbonate spectra and the argillic alteration in Mahd Adh Dhahab are expected to be very similar in the 2.2 um region.

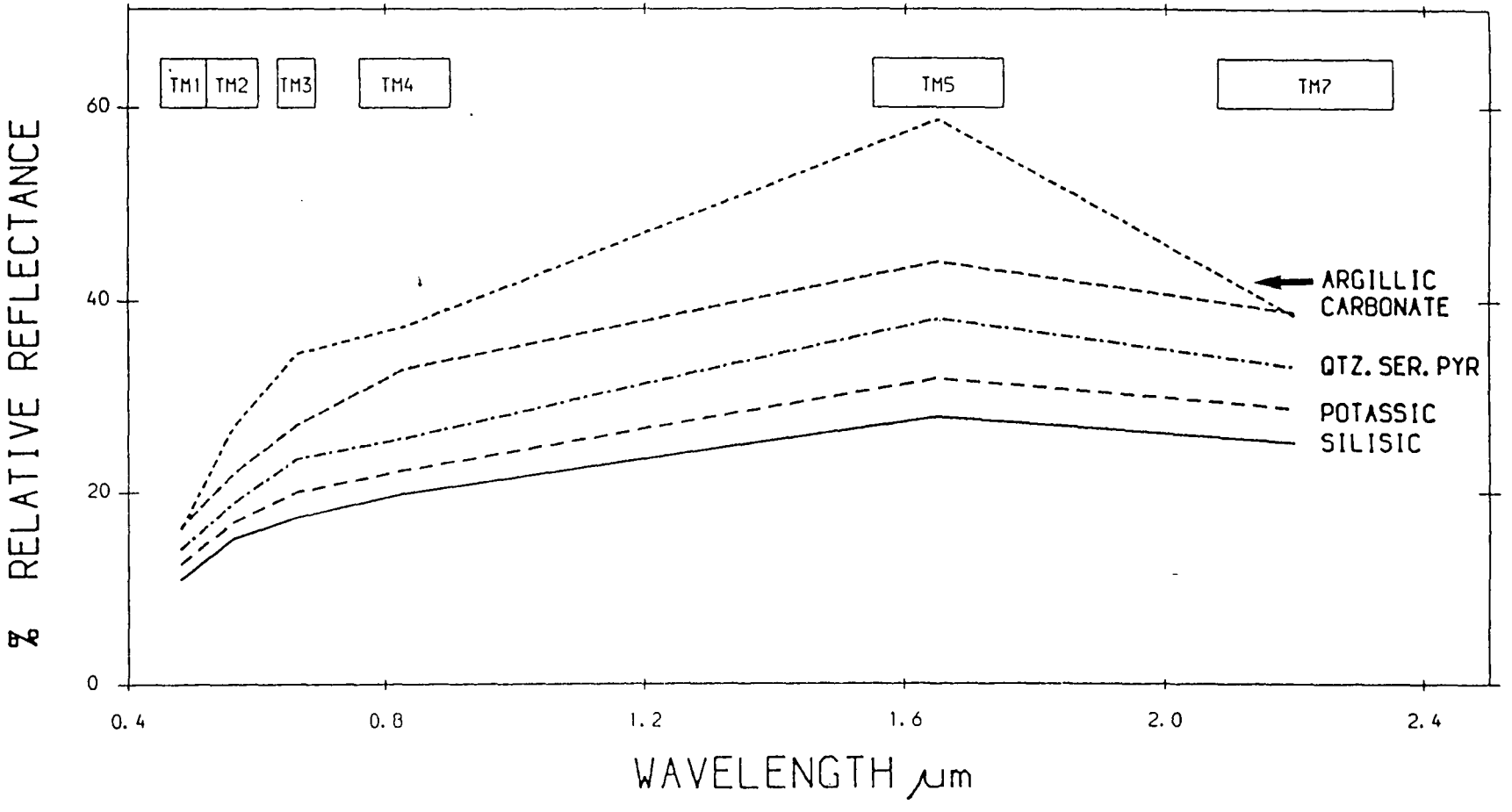

Fig. 7.1 Average HHRR spectra from Mahd Adh Dhahab area.

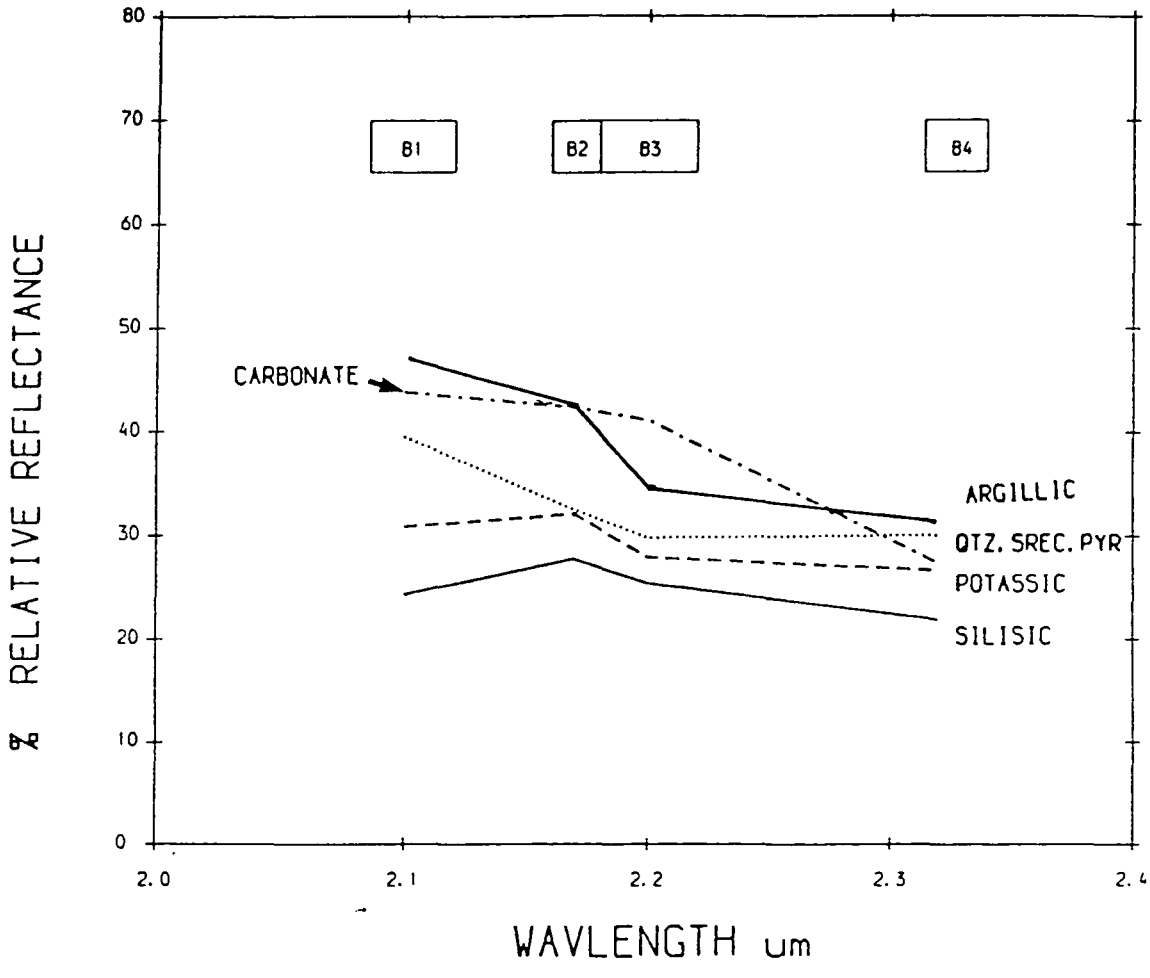

Fig. 7.2 Average HHRR narrow bands spectra from Mahd Adh Dhahab area.

This was tested using HHRR data, band equivalent to TM bands (Fig. 7.1). The shape of carbonate rock spectrum is similar to the spectra of silicic alteration, potassic alteration with different albedo. The argillic alteration spectrum coincided with the spectrum of carbonate rock in the same point at band 7 (2.08 - 2.35 um). This means that it is impossible to separate the argillic alteration from the carbonate rock using TM 7 (2.08 - 2.35 um).

The HHRR which was used in this study was equipped with four band filters cover the range between 2.0884 - 2.340 um (Table 3.17) and (Appendix C). Using these four narrow bands the spectra of the alteration zone and carbonate rocks were measured in situ and the results are presented in Fig. 7.2 The carbonate rock exhibits very specific absorption features compared with the spectra from alteration zone. All the altered rocks exhibit absorption features at 2.2 um indicating the presence of Al-oH + Mg-oH bearing minerals. The carbonate rock is the only lithology to exhibit absorption features at 2.35 um. From the above discussion, it is clear that the data from the narrow bands centred at 2.2 um are very helpful in discriminating carbonate rock from alteration zone (Fig. 7.3).

Lithological mapping could be improved substantially by acquiring and analysing high spectral resolution data; particularly for separating carbonate rocks from alteration zones, and also for discriminating different types of alteration within alteration zones.

The HHRR narrow bands and IRIS spectroradiometer data

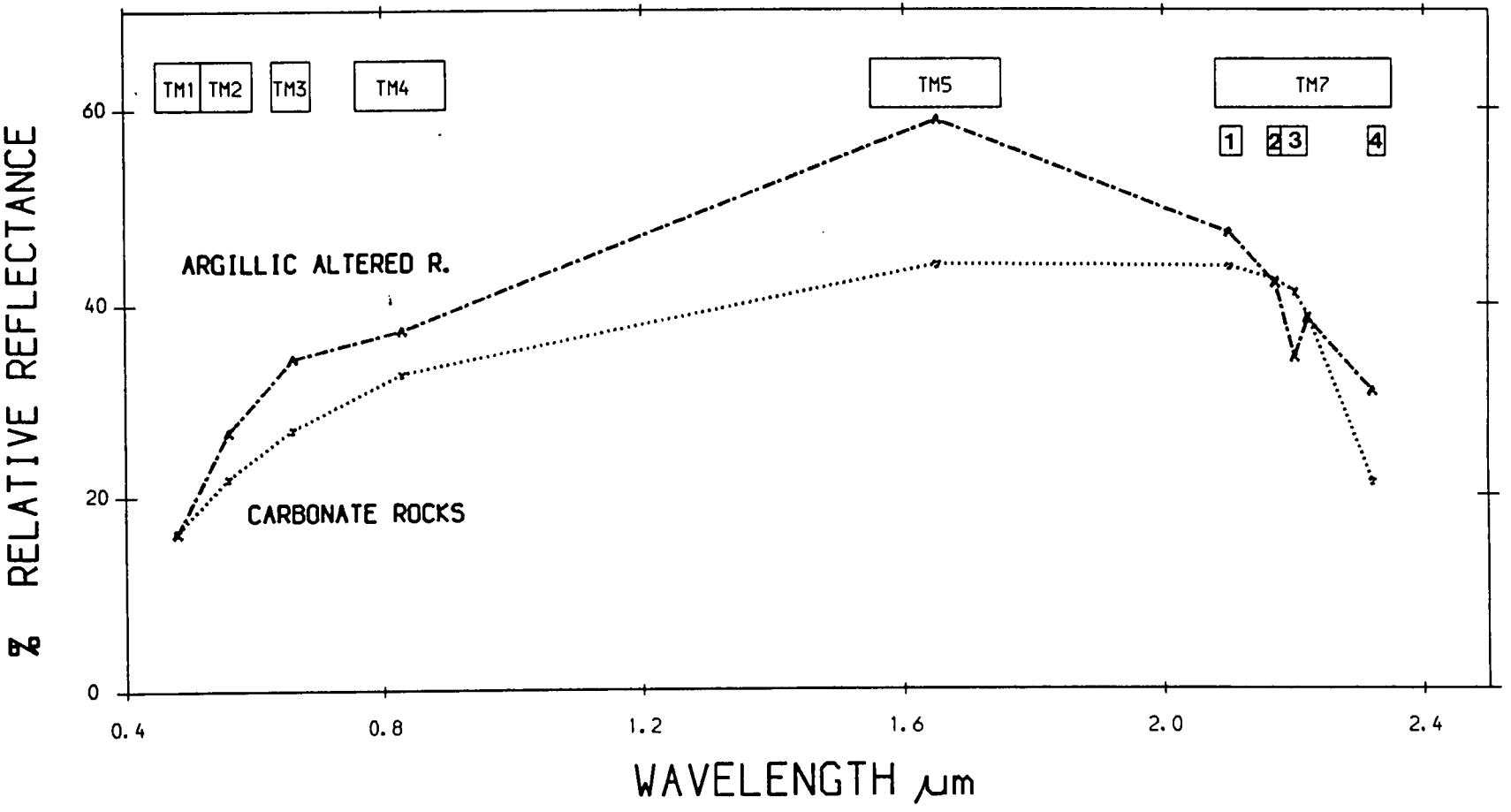

Fig. 7.3 Average HHRR spectra from Mahd Adh Dhahab area, using the TM bands and four narrow bands.

show the potential of high spectral resolution sensors for geological mapping in the Arabian Shield. When high spectral resolution image data becomes available for this area, it will complement many of the techniques and results presented in this thesis.

REFERENCES

The Arabian Aerosurvey Co. Ltd. 1984. Makkah North: Airborne Thematic Mapper Survey Report on Acquisition, Processing and Geological Interpretation. For Directorate General of Mineral Resources, Saudi Arabia.

Abrams, M.J., Conel, J.E., Lang, H.R. 1984. The joint NASA/GEOSAT Test Case Project. Final report, Helen N. Paley (Ed.). AAPG, Tulsa.

Abrams, M.J. & Siegal, B. 1980. Lithological Mapping. In: B. Siegal (Ed.). Remote Sensing in Geology. John Wiley & Sons, New York.

Abrams, M.J., Brown, D., Lepley, L. and Sadowski, R. 1983. Remote Sensing for copper exploration in Southern Arizona. Econ. Geology. 78, No. 4, 591-604.

Abrams, M. 1986. Mapping the Oman Ophiolite using TM data. Fifth Thematic Conference: Remote Sensing for Exploration Geology, Reno Nevada.

Abrams, M., Sadowski, R. & Prost, G. 1984. Porphyry Copper in Helvita, Arizona. In: the NASA/GEOSAT Test Case Project. AAPG, Tulsa.

Abrams, M. & Brown, D. 1984. Porphyry Copper at Silverbell in Arizona. In: The Joint NASA/GEOSAT Test Case Project. AAPG, Tulsa.

Abrams, M.J. 1984. Landsat-4 Thematic Mapper and Thematic Mapper Simulator data for a porphyry Copper Deposit. Photogrammetric Engineering and Remote Sensing, 50, no. 8, 1171-1173.

Abrams, M. 1982. Effects of Spatial Resolution. In: M. Settle (Ed.). Workshop on the future Multispectral Imaging Capability for lithological mapping. JPL, Caltech.

Abrams, M.J. & Rowan, L.C. 1979. Discrimination of altered rocks using spectral data from 0.45 to 2.45 micrometre wavelength region. Proc. 13th Int. Symp. Remote Sensing Env. Ann Abor, Michigan, 73-74.

Abrams, M.J., Ashley, R.P., Rowan, L.C., Goetz, A. & Kahle, A.B. 1977. Mapping of hydrothermal alteration in the cuprite mining district, Nevada, using aircraft scanner images for the spectral region 0.46-2.36um. Geology 5, 713-718.

Aguttes, J. & Duhamel, M. 1971. Geology and Mineral exploration of the Jabal Said quadrangle. Bureau de Recherches Geologiques et Minieres Technical Record 71, JED-2, 63pp.

Al-Hinai, K.G. 1988. Quaternary Aeolian Sand Mapping in Saudi Arabia. Unpublished Ph.D. Thesis, Imperial College of Science & Technology, London.

Anderson, J.R. 1971. Land use classification schemes used in selected recent geographic applications of remote sensing. Photogramm. Eng. 37(4), 379-387.

Ashley, R.P. & Abrams, M. 1980. Alteration mapping using multispectral images - cuprite mining district, Esmerelda County, Nevada. U.S. Geological Survey Open File Report 80, 367.

Bailey, J. 1976. Trace element techniques in the Institute for Petrology, University of Copenhagen. In: Bailey, J. & Sorensen, I. (eds) X-ray fluorescence analysis, Internal Report, University of Copen Hagen.

Ballew, G.I. 1977. Alteration mapping at Gold Field, Nevada by cluster and discriminant analysis of Landsat digital data. Proc. 11th Int. Symp. Remote Sensing Env., Ann Arbor, Michigan, 783-790.

Barringer. 1981. Manual of Ratioing Radiometer Hand Held Reflectance Radiometer for earth sciences. Barringer Research Ltd. Golden, Colorado, U.S.A.

Bird, A.C., Garrard, C.R., Lles, A.R., Loughlin, W.P., Tawfiq, M., & Legg, C. 1985. An investigation of spectral signatures from mineralised rock outcrops as defined by Airborne TM data of the Saudi Arabian Shield. Proc. 3rd International colloquium on spectral signatures of objects in remote sensing, Les Arcs, France.

Blom, R.G., Abrams, M.J. & Adams, H.G. 1980. Spectral reflectance and discrimination of plutonic rocks in the 0.45 to 2.45um region. J. Geophys. Res. 85, 2638-2648.

Boldget, Gunther, F.J., Podwysocki, M.H. 1978. Discrimination of rock classes and alteration products in southwestern Saudi Arabia with computer enhanced Landsat data. NASA Technical paper 1327, NASA scientific and technical information office.

Bournat, G. 1981. Jabal Said Copper-zinc deposit, synthesis of work and results 1971-1974. Saudi Arabian Deputy Ministry for Mineral Resources, open file Report BRGM-OF-01-07, 92pp.

Bowden, R.A. & Smith, G.H. 1981. An overview study of the Jabal Said district, Saudi Arabia. Saudi Arabian Deputy Ministry for Mineral Resources, Technical Record RF-TR-01-2.

Brown, G.F., Jackson, R.O., Bague, R.G. & Maclean, W.H. 1963. Geological map of the southern Hijaz quadrangle. U.S. Geological Survey Miscellaneous Investigations Map I-210A, scale 1:500,000.

Buckingham, W.F. & Sommer, S.E. 1983. Mineralogical characterization of rock surface formed by Hydrothermal alteration and weathering - application to remote sensing. Economic Geology, 78, no. 4, 664-674.

Chan, K.M. 1980. Report on the geology, mineral prospects and potential of the Mahd Adh Dhahab concession held by Goldfields Mahd Adh Dhahab Limited, Kingdom of Saudi Arabia.

Clavez, J.Y. & Kemp, J. 1982. Geochronological investigations in the Mahd Adh Dhahab quadrangle, Central Arabian Shield. Saudi Arabian Deputy Ministry for Mineral Resources. Technical Record BRGM-TR-02-5, 41pp.

Conel, J.G., Abrams, M.J. & Baird, K.W. 1980. Uranium; spectral discrimination of alteration phenomena in sediments. Modern Geol. 7, 115-135.

Conel, J.G., Lang, H.R., Paylor, E.D. & Alley, R.E. 1985. Preliminary spectral and geologic analysis of Landsat-4 thematic mapper data, Wind River Basin Area, Wyoming. IEEE Transaction on Geoscience and Remote Sensing, GE-23, No. 4.

Conel, J.E., Abrams, M.J. & Goetz, A.F.H. 1978. A study of alteration associated with Uranium occurrences in sandstone and its detection by remote sensing methods. J.P.L. Publication 78-66, Vol. 1.

Collins, W. 1978. Remote sensing of crop type and maturity. Photogramm. Eng. & Remote Sensing 44, 43-55.

Collins, W. & Chang, S.H. 1982. Mapping the distribution and mineralogy of hydrothermally altered rocks by using airborne multispectral scanner and spectroradiometer data, Marysvale, Utah. Int. Symposium Remote Sensing of Environment, Fortworth, U.S.A.

Collins, W., Chang, S.H., Raines, G., Canney, F., & Ashley, R. 1983. Airborne biogeochemical mapping of hidden minerals deposits. Economic Geology, 78, 737-749,

Crane, K. & Bonatte, E. 1987. The role of Fracture zones during early Red Sea rifting: structural analysis using space shuttle radar and Landsat Imagery. J. geol. Soc. Lond., 144, 407-420.

Davis, J.C. 1975. Statistics and data analysis in geology. J. Wiley & Sons, New York, 550pp.

Daedalus Scanner Applications worldwide. 1982. Daedalus Enterprises Inc. Ann Arbor, U.S.A.

Delfour, J. 1970. Sulphide mineralisation at Nugrah and Jabal Said. B.R.G.H. Technical record 70-JED-22.

Dirom, G.A. 1947. Geological report - Mahd Dahab. Saudi Arabian Dir. Gen. Mineral Resources Files. SAMS Unpublished Report, 15pp.

Doebrich, J.L. & Leanderson, J.P. 1984. Geology and hydrothermal alteration of the Mahd Adh Dhahab epithermal precious-metal deposit, Saudi Arabia. Deputy Ministry for Mineral Resrouces Openfile Report USGS-OF-04-32.

Doebrich, J.L. and Leanderson, P.J. 1984. Supporting data for geology and hydrothermal alteration at Mahd Adh Dhahab epithermal precious-metal deposit, Kingdom of Saudi Arabia: Implications for genesis of the deposit. Deputy Ministry for Mineral Resources data file USGS-DF-04-23.

Donoghue, D. and Hook, S.J. 1986. Preprocessing of airborne multispectral data: a necessity for quantitative remote sensing. Proc. of NERC Airborne Campaign Workshop.

Dottin, O. 1974. Revised Geology of the Sufaynah Quadrangle 23/40D, Saudi Arabia. B.R.G.M. Open file Report 75-JED-29.

Dozier, J. & Strahler, A. 1983. Ground Investigations in support of remote sensing. In: Colwell, R.N. (ed.), Manual of Remote Sensing, 1. Am. Soc. of Photogrammetry, p.959.

Doubner, L. et al. 1981. A hand-held ratioing radiometer for remote sensing measurements. 7th Canadian Symposium of Remote Sensing, Winnipeg, 423-478.

Gladwell, D.R., Lett, R. & Lawrence, P. 1983. Application of reflectance spectrometry to mineral exploration using portable radiometers. Economic Geol. 78, 669-710.

Gettings, M.E. 1981. Geophysical investigations in the Mahd Adh Dhahab District, Saudi Arabia. U.S. Geological Survey Open File Report 81-828.

Gillespie, A. & Kahle, A. 1986. Colour enhancement of highly correlated images: I Decorrelation and HSI stretches. Remote Sensing of the Environment 20, 209-255.

Gillespie, A. 1980. Digital Techniques of image enhancement, Chapter 6. In. Remote Sensing in Geology, John Wiley, London.

Gillespie, A.R. and Kahle, A.B. 1977. Construction and Interpretation of a digital thermal Inertia

Image. Photogram. Metr. Eng. 43, 983-1000.

Goetz, A.F.H., Barrett, Rock, N. & Rowan, L.C. 1983. Remote sensing for exploration: an overview. Econ. Geol., 78(4), 573-590.

Goetz, A., Vane, G., Solomon, J., & Rock, B. 1985. Imaging Spectrometry for Earth Remote Sensing. Science, Vol. 228, 1147-1153.

Goetz, A.F.H. & Rowan, L.C. 1981. Geological Remote Sensing. Science, Vol. 211, 781-791.

Goetz, A.F.H., Siegal, B.S. & Rowan, L.C. 1975. Qunatitative spectral techniques and computer image processing as applied to lithological mapping proceedings. 14th IEEE Conference on Decision & Control, Houston, Texas. 412-413.

Goldsmith, R. & Kother, J. 1971. Geology of Mahd Adh Dhahab - Umm ad Damar area, Kingdom of Saudi Arabia, Saudi Arabia Dir. Gen. Mineral. Resources Bull., 6, 20pp.

Greenbaum, D. 1987. Lithological discrimination in Central Snowdonia using airborne multispectral scanner Imagery. Int. J. Remote Sensing, 8, no. 6, 799-816.

Gustafson, L.B. & Hunt, J.P. 1975. The Porphyry Copper Deposit at El Salvador, Chile. Economic Geology, 70, 857-912.

Hadley, D.G. 1974. Geological map of the Wayban Quadrangle, Saudi Arabia. Ministry of Petroleum & Mineral Resources, DGMR, Map GM-7, Scale 1:100,000.

Hadley, D.G. 1973. Geology of Sahl al Matran quadrangle, northwestern Hijaz, Kingdom of Saudi Arabia. Ministry of Petr. & Mineral. DGMR, Map G-6, Scale 1:100,000.

Hakim, H.D. 1988. Personnel communications.

Hilpert, L.A. Roberts, R.J. & Dirom, G.A. 1982. Geology of Mine Hill and the underground workings. Mahd Adh Dhahab Mine, Saudi Arabia. Unpubl. USGS Saudi Arabia Mission Report.

Hopwood, T. 1979. An exploration study of metal deposits in the Jabal Said region, Kingdom of Saudi Arabia. Riofinex Ltd. RF0-1979-9.

Howes, D.R. & Sanderson, P.M. 1985. Prospecting for Gold in Mahd Group Rocks, North Kish area, Saudi Arabia. Deputy Ministry for Mineral Resources, Jeddah, Open File Report, RF-OF-05-3.

Huckerby, J.A., Magee, R., Moor, J.McM., & Coates, D. 1986. Thematic Mapper applied to alteration zone mapping for gold exploration in Southeast Spain. The Fifth Thematic Conference: Remote Sensing for Exploration Geology, Reno, Nevada, U.S.A.

Huckerby, J.A. 1984. Structural setting and mineralisation at the Madh Adh Dhahab gold mine, Western Saudi Arabia. Unpublished Ph.D. thesis, Imperial College of Science & Technology, London.

Huckerby, J.A., Moor, J. Davis, Lewis, P.J. & Martin, G.J. 1984. Mahd Adh Dhahab deposit, Saudi Arabia - Discussions. Trans. Inst. Mining & Metallurgy, Section B, v. 93.

Huckerby, J., Moor, J. & Davis, G. 1983. Tectonic control of mineralization at Mahd Adh Dhahab gold mine, Western Saudi Arabia. Trans. Inst. Mining & Metallurgy, Section B, v. 92.

Hunt, G.R. 1979a. Spectral signatures in the 0.4 to 1.1um region, Sec. 3.7, p. 3-97 to 3-116. In: ORI Inc.. Multispectral Resources Sampler: Summary Report of Workshop, Colorado State Univ.

Hunt, G.R. 1979b. Near Infrared (1.3-2.4um) spectra of alteration minerals - potential for use in remote sensing. Geophysics, 44 (12), 1974-1986.

Hunt, G.R. 1980. Electromagnetic radiaiton: Tech. Communication link in remote sensing. In: Remote Sensing in Geology, B.S. Siegal and A.R. Gillespie (Eds.), John Wiley, New York, 5-45.

Hunt, G.R. & Ashley, R.P. 1979. Spectra of altered rocks in the visible and near-infrared. Economic Geology, 74, 1613-1629.

Hunt, G.R. & Salisbury, J.W. 1978. Assessment of Landsat filters for rock type discrimination, based on intrinsic information in Laboratory spectra. Geophysics, 43(4), 738-747.

Hunt, G.R. & Salisbury, J.W. 1970. Visible and near infrared spectra of minerals and rocks: I. Silicate minerals. Modern Geology, 1, 283-300.

Hunt, C.R., Salisbury, J.W. and Lenhoff, C.J. 1971a. Visible and near infrared spectra of minerals and rocks: III oxides and hydroxides. Modern Geology, 2, 195-205.

Hunt, G.R. & Salisbury, J.W. 1971. Visible and near infrared spectra of minerals and rocks: II Carbonates. Modern Geology, 2, 23-30.

Hunt, G.R., Salisbury, J.W. & Lenhoff, C.J. 1972. Visible and near infrared spectra of minerals and rocks. V. Halides, phosphates, aisenates, vanadates and borates. Modern Geology, 3, 121-132.

Hunt, G.R., Salisbury, J.W. & Lenhoff, C.J. 1971b. Visible and near infrared spectra of minerals and rocks. IV sulphates and sulphides. Modern Geology, 3, 1-14.

Hunt, G.R., Salisbury, J.W. & Lenhoff, C.J. 1973a. Visible and near infrared spectra of minerals and rocks. VI additional silicates. Modern Geology, 4, 85-106.

Hunt, G.R., Salisbury, J.W. & Lenhoff, C.J. 1974a. Visible and near infrared spectra of minerals and rocks. VIII intermediate igneous rocks. Modern geology, 4, 237-244.

Hunt, G.R. & Salisbury, J.W. 1976. Visible and near infrared spectra of minerals and rocks. XI Sedimentary rocks. Modern Geol. 5, 211-217.

Hunt, G.R., Salisbury, J.W. & Lenhoff, C.J. 1974b. Visible and near infrared spectra of Minerals and rocks: IX basic and ultrabasic rocks. Modern Geology, 5, 15-22.

Hunt, G.R., Salisbury, J.W. and Lenhoff, C.J. 1973b. Visible and near infrared spectra of minerals and rocks: VII acidic igenous rocks. Modern Geology, 4, 217-224.

Hunt, G.R. 1977. Spectral signatures of particulate minerals in the visible and near-infrared. Geophysics, 42, 3, 501-513.

Hunt, G.R. and Salisbury, J.W. 1976. Visible and near infrared spectra of minerals and rocks. XII. metamorphic rocks. Modern Geology, 5, 219-228.

Hunting Co., 1984 in Makkah north Airborne thematic mapper survey. Report on Acquisition, Processing and geological interpretation. Prepared for Directorate General of Mineral Resources by Jeddhah by the Arabian Aerosurvey Co. Ltd., Riyadh - Saudi Arabia.

Irons, J.R. & Labovitz, M.L. 1982. A data analysis approach to Look-angle Radiance Adjustment. Journal of Applied Photographic Engineering, 8, 128-137.

Irons, J.R., Markham, B.L., Nelson, R.F., Toll, D.L., Williams, D.F., Latty, R.S. & Stauffer, M.L.

1985. The effects of spatial resolution on the classification of thematic mapper data. Int. J. of Remote Sensing, 6, 1385-1404.

Jurde, G., 1976. Jabal Said Copper Deposit - Saudi Arabia. Progress Report No. 4, Joint Venture SEREM/US Steel Corporation Open file Report.

Jackson, R., Printer, P., Reginato, R., & Idso, S. 1980. Hand-held Ratiometry. A set of notes developed for use at the workshop on hand-held radiometry. Phoenix, Arizona. U.S. Dept. of Agriculture, Science Education Administration, ARM-W-19.

Kahle, A.B. & Rowan, L.C. 1980. Evaluation of multispectral middle infrared aircraft images for lithological mapping in the east Tintic Mountains, Utah. Geology, 8, 234-39.

Kahle, A.B., Goetz, A.F., Palley, H.N., Alley, R.E. & Abbott, E.A. 1981. A data base of geological field spectra. Proc. 15th Int. Symp. Remote Sensing Env. Ann Arbor, Michigan, 329-337.

Kahle, A.B. & Goetz, A.F. 1983. Mineralogic information from a new airborne thermal infrared multi-spectral scanner. Science, 222, 4619.

Kahle, A.B., 1982. Spectral Remote Sensing of rocks in arid lands. Int. Symp. Remote Sensing of Env. 1st Thematic Conference: Remote Sensing of arid and semi-arid lands, Cairo, 279-295.

Kahle, A.B., Rowan, L.C. & Madura, D.P. 1979. Rock and mineral discrimination using Mid-IR spectral emittance data combined with visible and near IR spectral reflectance data. Thirteenth International symposium on Remote sensing of the Environment.

Kaufman, H. & Pfeiffer, B. 1988. Image optimization versus classification - An application oriented comparison of different methods by use of Thematic mapper data. Photogrammetria, 42-5/6 311-324.

Kemp, J., Cros. Y., and Prian, J. 1982. Geological map of the Mahd Adh Dhahab Quadrangle, Sheet 23E, Kingdom of Saudi Arabia (Map GM-64, A, B and C). Deputy Ministry for Mineral Resources, Saudi Arabia. Scale 1:250,000.

Kendall, M.G. 1972. A Course on Multivariate Analysis. 5th Edition. Griffin, London.

Killsgard, T.H. 1975. Summary of activities, US Geological Survey, Saudi Arabian Project 1950-1975, U.S. Geological Survey Saudi Arabian Project Report 200, 50pp.

Klecka, W.R. 1975. Discriminant analysis, Ch. 23, p. 434-467. In: SPSSX statistical package for social sciences. (Nie, N.H., Hull, C.H., Jenkins, J.G., Steinbrenner, K, & Brent, D.H. (eds)) McGraw-Hill, New York.

Lee, K. 1985. Interactive digital image analysis of Landsat MSS Images for mapping hydrothermal limonite. 4th Thematic Conference: Remote Sensing for Exploration Geology, San Francisco, California.

Lees, R.D., Bettis, W.R. & Bernstein, R. 1985. Evaluation of Landsat thematic mapper imagery for geological applications. Proc. of the IEEE, vol. 73, no. 6.

Legg, A.C. 1985. Application of the Airborne Thematic Mapper to the Study of Alteration zones at Jabal Said (23/40B). Open File Report DGMR-OF-05-47. Deputy Ministry for Mineral Resources Jeddah, Saudi Arabia.

Lepley L. 1985. Porphyry Copper in Salford Arizona. In Joint NASA/GEOSAT Test Case Study Project. AAPG.

Lillesand, T.M. & Kiefer, R.W. 1987. Remote Sensing and Image Interpretation. John Wiley & Sons - New York.

Longshaw, T.G. 1974. Field spectroscopy for Multispectal Remote Sensing: An analytical approach. Applied Optics, 13(6), 1487-1493.

Longshaw, T.G. 1972. Spectral reflectance measurement for multispectral remote sensing. Proc. Symp. Remote Sensing, Pretoria, 25-31.

Loughlin, W.P. & Tawfiq, M. 1985. Discrimination of Rock Types and Alteration zones from Airborne MSS Data: The Samran-Shayban and Mahd Adh Dhahab areas of Saudi Arabia. Fourth Thematic Conference: Remote Sensing for Exploration Geology, San Francisco, California.

Lowell, J.D. & Guilbert, J.M. 1970. Lateral and vertical alteration - mineralization zoning in porphyry ore deposits. Economic Geology, 65 (4), 373-408.

Luce, R.W., Bagdady, A.Y. & Roberts, R.J. 1975. Geology and ore deposits of the Mahd Adh Dhahab district, Saudi Arabia. U.S. Geological Survey, Saudi Arabia Project Report, SA(IR) - 195.

Markham, B.L. & Townshend, J.R.G. 1981. Land cover classification accuracy as a function of sensor spatial resolution. Fifth Int. Sumposium on Remote Sensing of Environment, Ann Arbor, Michigan, U.S.A.

Milton, E.J. 1987. Principles of field spectroscopy. Int. J. of Remote Sensing, 8(12), 1807-1827.

Munday, T. 1985. Multispectral Remote Sensing of surficial materials in an arid environment. Unpublished Ph.D. Thesis, University of Reading.

Marsh, S. & McKeon, J. 1983. Integrated analysis of high resolution field and airborne spectro-radiometer data for alteration mapping. Economic Geology, 78, 4, 618-632.

Magee, R.W., Moor, J.M. & Brunner, J. 1986. Thematic mapper data applied to mapping hydrothermal alternation in Southwest New Mexico. Fifth Thematic Conference "Remote Sensing for Exploration Geology", Reno, Nevada, U.S.A.

Mayer, C. & Hemley, C. 1967. Wall rock alteration. In: H.L. Barnes (ed.) Geochemistry of hydrothermal ore deposits. Hult, Rinehart & Winston, New York.

Milton, E.J. 1980. A portable multiband radiometer for ground data collection in remote sensing. Int. J. Remote Sensing, 7(2), 153-165.

Mather, P.M. 1976. Computational Methods of Multivariate analysis in Physical geography. Wiley, New York, 532pp.

Mather, P. 1987. Computer processing of remotely-sensed images - An Introduction. John Wiley & Sons, New York.

Mermbeck, B.F. & Turner, B.J. 1980. Directed canonical analysis and the performance of classifiers under its associated linear transformation. IEEE, Trans. Geosci. and Remote Sensing, Vol.EG-18, 190-196.

Markham, B.L. & Townshend, J.R. 1981. Land cover classification accuracy as a function of sensor

spatial resolution. 15th Int. Symp. on Remote Sensing of Environment. Ann Arbor, Michigan, U.S.A.

Minarik, L., Absolon, K., Kollnerova, Z. & Klecka, M. 1983. Chemical changes of granite during its weathering. In: Leaching and diffusion in rocks and their weathering products. Augustithis (ed.). Theophrastus Publications, Athens.

Morrison, D.F. 1967. Mutivariate Statistical Methods. McGraw-Hill, New York.

Mosser, C.H., 1979. Elements traces dans quelques Argiles des alterations et des sediments. In: L.H. Ahrens (Ed.) Origin and distribution of the elements. Pergamon Press, Oxford, 315-329.

NASA, 1972. Data User Handbook for Earth Resources Technology Satellite. NASA, Goddard Space Flight Centre.

Paylor, E.D., Abrams, M.J., Conel, J.E., Kahle, A.B. & Lang, H.R. 1985. Performance evaluation and geological utility of Landsat-4 Thematic Mapper data. NASA/JPL Publication 85-66 Pasadena, California.

Podwysocki, H., Gunther, F.J. & Blodget, H.W. 1977. Discrimination of rock and soil types by digital analysis of Landsat data. NASA TMX-71290.

Podwysocki, M.H., Gunther, F.J., Blodgt, H.W. & Anderson, A.T. 1979. A comparison of rock discriminating capabilities based on present and future Landsat satellite systems - Summaries. Thirteenth International Symposium on Remote Sensing of the Environment.

Podwysocki, M.H., Segal, D.B. & Abrams, M.J. 1983. Use of multispectral scanner images for assessment of hydrothermal alteration in the Marysvale, Utah mining area. Economic Geology, 78, 678-687.

Podwysocki, M.H., Power, M.S. & Jones, O.D. 1985. Preliminary evolution of the Landsat-4 Thematic mapper for mineral exploration. Adv. Space Res. 5(5), 13-20.

Power, R.W., Ramirez, L.F., Redmond, C.D. & Elberg, E.L. (1966). Geology of Arabian Peninsula, sedimentary geology of Saudi Arabia. USGS Professional Paper 5600: 1-147.

Price, C.V., Birnie, R., Logan, T. & Rock, B. 1985. Discrimination of lithological units on the basis of botanical association units and Landsat TM spectral data in the ridge and valley province, Pennsylvania. Fourth Thematic Conference, San Franciso, U.S.A.

Prost, G.L. 1980. Alteration mapping with airborne multispectral scanners. Economic Geology, 75, 894-906.

Pruett, F.D. & Vandenakker, J. 1985. Exploration use of Remote Sensing within the Middle East. Fourth Thematic Mapper Conference, San Francisco, California, U.S.A.

Purdy, T.L. et al. 1985. Use of Thematic Mapper data for alteration and geological mapping in South-central Nevada. Fourth Thematic Mapper Conference, San Francisco, Vol. 2, 631.

Raines, G.L. & Lee, K. 1974. Spectral reflectance measurements. Photogramm. Eng. Remote Sensing, 40, 547-550.

Rehaile, M. & Warden, A.J. 1978. Comparison of the Bir Umq and Hamdan Ultrabasic complexes, Saudi

Arabia. In: Evolution and Mineralization of the Arabian-Nubian Shield. Inst. Appl. Geol. Jeddah. Bull. 3(4), 143-156.

Riofinex Geological Mission. 1984. Jabal Said District overview study. Technical Record RF-TR-01-2 Jeddah, Saudi Arabia.

Robinson, B.F. & Biehl, L.L. 1979. Calibration procedures for measurement of Reflectance factor in remote sensing field research. Soc. of Photo-optical instrumentation engineers, 196, Measurements of optical radiations, 16-26.

Rothery, D.A. 1984. Reflectances of ophiolite rocks in the Landsat MSS bands: relevance to lithological mapping by remote sensing. J. Geol. Soc. Lond. 141, 933-939.

Rothery, D.A. 1987. Improved discrimination of rock units using Landsat Thematic Mapper of the Oman ophiolite. J. Geol. Soc. Lond. 144, 587-597.

Rothery, D.A. & Milton, E.J. 1981. Lithological discrimination in ophiolite terrain: Landsat MSS imagery and reflectance measurements in Oman. In: Allen, J.A. & Bradshaw, M.J. (Eds), Geological and terrain analysis. Applications of remote sensing. Proc. of the 8th Annual Conference of the Remote Sensing Society.

Rowan, L.C. & Abrams, M.J. 1978. Evaluation of Landsat multispectral scanner images for mapping altered rocks in the east Tintic Mountains, Utah. U.S.G.S. Open file Report, 78-736, 73pp.

Rowan, L.C., Goetz, A.M. & Abbott, E. 1987. Analysis of Shuttle Multispectral infrared Radiometer measurements of the western Saudi Arabian Shield. Geophysics, 52(7), 907-923.

Rowan, Goetz A.M., & Ashley, R. 1977. Discrimination of hydrothermally altered and unaltered rocks in visible and near infrared multispectral images. Geophysics, 42(3), 522-535.

Rowan, L.C., Wetlaufer, P.H., Goetz, A.F., Billingsely, F.C. & Stewart, J.H. (1974). Discrimination of rock types and detection of hydrothermally altered area in South Central Nevada by use of computer-enhanced ERTS. U.S.G.S. Professional paper 883, 35p.

Rowan, L.C. & Lathram, E. 1980. Mineral Exploration. In: Remote Sensing in Geology. Siegal, B. & Gillespie A. (eds.) John Wiley in New York, 553pp.

Rowan, L.C. & Kahle, A. 1982. Evaluation of 0.46-2.36um multispectral scanner images of the east Tintic mining district, Utah, for mapping hydrothermally altered rocks. Economic Geology, 77(2), 441-452.

Sabir, H. 1981. Geology and Mineralogy of the Polymetallic sulphide mineralization at Jabal Said, Saudi Arabia. Deputy Ministry for Mineral Resouces, Jeddah, Bulletin 26.

Salisbury, J.W., Hunt, G.R. and Lenhoff, C.J. 1975. Visible and near infrared spectra: X. Stony meteorites. Modern Geology, 5, 115-126.

Settle, M. (Ed.) 1982. Workshop on the use of future multispectral imaging capabilities for lithological mapping. JPL publication 82-93, Pasadena, California.

Siegal, B.S. and Abrams, M.J. 1976. Geological mapping using Landsat Data. Photogramm. Eng. Remote Sensing, 42(3), 325-337.

Siegal, B., & Gillespie, A. (ed.) 1980. Remote Sensing in Geology. John Wiley & Sons, New York.

Siegrist, A.W. and Schnetzler, C.C. 1980. Optimum spectral bands for rock discrimination. Photogramm. Eng. Remote Sensing, vol. 46(9), 1207-1215.

Silva, L. 1978. Radiation and Instrumentation in remote sensing. Chapter in Remote Sensing: Quantitative approach. P. Swain (ed.), McGraw-Hill, New York.

Shih, E.H. & Schowengerdt, R.A. 1983. Classification of arid geomorphic surface using Landsat spectral and textural features. Photogramm. Eng. and Remote Sensing, 49, No. 3, 337-347.

Smith, E.A., Barnes, D.P., Johnson, P.R., Bognar, B., Garfield, L. & Scheibner, E. A review of the Geology Mineralisation and mineral resources potential of the Kingdom of Saudi Arabia. Saudi Arabian Deputy Ministry for Mineral Resouces Open File Report RF-OF-05-1.

Smith, W. (ed.). 1977. Remote Sensing Applications for mineral exploration. Dowding, Hutchinson & Ross, Inc., Stroudsburg.

Soha, J.M. & Schwartz, 1978. Multispectral histogram normalization contract enhancement. The 5th Canadian Symposium on Remote Sensing.

Suits, G.H. 1983. The nature of electromagnetic radiation. In: Colwell, R.V. (ed.) Manual of remote sensing, 1. 37pp. American Society of Photogrammetry.

Sultan, M., Arvidson, R., Sturchio, N. & Guinness, E. 1987. Lithological Mapping in arid regions with Landsat thematic mapper data: Meatiq dome, Egypt. Geological Society of America Bulletin, 99, 748-762.

Sultan, M. & Sturchio, N. 1986. Mapping of Serpentinites in the Eastern District of Egypt by using Landsat thematic mapper data. Geology, 14, 995-999.

Swain, P.H. & Davis, S.M. (eds.) 1978. Remote Sensing: the quantitative approach. McGraw-Hill In. New York, 396pp.

Thaker, F. 1988. Faculty of Earth Sciences, Jedda, Saudi Arabia, Pers. Comm.

Theobald, P.K. Jnr. 1965. Geological Status Report, April 1965, Mahd Adh Dhahab area, Saudi Arabia, US Geological Survey, Saudi Arabian Project Technical Letters 15, Open File Report 11pp.

Townsend, T.E., 1984. Discrimination of Iron alteration Minerals in Remote Sensing Data. Unpublished Ph.D. Thesis, Department of Applied Earth Sciences, Stanford University, USA.

Townshend, J.R.G., 1980. The spatial resolution power of earth resources satellites: a review. Technical memorandum 82020 NASA. Goddard Space Flight Center.

Townshend, J.R.G & Justice, C.O. 1988. Selecting the spatial resolution of satellite sensors required for global monitoring of Land transformations. Int. J. Remote Sensing, 9(2), 187-236.

Twitchell, K.S. 1958. Saudi Arabia with an account of the development of its natural resources. Princeton University Press, 268pp.

Twitchell, S.T. 1983. Weathering and erosion. Butterworths, London.

U.S.G.S. 1984. Preliminary Landsat Image map of the southern Hizaz quadrangle, Kingdom of Saudi Arabia. Saudi Arabian Deputy Ministry for Mineral Resources. Technical Records USGS-TR-04-6, Scale 1:500,000.

U.S.G.S. 1984. Landsat Image map of the AlMadinah quadrangle, sheet 24D, Kingdom of Saudi Arabia.

Saudi Arabian Deputy Ministry for Mineral Resources Open File Report USGS-OF-02-80, Scale 1:250,000.

Vincent, R.K. & Thompson, F.J. 1972. Rock type discrimination from ratioed infrared scanner images of Pisgah Crater, California. Science, 175, 986.

Whitney, G., Abrams, M. & Goetz, A. 1983. Mineral Discrimination using a portable Ratio-Determining Radiometer. Economic Geology, 78(4), 688-698.

Wiersma, D.J. & Landgrebe, D.A. 1978. The analytical design of spectral measurement for multispectral remote sensor systems. LARS Tech. Report 122678. West Lafayette, Indian, Laboratory for Applications of Remote Sensing.

Worl, R.G. 1979. Ore Controls at the Mahd Adh Dhahab gold mine, Kingdom of Saudi Arabia. In: Evolution and Mineralization of the Arabian-Nubian Shield: King Abdulaziz Unviersity, Institute of Applied Geology, Bulletin 3, v. 2. Pergammon Press, Oxford & New York, 93-106.

APPENDICES

APPENDICES

Appendix A1	MSS
Appendix A2	TM
Appendix A3	ATM
Appendix B	IRIS
Appendix C	HHRR
Appendix D	Detailed spectra for lithologies in Mahd Adh Dhahab.
Appendix E	Detailed spectra for lithologies in Jabal Said.

APENDIX A1

LANDSATS 1, 2 and 3

ch:
sat 1: 23 July 1972
eration ended: 6 January
'8
sat 2: 22 January 1975
eration ended:
February 1982
sat 3: 5 March 1978
ndby mode: 31 March
3

al parameters:
: near polar
synchronous
de: 919 km
ation: 99.09°.
rage: 82°N to 82°S.
d: 103 minutes, crossing
equator at 9.30hrs local
e.
at cycle: 18 days.

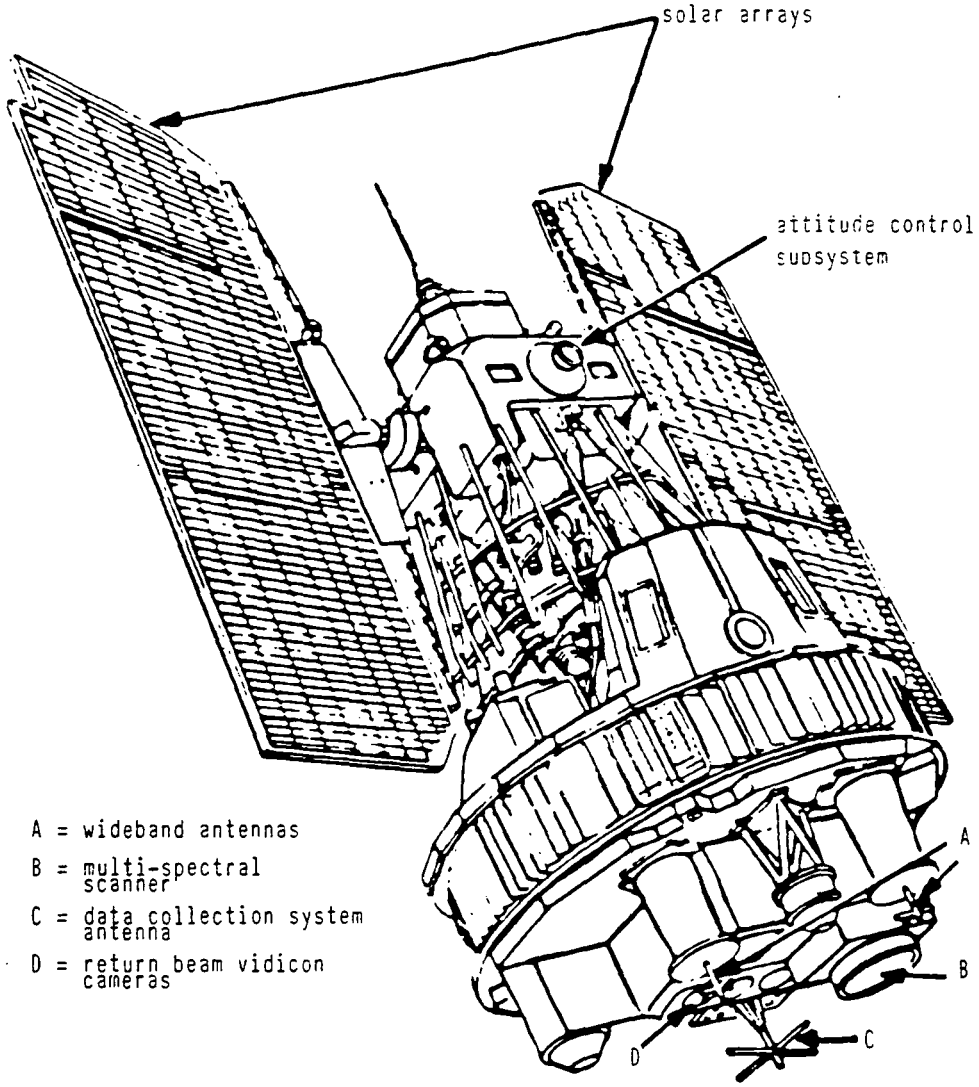

llites and sensors

sat-1 was the first satellite
ned to collect data about the
s surface and resources.
satellites, initially called
Resources Technology
ites (ERTS), launched by
A between 1972 and 1978
rised the first generation of
ndsat series.

atellites' payload consisted
o sensors:

urn beam vidicon (RBV)
neras

our band multi-spectral
nner system (MSS)

ata were either transmitted
y to specially equipped
d stations or stored on tape
lers for later transmission to
entres in the U.S.A. The
at receiving stations
ng the U.K. and Europe are
ino in Italy and Kiruna in
en, both are part of the
net programme.

Return Beam Vidicon Camera (RBV)

	Wavelength (μm)	Resolution	Image format and comments
Landsats 1 and 2 – three RBVs:			Simultaneous view from three cameras of a scene 185 x 185 km with 14% side overlap at the equator and 10% forward overlap.
Band 1	0.475-0.575 (blue-green)	80m	
Band 2	0.580-0.680 (yellow-red)	80m	
Band 3	0.690-0.830 (red-near IR)	80m	
Landsat 3 – two RBVs, single band:	0.505-0.750 (visible to near IR – panchromatic)	40m	Two side-by-side images, 98 x 98km, four RBV images approximately coinciding with scene.

Multi-spectral Scanner (MSS)

	Wavelength (μm)	Resolution	Image format and comments
Landsats 1, 2 and 3:			185 x 185km images with 10% forward overlap and 14% side overlap at the equator, increasing towards the poles.
Band 4	0.50-0.60 (green)	80m	
Band 5	0.60-0.70 (red)	80m	
Band 6	0.70-0.80 (red-near IR)	80m	
Band 7	0.80-1.10 (near IR)	80m	
Landsat 3 only:			Range of thermal sensitivity: Only a few scenes available of limited area.
Band 8	10.40-12.50 (thermal IR)	120m	

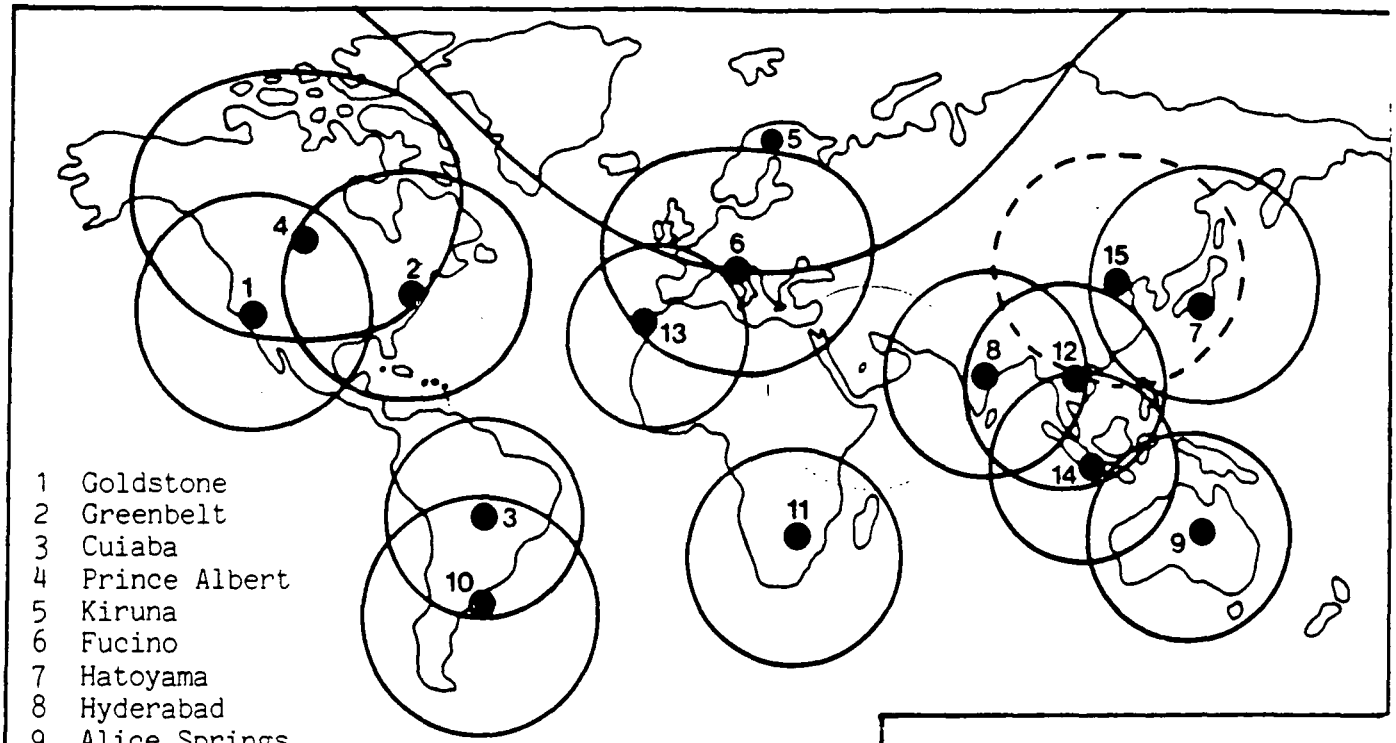

Landsat receiving stations.

The first generation of Landsat satellites were launched into a sun synchronous, near-polar orbit, at an altitude of approximately 900km. The angle between the Sun, the centre of the Earth and the satellite was maintained at 37.5° as the Earth orbits the Sun, and the orbital plane is inclined at 99° to the equator. This type of orbital configuration ensures repeatable sun illumination conditions, aiding the comparison of yearly changes in vegetation and mosaicing of adjacent tracks.

The satellite crosses the equator every 103 minutes. During this time, the Earth rotates a distance of 2760km under the satellite at the equator. When the satellite has completed 14 orbits, 24 hours has elapsed and the next westward track of data is acquired. In 18 days one satellite obtained coverage of nearly the entire Earth's surface, weather conditions permitting. The coverage pattern and overhead crossing time of one Landsat satellite during the period 1972 to 1983 are shown on the adjacent map. When two satellites were operational they were positioned nine days apart to allow a regular and more frequent data acquisition capability.

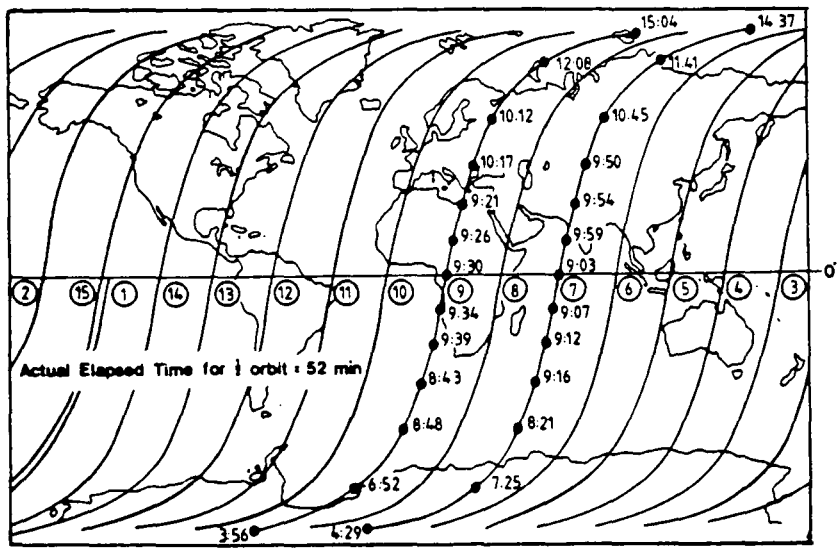

Landsat orbital tracks for one day of coverage indicating variations in local time of data acquisition.

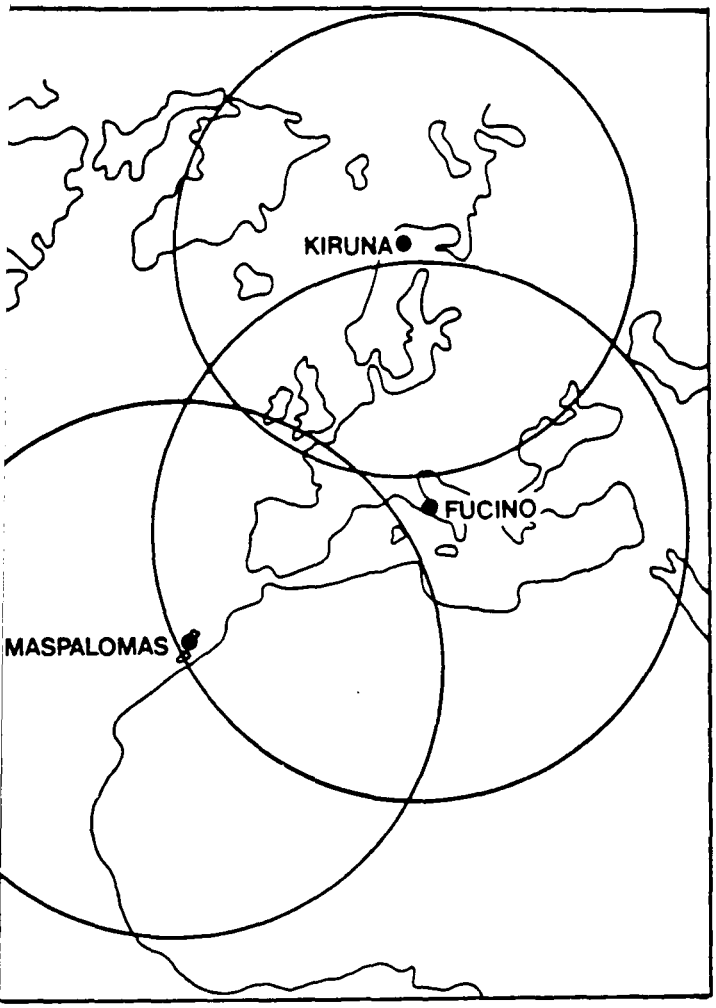

Applications

The main application fields of the individual MSS bands were identified as:-

Band 4: mapping of sediment ladened water and delineation of shoals and reefs in shallow water.

Band 5: identification of cultural features – urban areas, roads, etc.

Band 6: vegetation studies and delineating boundaries between landforms, land and water.

Band 7: vegetation mapping and water/land separation. This band provides the best penetration of atmospheric haze.

Applications of Landsat data have been widespread in many fields, including:

- geology
- mineral and petroleum exploration
- forestry and agriculture
- hydrology
- coastal processes
- land use and land cover
- mapping environmental changes
- resources inventories
- pollution monitoring

The best use of satellite data such as that from the Landsat missions, has been made when the imagery is interpreted in conjunction with existing information and good ground knowledge of the area under investigation.

Data acquisition

The National Remote Sensing Centre is able to acquire Landsat data from the Earthnet coverage area outside the U.K., from the U.S. data centres and also from individual ground stations and centres around the world. Accounts are held at certain data centres to permit the acquisition of imagery in the shortest possible time.

Data coverage

Coverage maps for both Landsats 1, 2 and 3 and Landsats 4 and 5 are included in Appendix 1, superimposed on these maps are the scenes held within the NRSC archive. A full listing of these scenes is provided in Appendix 2 with details of path/row, sensor, acquisition date, cloud cover, scene centre and country location.

NRSC archive

The Landsat archive at the National Remote Sensing Centre is one of the largest digital data archives outside of the U.S.A. It mainly comprises data from the Earthnet ground stations, as it is NRSC policy to acquire all cloud-free or low cloud cover scenes of the U.K. However, over recent years the worldwide archive has also been expanded.

Both digital data and photographic products can be supplied from the NRSC. The various products and services available are described elsewhere in the Data Users Guide, but for further information and price lists contact the NRSC.

EARTHNET PRODUCTS

Digital products

0100 MSS (Multispectral Scanner) raw data CCT (Computer compatible Tape)

MSS System Corrected CCT

0200 With absolute radiometric corrections
0201 With statistical radiometric corrections
0202 With both absolute and statistical corrections
0300 RBV (Return Beam Vidicon) CCT one subscene (number 1, 2, 3 or 4 upper left, upper right, lower left, lower right)
0400 Copy CCT ordered together with first CCT

Photographic products

MSS quick-look print

0601 Single print (one scene)
The Quick look hard copy print is an uncorrected band 7 (or band 4 for Landsat-4 and -5) image; scale is approximately 1:1.500.000. Its main purpose is the evaluation of cloud content and radiometric quality of the image.
0602 Yearly subscription, set of prints of one scene, all passes of the year. The yearly Q/L subscription relates to all passes over a given scene for the year in question. With an 18-day Landsat 1-2-3 cycle (or a 16-day Landsat 4-5 cycle) this means on average 20 prints.

B/W MSS Images (per band)

0801 240mm print scale 1:1.000.000
0802 Additional copy of 0801
0803 240mm film positive scale 1:1.000.000
0804 Additional copy of 0803
0805 240mm film negative scale 1:1.000.000
0806 Additional copy of 0805
0807 480mm print scale 1:500.000
0808 Additional copy of 0807
0809 480mm film positive scale 1:500.000
0810 Additional copy of 0809
0811 960mm print scale 1:250.000
0812 Additional copy of 0811

B/W RBV Images (per subscene)

Available in either positive or negative form the images relate to a 99 x 99km subscene.

0901 240mm print
0902 Additional copy of 0901
0903 240mm film positive
0904 Additional copy of 0903
0905 240mm film negative
0906 Additional copy of 0905
0907 480mm print
0908 Additional copy of 0907
0909 480mm film positive
0910 Additional copy of 0909
0911 960mm print
0912 Additional copy of 0911

MSS colour composites

(bands 4-5-7 or 4-6-7: Landsat 1-2-3)
(bands 1-2-4 or 1-3-4: Landsat 4-5)

1001 240mm print, full price
1002 240mm print, reduced price
1003 240mm film positive, full price
1004 240mm film positive, reduced price
1005 480mm print, full price
1006 480mm print, reduced price
1007 960mm print, full price
1008 960mm print, reduced price

This table also refers to Landsat 4 and 5 MSS products.

APENDIX A2

LANDSATS 4 and 5

.aunch:
.andsat 4: 16 July 1982
.andsat 5: 1 March 1984

)rbital parameters:
)rbit: near polar
sun synchronous
\ltitude: 705 km
nclination: 98.2°.
Coverage: 81°N to 81°S.
'eriod: 99 minutes, crossing the equator at 9.45hrs local time.
Repeat cycle: 16 days.

Satellites and sensors

The second generation of NASA's andsat series was initiated in uly 1982 with the launch of andsat 4. In addition to the onventional multi-spectral canner system (MSS – four vavebands and 80m ground esolution) familiar to all users of he earlier Landsats, the payload ncluded the Thematic Mapper TM), which recorded data in even wavebands with a esolution of 30m in the visible, ear and middle infra-red vavebands and 120m in thermal nfra-red. Unfortunately power upply problems terminated the eception of TM data in February 983, although MSS acquisition ontinues. However, Landsat 5 as launched on 1 March 1984 nd both MSS and TM sensors, re operational.

Multi-Spectral Scanner

he MSS on Landsats 4 and 5 are milar to those flown on earlier andsat missions. The ground ixel resolution is 80 by 80m. owever, the four spectral bands re identified by a new numbering ystem – although the spectral overage remains unchanged.

Landsats 1, 2 and 3		Landsats 4 and 5
Band 4	→	Band 1
Band 5	→	Band 2
Band 6	→	Band 3
Band 7	→	Band 4

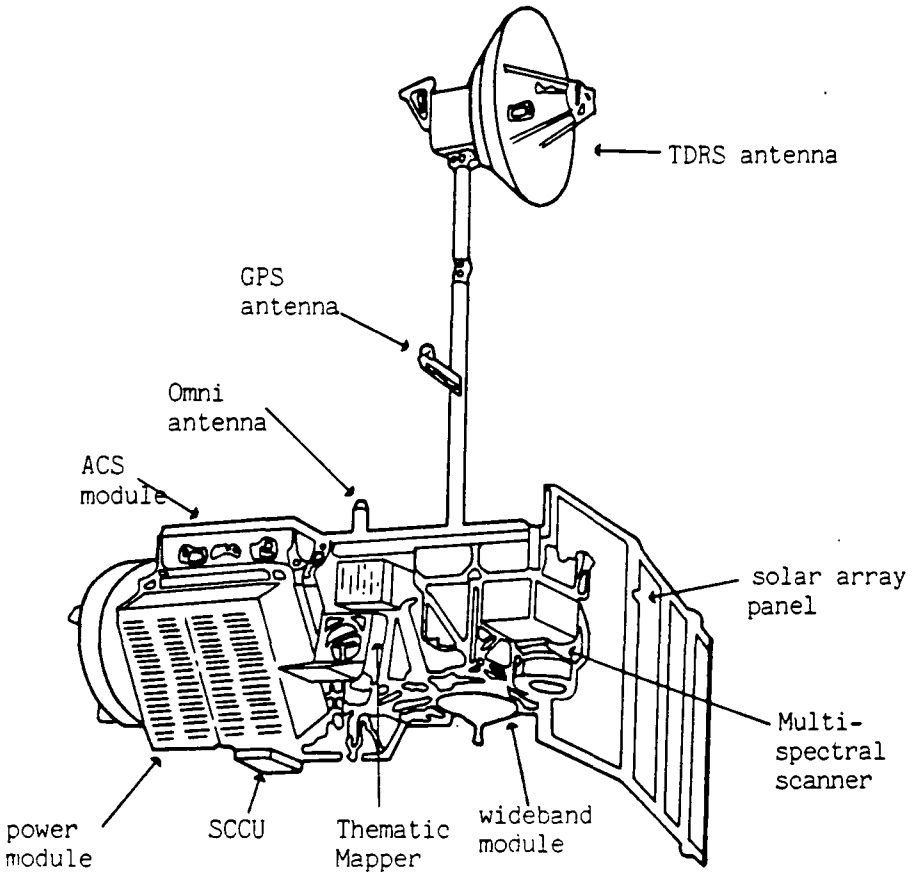

Multi-Spectral Scanner (MSS)

	Wavelength (μm)	Resolution
Band 1	0.50-0.60 (green)	80m
Band 2	0.60-0.70 (red)	80m
Band 3	0.70-0.80 (red-near IR)	80m
Band 4	0.80-1.10 (near IR)	80m

Thematic Mapper

	Wavelength (μm)	Resolution
Band 1	0.45 - 0.52	30m
Band 2	0.52 - 0.60	30m
Band 3	0.63 - 0.69	30m
Band 4	0.76 - 0.90	30m
Band 5	1.55 - 1.75	30m
Band 6	10.40 - 12.50	120m
Band 7	2.08 - 2.35	30m

Both sensors provide image data with 185 x 185km coverage, with 5.4% forward overlap and 7.3% side overlap at the equator increasing at higher latitudes.

Orbit

The orbital configuration of the satellites creates a 16-day repeat cycle for each satellite. In other words, a specific satellite will travel along a particular ground track once every 16 days. The orbits of the two satellites are eight days out of phase. For either one of these satellites, the time interval between adjacent tracks is seven days. This arrangement contrasts with the 18-day orbital cycles of the first three Landsat satellites which resulted in a one day interval between orbits over adjacent tracks.

The MSS and TM sensors are aligned to scan the same geographical area of 185km wide directly below the oribtal path of the satellite.

There is a minimum side lap of 7.3% between adjacent orbits at the equator, increasing to a maximum of 84% at 80°N/S.

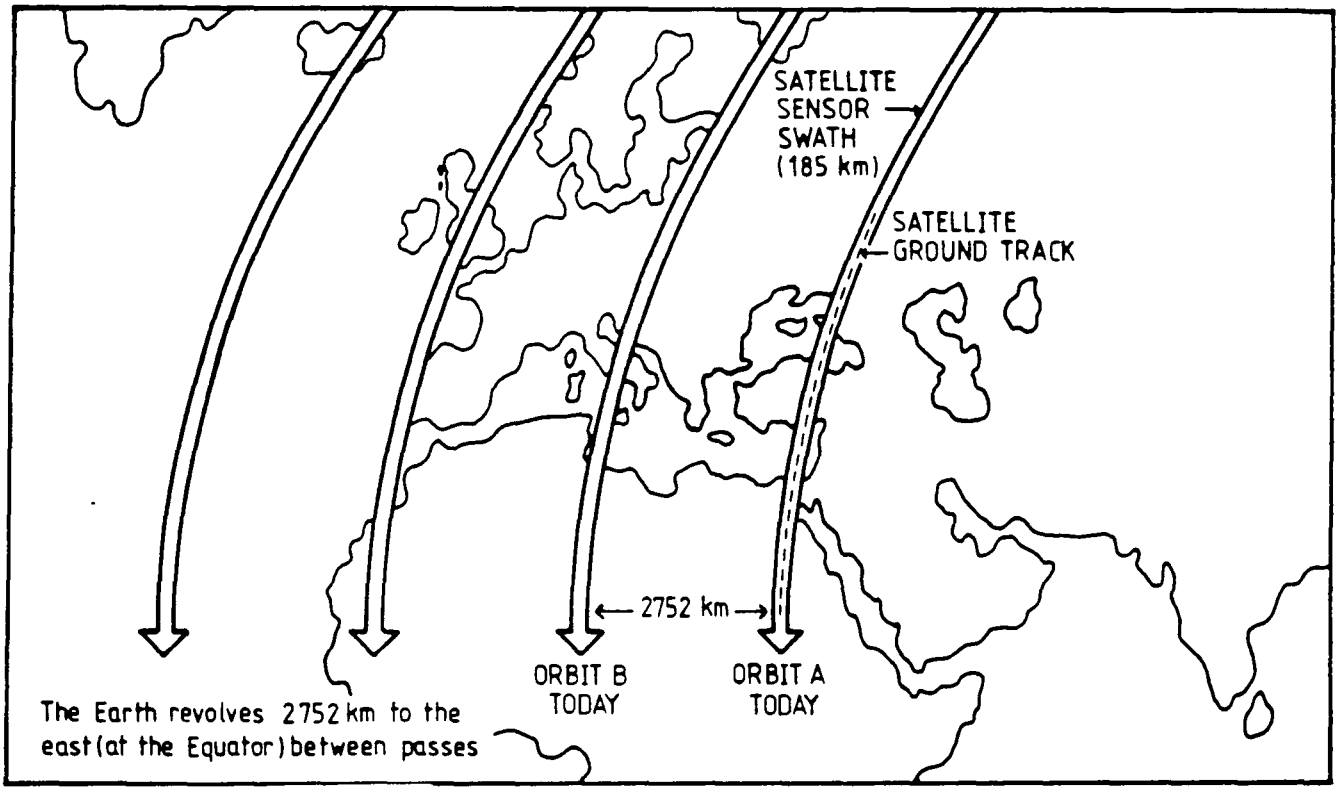

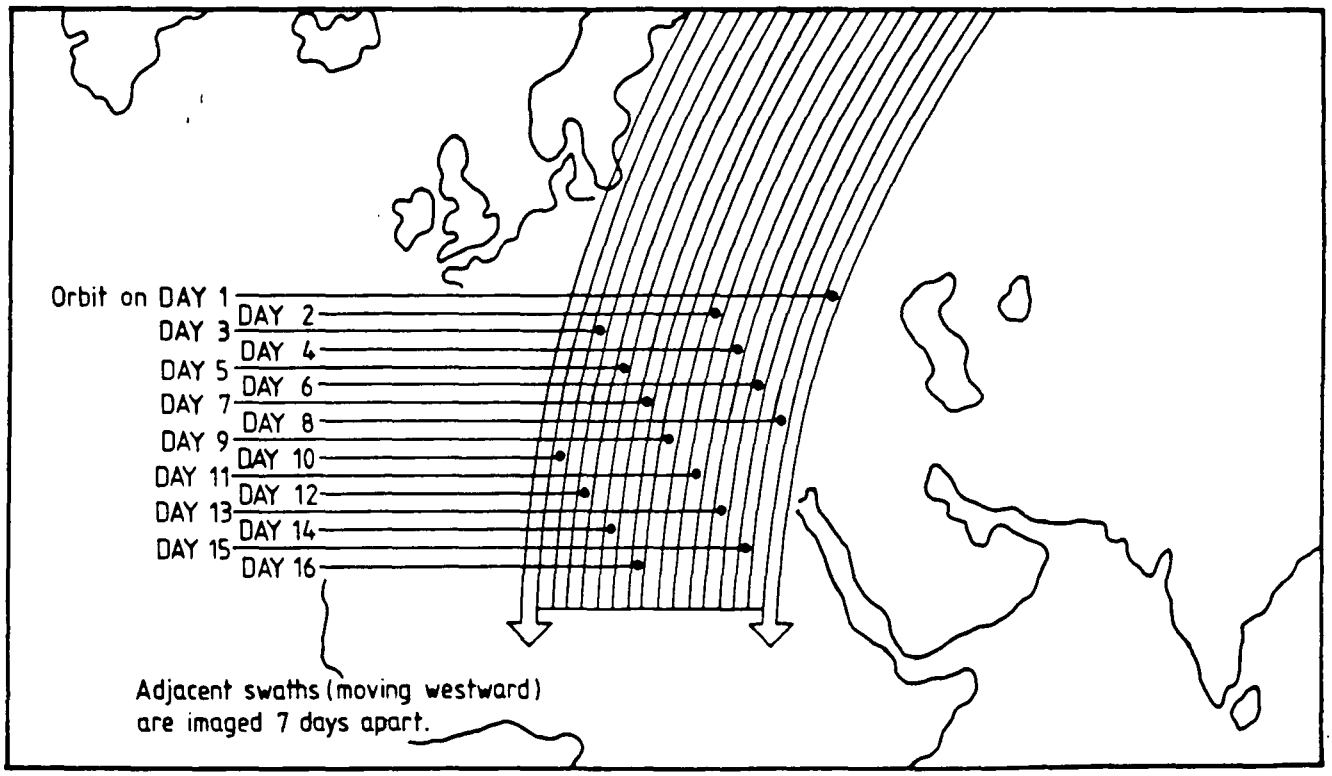

overage

ndsat 4 and 5 pass over the same ground track ter completing 233 orbits of the Earth. This orbital peat cycle is incompatible with the 251-orbit orldwide Reference System (WRS) used to index SS data from the previous Landsat satellites. A ew system of path and row indices has been esigned for both MSS and TM data from Landsat 4 nd 5. A path index number is assigned to the ound track of each orbit. The new system consists 233 orbital paths numbered east-to-west with the ntre point of path 001 crossing the equator at .95 degrees west longitude. The data for each ene consist of the data acquired during a .87-second increment of the orbital motion of the tellite. This increment corresponds to pproximately 5700 scan lines of image data. Both e MSS data and the TM data for each scene cover surface area approximately 170km along-track by 5km across-track. A row index is assigned to each ene centre. Row one of each path starts at 80°51′ rth latitude and the numbering increases uthward through the equator (row 60) to 81°51′ uth latitude (row 122). The satellites then travel rthward for the ascending (night time) portion of ch orbit, and row numbers increase from south-to-rth through the equator (row 184) to 81°51′ north titude (row 246). Thus, row indices 123 through 6 refer to scenes of night time TM thermal data hich are not acquired on a routine basis.

The first three Landsat satellites relied upon onboard tape recorders to store data until the satellite passed within range of a ground station. These recorders were often the first component to fail. Landsat 4 and 5 use a new communications system, called the Tracking and Data Relay Satellite System (TDRSS), which eliminates the need for onboard recorders. TDRSS will eventually consist of two satellites (plus an in-orbit spare satellite) in geosynchronous orbits and a centralised ground receiving station located at White Sands, New Mexico. The first TDRSS satellite (TDRS-East) was launched on April 4, 1983 aboard NASA's space shuttle Challenger (mission STS-6). After overcoming problems caused by a malfunction of its booster rocket, the satellite reached its permanent station on October 17, 1983. TDRS-East is currently in geosynchronous orbit over the equator at 41° west longitude at an altitude of 35,890km.
for launch

The second TDRSS satellite was lost on board the Challenger disaster in January 1986 – further setting back an urgent programme that was already delayed by a year.

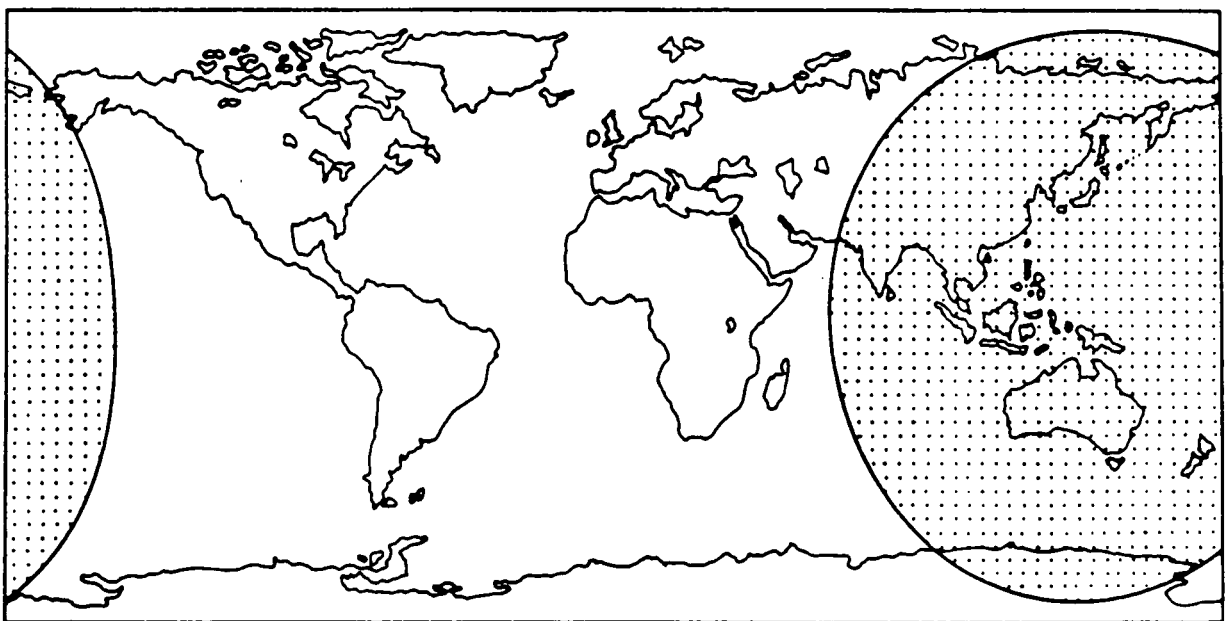

Shaded area indicates regions where data acquisition via TDRS-East is not possible

Thematic Mapper

Several major differences exist between the basic design of the MSS and the design of the TM. First, the TM acquires data during both the forward (west-to-east) and reverse (east-to-west) sweeps of its scan mirror. This bidirectional approach was adopted to reduce the rate of oscillation of the scan mirror and increase the dwell time of individual detectors upon the Earth's surface.

The TM does not rely on fibre optics, as does the MSS, to direct incoming electromagnetic energy onto photosensitive detectors. Fibre optics are incapable of transmitting 100 per cent of the incident energy from the focal plane to the sensor's detectors. Instead the TM focuses incident radiation directly onto detectors within a prime focal plane assembly. This assembly contains four sets of 16 detectors for four spectral bands in the visible and near infra-red portions of the spectrum. A cooled focal plane assembly contains two arrays of 16 indium antimonide (InSb) photodiodes for two middle infra-red spectral bands and four mercury cadmium telluride (HgCdTe) detectors for a thermal band.

The use of multiple detectors for each spectral band results in the generation of 16 scan lines of data for the six reflective bands and four lines of data for the thermal band during each sweep of the scan mirror. At any one instant, surface radiance is sensed by a total of 100 TM detectors.

The TM also offers improved radiometric sensitivity over the MSS, even though the spectral bandwidth and the IFOV of the TM detectors is significantly less than that of the MSS. In conjunction with the improved sensitivity, TM data are quantised to eight bits (256 digital counts) while MSS data are quantised to six bits (64 digital counts). This effectively corresponds to a four-fold increase in the grey scale being used to measure the intensity of Earth radiation in each discrete spectral band.

Applications

Band

- **1** Sensitive to chlorophyll and cartonoid concentrations for soil/vegetation differentiation, deciduous/coniferous differentiation. Coastal water mapping.
- **2** Sensitive to green reflectance by healthy vegetation.
- **3** Sensitive to chlorophyll absorption for plant species differentiation.
- **4** Sensitive to near infra-red reflectance of healthy vegetation for biomass surveys.
- **5** Sensitive to vegetation moisture and snow/cloud reflectance differences.
- **6** Thermal mapping.
- **7** Sensitive to vegetation moisture and to hydroxyl ions in minerals for geological mapping.

The TM acquires data in seven spectral bands. Four of these bands are located in portions of the spectrum not sensed by the MSS. The location and width of the seven bands were carefully chosen for sensitivity to certain natural phenomena and to minimise the attenuation of surface energy by atmospheric water. The table lists the spectral bands along with the rationale for selecting each band.

Another advanced feature of the TM is its spatial resolution. The TM instantaneous-field-of-view (IFOV) is 30m x 30m for the six reflective spectral bands (bands TM1 to TM5 and TM7) and 120m x 120m for the thermal band (band TM6). The MSS provides a resolution of approximately 80m x 80m in all bands.

EARTHNET PRODUCTS
THEMATIC MAPPER-TM-data
(LANDSAT 4-5)

Digital products

Raw data
1101 CCT full scene
1102 CCT quarter scene (1, 2, 3 or 4, left-right, left-right)
1103 CCT full scene, one band

System Corrected data
1201 CCT full scene
1202 CCT quarter scene (1, 2, 3 or 4, left-right, left-right)
1203 CCT full scene, one band

Photographic products

Quick-look print
1301 per print
1302 yearly subscription, set of prints of one scene, all passes of the year

TM B/W Images (full scene or quarter scene)
1401 240mm print
1402 Additional copy of 1401
1403 240mm film positive
1404 Additional copy of 1403
1405 240mm film negative
1406 Additional copy of 1405
1407 480mm print
1408 Additional copy of 1407
1409 480mm film positive
1410 Additional copy of 1409
1411 960mm print
1412 Additional copy of 1411

TM Colour composites
1501 240mm print
1502 240mm film
1503 480mm print
1504 960mm print

APENDIX A3

Airborne Thematic Mapper

AADS1268

ATM

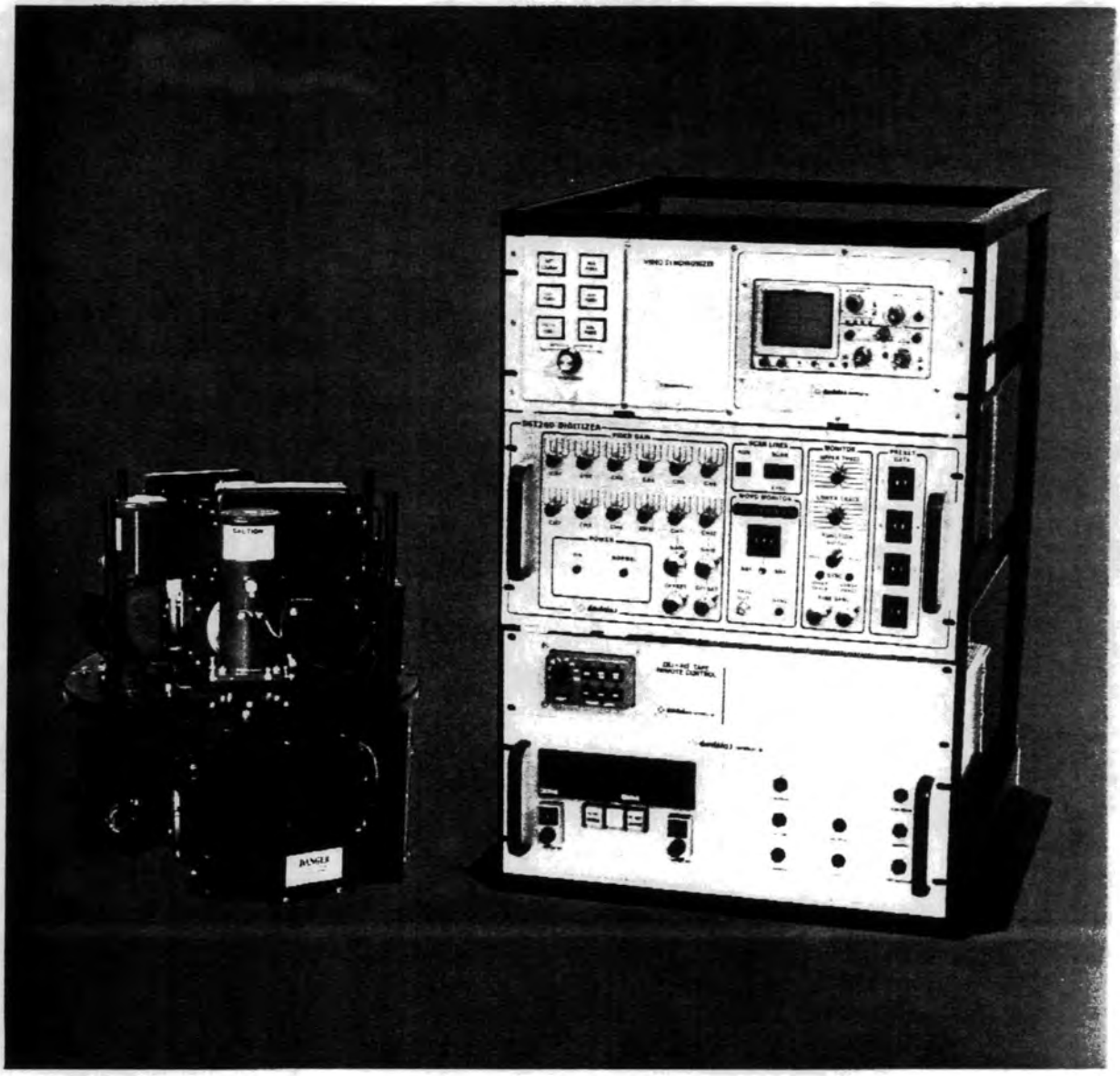

DAEDALUS ENTERPRISES, INC. P.O. Box 1869, Ann Arbor, Michigan 48106 TELEX 230530

daedalus

Daedalus Airborne Thematic Mapper Scanner

Daedalus offers a totally new scan head configuration to acquire data in the NASA-selected thematic mapper bands and to achieve a highly versatile foundation for the multispectral research requirements of the 1980's. The Daedalus system (designated the AADS1268), Airborne Thematic Mapper (ATM), combines this state of the art scan head with proven electronic assemblies of the AADS1260 system.

The prototype scan head was flown operationally for the first time in October 1981, during an extensive high altitude data acquisition program in the western United States.

At an altitude of 12.5 kilometers, the ATM spatial resolution of 2.5 milliradians produces approximately the same pixel size as the Landsat-D Thematic Mapper (30 meters x 30 meters).

Sophisticated image processing of ATM data collected over semiarid terrain enables geologists to obtain important new information for petroleum and mineral exploration. Whereas properly processed Landsat 1, 2 and 3 data can be used to map iron oxides, ATM can be used to segregate iron oxides into primary and secondary categories, as well as to map surface exposures of clay minerals. Since both secondary iron oxides and clay minerals are associated with basic metal deposits, the ATM offers exciting new capabilities for gold, silver, uranium, copper, lead, zinc, and other metal exploration. It also offers new capabilities for mapping surface soil alterations and vegetative anomalies which are sometimes related to ancient oil and gas seeps.

Daedalus customers who own AADS1260 Digital MSS Systems can convert to an AADS1268 ATM configuration; however, this configuration must be accomplished at the Daedalus facilities in Ann Arbor, Michigan, U.S.A.

Major improvements offered in the AADS1268 are:

1. Versatile optical design, which can accommodate a great variety of combinations of spectrometer configurations as future needs arise.
2. Precise registration of pixels from all channels.
3. Combination of spectral bands, e.g., thematic mapper bands, not previously achievable.
4. Optional 1.25 mrad IFOV field stop aperture assembly.
5. Higher performance optics and coatings.
6. Improved laboratory calibration equipment.

The first production AADS1268 was delivered to NASA Ames in March 1982, as a modification of their AADS1260 System, for 1.25 mrad operation in their Lockheed ER-2 high altitude research aircraft.

The principal AADS1268 system specifications for a 2.5 mrad configuration are as follows:

OPERATING WAVELENGTHS AND PERFORMANCE PARAMETERS

Channel Band Edges in μm	12.5 scans/sec.		50 scans sec.	
	NER[1]	NEΔρ[2]	NER[1]	NEΔρ[2]
0.42 - 0.45	< 1.0	< 0.5	< 2.0	< 1.0
*0.45 - 0.52	< 0.2	< 0.1	< 0.5	< 0.2
*0.52 - 0.60	< 0.15	< 0.05	< 0.3	< 0.15
0.605 - 0.625	< 0.3	< 0.15	< 0.5	< 0.2
*0.63 - 0.69	< 0.2	< 0.06	< 0.3	< 0.1
0.695 - 0.75	< 0.2	< 0.2	< 0.3	< 0.2
*0.76 - 0.90	< 0.1	< 0.1	< 0.2	< 0.2
0.91 - 1.05	< 0.3	< 0.3	< 0.5	< 0.5
*1.55 - 1.75	< 0.15	< 0.3	< 0.3	< 0.7
*2.08 - 2.35	< 0.05	< 0.3	< 0.1	< 0.7
*8.5 - 13.	< 0.2°C NEΔT[3]		< 0.3°C NEΔT[3]	

* Thematic Mapper Bands, except thermal band broadened for airborne operation.

① Noise Equivalent Radiance in $Wx10^{-7}$-cm^{-2}-nm^{-1}-sr^{-1}.

② Noise Equivalent Reflectance Change (in %) P. Moon Value: Ref: NASA Tech. Paper #1575, Dec. 1979.

③ Noise Equivalent Temperature Change.

Instantaneous Field of View (IFOV)	2.5 mrad (1.25 mrad optional)
Digitized Field of View	85.92° (2.5 mrad IFOV) or 42.96° (1.25 mrad IFOV)
Scan Rate	12.5; 25; 50 scans sec.
Velocity Height Ratio	0.031; 0.062; 0.125 radians sec. corresponding to 12.5; 25; and 50 scans sec., respectively (2.5 mrad IFOV)
Roll Correction	± 15°
Infrared Reference Source	2 controllable thermal blackbodies with a temperature range of − 15°C to + 50°C with respect to scan head heat sink temperature.

PHYSICAL DIMENSIONS:

AADS1268 Scanner System:	HEIGHT in.	HEIGHT cm	WIDTH in.	WIDTH cm.	DEPTH in.	DEPTH cm.	WEIGHT lbs.	WEIGHT kg.
Scan Head w/Spectrometer (AB115/AB180)	18	45	16	40	16	40	100	46
Operator Console (AB244A)	7	18	19	48	14	34	25	11.4
Power Distributor/Reference Controller (ABDE221)	7	18	19	48	19	48	38	17.3
Digitizer (ABDE260)	8.75	22	19	48	19	48	59	27
Data Recording System:								
Tape Machine (14-Track) (typical)	21.3	54	17.5	44.5	10.2	26	85	39

ENVIRONMENTAL CONDITIONS:

	TEMPERATURE	HUMIDITY (Non-Condensing)	ALTITUDE
Scan Head (Operating)	− 55°C to + 70°C	0-95%	0-50,000 ft. (15,000m)
Electronics (Operating)	+ 10°C to + 50°C	0-95%	0-15,000 ft. (4,000m)
Electronics (Non-operating)	− 40°C to + 70°C	0-95%	0-15,000 ft. (4,000m)

TOTAL SYSTEM POWER REQUIRED:

AADS1268 Scanner System	28 volts DC/45 amps.
Tape Machine (14-Track)	28 volts DC/10 amps.

Daedalus Enterprises, Inc.
P.O. Box 1869
Ann Arbor, MI 48106

Telex — 230530
Phone — 313-769-5649

APENDIX B

IRIS

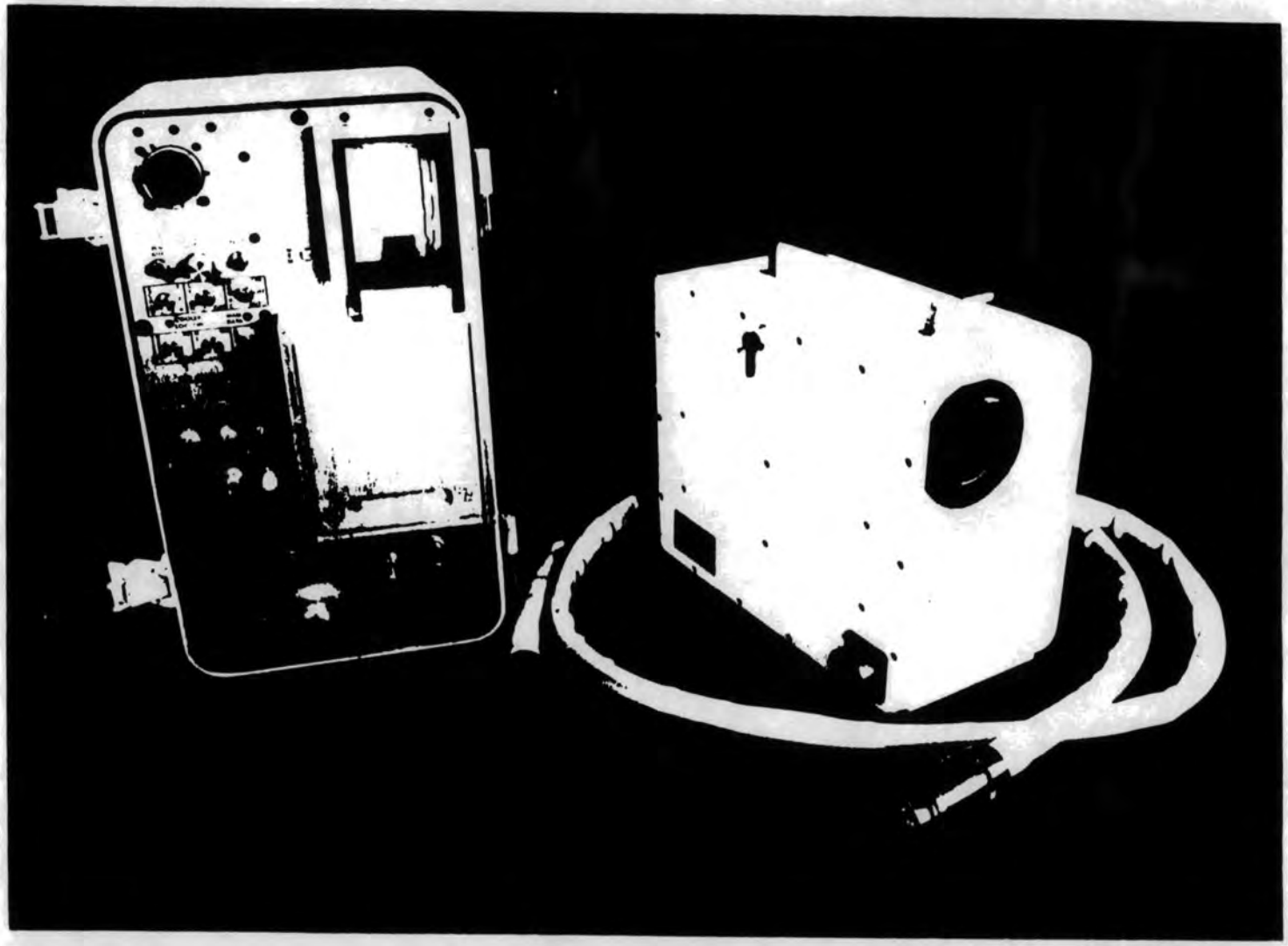

Figure 1. The Geophysical Environmental Research Inc. IRIS Mk IV Spectrometer.

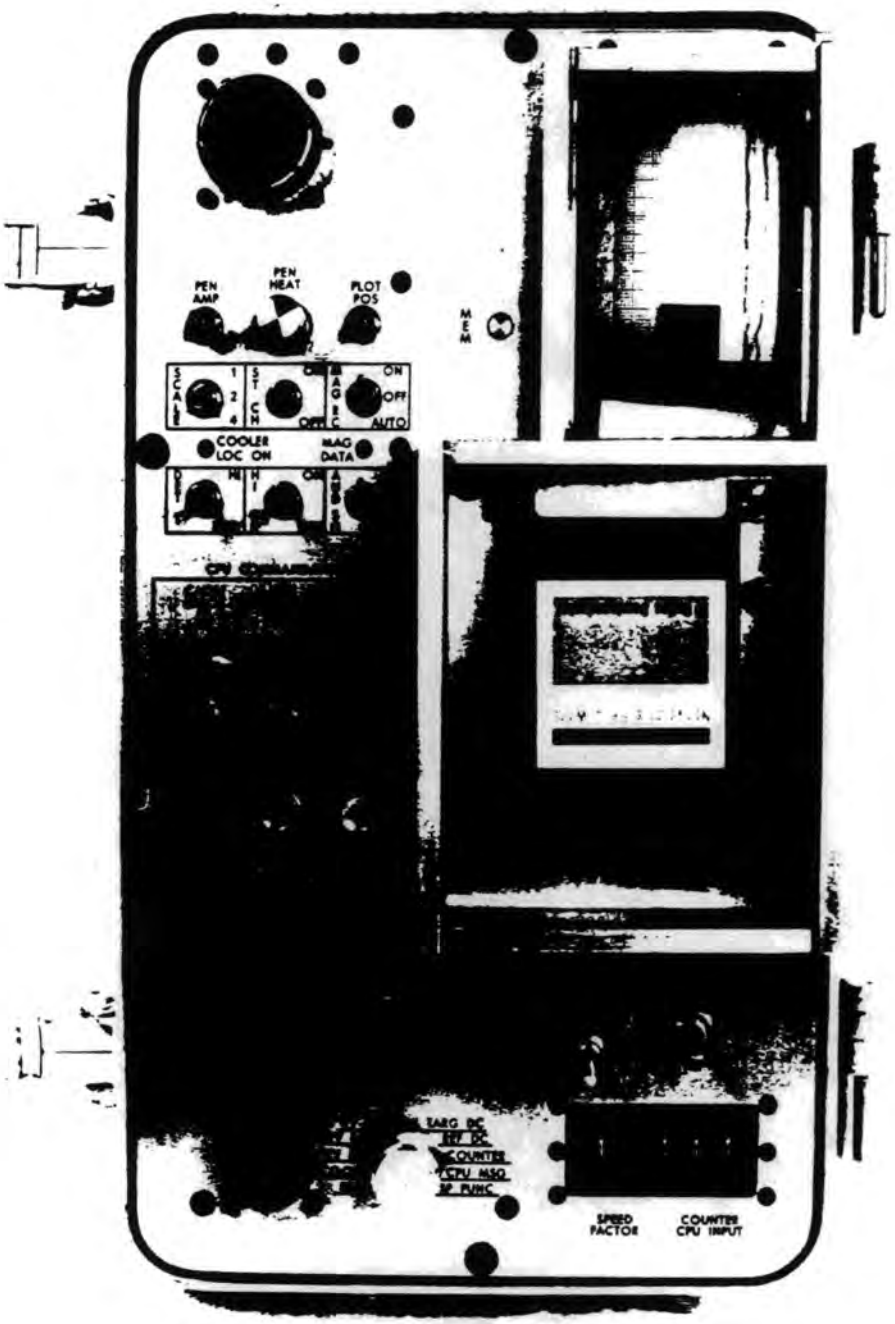
PEN AMP
PEN HEAT
PLOT POS
MEM
SCAN
ST CH
MAG DC
ON
OFF
AUTO
COOLER LOC ON
MAG DATA
SPEED FACTOR
COUNTER CPU INPUT

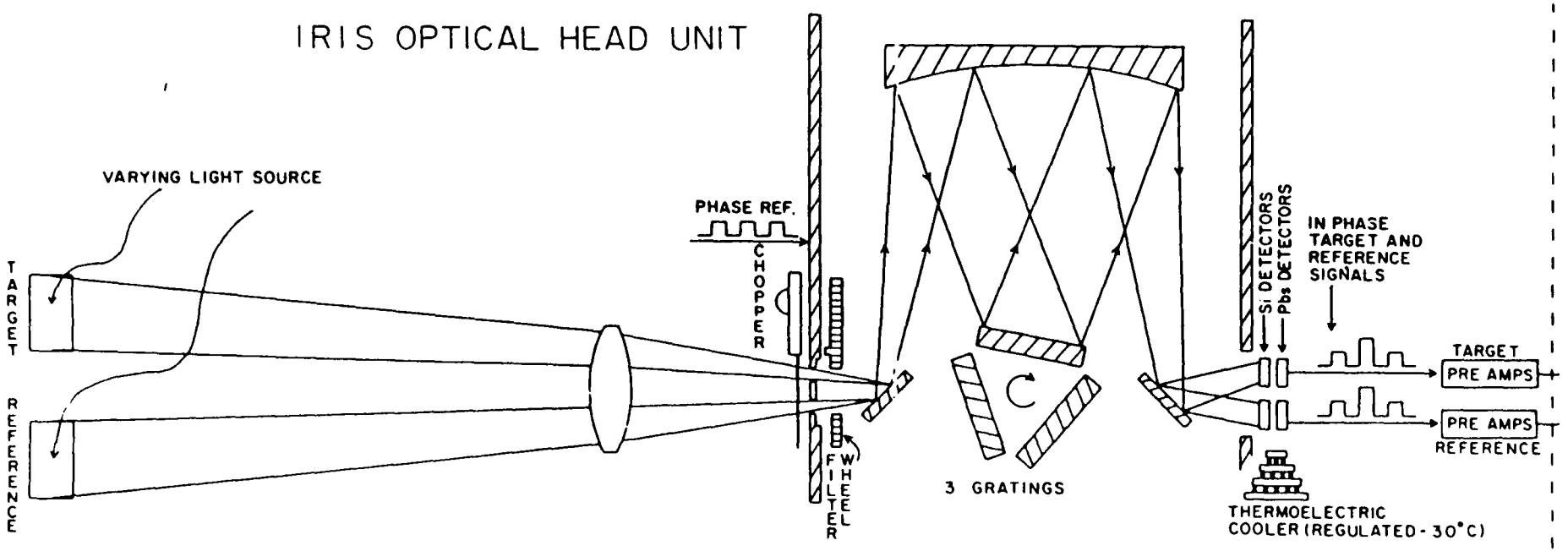

Figure 2. Schematic diagram of the IRIS Optical Head.

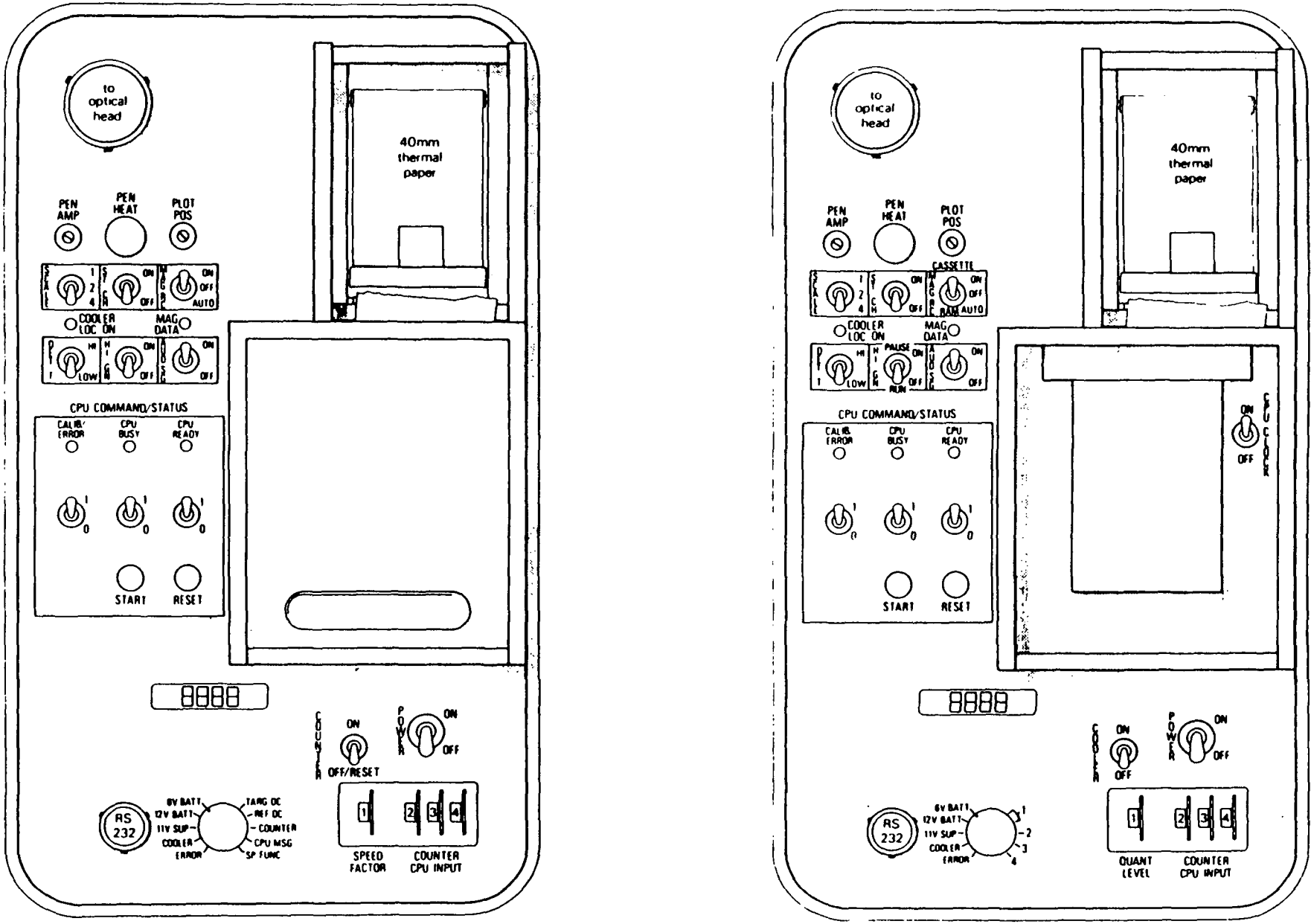

Figure 3. The IRIS Mk IV Control Unit. a) External details.

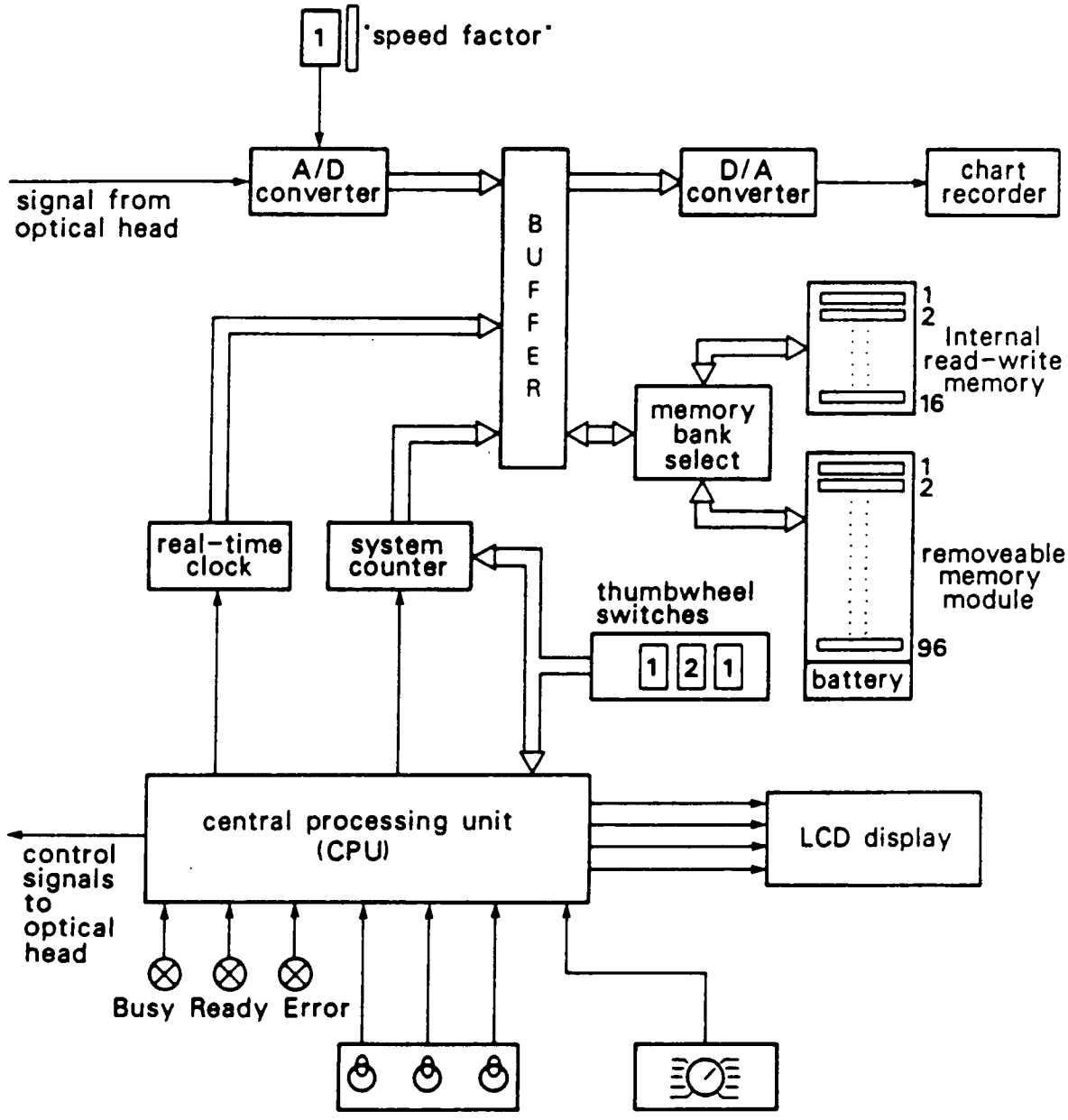

Figure 3. The IRIS Mk IV Control Unit. b) Internal schematic.

APENDIX C

HHRR

BARRINGER RESEARCH

RATIOING RADIOMETER*
Hand Held Reflectance Radiometer for the Earth Sciences

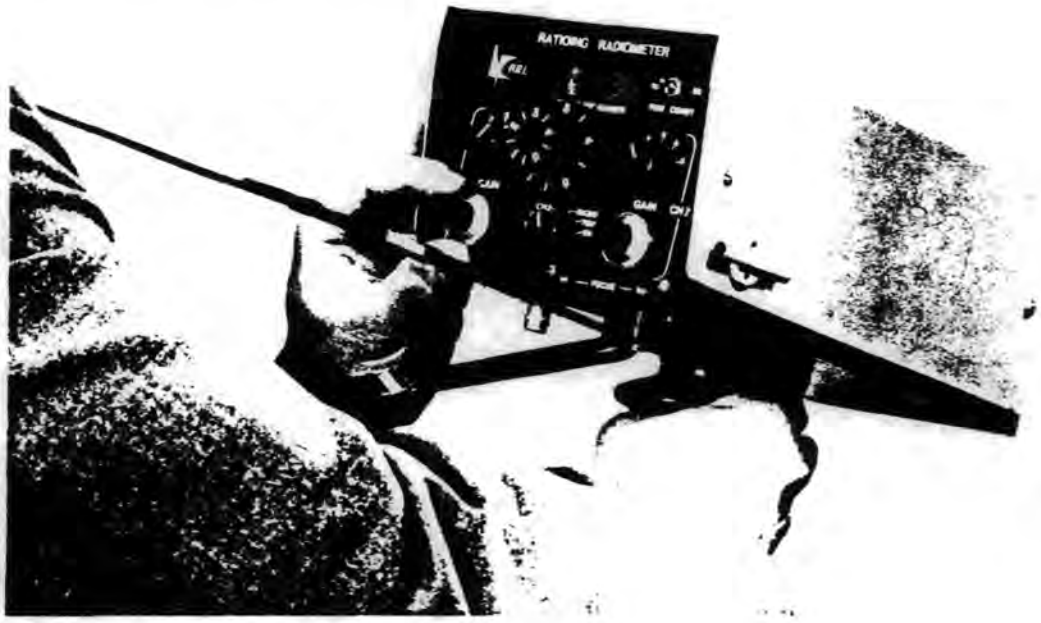

DESCRIPTION

The instrument is a self-contained, dual beam ratioing radiometer with two optical trains directed at the same target. It provides a continuous digital readout of ratio values from the two optical trains each of which includes a separate filter for selection of the narrow spectral bands to be ratioed for identification of the presence of a particular target, on the basis of known spectral characteristics of the target.

Positive target identification can be achieved by measuring the ratio of the two most prominent spectral peaks characterizing the target. The instrument can provide a selective ratio of such spectral peaks in any of up to 25 pairs of pre-selected narrow bands in the spectral range from 0.4 micrometres to 2.5 micrometres.

The radiometer is simple to operate with minimal skill required. Field calibration is carried out infrequently with solar radiation or an artificial source, such as a quartz-iodine lamp and a highly reflective reference material having a uniform spectral reflectance in the region of interest.

The portable radiometer system comprises the Ratioing Radiometer Head, a Battery Pack, a Standard Reflectance Target Package, and a carrying case. Sets of Narrow Band Filters are available to suit a wide variety of applications.

**Developed by California Institute of Technology at Jet Propulsion Laboratory during research sponsored by NASA. Manufactured and sold by Barringer under exclusive license from California Institute Research Foundation.*

SPECIFICATIONS:

RADIOMETER HEAD

Spectral Range:	0.4 - 2.5 micrometres (Extended range 0.3 - 3.5 micrometres is optional).
Filters:	Not included. To be selected from available stock or custom ordered, Barringer will make a preliminary filter evaluation for any customer application.
Light Sources:	Scattered solar radiation, or artificial source.
Optics:	Standard unit has a 2° x 12° FOV
Noise Equivalent Reflectance:	1.5% @ 1 sec. response time and 60° solar zenith angle.
Dynamic Range:	Typically three orders of magnitude.
Response Time:	Typically selectable 1 second or 5 seconds; can be modified to suit customer requirements.
Display:	Reflectance ratio, or individual radiometer signal, or battery voltage or detector temperature on 4 digit LCD.
Analog Outputs:	Reflectance ratio signal and radiometer outputs: 0 to 10 VDC at 10 k output resistance.
Mechanical:	Size — 4" x 5.5" x 9" (10 cm x 14 cm x 24 cm) approximate Weight — 6 lbs (2.8 kg) approximate Pistol grip handle, shoulder strap.
Environmental:	Ambient temperature range: 0 to 40°C Dust sealed, splash & rain proof.
Power Requirements:	+ 6V DC: (8 hours operation from battery pack).
BATTERY PACK:	Belt mounted 6V rechargeable pack. 2" x 5" x 7" (5 x 13 x 18 cm) 4.5 lbs (2 kg).
REFLECTANCE TARGET PACKAGE:	Non water absorbing standard reflectance sample, belt mounted. 1" x 4.5" x 12.5" (2.5 x 11.5 x 32 cm) 1 lb. (0.5 kg).
SHIPPING/CARRYING CASE:	16" x 20" x 9" (41 x 51 x 23 cm), 12 lbs (5.5 kg) net.

OPTIONS:

A wide range of options available to suit individual requirements.
Narrow band filters. A list of standard and stock filters is available.
Artificial illuminator.
Tripod adaptor.

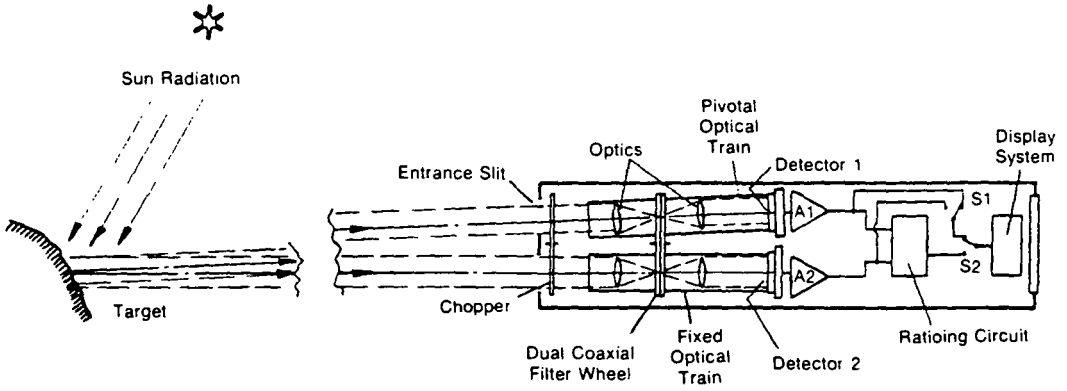

Ratioing Radiometer Simplified Schematic.

TYPICAL APPLICATIONS:

General Studies	Water quality; soil moisture content; ground truthing for remotely sensed data, (covers NASA Thematic Mapper and LANDSAT bands):
Agriculture	Crop health and vigour; maturity and stress; agricultural land use; grazing lands analysis; pollution effects on forest cover; forest speciation;
Geobotany	Spectral reflectance changes caused by mineralization induced stress
Geochemistry	Detection of geochemical alteration haloes
Geology	Outcrop detection and geological mapping; soil, overburden and rock classification; stratographical studies; examination of lithological facies changes
Exploration	Hydrothermal alteration patterns; diamond drill core and oil well drill cutting logging
Oceanography	Coastal and estuarine studies; water colour; algae growths; shoaling; limnological studies and turbidity; hydrology stress
GeoTechnology	Soil mechanics; earth stability studies; engineering geology; clay content of ores.

Barringer staff will be pleased to discuss other applications, and have a large library of spectral signatures to call upon.

A scanning field reflectance spectrometer covering the same working spectral range of this instrument, 0.4 to 2.5 microns, is available to enable correct selection of filters for various user applications.

DESIGN FEATURES:

- Chopper provides AC signal to the two detector channels.
- Two balanced detectors simultaneously measure radiance through pairs of reference filters.
- Signal obtained by ratioing the detector outputs after amplification and rectification.
- Continuous digital readout of radiometric signal on a liquid crystal display. Analog output available for recording.
- Readout of either channel separately or radiometric ratio switch selectable.
- External reflectance reference target verifies balance and calibration of the instrument.
- Common field of view (FOV) for both channels, 4 feet to infinity (parallax compensation).
- Light weight, hand held, battery operated, truly portable. Rugged construction for field service.
- Liquid crystal display visible in full daylight of radiometric ratio, single channel radiance, detector temperature and battery state via switch selection.
- LCD indicator of chopper out of lock; detector cooler failure; and battery low voltage.
- Both sections of the filter wheel accommodate 5 filters each in snap-in mounts for easy exchange in the field.

OPERATIONAL FEATURES:

- Ratio operation compensates for illumination changes.
- Calibration against standard reference target compensates for solar/sky spectral changes.
- Solar radiation or artificial source may be used.
- Insensitive to thermal drifts and gradients within the unit.
- Wide selection of filters available for different applications.
- Simple to use, calibrate and interpret.
- Filter positions in either channel easily switch selectable to move independently or as preset matched pairs.

NORMALIZED BAND-RATIOS OF CALCULATED RESPONSES TO LABORATORY REFLECTANCE DATA FOR HHRR FILTER BANDPASS

BAND-RATIO	ALUNITE	KAOLINITE	MONTMORILLONITE	CALCITE
2.10/2.17	1.47	1.59	1.04	1.02
2.10/2.22	0.86	1.41	1.19	1.04
2.17/2.20	0.80	1.10	1.20	1.00
2.17/2.22	0.59	0.88	1.14	1.02
2.20/2.22	0.74	0.80	0.94	1.03
2.20/2.35	0.74	0.95	1.01	1.27

SPECTRA OF ALTERED ROCKS

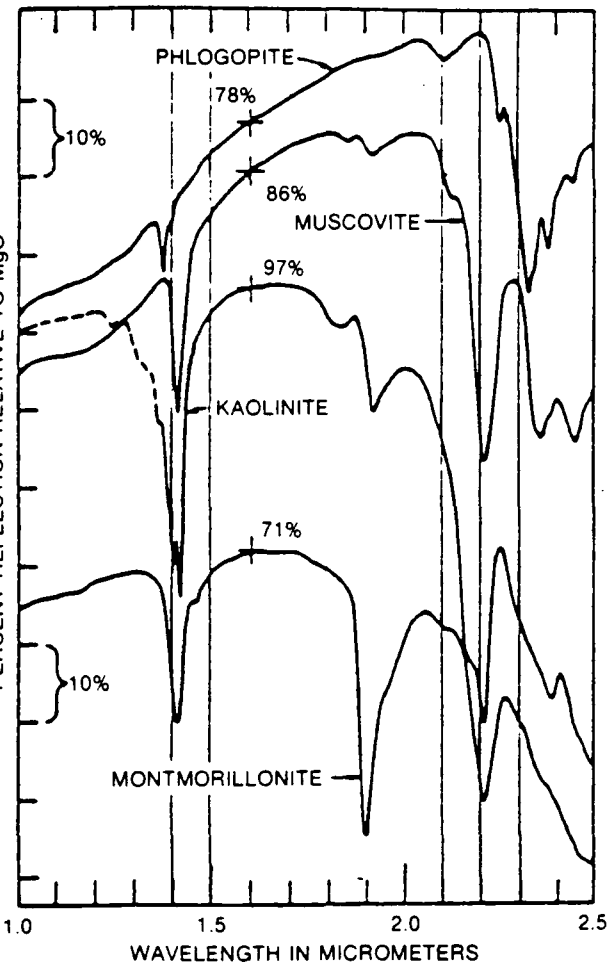

Features due to vibrational processes in the spectra of four hydroxyl-bearing minerals commonly present in hydrothermally altered rocks. Spectra are displaced vertically. Reflection values are indicated on the curves at 1.6 μm.

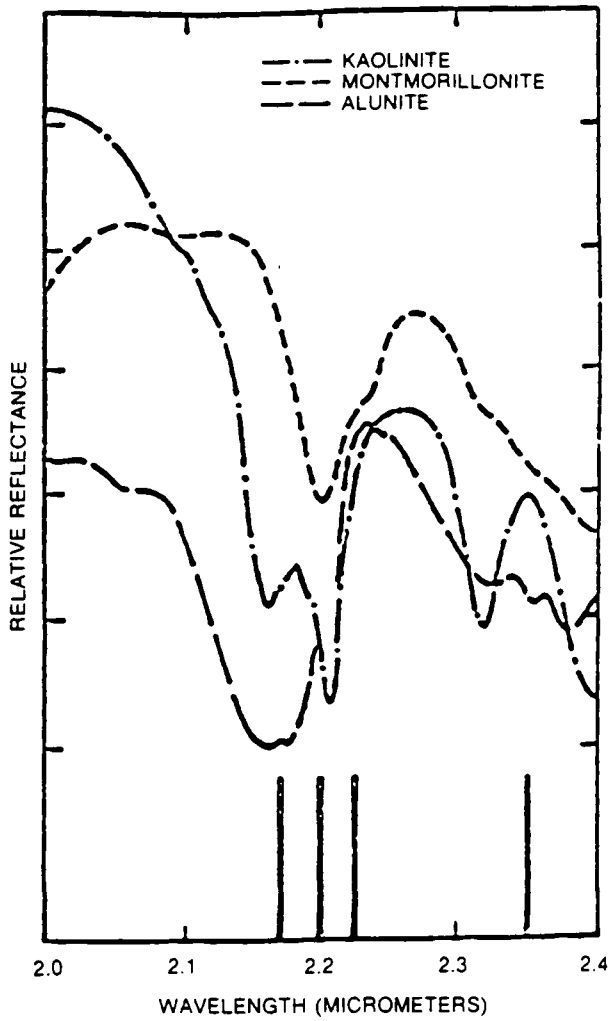

Laboratory spectra of selected minerals (layer silicate) from Hunt (USGS). The bars on the ordinate indicate location of centres of four of the radiometer channels.

Through the selection of the two filters for ratioing, a wide range of applications can be addressed. Thus the two filters can be closely set together for detecting very subtle fine structures, as in clay minerals, as illustrated to the left.

Alternatively the filters can be spaced far apart. Filter position selection depends upon the application.

Selected Bibliography

1) G. R. Hunt, R. P. Ashley, 1979 Econ. Geol. 74, 1615, 1629

2) Hunt & Salisbury, Modern Geology, 1970, 283-300; 1971, 23-30, 195-205; 1973, 85-106, 217-224, 237-244; 1974, 15-22; 1976, 211-217

3) Hunt & Wynn, 1979, Geophys.

4) Hunt, 1977, Geophys. 42, No. 3, 501-513

5) Blom, Abrams, Adams, 1980, Spectral Reflection Plutonic Rocks, Geophys. in press.

6) Daubner, Davies, Dick, Till, 1981 15th International Symposium of Remote Sensing, Ann Arbour Michigan, May 1981

7) Barringer, Davies, Henderson, 1981, in press.

For further information contact:

Barringer Research Limited
304 Carlingview Drive
Metropolitan Toronto
Rexdale, Ontario, Canada M9W 5G2
Phone: 416-675-3870
Telex: 06-989183
Barringer Resources Inc.
1626 Cole Blvd.
Golden, Colorado 80401
Phone: 303-232-8811
Telex: 45810

2M 1-81

MECHANICAL LAYOUT

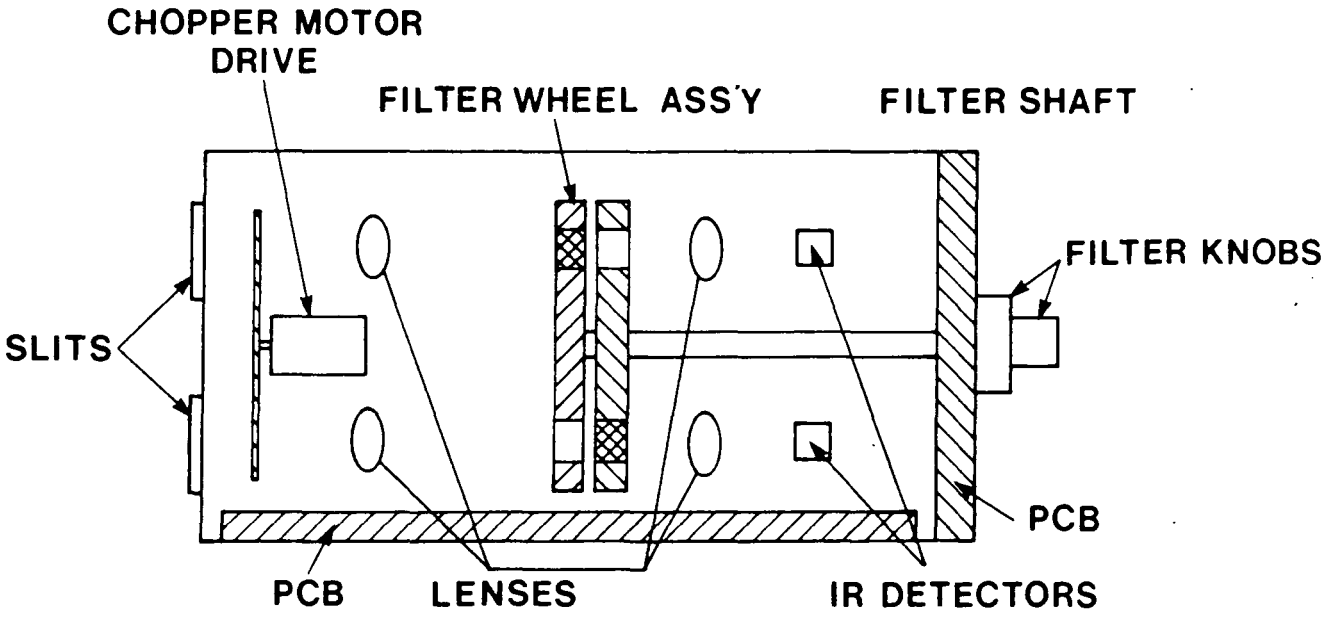

plan view

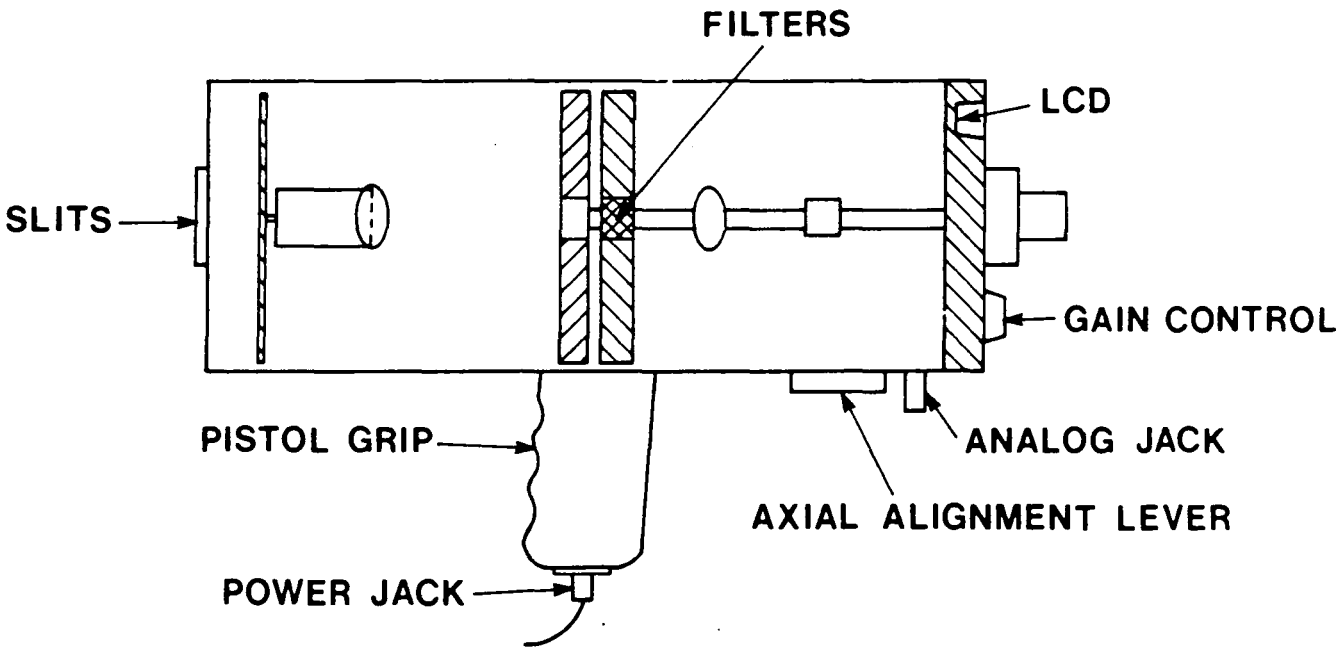

side view

(source : Barringer 1982)

SCHEMATIC OF RATIOING RADIOMETER

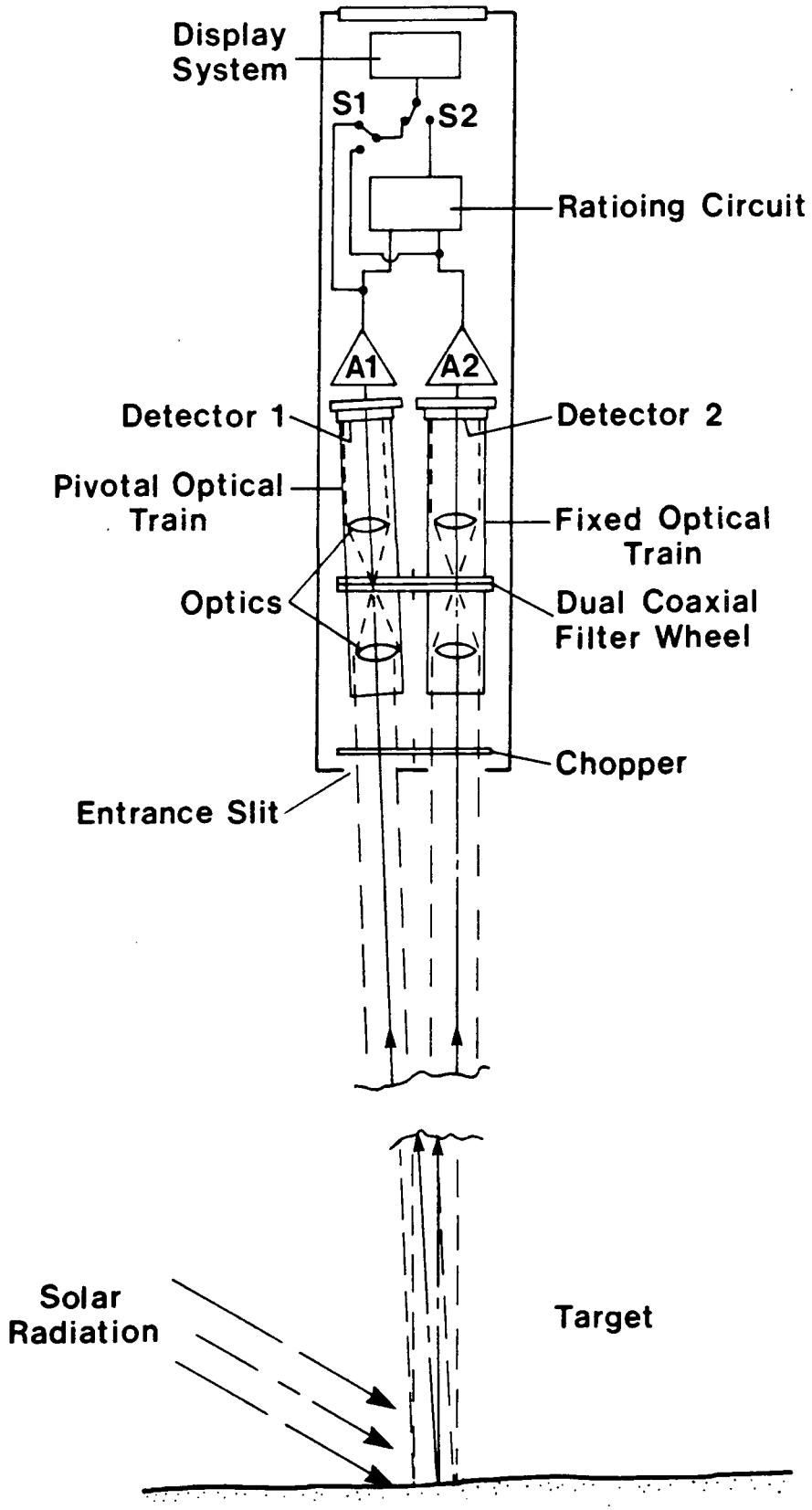

(source: Barringer 1982)

ELECTRONICS SIGNAL PROCESSING

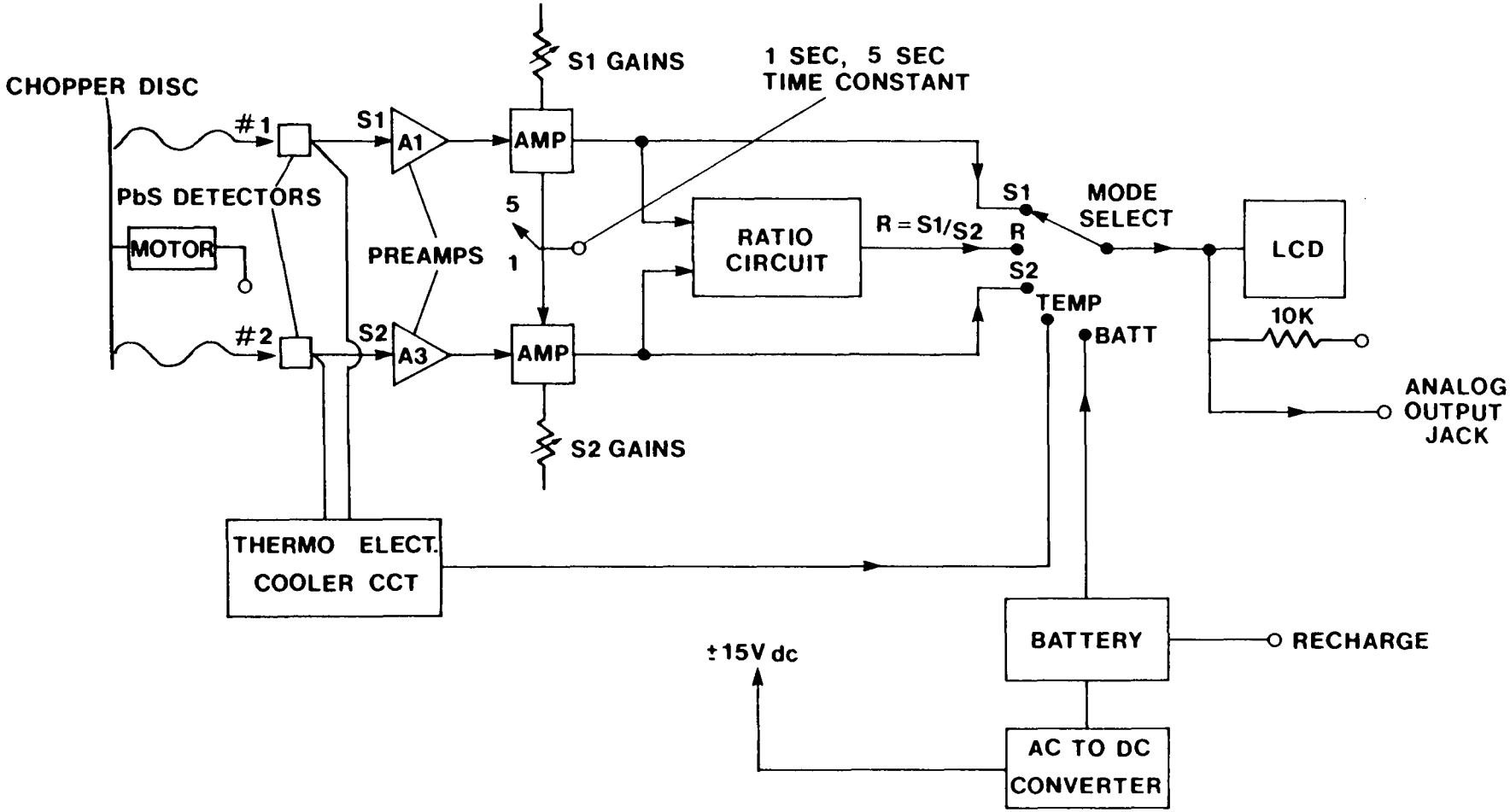

(source : Barringer 1982)

Field Spectra using HHRR

AREA NAME:

SITE NAME:

SITE DESCRIPTION:

LITHOLOGY:

PHOTO: NO:

DATE: TIME:

WEATHER CONDITIONS:

INSTRUMENT: REFERENCE PLATE:

OPERATOR:

TM1 [SURFACE]		BAND 1 [SURFACE]	
TM1 [REFERENCE]		BAND 1 [REFERENCE]	
TM2 [SURFACE]		BAND 2 [SURFACE]	
TM2 [REFERENCE]		BAND 2 [REFERENCE]	
TM3 [SURFACE]		BAND 3 [SURFACE]	
TM3 [REFERENCE]		BAND 3 [REFERENCE]	
TM4 [SURFACE]		BAND 4 [SURFACE]	
TM4 [REFERENCE]		BAND 4 [REFERENCE]	
TM5 [SURFACE]			
TM5 [REFERENCE]			
TM7 [SURFACE]			
TM7 [REFERENCE]			

COMMENTS:

APENDIX D

DETAIL SPECTRA OF LITHOLOGIES

MAHD ADH DHAHAB

AREA

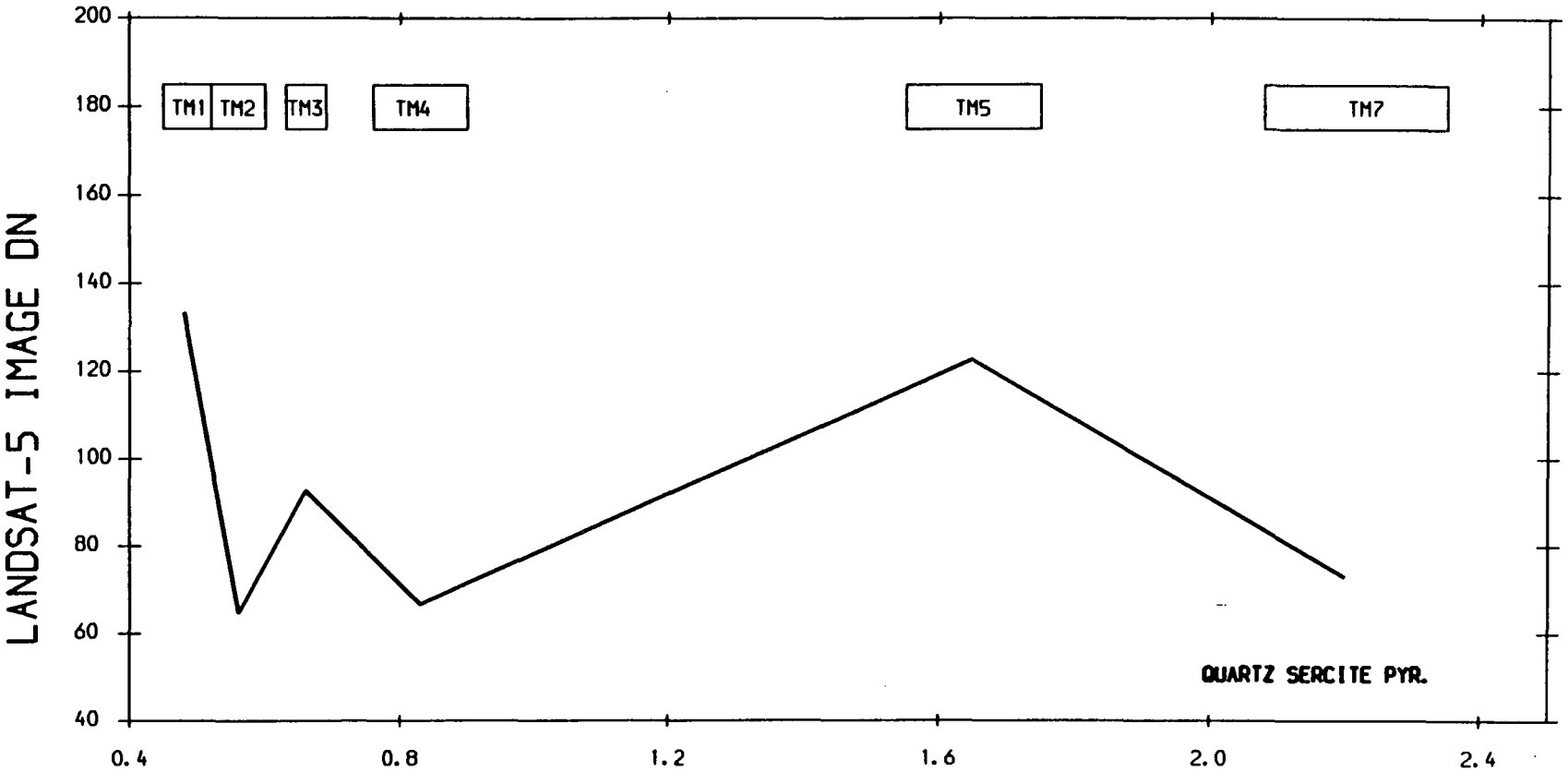

LANDSAT TM UNCALIBRATED DATA

MAHD ADH DHAHAB- SAUDI ARABIA

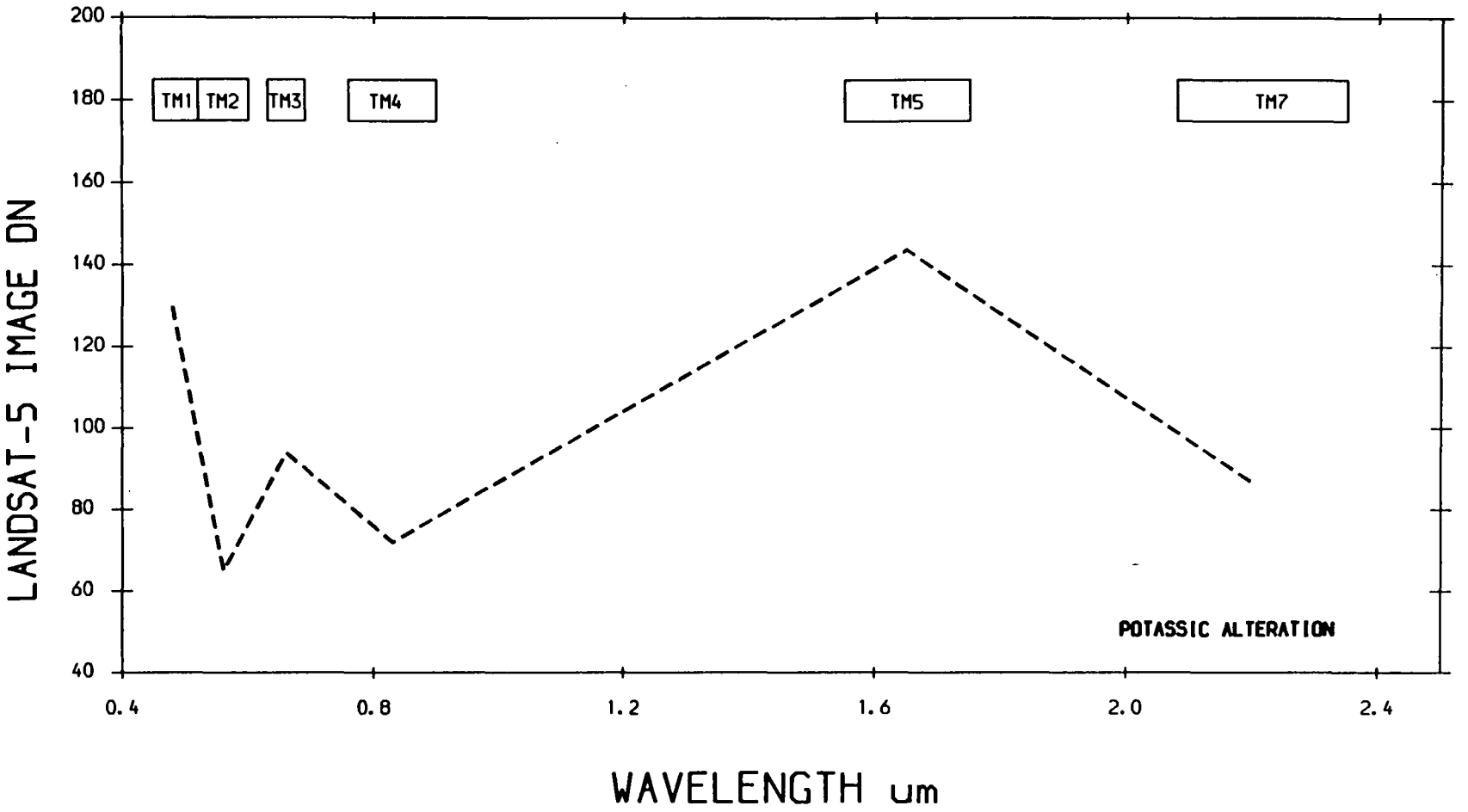

LANDSAT TM UNCALIBRATED DATA

MAHD ADH DHAHAB- SAUDI ARABIA

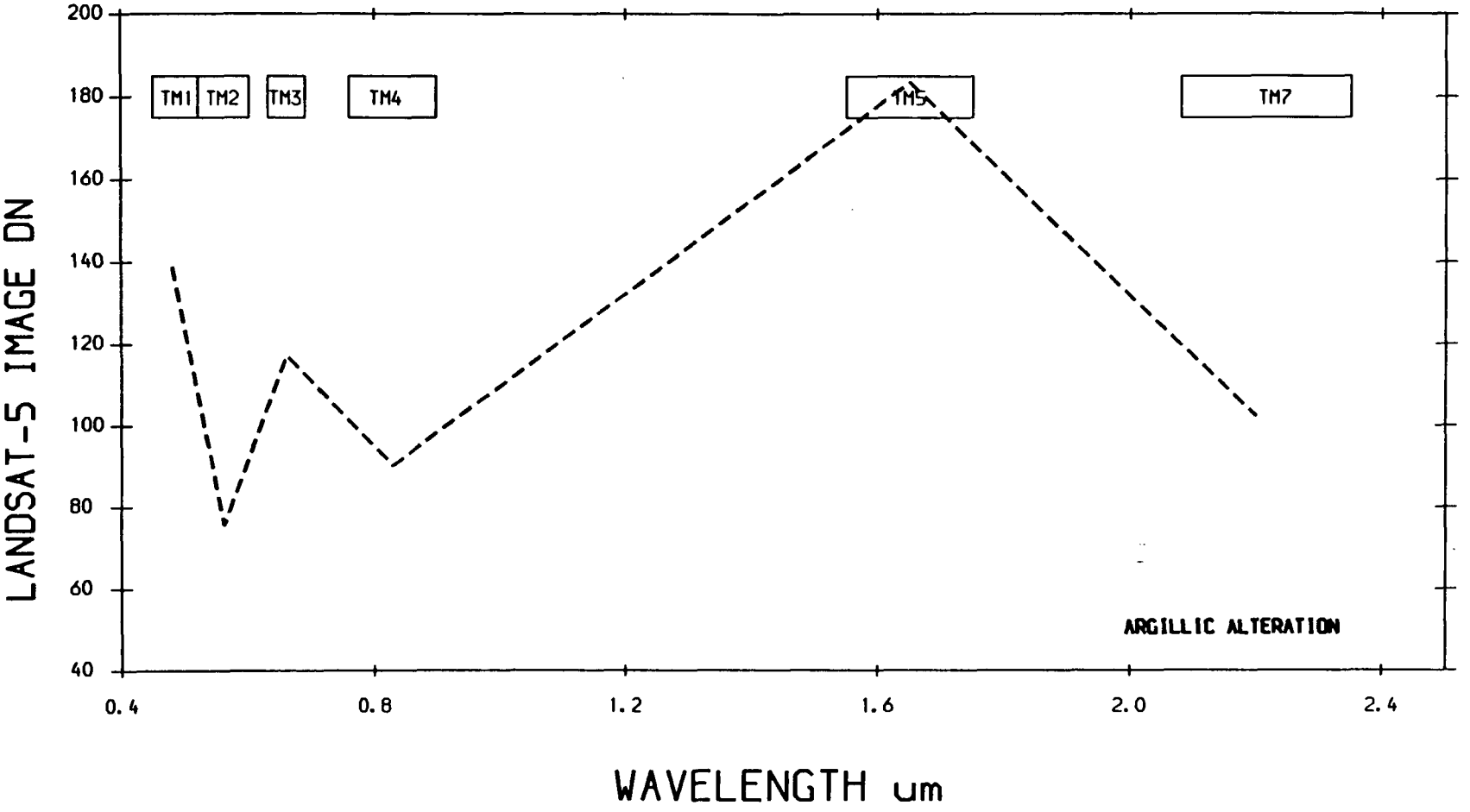

LANDSAT TM UNCALIBRATED DATA

MAHD ADH DHAHAB- SAUDI ARABIA

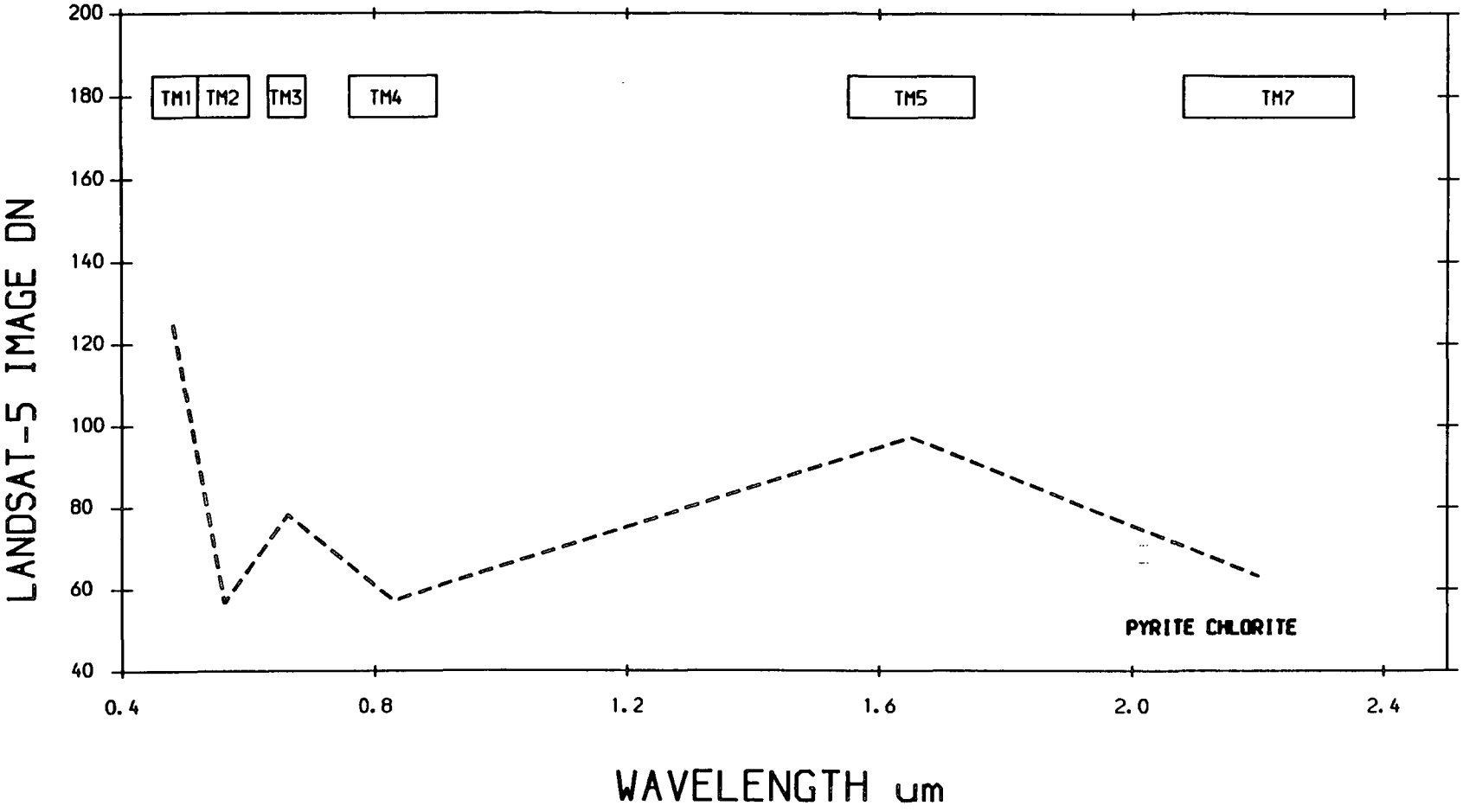

LANDSAT TM UNCALIBRATED DATA

MAHD ADH DHAHAB- SAUDI ARABIA

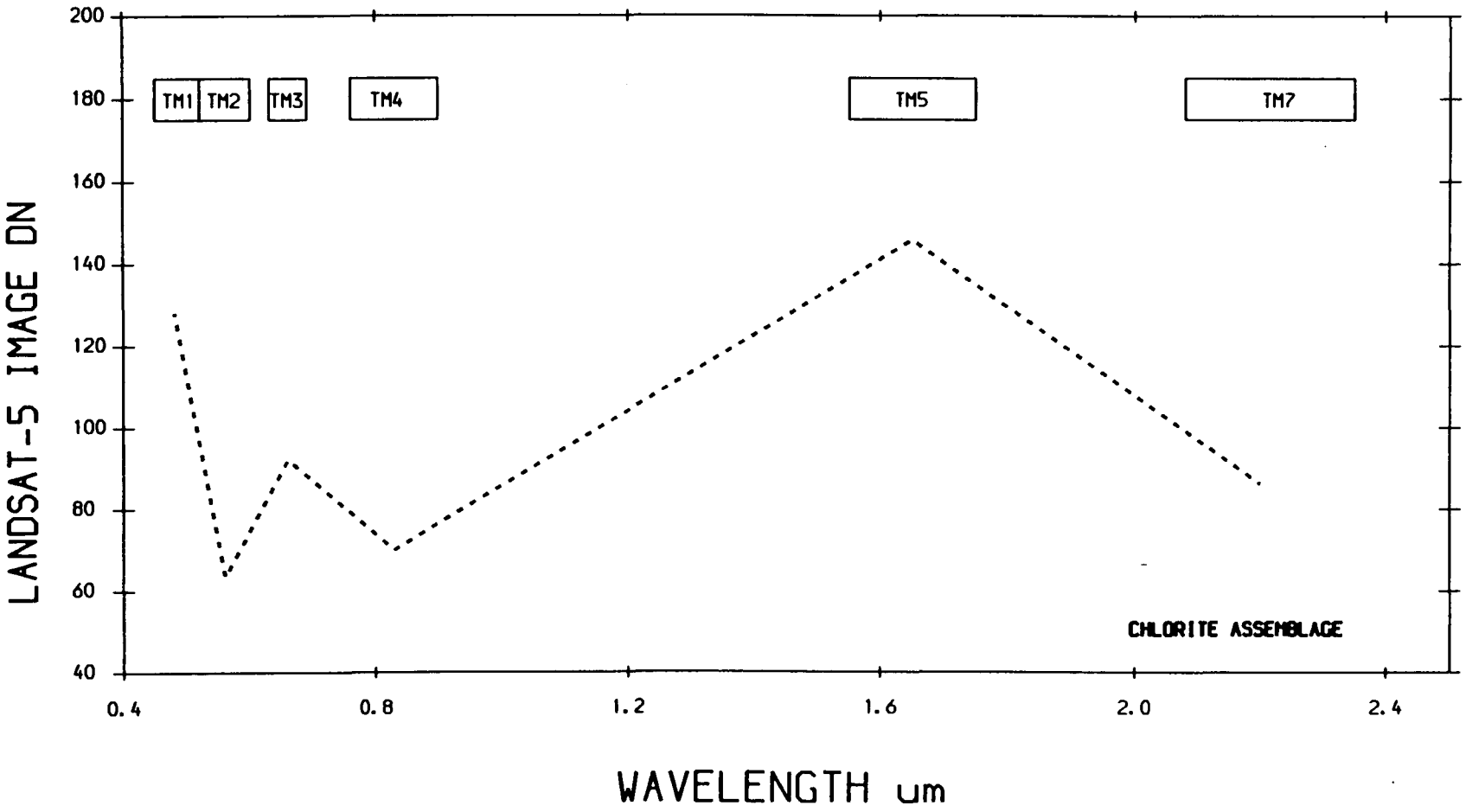

LANDSAT TM UNCALIBRATED DATA

MAHD ADH DHAHAB- SAUDI ARABIA

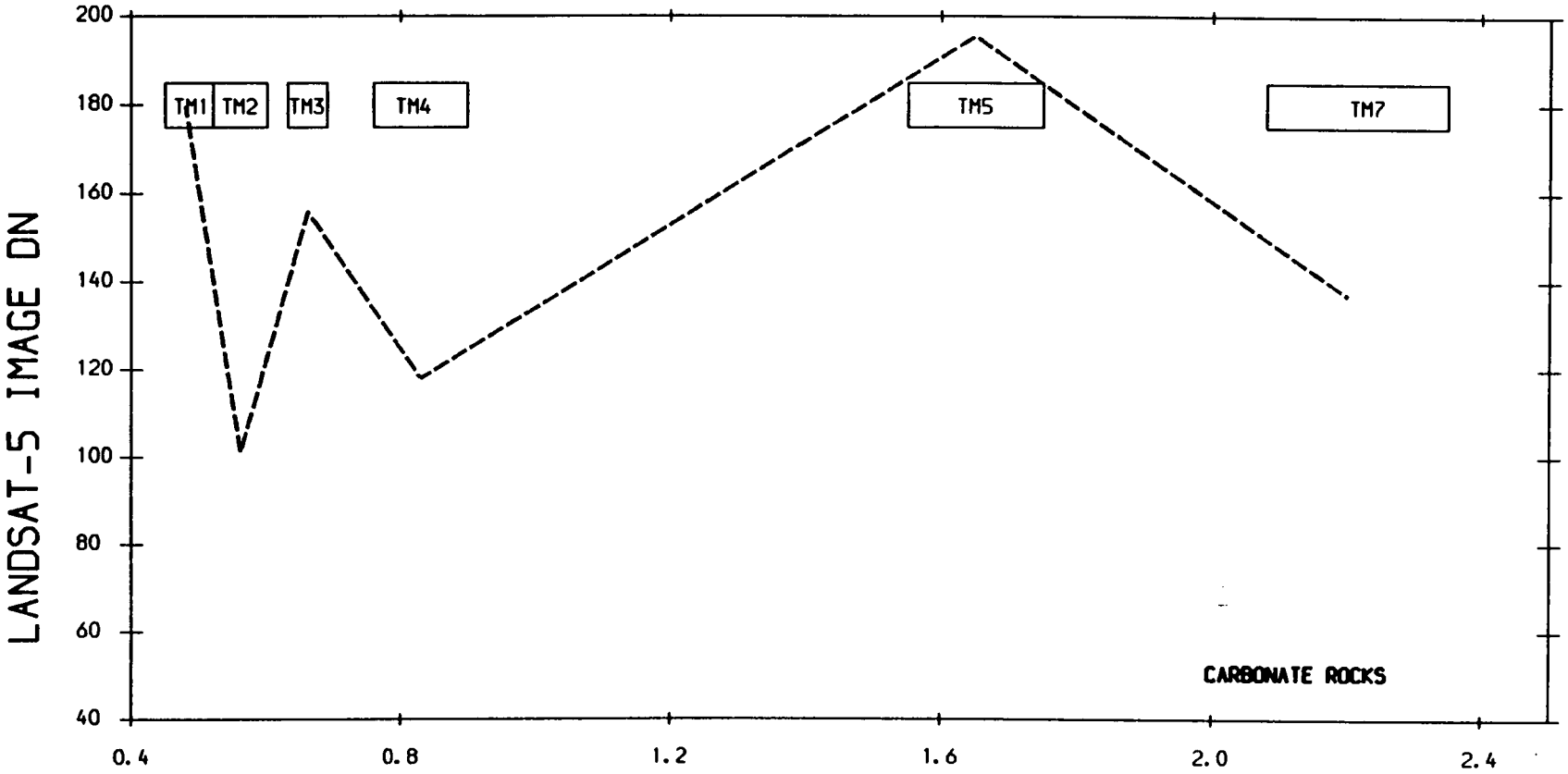

LANDSAT TM UNCALIBRATED DATA

MAHD ADH DHAHAB- SAUDI ARABIA

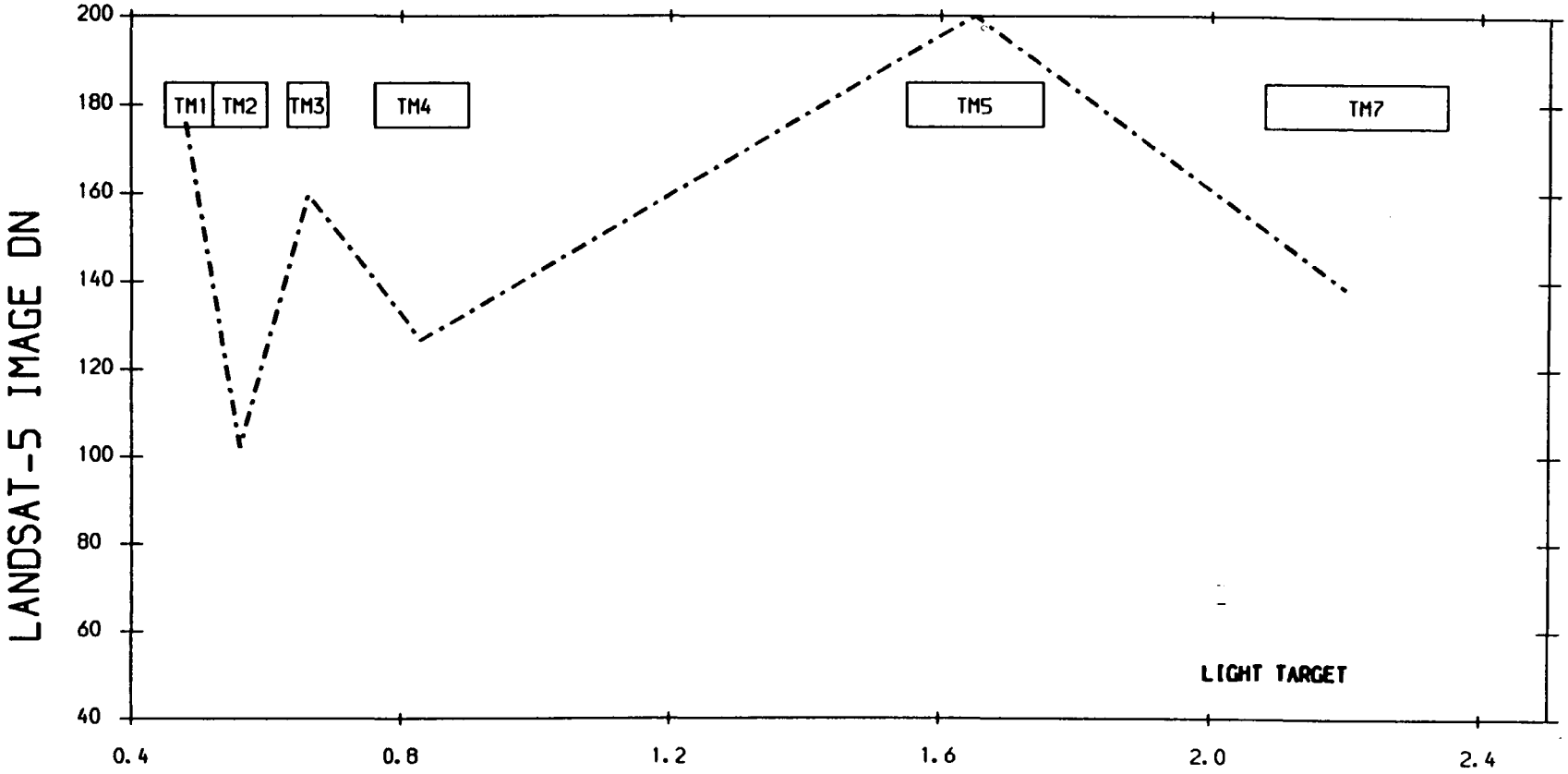

LANDSAT TM UNCALIBRATED DATA

MAHD ADH DHAHAB- SAUDI ARABIA

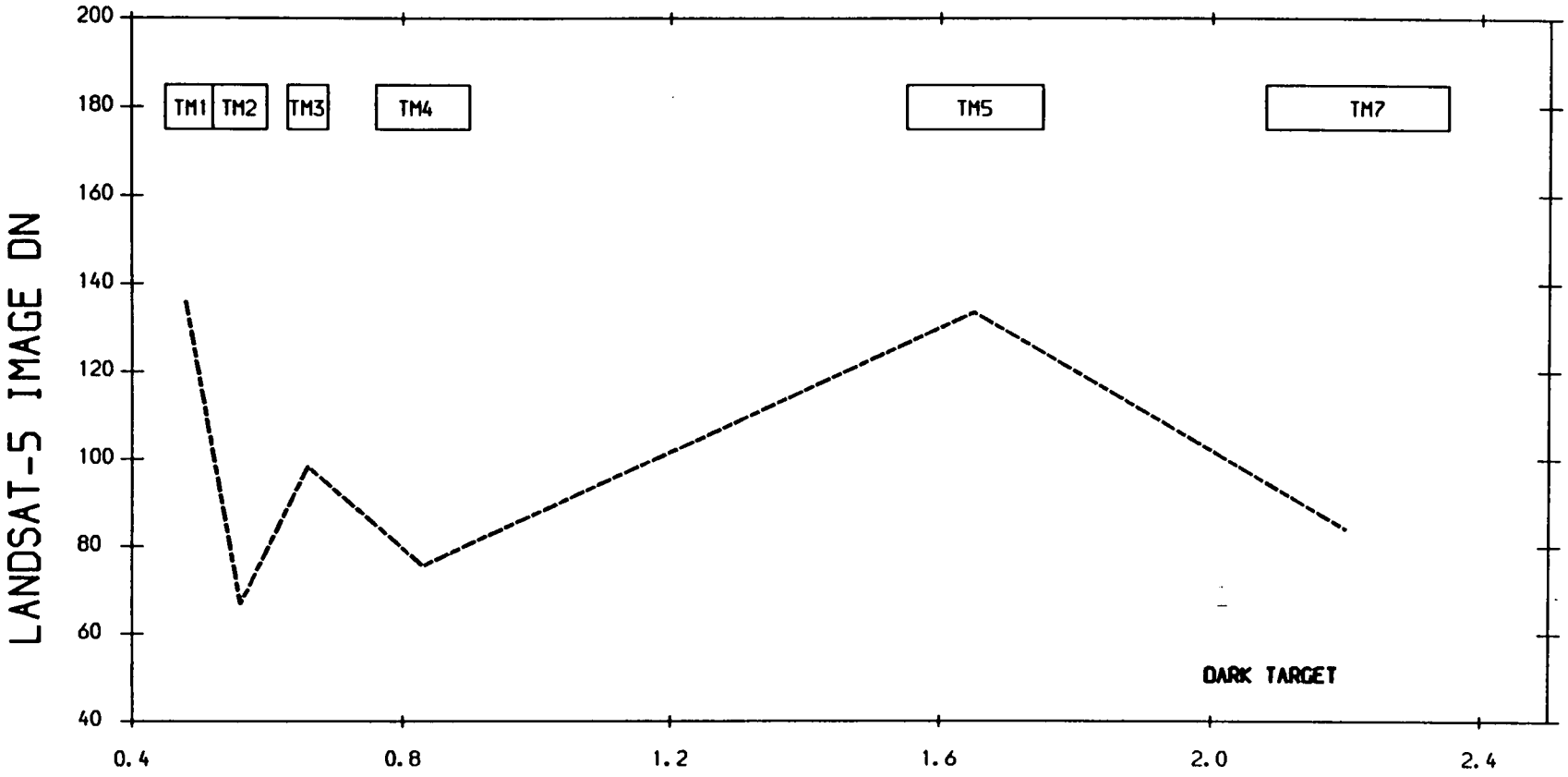

LANDSAT TM UNCALIBRATED DATA

MAHD ADH DHAHAB- SAUDI ARABIA

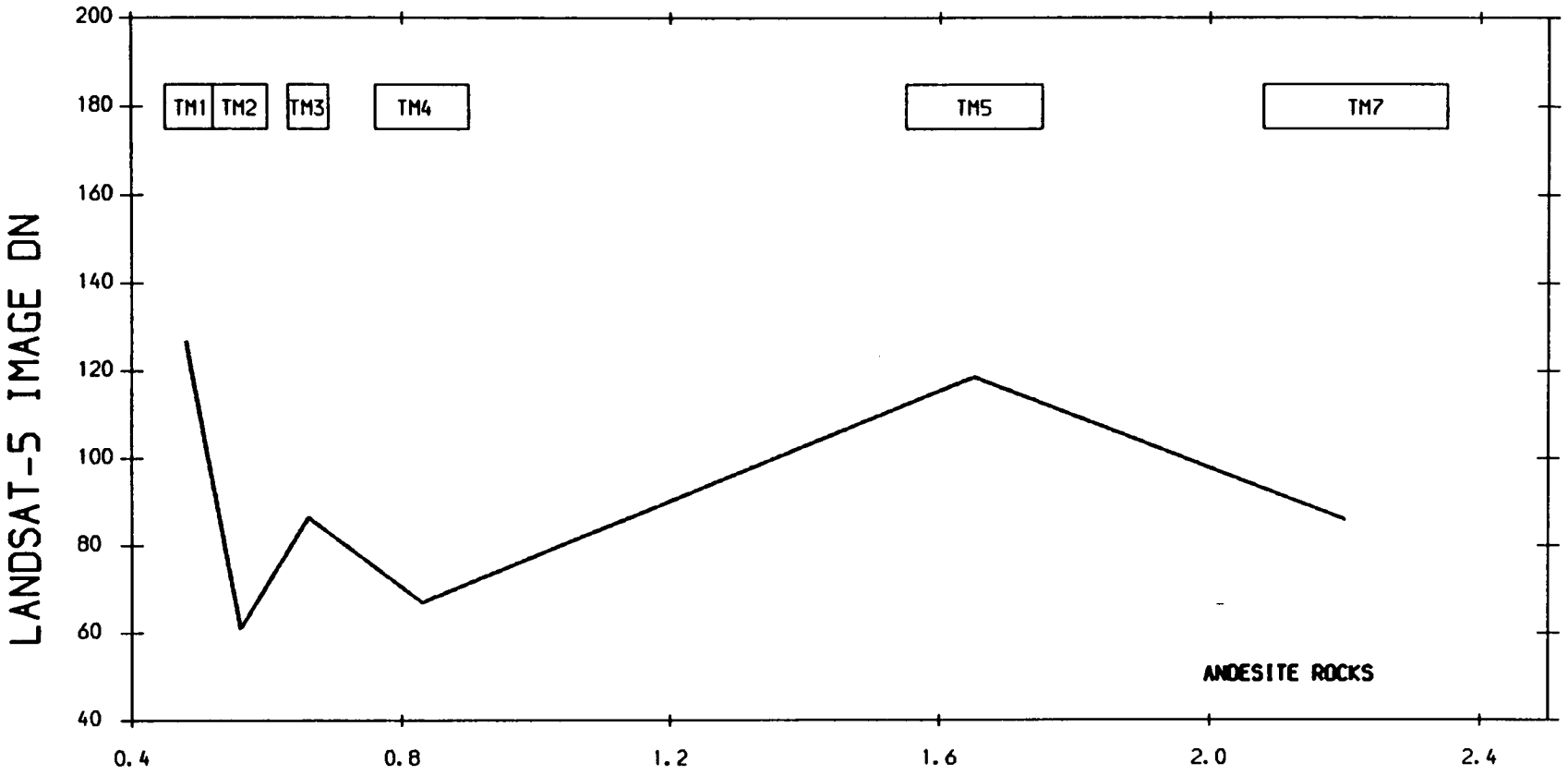

LANDSAT TM UNCALIBRATED DATA

MAHD ADH DHAHAB- SAUDI ARABIA

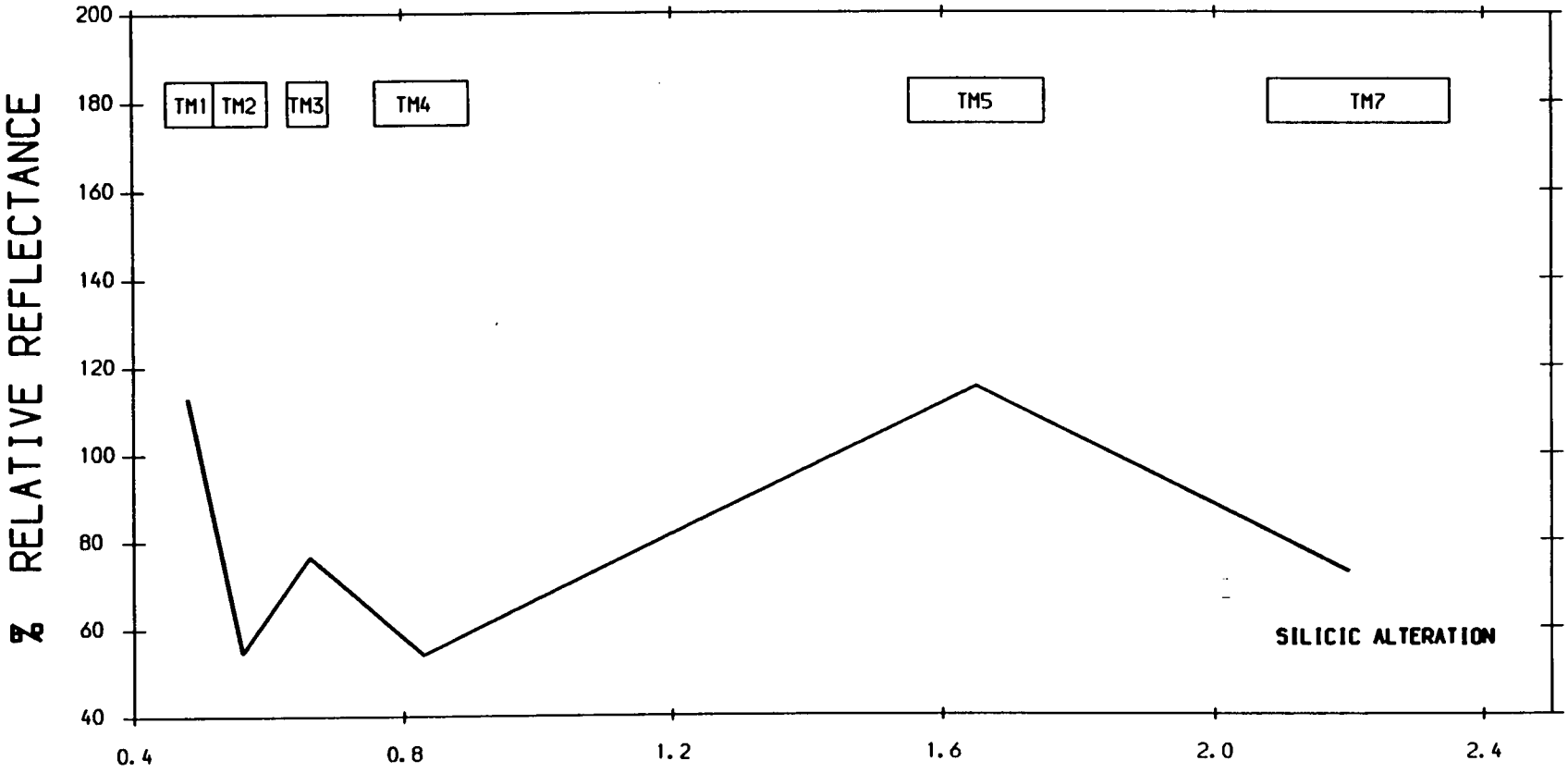

LANDSAT TM UNCALIBRATED DATA

MAHD ADH DHAHAB- SAUDI ARABIA

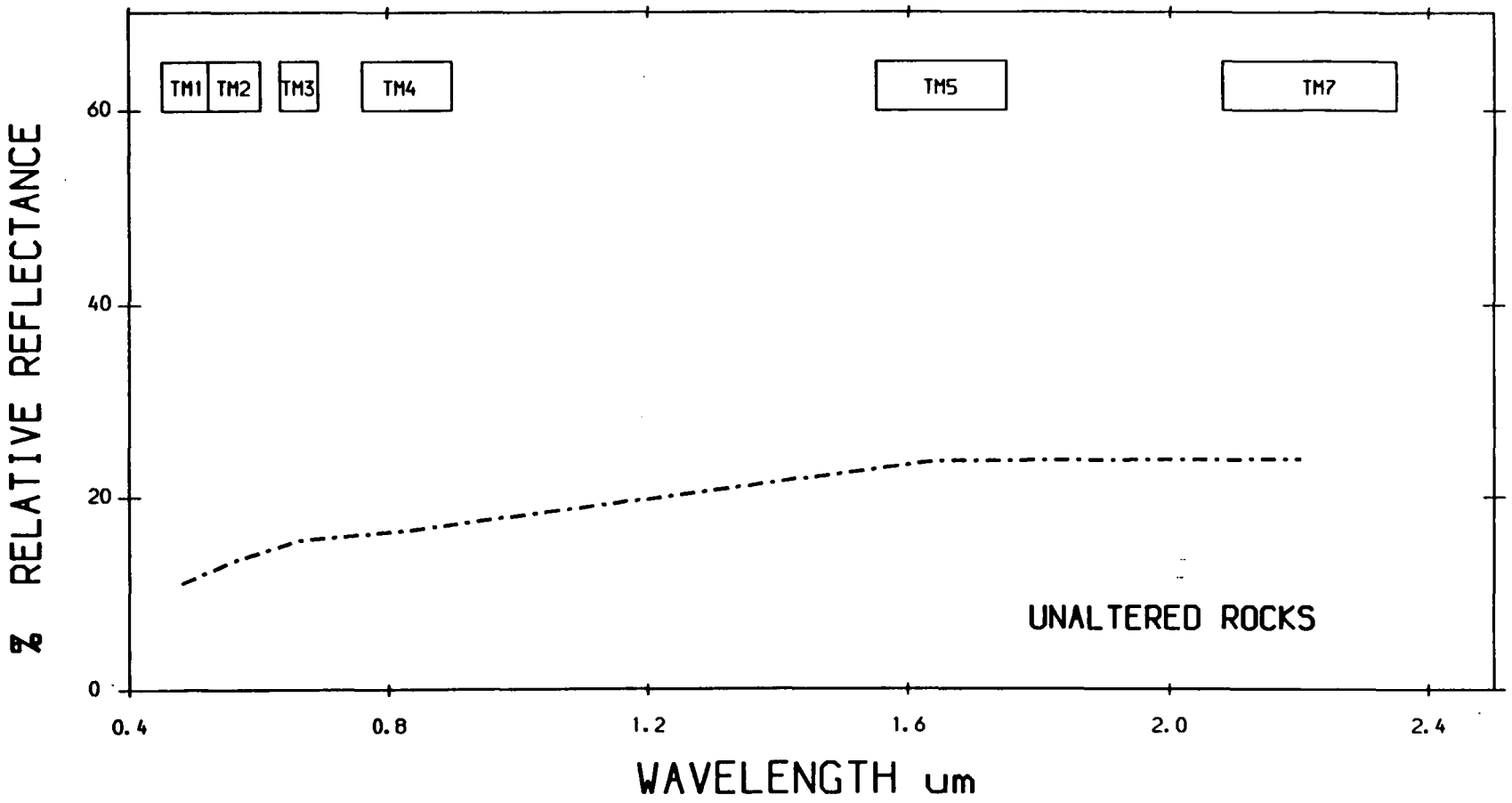

LANDSAT TM CALIBRATED TO RELATIVE REFLCTANCE

MAHD ADH DHAHAB- SAUDI ARABIA

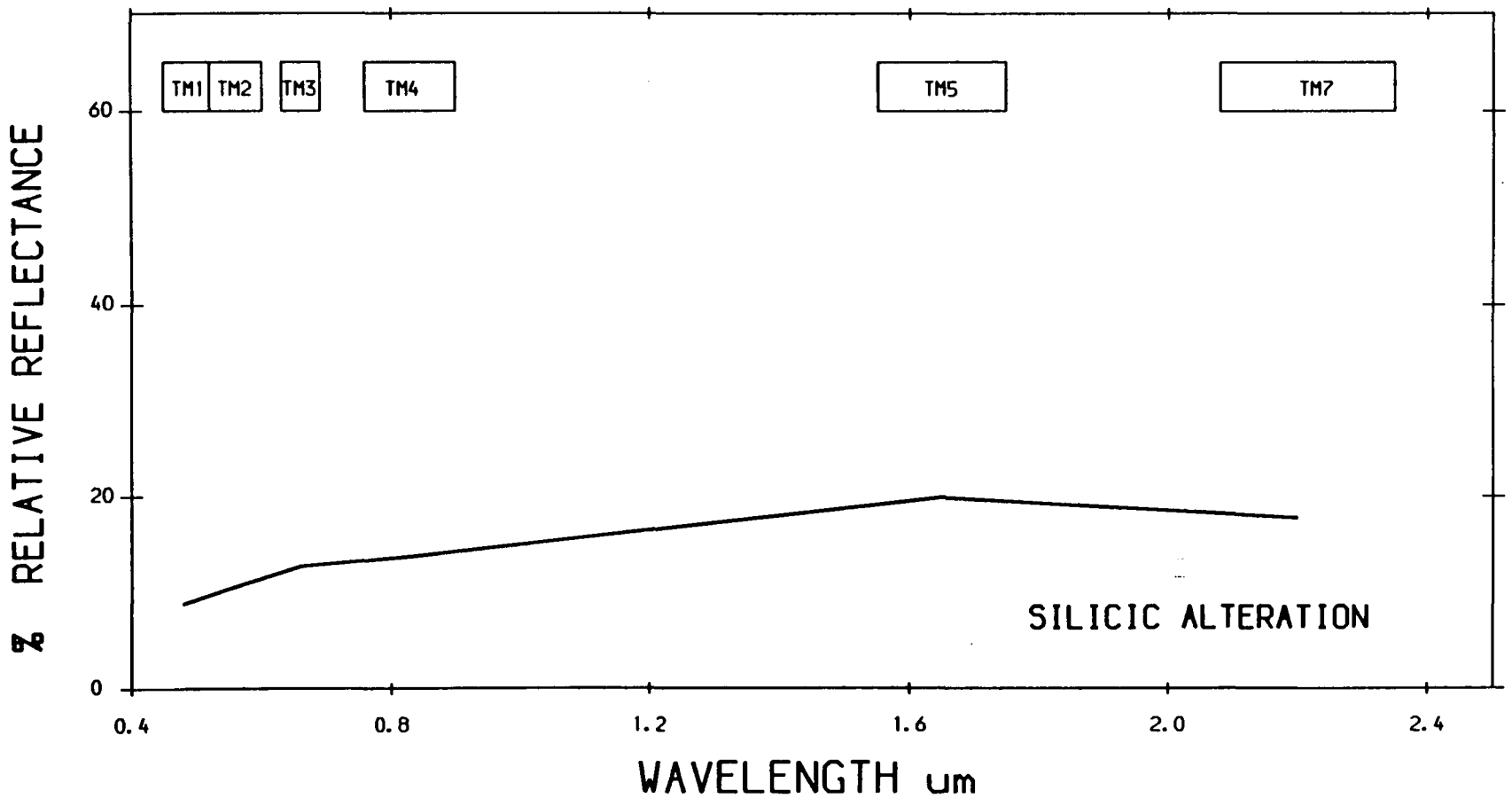

LANDSAT TM CALIBRATED TO RELATIVE REFLCTANCE

MAHD ADH DHAHAB- SAUDI ARABIA

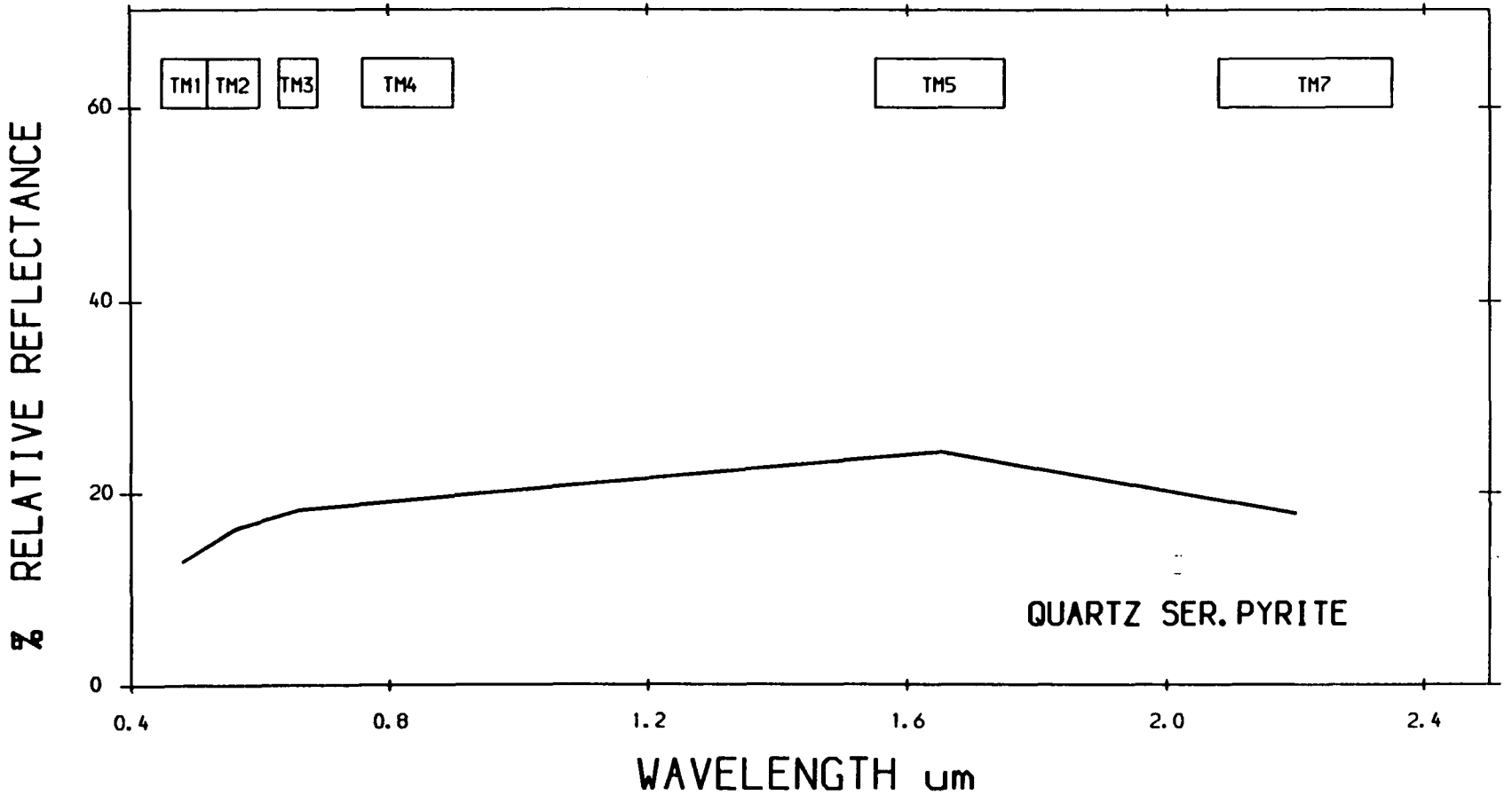

LANDSAT TM CALIBRATED TO RELATIVE REFLCTANCE

MAHD ADH DHAHAB- SAUDI ARABIA

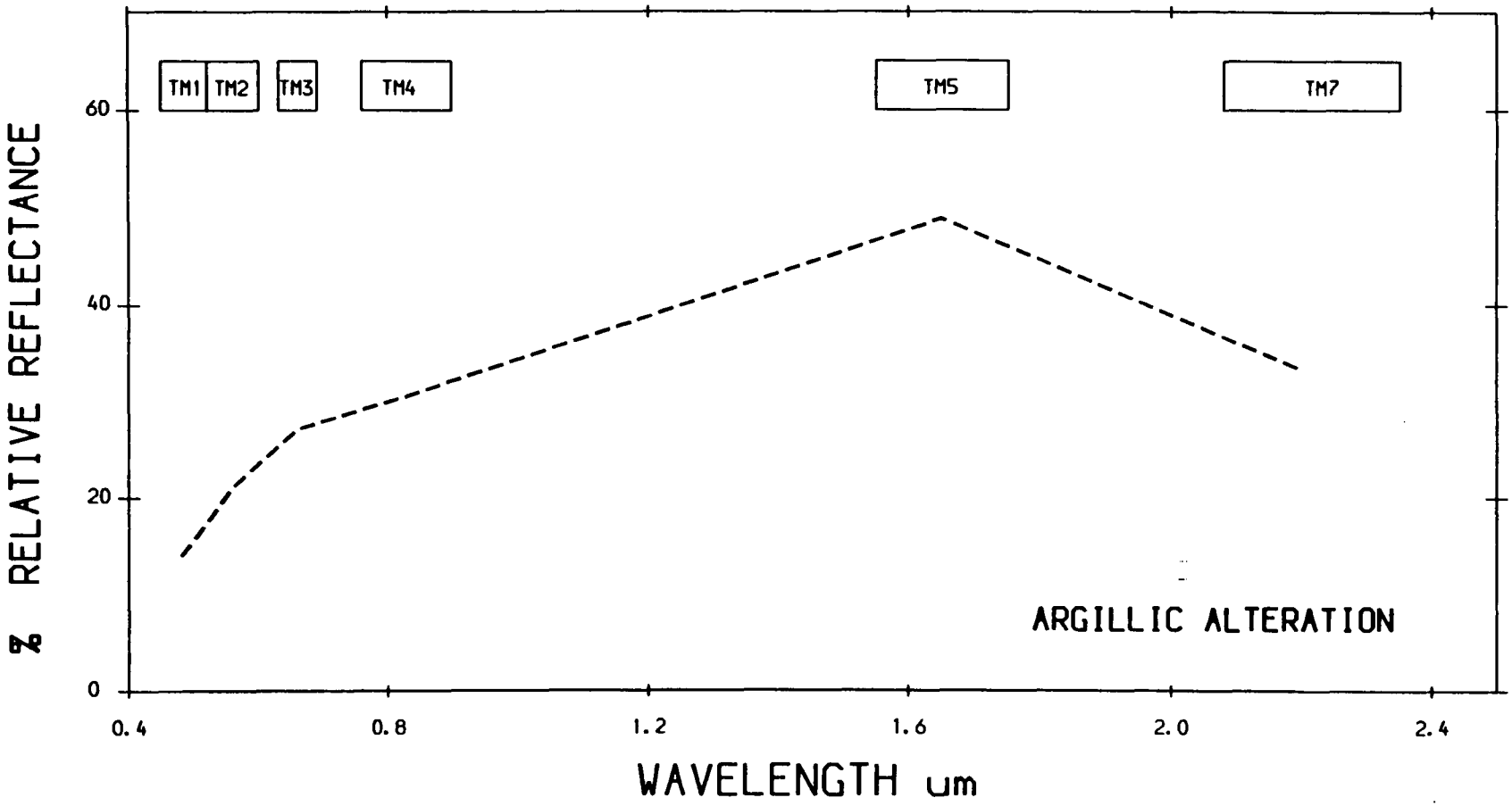

LANDSAT TM CALIBRATED TO RELATIVE REFLCTANCE

MAHD ADH DHAHAB- SAUDI ARABIA

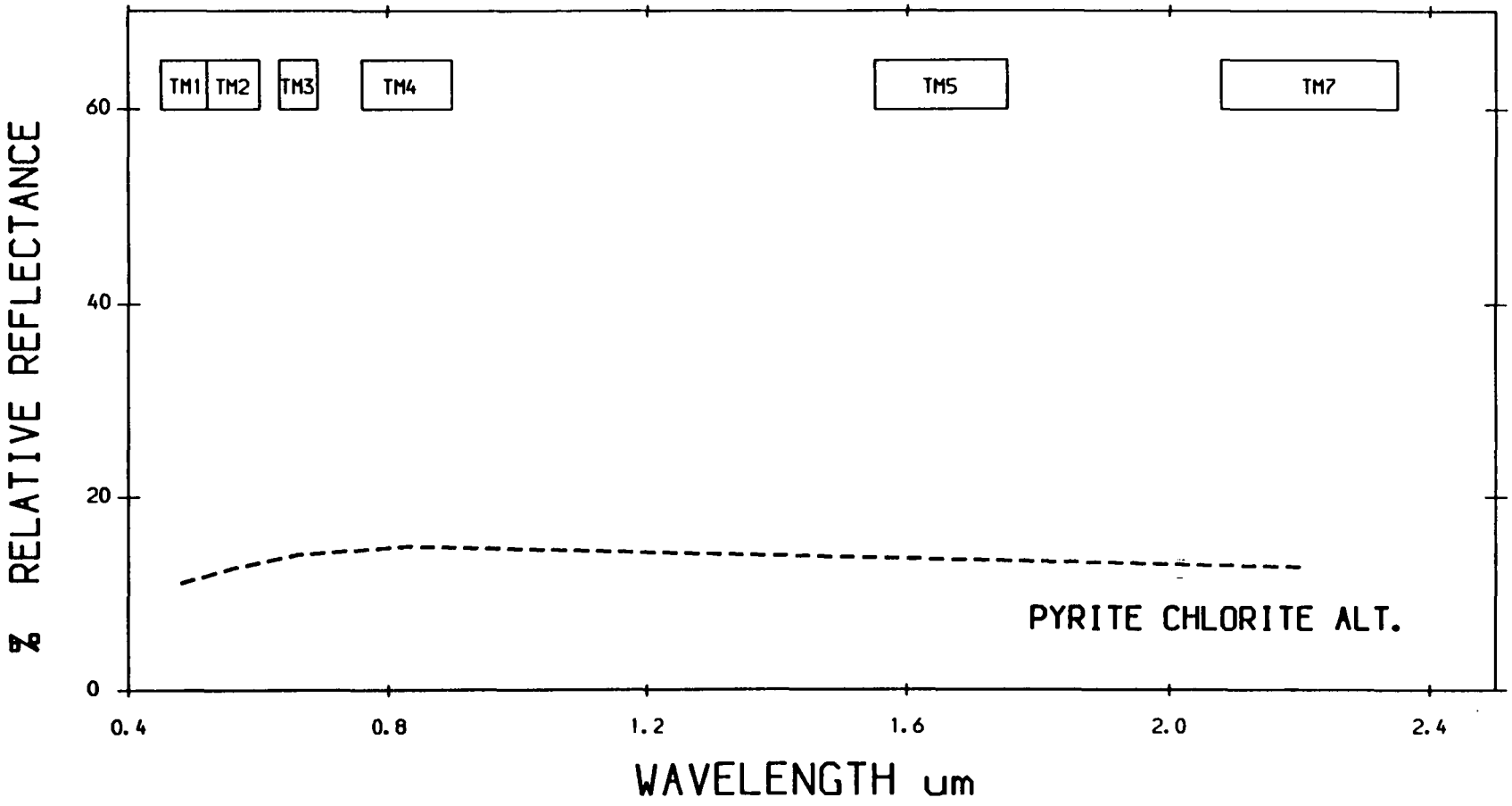

LANDSAT TM CALIBRATED TO RELATIVE REFLCTANCE

MAHD ADH DHAHAB- SAUDI ARABIA

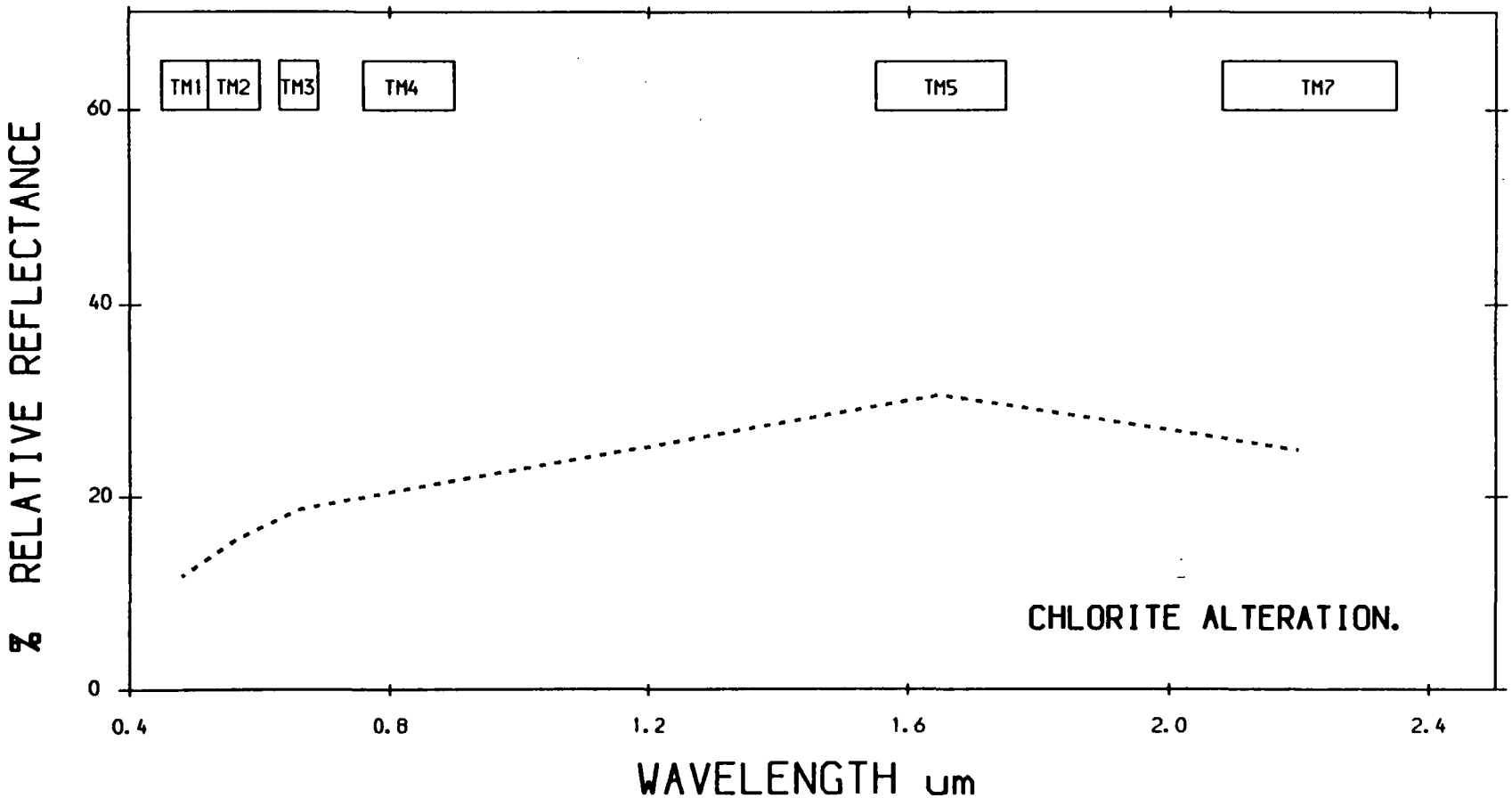

LANDSAT TM CALIBRATED TO RELATIVE REFLCTANCE

MAHD ADH DHAHAB- SAUDI ARABIA

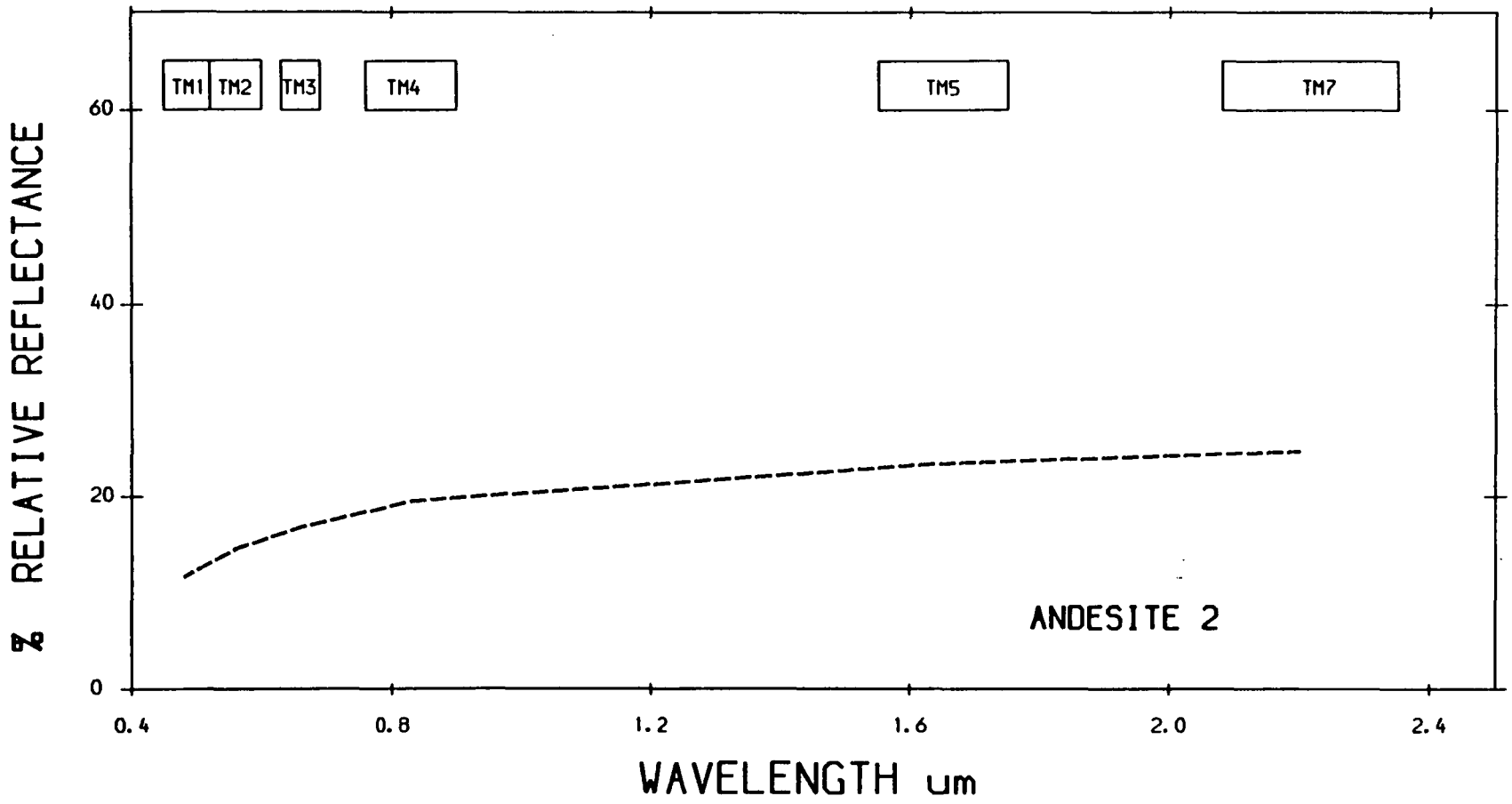

LANDSAT TM CALIBRATED TO RELATIVE REFLCTANCE

MAHD ADH DHAHAB- SAUDI ARABIA

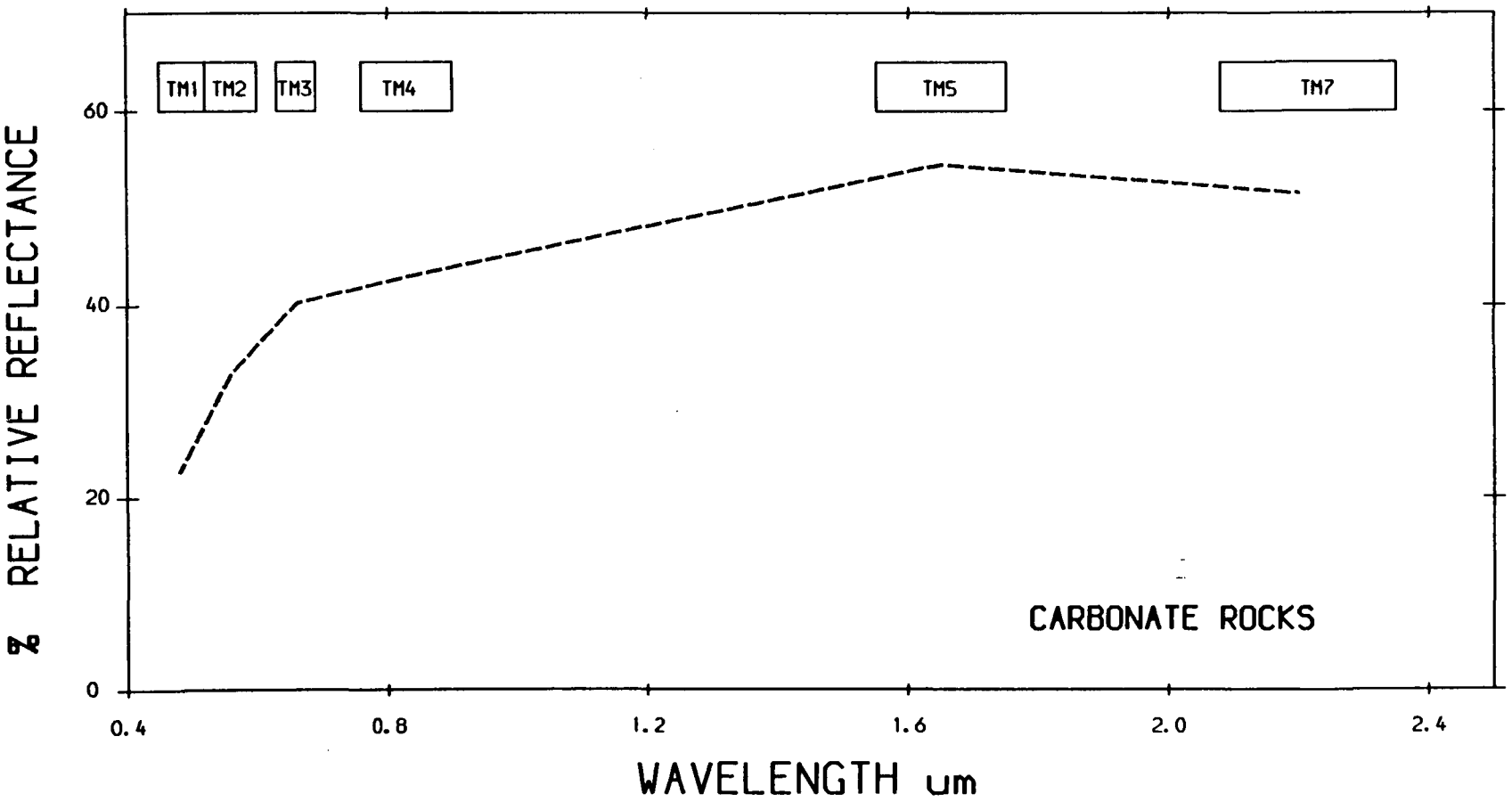

LANDSAT TM CALIBRATED TO RELATIVE REFLCTANCE

MAHD ADH DHAHAB- SAUDI ARABIA

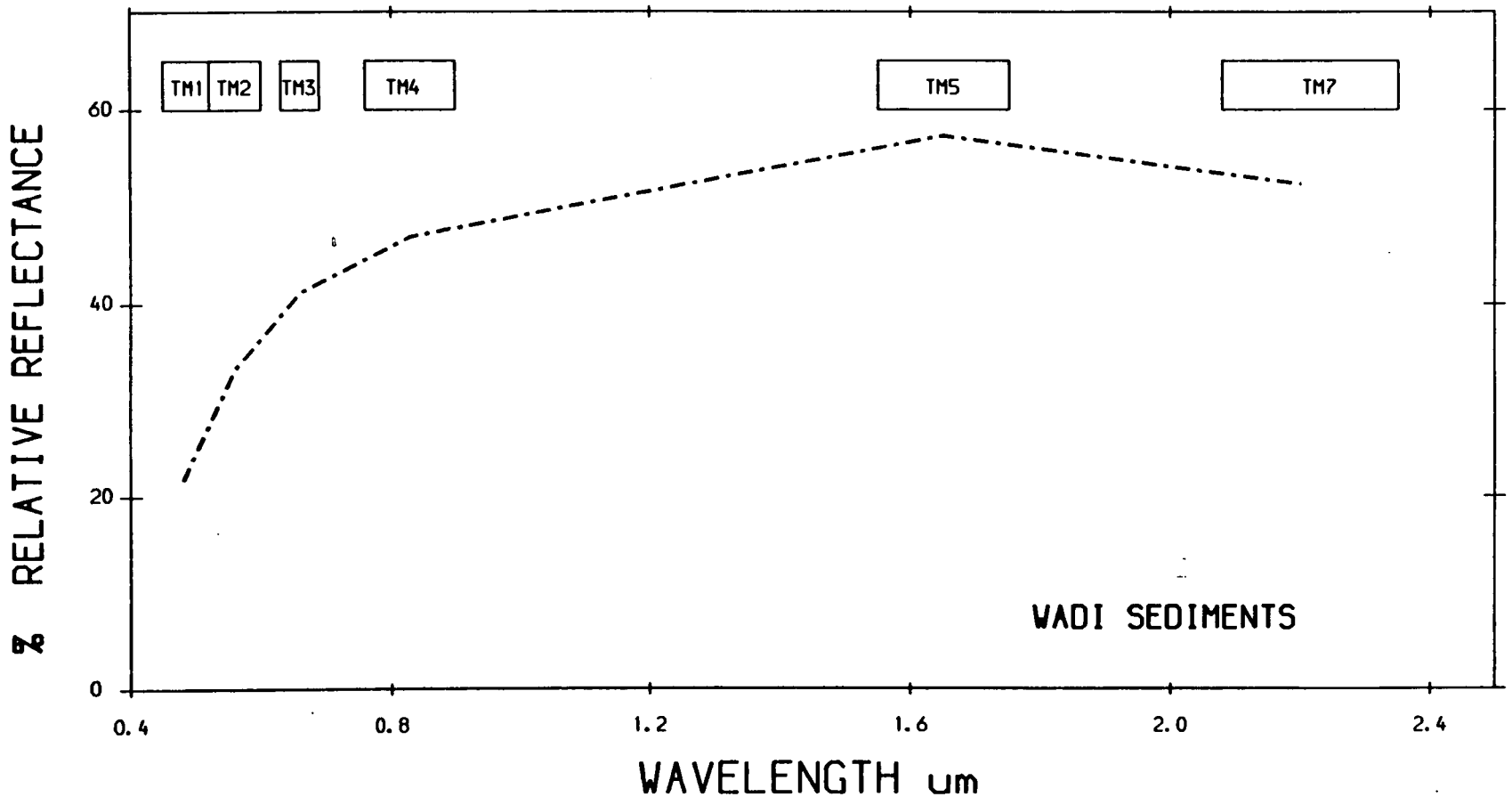

LANDSAT TM CALIBRATED TO RELATIVE REFLCTANCE

MAHD ADH DHAHAB- SAUDI ARABIA

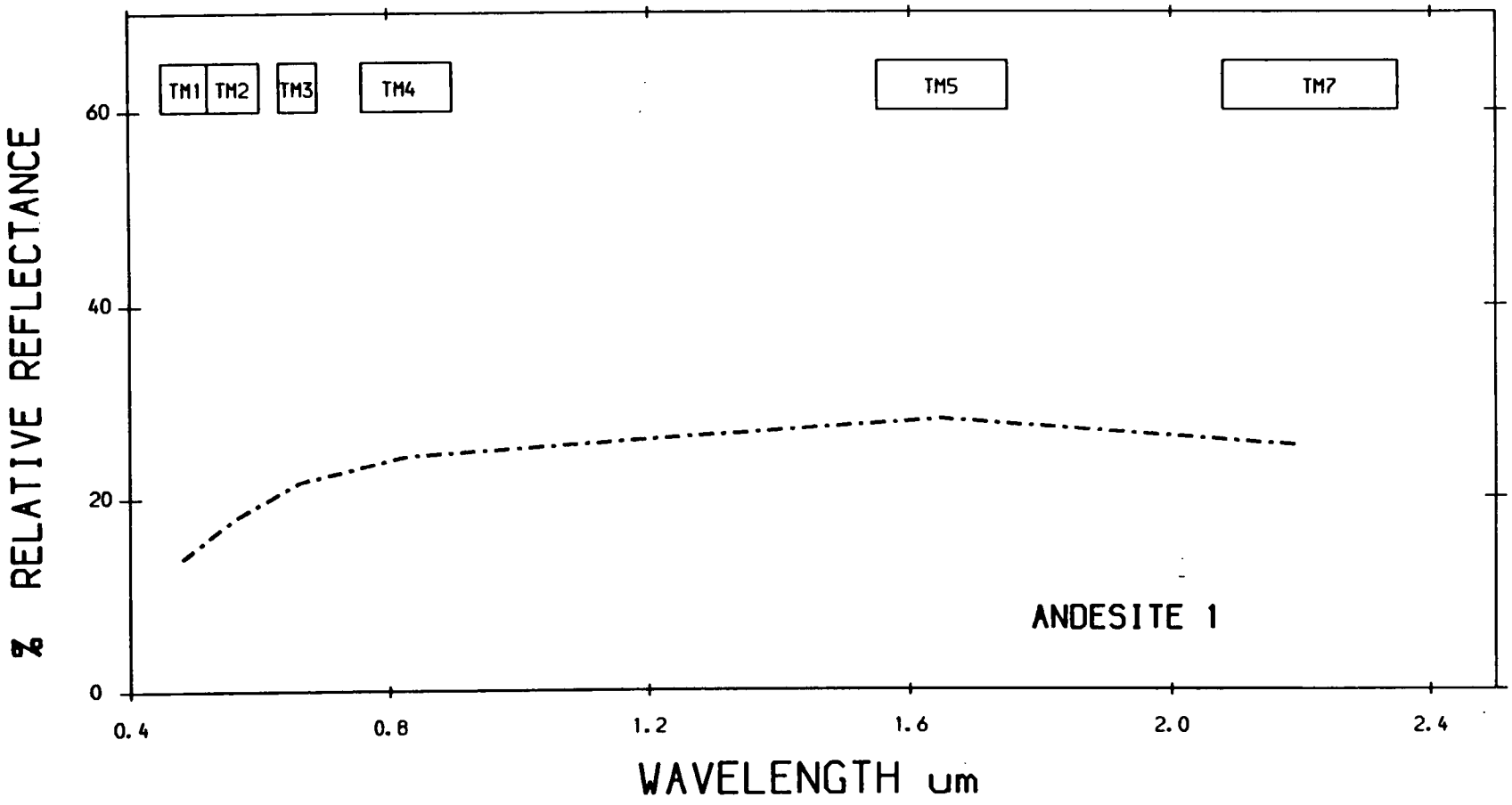

LANDSAT TM CALIBRATED TO RELATIVE REFLCTANCE

MAHD ADH DHAHAB- SAUDI ARABIA

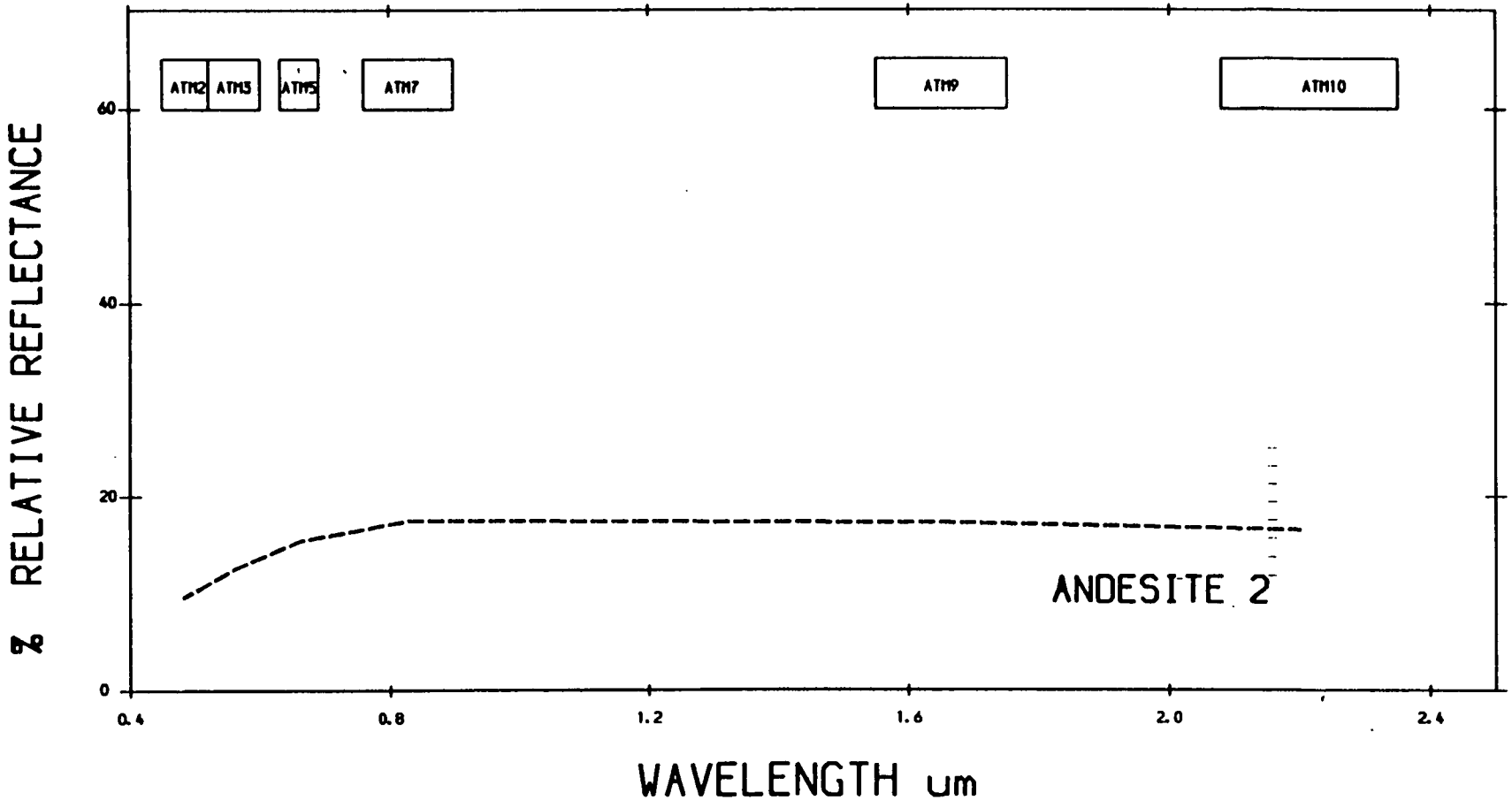

ATM 3000 M BAND EQUIVALENT TO TM CALIBRATED TO RELATIVE REFLECTANCE USING CALIBRATION CUR

MAHD ADH DHAHAB- SAUDI ARABIA

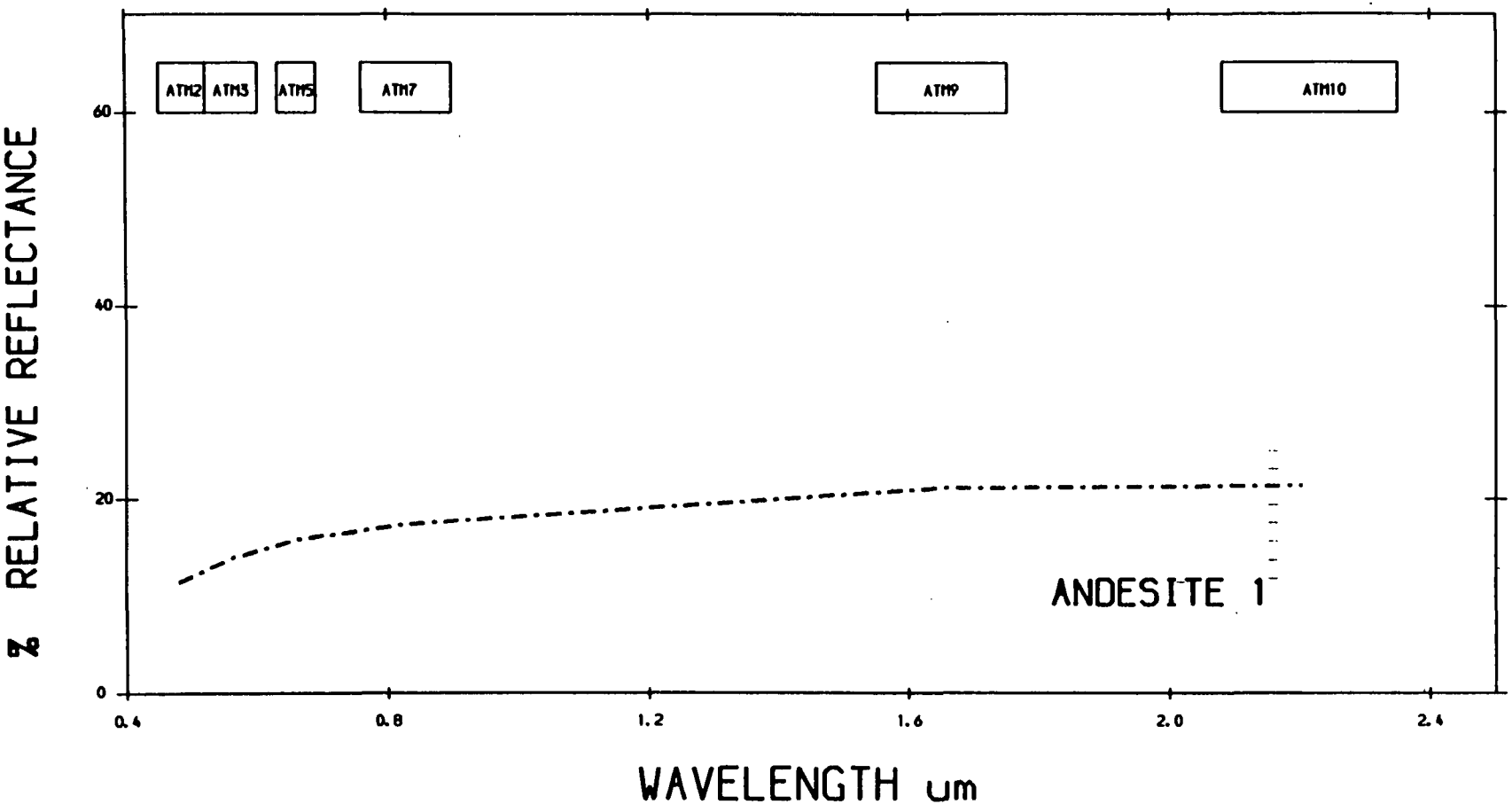

ATM 3000 M BAND EQUIVALENT TO TM CALIBRATED TO RELATIVE REFLECTANCE USING CALIBRATION CUR

MAHD ADH DHAHAB- SAUDI ARABIA

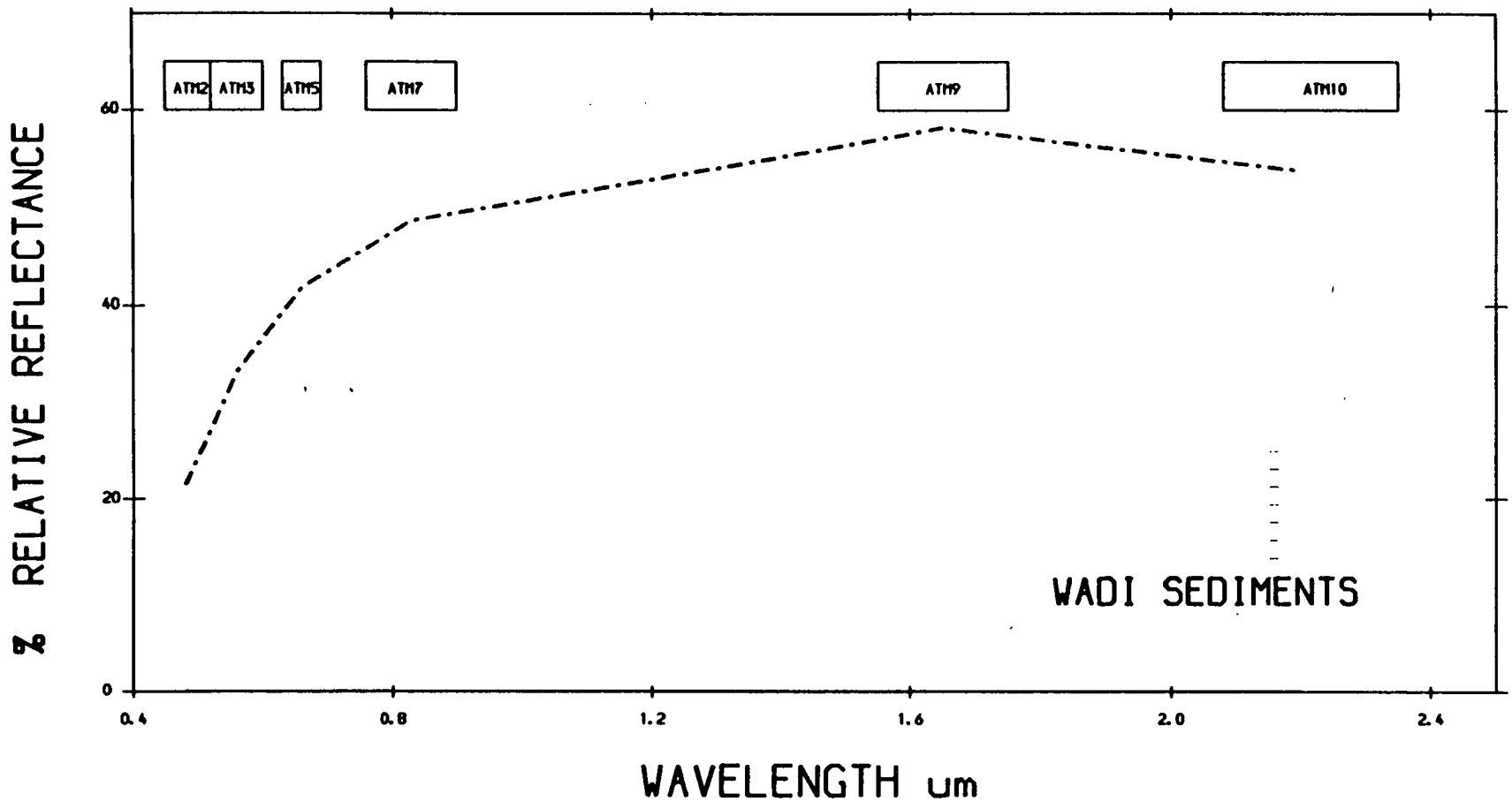

ATM 3000 M BAND EQUIVALENT TO TM CALIBRATED TO RELATIVE REFLECTANCE USING CALIBRATION CUR

MAHD ADH DHAHAB- SAUDI ARABIA

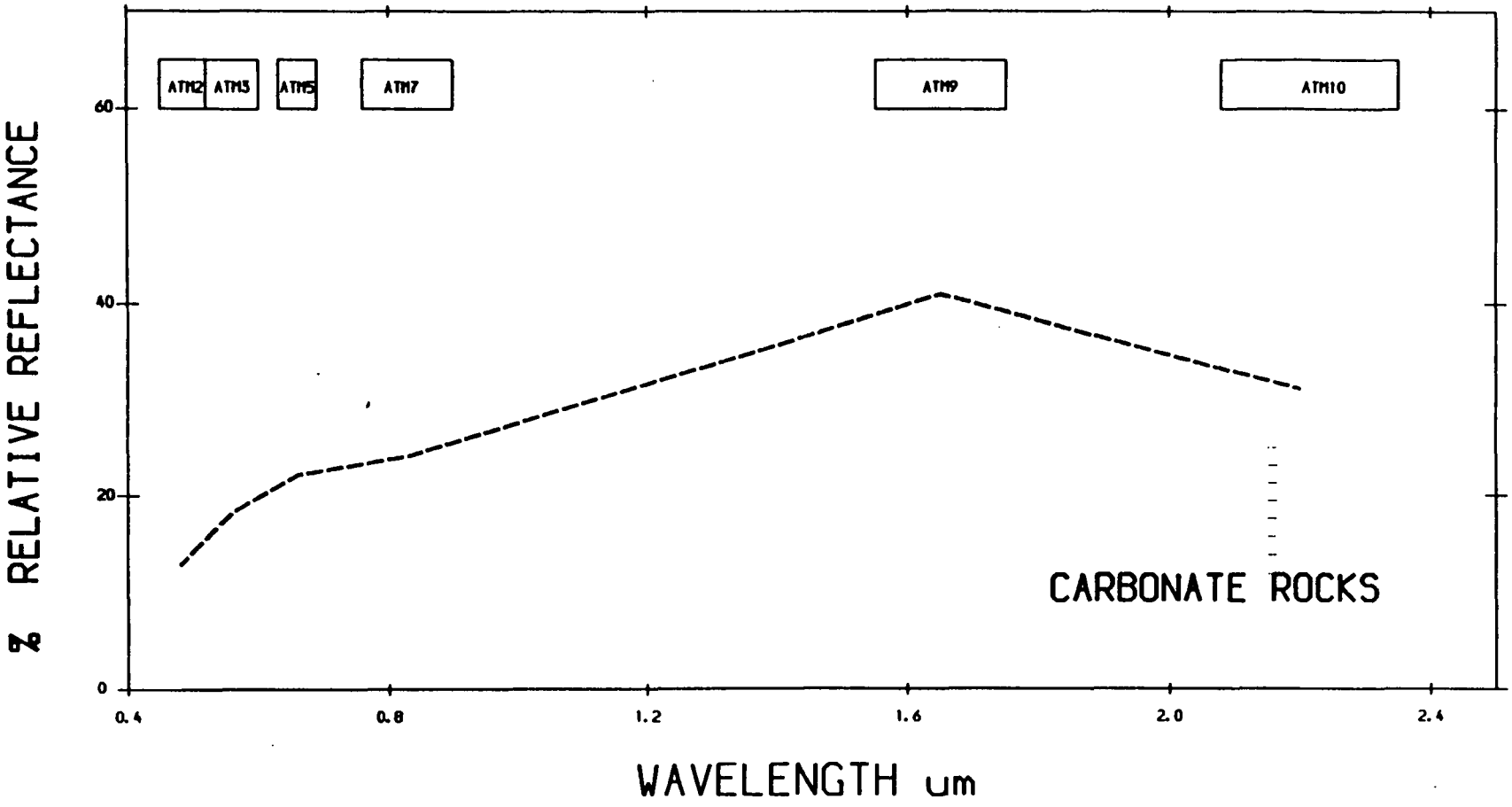

ATM 3000 M BAND EQUIVALENT TO TM CALIBRATED TO RELATIVE REFLECTANCE USING CALIBRATION CUR

MAHD ADH DHAHAB- SAUDI ARABIA

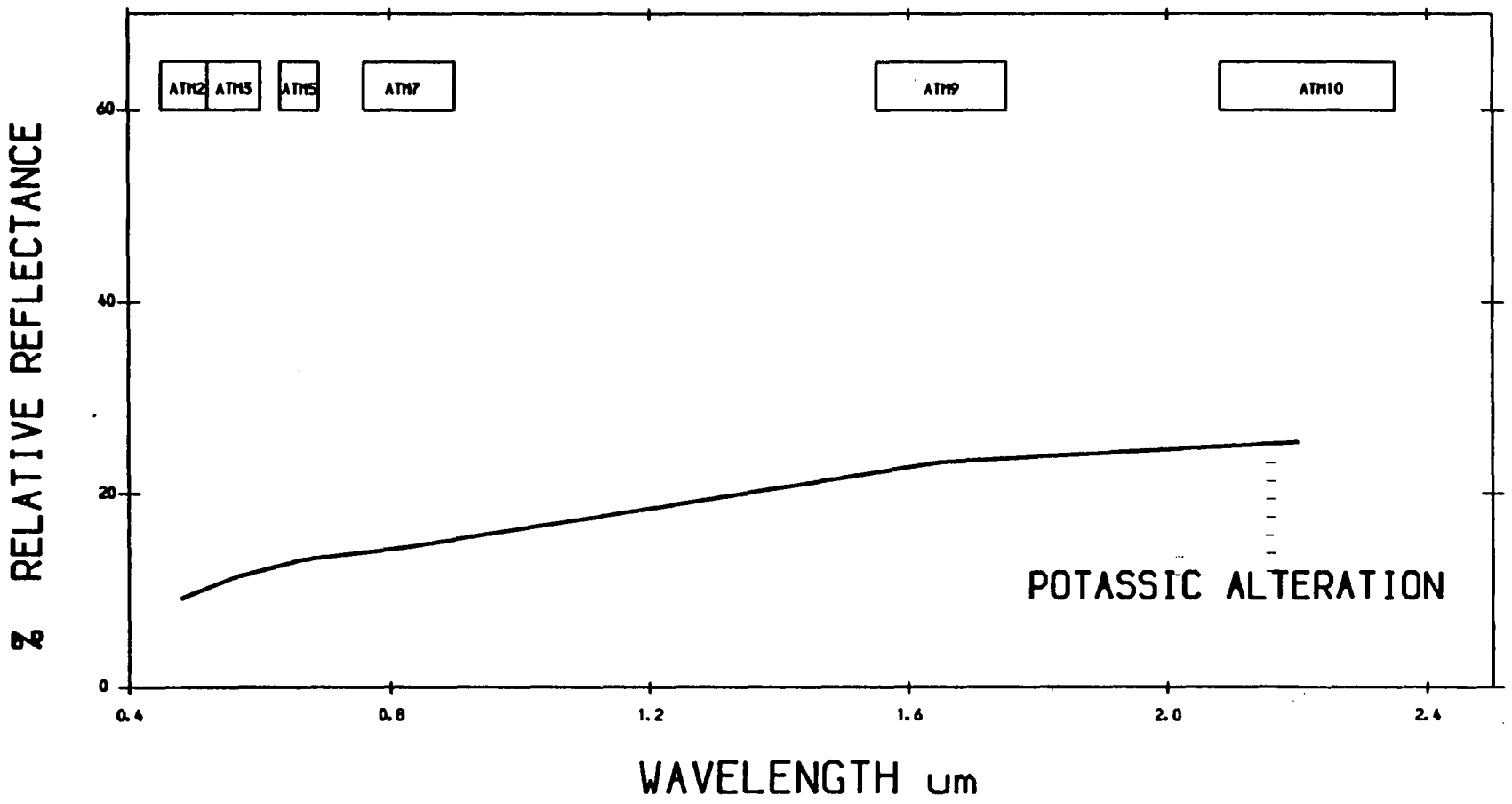

ATM 1000 M BAND EQUIVALENT TO TM CALIBRATED TO RELATIVE REFLECTANCE USING CALIBRATION CURVE

MAHD ADH DHAHAB- SAUDI ARABIA

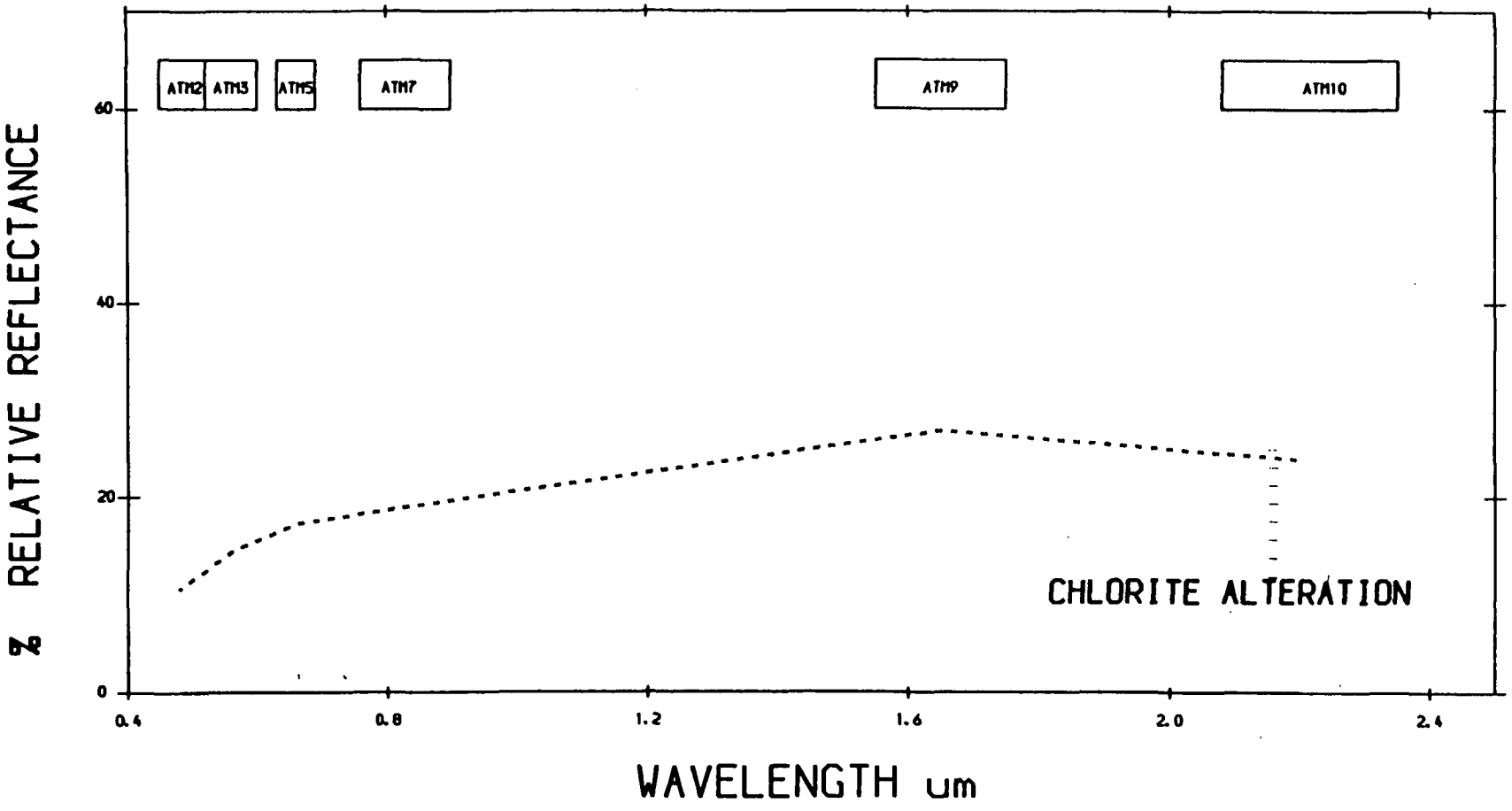

ATM 3000 M BAND EQUIVALENT TO TM CALIBRATED TO RELATIVE REFLECTANCE USING CALIBRATION CUR

MAHD ADH DHAHAB- SAUDI ARABIA

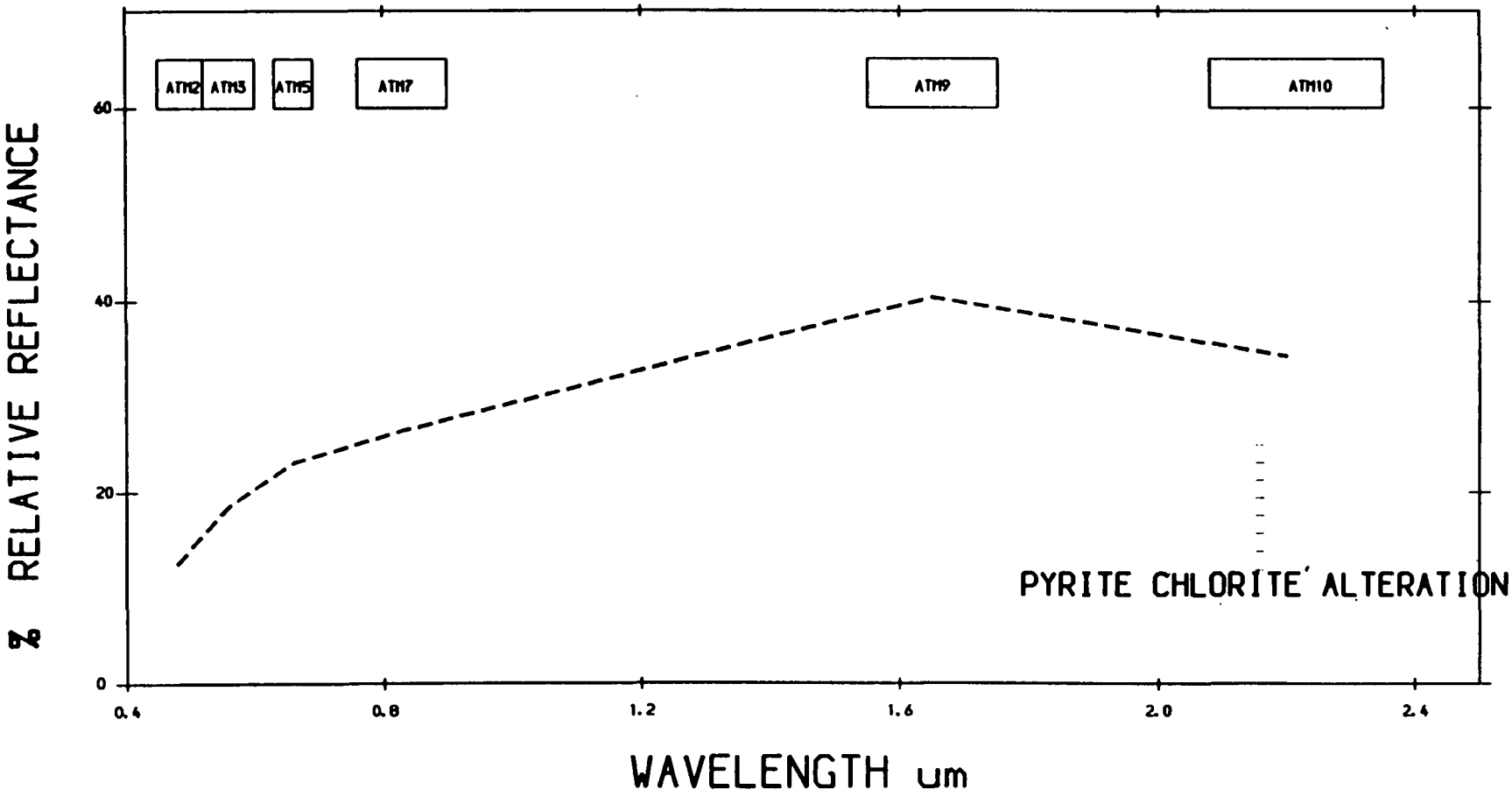

ATM 3000 M BAND EQUIVALENT TO TM CALIBRATED TO RELATIVE REFLECTANCE USING CALIBRATION CUR

MAHD ADH DHAHAB- SAUDI ARABIA

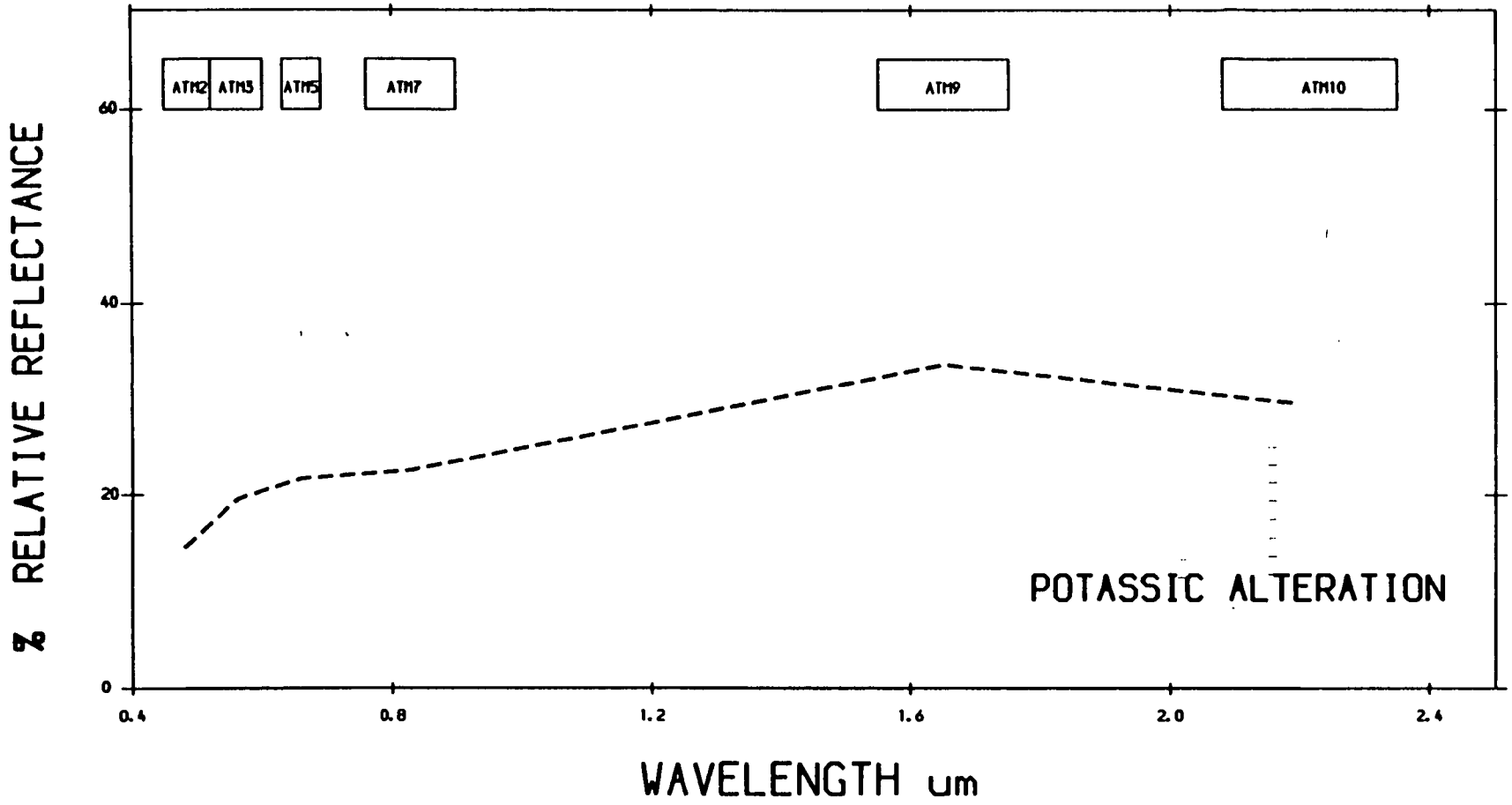

ATM 3000 M BAND EQUIVALENT TO TM CALIBRATED TO RELATIVE REFLECTANCE USING CALIBRATION CUR

MAHD ADH DHAHAB- SAUDI ARABIA

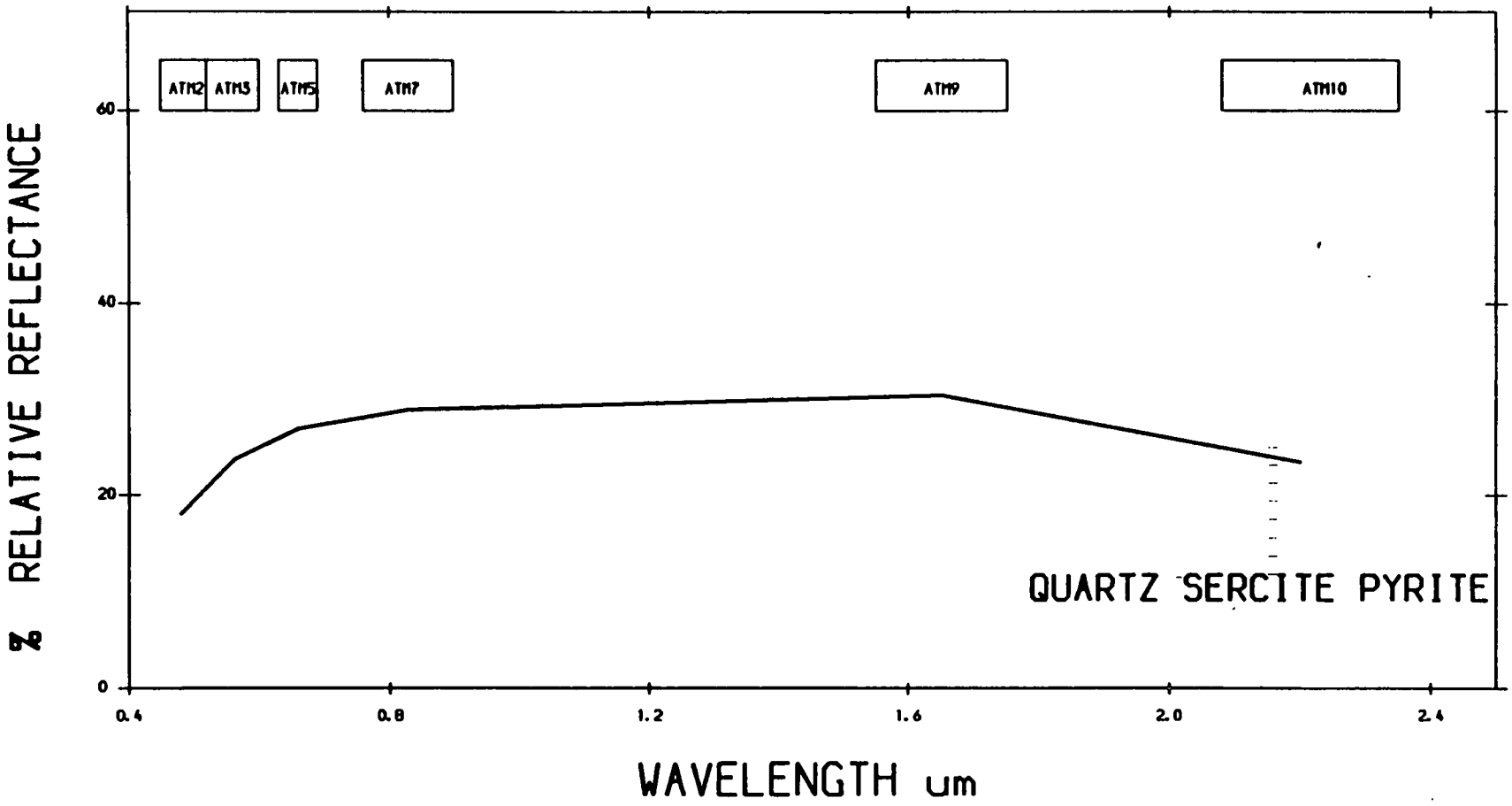

ATM 3000 M BAND EQUIVALENT TO TM CALIBRATED TO RELATIVE REFLECTANCE USING CALIBRATION CUR

MAHD ADH DHAHAB- SAUDI ARABIA

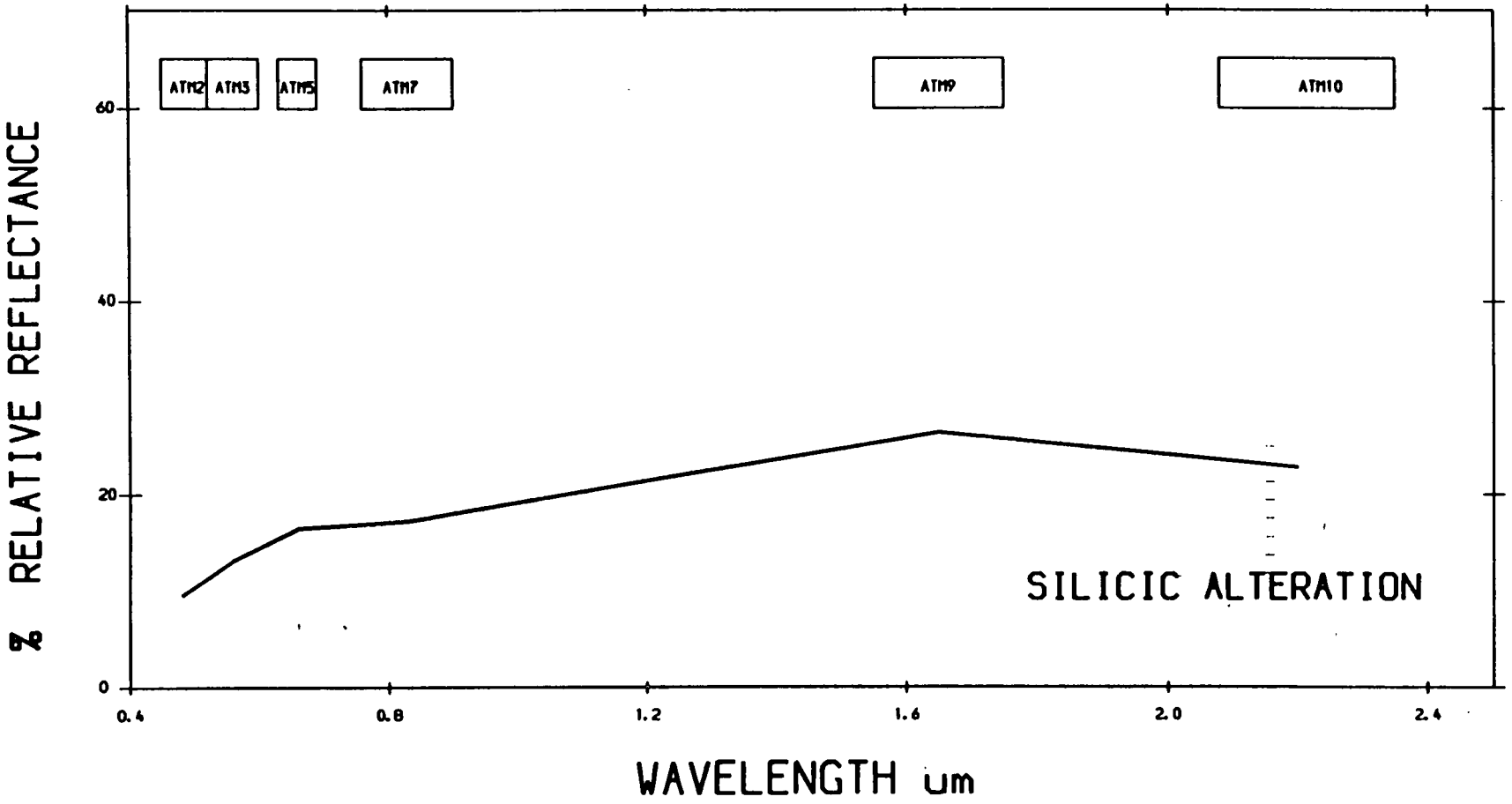

ATM 3000 M BAND EQUIVALENT TO TM CALIBRATED TO RELATIVE REFLECTANCE USING CALIBRATION CUR

MAHD ADH DHAHAB- SAUDI ARABIA

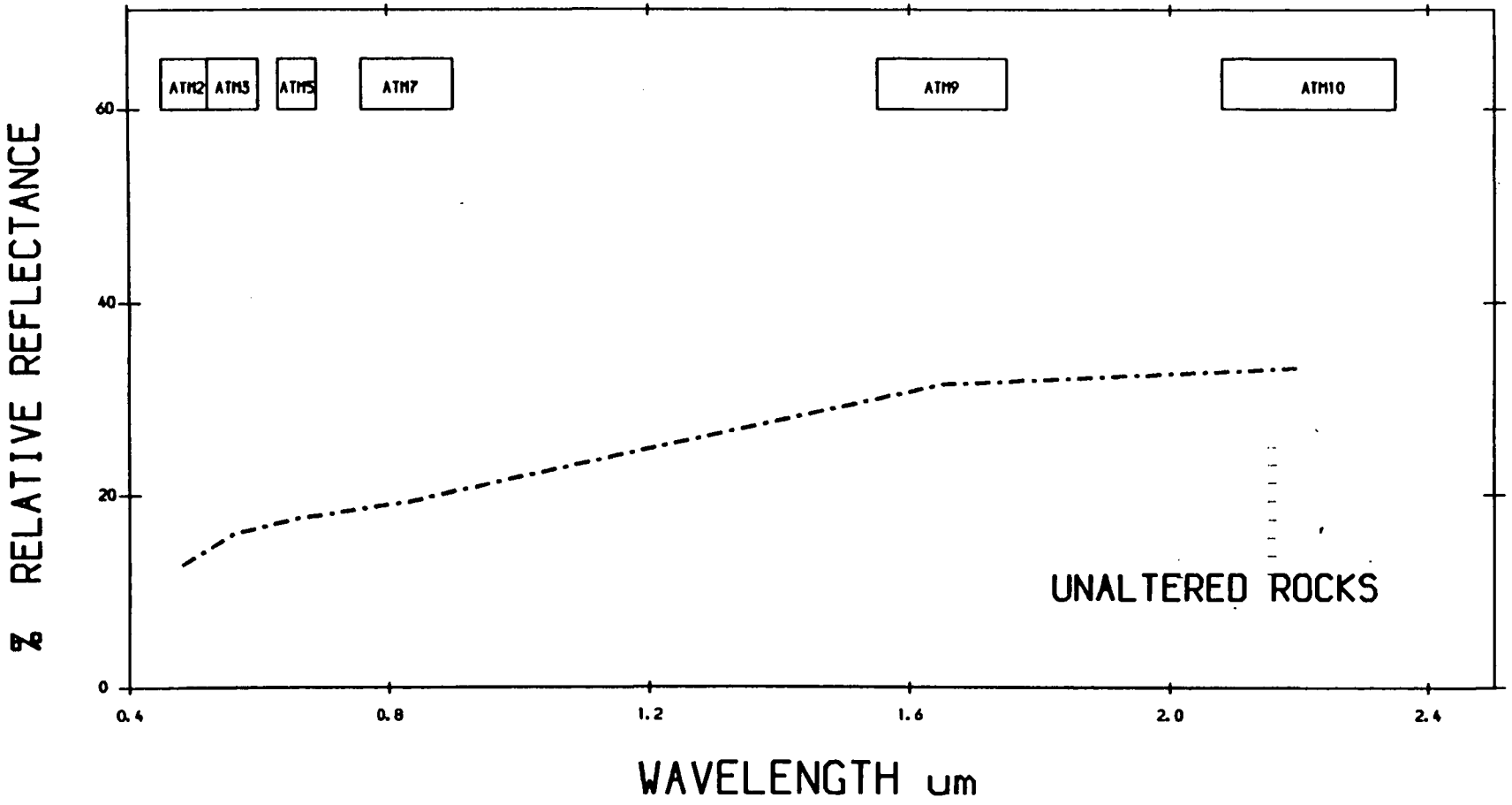

ATM 3000 M BAND EQUIVALENT TO TM CALIBRATED TO RELATIVE REFLECTANCE USING CALIBRATION CUR

MAHD ADH DHAHAB- SAUDI ARABIA

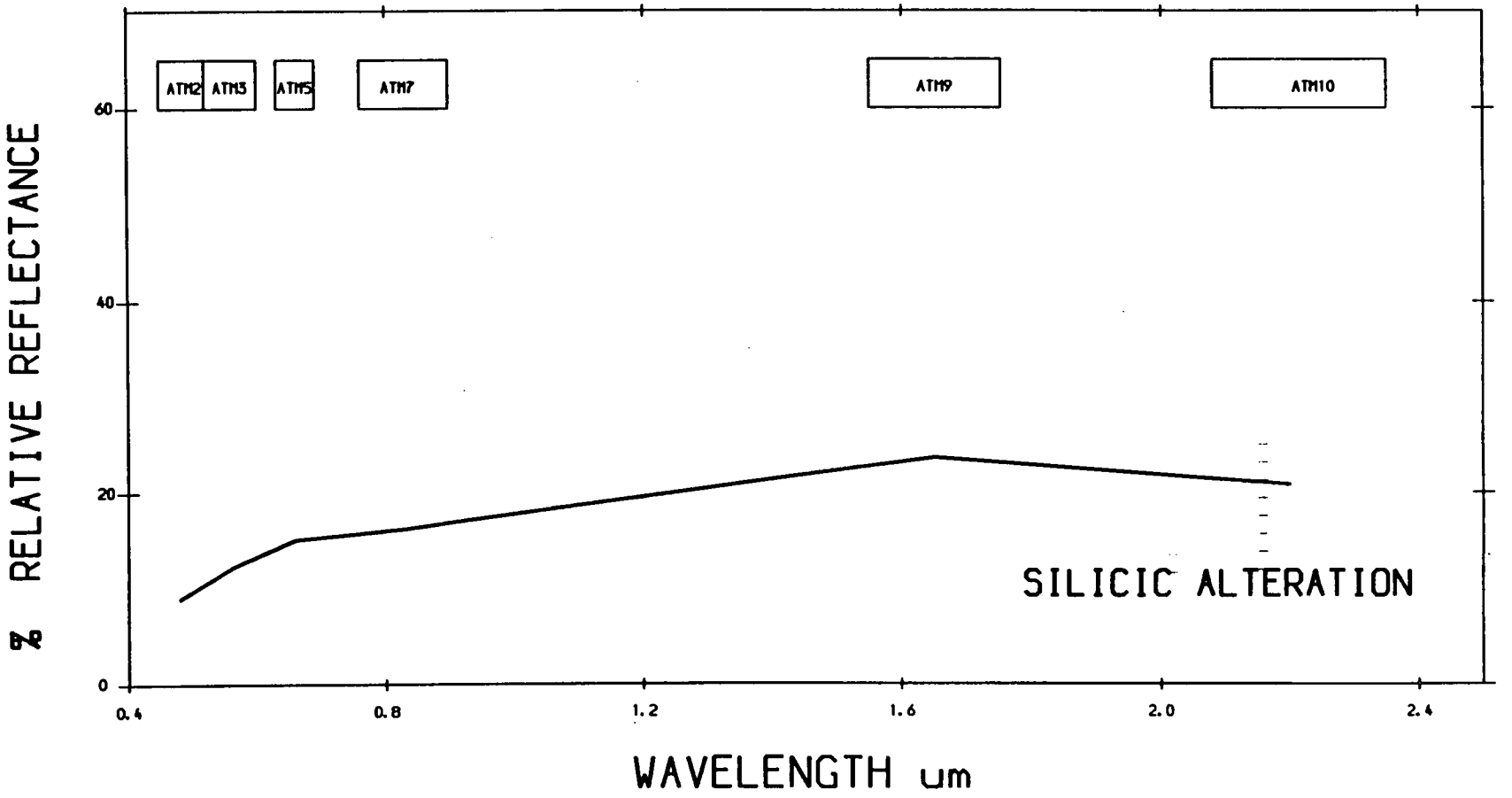

ATM 2000 M BAND EQUIVALENT TO TM CALIBRATED TO RELATIVE REFLECTANCE USING CALIBRATION CURVE

MAHD ADH DHAHAB- SAUDI ARABIA

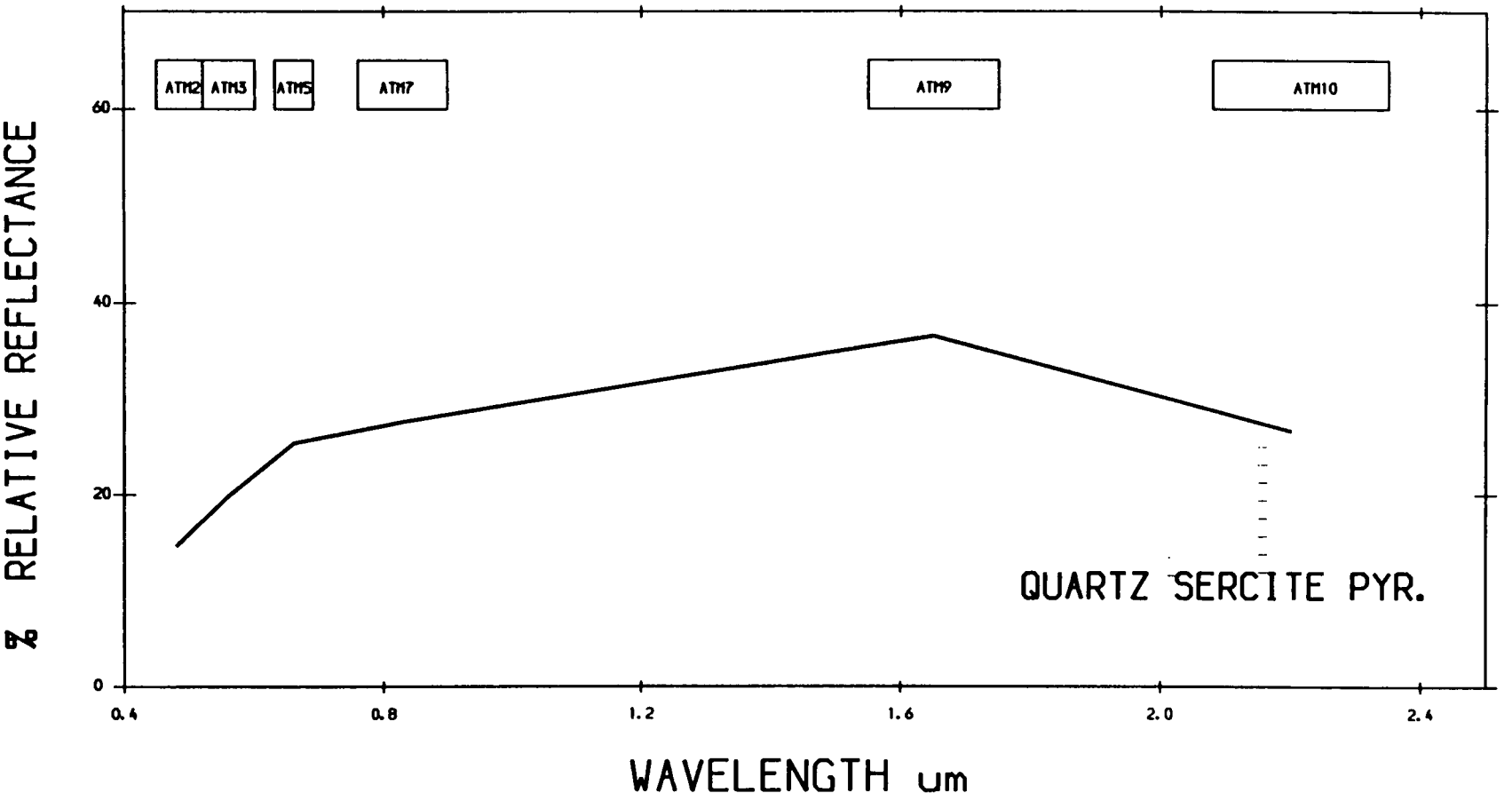

ATM 2000 M BAND EQUIVALENT TO TM CALIBRATED TO RELATIVE REFLECTANCE USING CALIBRATION CURVE

MAHD ADH DHAHAB- SAUDI ARABIA

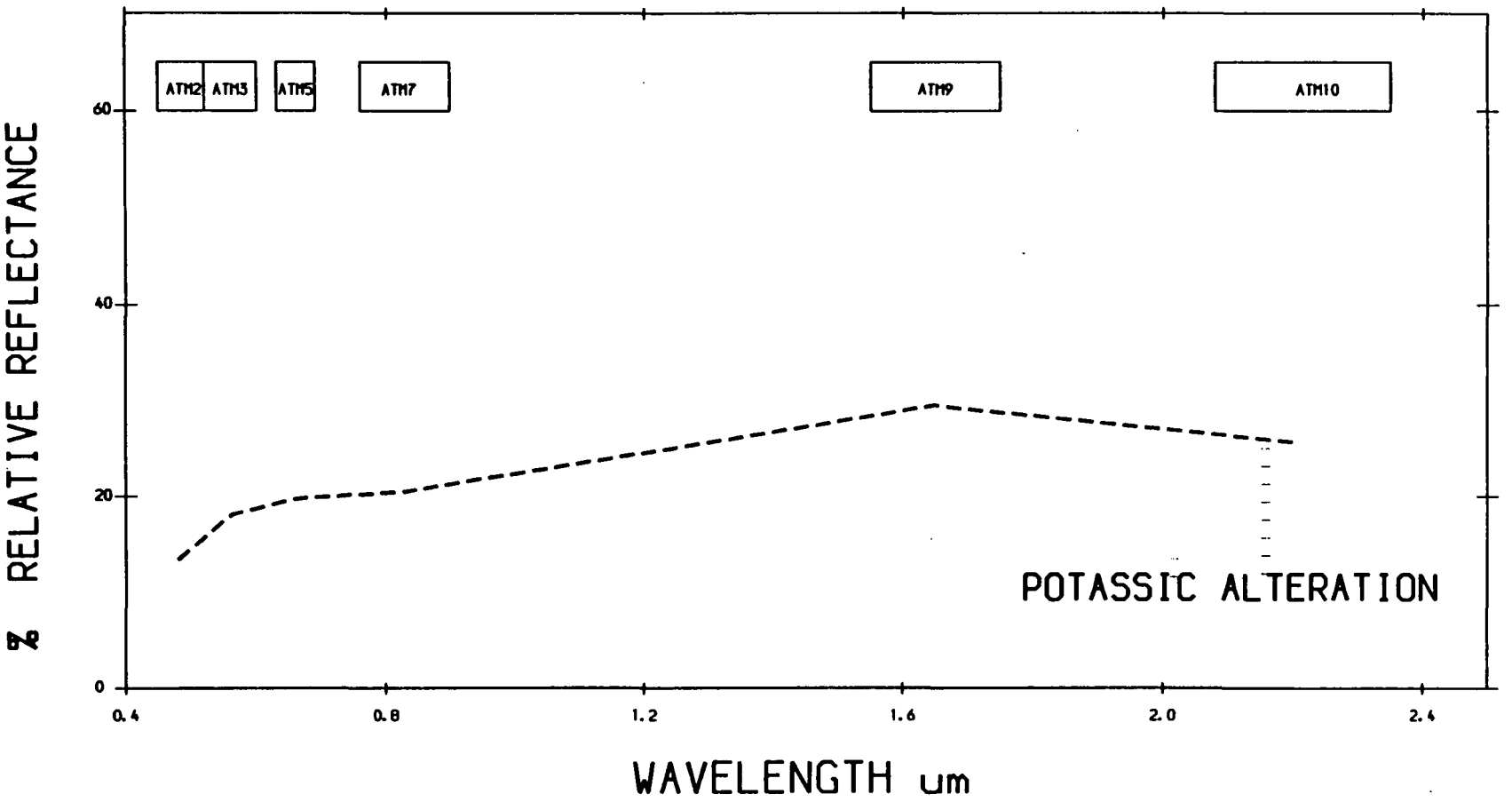

ATM 2000 M BAND EQUIVALENT TO TM CALIBRATED TO RELATIVE REFLECTANCE USING CALIBRATION CURVE

MAHD ADH DHAHAB- SAUDI ARABIA

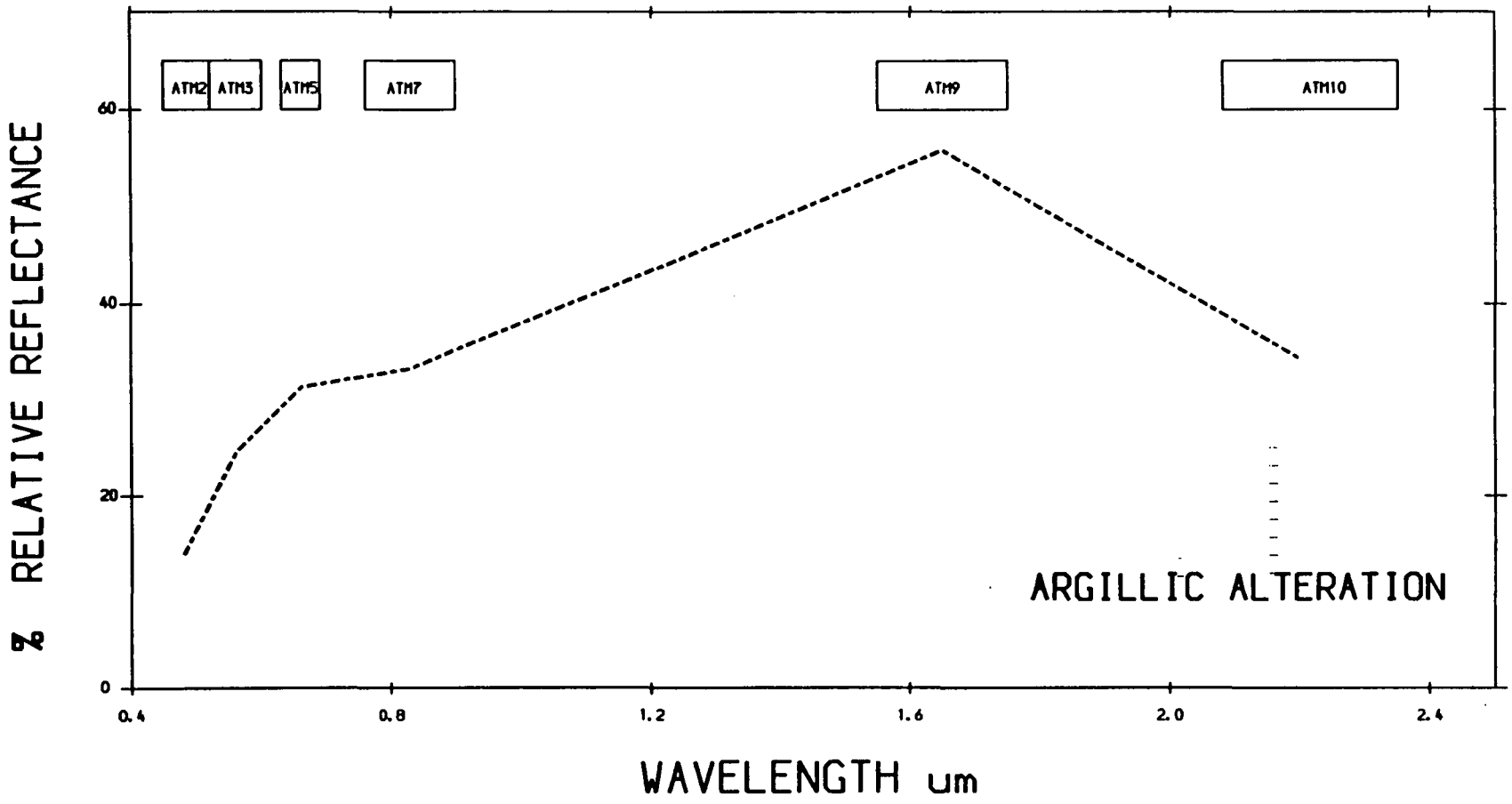

ATM 2000 M BAND EQUIVALENT TO TM CALIBRATED TO RELATIVE REFLECTANCE USING CALIBRATION CURVE

MAHD ADH DHAHAB- SAUDI ARABIA

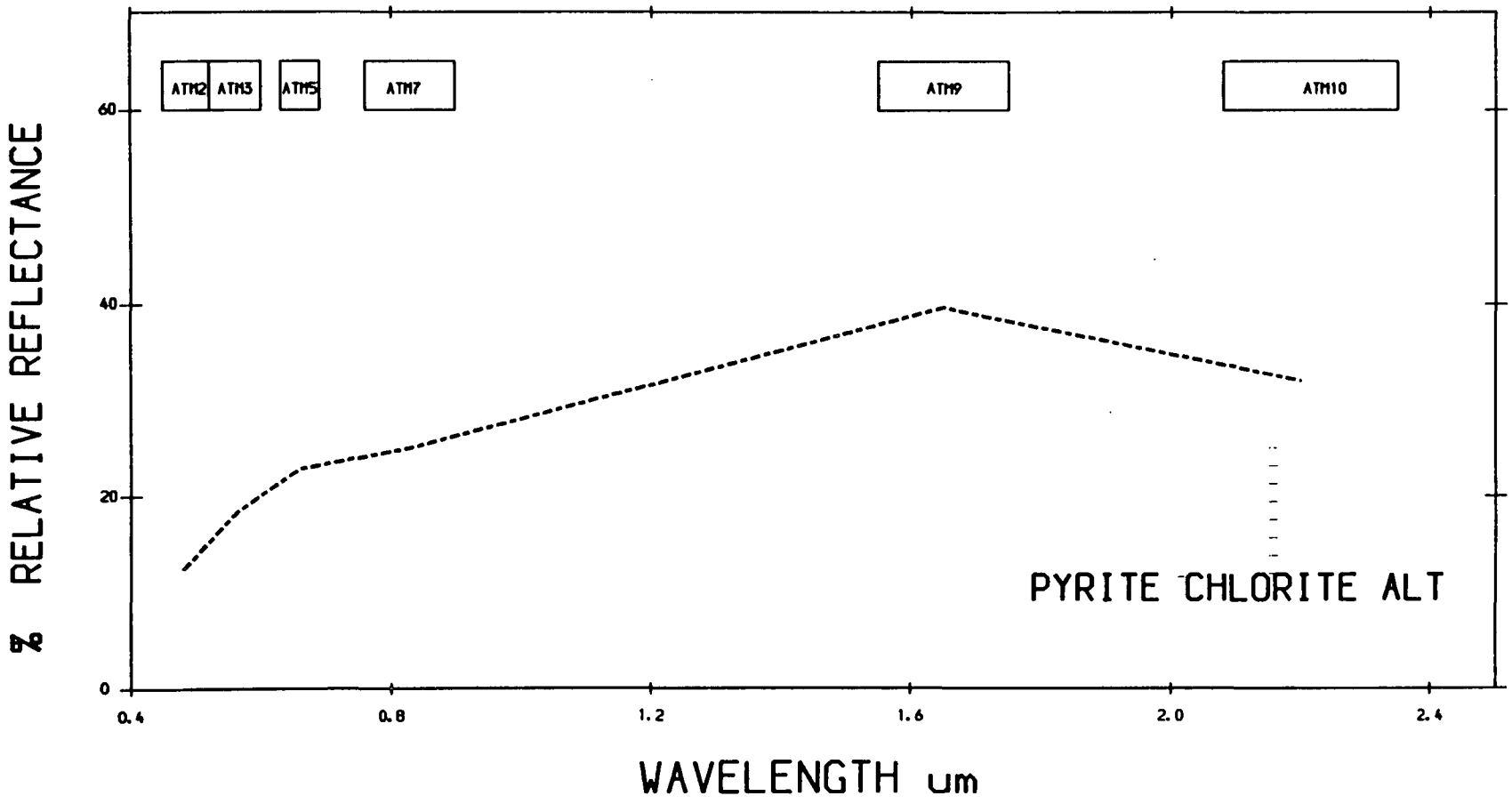

ATM 2000 M BAND EQUIVALENT TO TM CALIBRATED TO RELATIVE REFLECTANCE USING CALIBRATION CURVE

MAHD ADH DHAHAB- SAUDI ARABIA

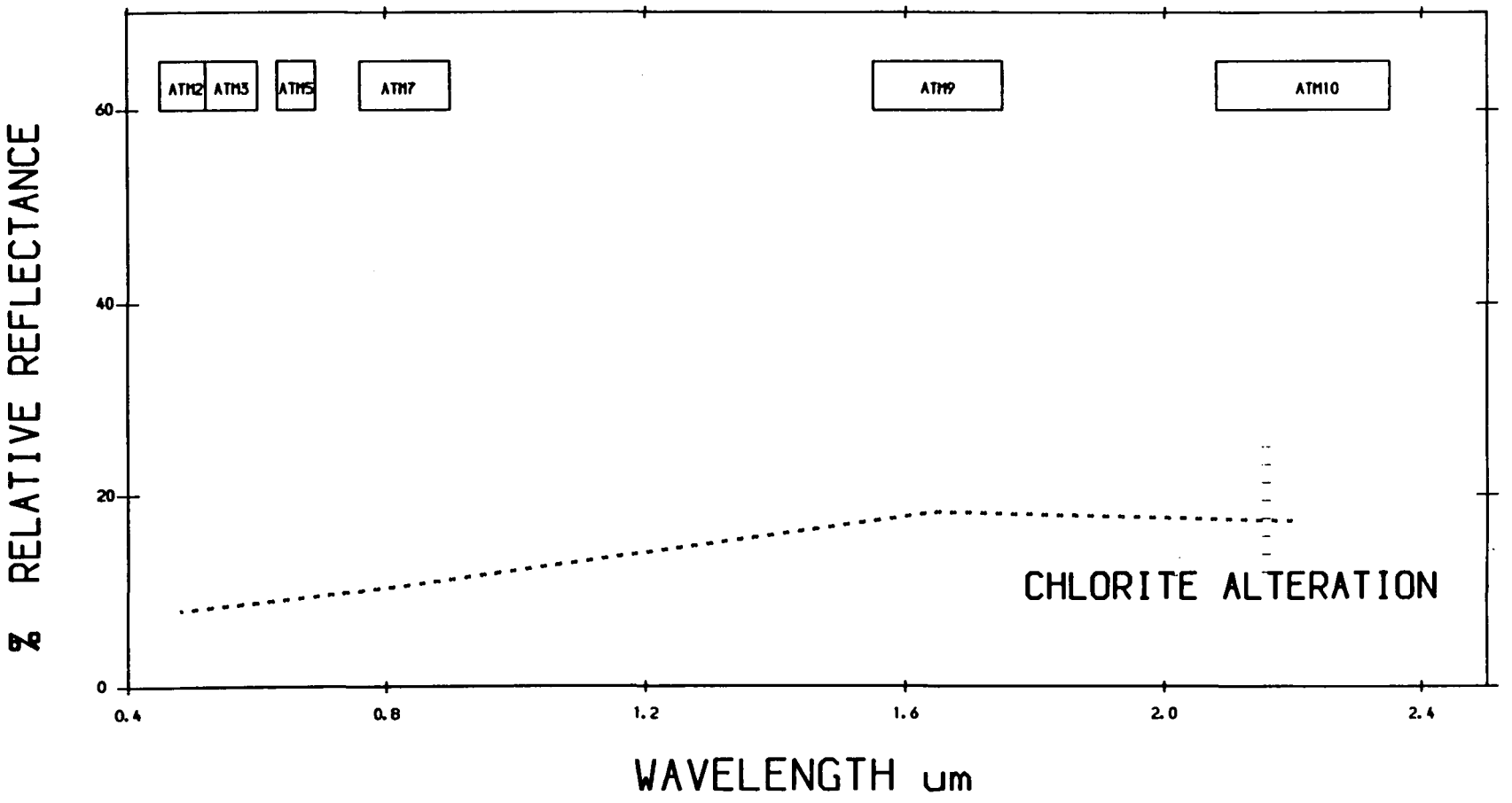

ATM 2000 M BAND EQUIVALENT TO TM CALIBRATED TO RELATIVE REFLECTANCE USING CALIBRATION CURVE

MAHD ADH DHAHAB- SAUDI ARABIA

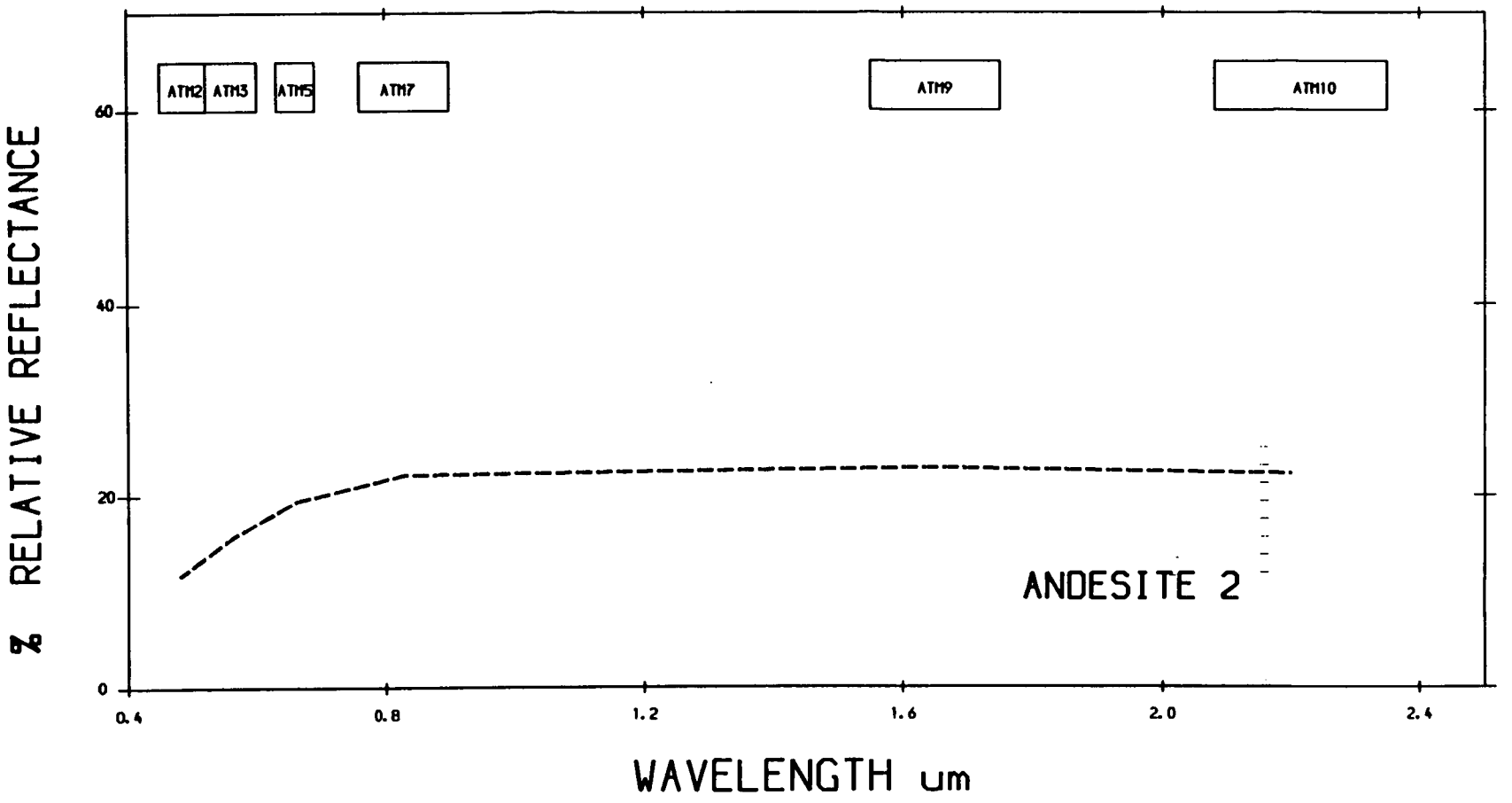

ATM 2000 M BAND EQUIVALENT TO TM CALIBRATED TO RELATIVE REFLECTANCE USING CALIBRATION CURVE

MAHD ADH DHAHAB- SAUDI ARABIA

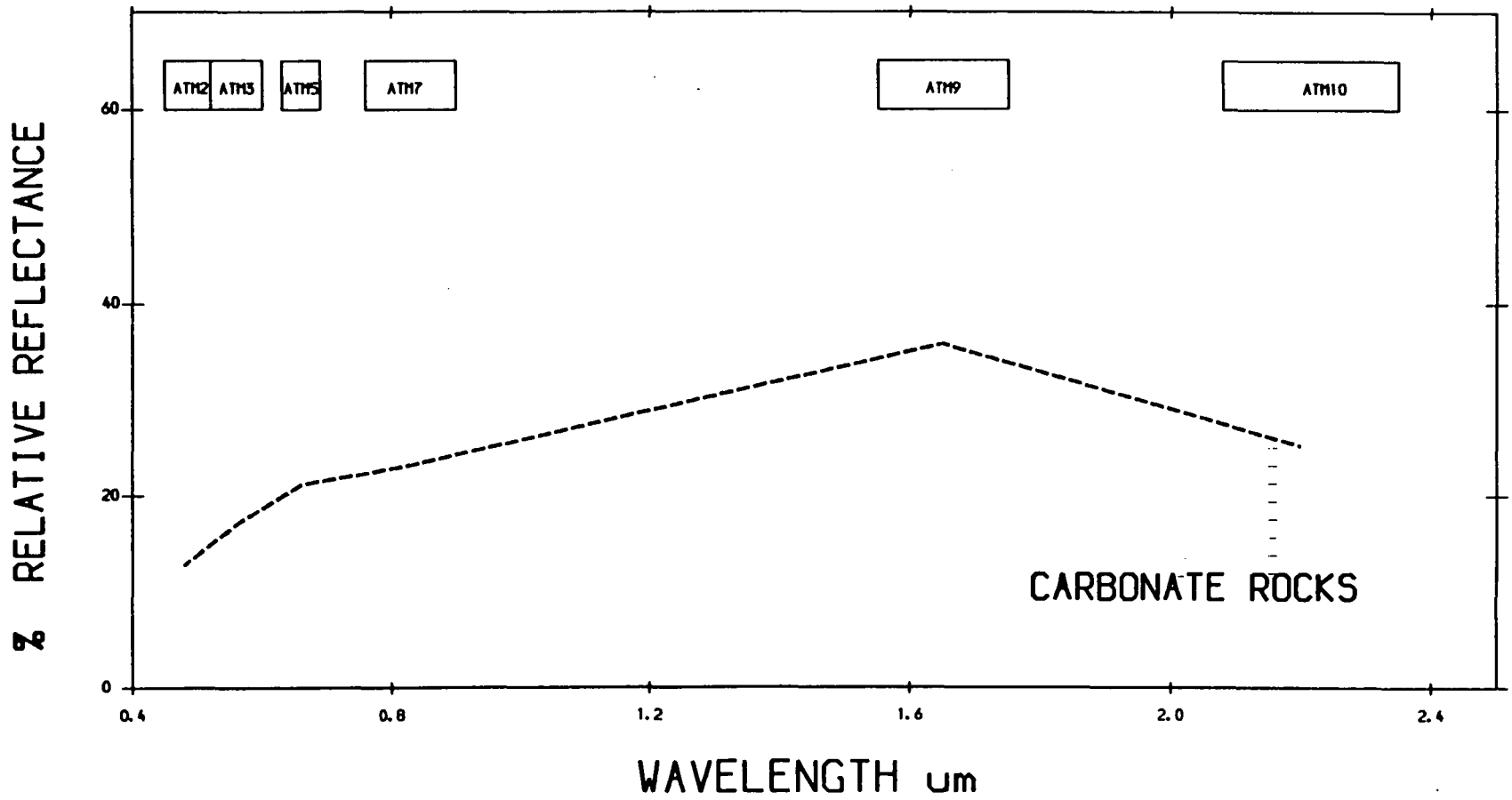

ATM 2000 M BAND EQUIVALENT TO TM CALIBRATED TO RELATIVE REFLECTANCE USING CALIBRATION CURVE

MAHD ADH DHAHAB- SAUDI ARABIA

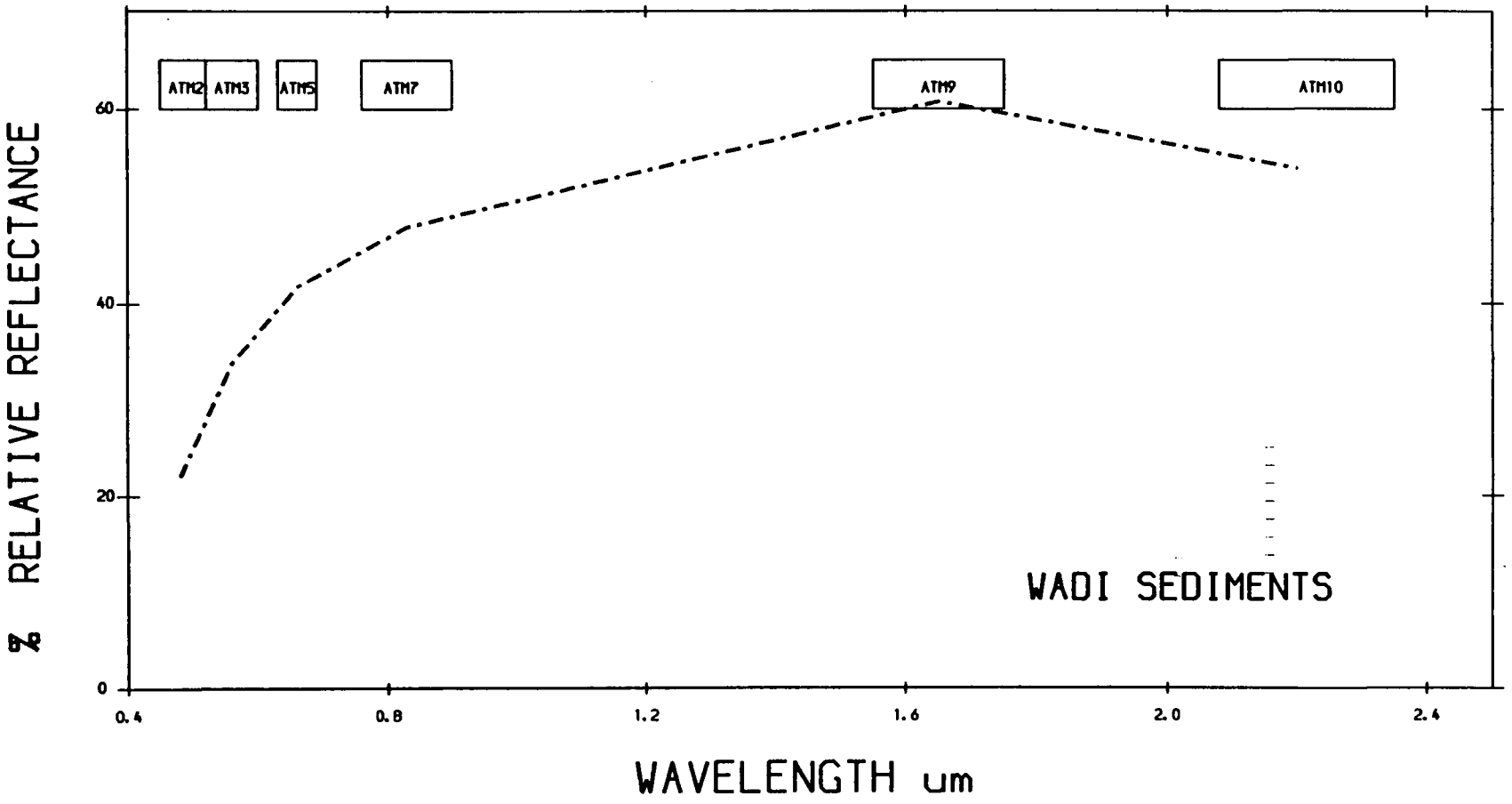

ATM 2000 M BAND EQUIVALENT TO TM CALIBRATED TO RELATIVE REFLECTANCE USING CALIBRATION CURVE

MAHD ADH DHAHAB- SAUDI ARABIA

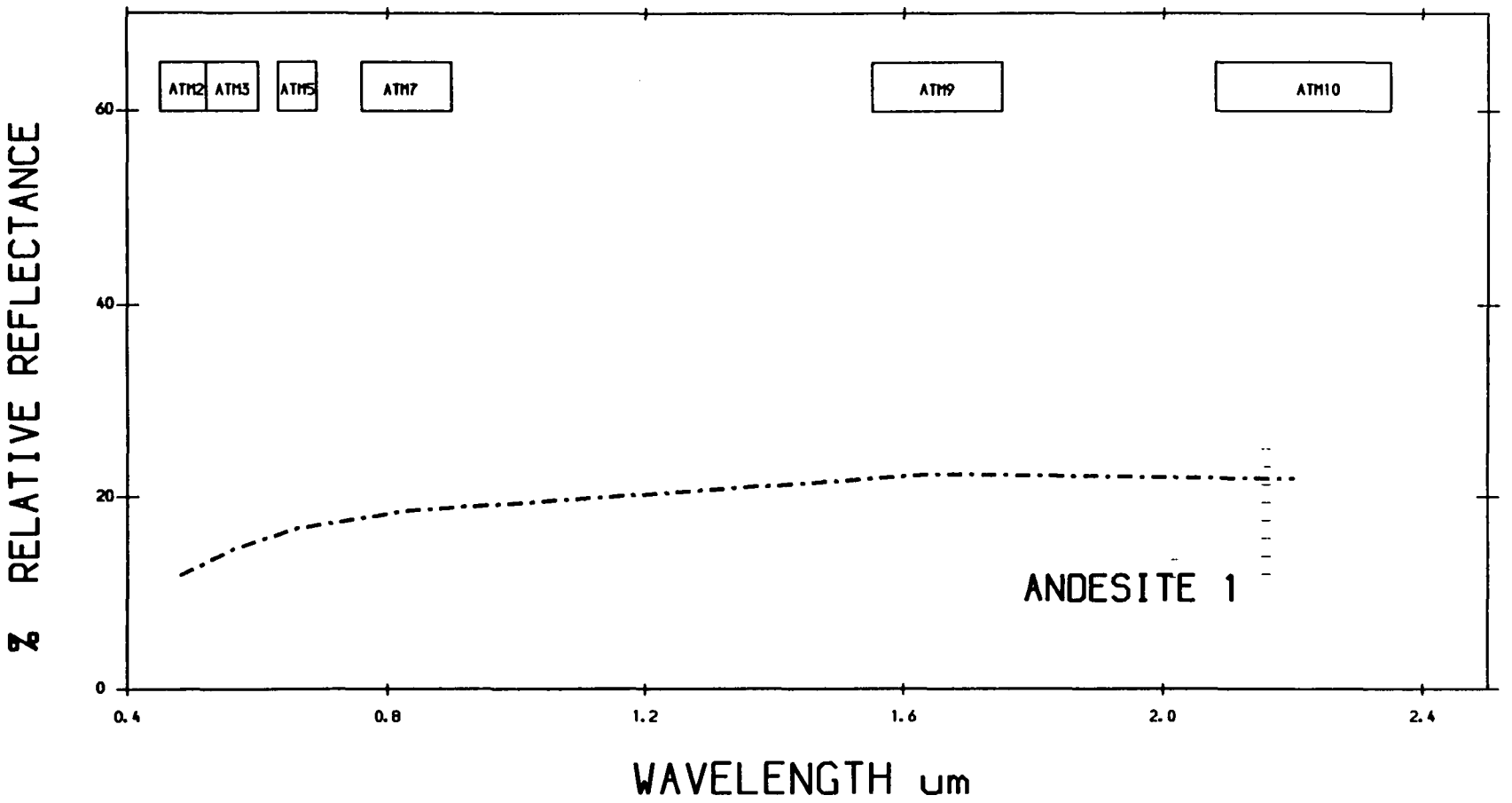

ATM 2000 M BAND EQUIVALENT TO TM CALIBRATED TO RELATIVE REFLECTANCE USING CALIBRATION CURVE

MAHD ADH DHAHAB- SAUDI ARABIA

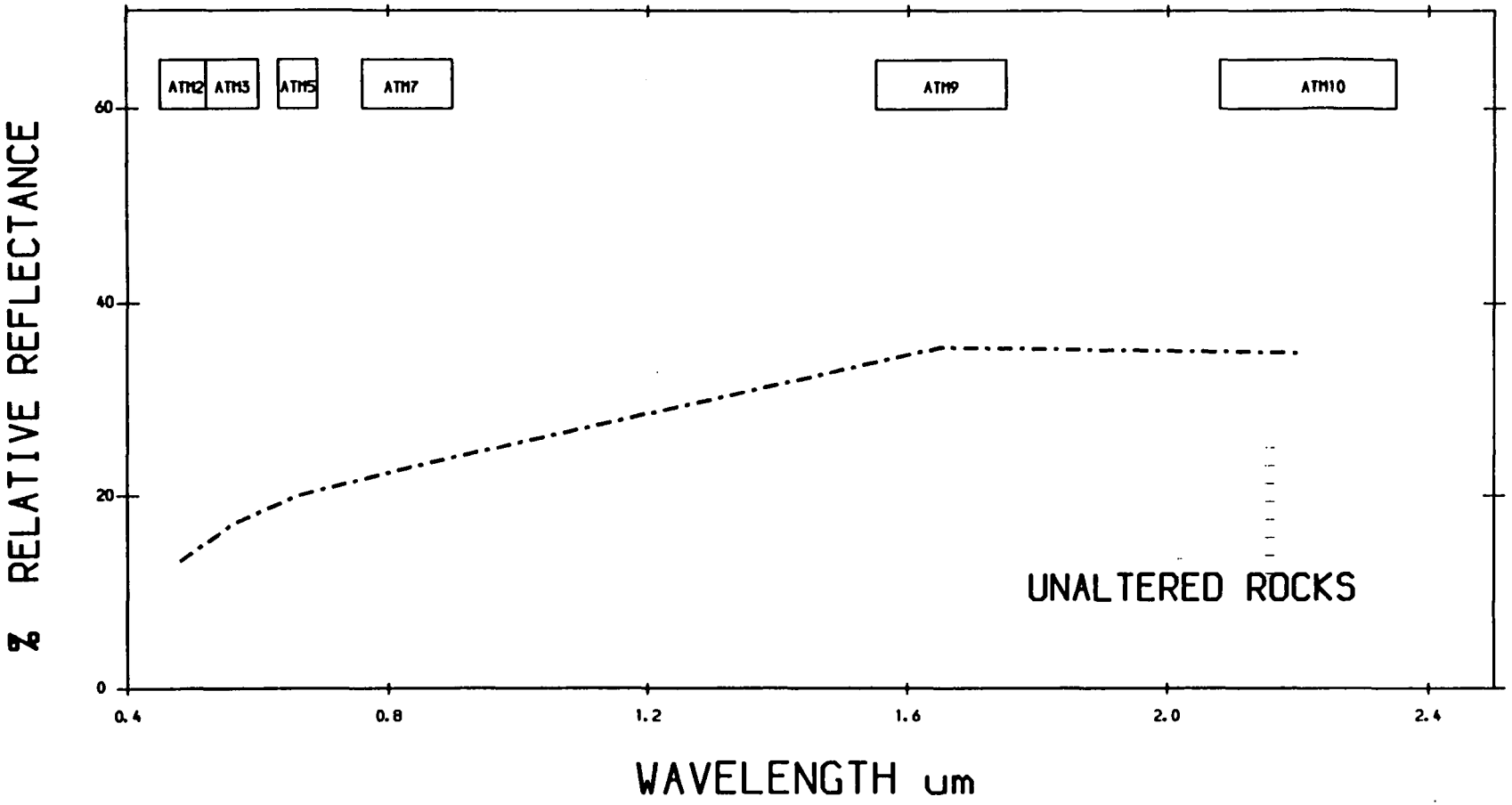

ATM 2000 M BAND EQUIVALENT TO TM CALIBRATED TO RELATIVE REFLECTANCE USING CALIBRATION CURVE

MAHD ADH DHAHAB- SAUDI ARABIA

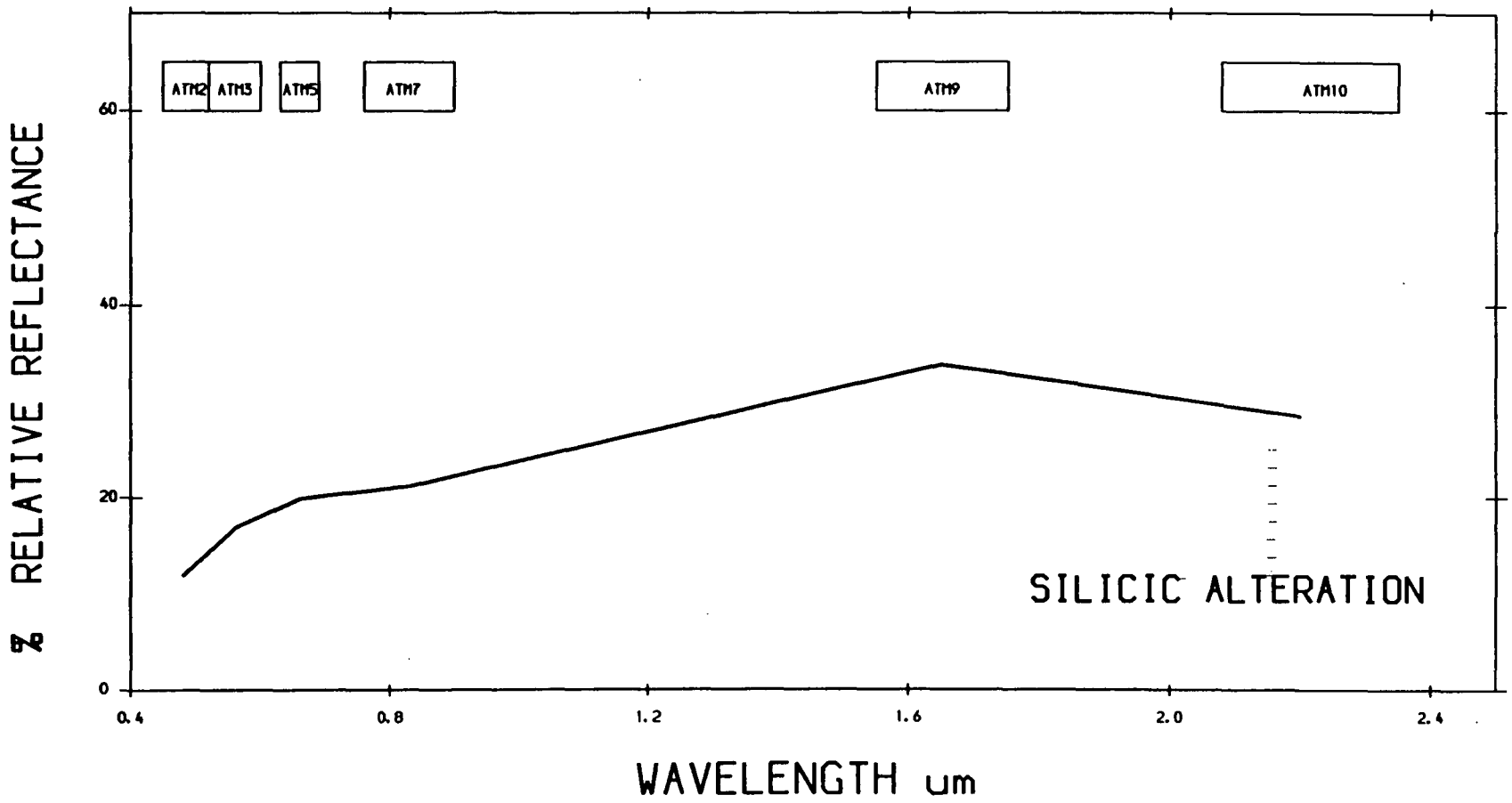

ATM 1000 M BAND EQUIVALENT TO TM CALIBRATED TO RELATIVE REFLECTANCE USING CALIBRATION CURVE

MAHD ADH DHAHAB- SAUDI ARABIA

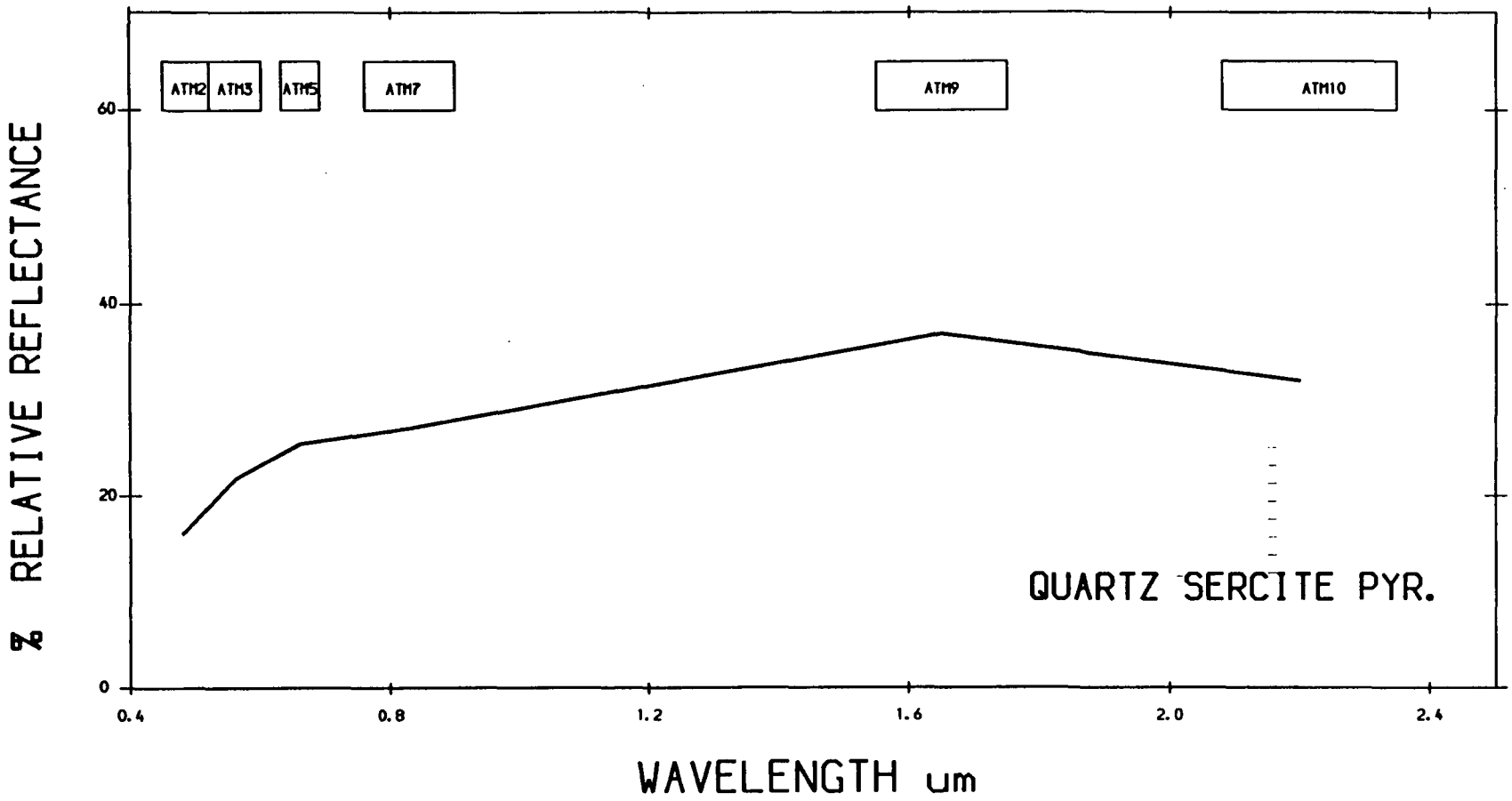

ATM 1000 M BAND EQUIVALENT TO TM CALIBRATED TO RELATIVE REFLECTANCE USING CALIBRATION CURVE

MAHD ADH DHAHAB- SAUDI ARABIA

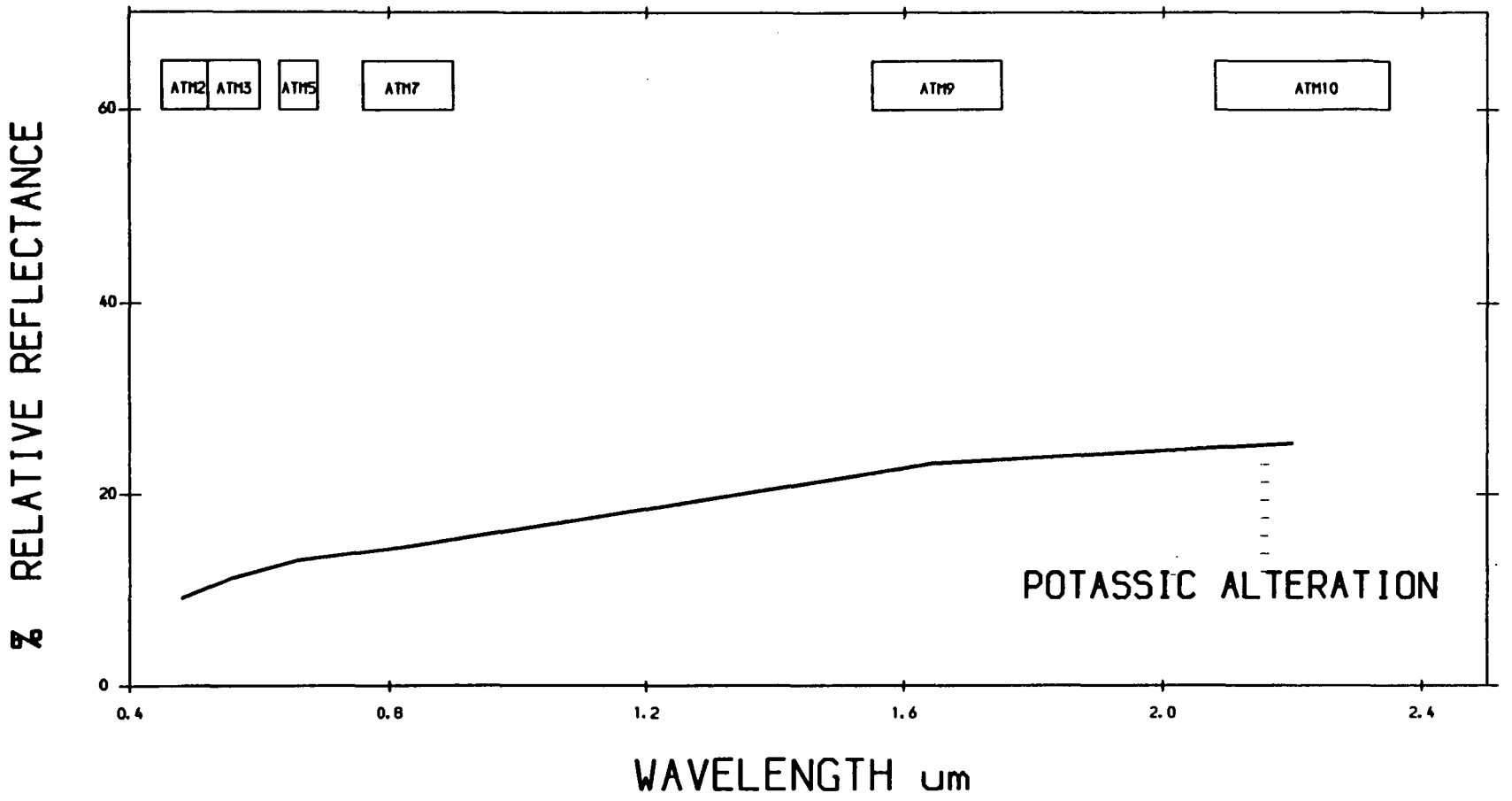

ATM 1000 M BAND EQUIVALENT TO TM CALIBRATED TO RELATIVE REFLECTANCE USING CALIBRATION CURVE

MAHD ADH DHAHAB- SAUDI ARABIA

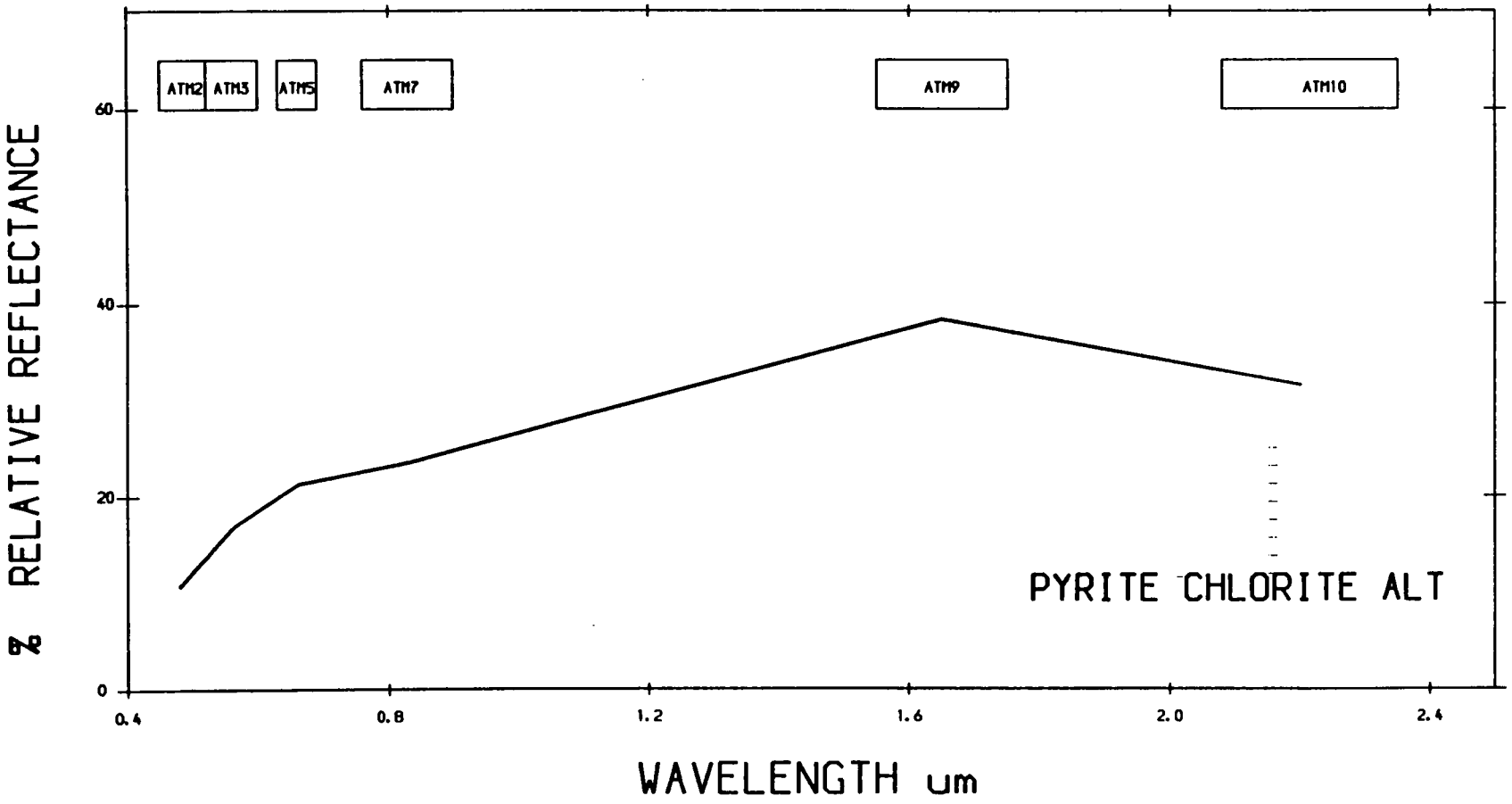

ATM 1000 M BAND EQUIVALENT TO TM CALIBRATED TO RELATIVE REFLECTANCE USING CALIBRATION CURVE

MAHD ADH DHAHAB- SAUDI ARABIA

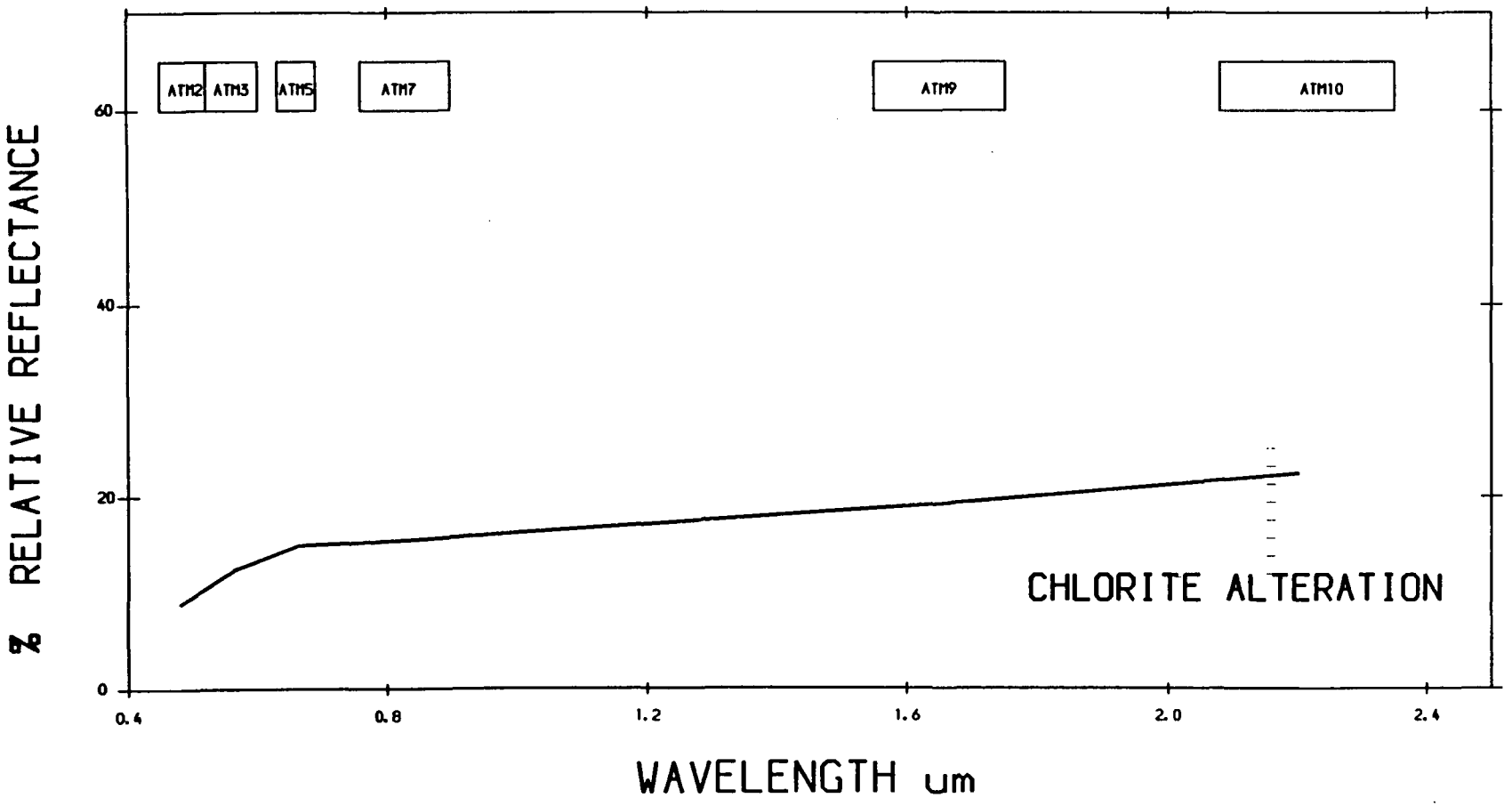

ATM 1000 M BAND EQUIVALENT TO TM CALIBRATED TO RELATIVE REFLECTANCE USING CALIBRATION CURVE

MAHD ADH DHAHAB- SAUDI ARABIA

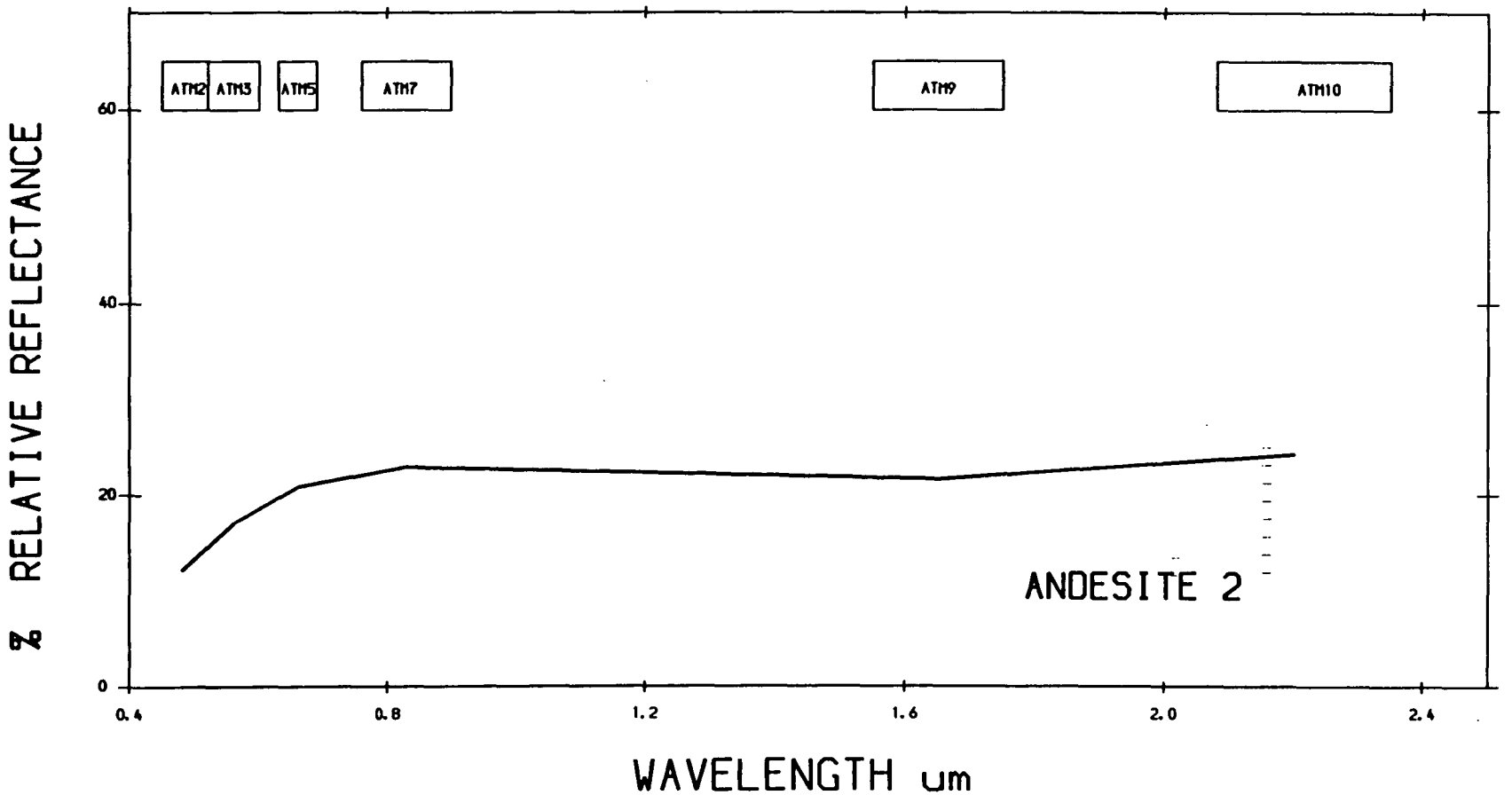

ATM 1000 M BAND EQUIVALENT TO TM CALIBRATED TO RELATIVE REFLECTANCE USING CALIBRATION CURVE

MAHD ADH DHAHAB- SAUDI ARABIA

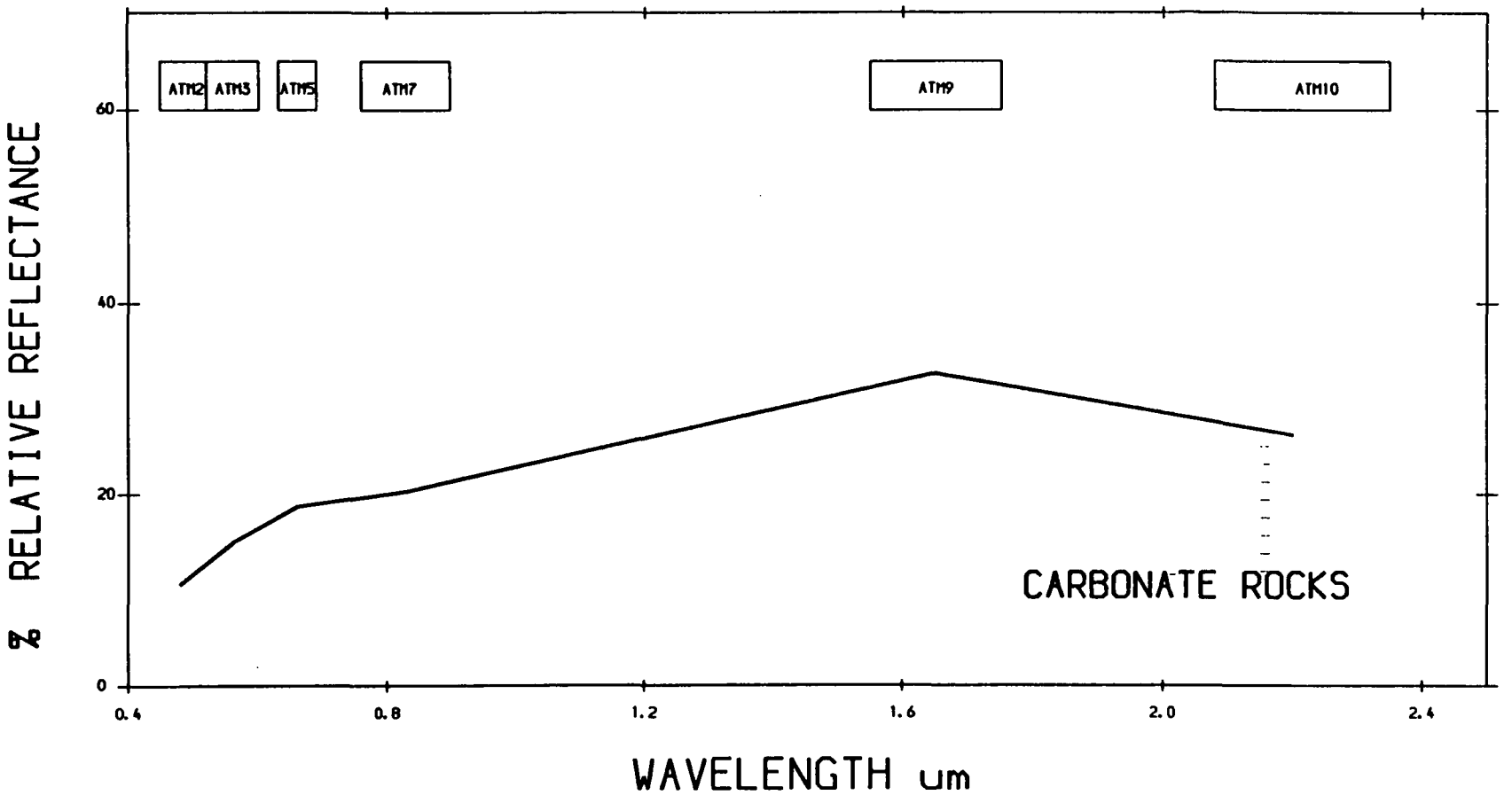

ATM 1000 M BAND EQUIVALENT TO TM CALIBRATED TO RELATIVE REFLECTANCE USING CALIBRATION CURVE

MAHD ADH DHAHAB- SAUDI ARABIA

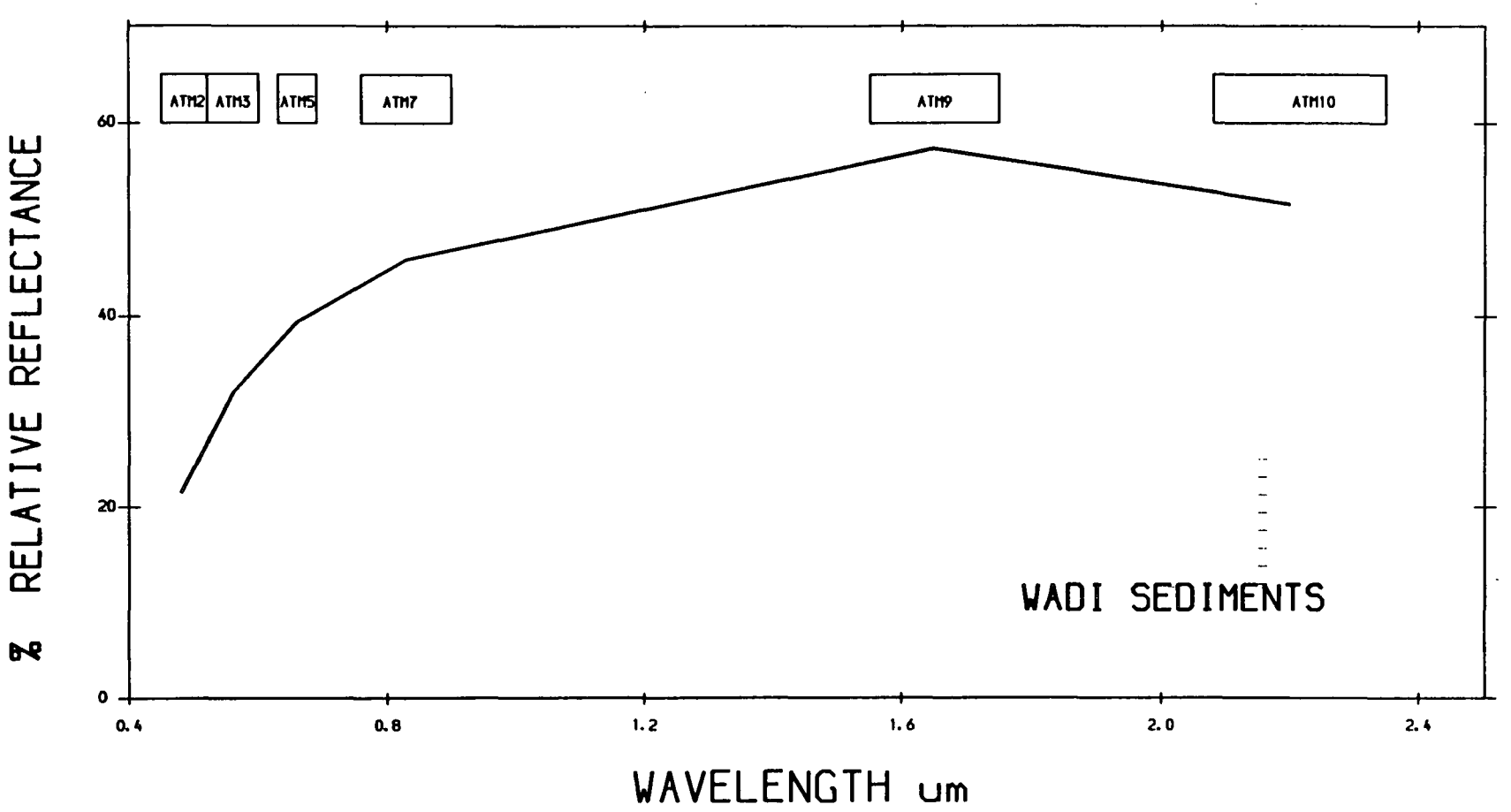

ATM 1000 M BAND EQUIVALENT TO TM CALIBRATED TO RELATIVE REFLECTANCE USING CALIBRATION CURVE

MAHD ADH DHAHAB- SAUDI ARABIA

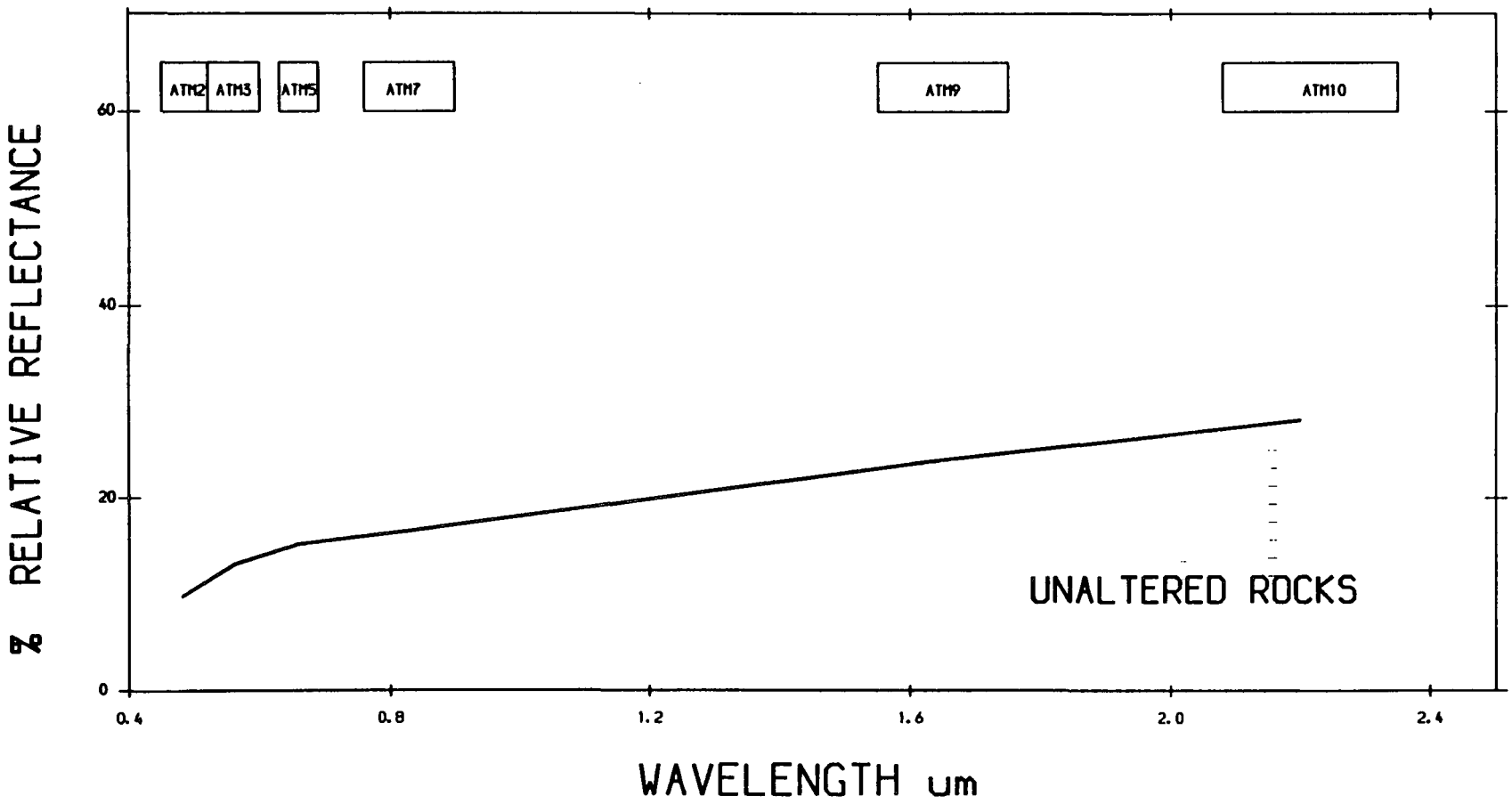

ATM 1000 M BAND EQUIVALENT TO TM CALIBRATED TO RELATIVE REFLECTANCE USING CALIBRATION CURVE

MAHD ADH DHAHAB- SAUDI ARABIA

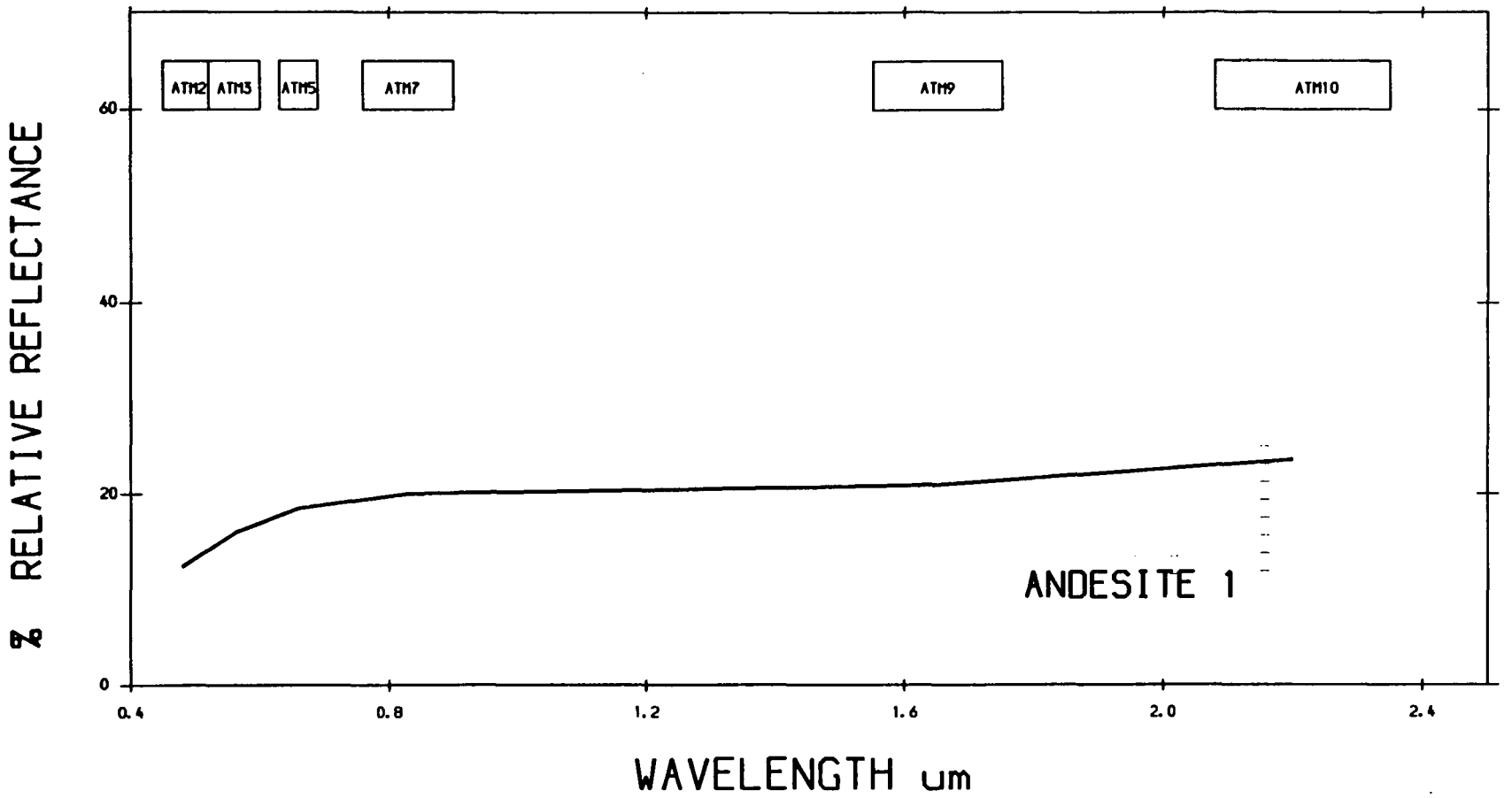

ATM 1000 M BAND EQUIVALENT TO TM CALIBRATED TO RELATIVE REFLECTANCE USING CALIBRATION CURVE

MAHD ADH DHAHAB- SAUDI ARABIA

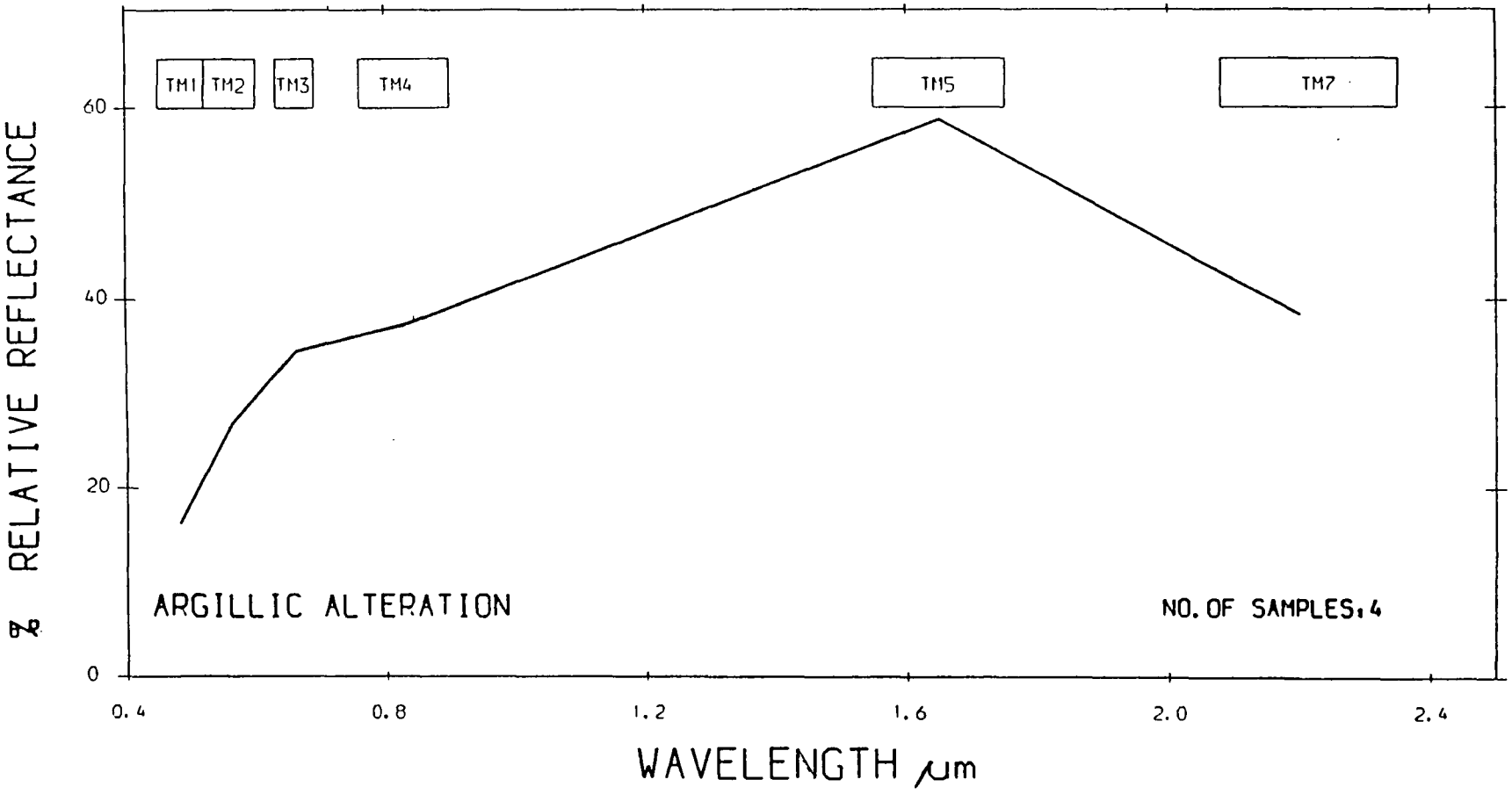

AVERAGE HHRR SPECTRA FROM MAHD ADH DHAHAB AREA

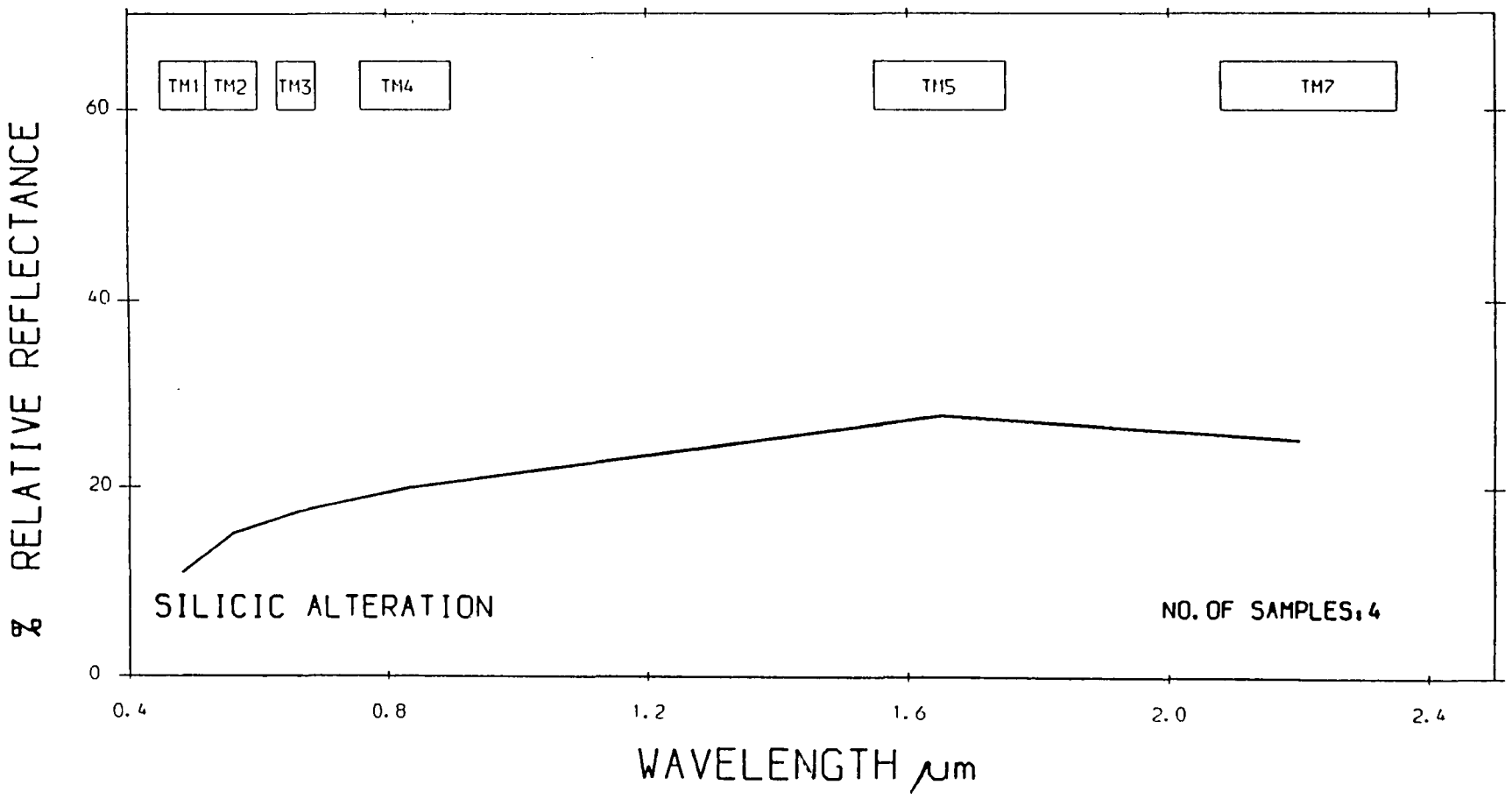

AVERAGE HHRR SPECTRA FROM MAHD ADH DHAHAB AREA

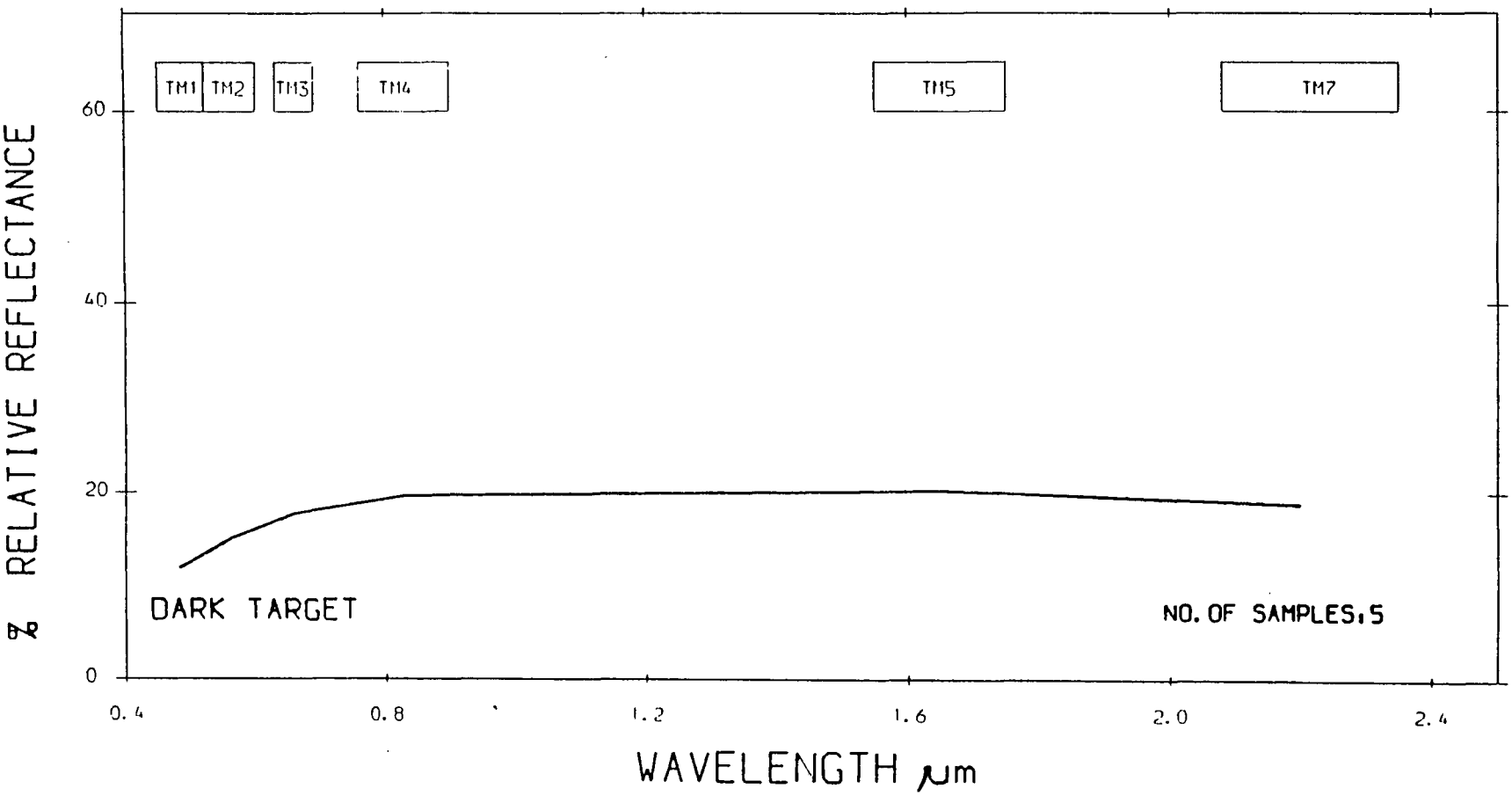

AVERAGE 'HHRR SPECTRA FROM MAHD ADH DHAHAB AREA

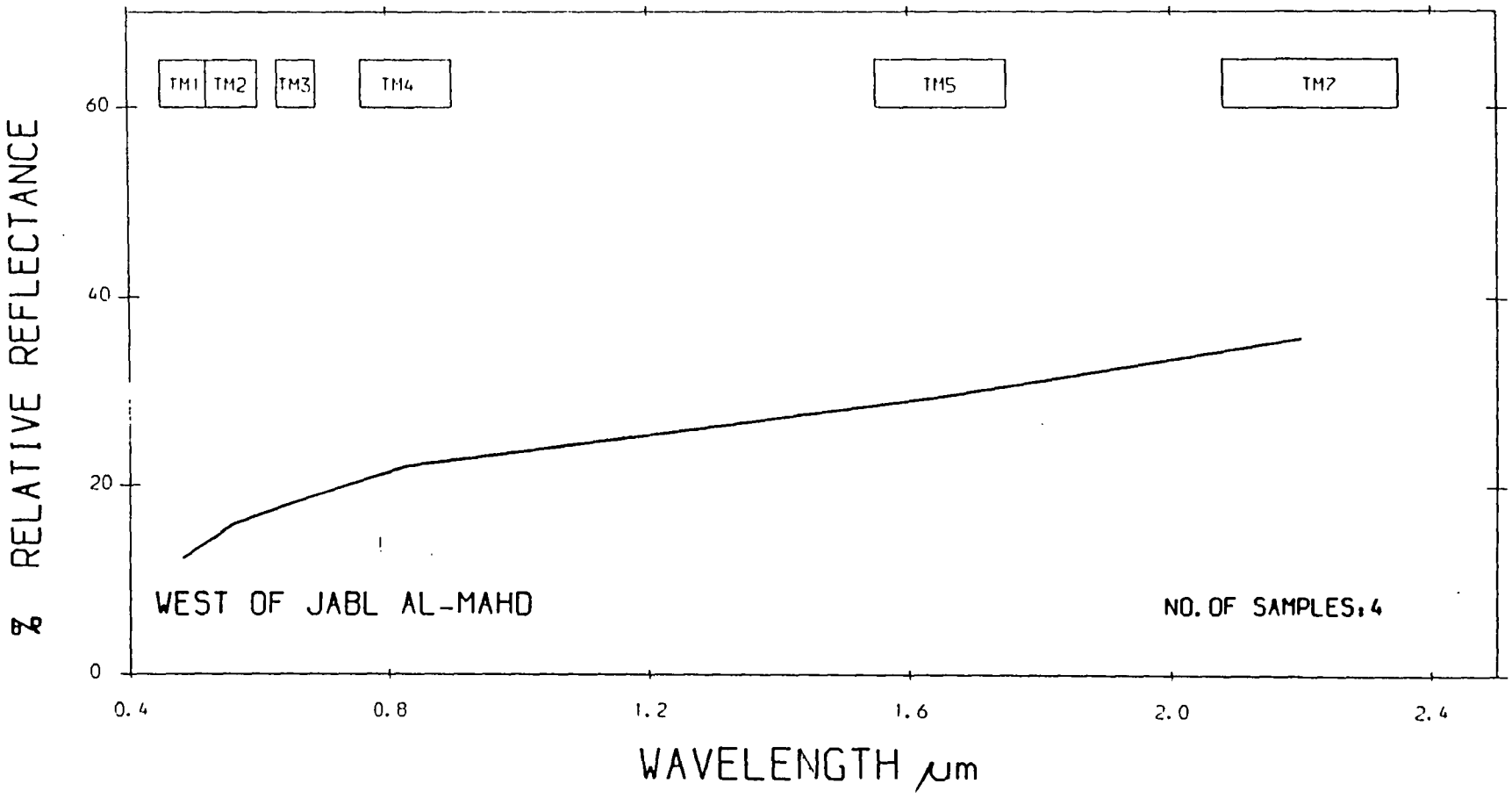

AVERAGE HHRR SPECTRA FROM MAHD ADH DHAHAB AREA

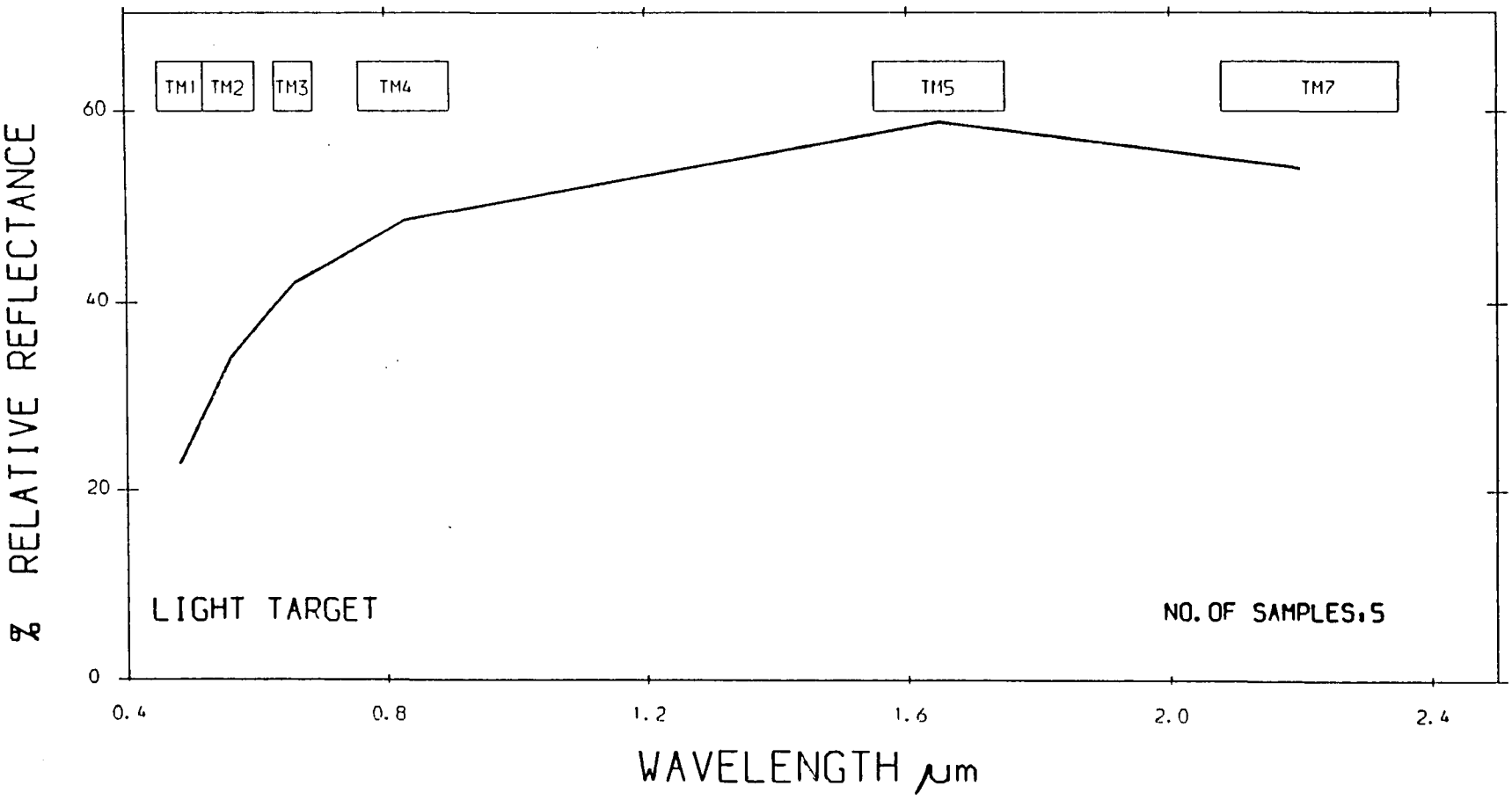

AVERAGE HHRR SPECTRA FROM MAHD ADH DHAHAB AREA

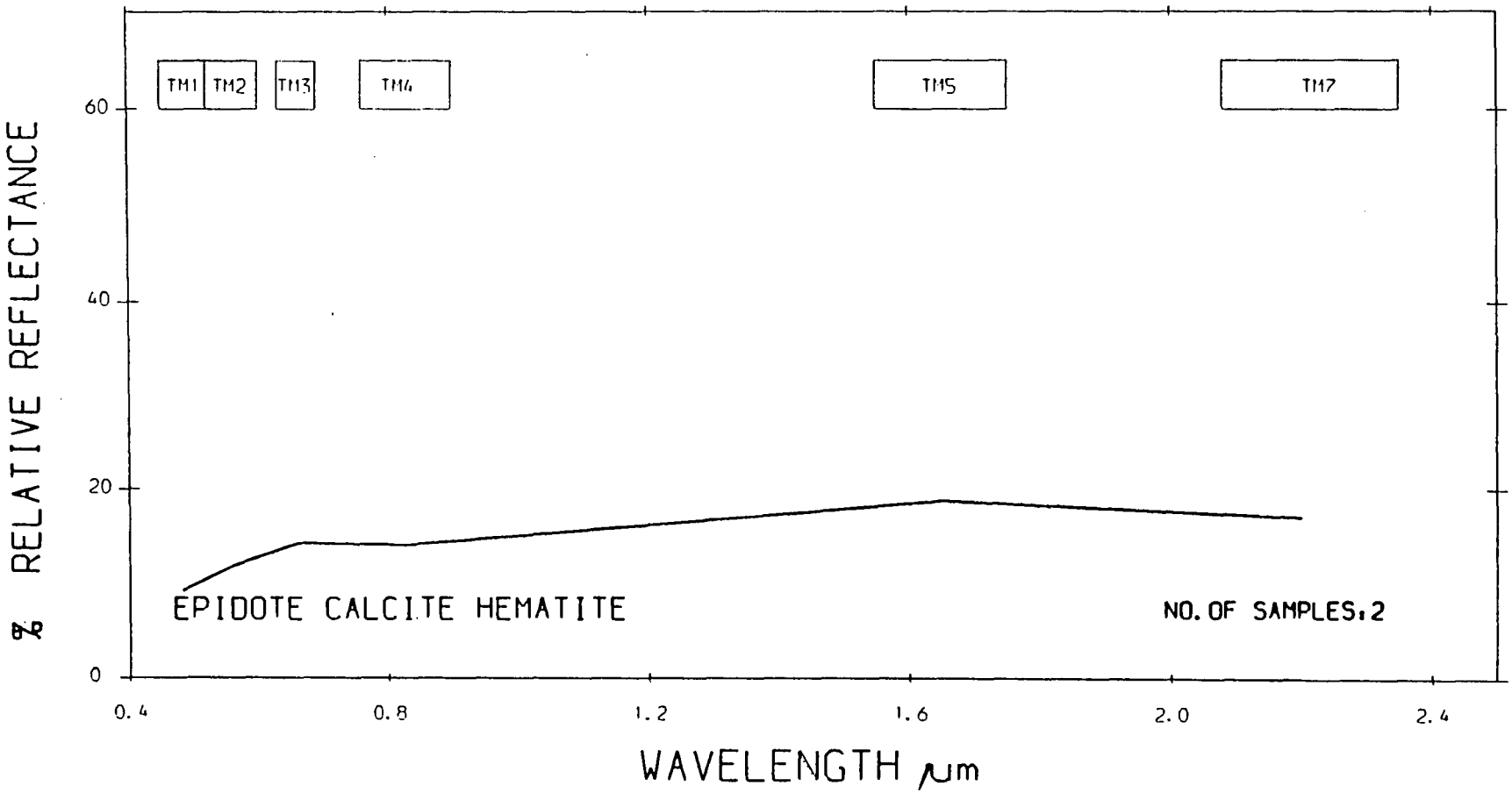

AVERAGE HHRR SPECTRA FROM MAHD ADH DHAHAB AREA

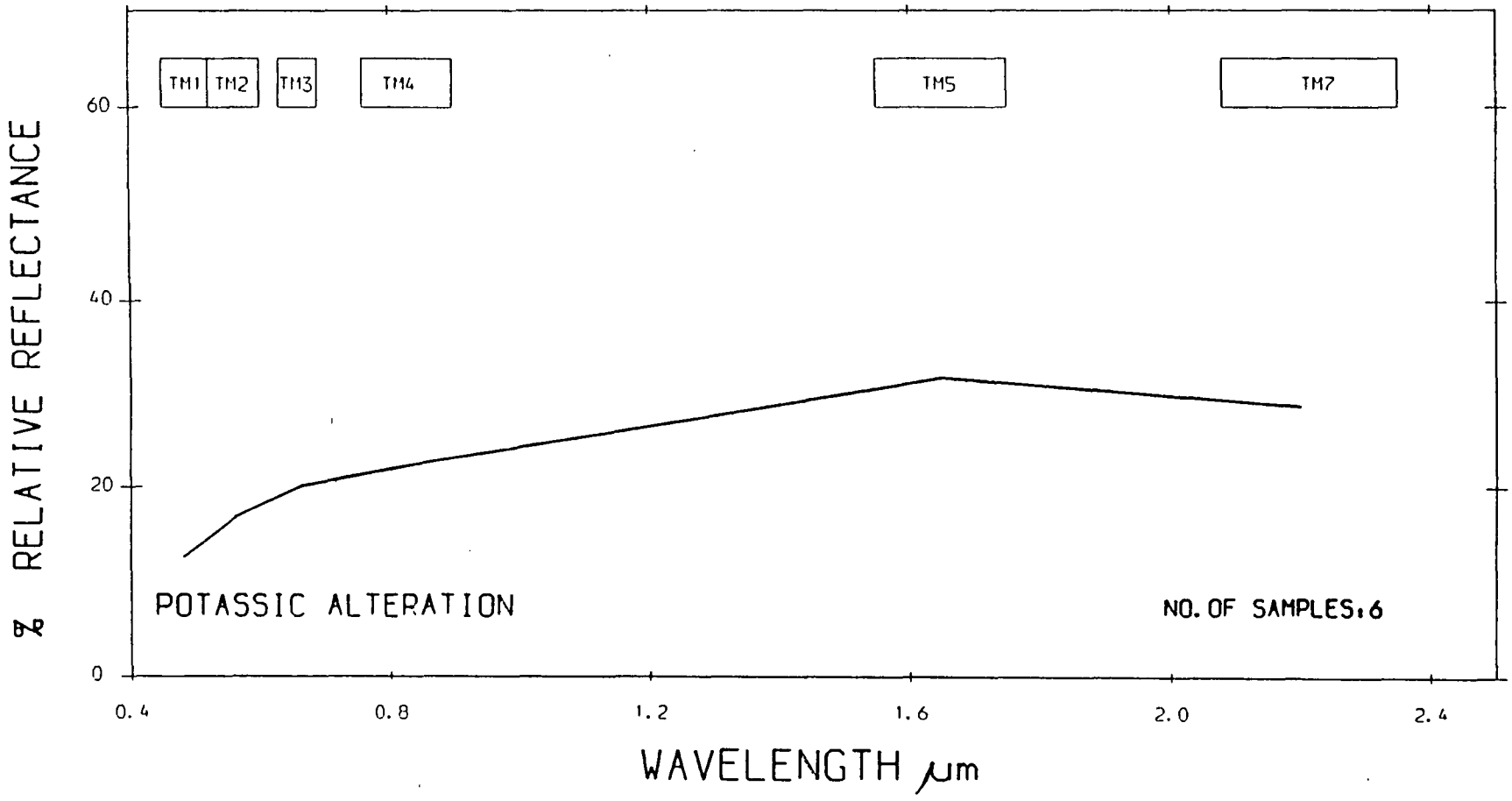

AVERAGE HHRR SPECTRA FROM MAHD ADH DHAHAB AREA

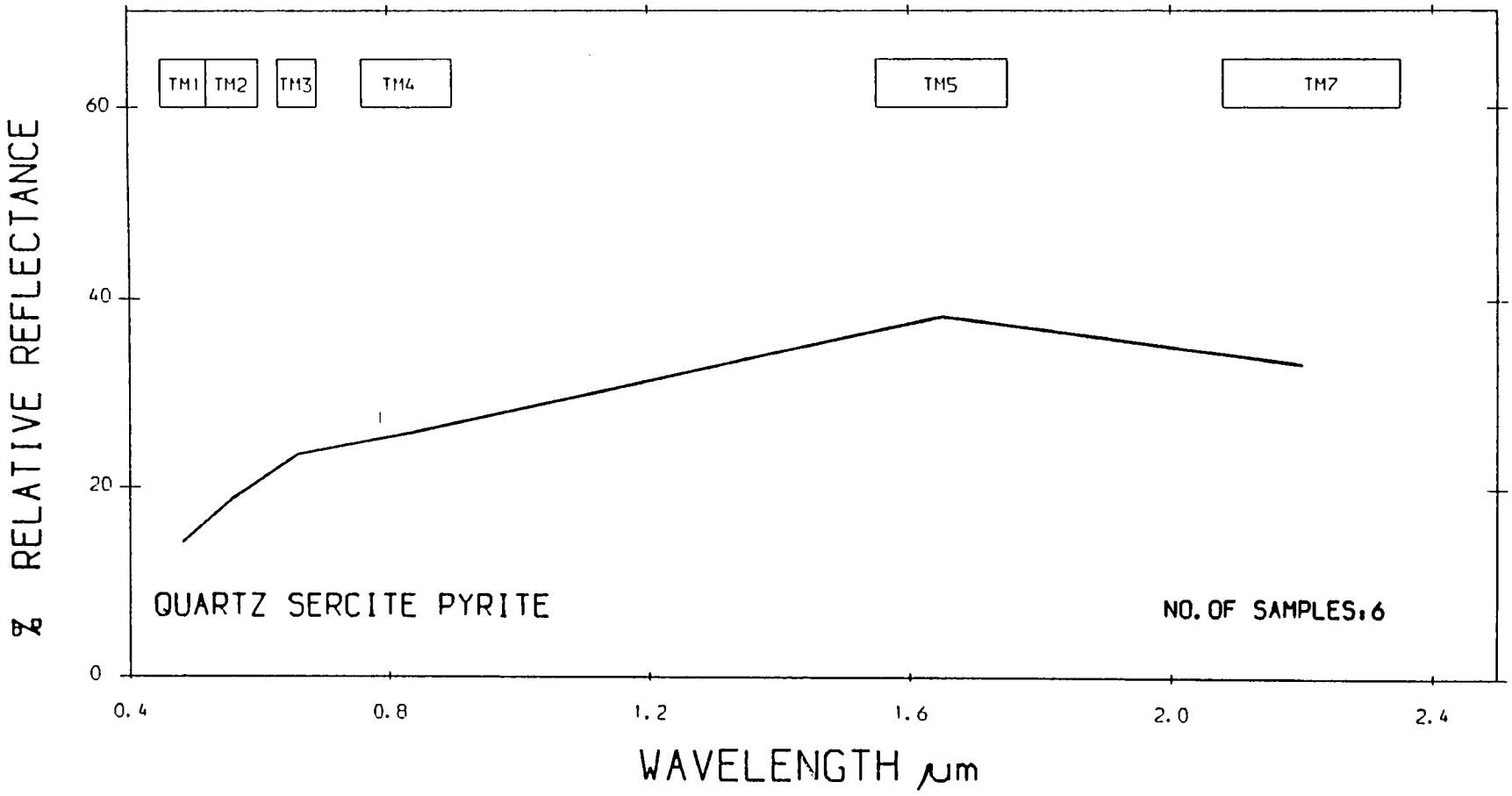

AVERAGE HHRR SPECTRA FROM MAHD ADH DHAHAB AREA

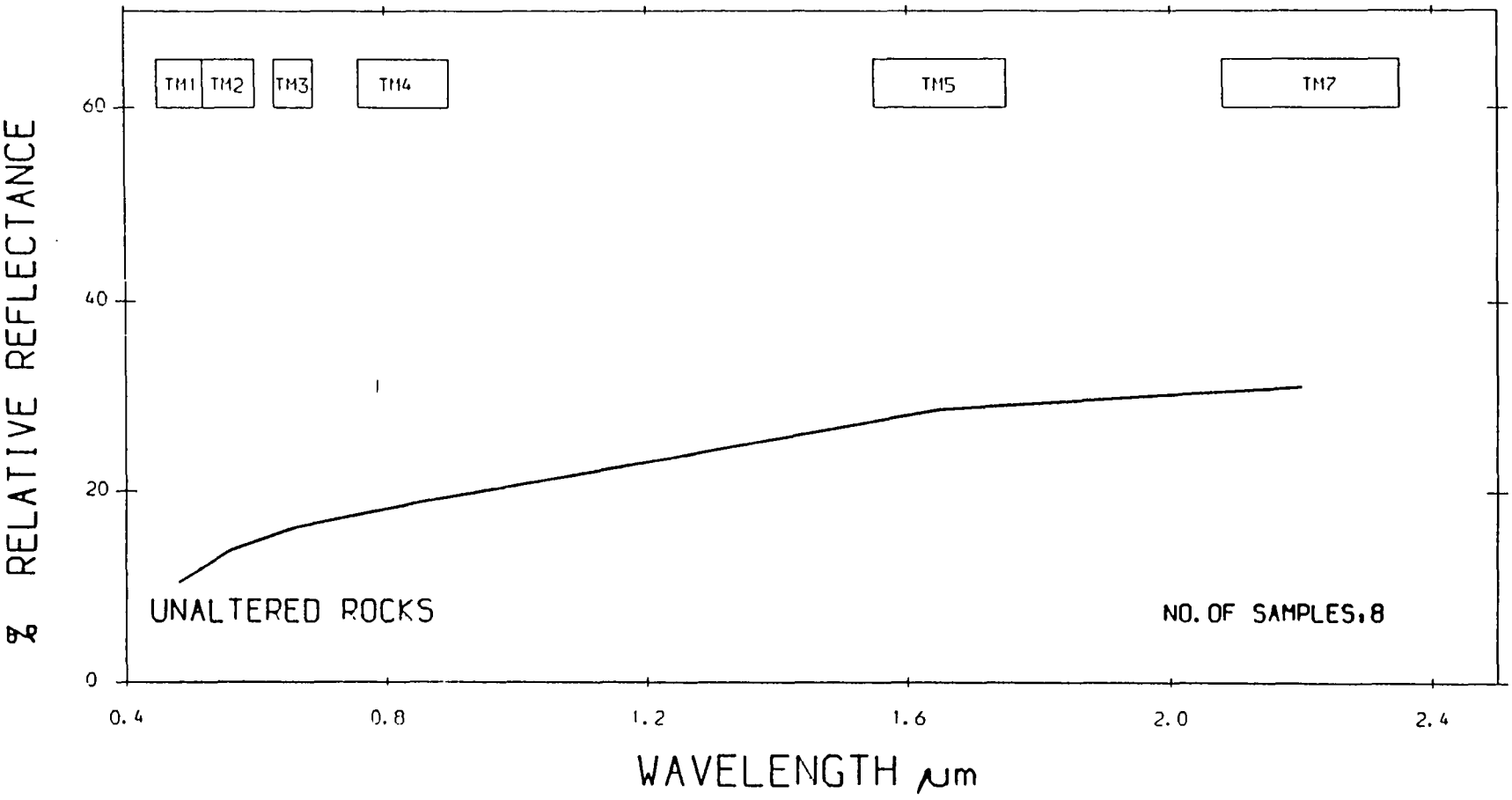

AVERAGE HHRR SPECTRA FROM MAHD ADH DHAHAB AREA

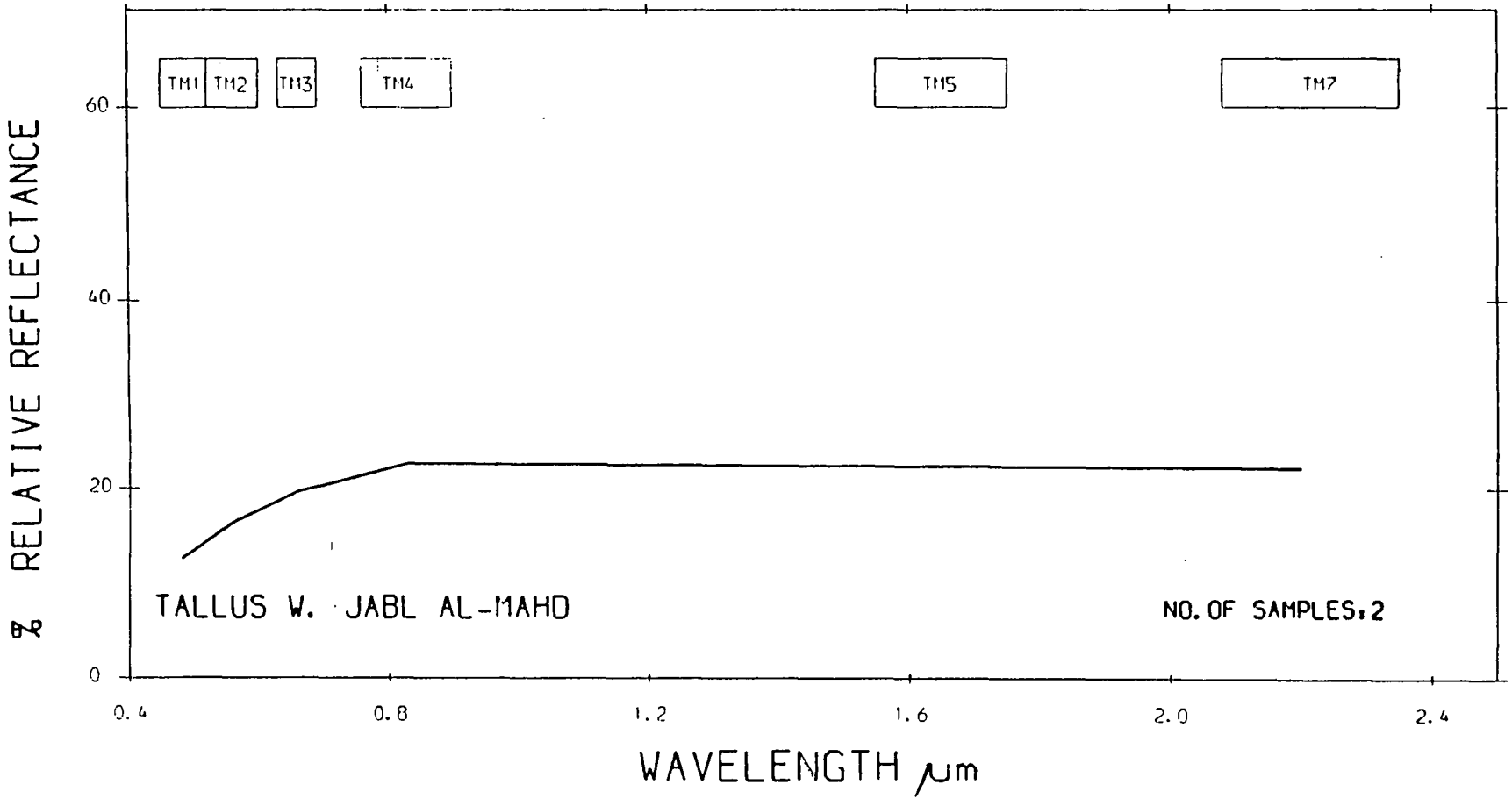

AVERAGE HHRR SPECTRA FROM MAHD ADH DHAHAB AREA

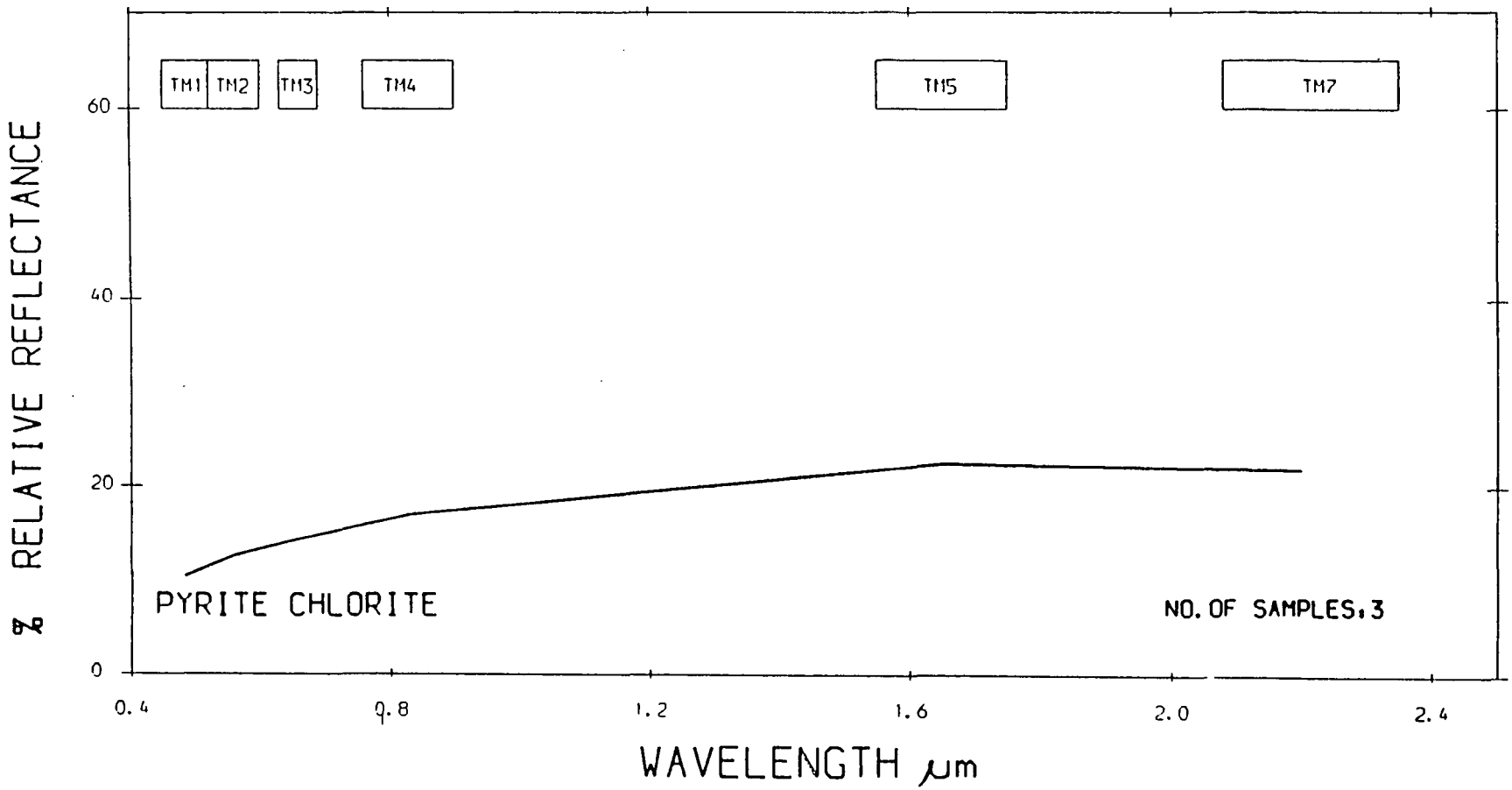

AVERAGE HHRR SPECTRA FROM MAHD ADH DHAHAB AREA

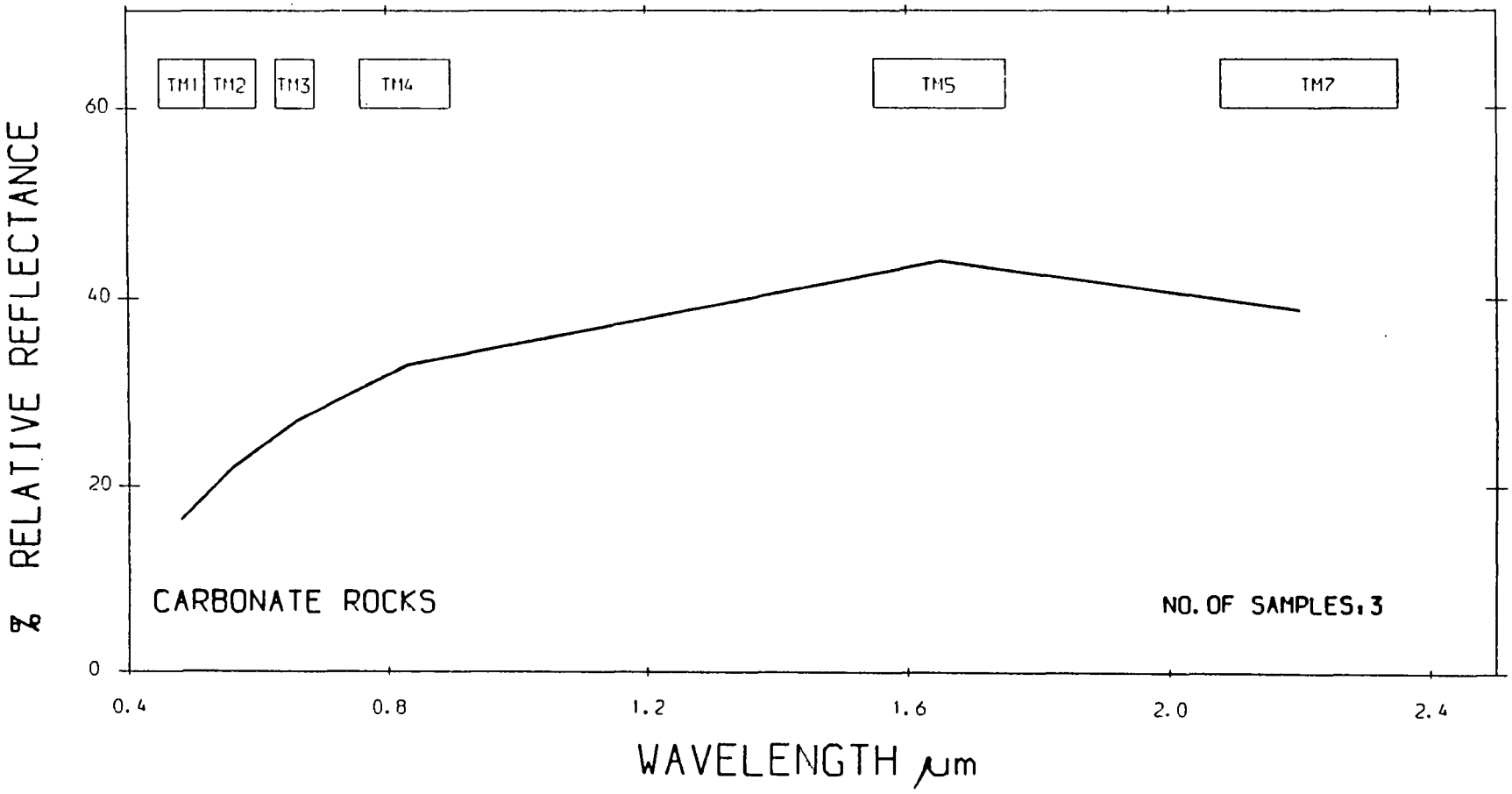

AVERAGE HHRR SPECTRA FROM MAHD ADH DHAHAB AREA

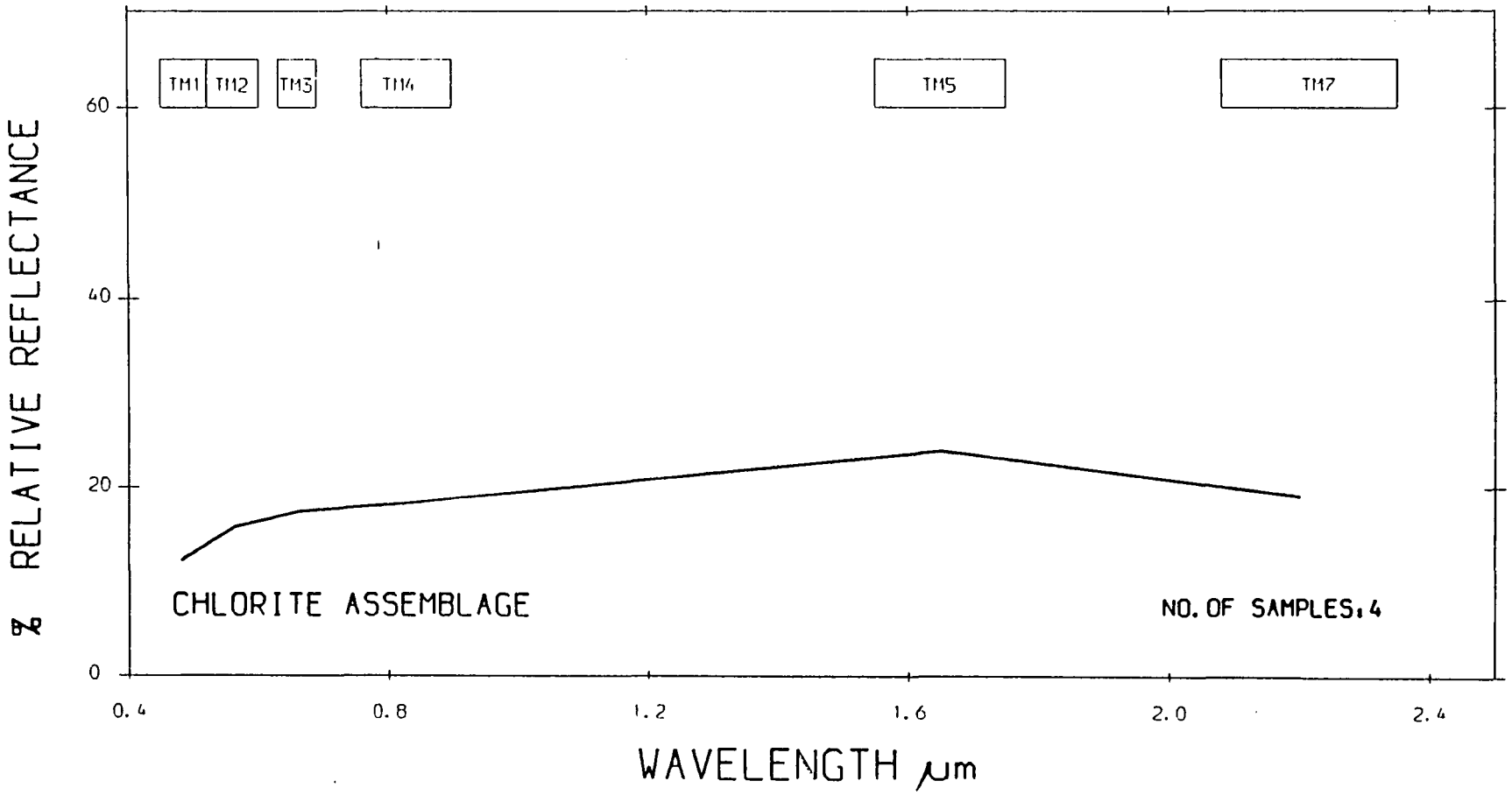

AVERAGE HHRR SPECTRA FROM MAHD ADH DHAHAB AREA

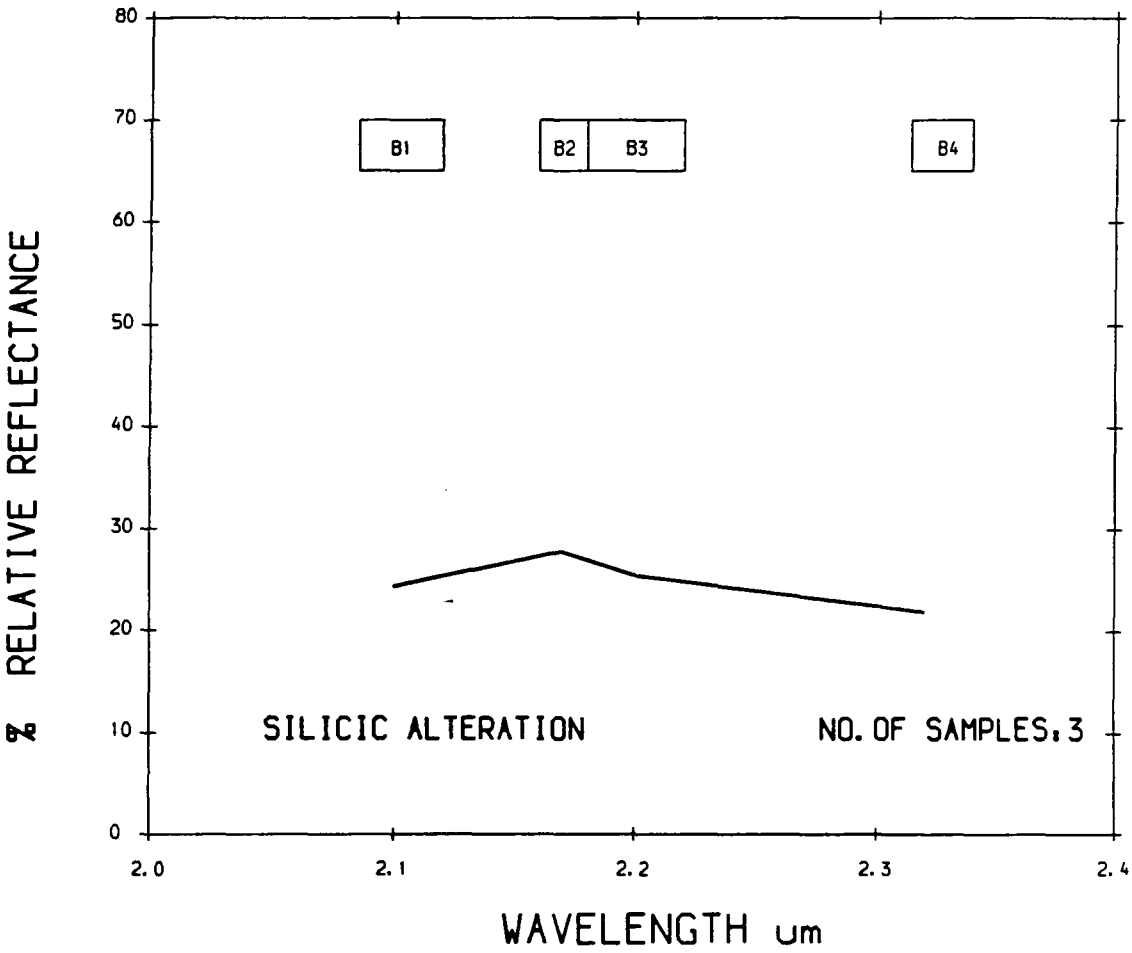

AVERAGE HHRR SPECTRA FROM MAHD ADH DHAHAB AREA

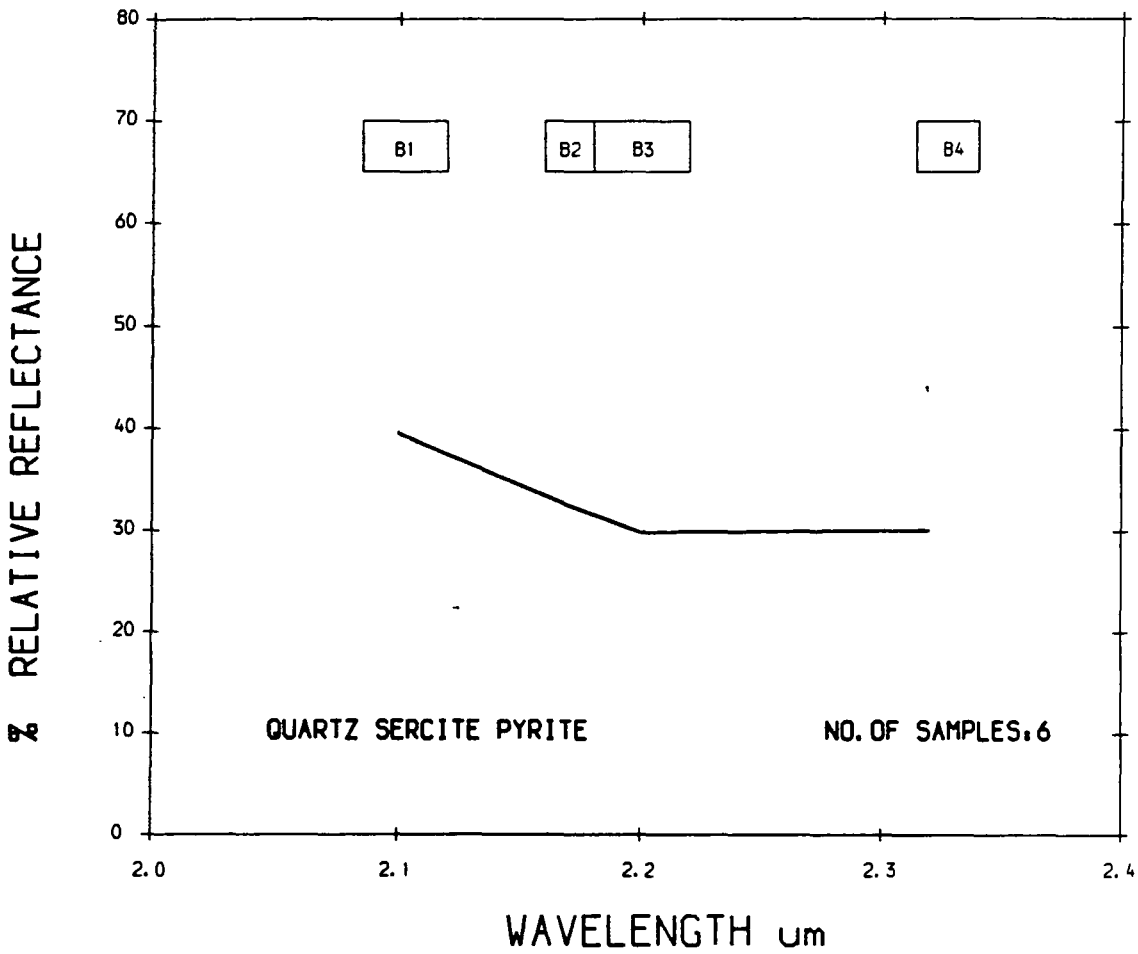

AVERAGE HHRR SPECTRA FROM MAHD ADH DHAHAB AREA

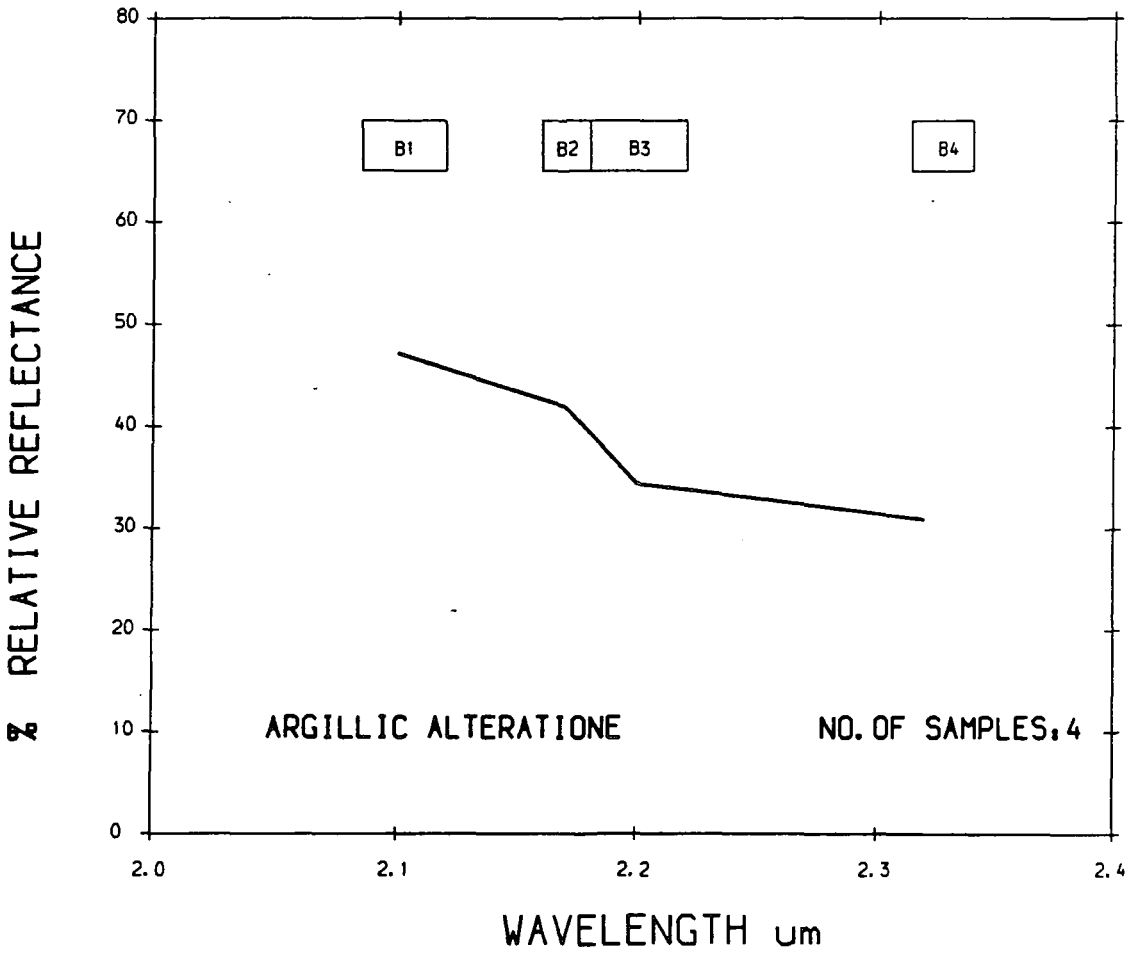

AVERAGE HHRR SPECTRA FROM MAHD ADH DHAHAB AREA

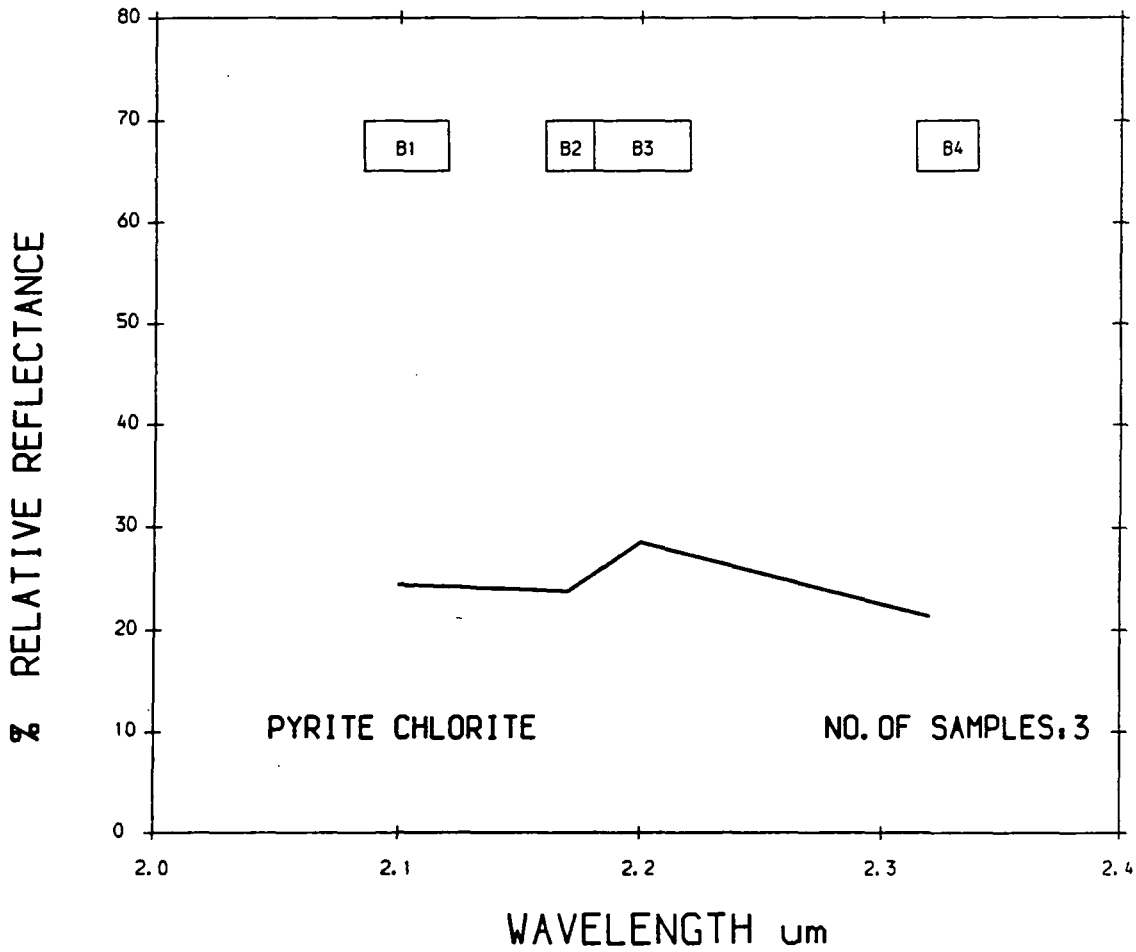

AVERAGE HHRR SPECTRA FROM MAHD ADH DHAHAB AREA

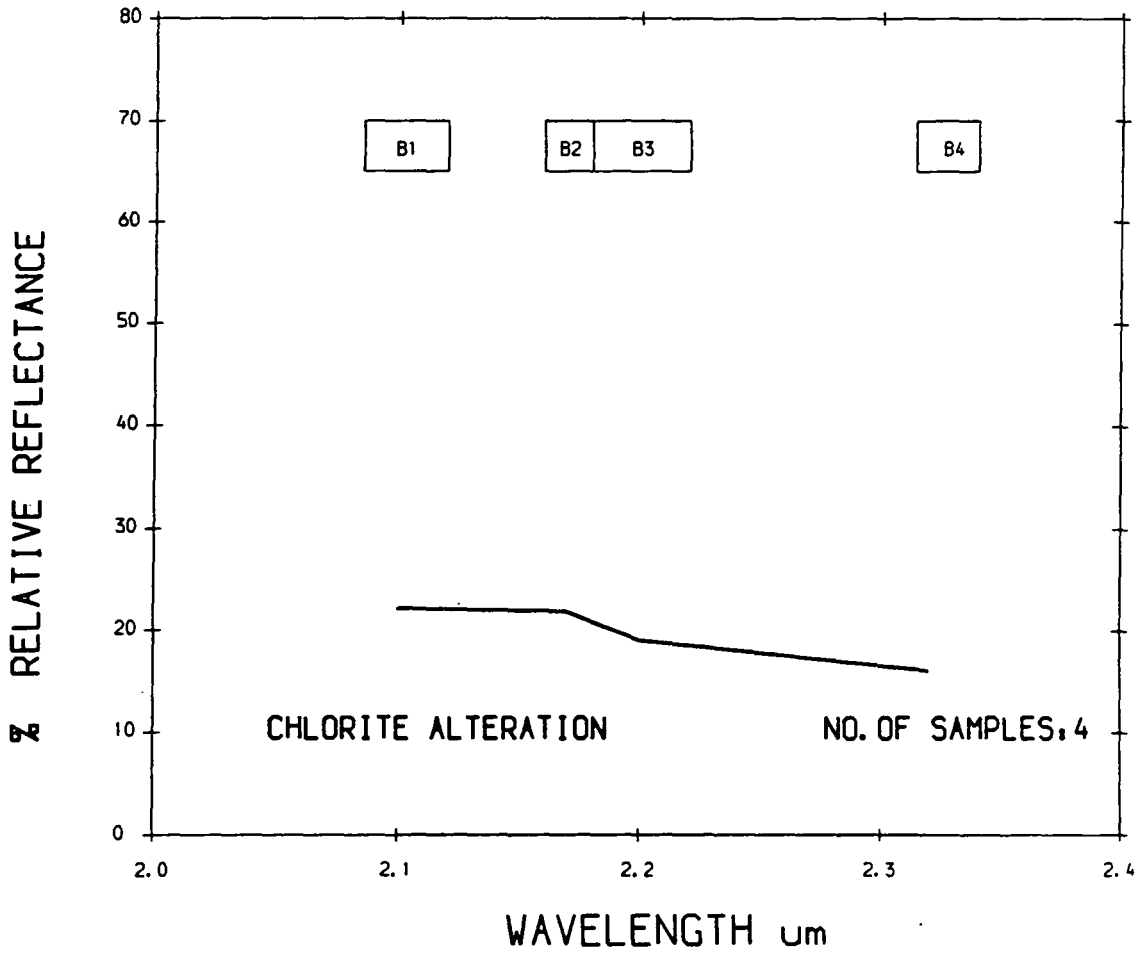

AVERAGE HHRR SPECTRA FROM MAHD ADH DHAHAB AREA

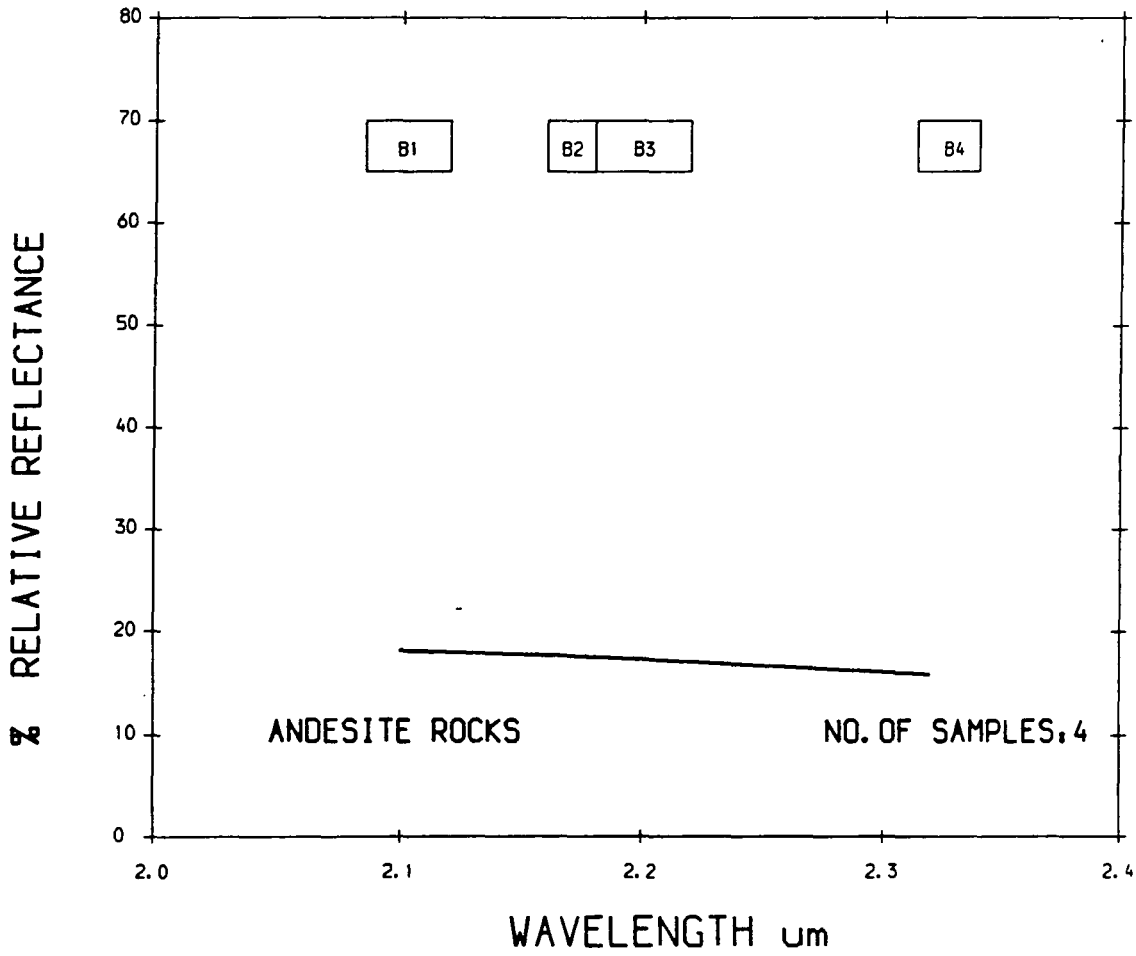

AVERAGE HHRR SPECTRA FROM MAHD ADH DHAHAB AREA

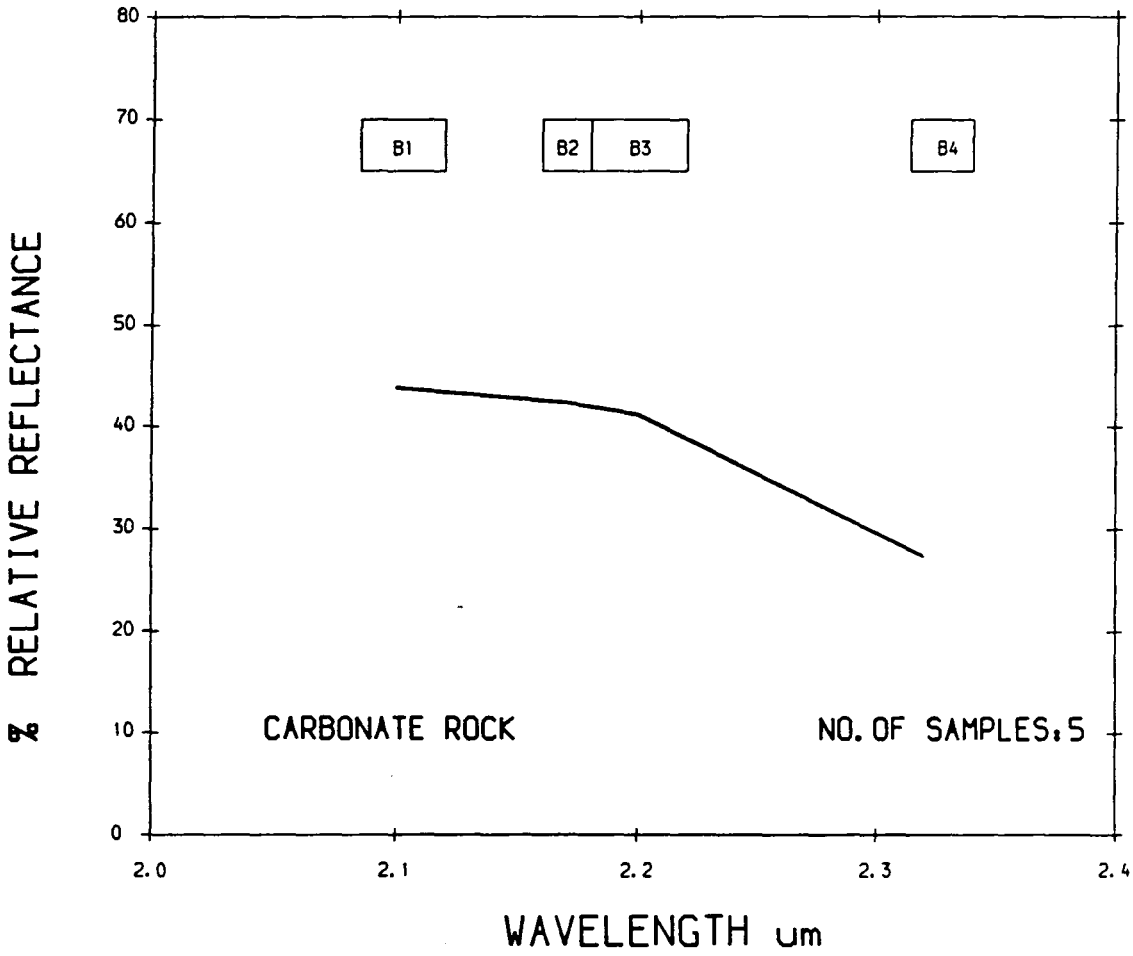

AVERAGE HHRR SPECTRA FROM MAHD ADH DHAHAB AREA

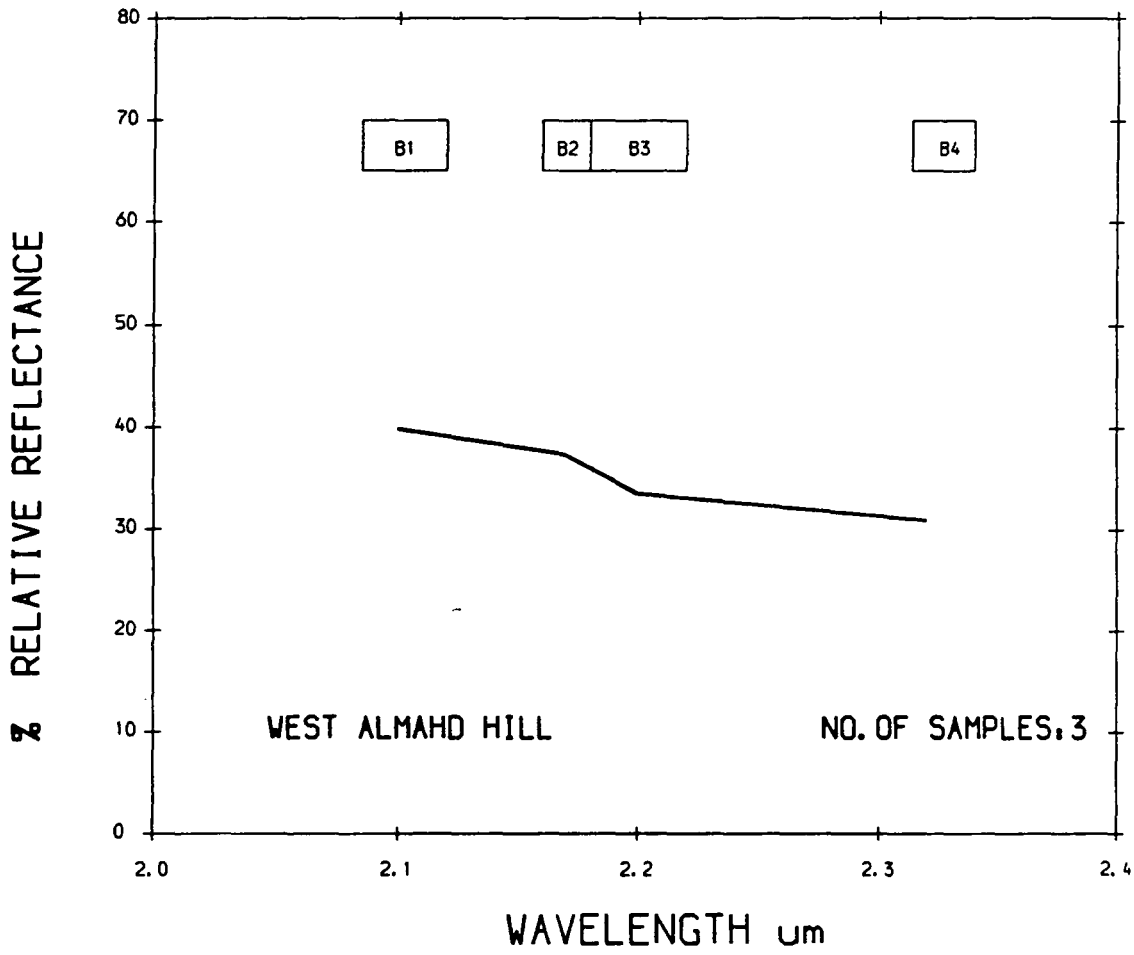

AVERAGE HHRR SPECTRA FROM MAHD ADH DHAHAB AREA

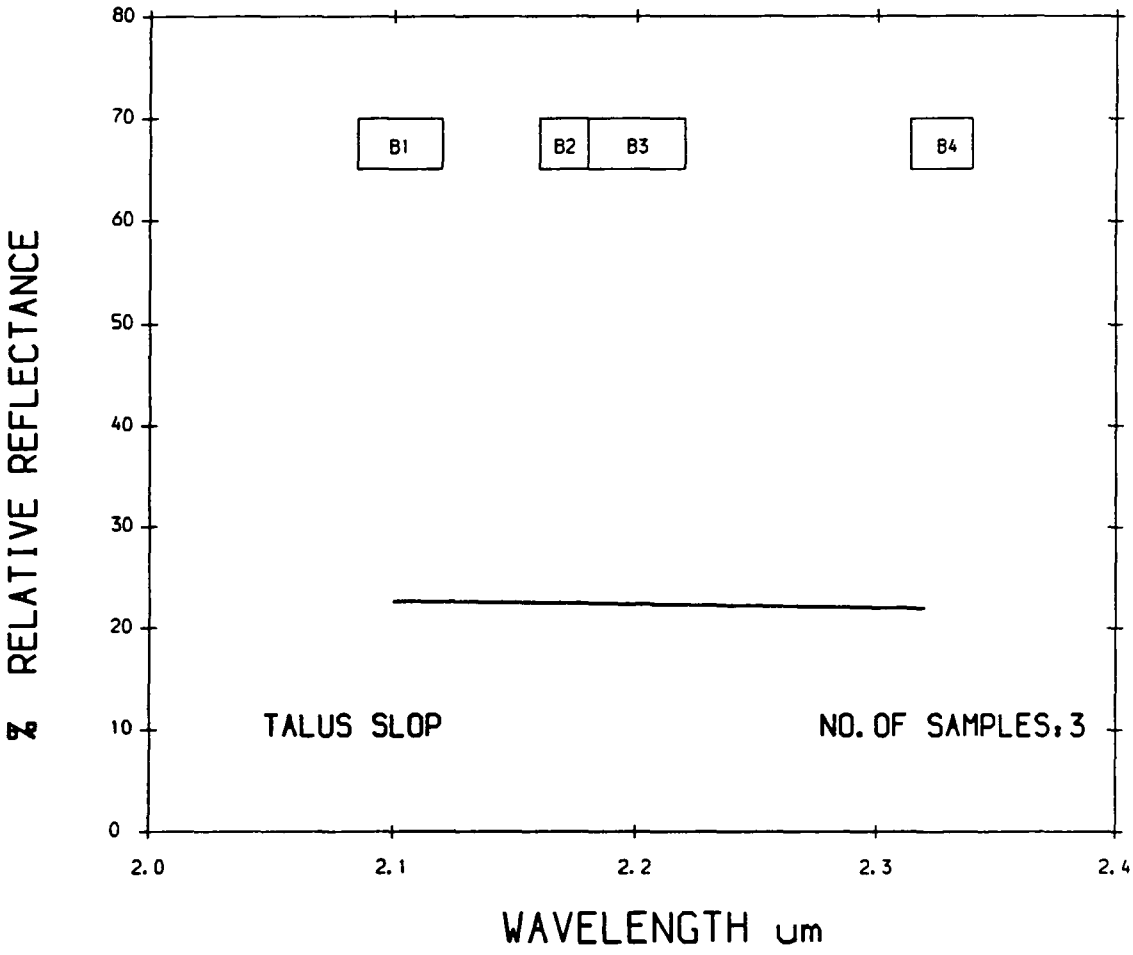

AVERAGE HHRR SPECTRA FROM MAHD ADH DHAHAB AREA

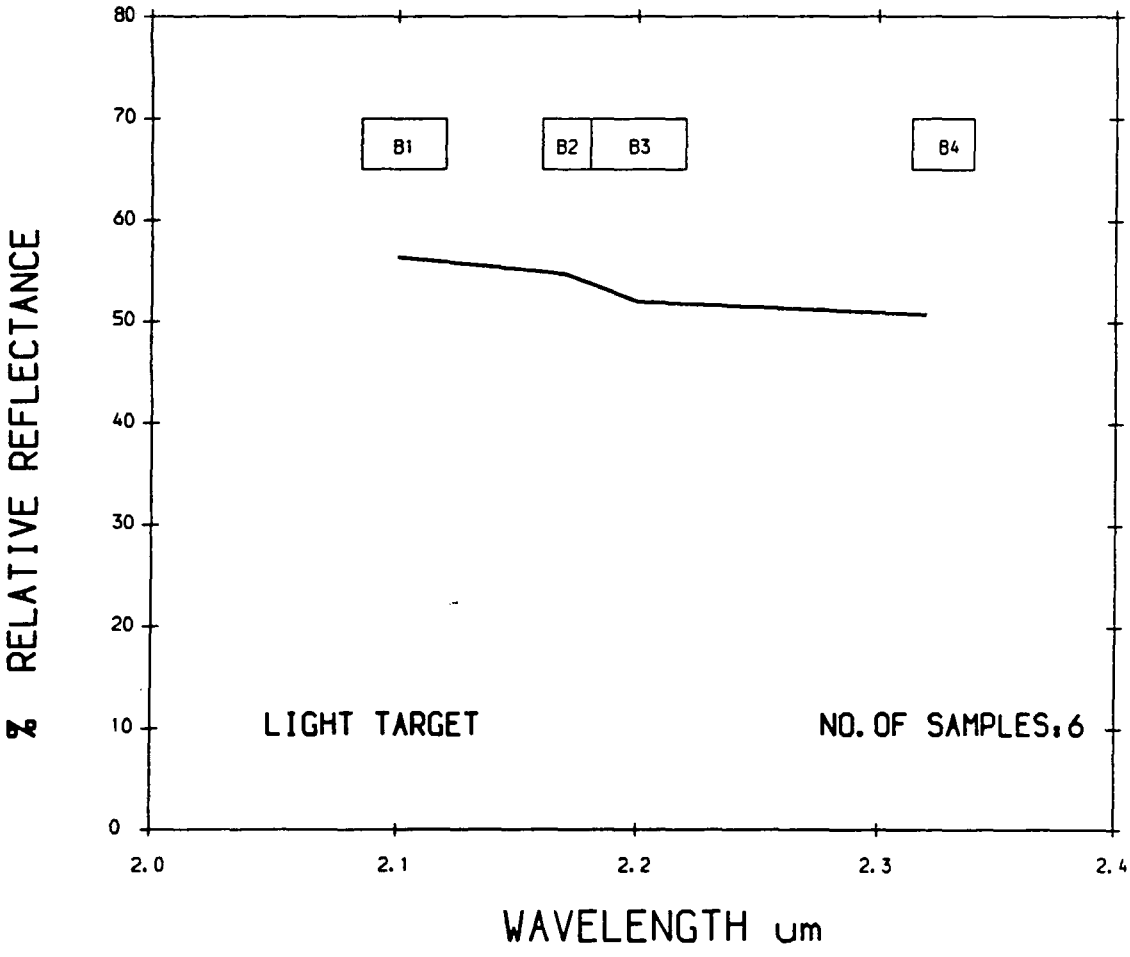

AVERAGE HHRR SPECTRA FROM MAHD ADH DHAHAB AREA

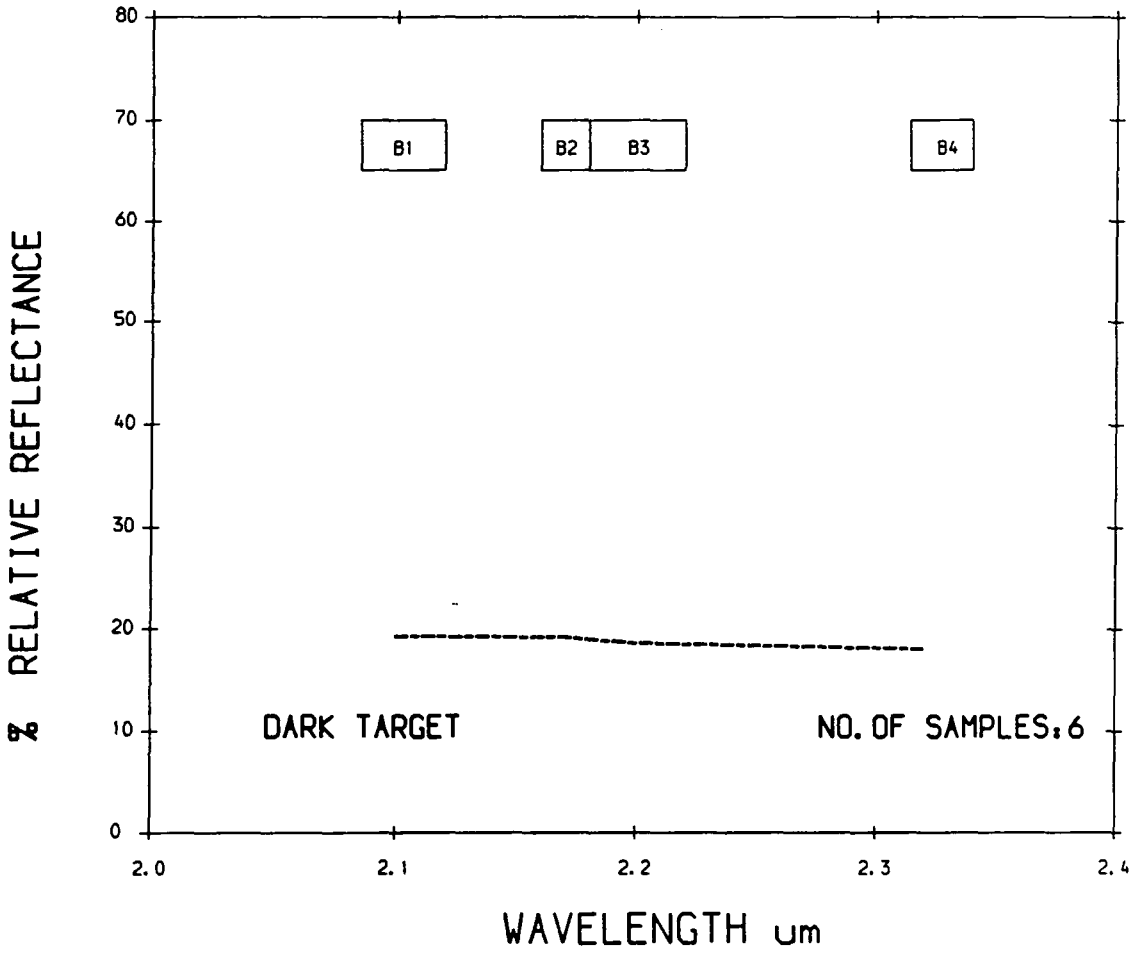

AVERAGE HHRR SPECTRA FROM MAHD ADH DHAHAB AREA

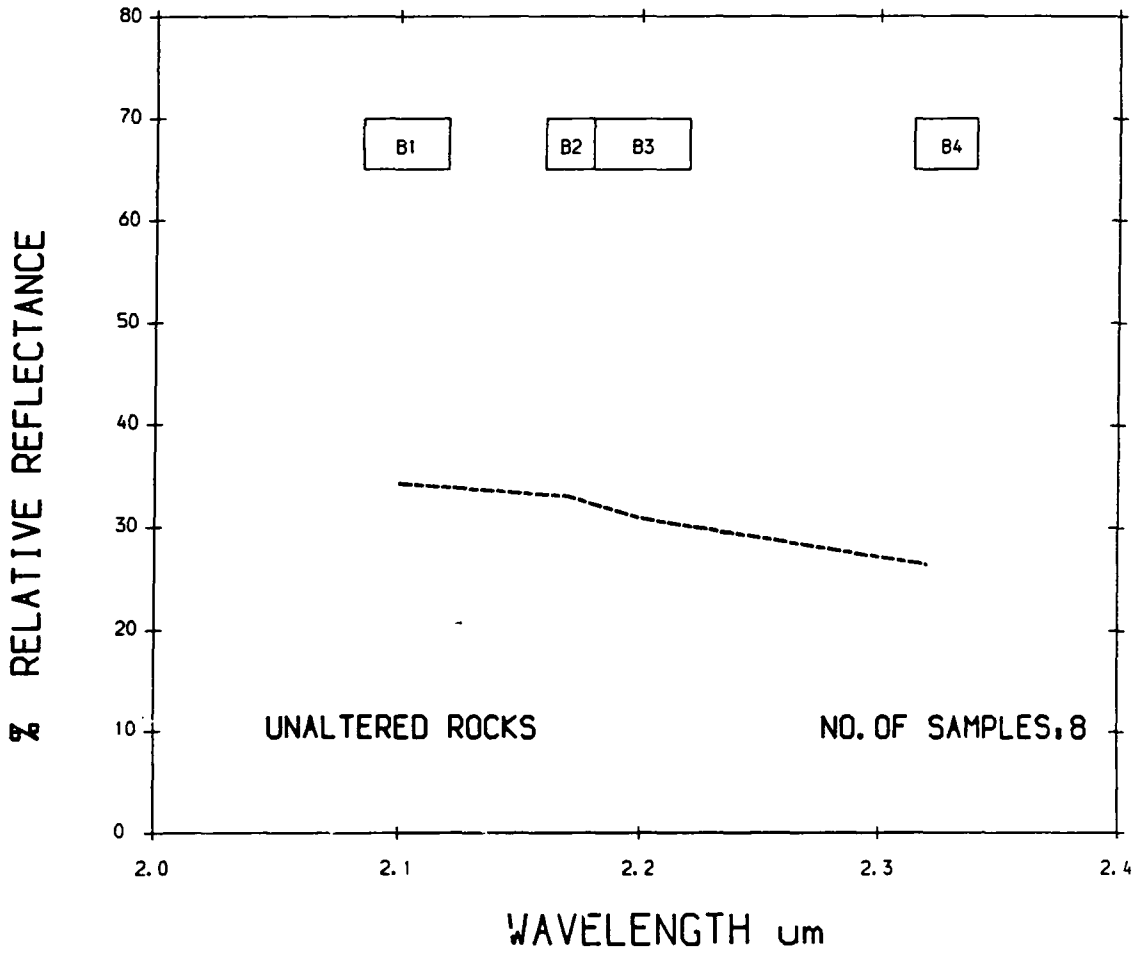

AVERAGE HHRR SPECTRA FROM MAHD ADH DHAHAB AREA

APENDIX E

DETAIL SPECTRA OF LITHOLOGIES

JABAL SAID AREA

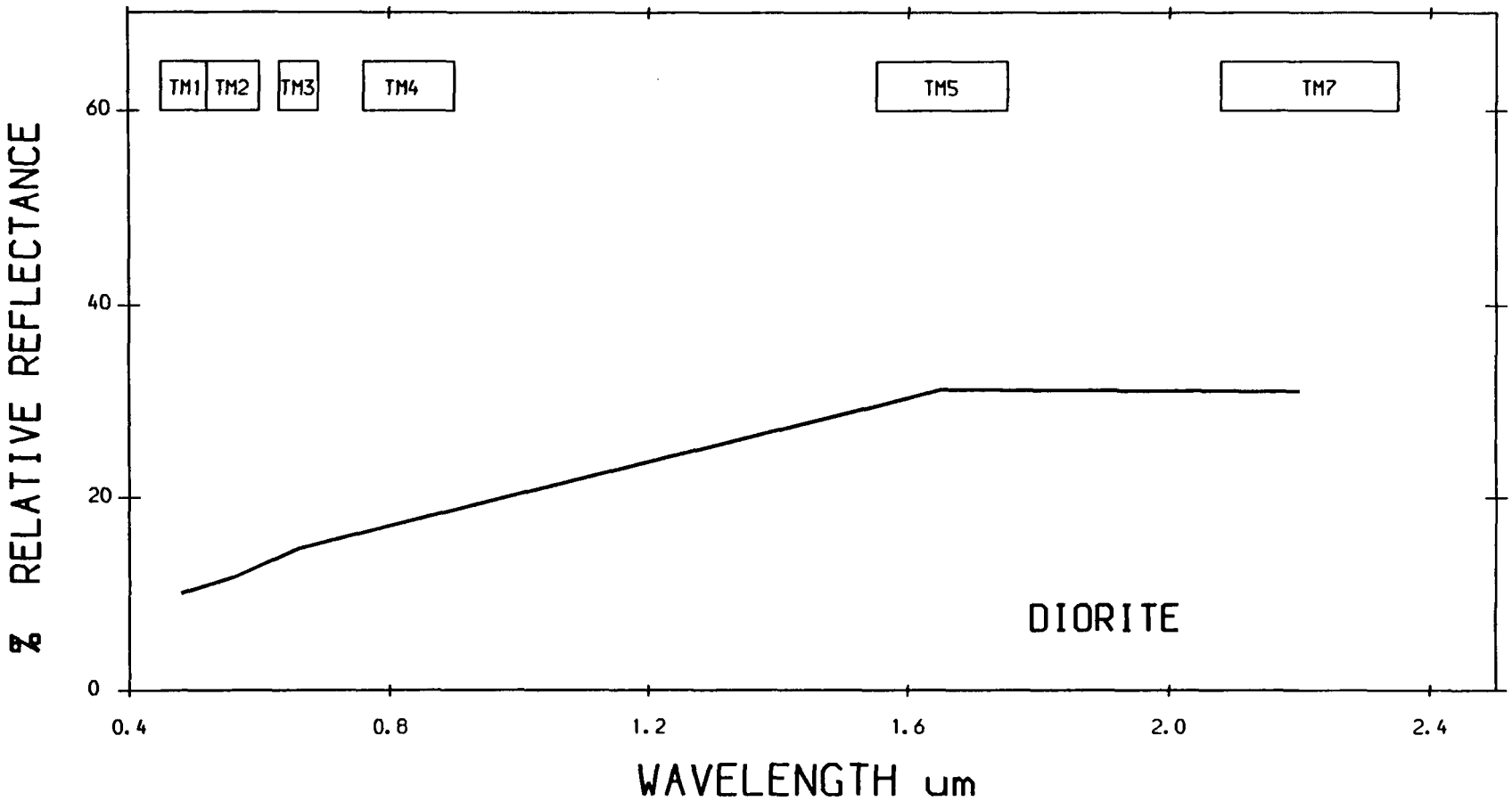

LANDSAT 5 TM CALIBRATED TO RELATIVE REFLCNCE

JABAL SAID AREA- SAUDI ARABIA

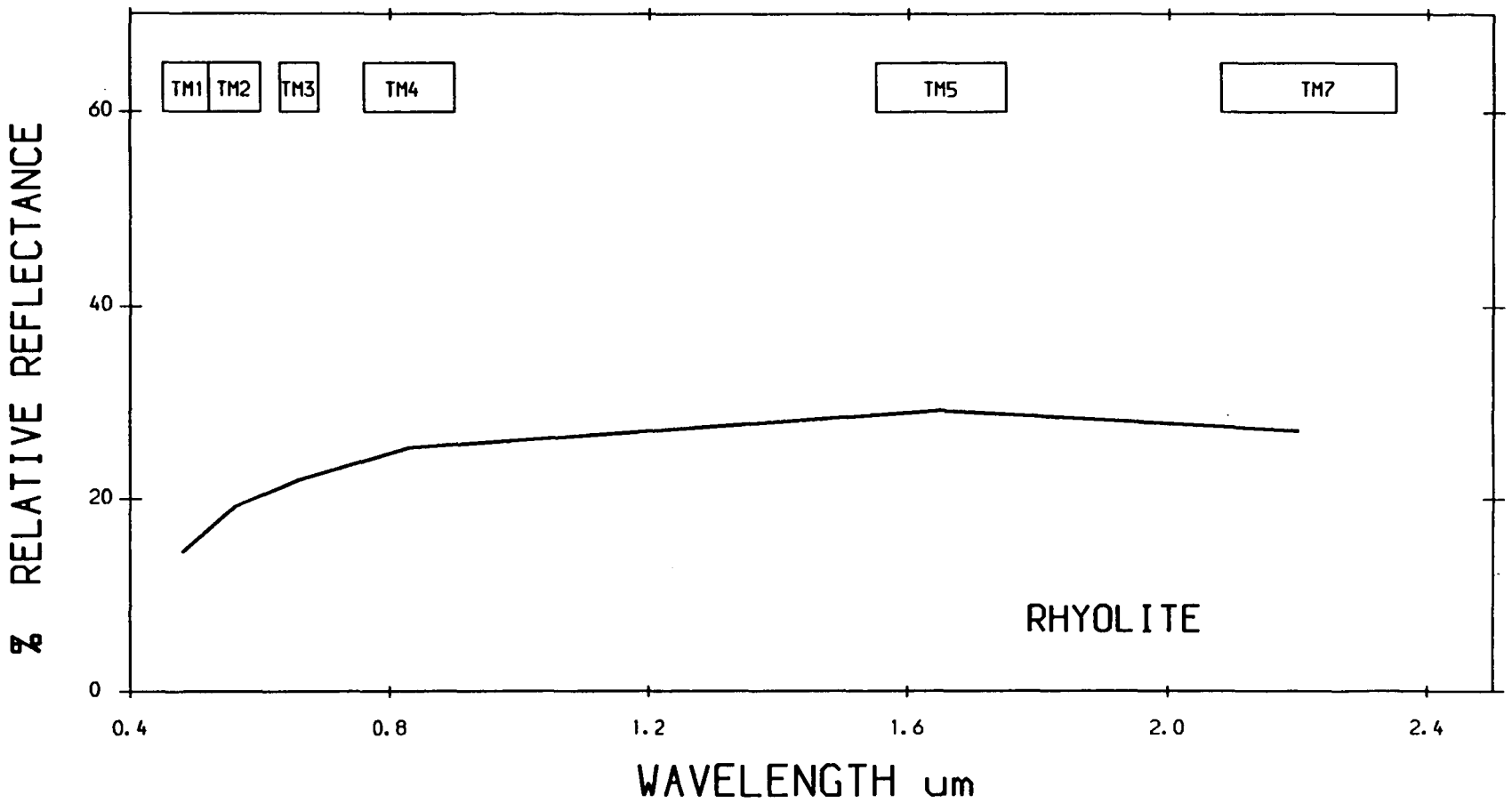

LANDSAT 5 TM CALIBRATED TO RELATIVE REFLCNCE

JABAL SAID AREA- SAUDI ARABIA

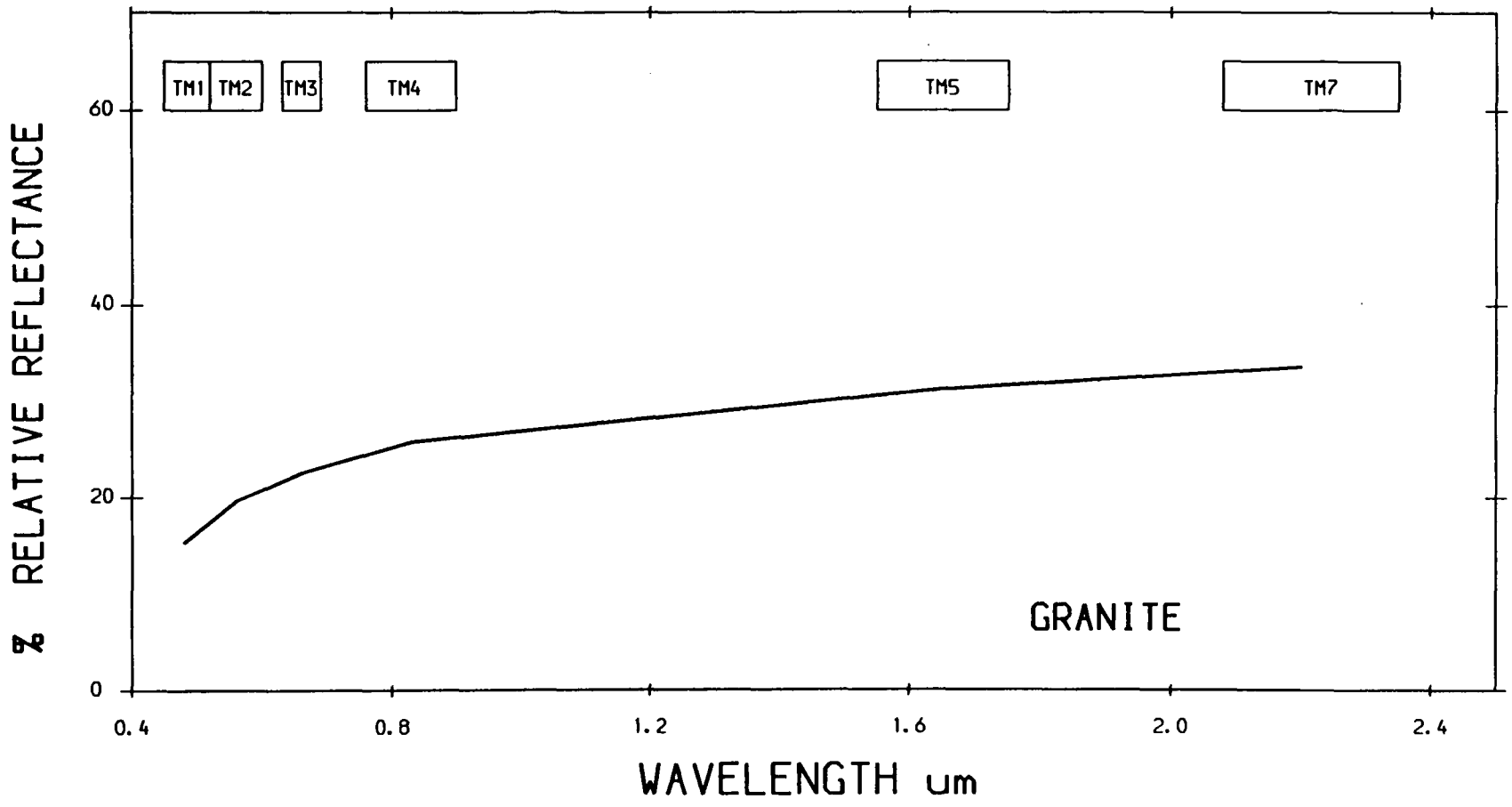

LANDSAT 5 TM CALIBRATED TO RELATIVE REFLCNCE

JABAL SAID AREA- SAUDI ARABIA

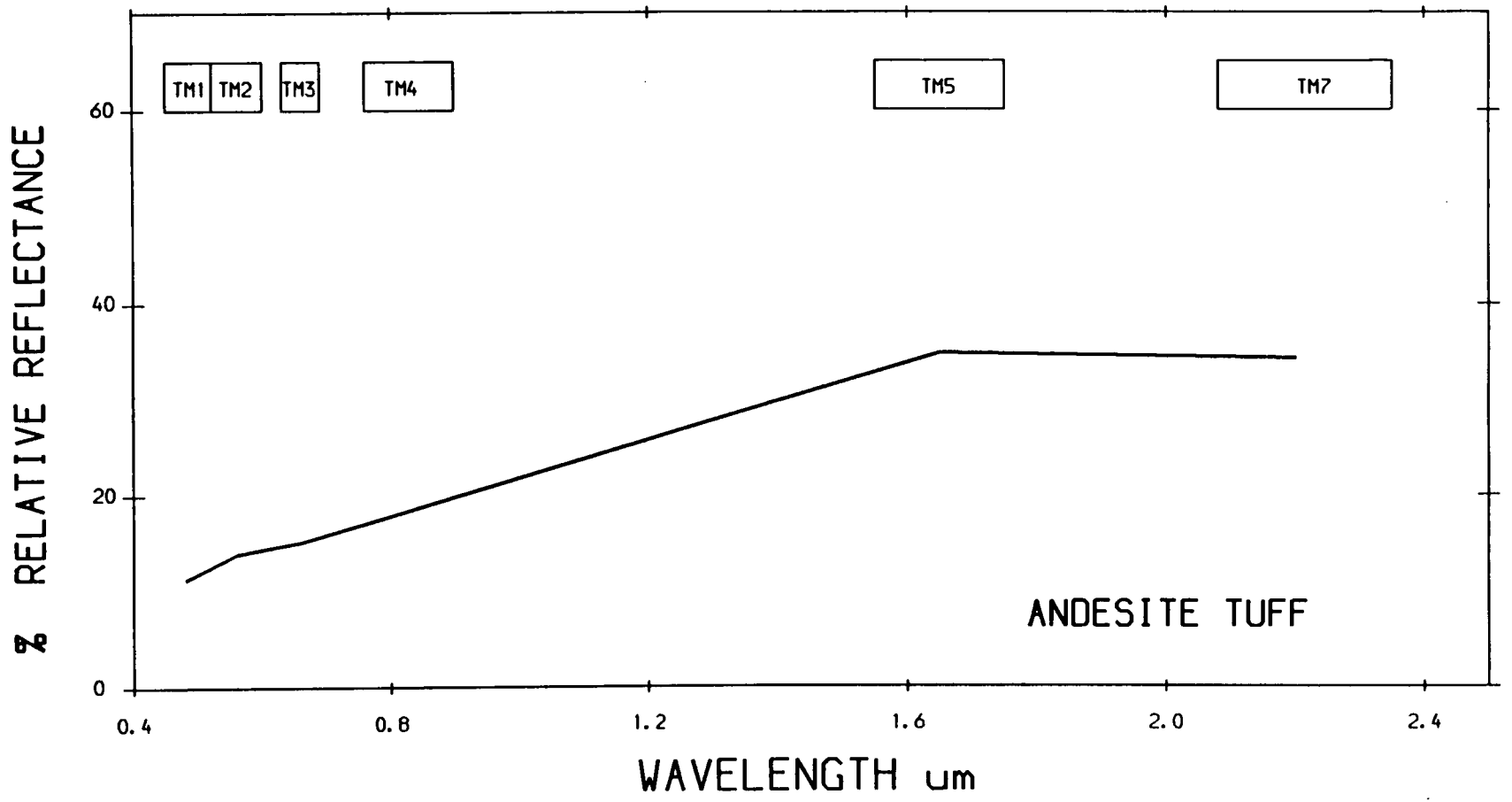

LANDSAT 5 TM CALIBRATED TO RELATIVE REFLCNCE

JABAL SAID AREA- SAUDI ARABIA

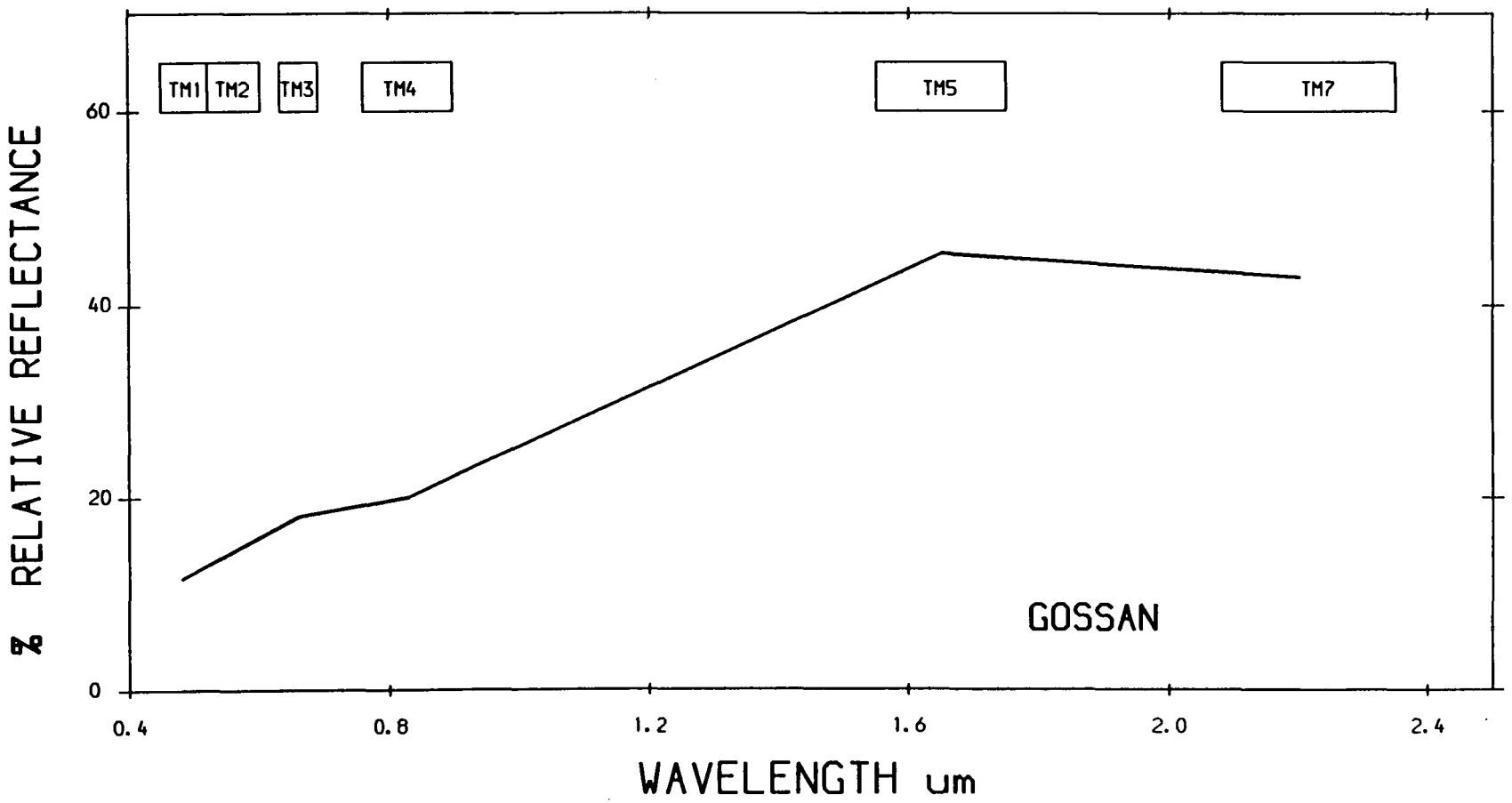

LANDSAT 5 TM CALIBRATED TO RELATIVE REFLCNCE

JABAL SAID AREA- SAUDI ARABIA

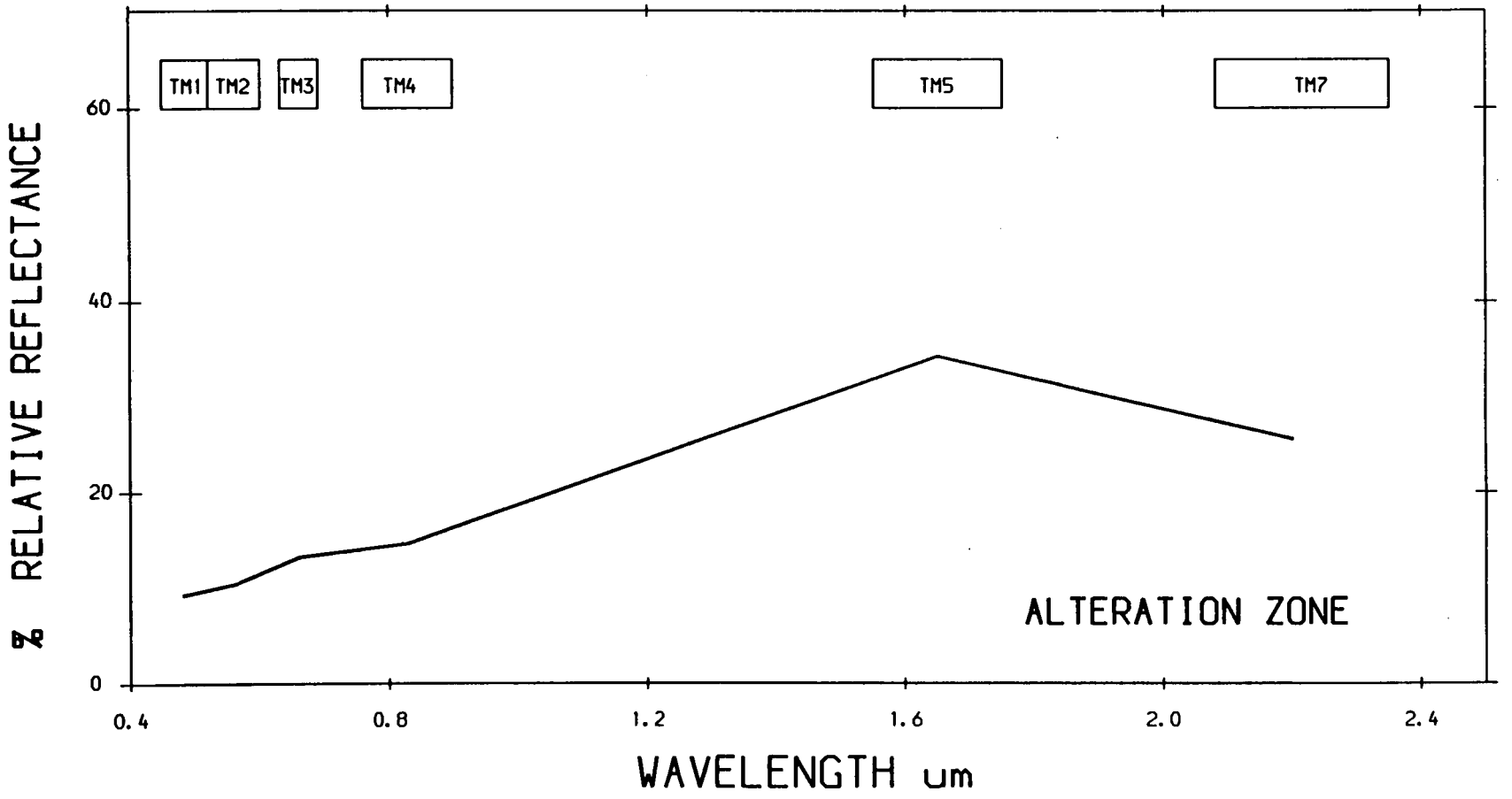

LANDSAT 5 TM CALIBRATED TO RELATIVE REFLCNCE

JABAL SAID AREA- SAUDI ARABIA

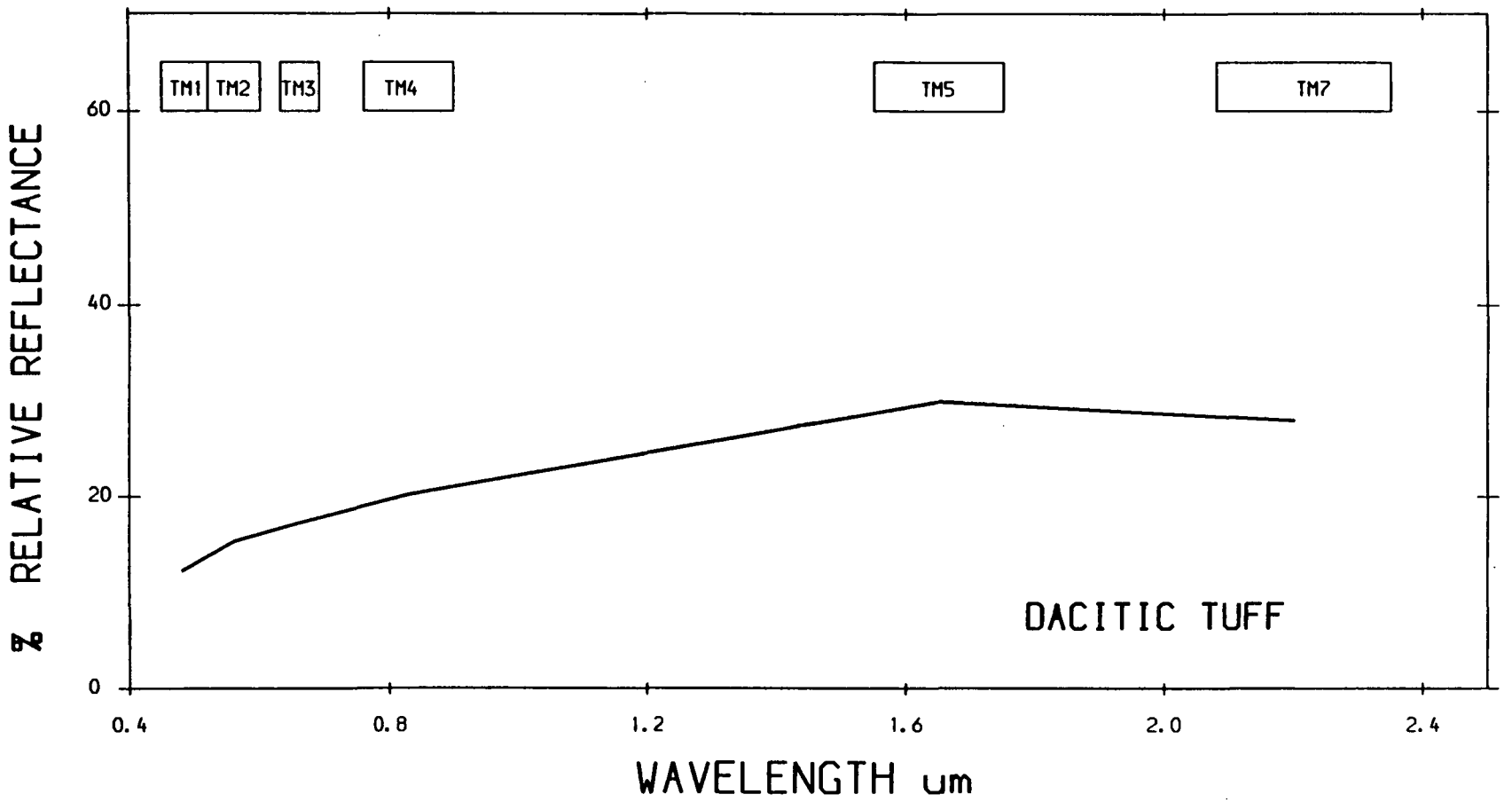

LANDSAT 5 TM CALIBRATED TO RELATIVE REFLCNCE

JABAL SAID AREA- SAUDI ARABIA

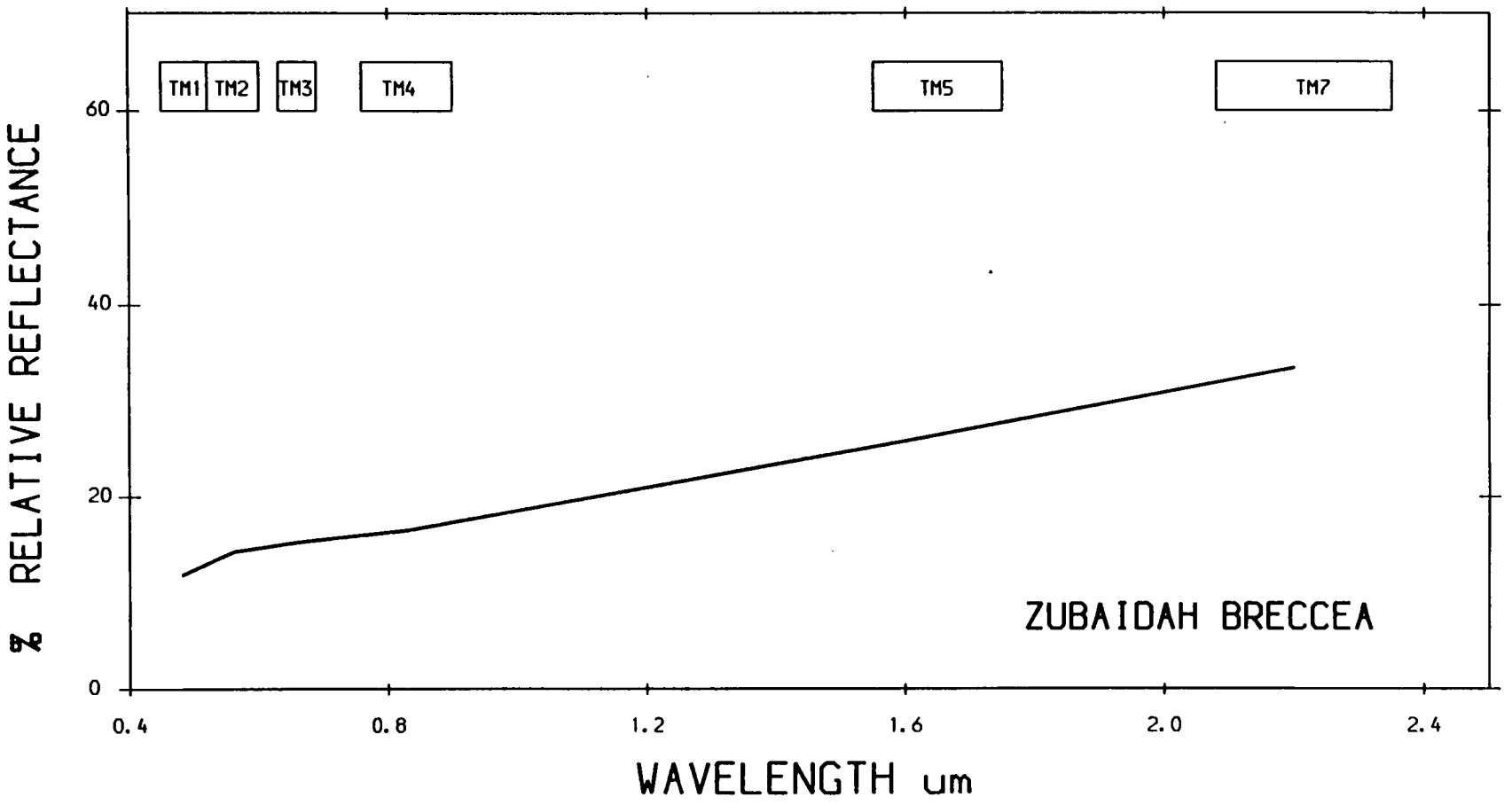

LANDSAT 5 TM CALIBRATED TO RELATIVE REFLCNCE

JABAL SAID AREA- SAUDI ARABIA

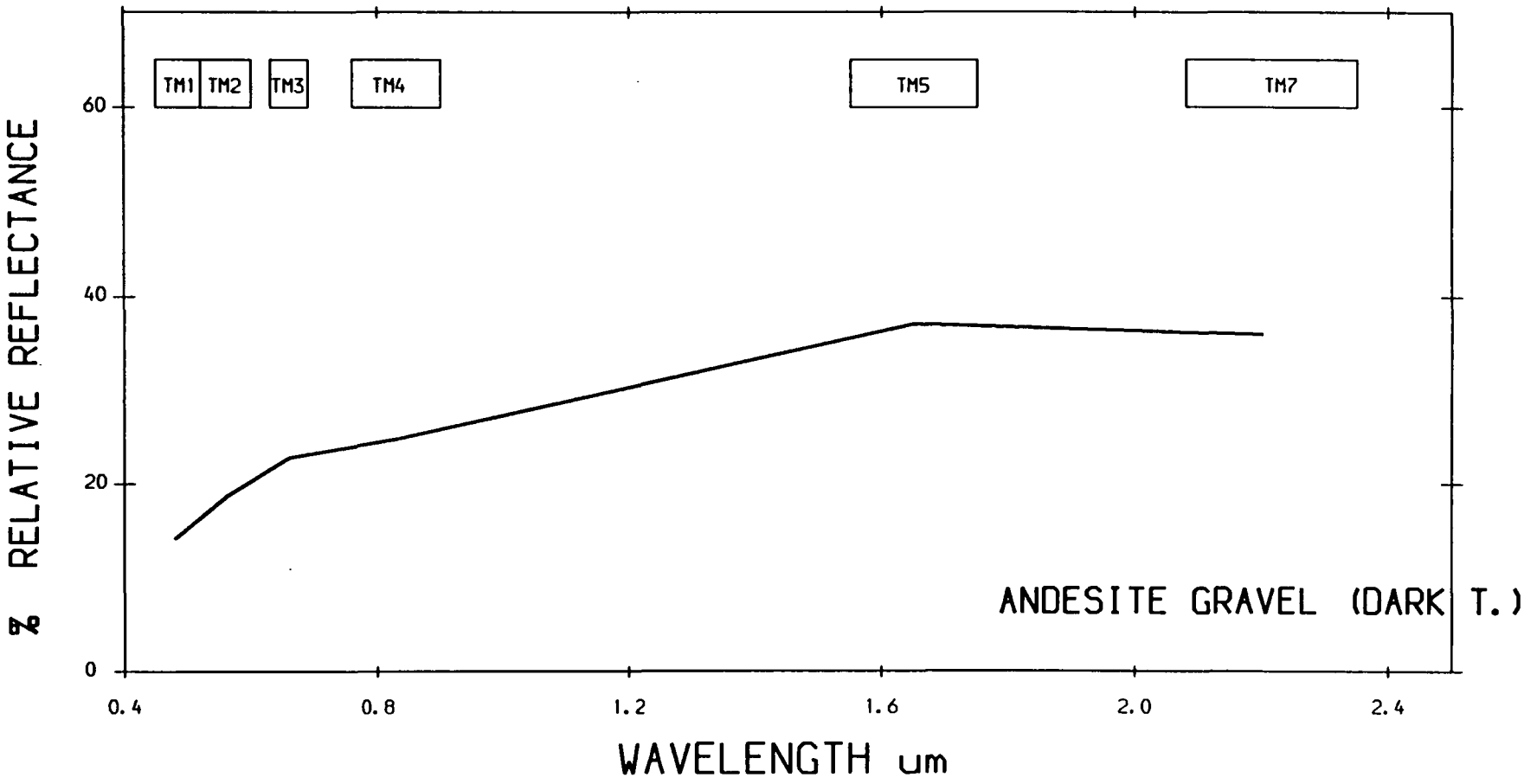

LANDSAT 5 TM CALIBRATED TO RELATIVE REFLCNCE

JABAL SAID AREA- SAUDI ARABIA

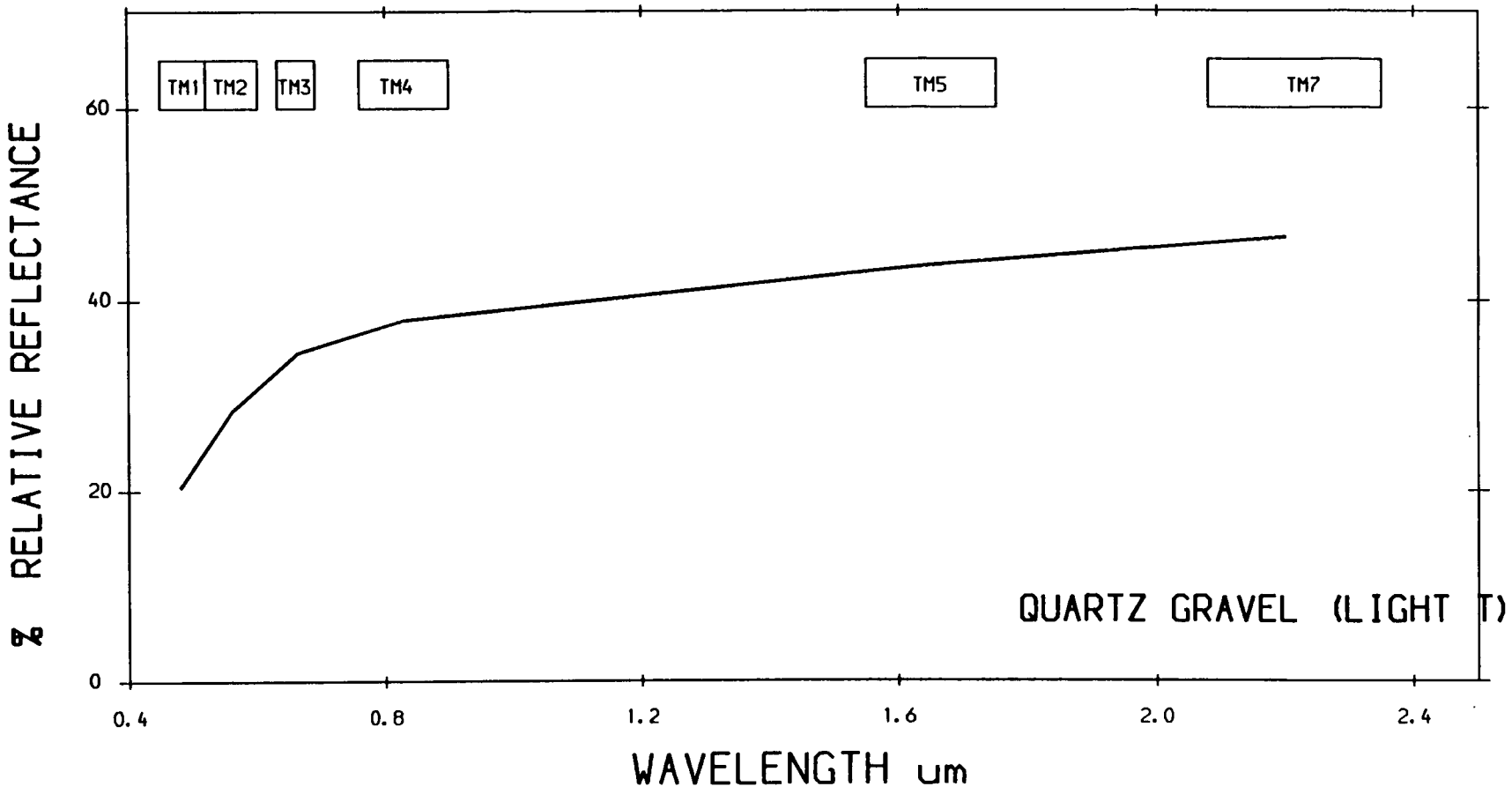

LANDSAT 5 TM CALIBRATED TO RELATIVE REFLCNCE

JABAL SAID AREA- SAUDI ARABIA

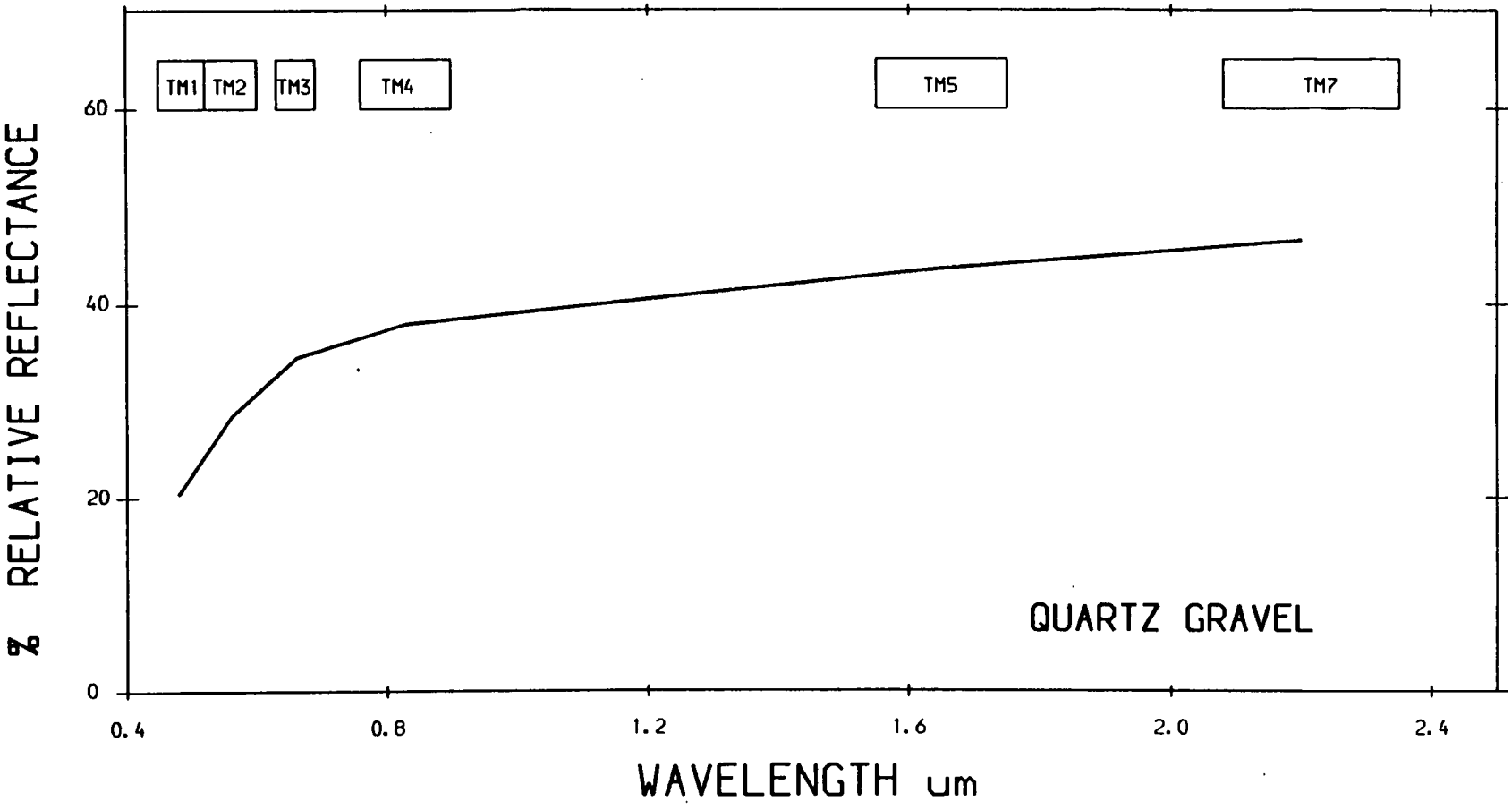

LANDSAT 5 TM CALIBRATED TO RELATIVE REFLCNCE

JABAL SAID AREA- SAUDI ARABIA

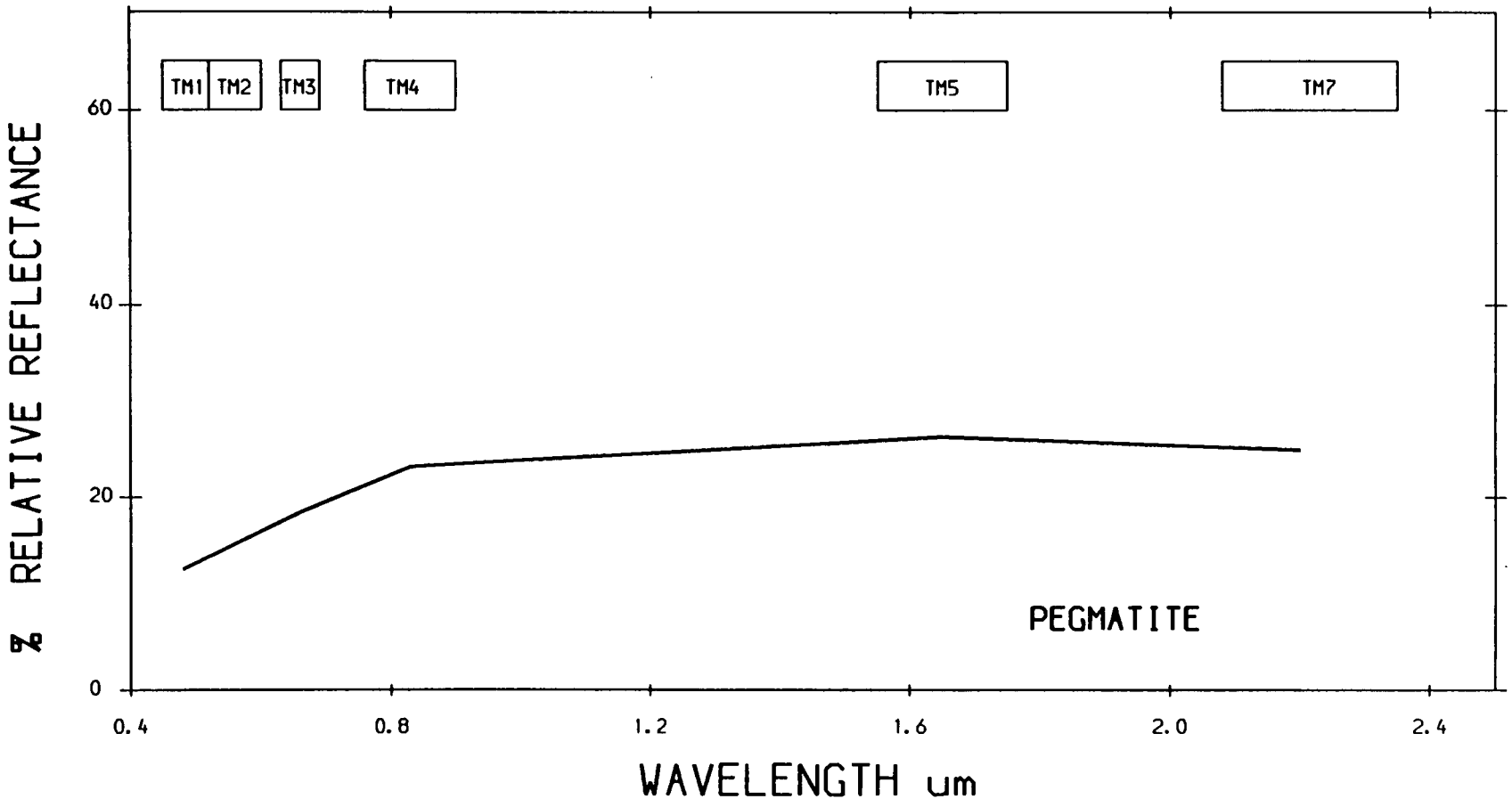

LANDSAT 5 TM CALIBRATED TO RELATIVE REFLCNCE

JABAL SAID AREA- SAUDI ARABIA

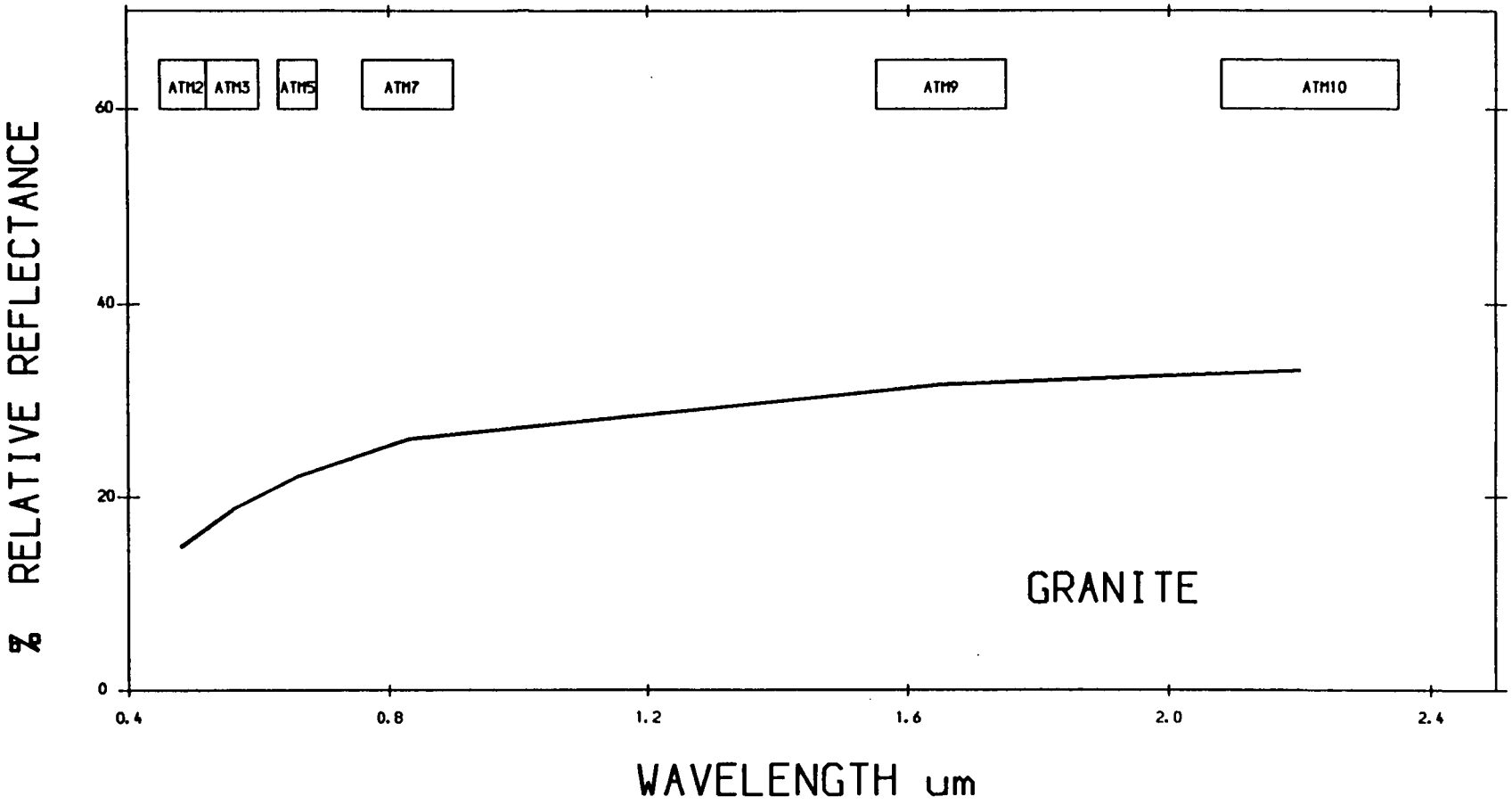

ATM 3000 M BAND EQUIVALENT TO TM CALIBRATED TO RELATIVE REFLECTANCE USING CALIBRATION CURVE

JABAL SAID AREA - SAUDI ARABIA

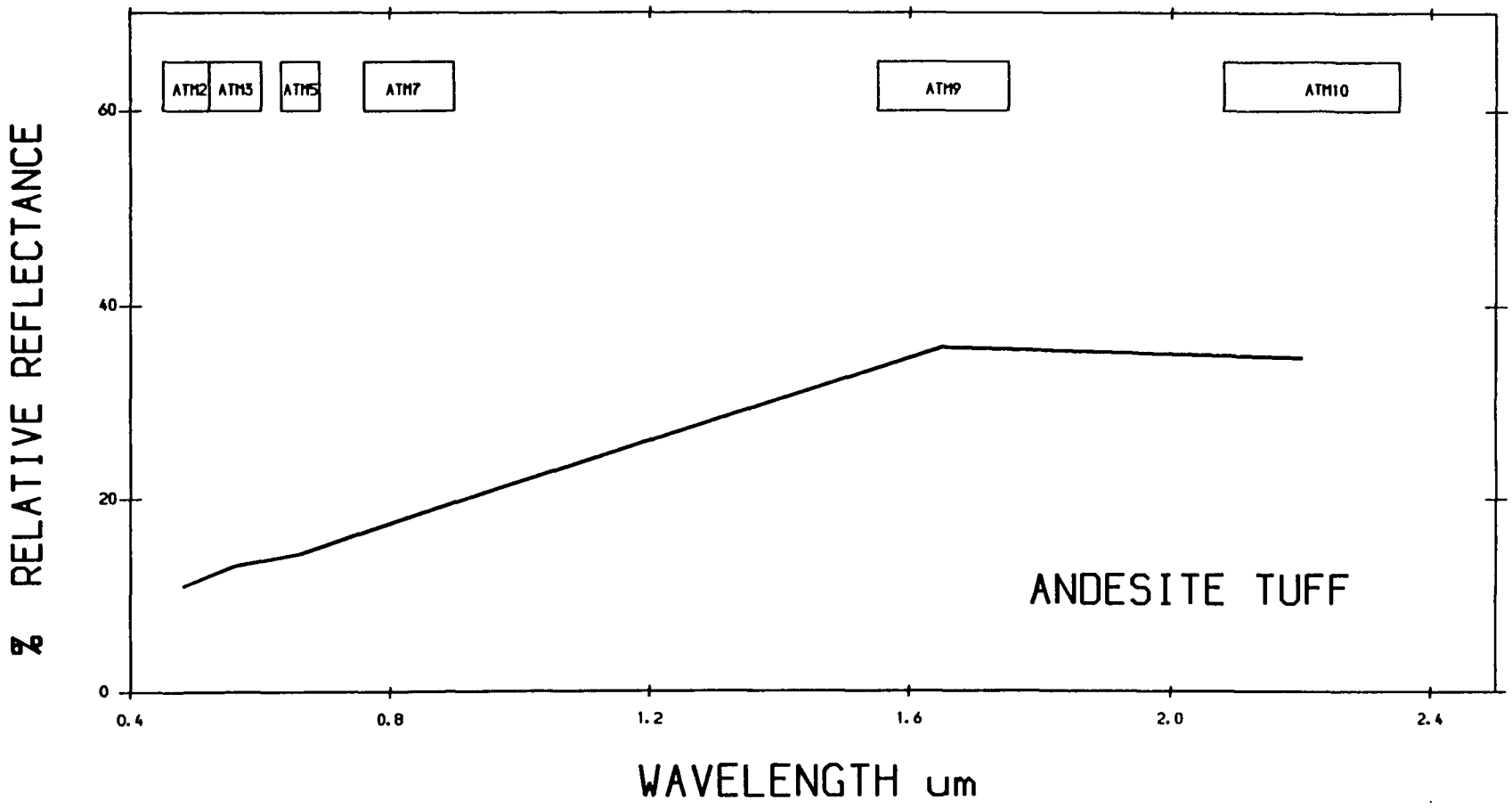

ATM 3000 M BAND EQUIVALENT TO TM CALIBRATED TO RELATIVE REFLECTANCE USING CALIBRATION CURVE

JABAL SAID AREA - SAUDI ARABIA

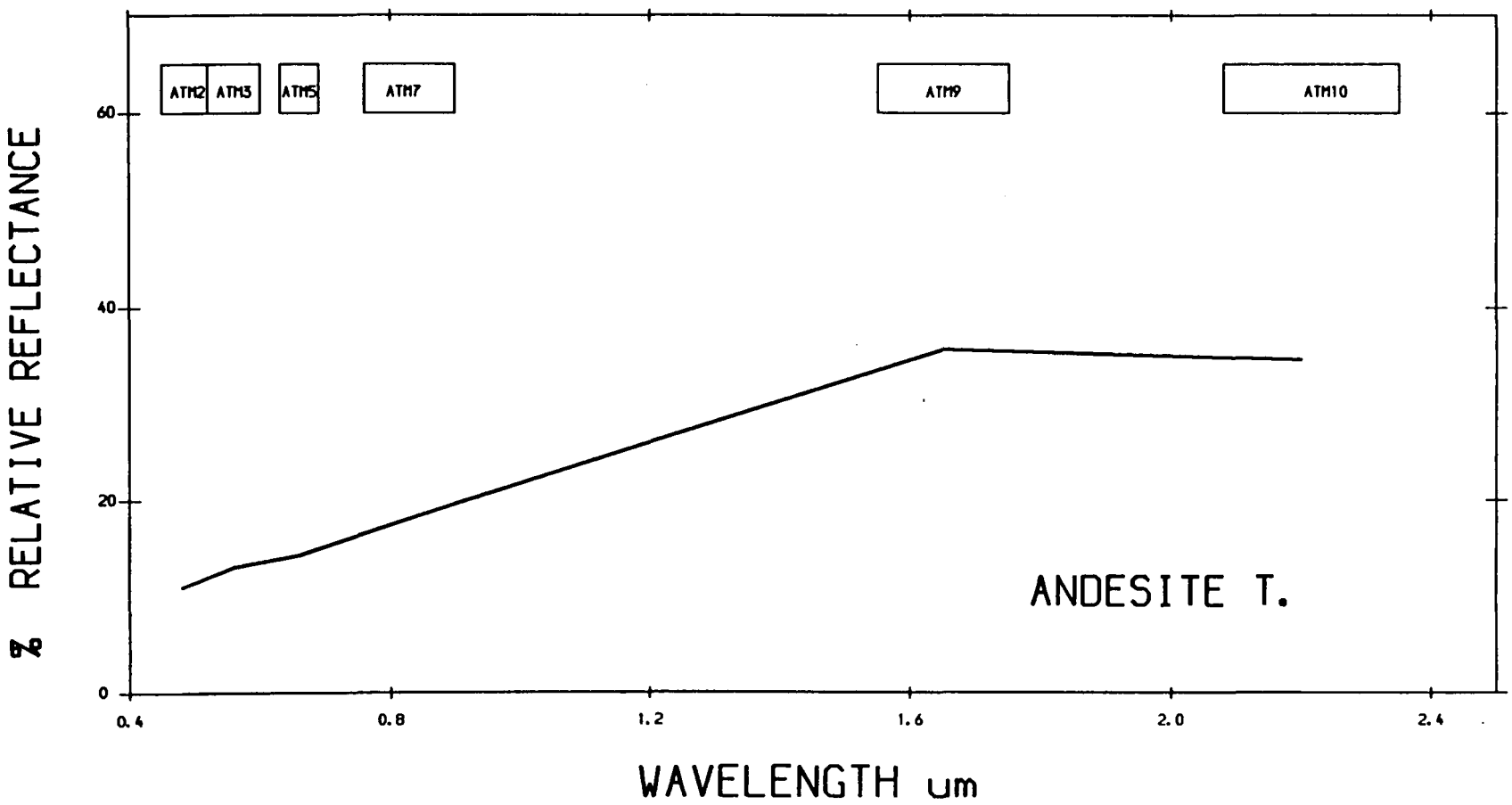

ATM 3000 M BAND EQUIVALENT TO TM CALIBRATED TO RELATIVE REFLECTANCE USING CALIBRATION CURVE

JABAL SAID AREA - SAUDI ARABIA

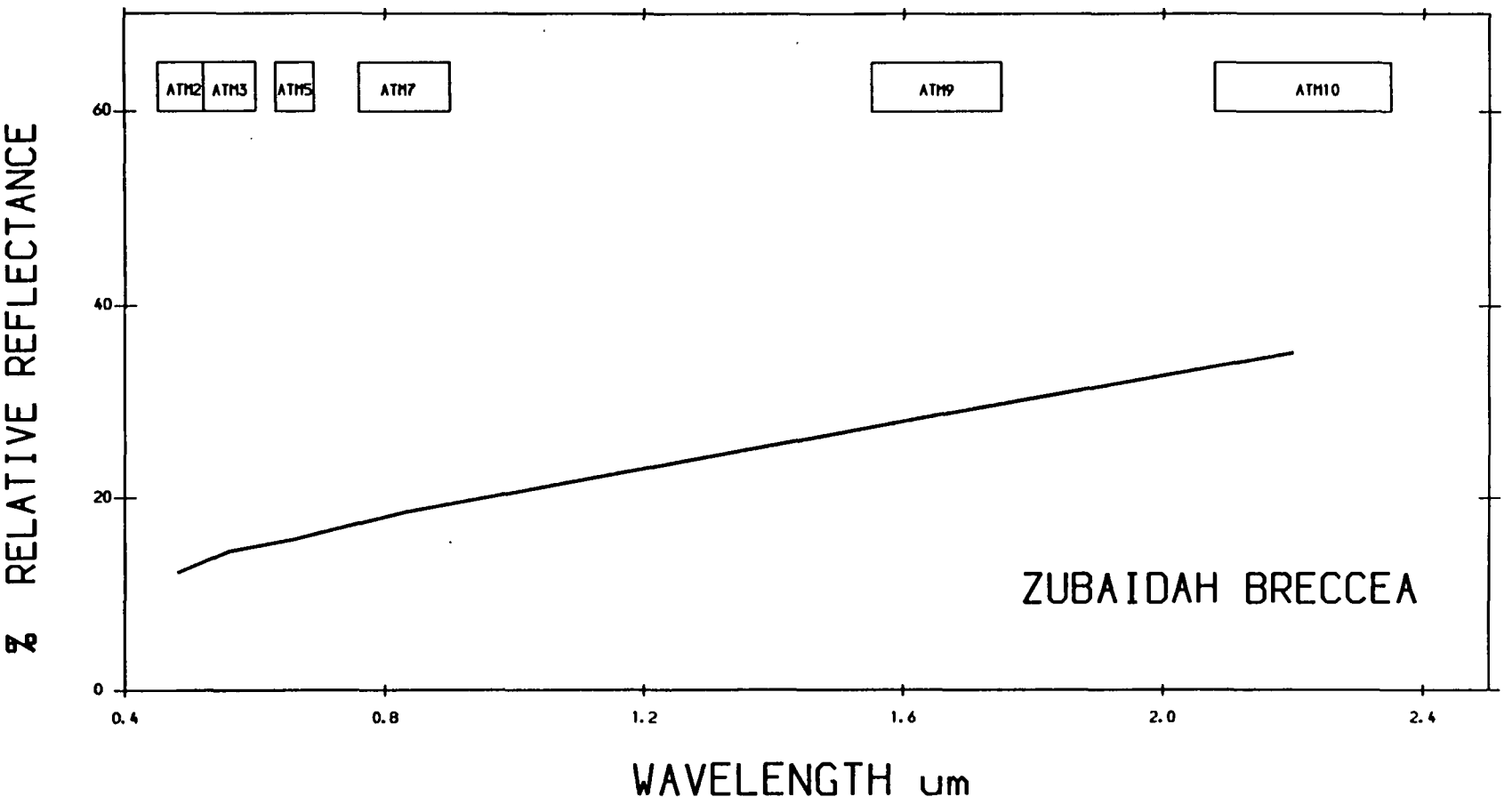

ATM 3000 M BAND EQUIVALENT TO TM CALIBRATED TO RELATIVE REFLECTANCE USING CALIBRATION CURVE

JABAL SAID AREA - SAUDI ARABIA

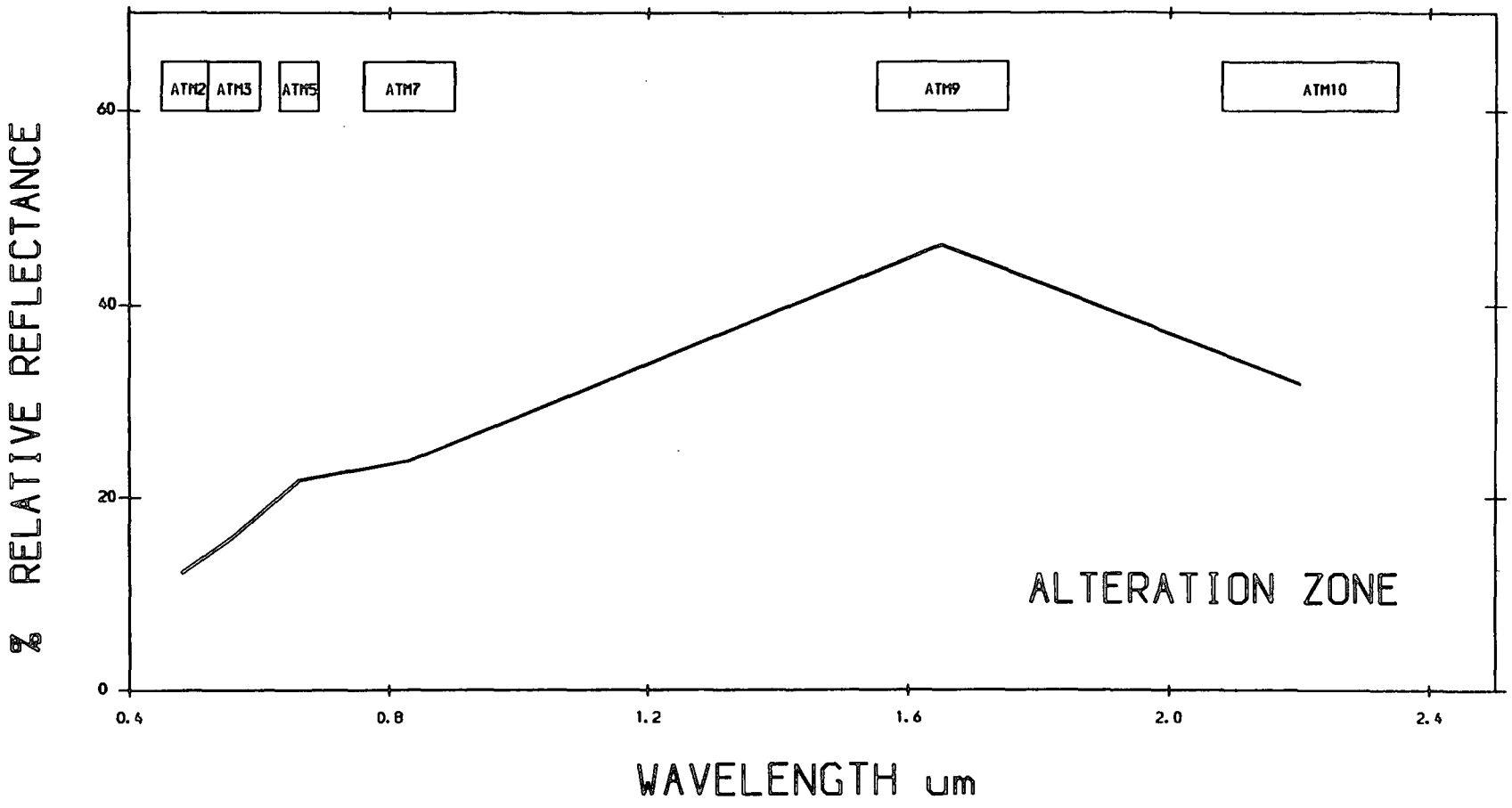

ATM 3000 M BAND EQUIVALENT TO TM CALIBRATED TO RELATIVE REFLECTANCE USING CALIBRATION CURVE

JABAL SAID AREA - SAUDI ARABIA

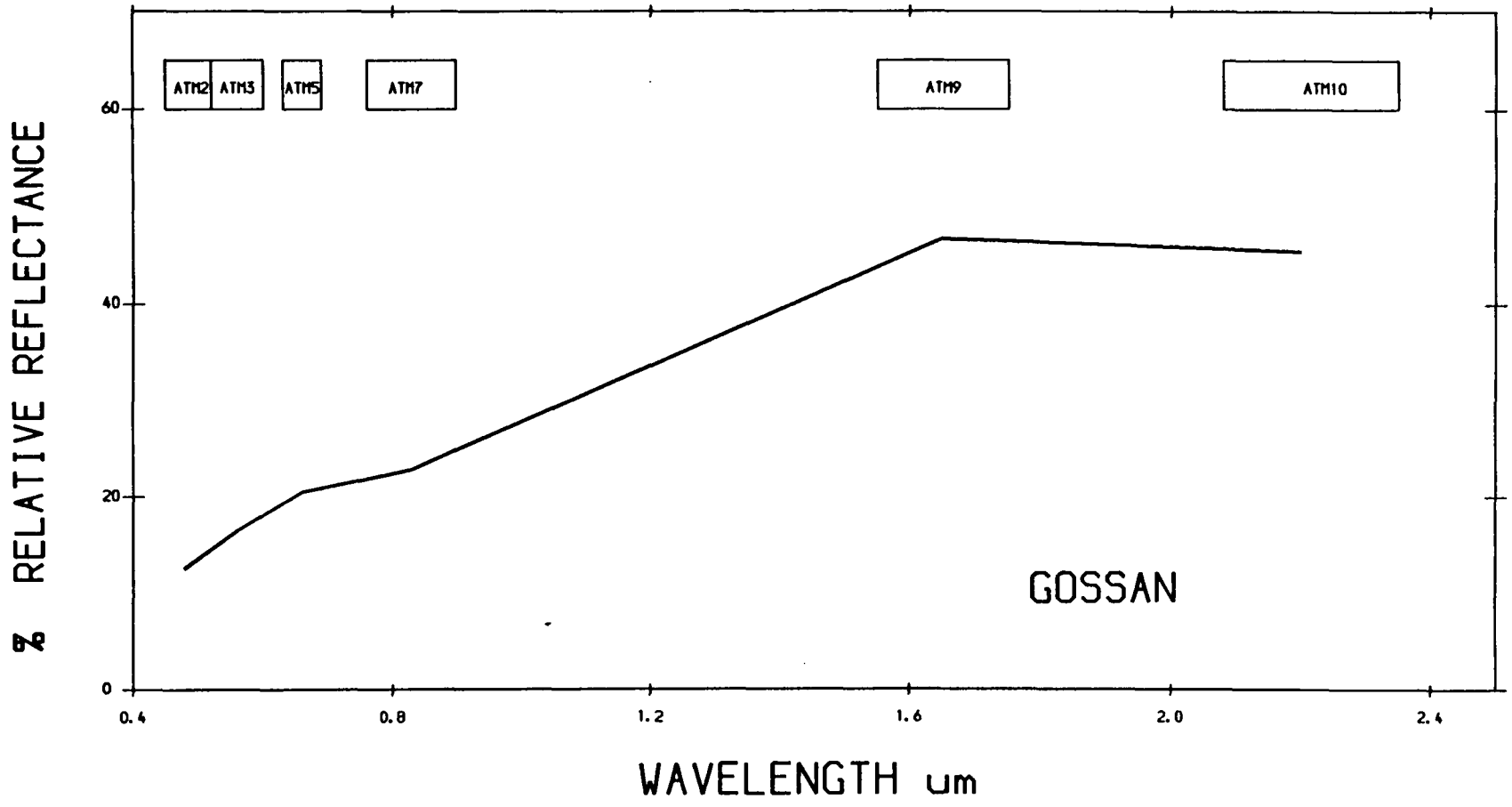

ATM 3000 M BAND EQUIVALENT TO TM CALIBRATED TO RELATIVE REFLECTANCE USING CALIBRATION CURVE

JABAL SAID AREA - SAUDI ARABIA

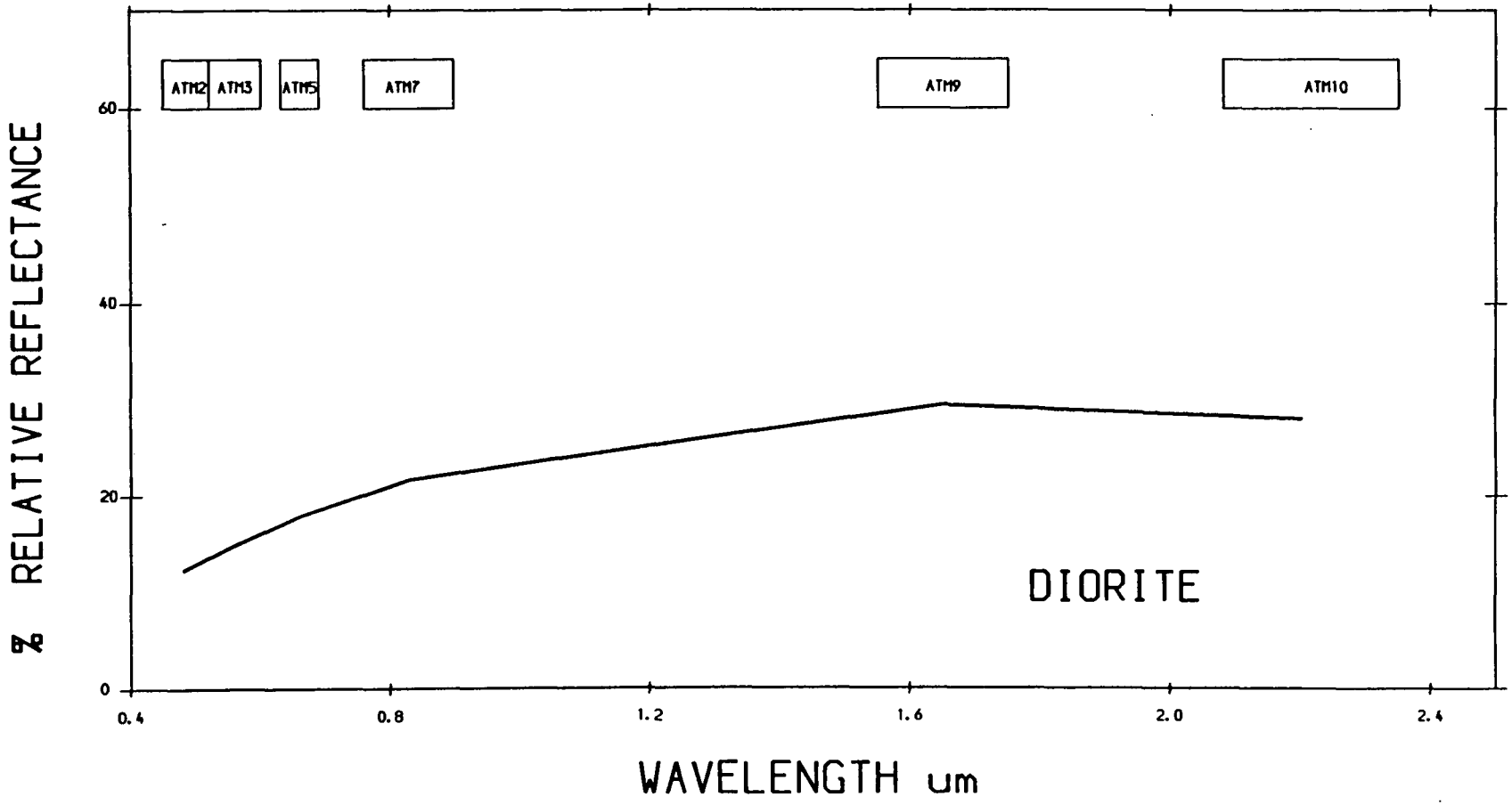

ATM 3000 M BAND EQUIVALENT TO TM CALIBRATED TO RELATIVE REFLECTANCE USING CALIBRATION CURVE

JABAL SAID AREA - SAUDI ARABIA

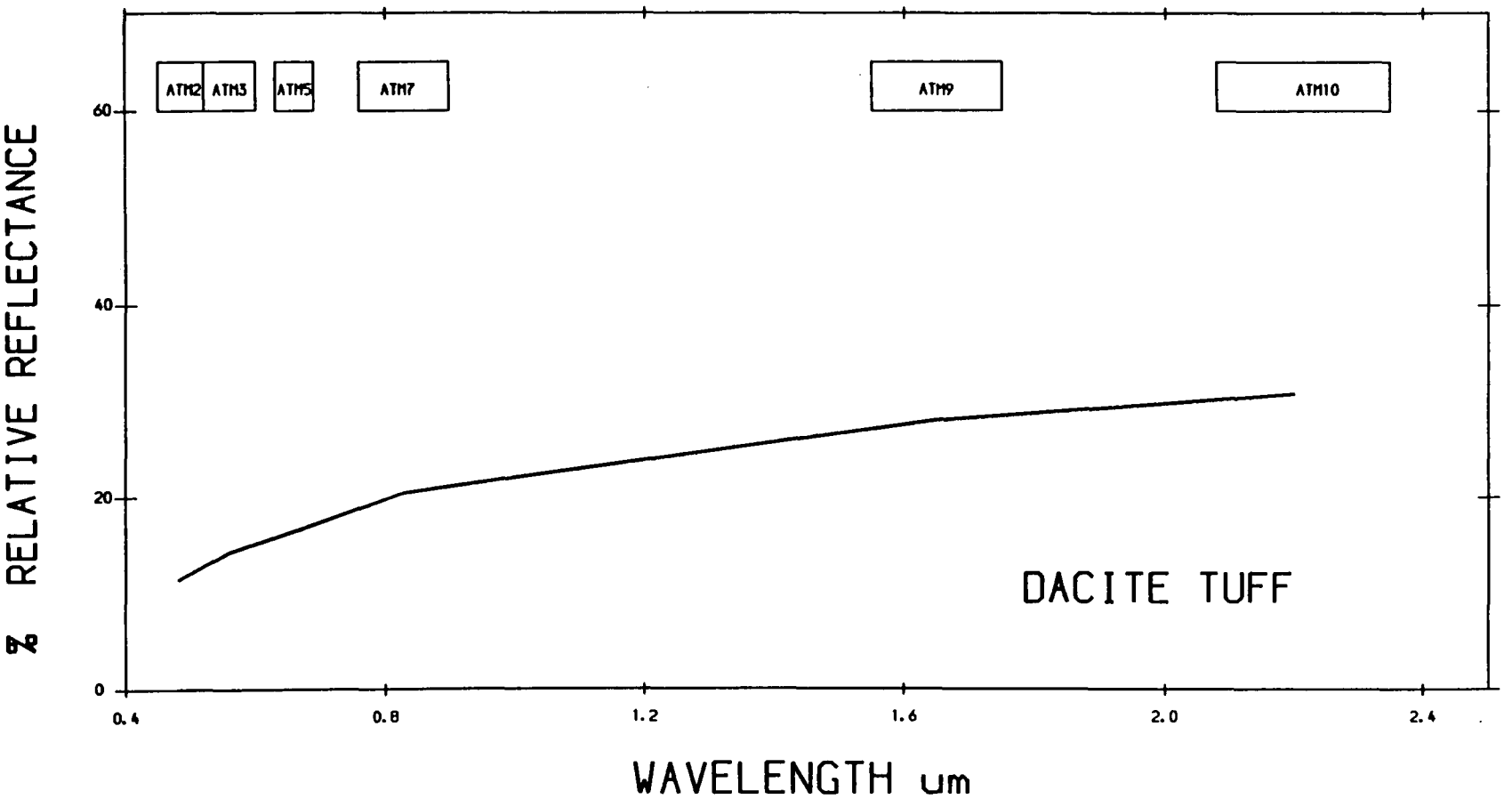

ATM 3000 M BAND EQUIVALENT TO TM CALIBRATED TO RELATIVE REFLECTANCE USING CALIBRATION CURVE

JABAL SAID AREA - SAUDI ARABIA

009

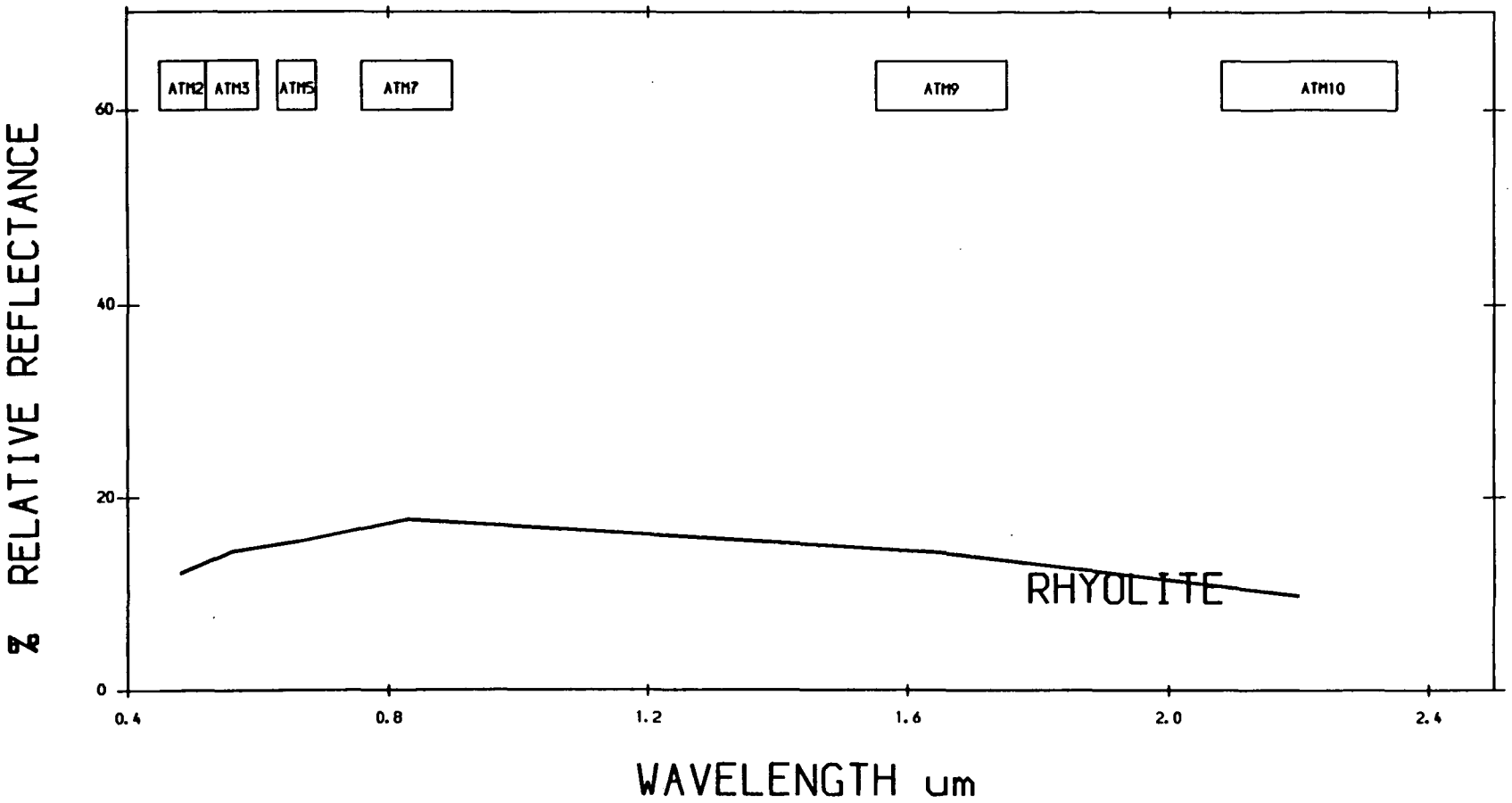

ATM 3000 M BAND EQUIVALENT TO TM CALIBRATED TO RELATIVE REFLECTANCE USING CALIBRATION CURVE

JABAL SAID AREA - SAUDI ARABIA

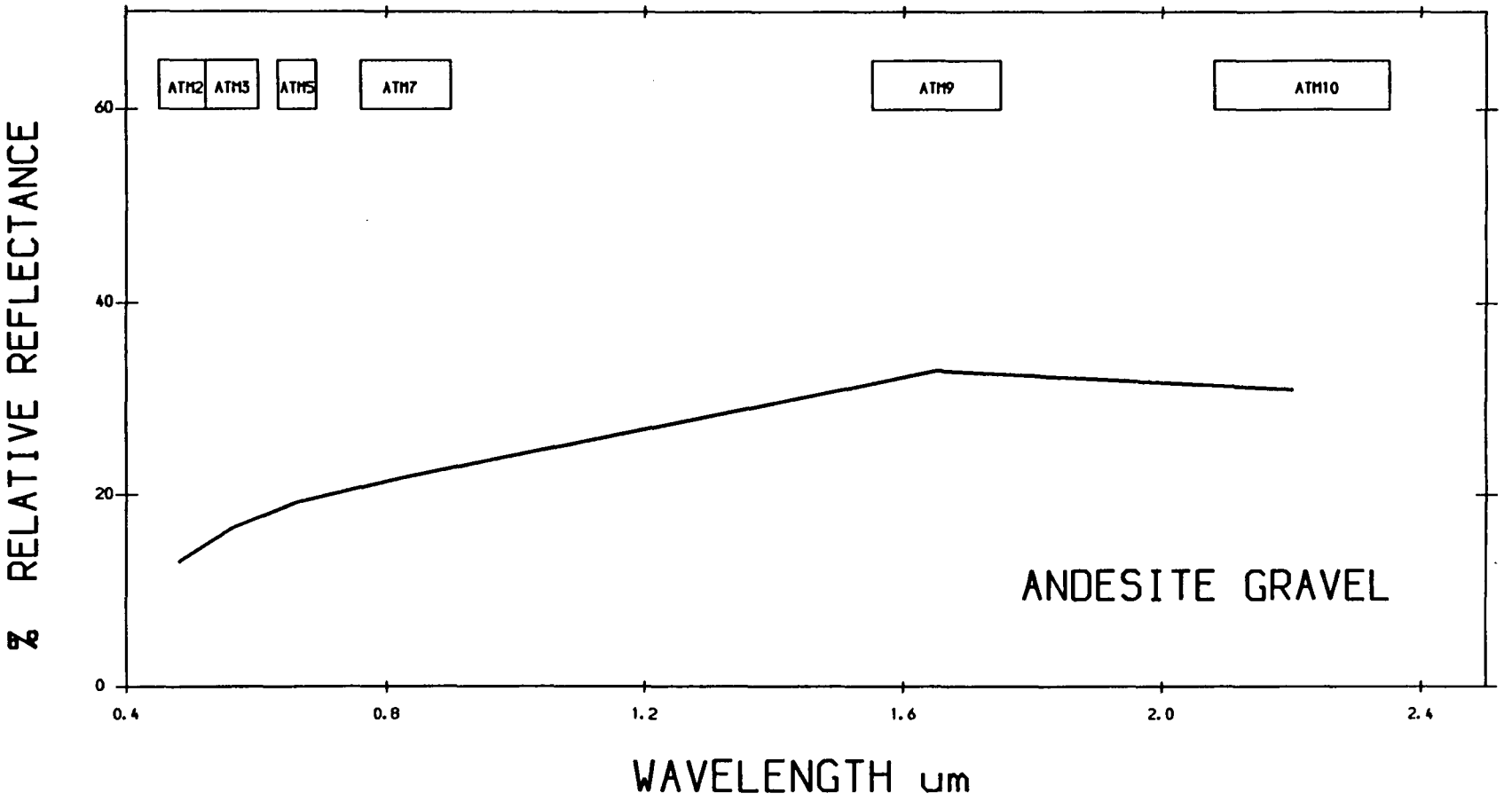

ATM 3000 M BAND EQUIVALENT TO TM CALIBRATED TO RELATIVE REFLECTANCE USING CALIBRATION CURVE

JABAL SAID AREA - SAUDI ARABIA

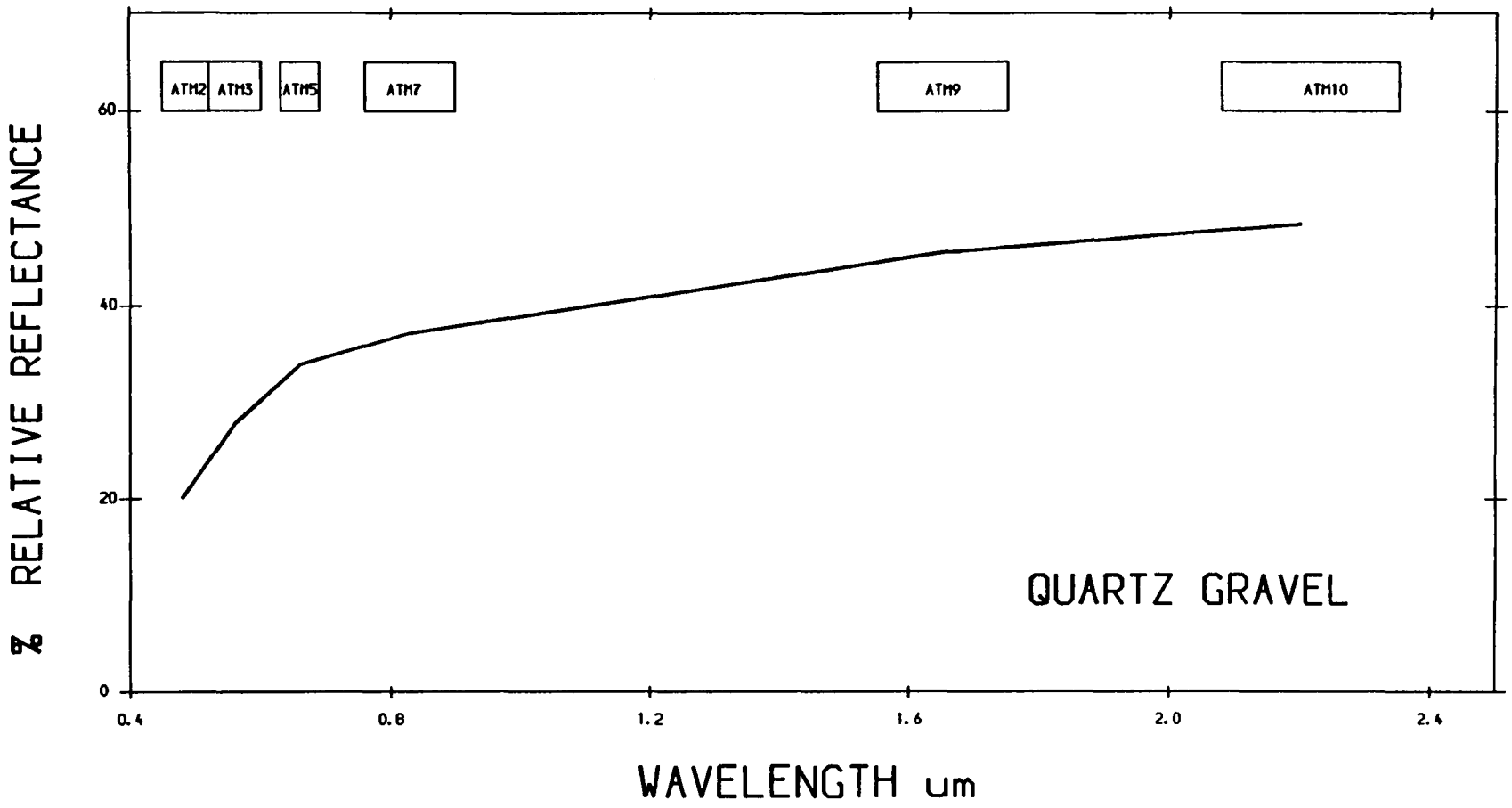

ATM 3000 M BAND EQUIVALENT TO TM CALIBRATED TO RELATIVE REFLECTANCE USING CALIBRATION CURVE

JABAL SAID AREA - SAUDI ARABIA

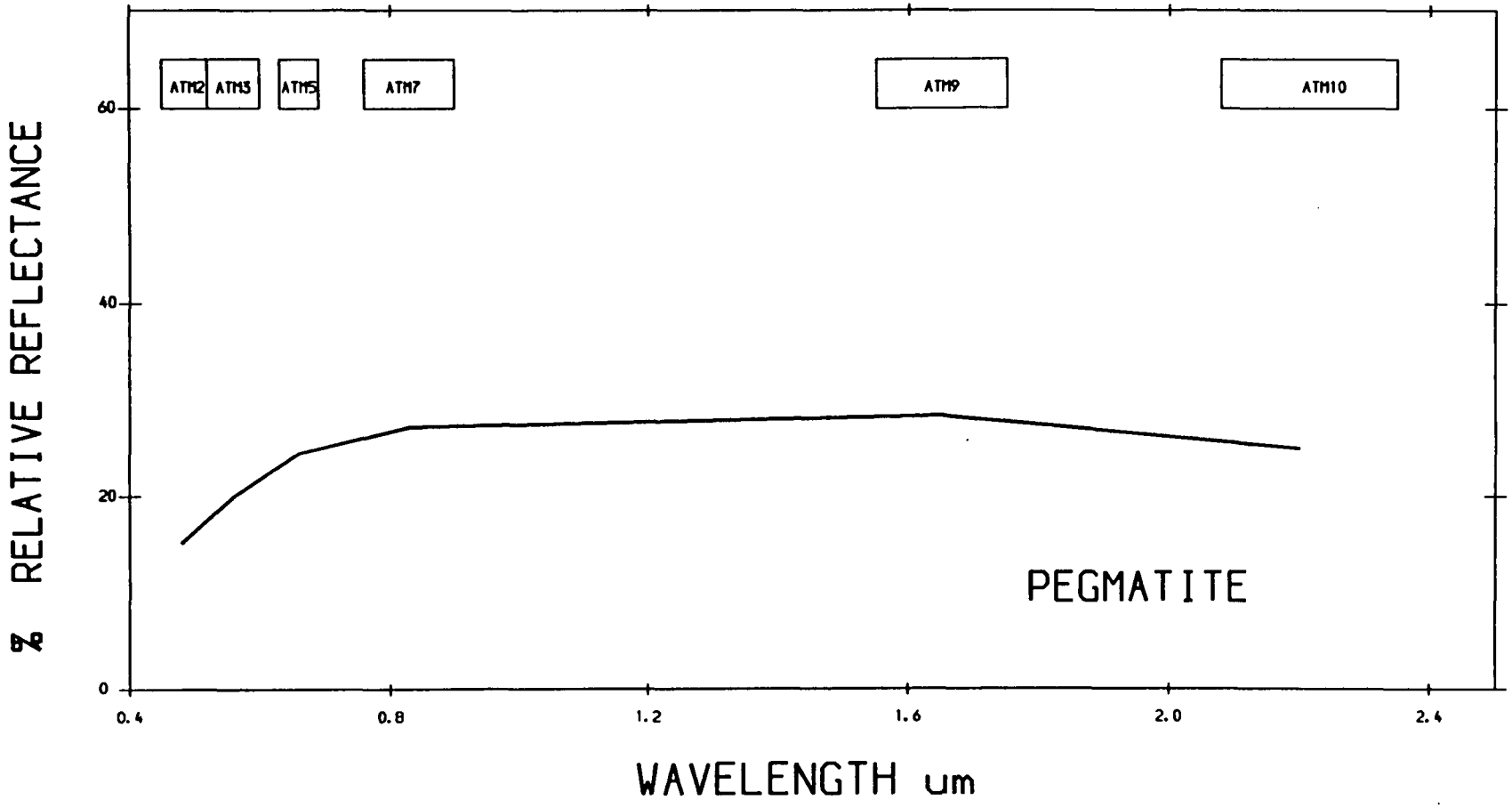

ATM 3000 M BAND EQUIVALENT TO TM CALIBRATED TO RELATIVE REFLECTANCE USING CALIBRATION CURVE

JABAL SAID AREA - SAUDI ARABIA

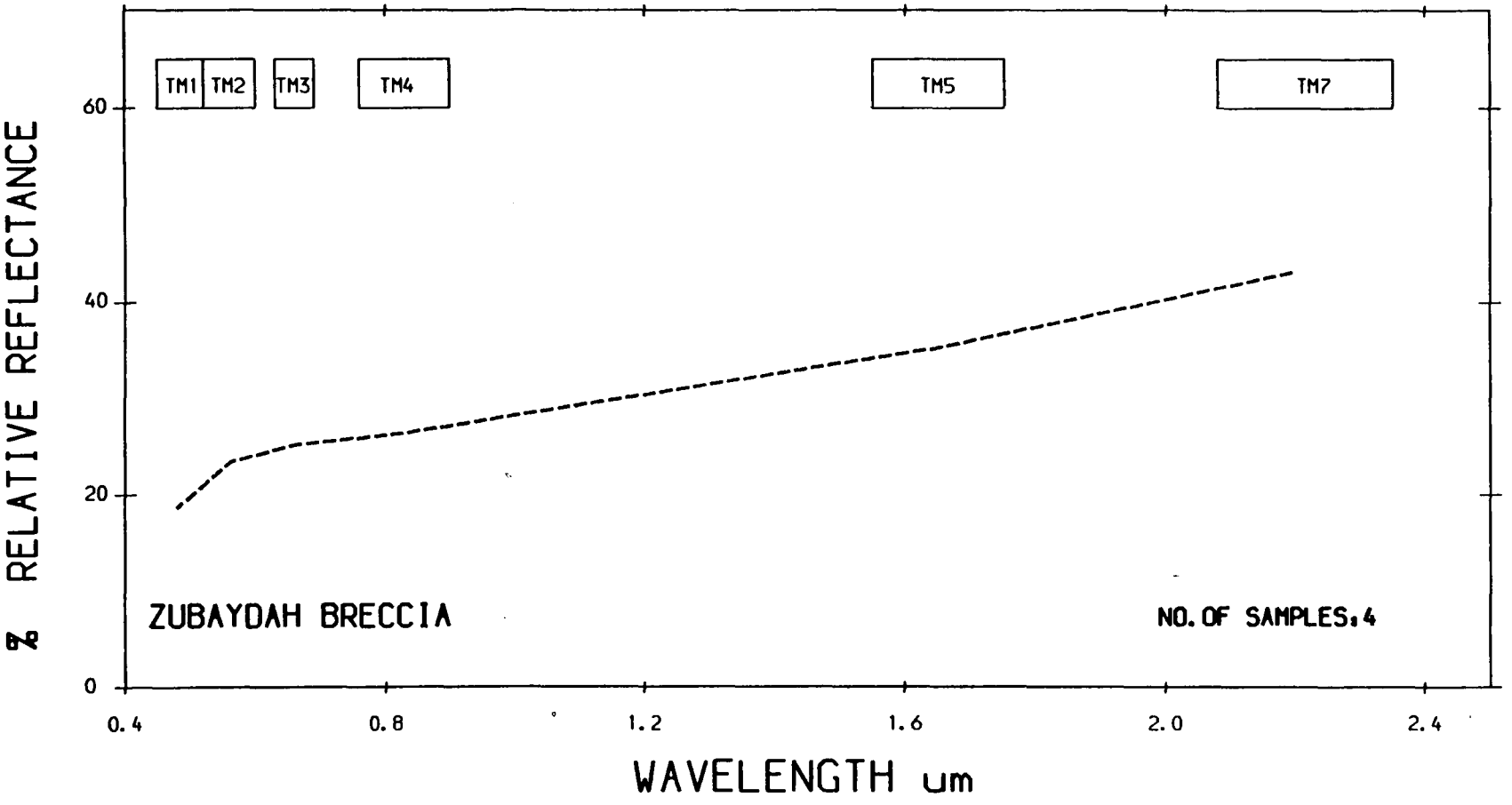

AVERAGE HHRR SPECTRA FROM JABAL SA`ID AREA

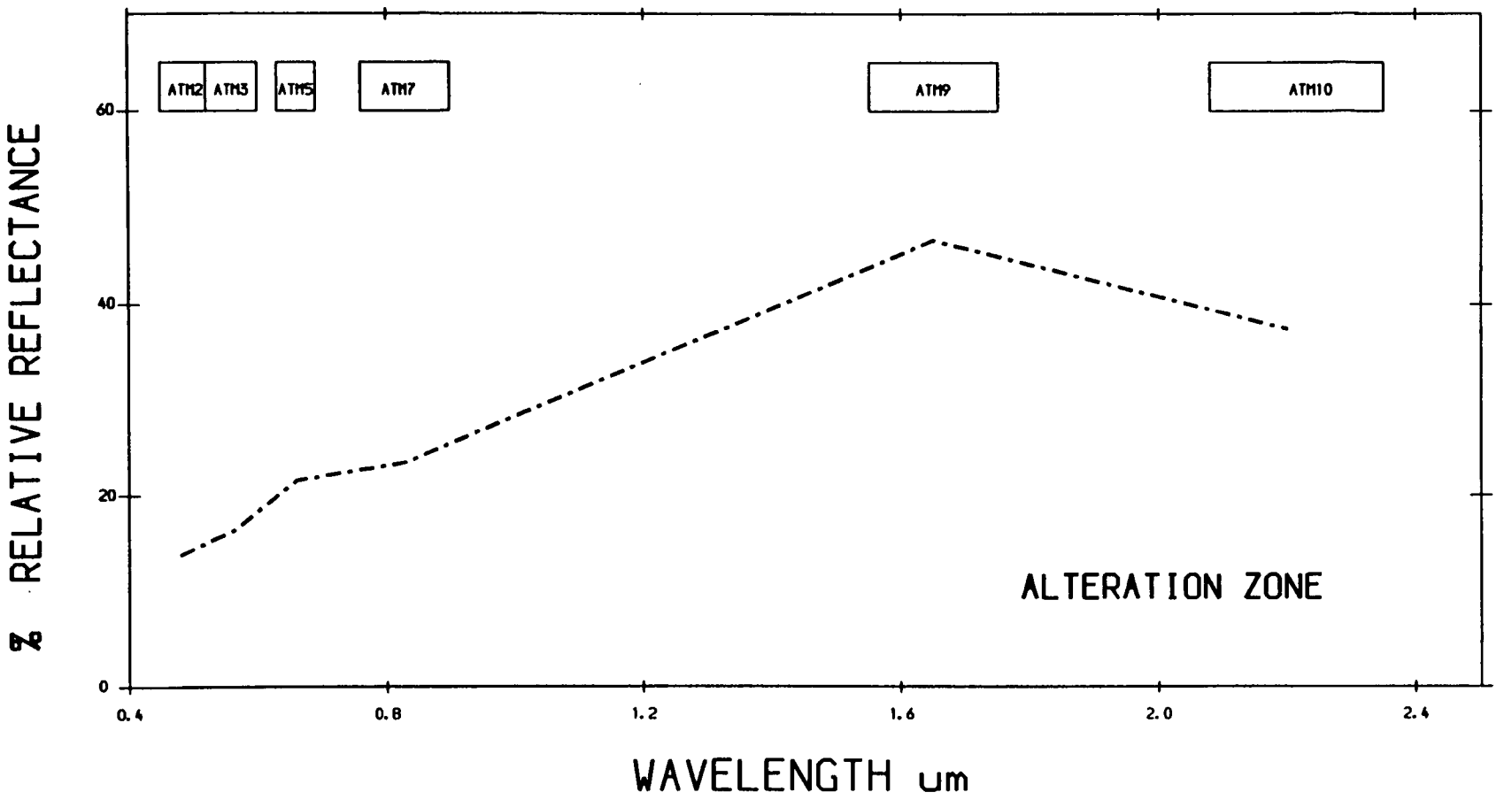

ATM 2000 M BAND EQUIVALENT TO TM CALIBRATED TO RELATIVE REFLECTANCE USING CALIBRATION CURVE

JABAL SAID AREA - SAUDI ARABIA

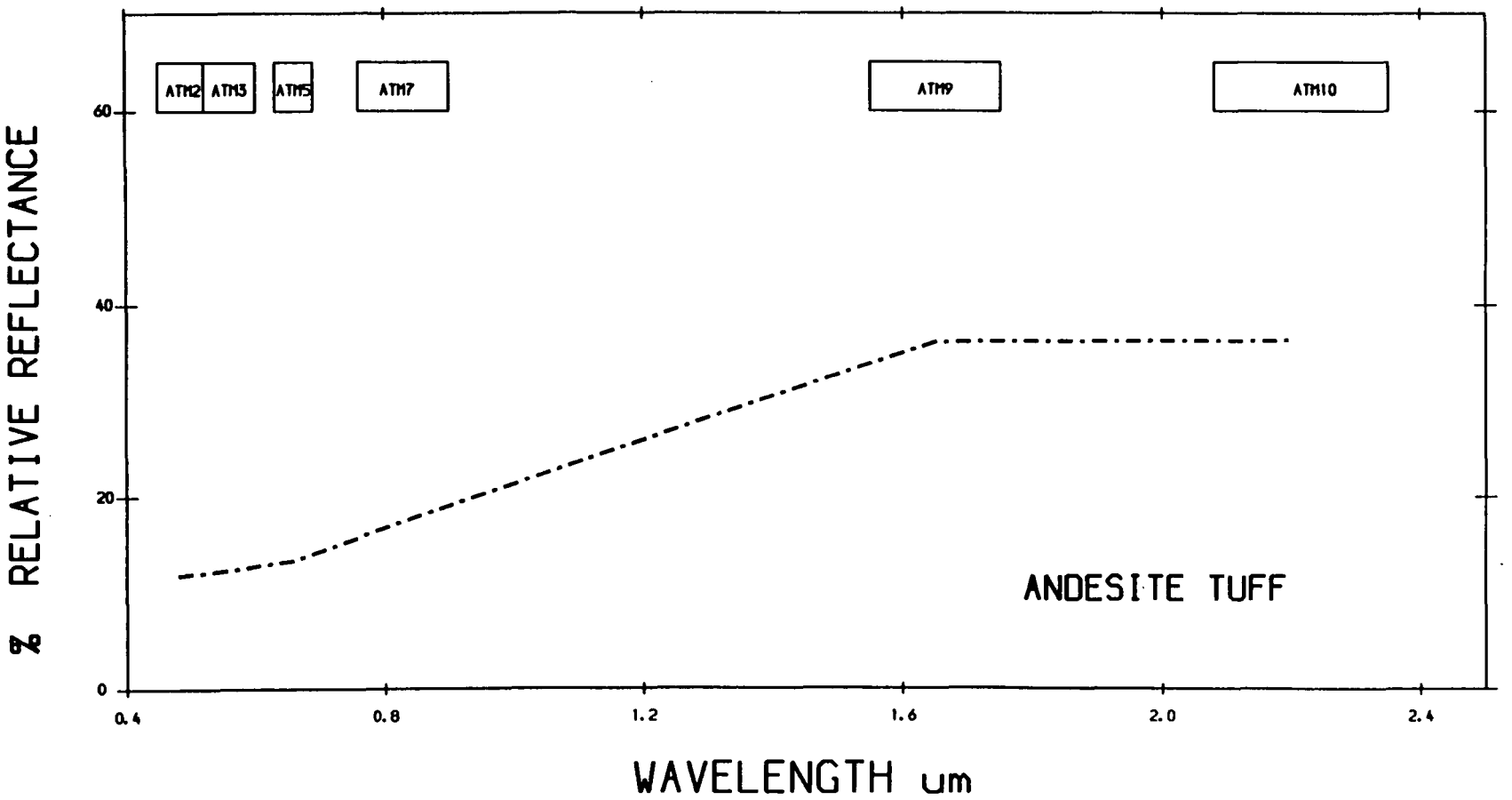

ATM 2000 M BAND EQUIVALENT TO TM CALIBRATED TO RELATIVE REFLECTANCE USING CALIBRATION CURVE

JABAL SAID AREA - SAUDI ARABIA

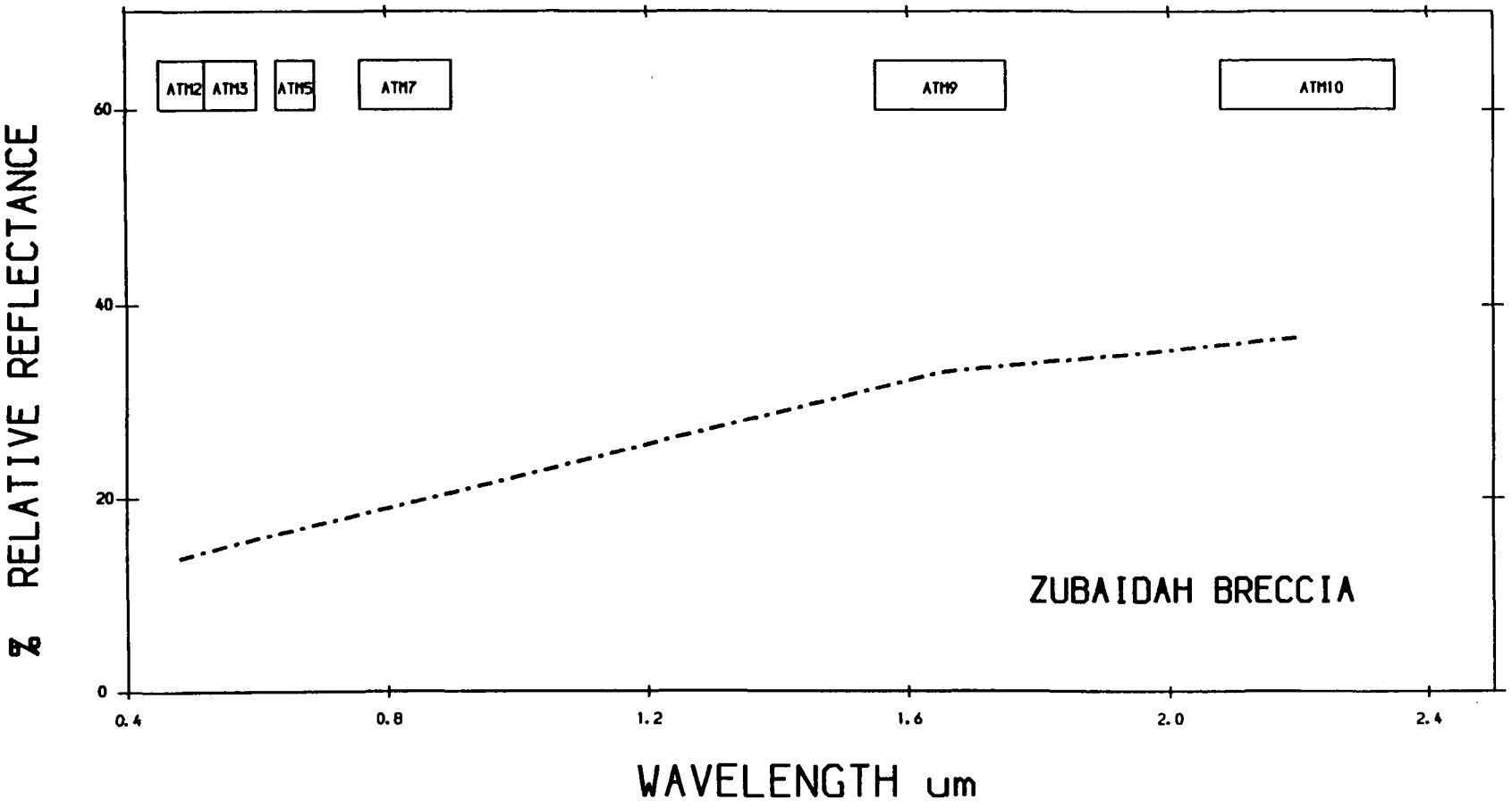

ATM 2000 M BAND EQUIVALENT TO TM CALIBRATED TO RELATIVE REFLECTANCE USING CALIBRATION CURVE

JABAL SAID AREA - SAUDI ARABIA

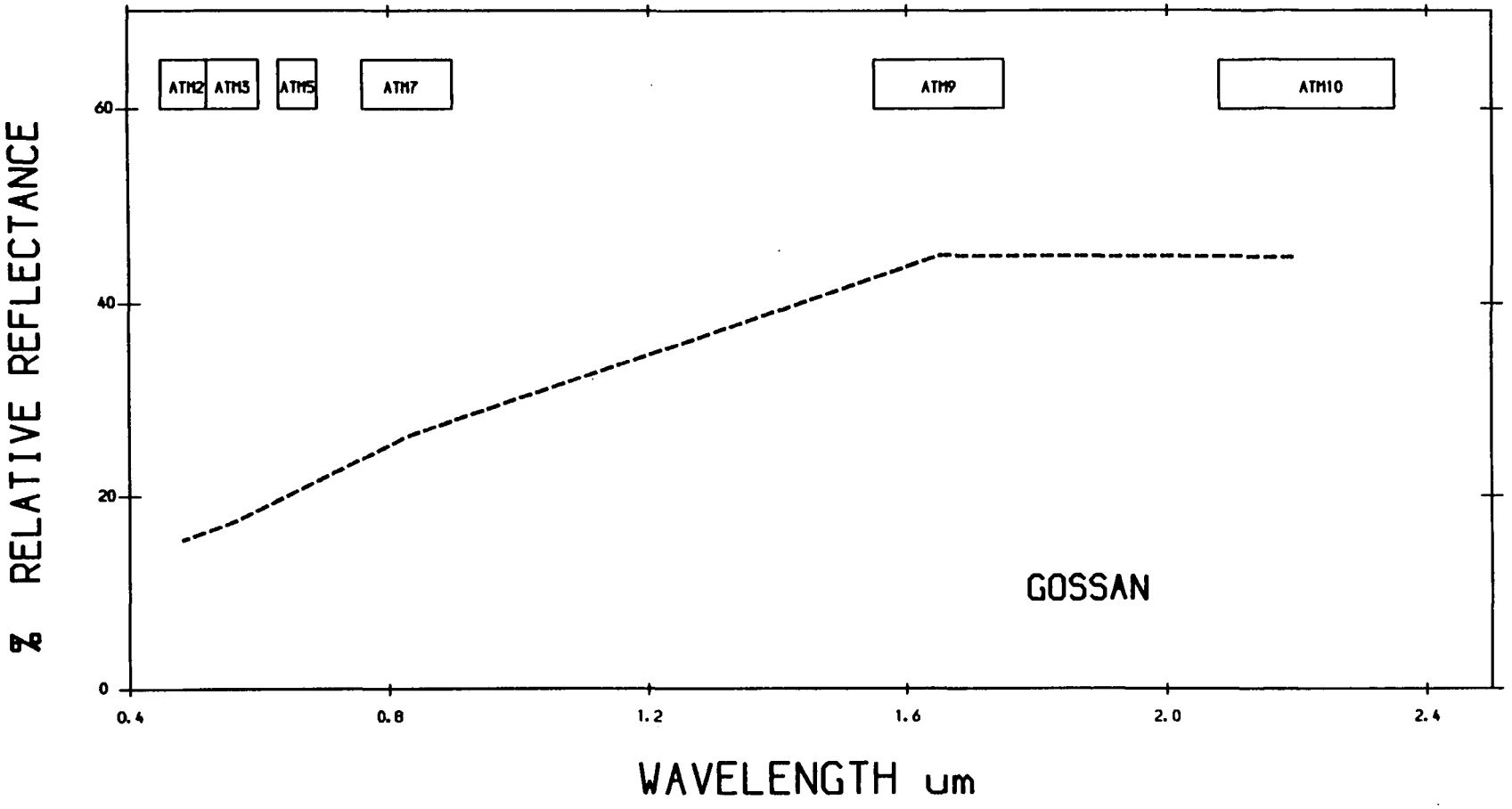

ATM 2000 M BAND EQUIVALENT TO TM CALIBRATED TO RELATIVE REFLECTANCE USING CALIBRATION CURVE

JABAL SAID AREA - SAUDI ARABIA

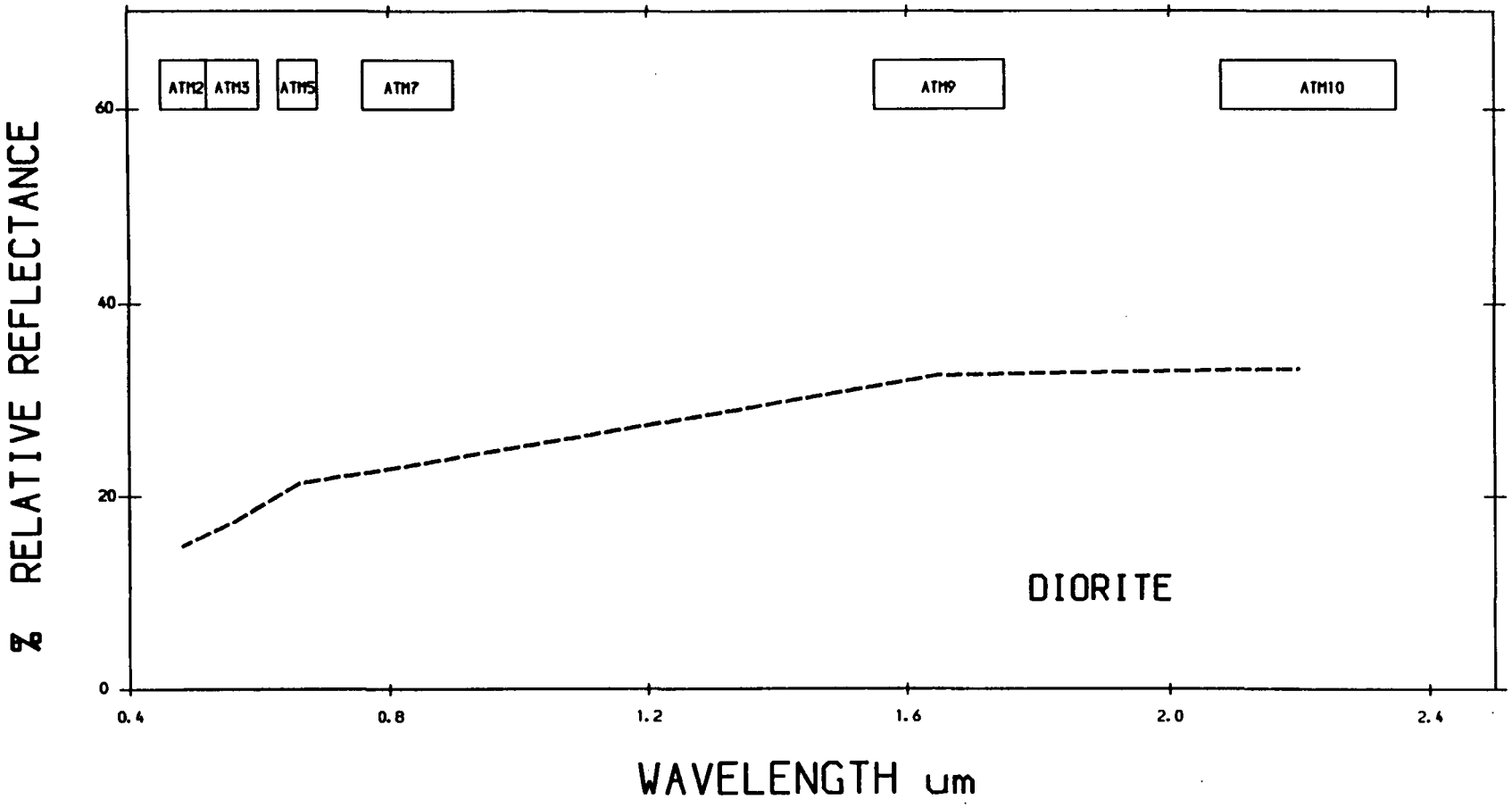

ATM 2000 M BAND EQUIVALENT TO TM CALIBRATED TO RELATIVE REFLECTANCE USING CALIBRATION CURVE

JABAL SAID AREA - SAUDI ARABIA

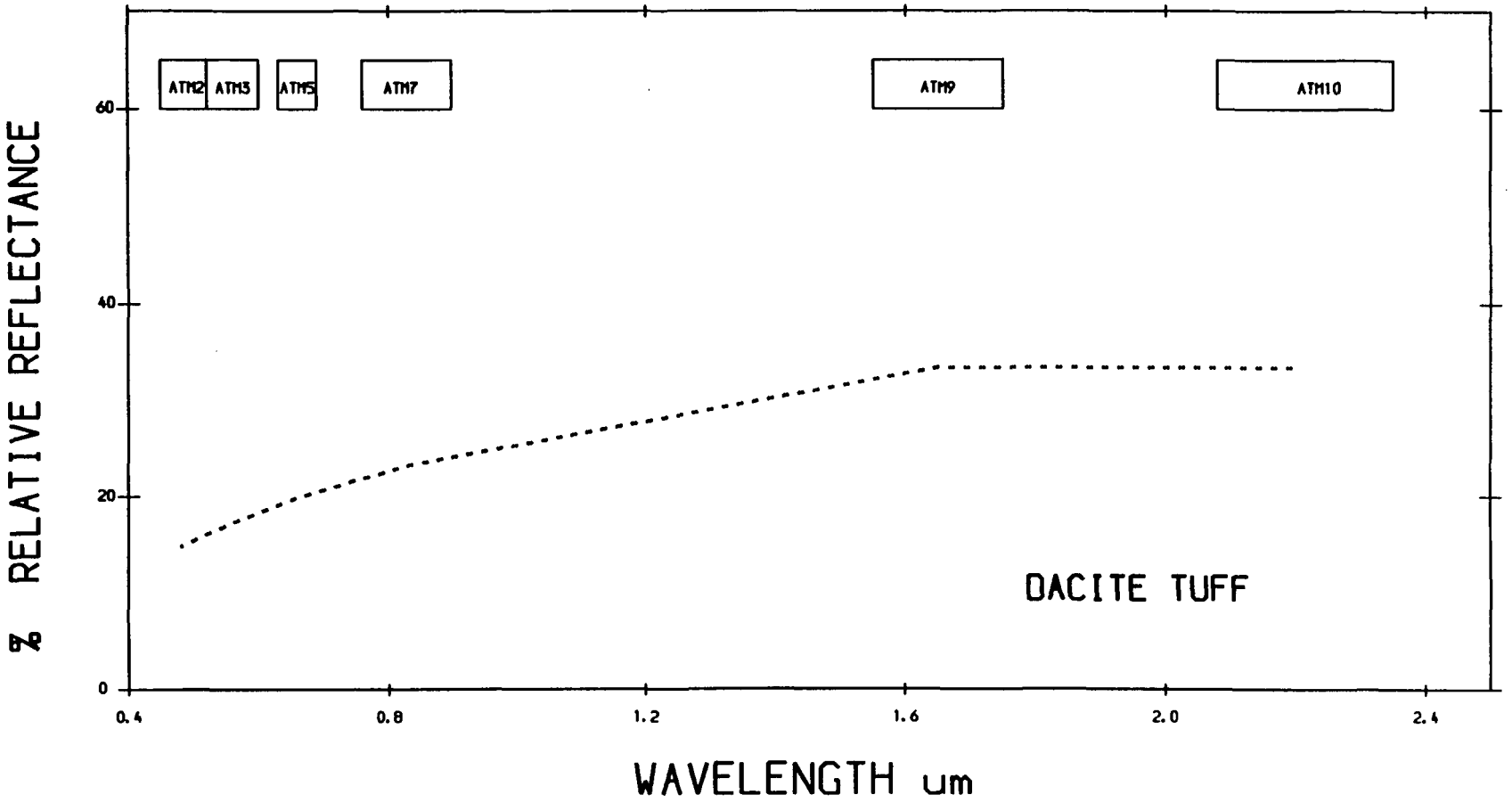

ATM 2000 M BAND EQUIVALENT TO TM CALIBRATED TO RELATIVE REFLECTANCE USING CALIBRATION CURVE

JABAL SAID AREA - SAUDI ARABIA

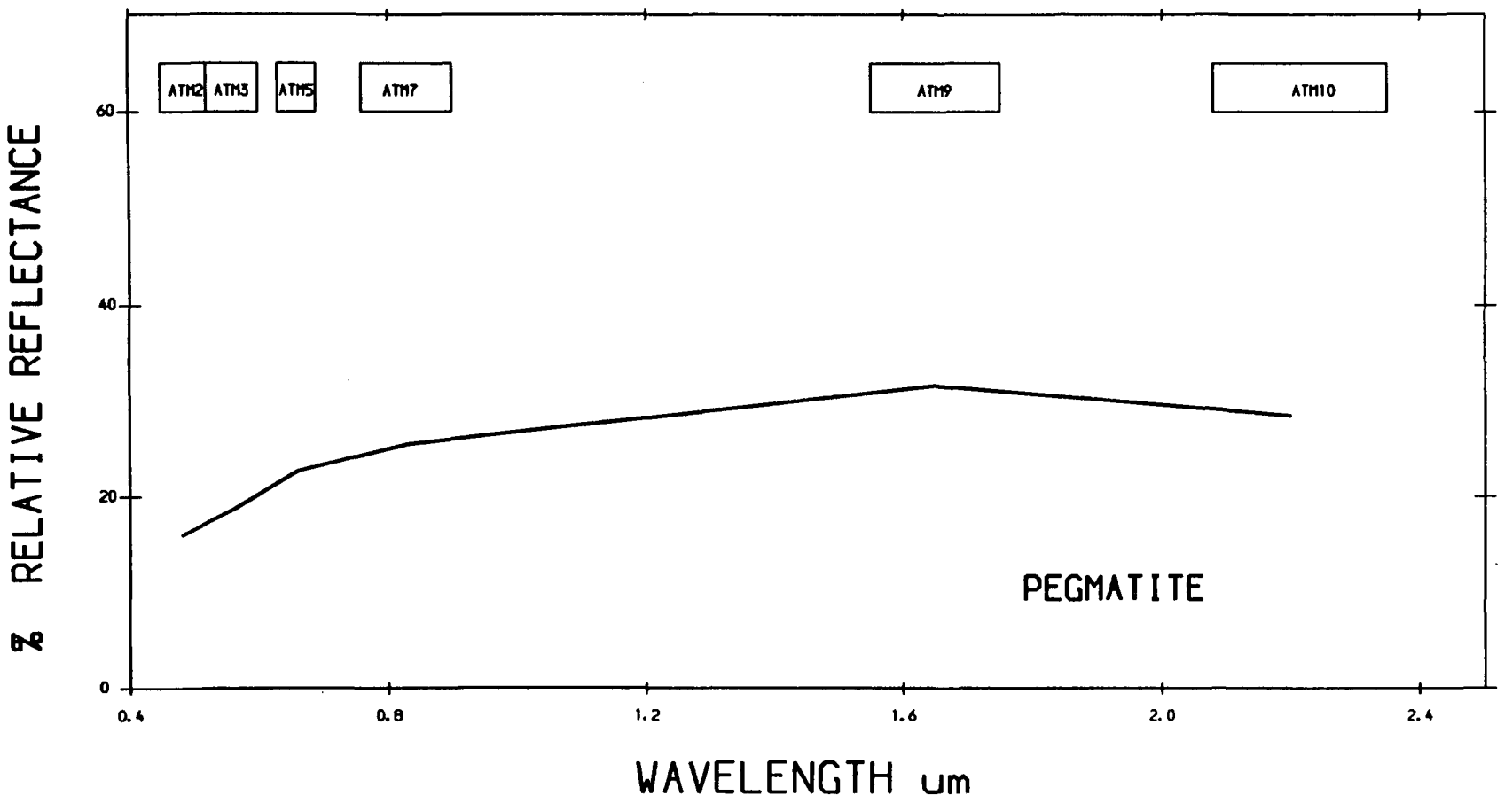

ATM 2000 M BAND EQUIVALENT TO TM CALIBRATED TO RELATIVE REFLECTANCE USING CALIBRATION CURVE

JABAL SAID AREA - SAUDI ARABIA

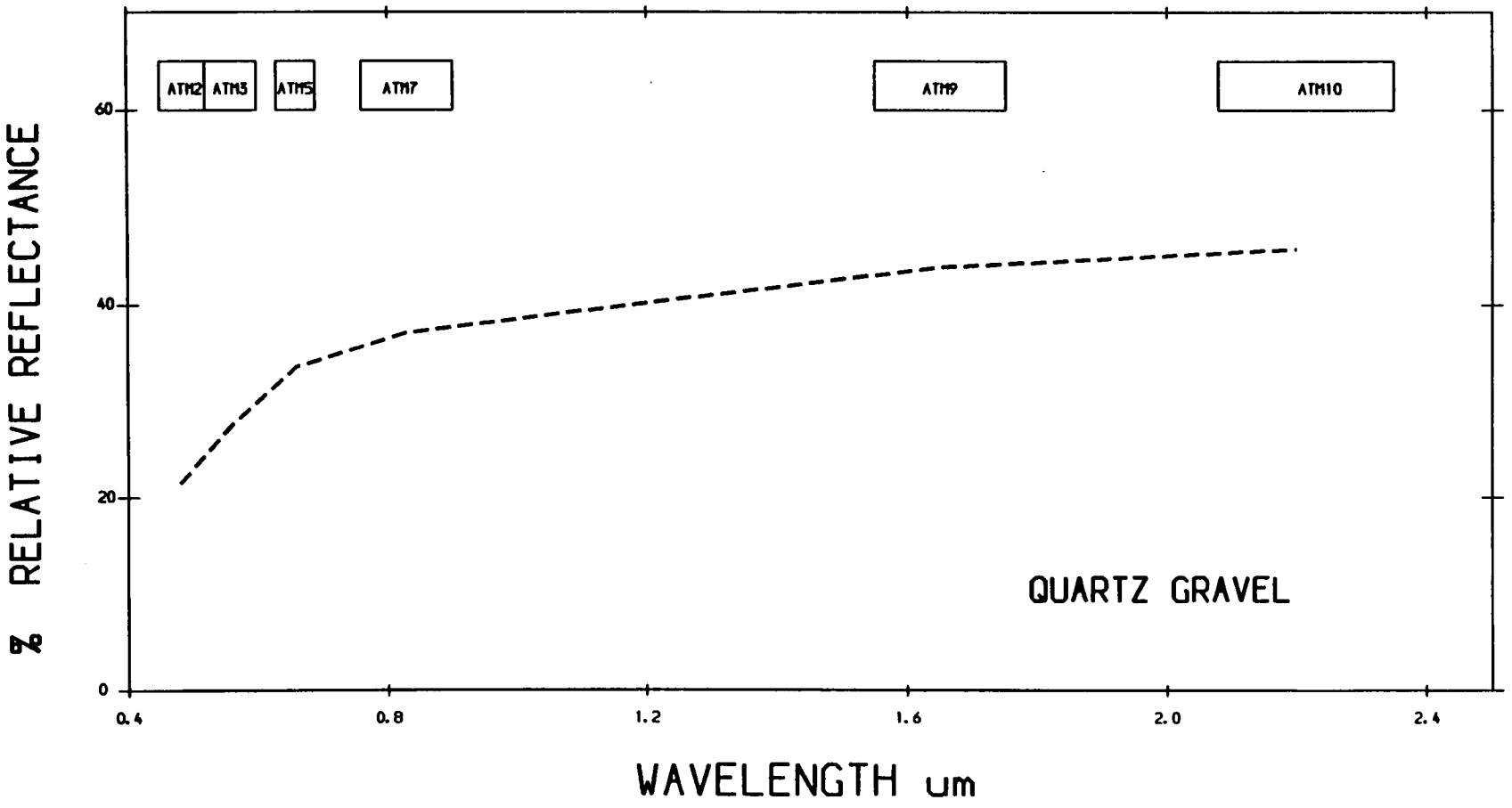

ATM 2000 M BAND EQUIVALENT TO TM CALIBRATED TO RELATIVE REFLECTANCE USING CALIBRATION CURVE

JABAL SAID AREA - SAUDI ARABIA

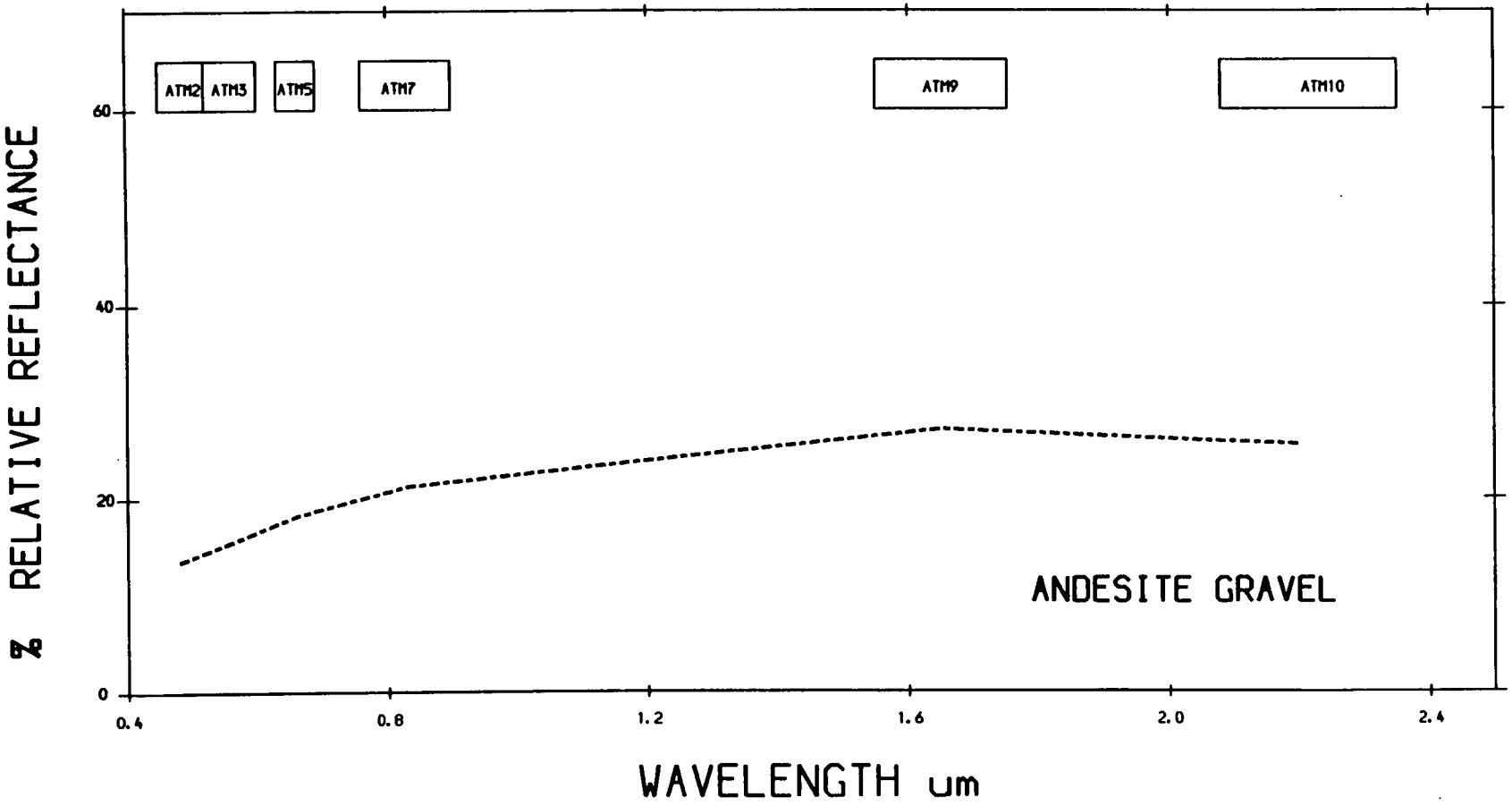

ATM 2000 M BAND EQUIVALENT TO TM CALIBRATED TO RELATIVE REFLECTANCE USING CALIBRATION CURVE

JABAL SAID AREA - SAUDI ARABIA

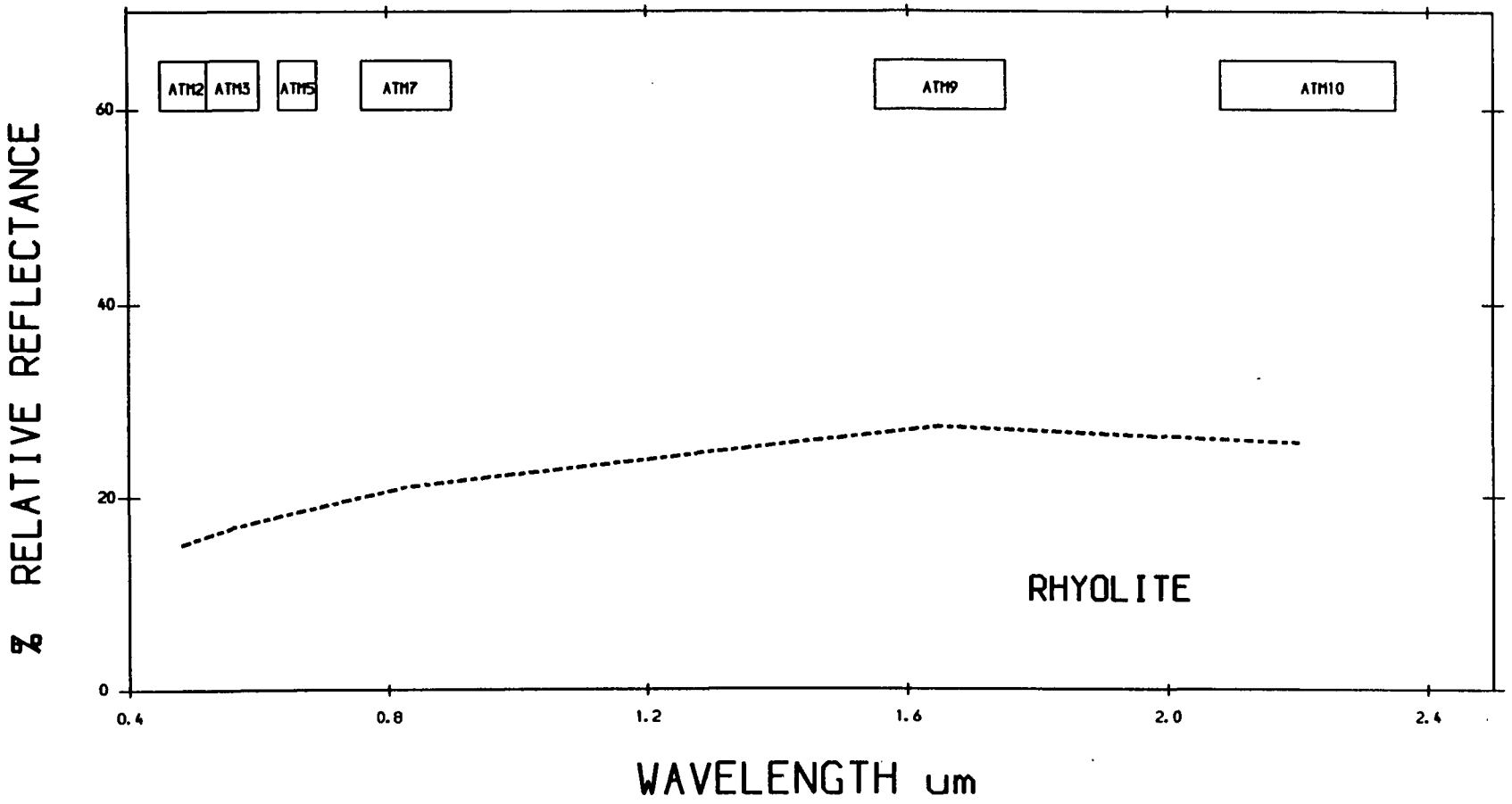

ATM 2000 M BAND EQUIVALENT TO TM CALIBRATED TO RELATIVE REFLECTANCE USING CALIBRATION CURVE

JABAL SAID AREA - SAUDI ARABIA

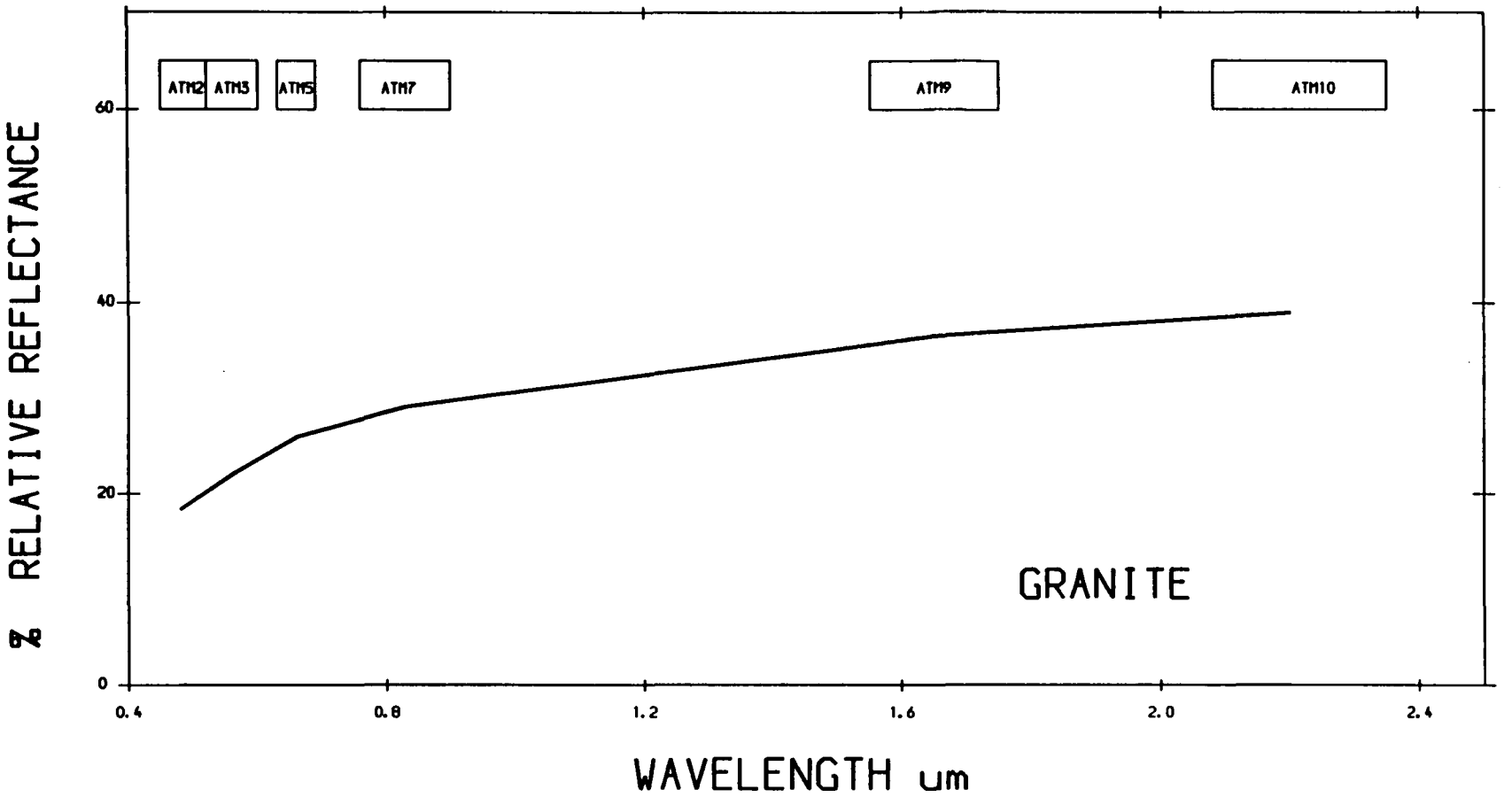

ATM 2000 M BAND EQUIVALENT TO TM CALIBRATED TO RELATIVE REFLECTANCE USING CALIBRATION CURVE

JABAL SAID AREA - SAUDI ARABIA

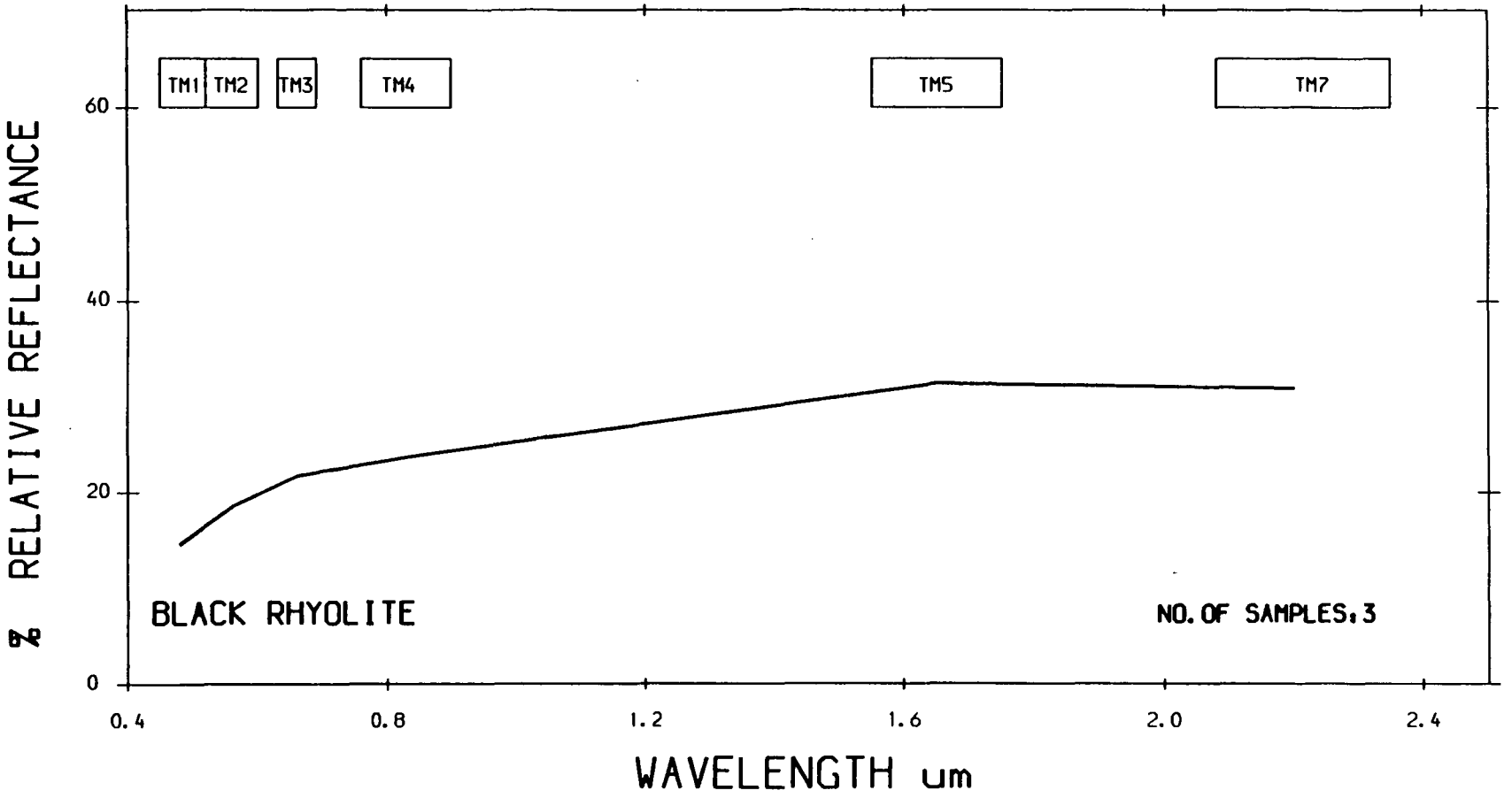

AVERAGE HHRR SPECTRA FROM JABAL SA`ID AREA

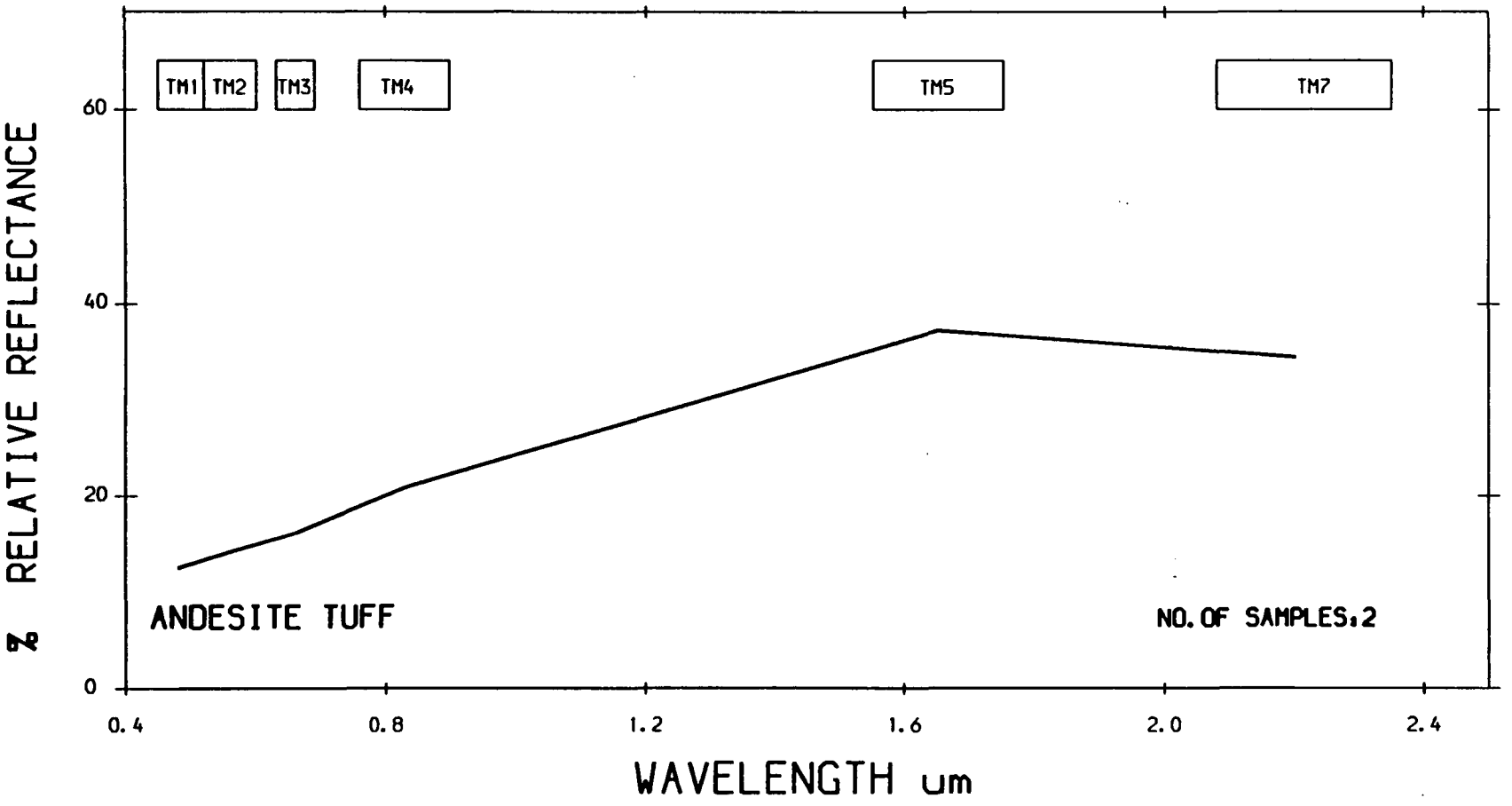

AVERAGE HHRR SPECTRA FROM JABAL SA`ID AREA

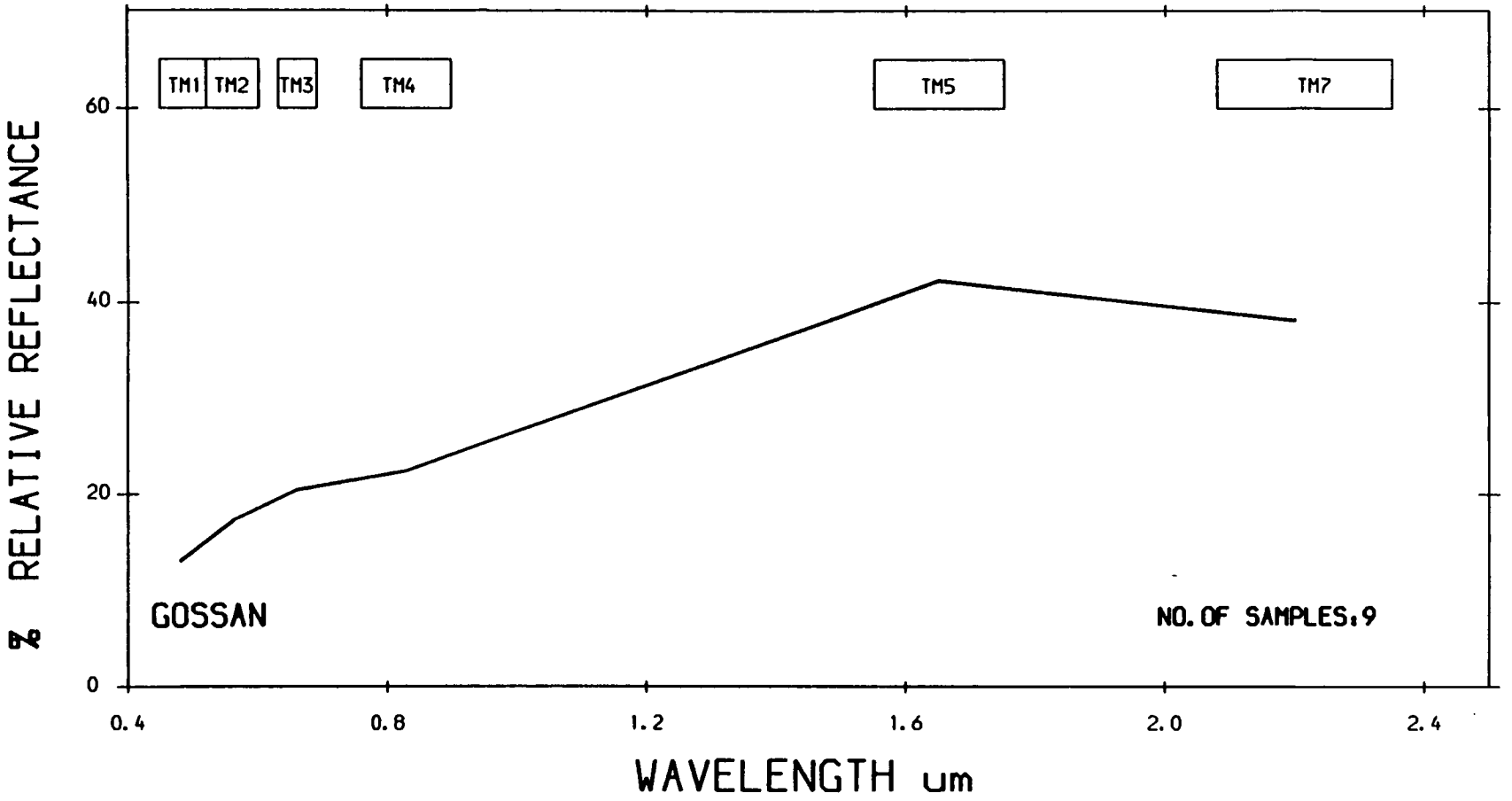

AVERAGE HHRR SPECTRA FROM JABAL SA`ID AREA

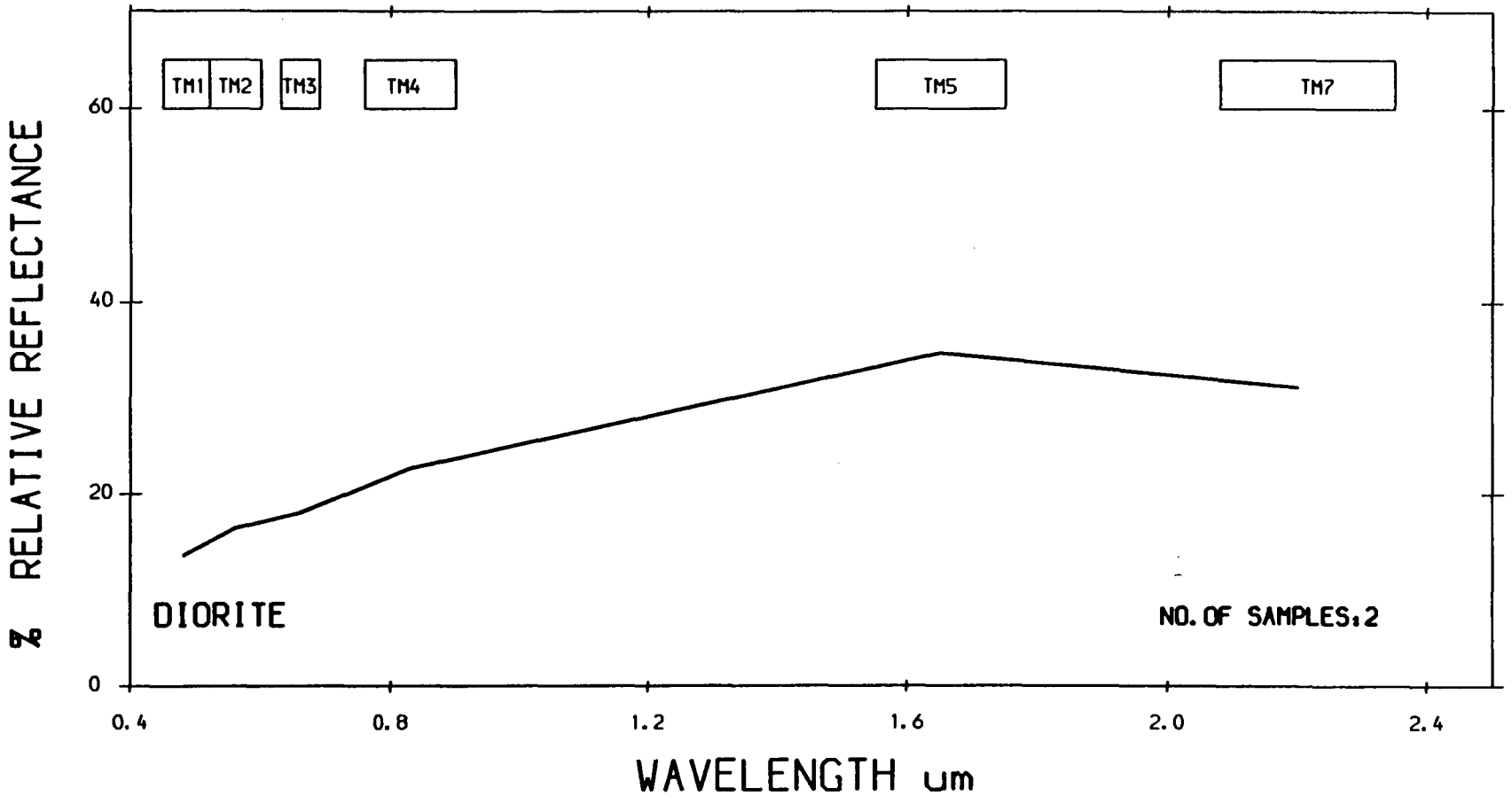

AVERAGE HHRR SPECTRA FROM JABAL SA`ID AREA

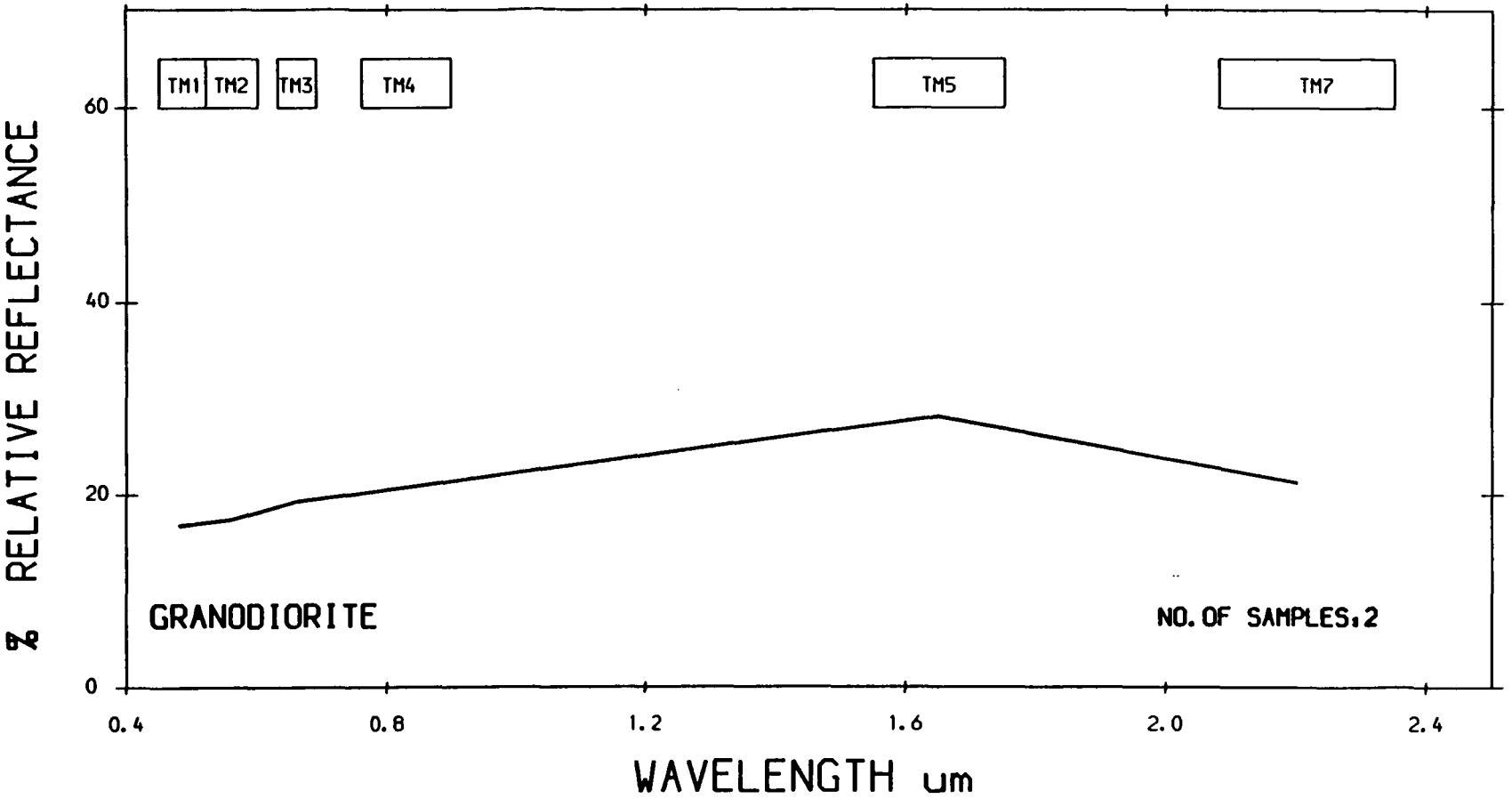

AVERAGE HHRR SPECTRA FROM JABAL SA`ID AREA

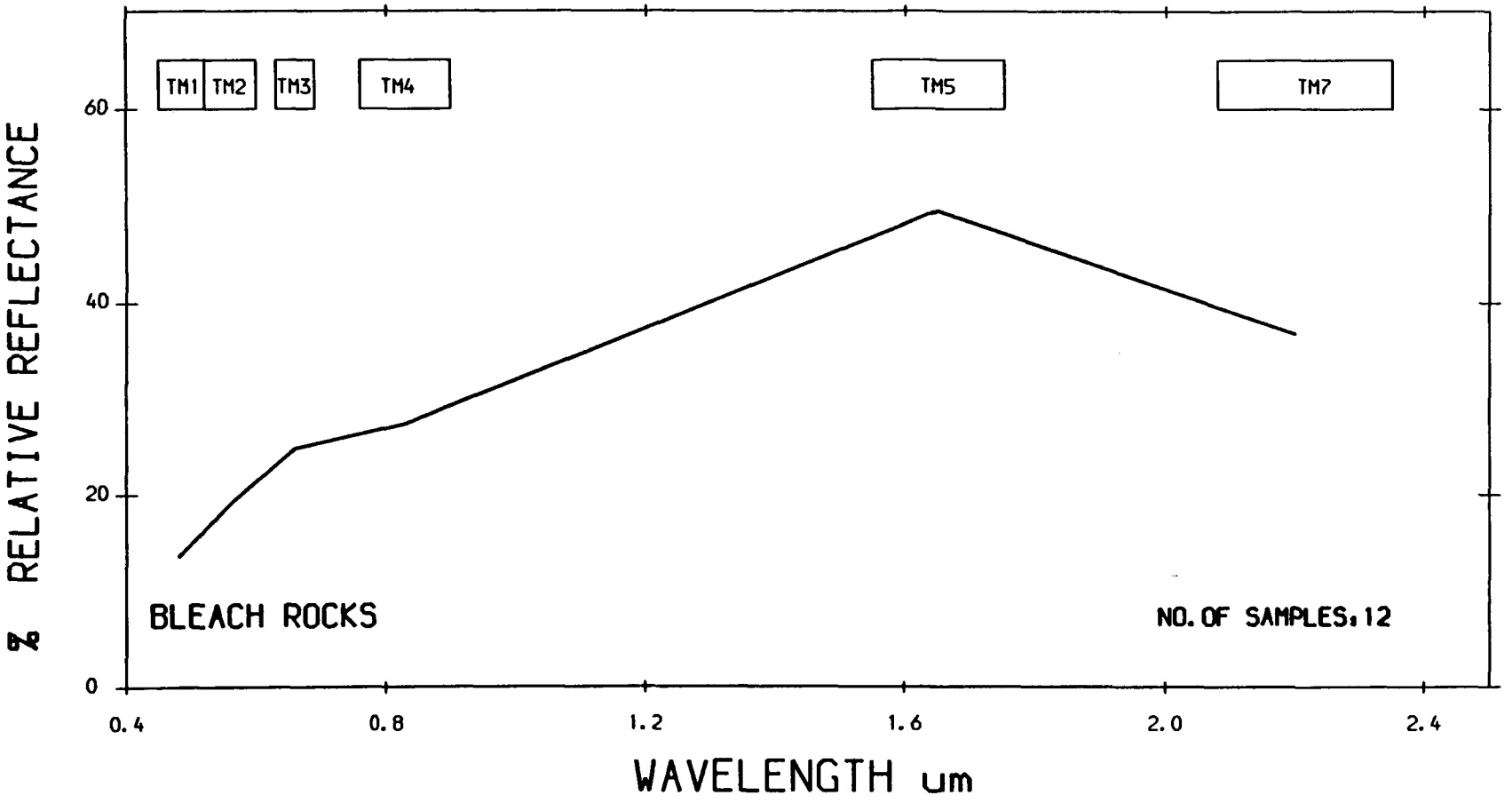

AVERAGE HHRR SPECTRA FROM JABAL SA`ID AREA

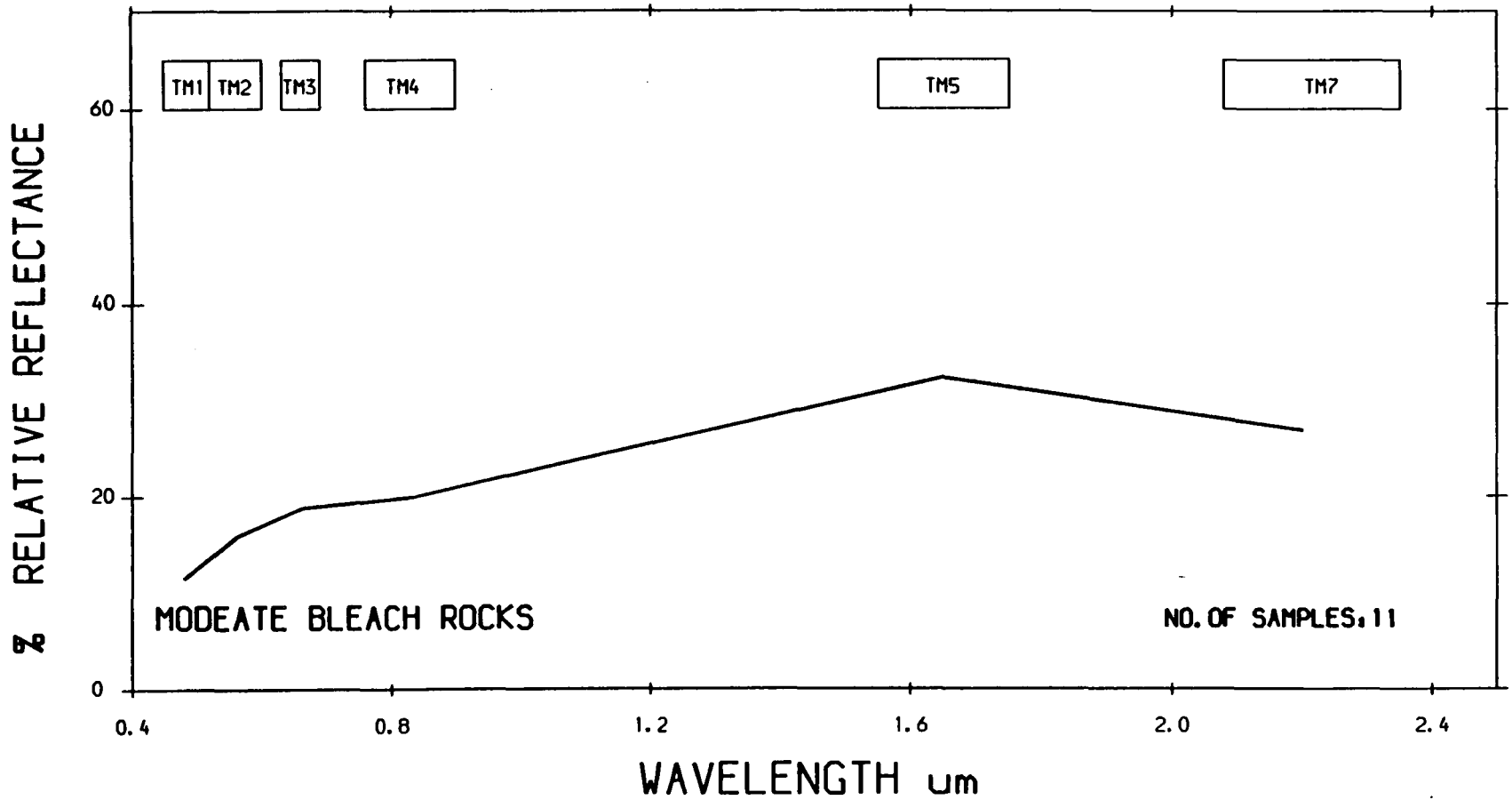

AVERAGE HHRR SPECTRA FROM JABAL SA`ID AREA

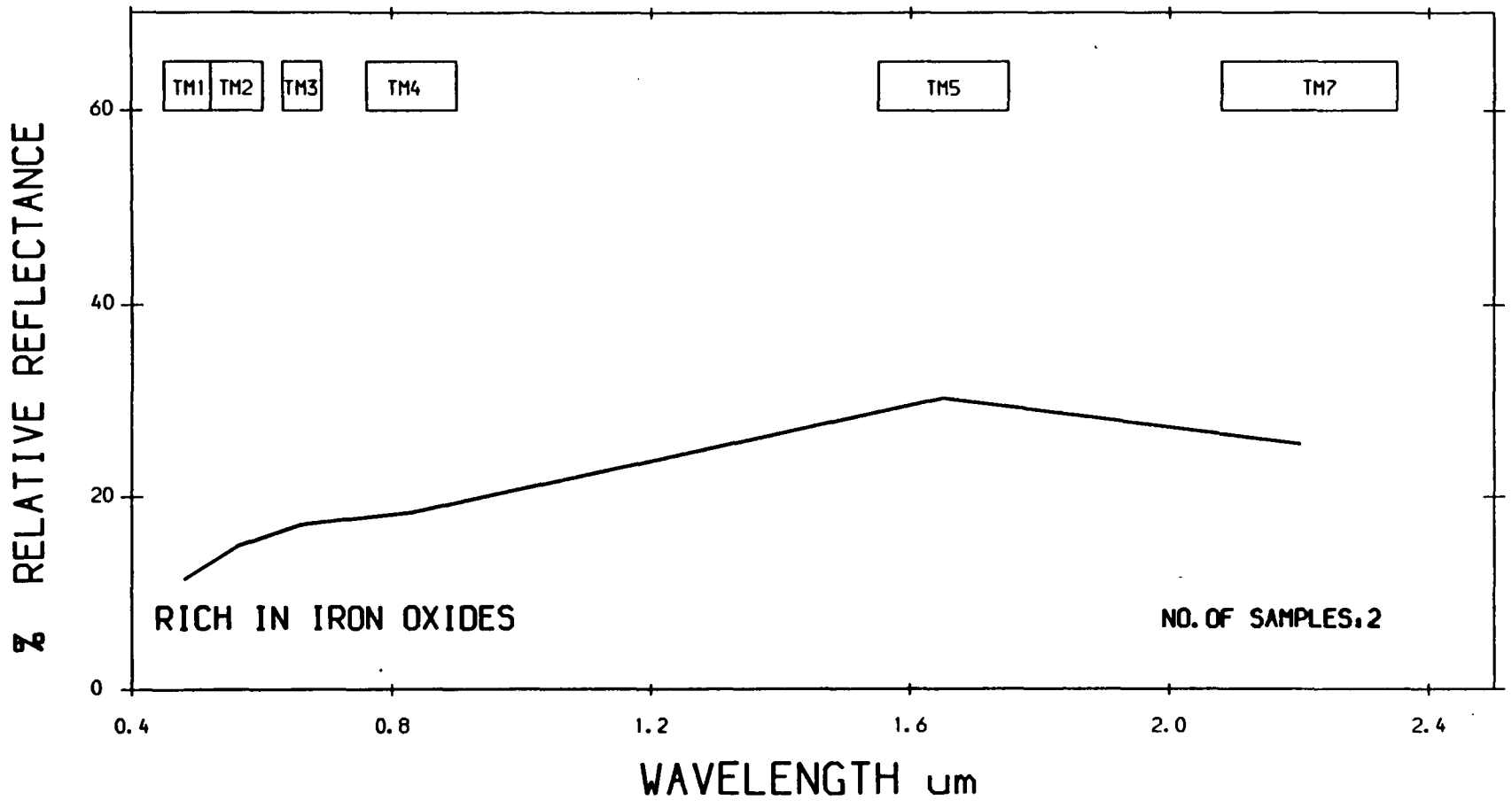

AVERAGE HHRR SPECTRA FROM JABAL SA`ID AREA

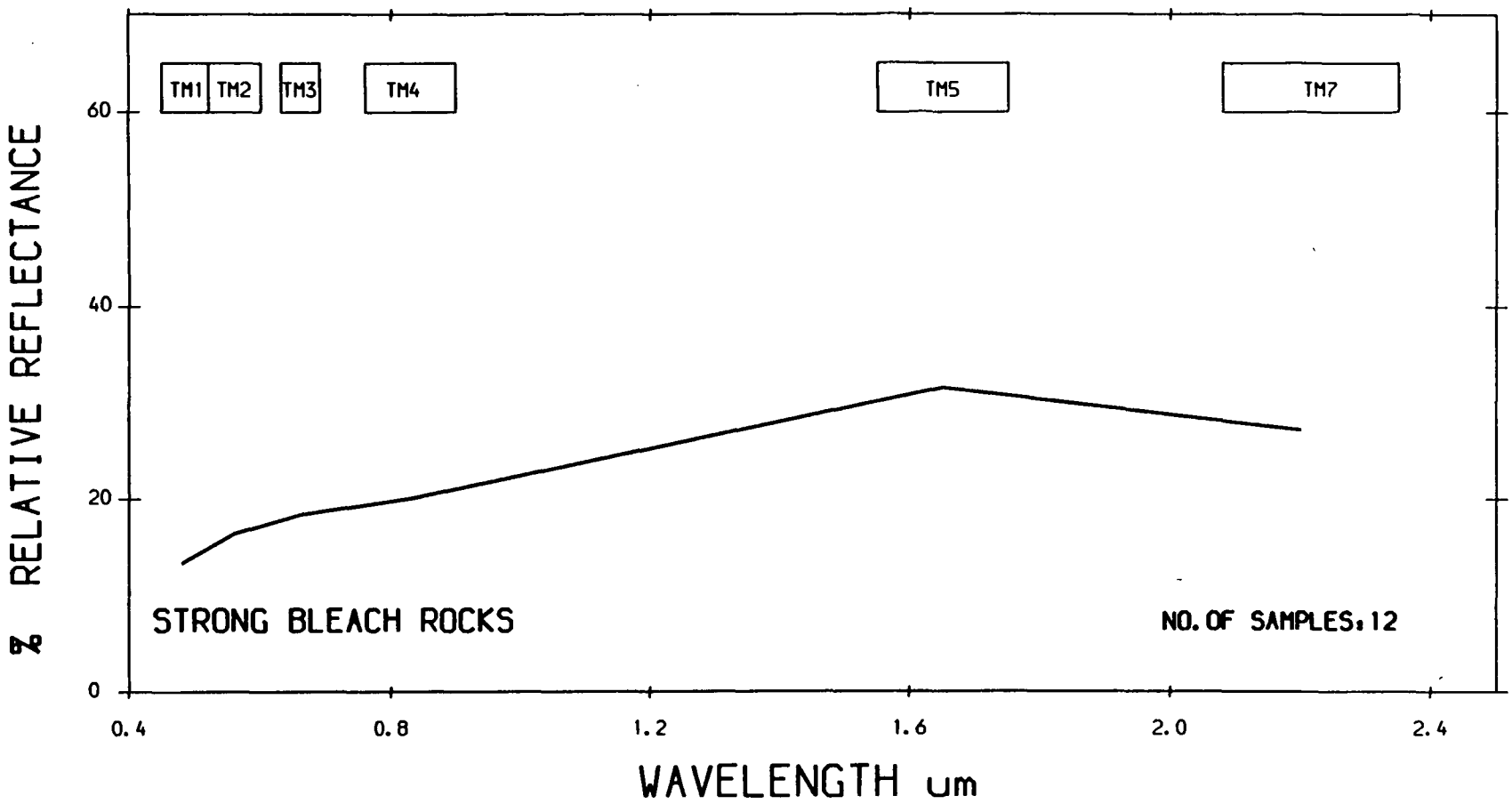

AVERAGE HHRR SPECTRA FROM JABAL SA`ID AREA

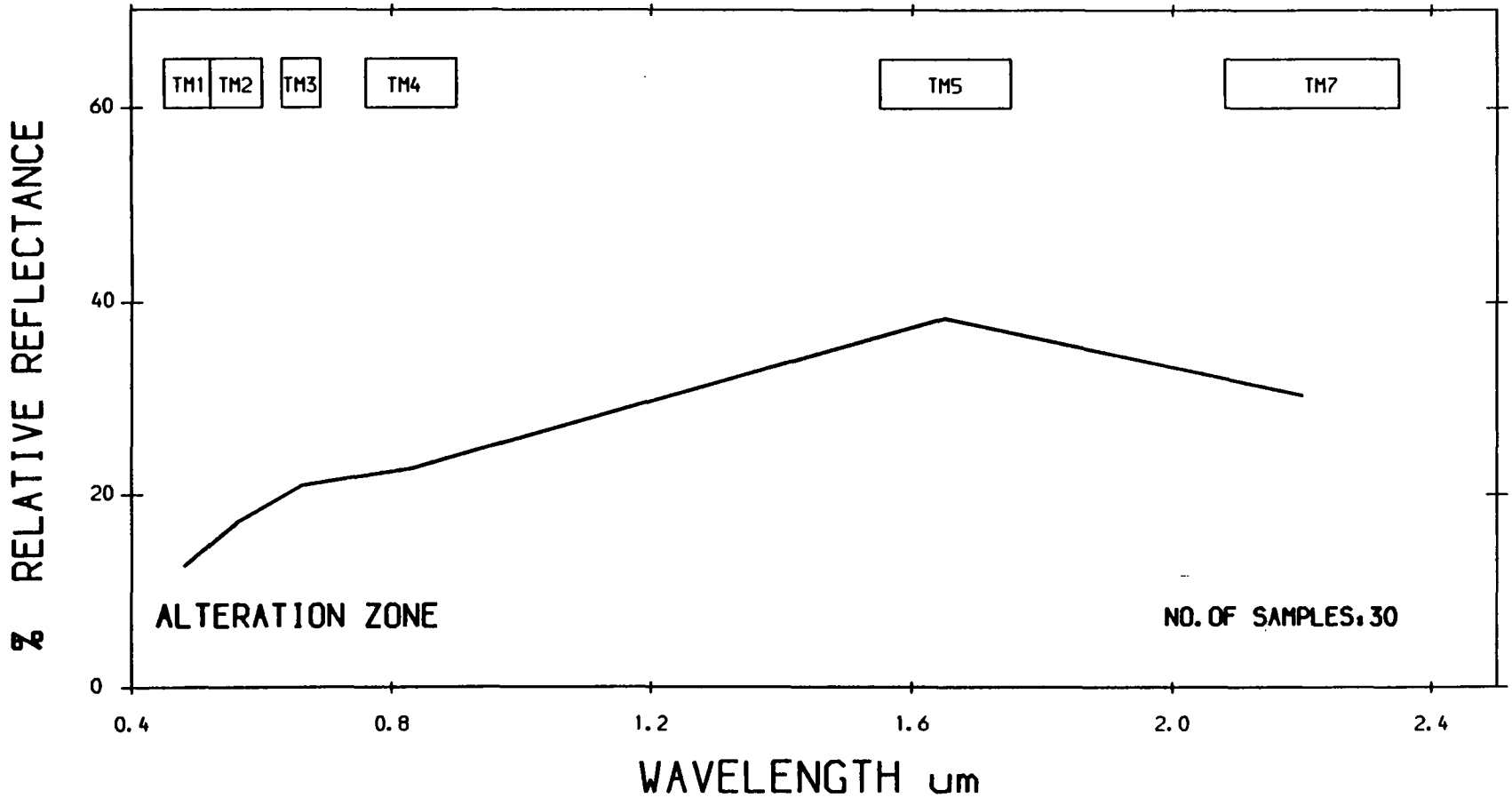

AVERAGE HHRR SPECTRA FROM JABAL SA`ID AREA

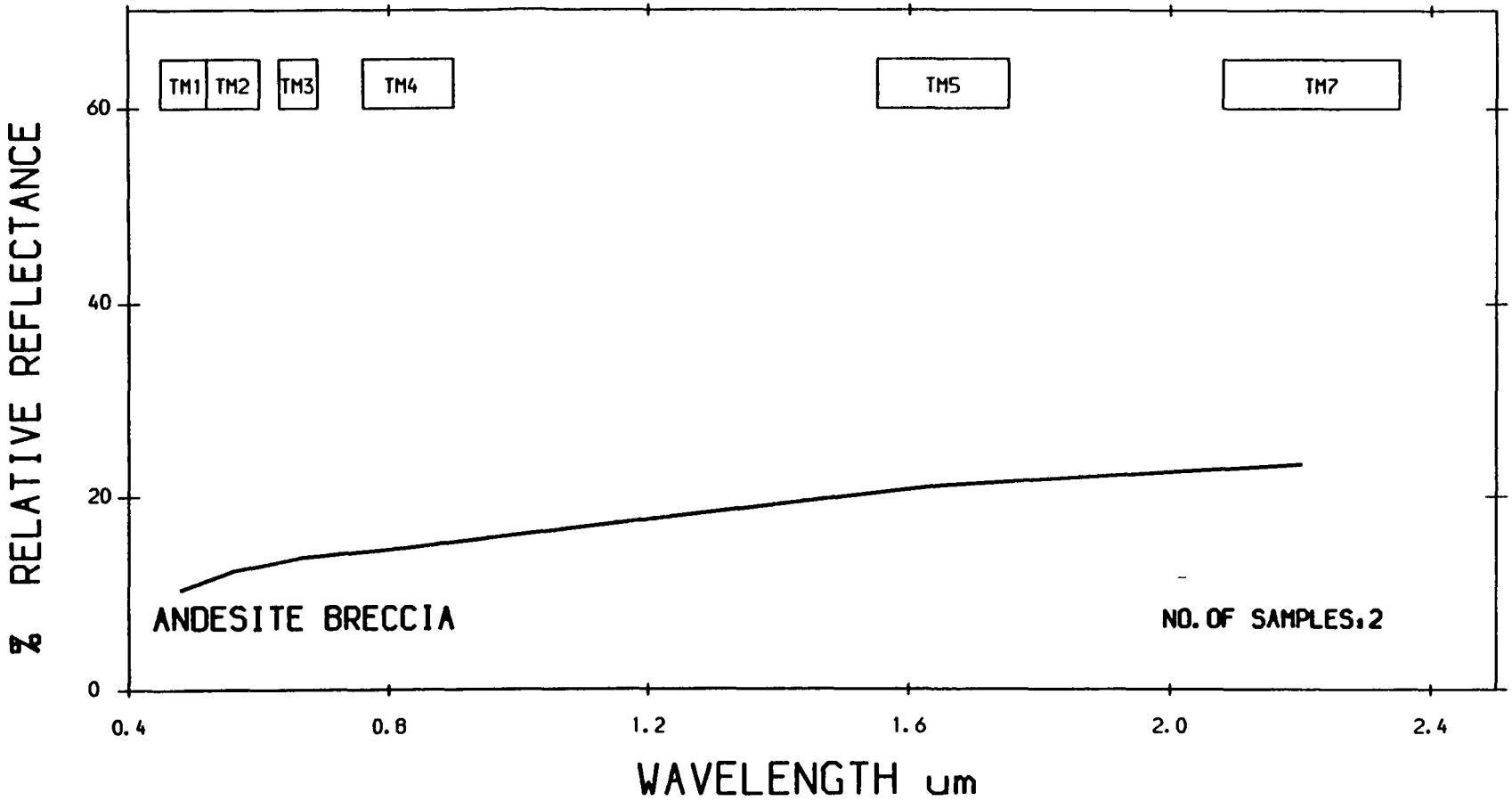

AVERAGE HHRR SPECTRA FROM JABAL SA`ID AREA

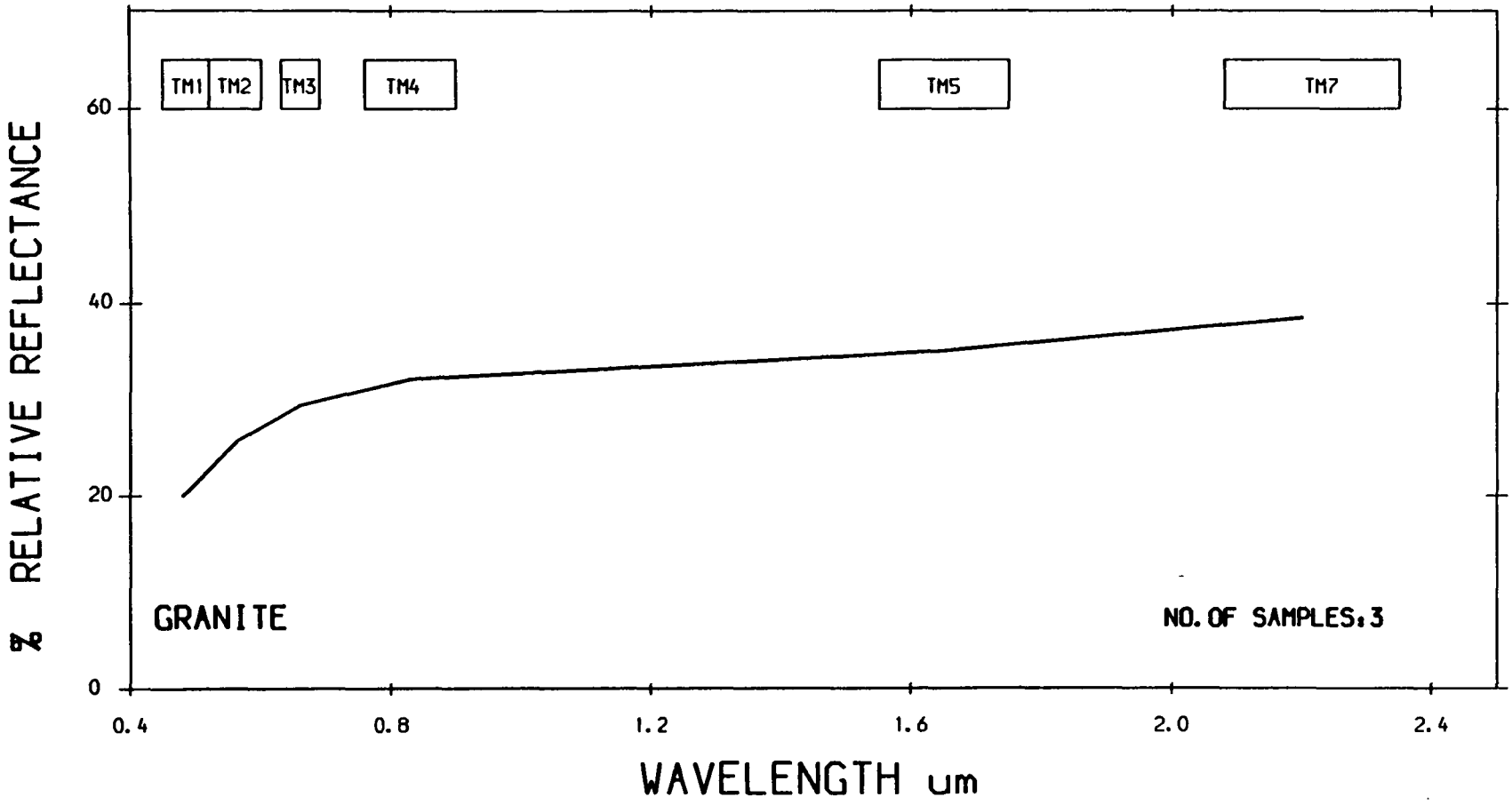

AVERAGE HHRR SPECTRA FROM JABAL SA`ID AREA

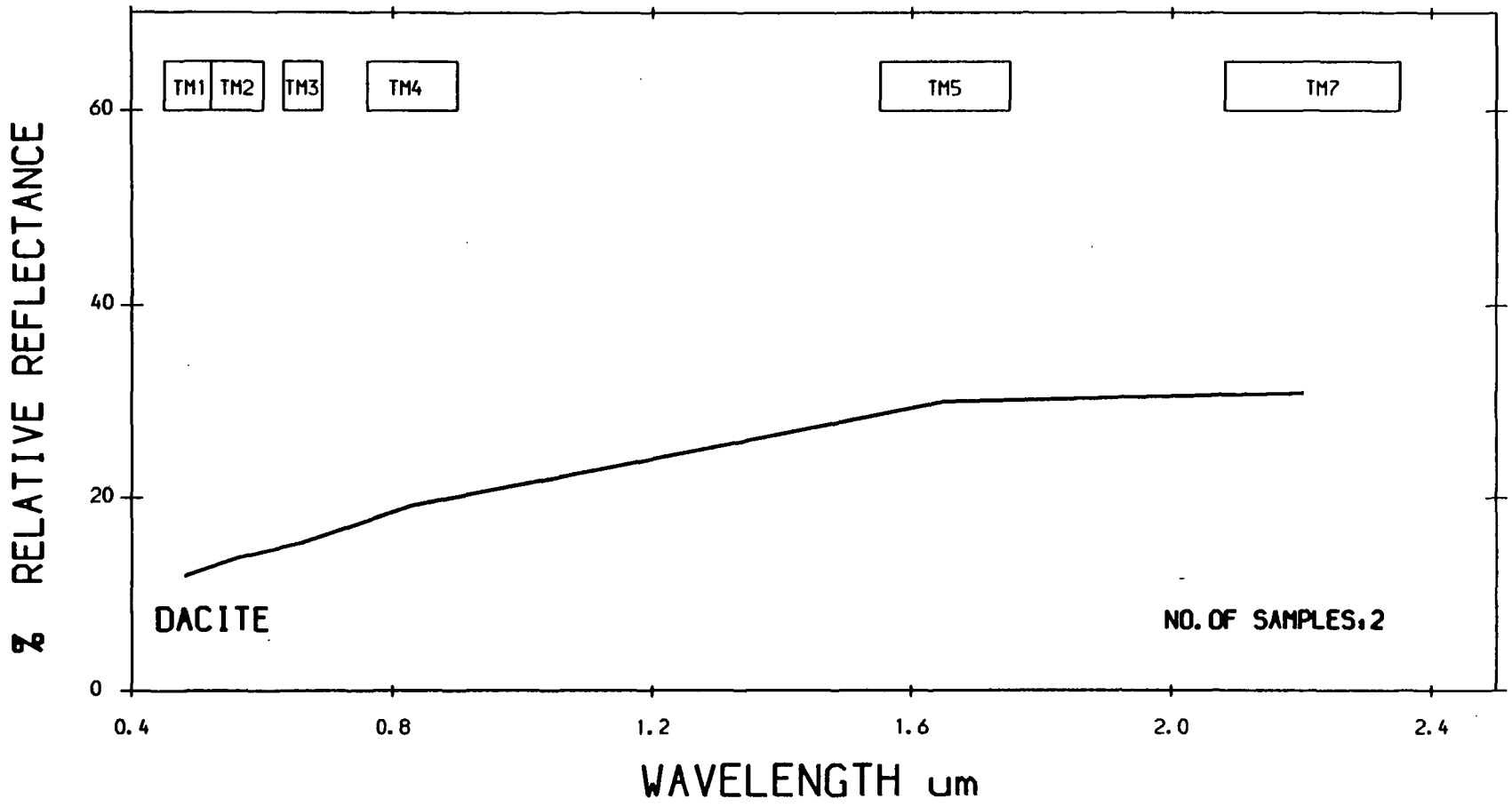

AVERAGE HHRR SPECTRA FROM JABAL SA`ID AREA

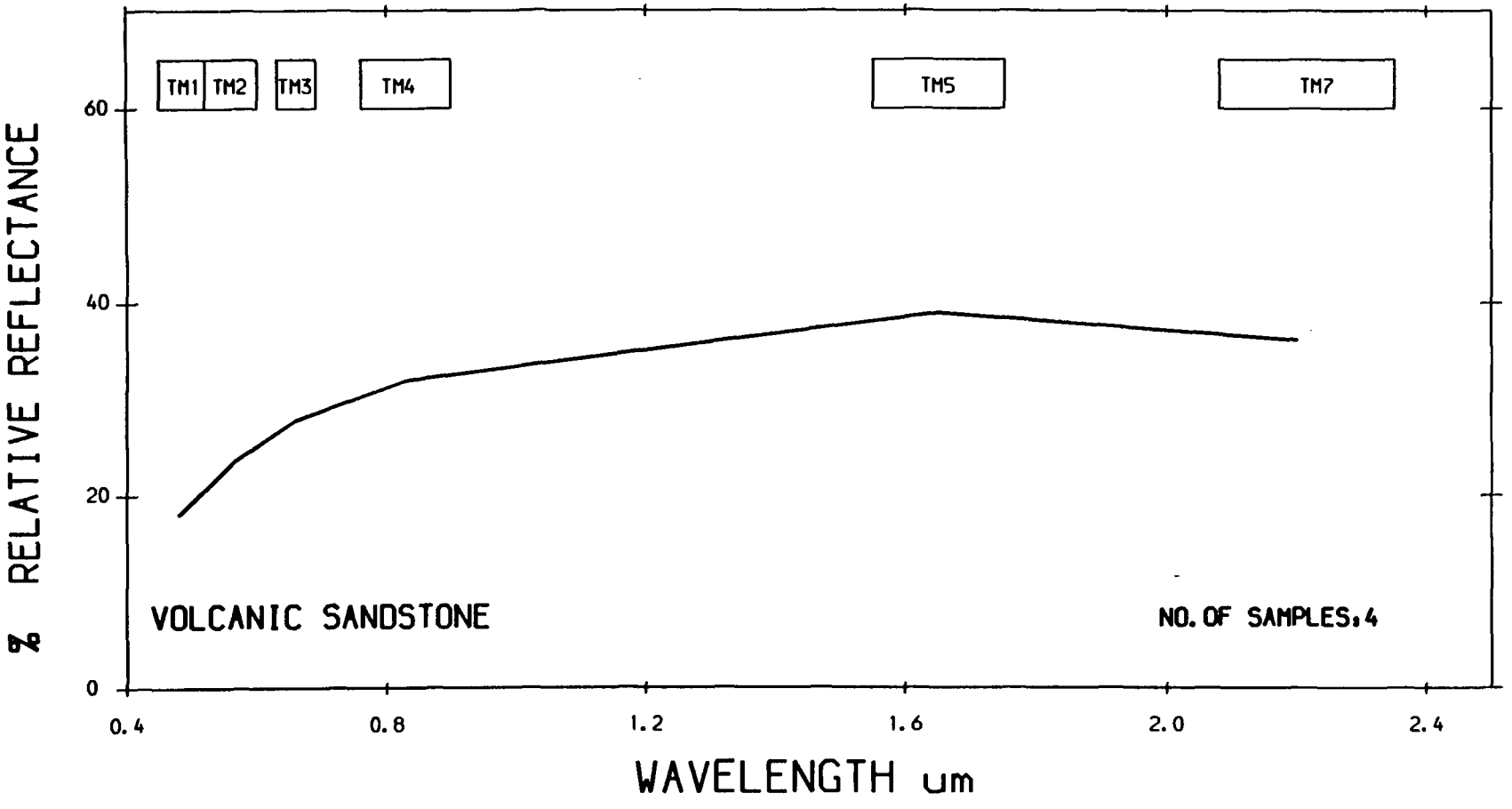

AVERAGE HHRR SPECTRA FROM JABAL SA`ID AREA

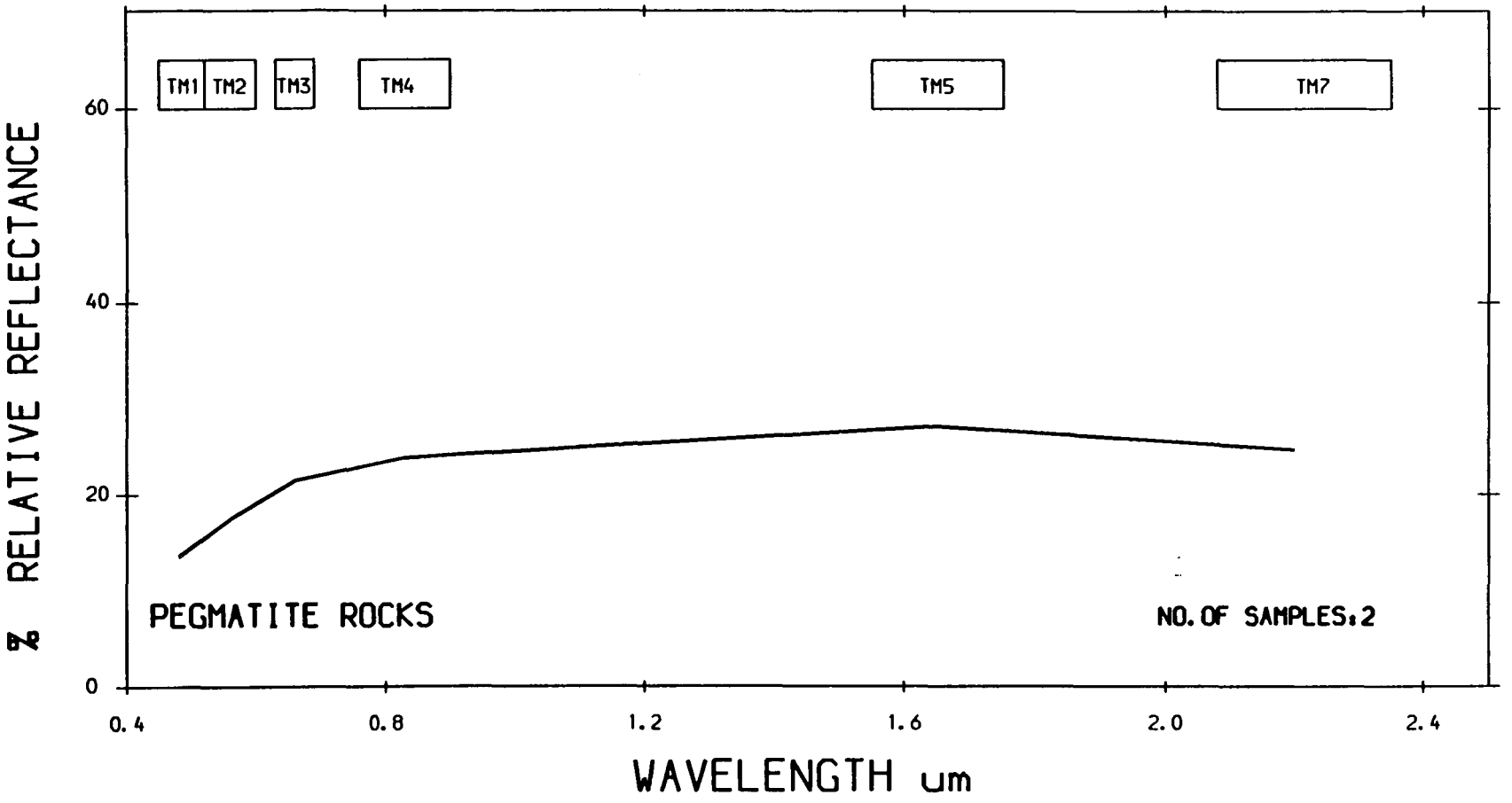

AVERAGE HHRR SPECTRA FROM JABAL SA`ID AREA

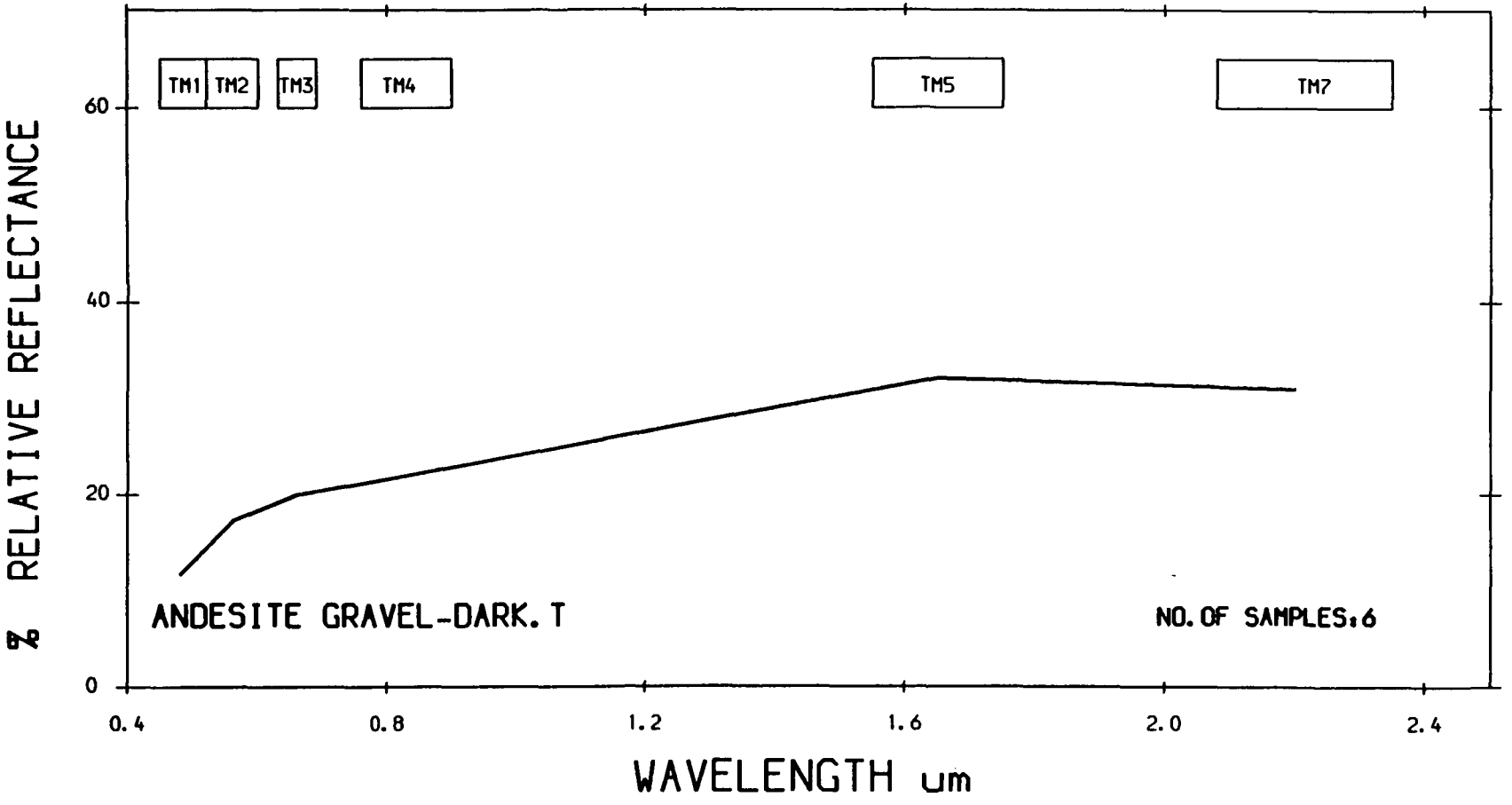

AVERAGE HHRR SPECTRA FROM JABAL SA`ID AREA

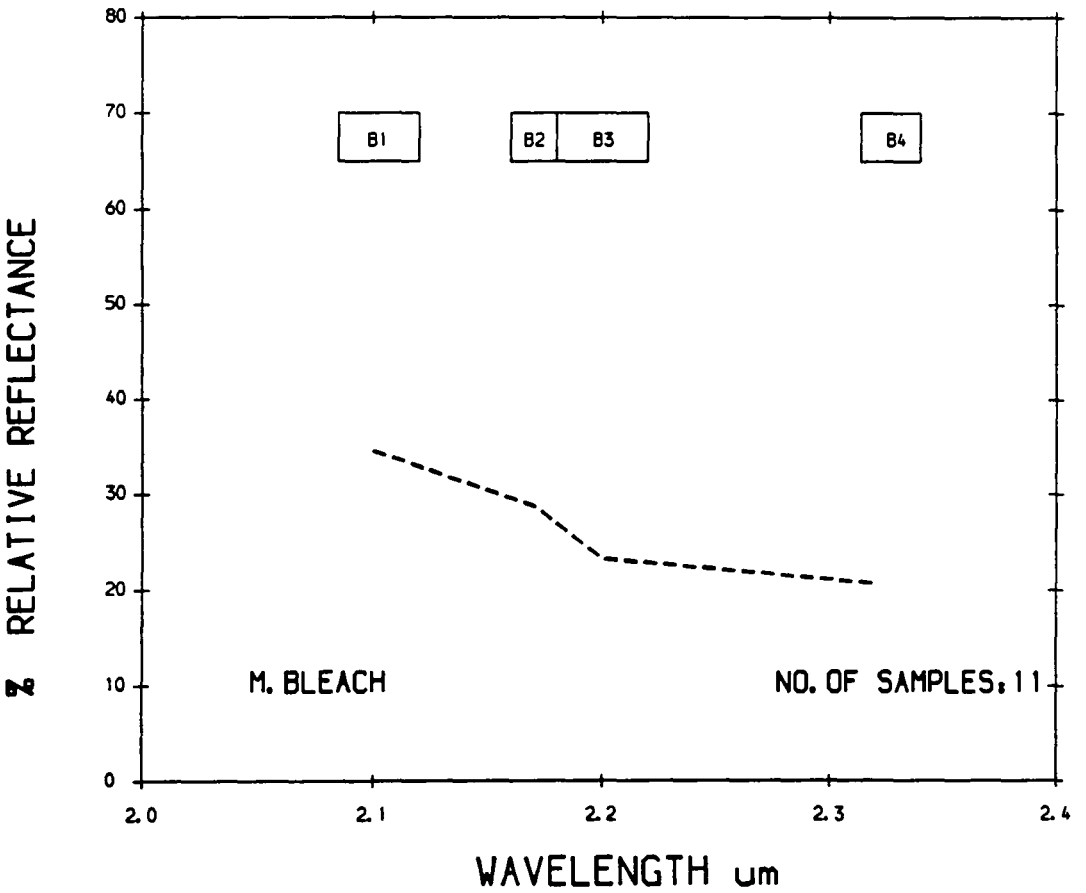

AVERAGE HHRR SPECTRA FROM JABAL SA`ID AREA

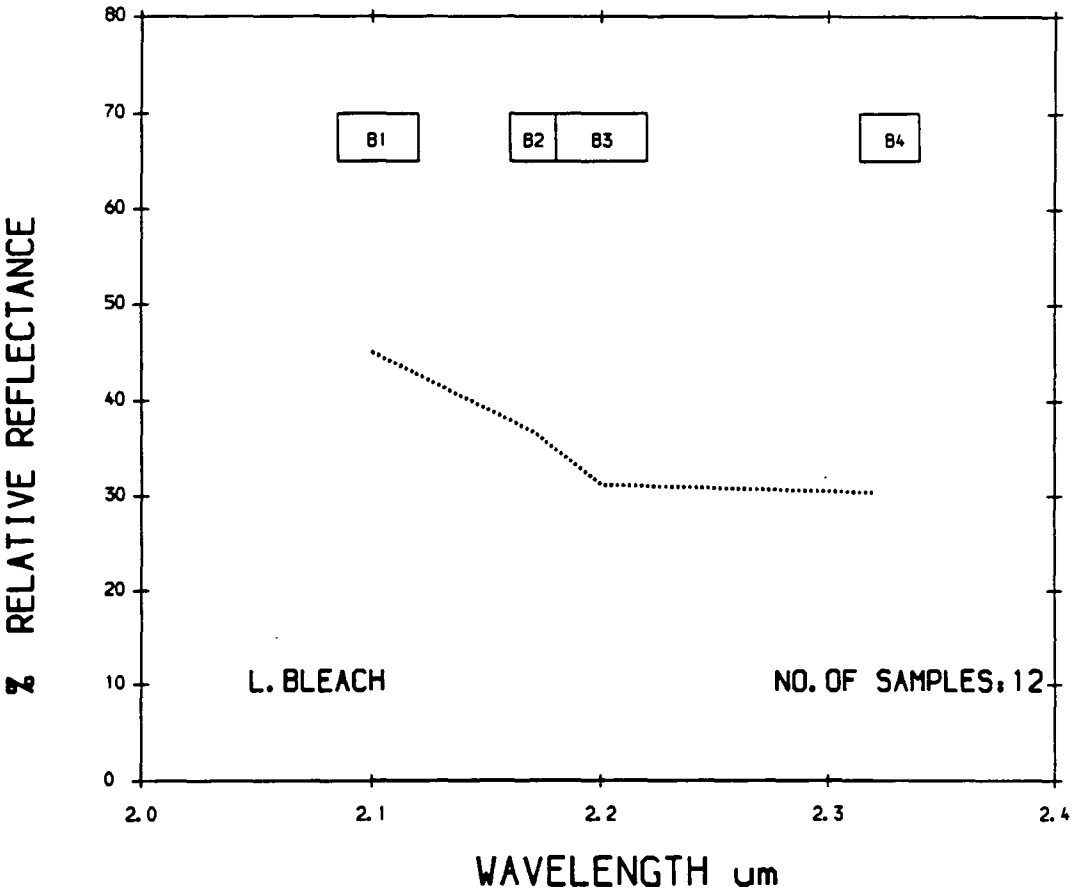

AVERAGE HHRR SPECTRA FROM JABAL SA`ID AREA

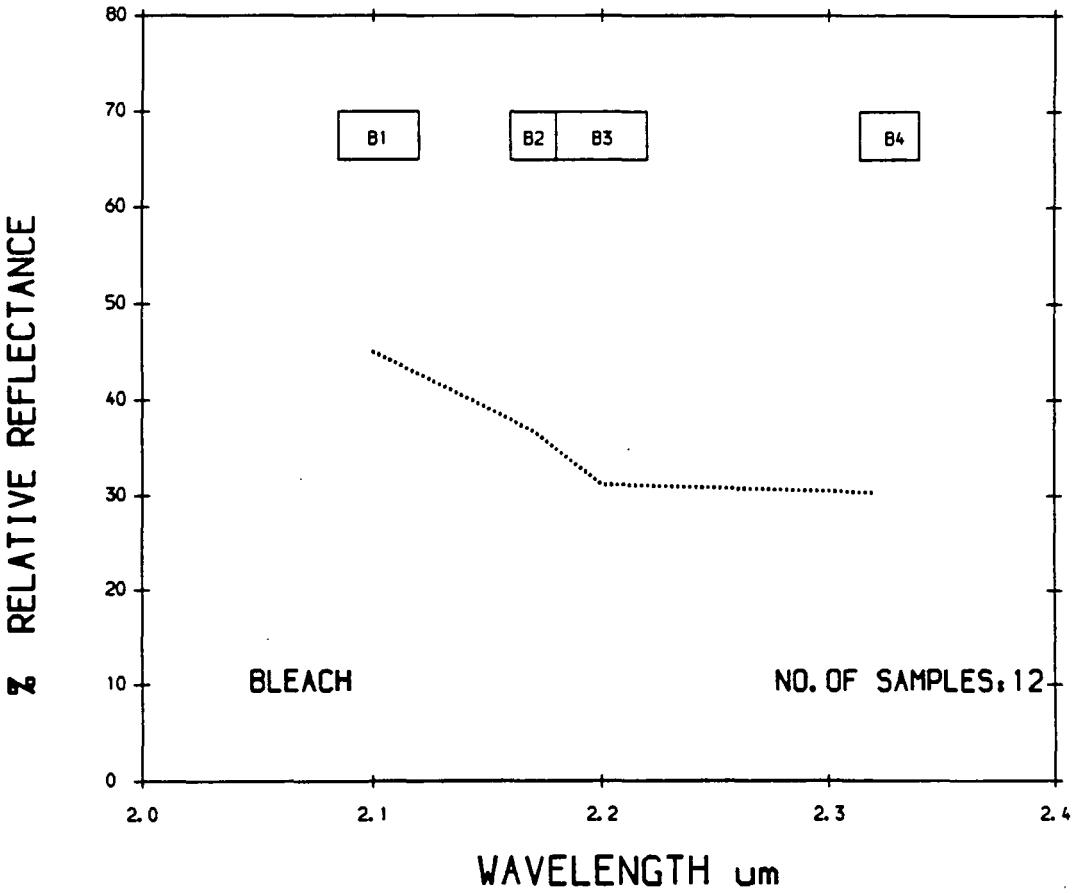

AVERAGE HHRR SPECTRA FROM JABAL SA`ID AREA

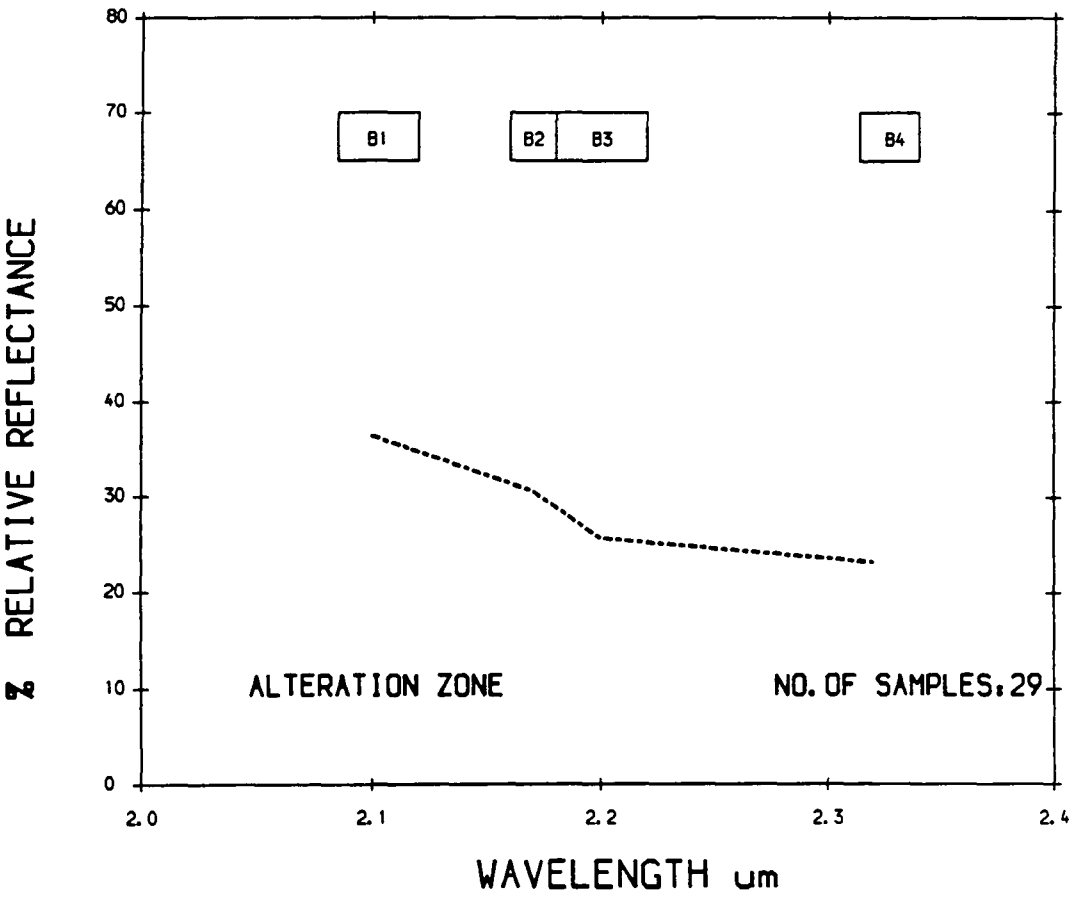

AVERAGE HHRR SPECTRA FROM JABAL SA`ID AREA

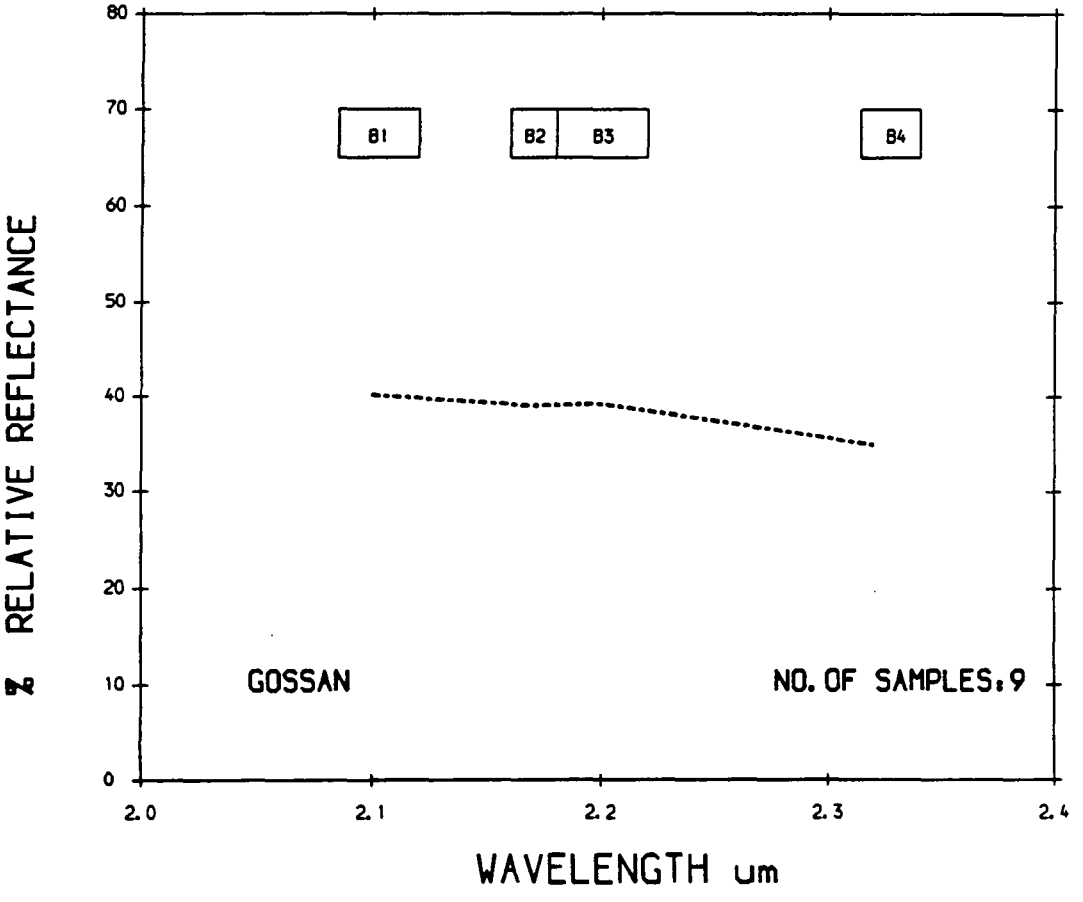

AVERAGE HHRR SPECTRA FROM JABAL SA`ID AREA

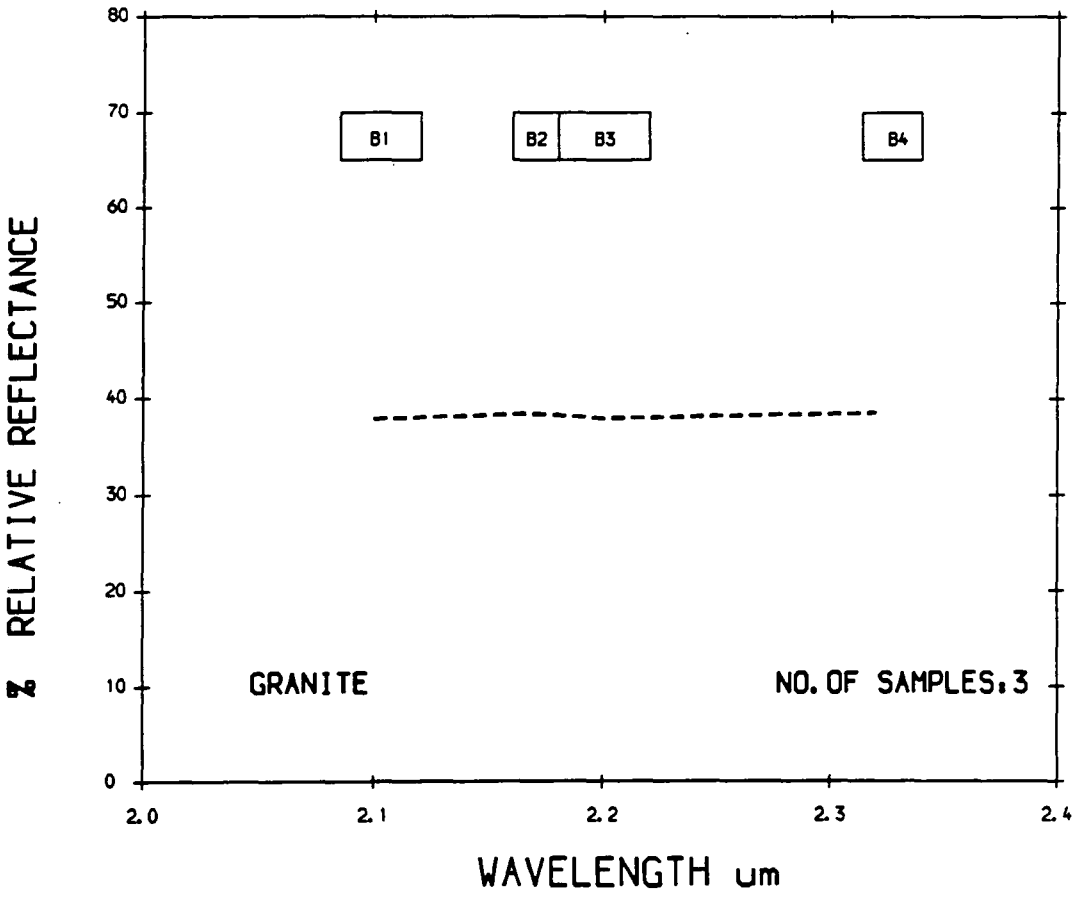

AVERAGE HHRR SPECTRA FROM JABAL SA`ID AREA

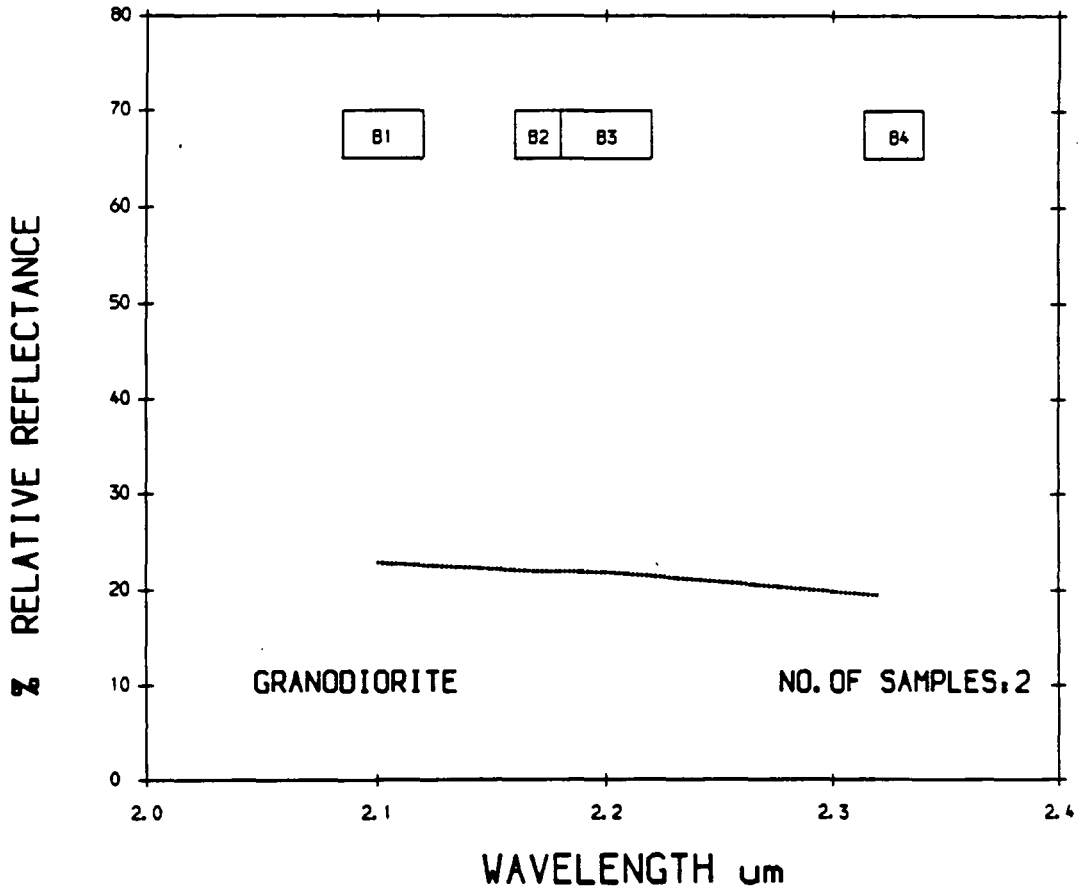

AVERAGE HHRR SPECTRA FROM JABAL SA`ID AREA

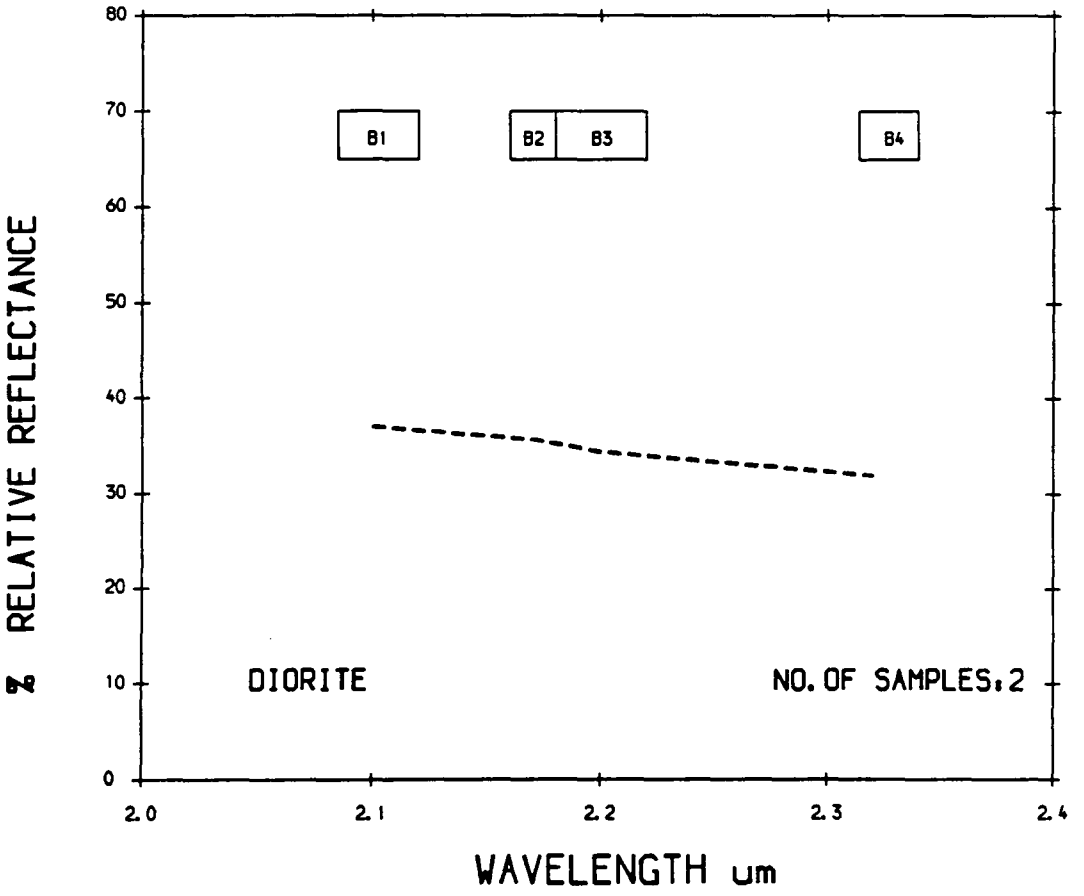

AVERAGE HHRR SPECTRA FROM JABAL SA`ID AREA

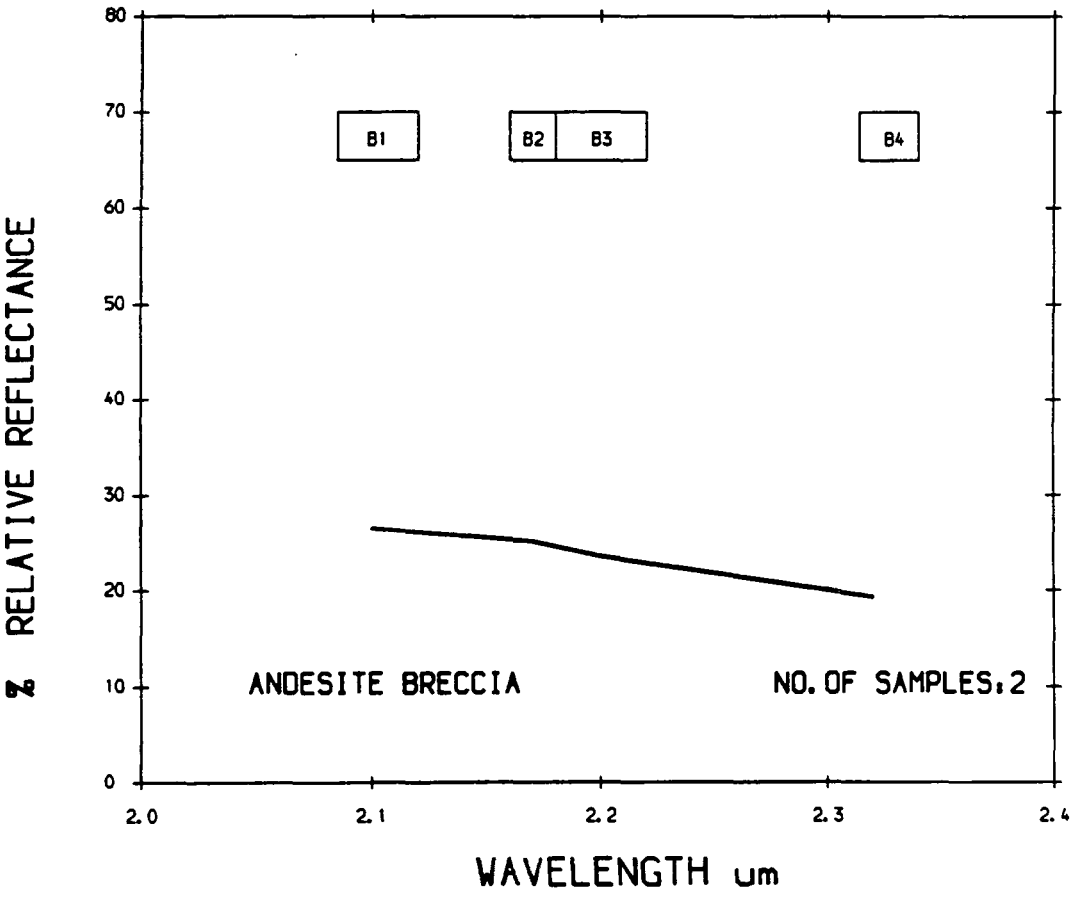

AVERAGE HHRR SPECTRA FROM JABAL SA`ID AREA

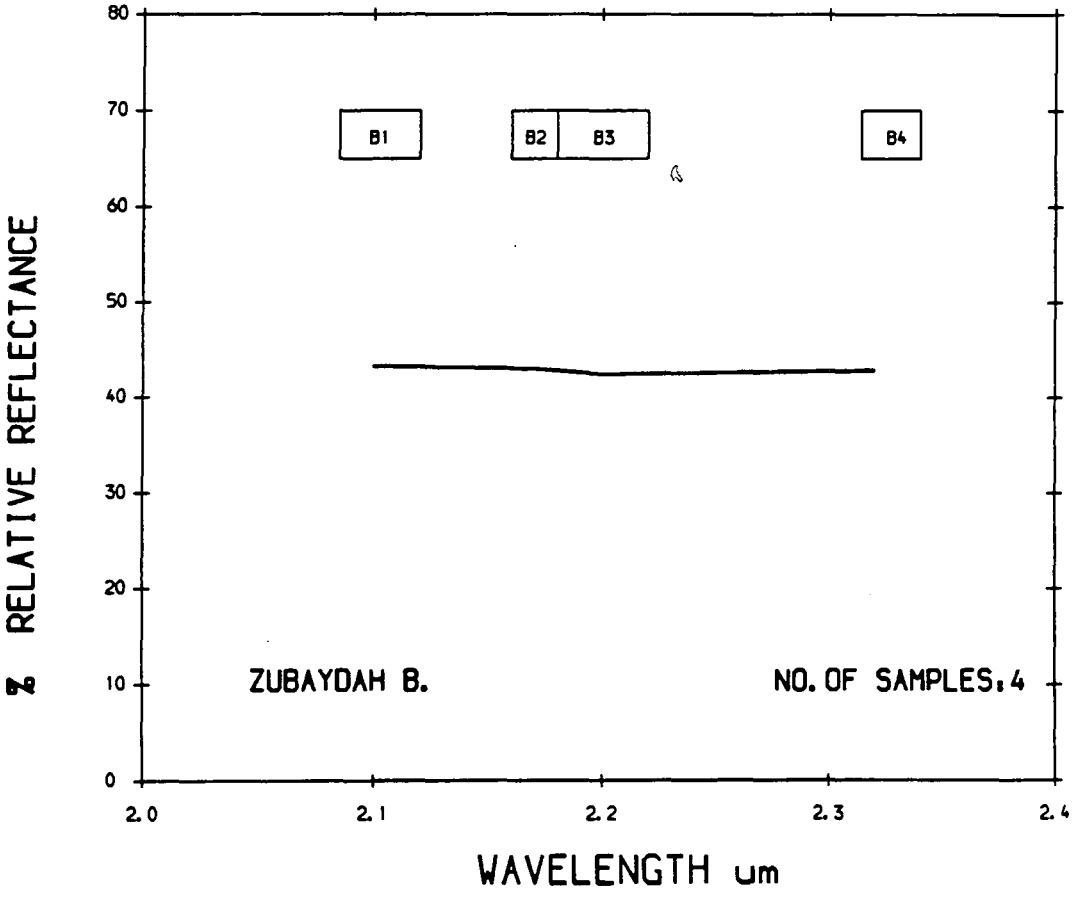

AVERAGE HHRR SPECTRA FROM JABAL SA`ID AREA

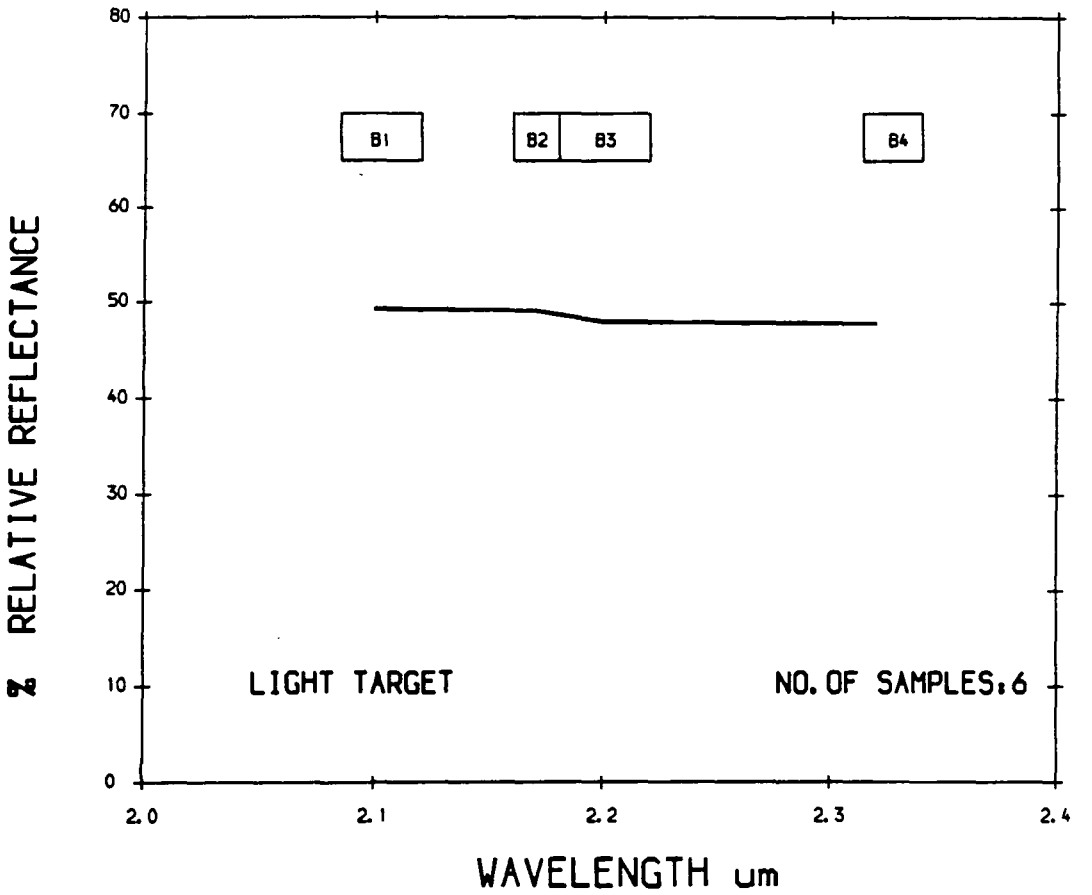

AVERAGE HHRR SPECTRA FROM JABAL SA`ID AREA

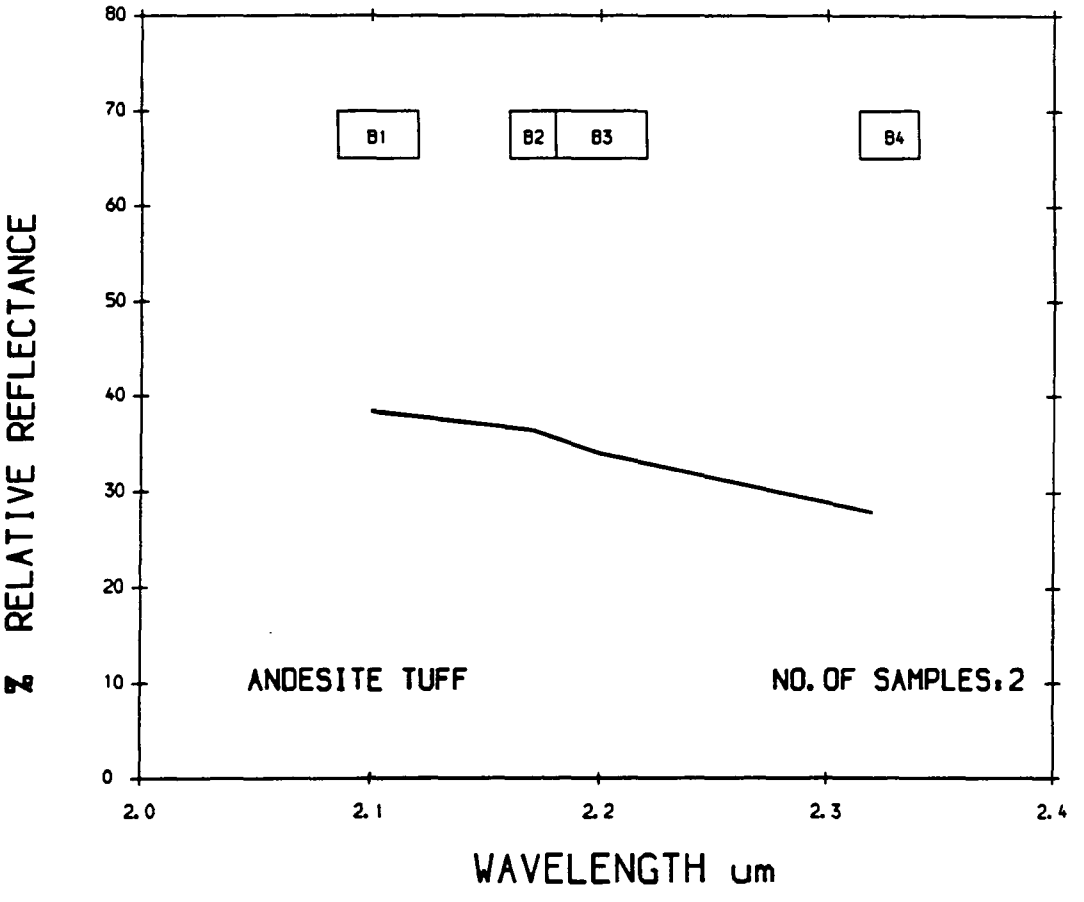

AVERAGE HHRR SPECTRA FROM JABAL SA`ID AREA

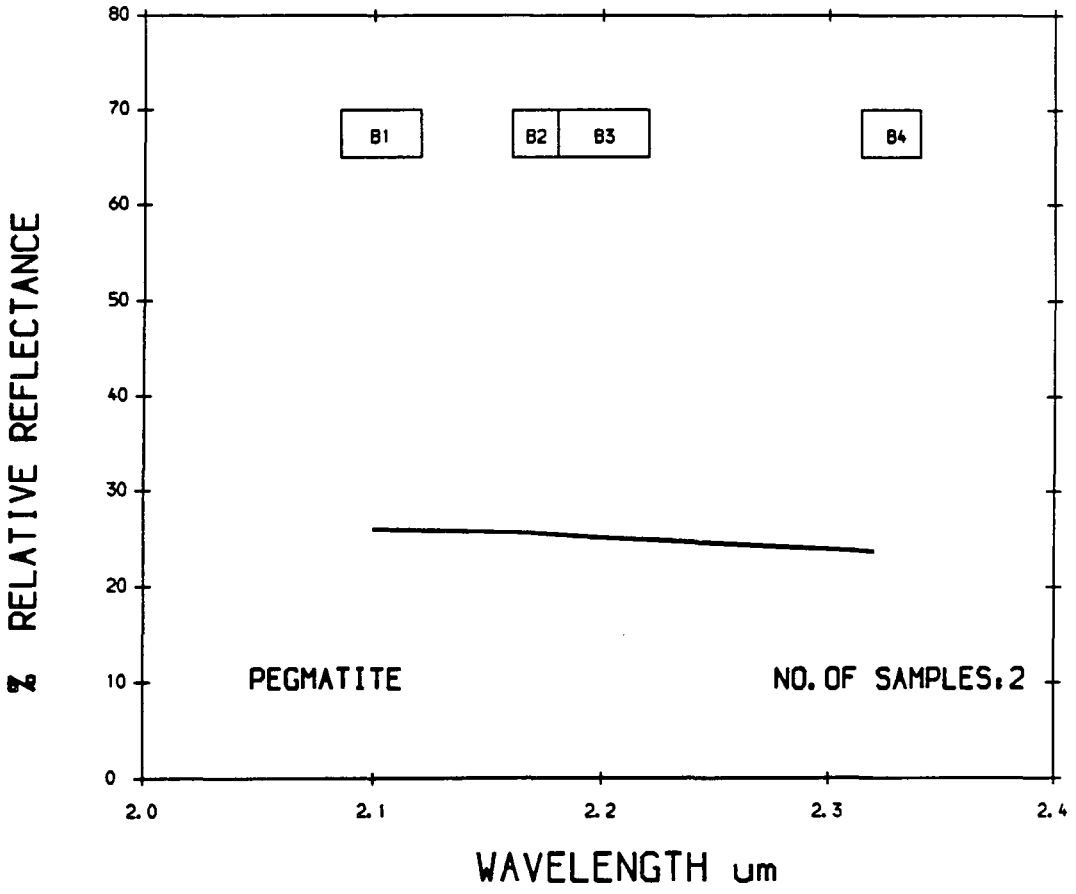

AVERAGE HHRR SPECTRA FROM JABAL SA`ID AREA